The impact of maternal glucose fluctuations in gestational diabetes on placental development

Abigail Rose Byford

Submitted in accordance with the requirements for

the degree of Doctor of Philosophy in Medicine

The University of Leeds

School of Medicine

September 2023

Intellectual Property and Publication Statement

The candidate confirms that the work submitted is her own and that appropriate credit has been given where reference has been made to the work of others.

Acknowledgements

Firstly, I would like to thank my supervisory team (Dr Karen Forbes, Professor Eleanor Scott, Dr Virginia Pensabene and Dr Nigel Simpson) for their support, advice, and assistance during my PhD. While Karen has been invaluable in the development and completion of this project, she has also been a great mentor and has introduced me to the field of placental research, which has inspired me to pursue a career in this area. Eleanor has provided me with her expert knowledge on glucose fluctuations in diabetic pregnancies and understanding the clinical applications of this project. Thank you to Virginia for her support with the microfluidics work, and for her continued efforts to train me on these new techniques even during Covid-19, when we could not meet in person. I would also like to thank Virginia's PhD student Elena Mancinelli for making and delivering me weekly microfluidic devices and for the advice when I was finding microfluidic cell culture a challenge. As well as Dr Kristina Haase and Dr Marta Cherubini at EMBL Barcelona for hosting me for 2 weeks to work with their triculture placental microvasculature model and helping me with these experiments. Additionally, thank you to the BHF for funding this project.

I would like to thank everyone in the Leeds pregnancy research group, particularly members of the Forbes and Forde labs, Manon Owen, Dr Rachel Quilang, Dr Maggie Kennedy, Georgia Fakonti, Rachel Farrelly, Dr Amanda Leow, Jessica Edge, and Haidee Tinning, for their friendship, knowledge, technical support (including help with medium changes, placenta collections and finding patient demographics). Thank you to those in the Forbes group who also helped me deliver my placenta lino printing at various events, including Jane Luk, who has been a great extended member of the Forbes group at conferences. To all the friends I have made at LICAMM, including all the other BHF-funded PhD students, you have made my time in LICAMM incredibly enjoyable. Especially Manon Owen, Katie Smith, and Jacob Kinsella for your support, friendship, and laughs. I would also like to thank the LICAMM SOT, Ruth Hughes and Sally Boxall in the Bioimaging facility for their flow cytometry and microscopy expertise and my mentor, Josie Fullerton at the University of Glasgow.

A massive thank you to all my family and friends, especially my partner Lewis, for putting up with my stress whilst living with me throughout the PhD. My mum, Julie, who has had a difficult time with her health over the last year, but never failed to support me and tell me how proud of me she is, as well as my incredibly supportive dad, Richard. Thank you to my sister, Chloe and partner Will, who have also given me my beautiful niece Bella, who has been lovely to spend time with on weekends at home when needing a break from my PhD. Thanks to my friends, Emily, Rachel, Ellen, Amy, as

well as Lewis' family. Finally, I would also like to thank my loving Nana and my late Grandad, who was always the most interested in hearing about my research.

Abstract

Background: Gestational diabetes (GDM) affects around 13% of pregnancies and is associated with an increased risk of infants being born large-for-gestational-age (LGA). LGA can lead to birth complications and infants are predisposed to developing future cardiometabolic disease. The prevalence of LGA remains high even when glycaemia is well controlled and continuous glucose monitoring (CGM) has demonstrated that women with GDM who deliver LGA infants have temporal periods of mild hyperglycaemia. It is unclear how this causes LGA, but LGA has been linked to altered placental development and function.

Aim: To determine whether temporal periods of mild hyperglycaemia associated with LGA in GDM impact on placental development and function.

Methods: Placental explants from uncomplicated pregnancies were cultured in glucose fluctuations mimicking *in vivo* levels in GDM. Further RNA sequencing, bioinformatics, immunohistochemistry and ELISAs were performed to predict the functional consequence. Two models were employed to assess the impact of glucose fluctuations on placental vascular development; endothelial-lineage differentiation of placental mesenchymal stromal cells (pMSCs) isolated from term placentae, and a perfusable 'on-a-chip' model of placental microvessels. Differentiation potential and microvessel function were assessed by RT-qPCR, and functional assays.

Results: Mild hyperglycaemia altered the placental transcriptome and differentially expressed genes (DEGs) were predicted to be associated with vascular development and an anti-inflammatory response. ELISAs and RT-qPCR confirmed downregulation of pro-inflammatory mediators and showed trends towards increased levels of vascular-regulatory M2-polarised placental macrophages (Hofbauer Cells; HBCs). Culture of pMSCs in mild hyperglycaemia had minimal impact on their endothelial-lineage differentiation, however vessel development and permeability were altered by glucose fluctuations in the microvessel model.

Conclusion: Fluctuations in maternal glucose in GDM can alter the placental transcriptome and may contribute to placental vascular dysfunction, directly and/or via HBCs. This may impact the ability of the placenta to transfer nutrients and gases to the fetus, resulting in LGA.

Table of Contents

Word Count: 89,346

List of Figures

List of Tables

List of Abbreviations

2DG	2-deoxyglucose
2DG6P	2-deoxyglucose-6-phosphate
4PL	Four Parameter Logistic
ABCG2	ATP-binding cassette super-family G member 2
ac-LDL	Acetylated low-density lipoprotein
ACOG	American College of Obstetrics and Gynaecology
ACTB	Actin β/β-actin
ADA	American Diabetes Association
AGA	Appropriate-for-gestational-age
AiDAPT	Automated insulin delivery amongst pregnant women with type 1 diabetes study
ALAS2	Erythroid-specific 5-aminolevulinate synthase
AMSC	Adipose Tissue MSC
Ang-1	Angiopoietin-1
ANOVA	Analysis of Variance
av-MSC	Amnion avascular MSC
B2M	β2-microglobulin
BCL2A1	Bcl-2-related protein A1
BM	Basal Membrane
BMI	Body mass index
BMP	Bone morphogenic protein
BMSC	Bone marrow MSC
BSA	Bovine serum albumin
Bv-MSCs	Placental Chorionic Blood Vessel MSCs
BWC	Birthweight Centile
CALD1	Caldesmon
CASP3	Caspase 3
CCL	Chemokine Ligand
CCN1	Calponin
CCNG2	Cyclin-G2
CCR	C-C chemokine receptor
CDH2	Cadherin 2
cDNA	Complementary DNA
CEBPB	CCAAT/enhancer-binding protein beta
CGM	Continuous Glucose Monitoring
CMSCs	Chorionic (Plate) MSCs

CONCEPTT	Continuous glucose monitoring in pregnant women with type 1 diabetes study
CPS1	Carbamoyl phosphate synthetase 1
CRH	Corticotropin-releasing hormone
CSH1	Chorionic somatomammotropin hormone 1
Ct	Cycle threshold
CXCR	CXC chemokine receptors
DAB	3,3′-Diaminobenzidine
DAPI	4′,6-diamidino-2-phenylindole
DCCT	Diabetes control and complications trial
DEGs	Differentially expressed genes
DM	Diabetes Mellitus
DMEM	Dulbecco's Modified Eagle Medium
DMSO	Dimethylsulfoxide
dNK	Decidual natural killer cell
DOHaD	Developmental Origins of Health and Disease
DPX	Dibutylphthalate Polystyrene Xylene
EC	Endothelial cell
ECFCs	Endothelial colony forming cells
ECM	Extracellular matrix
ECSCR	Endothelial Cell Surface Expressed Chemotaxis and Apoptosis Regulator
EGF	Epidermal growth factor
EGFR	Epidermal growth factor receptor
EGM	Endothelial growth medium
EL	Endothelial lipase
EndMT	Endothelial-to-Mesenchymal transition
eNOS	Endothelial nitric oxide synthase
EPCAM	Epithelial cell adhesion molecule
ER	Enrichment ratio
EVM	Extravascular gel matrix
EVs	Extracellular vesicles
EVT	Extravillous trophoblast
FABP	Fatty acid binding protein
FATP	Fatty acid transport protein
FBS	Fetal bovine serum
FCGR2B	Fc gamma receptor IIb
FcR	Fc Receptor

FDA	Functional Data Analysis
FDR	False Discovery Rate
FFPE	Formalin Fixed Paraffin Embedded
FGF	Fibroblast growth factor
FGR	Fetal growth restriction
FI	Flow index
FLT1/VEGFR1	Fms related receptor tyrosine kinase
FpECs	Fetoplacental endothelial cells
FSC-A	Forward scatter area
FSC-H	Forward scatter height
GAPDH	Glyceraldehyde 3-phosphate dehydrogenase
GATM	Glycine amidinotransferase
GCM1	Chorion-specific transcription factor GCMa
GDM	Gestational Diabetes Mellitus
gDNA	Genomic DNA
GelMA	Methacrylated gelatin membrane
GEO	Gene Expression Omnibus
GHRL	Ghrelin-obestatin prepropeptide
GLUT	Glucose Transporter
GO	Gene Ontology
GPC3	Glypican-3
GPR183	G-protein coupled receptor 183
GROW	Gestation Related Optimal Weight
GUSB	β-glucuronidase
H&E	Haematoxylin and Eosin
HAPLN2	Hyaluronan and Proteoglycan Link Protein 2
HAPO	Hyperglycaemia and adverse pregnancy outcome study
HbA1c	Glycosylated haemoglobin
HBA2	Haemoglobin subunit alpha 2
HBC	Hofbauer Cell
HBSS	Hanks Balanced Salt Solution
HCAM1/CD44	Homing cell adhesion molecule
hCAT-1	Human cationic amino acid transporter 1
hCG	Human chorionic gonadotrophin
hENT	Human equilibrative nucleoside
HGF	Hepatocyte growth factor
HK2	Hexokinase 2

HLA	Human leukocyte antigen
HLA-DR	Major histocompatibility complex class II DR
HPAEC	Human placental arterial endothelial cell
HPC	Haematopoietic stem cell
HPF	Human placental fibroblast
HPP	Human placental pericyte
HPRT1	Hypoxanthine phosphoribosyltransferase 1
HPVEC	Human placental venous endothelial cell
HUVEC	Human umbilical vein endothelial cell
ICAM-1	Intercellular adhesion molecule 1
IDF	International diabetes federation
IGF	Insulin-like growth factor
IGFBP	IGF-binding protein
IHM	Interhemal membrane
IL	Interleukin
IL36RN	Interleukin 36 receptor antagonist
ILRL1	Interleukin 1 receptor-like 1
INSL4	Early placenta insulin-like peptide
IPA	Ingenuity pathway analysis
ISCT	International society of cellular therapy
IUGR	Intrauterine growth restriction
IVS	Intervillous space
JCAD	Junctional cadherin 5 associated
KDR/VEGFR2	Kinase insert domain receptor
KEGG	Kyoto Encyclopaedia of Genes and Genomes
KISS1	KISS1 metastasis inhibitor
LAT	Large neutral amino acid transport
LDH	Lactate dehydrogenase
LDLs	Low-density lipoproteins
LDS	Lithium dodecyl sulfate
LEP	Leptin
LGA	Large-for-gestational age
Log_2FC	Log_2 Fold Change
LPL	Lipoprotein lipase
LPS	Lipopolysaccharide
LYPD6	PLAUR domain-containing protein 6
MAGiC	Maternal Glucose in Pregnancy Study

MAPK	Mitogen-activated protein kinase
MCAM/CD146	Melanoma cell adhesion molecule
MHC	Major histocompatibility complex
miRNAs	Micro RNAs
MMP	Matrix Metalloproteinase
MRC1/CD206	C-type mannose receptor 1
MSC	Mesenchymal stromal/stem cell
MVM	Microvillous membrane
MYH11	Myosin 11
MYOCD	Myocardin
MyoD	Myoblast determination protein 1
NAMPT	Nicotinamide phosphoribosyltransferase
Nanog	Homeobox protein Nanog
NBF	Neutral buffered formalin
NEAA	Non-Essential Amino Acids
NEFAs	Non-esterified fatty acids
NGS	Next Generation Sequencing
NICE	National Institute for Clinical Excellence
NLRP1	NLR family pyrin domain containing 1
NO	Nitric oxide
NPID	National Pregnancy in Diabetes Audit
NR3C1	Glucocorticoid receptor
NR4A1	Nuclear receptor subfamily 4 group A member 1
NRT	No reverse transcriptase Control
NT5E/CD73	Ecto-5′-nucleotidase
NTC	No template control
Oct4	Octamer-binding transcription factor 4
OGTT	Oral glucose tolerance test
ORA	Over Representation Analysis
PAX	Paired box gene
PBS	Phosphate buffered saline
PCA	Principle Component Analysis
PDGFD	Platelet derived growth factor D
PDGFRβ	Platelet derived growth factor receptor beta
PDMS	Polydimethylsiloxane
PECAM1/CD31	Platelet endothelial cell adhesion molecule
PFA	Paraformaldehyde

PGDH	Hydroxyprostaglandin dehydrogenase
PGE2	Prostaglandin E2
PI	Pulsatility Index
PIK3R1	Phosphatidylinositol 3-kinase regulatory subunit 1
PLAC1	Placenta-specific protein 1
PlGF	Placental growth factor
pMSCs	Placental mesenchymal stromal cell
PPARγ	Peroxisome proliferator-activated receptor γ
proMMP-9	TIMP-deficient matrix metalloproteinase-9 zymogen
PSG	Penicillin, streptomycin, and glutamine
PTGS2/COX2	Prostaglandin-endoperoxide synthase 2
PVDF	Polyvinylidene fluoride
QQ	Quantile Quantile
Q_{uv}	Umbilical vein volume blood flow
RAMP2	Receptor Activity Modifying Protein 2
RCT	Randomised controlled trial
RFP	Red fluorescent protein
RIPA	Radioimmunoprecipitation assay buffer
ROI	Region of Interest
ROX	5-carboxy-X-rhodamine
RPL13A	60S ribosomal protein L13a
RPLP0	60S acidic ribosomal protein P0
SELL	L-Selectin
sEng	Soluble endoglin
sFLT1	Soluble fms-like tyrosine kinase 1
SGA	Small-for-gestational age
SHEDs	Stem cells from human exfoliated deciduous teeth
SMBG	Self-monitoring of blood glucose
SNAT	Small neutral amino acid transport
SOX2	SRY (sex determining region Y)-box 2
SPHK1	Sphingosine kinase 1
SRRT	Serrate RNA effector molecule homolog
SSC-A	Side scatter area
STAT3	Signal transducer and activator of transcription 3
STC1	Stanniocalcin-1
STZ	Streptozotocin
SV40	Simian virus 40 large T antigen

T1DM	Type 1 Diabetes Mellitus
T2DM	Type 2 Diabetes Mellitus
TAGLN	Transgelin
TAR	Time Above Range
TAT	T amino acid transporter
TBR	Time Below Range
TBS	Tris Buffered Saline
TBST	Tris Buffered Saline with Tween
TEER	Transepithelial electrical resistance
TGF β	Transforming growth factor β
Th1	Type 1 helper T cell
Th2	Type 2 helper T cell
THY1/CD90	Thymocyte differentiation antigen 1
TIMP1	Tissue inhibitor of metalloproteinases-1
TIR	Time in Range
T_m	Melting Temperature
TMT	Tandem Mass Tagging
TNFAIP8	Tumour necrosis factor-α–induced protein 8
TNF-α	Tumour necrosis factor α
TOP1	Topoisomerase 1
TUNEL	Terminal deoxynucleotidyl transferase dUTP nick end labelling
uMAP	Uniform Manifold Approximation and Projection
UMSC	Umbilical Cord MSC
VCAM-1	Vascular cell adhesion molecule 1
VE-Cadherin/CDH5	Vascular endothelial cadherin
VEGF	Vascular endothelial growth factor
VEGFR	VEGF receptor
VFI	Vascular flow index
VI	Placental vascular index
VLDL	Very low-density lipoprotein
VSC	Vascular stem cell
VSIG4	V-set and immunoglobulin domain containing 4
VSMC	Vascular smooth muscle cell
VT	Villous trophoblast
VTN	Vitronectin
vWF	von Willebrand factor

WHO	World health organisation
WNT11	Wnt Family Member 11
XIAP	X-linked inhibitor of apoptosis protein
YWHAZ	14-3-3 protein zeta/delta
αSMA	α smooth muscle actin
ΔΔCt	Delta-Delta Ct

Publications relating to this thesis

Published review articles:

- Byford AR, Forbes K, Scott EM. (2022). Glucose Treatment Targets in Pregnancy - A Review of Evidence and Guidelines*. Current Diabetes Reviews,* 19(2).
- Byford A, Baird-Rayner C, Forbes K. (2021). Don't sugar coat it: the effects of gestational diabetes on the placental vasculature. *The Biochemist,* 43(2): 34-39.

Published abstracts:

- Byford A, Walsh K, Scott EM, Forbes K. (2022) Temporal periods of mild hyperglycaemia in pregnancies complicated by gestational diabetes and LGA alter placental transcriptomic networks associated with vascularisation and M2 Hofbauer cell polarisation. Endocrine Abstracts, 86: P199. Poster presentation at the Society for Endocrinology annual conference, Harrogate, UK.
- Byford A, Walsh K, Scott EM, Forbes K. (2022) Temporal periods of maternal hyperglycaemia in gestational diabetes alter placental transcriptome networks associated with inflammation and vascular development. Placenta, 122. Poster presentation at Sociedad Latinoamericana de Interacción Materno-Fetal y Placenta (SLIMP) conference.
- Byford A, Walsh K, Scott EM, Forbes K. (2021) An ex-vivo human placental model demonstrates that temporal fluctuations in maternal glucose in gestational diabetes alter placental transcriptome networks associated vascular development and angiogenesis. Endocrine Abstracts, 77: OP3.2. Poster presentation and oral flash talk at the at the Society for Endocrinology annual conference Edinburgh, UK.
- Byford A, Walsh K, Scott EM, Forbes K. (2021) Temporal fluctuations in maternal glucose levels alter placental transcriptome in pregnancies complicated by gestational diabetes'. Placenta, 112:e65. Poster presentation at the International Federation of Placenta Associations (IFPA) conference.

Chapter 1 – General Introduction

1.1 Diabetes mellitus in pregnancy

Diabetes mellitus (DM) is a metabolic disorder that results from impaired insulin secretion, insulin resistance or a combination of both[1]. Type 1 Diabetes (T1DM) is typically caused by autoimmune damage to the insulin-producing β-cells of the pancreas, whereas Type 2 Diabetes (T2DM) can occur due to insulin resistance and subsequent varying degrees of β-cell failure[2]. The inability of insulin to control blood glucose levels can lead to hyperglycaemia, which can subsequently cause β-cell dysfunction, impairing insulin secretion, resulting in a cycle of hyperglycaemia[3]. In 2017, the International Diabetes Federation (IDF) estimated that 451 million adults live with diabetes worldwide, which is expected to increase to 693 million by 2045, making it one of the largest public health concerns[4]. Secondary complications of diabetes include retinopathy, neuropathy, nephropathy and cardiovascular complications, which arise following progressive tissue and vascular damage[1]. A particular concern is the increased rates of diabetes in the younger population, including women of reproductive age[5].

Diabetes in pregnancy can arise due to pre-gestational diabetes (T1DM or T2DM), or gestational diabetes (GDM). GDM, is diabetes that first manifests during pregnancy and usually resolves post-partum[6]. In normal pregnancies, as gestation advances, insulin resistance increases, due to changes in placental hormones, such as oestrogen and progesterone[7]. Additionally, the β-cells undergo hyperplasia and hypertrophy to meet the metabolic demands of pregnancy[8]. In women with GDM, maternal glucose regulation is compromised, which occurs as a result of β-cell dysfunction[8]. Here, β-cells fail to compensate for the demands of pregnancy, which when combined with insulin resistance, results in hyperglycaemia[8]. Additionally, increased maternal adipose deposition, reduced exercise, and increased caloric intake contribute to relative glucose intolerance in GDM[9]. In 2019, it was reported that the overall rate of hyperglycaemia in pregnancy was 15.8%, with GDM and pre-gestational diabetes accounting for 12.8% and 2.6%, respectively[10]. Rates of pre-gestational diabetes in pregnancy and GDM are rising worldwide, due to the increased levels of obesity and T2DM associated with unhealthy lifestyles[5,11]. For example the proportion of diabetic pregnant women that have T2DM has increased to 50% in 2016, compared to 27% in 2002-2003[12].

1.1.1 Diagnosis and treatment

GDM is currently diagnosed by an oral glucose tolerance test (OGTT) conducted between 24-28 weeks' gestation, where 75g of glucose is ingested and blood glucose measured after 2 hours[13]. A patient is diagnosed with GDM if they have a fasting plasma glucose level of 5.6 mM or above, or a 2-hour plasma glucose level of 7.8 mM or above[14]. There are also several risk factors for developing GDM, including an ethnicity with high diabetes prevalence, family history of diabetes, previous GDM, body mass index (BMI) above 30 kg/m^2 and a previous baby weighing over 4.5 kg[14]. GDM is initially managed by lifestyle modifications, such as diet and exercise. If patients still fail to achieve glycaemic control, then pharmacological interventions are used, such as insulin or metformin, which when used in combination, or individually, can normalise blood glucose levels[6].

1.1.2 Adverse maternal and fetal outcomes

Prenatal exposure to maternal diabetes has been associated with an increased risk of complications for both the mother and the fetus. Complications that occur and are widely studied in pregnancies complicated by diabetes include spontaneous abortions/miscarriage, still birth, and pathological fetal growth[15–18]; as well as maternal complications, such as preeclampsia and hypoglycaemia[19]. Appropriate glycaemic control is paramount in reducing the risk of these adverse obstetric and neonatal outcomes[12]. Pre-gestational diabetes in pregnancy, and GDM (to a lesser extent) can also result in the development of congenital abnormalities, including congenital heart disease[20]. Organogenesis occurs between 5-8 weeks gestation[21]; therefore, the increased risk of congenital abnormalities could be linked to the onset of diabetes in pregnancy, given that poor glycaemic control could be present at conception and early pregnancy in women with pre-gestational diabetes. Although GDM is detected later in pregnancy, undetected poor glycaemic control could be present earlier, when the teratogenic affect could occur, resulting in a slightly higher risk of congenital anomalies, than the normal population[22]. Adverse outcomes in diabetic pregnancies can also lead to increased risk of cardiometabolic diseases later in life, in the mother and offspring[23]. Particularly, GDM has major long-term implications for maternal cardiovascular health, including a greater risk of heart failure, stroke, and ischemic heart disease[24]. In a recent study, MRI imaging during pregnancy revealed that women with GDM had impaired myocardial contractility and higher left ventricular mass, compared to women with healthy pregnancies. This was also associated with reduced myocardial energetics, demonstrating that the potential for GDM to impact maternal cardiovascular health likely occurs during pregnancy[24].

1.1.3 Pathological fetal growth

Complications of fetal growth occur in GDM, with large-for-gestational age (LGA) infants being the most common, while fetal growth restriction (FGR) and small-for-gestational age (SGA) are also observed, but to a lesser extent[25]. LGA and SGA are defined as infants that weigh above the 90th percentile, or below the 10th percentile for their gestational age, respectively[26]. Some studies refer to fetal overgrowth as 'macrosomia', which usually refers to birthweight above 4000 g, and is irrespective of gestational age[27]. LGA can cause complications in delivery, including prolonged labour, vaginal tearing and shoulder dystocia; therefore, LGA infants are often delivered early by a caesarean section, which has its own associated risks[27,28]. Both SGA and LGA newborns are predisposed to developing T2DM, cardiovascular disease and obesity later in life[8,27,29]. These cardiometabolic complications increase the risk of offspring themselves developing GDM in pregnancy[8], resulting in a self-perpetuating cycle of cardiometabolic disease. This also demonstrates that the *in utero* exposure to maternal diabetes leads to fetal programming, resulting in long-term health complications. This is a concept known as the 'Developmental Origins of Health and Disease' or DOHaD[30]. This has been linked to epigenetic changes, which have long-lasting effects on gene expression and increase the risk of developing non-communicable diseases, such as cardiometabolic diseases. Epigenetic DNA imprinting activity is the most active pre-conception to early infancy and thus is thought to contribute to developmental programming[31].

The hyperglycaemia and adverse pregnancy outcome (HAPO) study was paramount in demonstrating the association between maternal hyperglycaemia and the development of LGA. This study showed that rates of LGA increased with increasing maternal glucose levels, even in women that were not clinically diagnosed with GDM[32]. Although mechanisms for LGA are unclear, in 1954, Pedersen proposed that when maternal glycaemic control is compromised, as in GDM, blood glucose can cross the placenta and initiate insulin production in the fetus[32]. This usually occurs in the second trimester when the fetal pancreas has developed. Hyperinsulinemia and hyperglycaemia lead to an increase in fetal adiposity, increasing fat and protein stores and consequently resulting in further growth of the fetus[33]. However, more recent theories have expanded on this, which suggest that in addition to glucose, maternal amino acids and lipids, lead to an increase in nutrient supply to the fetus, elevating fetal insulin and growth[34]. In line with this, the prevalence of LGA remains high, even when pregnancies are considered well-controlled clinically, using standard methods of monitoring (self-monitoring of blood glucose [SMBG] and glycosylated haemoglobin [HbA1c]). Therefore, it is thought

that either factors other than glucose are involved and/or that these methods fail to detect the glucose variations that may result in LGA[35–37].

1.1.4 Methods of monitoring blood glucose during pregnancy

Glucose monitoring, used to assess glycaemic control, is the foundation of self-management in diabetes. The currently used methods of glucose monitoring during pregnancy include HbA1c, SMBG and continuous glucose monitoring (CGM).

HbA1c takes an overview of glycaemia from the preceding 60-90 days[38,39]. The Diabetes Control and Complications Trial (DCCT) in 1993 reported that the normal reference range of HbA1c in non-diabetic individuals is 4-6% (20-42 mmol/mol)[40,41] and that glycaemic control as close to this range as possible, can slow the progression of diabetic complications, such as retinopathy, nephropathy and neuropathy[39,41]. HbA1c is mainly used pre-conception to ensure adequate blood glucose control prior to pregnancy in women with pre-existing diabetes. In pregnancy, HbA1c levels are lower due to haemodilution and increased red blood cell turnover[21] and therefore is not the most useful method and it is seen as a secondary measurement for glycaemic monitoring. Moreover, HbA1c does not provide information about short term changes in glycaemia, for example post-prandially[21]. In guidelines from various societies, including the National Institute for Clinical Excellence (NICE), American College of Obstetrics and Gynaecology (ACOG) and the American Diabetes Association (ADA), HbA1c is recommended to be below 6-6.5% pre-pregnancy, if possible, without causing hypoglycaemia. However, NICE and ACOG do not recommend that HbA1c should be used during pregnancy[14,21,42–48].

SMBG is recommended for women with diabetes in pregnancy to monitor their blood glucose throughout gestation. Measurements include fasting, pre-prandial (prior to meals) and 1-2 hours post-prandial (after meals). This is important so that insulin and other pharmacological treatments can then be adapted to control fluctuations in blood glucose throughout the day[39,49]. Many studies have shown that SMBG can improve glycaemic control and pregnancy outcomes, as well as economic parameters (number of hospital stays and patient expenses)[50–52]. The NICE guidelines state that fasting glucose should be below 5.3 mM, and 1- and 2-hour post-prandial glucose should be below 7.8 and 6.4 mM, respectively[14,53], with similar guidelines from other societies[14,21,42–48].

HbA1c and SMBG provide only a snapshot of the glucose profile, at limited times during the day[35–37]. CGM, on the other hand, monitors interstitial glucose continuously and can provide more detailed glucose profiles and glycaemic excursions across the

24-hour day[54,55]. CGM devices generate an extensive amount of data, and many summary metrics can be calculated from this, including, mean glucose over time, time in range (TIR), time above range (TAR) and time below range (TBR), and measures of glycaemic variability (such as standard deviation and coefficient of variation)[54,55].

Recent studies have shown that CGM use significantly improves pregnancy outcomes, including the large, multicentre CGM randomised controlled trial (RCT) in pregnant women with T1DM on intensive insulin therapy, known as CONCEPTT[56]. The findings from this study showed that CGM use in pregnancy was associated with lower rates of LGA infants, with women in the CGM group spending more TIR (3.5-7.8 mmol/L) and lower TAR. This was achieved without increasing the rate of hypoglycaemia, gestational weight gain or insulin dose. In GDM pregnancies, CGM use has been shown to improve gestational weight gain, and influenced pharmacotherapy treatment in pregnancy to correct for hyper- or hypo-glycaemia[57–59].

The TIR target for CGM is 3.5-7.8 mmol/L for both pre-gestational diabetes in pregnancy and GDM. The upper limit of 7.8 mmol/L is in line with most SMBG post-prandial targets. The lower limit is based on the most recent studies in T1DM pregnancies, including CONCEPTT[56,60]. While it is primarily used in T1DM pregnancies, CGM guidelines are currently in the process of being updated to accommodate this new evidence and enable more widespread uptake of this method of monitoring[54,55].

1.1.5 Maternal glucose fluctuations associated with LGA

Given that CGM can provide detailed glucose profiles and glycaemic excursions across the 24-hour day[54,55], functional data analysis (FDA) can be applied to assess differences in temporal glucose profiles in relation to clinical outcomes. This has been utilised by several studies to give additional information about glucose levels in pregnancy using CGM[36,61,62]. For example, previous studies utilising CGM in pre-gestational diabetic pregnancies[37,63] were re-analysed by Law *et al*. (2015)[36] using FDA. While mean HbA1c was similar between women who delivered LGA and non-LGA infants, LGA was associated with a lower mean glucose in the first trimester (7 vs 7.1 mM; $p<0.01$) and higher mean glucose in the second and third trimesters (7 vs 6.7 mM; $p<0.001$ and 6.5 vs 6.4 mM; $p<0.01$, respectively). FDA showed that in the first trimester glucose values were significantly lower midmorning (09:00-11:00) and early evening (19:00-21:30).

In a recent study, Law *et al.* (2019) performed FDA on 153 women with GDM and performed masked-CGM for 7 days between 30-32 weeks' gestation. Mean glucose

over time was significantly higher in mothers that had LGA infants (6.2 mM), in comparison to their counterparts that had appropriately grown (AGA) infants (5.8 mM; p=0.025). Using functional data analysis, they observed that women with LGA infants had a higher nocturnal glucose (6.0±1.0 mM) for 6-hours overnight (00:30-06:30), compared to mothers of AGA infants (5.5±0.8 mM; p=0.005) (Figure 1.1)[62]. While these levels are only subtle increases (mild hyperglycaemia) and are not above the CGM target range (3.5-7.8 mM)[55], this accounts for 25% of the 24-hour day where the fetus is exposed to higher maternal glucose and this associated risk of LGA.

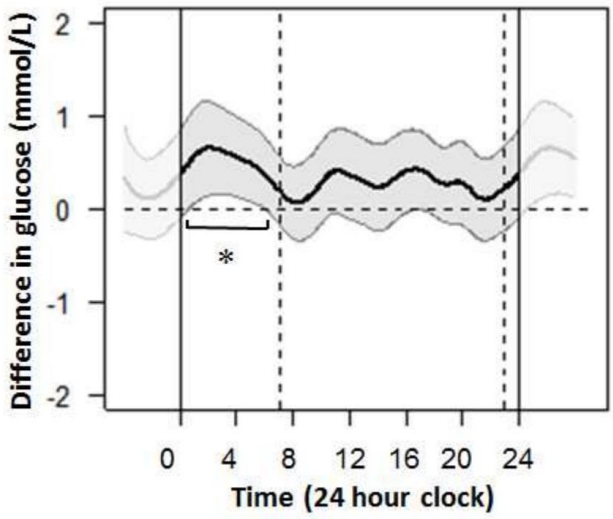

Figure 1.1 – Continuous Glucose Monitoring (CGM) profile of GDM mothers with LGA and AGA infants over a 24-hour period. Difference in mean temporal glucose levels between GDM mothers with LGA infants (dark wavy line) and GDM with AGA infants (horizontal dotted line). The grey area represents 95% confidence intervals, *p<0.05 (n=153, sensors worn for ~6 hours, 30-32 weeks' gestation)[62].

1.2 The placenta

Many of the complications that occur in GDM are thought to be linked to abnormal development of the placenta[64]. The placenta is a temporary organ that supports the development of the fetus during pregnancy by exchanging nutrients, including glucose, waste and gases between the mother and fetus[65]. The placenta is also an endocrine organ, which secretes hormones and growth factors responsible for sustaining pregnancy, such as human chorionic gonadotrophin (hCG) and progesterone[66]. To carry out its role, the placenta is highly vascularised and is comprised of two separate circulatory systems, the fetoplacental and uteroplacental circulation. The fetoplacental circulation includes the umbilical cord, which connects the placenta to the fetus and contains two umbilical arteries and one umbilical vein[67]. These umbilical vessels branch into the chorionic villi, which contain the fetal vessels and provide a large surface area to allow for efficient exchange of nutrients and gases[65,67]. The uteroplacental circulation is the flow of maternal blood from the uterine arteries into the intervillous space (IVS), which are spaces between the chorionic villi[68] (Figure 1.2).

1.2.1 Normal placental development

In early embryogenesis the blastocyst comprises of the embryoblast (inner cell mass) and the trophectoderm. The zona pellucida, which surrounds the blastocyst degenerates around 6-days post-conception, allowing the blastocyst to implant into the uterine wall[69]. The placenta comprises of two cell lineages, the trophoblast lineage, derived from the trophectoderm and the endothelial cell lineage, derived from the extra-embryonic mesoderm of the inner cell mass. The extra-embryonic mesoderm forms the allantois, a sac-like structure; blood vessels differentiate from the allantois mesodermal wall, giving rise to the umbilical cord[70].

The trophoblast cell lineage can differentiate into two cell types, the syncytiotrophoblast and the cytotrophoblast. Cytotrophoblasts are the resident stem cells of the placenta, which proliferate and cover the mesenchyme and fetal vessels that form the chorionic villi. Fusion of cytotrophoblast then generates and continuously replenishes the syncytiotrophoblast, a continuous outer single multinucleated epithelial cell layer[70,71]. The syncytium is the outermost layer of the chorionic villi, in contact with the maternal blood. It also contains microvilli, which increase the surface area and allow more time for absorption of nutrients[72] (Figure 1.2 Inset). Cytotrophoblasts also give rise to extravillous trophoblasts (EVTs), which anchor the placenta to the maternal decidua and transform the maternal spiral arteries into low-resistance vessels to increase blood flow to the growing fetus[71].

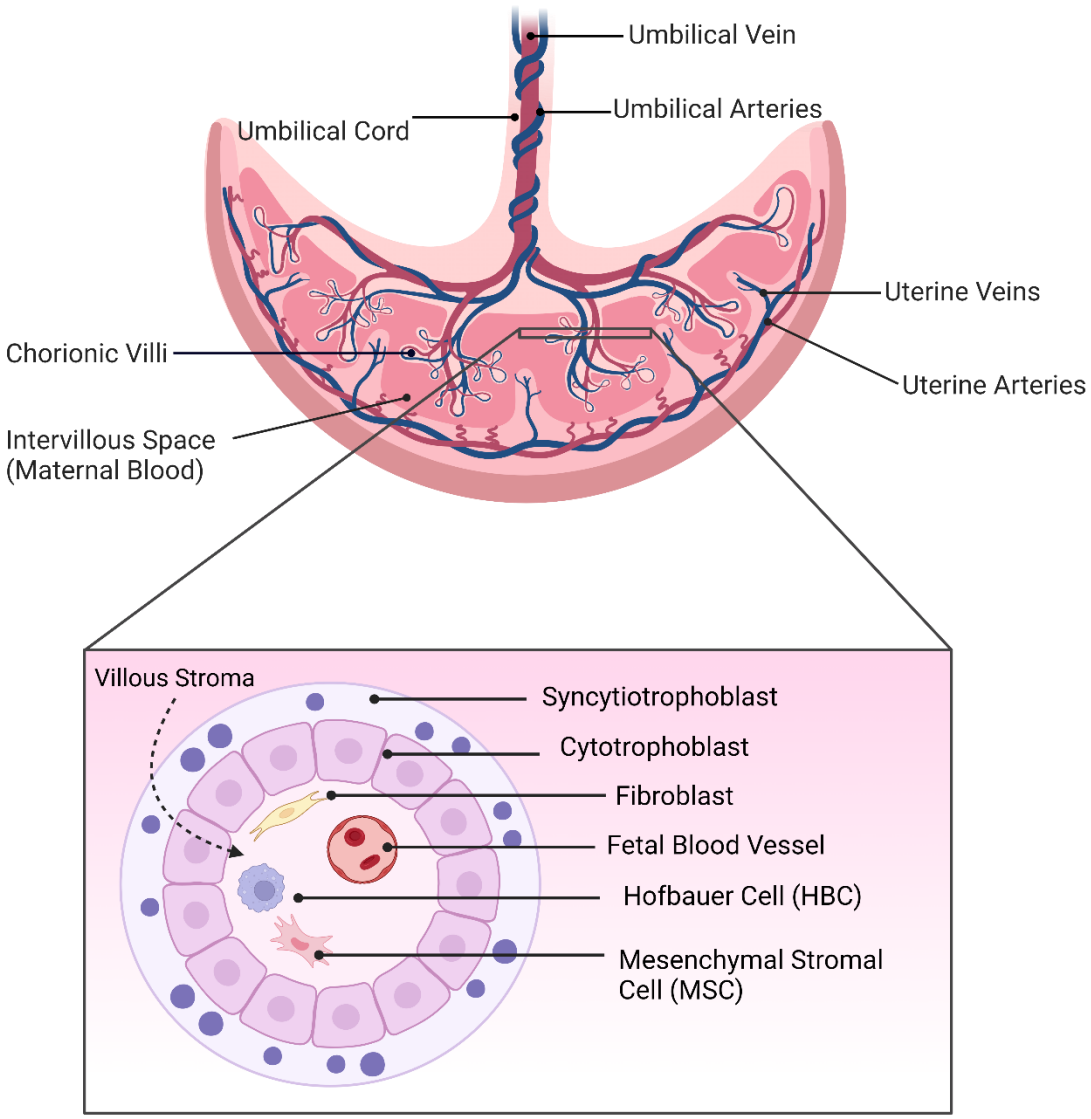

Figure 1.2 - Schematic representing the structure of the placenta. The key parts of the placenta are labelled. The inset depicts a cross section of the chorionic villi, showing the key cell types within the placenta. Image created with Biorender.com.

1.2.2 Establishment of the uteroplacental circulation

When the blastocyst is implanted in the endometrium, its nutrient supply is provided by the endometrial glands, and blood flow to the placenta is restricted, which creates a hypoxic environment[73,74]. During this time, EVTs become invasive and transform the spiral arteries. Spaces then form in the syncytium, which amalgamate to create the IVS[75]. In an early *ex vivo* study of hysterectomy specimens, Jaffe *et al.* (1997) observed a continuous trophoblastic shell at the uterine-intervillous boundary[76]. These 'trophoblast plugs' occlude uterine spiral arteries in early pregnancy, preventing blood flow into the IVS. In these early studies it was thought that these plugs become loose at 12-13 weeks' gestation, and enable blood flow[76,77]. However, in more recent histological analyses, channels were observed in trophoblast plugs from 7 weeks' gestation, and the lumen of these channels increased with gestation. Maternal red blood cells were also visible in the IVS at this time point, suggesting the uteroplacental circulation is established earlier than previously described[78]. Further studies have proposed that the increased flow through spiral arteries can lead to enhanced cell recruitment, which causes the channels to form and loss of trophoblast plug integrity, or the plug remains as a cohesive mass that is pushed away as blood flow increases throughout gestation[79].

1.2.3 Establishment of the fetoplacental circulation

The chorionic villi begin to develop 13-days post-conception when trophoblasts form extensions into the intervillous space. These projections are known as primary villi, comprised of only trophoblast cell lineages. Approximately 21-days post-conception, the primary villi are occupied by allantoic mesenchyme converting them into secondary villi. These villi become tertiary villi, including stem and terminal villi, following the development of fetal blood vessels. Stem villi connect to the chorionic plate and contain large vessels and microvessels. These are linked to terminal villi by intermediate structures. Terminal villi have many capillaries, which are separated from the syncytiotrophoblast by a thin basement membrane, with minimal maternal-fetal diffusion distance, and are therefore functional unit of the placenta[68]. This relies on the *de novo* formation of blood vessels, through vasculogenesis, and the branching of existing vessels, by angiogenesis[75].

1.2.3.1 Vasculogenesis and angiogenesis

During vasculogenesis, placental mesenchymal stromal cells (pMSCs) differentiate into haemangiogenic stem cells, which give rise to angioblast cells and haemangioblast cells, which are endothelial cell (EC) and haematopoietic cell progenitors, respectively[80]. Angioblast cells then form cell cords and eventually intercellular clefts, which creates the blood vessel lumen. These first capillaries eventually form the primitive capillary network[81].

In the third trimester, a switch to angiogenesis occurs, which is either 'branching' or 'non-branching', the sprouting or elongation of existing vessels, respectively[65,81]. Once the primitive capillary network has formed, branching angiogenesis takes place. During this process, vasodilation occurs, which increases vascular permeability. Proteases are activated and break down the basement membrane, allowing EC proliferation and migration. A stable vessel is the formed as the EC assemble, creating a lumen, and perivascular cells are recruited, such as pericytes and vascular smooth muscle cells (VSMCs)[65,81]. VSMCs are thought to compose a separate layer within the vascular wall, separated from the vascular basement membrane by MSCs, whereas pericytes are embedded into the endothelial basement membrane[82]. Pericytes contribute to vessel maturation and the expression of pericyte markers (α smooth muscle actin [αSMA] and platelet derived growth factor receptor β [PDGFRβ]) gradually increase and extend from the chorionic plate to peripheral villous branches[83]. VSMCs are important for determining vascular structure and are essential for regulating blood flow through the maternal and fetal villous networks[84]. Further into the third trimester, non-branching angiogenesis occurs through extension of existing capillaries, known as elongation, which may be proliferative or intercalative, through EC proliferation or incorporation of circulating endothelial or progenitor cells, respectively[65].

The processes of vasculogenesis and angiogenesis need to be tightly regulated during pregnancy, which involves several growth factors, such as vascular endothelial growth factor (VEGF), placental growth factor (PlGF) and fibroblast growth factor (FGF)[65,81]. FGF is responsible for the recruitment of angioblast cells early in pregnancy[81]. VEGF appears to be critical for all stages of placental vasculogenesis as inactivation of VEGF, or disruption of genes encoding VEGF receptors causes abnormal blood vessel development and embryonic lethality[85–87]. PlGF acts synergistically with VEGF to develop the placental vascular network[65]. VEGF also plays a multitude of roles in angiogenesis, including activating proteases and collagenases that breakdown the extracellular matrix (ECM) to allow for EC migration and proliferation[88,89]. It also stimulates endothelial nitric oxide (NO) production, a vasodilator and placental

angiogenic factor[90], as well as recruitment of pericytes to new vessels[82]. Other important signalling molecules include angiopoietin. ECs and pericytes are thought to communicate via angiopoietin/Tie-2 during placental vascular development[91]. Activation of Tie-2 receptors is also thought to inhibit EC apoptosis, stabilising the vessels[81,92] (Figure 1.3).

1.2.3.2 Paracrine signalling by other placental cells

Paracrine signalling by other cell types in the placenta, including fibroblasts, placental macrophages (Hofbauer Cells; HBCs) and trophoblast can contribute to placental vascular development. Trophoblast cells and HBCs are found within close proximity to developing blood vessels and have the ability to release angiogenic factors[93,94]. For example, trophoblast cells are known to release VEGF[95], FGF-2[96], PlGF[97], KISS1 metastasis inhibitor (KISS1)[98], Matrix Metalloproteinase 9 (MMP9)[99] and pigment epithelium derived factor (PEDF)[100]. HBCs and fibroblasts reside in the villous stroma[101,102]. In other organs, fibroblasts are known to regulate blood vessel formation through expression of growth factors and morphogens, such as FGF and transforming growth factor β (TGFβ), as well as ECM molecules[101]. HBCs, isolated from first trimester and term placentae, secrete VEGF-A and FGF-2[103,104]. In line with this, HBC levels have been correlated with the number of vasculogenic structures[94], and VEGF is strongly expressed in HBCs during the very early stages of pregnancy, when vasculogenesis is predominantly occuring[105]. HBCs are also known to release inflammatory mediators, such as, interleukin (IL)-8 and chemokine ligands (CCL)-2, -3 and -4[104], which are also reported to have angiogenic functions[106–112]. In *in vitro* studies, conditioned medium from HBCs increases the tubular formation in primary fetoplacental ECs[103].

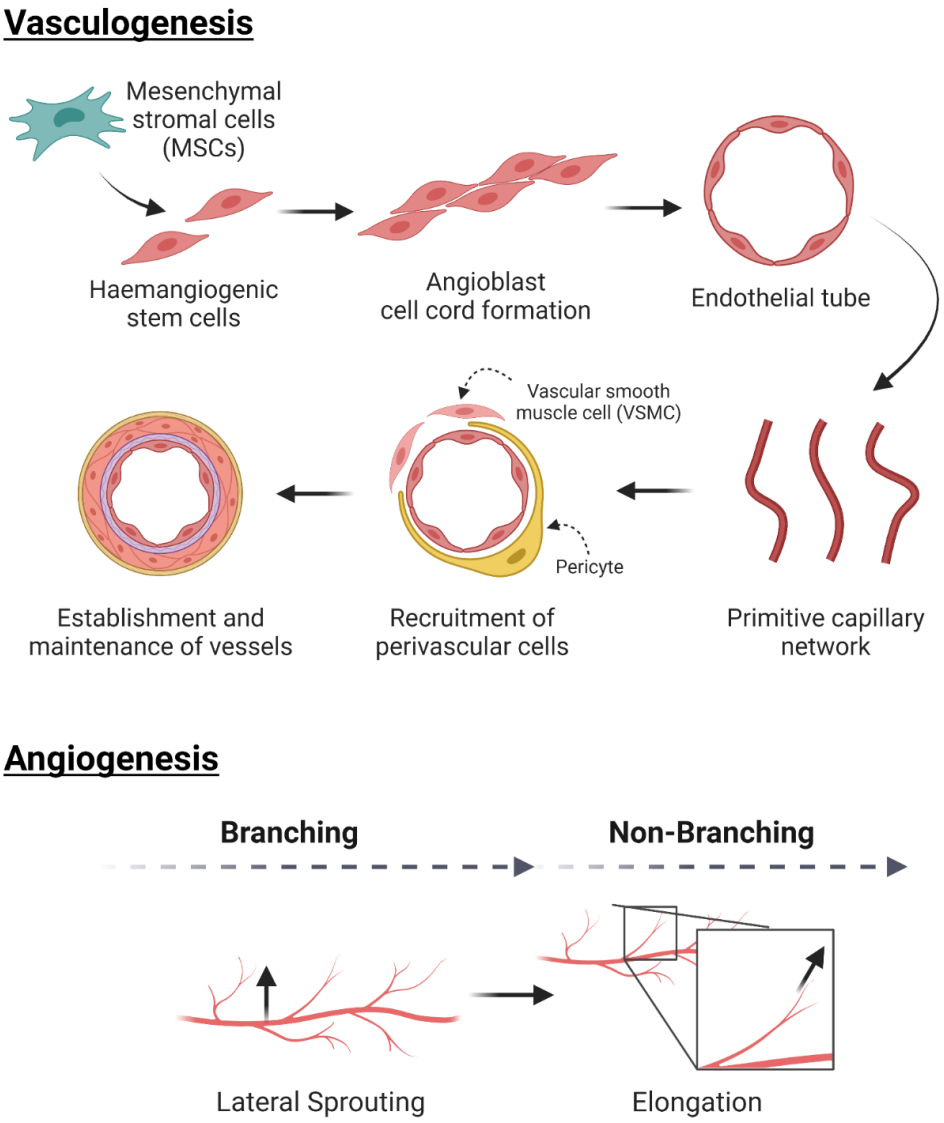

Figure 1.3 - Schematic demonstrating placental vascular development. During the first trimester of pregnancy the *de novo* formation of blood vessels occurs via vasculogenesis. Later in pregnancy, a switch to angiogenesis occurs to expand the placental vascular network. Image created with Biorender.com.

1.2.4 Placental blood flow and shear stress

The uteroplacental blood flow is predicted to be between 600-750 mL/min at term[68,113]. The remodelling of the uterine spiral arteries reduces the smooth muscle and elastic lamina of the vessel wall, which causes a 5-10 fold dilation at the vessel mouth and reduces the speed of blood flow into the IVS to 10 cm/s, in comparison to upstream values of 2-3 m/s. Based on the radius of these vessels, the dilated end is predicted to provide 0.37 mL/s (22.2 mL/min), and therefore it is estimated that 30-60 spiral arteries are required to provide a total uterine blood flow of 750 mL/min[113]. The laminar blood flow that enters the placenta from the uterine spiral artery disperses radially between the chorionic villi and becomes turbulent[114]. There is little impedance to blood flow as the IVS is a large space, unlike the systemic circulation where blood passes from arteries via capillary beds to veins[113]. Calculating specific flow rates within the IVS is difficult, as the maternal blood flow is thought to be reduced as it passes the villi and increase as it returns to the uterine veins. Therefore, the flow in the IVS is not uniform, and is dependent on the position of the villi, in relation to the spiral arteries and uterine veins[115].

The force of flowing blood on the endothelial surface of a blood vessel is known as the shear stress[116]. The shear stress of the maternal blood flow through remodelled spiral arteries is thought to be 1-10 dyn/cm^2 (0.1-1 Pa), which is reduced to 0.001-0.1 dyn/cm^2 as it enters the wide cavity of the IVS. The maternal blood will also exert a shear stress on the syncytium, as it is in direct contact. However, similar to the flow rate, the level of shear stress will vary depending on the position of the villi, as well as whether the villi are free-floating or anchoring[114]. Dynamic MRI has shown that velocities in the IVS are 1 mm/s in the third trimester of pregnancy. These findings were then applied to a computational model, which predicted a wall shear stress of 0.5 to 2.3 dyn/cm^2 (0.05 to 0.2 Pa), suggesting that the average wall shear stress on the surface of the villi is relatively low[117].

The most common method of measuring fetoplacental blood flow is the umbilical vein volume blood flow (Q_{uv}). Umbilical artery flow is not often used as there are inaccuracies with the diameter measurements of small pulsating blood vessels, and flow can be different between the two umbilical arteries. Several different studies have measured Q_{uv} in normal fetuses using Doppler ultrasonography, ranging between 1-539 mL/min (reviewed by [118]). Fetoplacental blood flow increases in the first half of pregnancy, then decreases around 24-25 weeks gestation until term, this is likely because initially the placenta grows faster than the fetus, then in the third trimester the fetus grows faster than the placenta[118]. There are limited studies assessing the flow

rate and levels of shear stress in fetoplacental capillaries. Tun *et al*. (2019) developed an anatomically based computational model of the placental vasculature, including both macro-level vessels and their interaction with a capillary structure. This model demonstrated that in the fetoplacental capillaries in normal pregnancies, the flow rate was predicted to be 0.13 µL/min with a shear stress of 0.05 Pa (0.5 dynes/cm^2)[119].

Placental blood flow and shear stress are also thought to contribute to placental vascular development[120,121]. In early pregnancy, the trophoblast plugs, which prevent blood flow into the IVS, are thought to result in shear stress conditions below 2 dyne/cm^2, upstream of their location, which promotes trophoblast-induced spiral artery remodelling[121]. Additionally, the force generated by blood flow in the fetoplacental capillaries applies shear stress to local endothelial cells, this causes mechanical stimulation important for differentiation as well as endothelial NO-mediated vasodilation[120].

1.2.5 Placental vascularisation in pregnancies complicated by maternal diabetes

The diabetic milieu, in pre-gestational diabetic pregnancies and GDM has been found to alter the vasculature of the placenta, which has been assessed using primarily histological methods. Placental lesions have been reported to be increased in placentae from pregnancies complicated by maternal diabetes, compared to uncomplicated pregnancies, which indicates chorionic villous immaturity[122]. Bhattacharjee *et al*. (2017) demonstrated that overt diabetic, gestational diabetic and mild hyperglycaemic placentae had villous immaturity (decreased formation of terminal villi and increased presence of immature intermediate villi)[123]. Other altered vascular morphologies reported, include reduced[124,125], and irregular/blunted microvilli in GDM[125] and thickening of the vasculo-syncytial membrane[124]. Both the vasculo-syncytial membrane, which is thinner region of the placental villous membrane[126], and the microvilli, which project from the syncytiotrophoblast into the IVS, increasing the surface area[127,128], are important for efficient exchange of nutrients and waste products between the mother and fetus. This suggests that these alterations in diabetic placentae may impair maternal-fetal exchange.

The level of placental vascularisation has also been investigated. These studies have reported increased angiosis, also known as hypervascularisation of the chorionic villi, in GDM[122,125,129], and T1DM[125]. In contrast, other studies have reported hypovascularisation of terminal villi in diabetes[130], or a combination of both hyper- and hypo-vascularised villi in T1DM[131] and GDM[132]. These contrasting findings have been

linked to glycaemic control. Calderon *et al*. (2007) reported hypervascularisation in mild hyperglycaemic placentae and hypovascularisation in GDM and overt diabetic placentae[132]. Moreover, Higgins *et al*. (2011) reported increased capillary volume with poor glycaemic control in T1DM and T2DM pregnancies[133]. Increased growth and branching of capillaries has also been observed[134,135], in addition to increased length, diameter and surface area of capillaries[136,137], in pregnancies complicated by maternal diabetes. However, other studies have reported no differences in the length[138] or decreased area of blood vessels[129].

Given that placental vascularisation may impact nutrient transfer across the placenta, and thus could influence fetal growth, these conflicting studies (demonstrating hyper- and hypo-vascularisation of the chorionic villi) may also explain why some infants are born LGA and some SGA. However, these studies do not take birthweight into consideration, and comparisons between AGA, LGA and SGA placentae have not been conducted. The above studies also use a varied range of techniques to fix and visualise placentas. If a placenta is not fixed soon after it is delivered, blood vessels begin to collapse[139], which will interfere with placental morphology. Where some studies have utilised perfusion fixing[138], to preserve the structure of placental vessels[139], many use standard formalin fixation and paraffin embedding. Nonperfused villi are also known to have alterations of syncytial microvilli, which is preserved with perfusion[139], and therefore may limit the findings on microvilli alterations in diabetic placentae discussed above. There are also maternal and fetal variables that are often not considered when assessing placental vasculature in diabetes, for example maternal BMI, fetal sex, diabetic treatment (e.g. metformin, insulin, diet) and mode of delivery. For example, male fetuses are known to develop larger placentas then females[140], and fetal sex has been linked to placental structure and postnatal outcomes[141]. Moreover, placental weight has been reported to be lower for infants born via caesarean section[140].

In addition to histological abnormalities, the balance between pro- and anti-angiogenic factors, which are involved in regulating vascular development of the placenta, are also thought to be altered in GDM. An increase in the pro-angiogenic factor, PlGF has been observed in the circulation of women with GDM[142–146], in T1DM[147] and non-insulin-dependent DM[143], with increased protein levels also reported in GDM, and overt diabetic placentae[144]. However, other studies did observe a decrease in GDM plasma[148] and unchanged levels in insulin-dependent DM[143]. Whereas, VEGF was reported to be unchanged in maternal plasma, as well as its placental mRNA and protein decreased[124,149,150] or unchanged[129] . An increase in the anti-angiogenic factor

soluble fms-like Tyrosine Kinase 1 (sFlt1), the soluble form of the VEGF receptor 1, has also been observed in maternal serum[144,151] and plasma[148].

1.2.6 Altered placental blood flow in pregnancies complicated by maternal diabetes

Uterine blood flow to the placenta is linked to fetal growth as a function of placental perfusion, and nutrient supply to the fetus[152]. Placental infarcts and decidual vasculopathy, reported in T2DM and GDM, lead to malperfusion of the placenta[153,154]. Many studies have assessed uterine artery velocimetry, as a measure of uteroplacental blood flow. Pietryga *et al*. (2005) reported abnormal dopplers in pre-gestational diabetes. Findings were also linked to birthweight, with a lower pulsatility index (PI) in macrosomic fetuses compared to normal weight infants, and a higher PI in SGA fetuses. There was also a correlation between HbA1c levels and umbilical and uterine artery PI, suggesting glycaemic control may influence blood flow[155]. Whereas other studies have shown no change, unless associated with pre-eclampsia[156,157]. Fetoplacental flow is impaired and vascular resistance increased in both T1DM and GDM pregnancies, in human and animal studies[158–162]. For example, Wong *et al*. (2019) assessed the placental vascular index (VI), which reports the tissue vascular density, flow index (FI), which measures the blood flow intensity, and vascular flow index (VFI), which considers both vascularisation and blood flow (VI x FI)[163]. These researchers found that VI and VFI were lower in patients with GDM in the first and second trimesters[158]. This is also in line with the time in placental vascular development when vasculogenesis is predominantly occurring[158]. Similar findings were observed in pre-gestational diabetes, but lower VI and VFI were observed between 35 and 40 weeks gestation[160].

Alterations in uteroplacental blood flow would also alter the shear stress exerted on the placental villi, and particularly the trophoblast barrier[117,164–167]. Given that the trophoblast is known to produce vasculogenic growth factors, shear stress may alter the production of these factors and hence placental vascular development[120,168,169]. Moreover, altered fetoplacental blood flow, would alter the shear stress applied to local ECs, which may alter endothelial function in diabetes, including vascular differentiation as well as endothelial NO-mediated vasodilation[120].

In FGR, uteroplacental resistance is high, with a high PI, which is indicative of abnormal trophoblast invasion and enhanced apoptosis[170,171]. Computational models of placental vasculature have also predicted elevated shear stress in placental microvasculature from FGR pregnancies. EC migration under these elevated shear

stress levels is reduced, which suggests that angiogenic branching may be impaired[172]. In the third trimester of pregnancy, higher umbilical and uterine artery vascular resistance have been associated with lower birthweight, fetal length, and weight. The higher umbilical artery resistance has also been linked to increased BMI, fat mass, systolic blood pressure and lower left ventricular mass in childhood[173].

In pregnancies complicated by LGA, umbilical vein blood flow at 11-14 weeks of pregnancy was found to be increased compared to AGA infants, which was mainly due to time-averaged maximum velocity values. In logistic regression, umbilical vein blood flow was associated with LGA[174]. This may be linked to hyperglycaemia, as Michelsen *et al*. (2018) demonstrated that fetal glucose consumption, calculated using umbilical blood flow and glucose measurements, was correlated with birthweight[175]. Furthermore, the umbilical vein blood flow is known to be responsible for the distribution of umbilical glucose to the fetal liver and fetal systemic circulation[176]. Similarly, Adanas Aydin *et al.* (2021) showed that acute hyperglycaemia (induced by a 50g OGTT) increased the umbilical artery PI[177], which is a measure of impedance and resistance to flow in the placental vasculature[178]. Thus, increased umbilical artery PI indicates reduced placental function, and is observed in FGR[179,180]. In contrast, Haugen *et al.* (2016) found that umbilical artery PI was decreased following a 75g OGTT. This decreased PI was correlated with abdominal circumference[181]. Although contrasting studies, these findings suggest that hyperglycaemia may lead to altered umbilical artery PI, which may be linked to altered fetal growth.

1.2.7 Endothelial dysfunction in pregnancies complicated by maternal diabetes

Endothelial dysfunction includes the altered capacity of the endothelium to uptake and metabolise the cationic amino acid L-arginine, an important substrate for NO synthesis by NO synthase (NOS). GDM has been associated with altered transport of L-arginine and NO synthesis. This has been linked to reduced adenosine transporters (human equilibrative nucleoside transporters [hENTs]), which increase extracellular nucleosides and activation of adenosine receptors on the endothelium[182]. This further increases NO production, endothelial NOS (eNOS) expression, and L-arginine transport by increasing human cationic amino acid transporter 1 (hCAT-1)[183]. For example, circulating adenosine is increased in GDM umbilical cord blood, compared to normal pregnancies and eNOS expression and activity and expression of *SLC7A1*, which encodes for hCAT-1, are increased in GDM human umbilical vein ECs (HUVECs)[182]. Moreover, isolated arteries and veins from GDM placentae have increased NO synthesis[184].

Other forms of endothelial dysfunction have been reported as Zhou *et al.* (2016) observed reduced proliferation, migration and tube formation of HUVECs isolated from GDM pregnancies compared to those from healthy pregnancies[185]. Endothelial activation is characterised by increased levels of cell adhesion molecules, such as intercellular adhesion molecule 1 (ICAM-1), vascular cell adhesion molecule 1 (VCAM-1) and E-Selectin[183]. In GDM, higher levels of soluble ICAM-1 (sICAM-1) have been reported, which has also been linked to development of T2DM[186]. HUVECs isolated from GDM pregnancies also have increased levels of ICAM-1 at the gene and protein level, demonstrating EC activation and dysfunction, in addition to reduced proliferation and increased VEGF gene expression and secretion. The transcriptome of GDM HUVECs were also altered, compared to non-diabetic HUVECs, and altered genes were associated with cell adhesion and the immune response[187].

1.2.8 Nutrient transport across the placenta and fetal growth

Oxygen transport across the placenta is limited by placental blood flow, whereas nutrient transport is also dependent on the presence of specific transport proteins, such as glucose, amino acid, and fatty acid transporters, which are critical to the development of the fetus[188,189]. Maternal-fetal exchange occurs across two cell layers, the fetal endothelium and the syncytiotrophoblast, which separate the fetal and maternal circulation. The syncytiotrophoblast is comprised of two polarised membranes, the maternal facing microvillous membrane (MVM) and the fetal facing basal membrane (BM), which contain different transporter proteins for maternal-fetal exchange[190]. The key nutrient transporter systems in the placenta are outlined in Figure 1.4. Given that fetal growth is dependent on the availability of nutrients in the fetal circulation, changes in the expression and activity of these transporters is associated with restricted and excessive fetal growth, including in diabetes[191].

1.2.8.1 Glucose transport

Glucose can diffuse across the placenta, or be transported by glucose transporters, down its concentration gradient (facilitated diffusion)[192]. The placenta has been shown to express several isoforms, GLUT- 1, 3, 4, 8, 9, 10. GLUT1 is the primary transporter, which is expressed in the syncytiotrophoblast, cytotrophoblast, ECs and the stroma. GLUT1 is known to be more highly expressed on the MVM in comparison to the BM[193]. GLUT3 is also thought to be expressed on the MVM, as well as the fetal endothelium, although the endothelial GLUT3 is not thought to be responsible for transplacental transport. Its expression levels are higher in first trimester, and then decline throughout pregnancy[194]. Based on this distribution of glucose transporters in the placenta, the

basal membrane is thought to be the rate-limiting step in trans-syncytial transport[192]. GLUT4 is an insulin-regulated transporter. Its expression is primarily detected in the cytoplasm of syncytial cells in the first trimester, which can rapidly be recruited to the cell surface. In the third trimester, GLUT4 expression is lower[195]. This is in line with insulin receptor expression in the placenta, as the insulin receptor is found on the MVM in the first trimester but is downregulated and localised to the fetal endothelium at term[192].

In pregnancies complicated by maternal diabetes, GLUT4 and GLUT9 have been found to be increased in insulin-treated women with GDM and pre-gestational diabetes. GLUT1 was also found to be increased in women with pre-gestational diabetes[196]. Similarly, GLUT1 at the BM was 2-fold higher in women with GDM or pre-gestational diabetes in pregnancy, compared to healthy pregnancies, suggesting increased uptake of glucose into the fetal circulation. Gaither *et al.* (1999) found that glucose transport activity was increased by 40% at the basal membrane in pre-gestational and gestational diabetic placentae. HbA1c measures showed that glycaemia was well controlled and concluded that GLUT1 expression is altered despite evidence for maternal hyperglycaemia. However, 8 of 25 diabetic fetuses were macrosomic and HbA1c would have been unable to detect any variations in maternal glucose, and potential periods of hyperglycaemia[197]. In contrast to fetal overgrowth, FGR has been associated with hypoglycaemia, and is not thought to be due to reduced glucose uptake or expression of GLUT1[193]. However, GLUT3 protein expression is increased in the cytotrophoblast of intrauterine growth restriction (IUGR) placentae, which is thought to contribute to increased consumption of glucose by the placenta itself[198].

1.2.8.2 Amino acid transport

Amino acids are required for protein accretion, metabolic processes, and biosynthetic pathways in the fetus[199]. Amino acid transport across the placenta is carrier-mediated, by members of the SLC superfamily, expressed on the MVM, BM or other placental cell types (reviewed by Cleal *et al*. [199]), which enable transport of the full range of amino acids to the fetus. The most studied in the placenta are the System A and System L amino acid transport systems. System A is sodium-dependent for small neutral amino acid transport (SNAT), such as alanine, serine, and glycine. System A transporters are found on the BM and MVM, but more highly expressed on the MVM. System L is a sodium-independent exchanger for large neutral amino acid transport (LAT), such as leucine[191]. Accumulative transporters, such as, SLC1 and SLC7 mediate uptake of amino acids across the MVM into the syncytiotrophoblast. This creates an amino acid

gradient, to stimulate further uptake of other extracellular amino acids, by amino acid exchange transporters. These exchange transporters swap amino acids in the syncytiotrophoblast for specific amino acids in the maternal blood. Whereas other transporters on the BM of the syncytiotrophoblast (e.g. SLC16A10 [TAT1] and SLC43 [LAT3/4]) mediate the transport of amino acids from the syncytium to the fetal circulation down their concentration gradient[199,200]. Other transporters (SLC1 and SLC38 [SNAT1/2/4] families) present on the BM can uptake fetal amino acids into the placenta[199]. For example, glutamate can be taken up into the placenta and metabolised to glutamine. Glutamine can then influence the placental transport of other amino acids, as well as nitrogen flux and cellular regulation[201].

In diabetic pregnancies, reduced system A activity was reported in the MVM of placentae from women with T1DM that delivered macrosomic infants[202]. However, in other studies, increased system A activity was observed in T1DM and GDM, independent of LGA[203], suggesting its alteration is associated with the diabetic milieu, and not fetal overgrowth. In GDM, system A activity was reported to be higher in the MVM, with and without LGA infants, compared to healthy controls and system L activity was higher in the MVM of GDM pregnancies with LGA infants, compared to controls[203]. The activity of the system A transporter was also found to be lower in placentae from SGA pregnancies (not diabetic)[204]. Other studies have shown that TAT1 (T amino acid transporter [TAT]) and LAT3 mRNA expression in the placentae was positively correlated with measures of fetal growth. For example, *SLC16A10* (TAT1) mRNA is increased with increasing birthweight and neonatal lean mass and *SLC43A1* (LAT3) mRNA was increased with increasing neonatal head circumference[200].

1.2.8.3 Fatty acid transport

The transport of fatty acids in the placenta requires the generation of non-esterified fatty acids (NEFAs) by lipases from maternal triglycerides, such as lipoprotein lipase (LPL) and endothelial lipase (EL), which are found on the MVM. NEFAs then cross the placenta by diffusion or facilitated diffusion by fatty acid carriers, such as CD36 (FAT) and fatty acid transport proteins (FATPs). Once in the cytoplasm the fatty acids bind to fatty acid binding proteins (FABPs)[205]. FABPs are responsible for cytosolic trafficking to sides for esterification, β-oxidation, and subsequent transfer to the fetus[191].

Fatty acid transport proteins are also thought to be altered in diabetes, which could lead to altered lipid deposition and metabolism in diabetes and pathological fetal growth. Protein expression of FABP1 was higher in GDM and insulin-dependent DM isolated MVMs, by 112% and 64%, respectively, compared to appropriate-for-

gestational age (AGA) infants from healthy pregnancies. MVM LPL activity was also reduced by 47% in pre-term IUGR[206]. Increased expression of EL has also been reported in T1DM pregnancies, particularly in those with poor metabolic control[207].

Overall, these studies suggest that altered placental nutrient transport could contribute to pathological fetal growth in diabetic pregnancies.

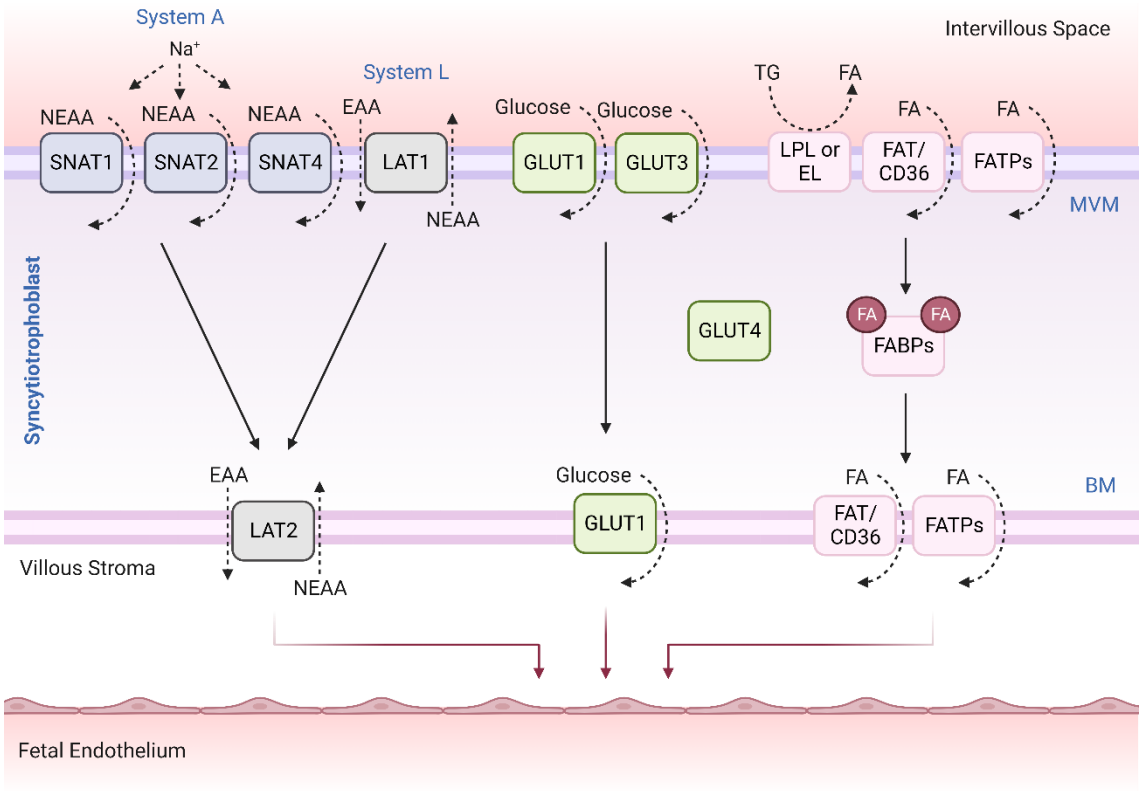

Figure 1.4 – Schematic outlining some of the key nutrient transporter systems in the placenta. Amino acids are transported by System A and System L transporters. Glucose is transported by glucose transporters (GLUTs) and fatty acids are transported by FATs and FATPs. Abbreviations: SNAT- Small Neutral Amino Acid Transporter; LAT- Large Neutral Amino Acid Transporter; EAA- Essential Amino Acid; NEAA- Non-Essential Amino Acid; LPL- Lipoprotein Lipase; EL- Endothelial Lipase; TG- Triglyceride; FA- Fatty Acid; FAT- Fatty Acid Transporter; FATP- Fatty Acid Transport Protein; FABP- Fatty Acid Binding Protein; MVM- Microvillous Membrane; BM- Basal Membrane. Image created with Biorender.com.

1.2.9 The placental immune system and fetal growth

In addition to regulated vascular development of the placenta, a successful pregnancy also involves interactions between the trophoblast and maternal decidual immune cells, which allow the fetus to develop in the uterus, with the mother's immune system intact[208]. When the EVT invade into the uterus during the first trimester of pregnancy, the decidua is populated by innate lymphocytes, decidual natural killer cells (dNK), which make up 70% of leukocytes. Other cell populations include decidual macrophages (~20%), dendritic cells and T-cells (~10-15%). The levels of these immune cells varies throughout pregnancy, with an increase in T-cells at term[209,210]. dNK cells secrete cytokines, chemokines and angiogenic factors[211]. In early pregnancy, there is an active Type 1 helper T cell (Th1) inflammatory response, which is important for embryo implantation[212]. Following this there is primarily an anti-inflammatory Type 2 helper T cell (Th2) response to tolerate the semi-allogeneic embryo, until a Th1 shift during labour[213]. Cytokines are proteins that act as immune mediators and regulators[214], and are expressed at the maternal-fetal interface[215,216]. In pregnancy, cytokines can mediate uterine receptivity, implantation, embryogenesis, fetal development, and the onset of labour. Modulatory cytokines, such as IL-3, IL-4, IL-5, and IL-10 minimise the Th1 responses in pregnancy. During labour, when there is a switch to the Th1 response, co-ordinated production of cytokines and prostaglandins occurs. Cytokines such as IL-6, IL-1β and IL-8 promote uterine smooth muscle contraction. Cytokines are also responsible for producing matrix metalloproteinases (MMPs) and therefore remodelling the ECM, which leads to rupture and dissociation of the fetal membranes[217]. Chemokines are a superfamily of small chemotactic cytokines, and along with their receptors are known to contribute to trophoblast invasion, decidualisation, immune cell recruitment in the placenta[218,219].

Maternally-derived macrophages reside in the decidua, and placental macrophages (HBCs), are derived from the fetus and reside in the villous core[220]. HBCs can be detected at around day 10 of pregnancy and are present throughout gestation, with levels higher in the first trimester (~50%) and lower levels in the third trimester (~20%)[209]. Macrophages are known to be either M1 or M2 polarised. M1 macrophages are pro-inflammatory and are activated by interferon-γ (IFNγ) and lipopolysaccharide (LPS). Whereas, M2 macrophages are activated by interleukins, and promote cell proliferation, angiogenesis, and ECM construction[103]. Hofbauer cells are thought to be primarily anti-inflammatory (M2 polarised) and express high levels of CD163, CD209 and CD206, as well as an increased secretion of IL-10 and TGF-β[103,221–224]. HBCs are therefore thought to elicit a regulatory function in the placenta based on this anti-

inflammatory phenotype[224]. Moreover, HBCs are thought to contribute to placental vascular development (Section 1.2.3.2). M2 macrophages can also be classified into further subtypes. Activation by IL-4 and IL-13 results in M2a macrophages, which have tissue repair and immunoregulatory properties. M2a HBCs are known to express CD209 and secrete IL1RN[103,225,226]. Immune complex activation results in M2b macrophages, which are responsible for humoral immunity and allergic reaction responses. M2b HBCs express CD86 and secrete TNF-α and IL-6, and therefore interestingly exhibit similar properties to M1 macrophages[103,225–227]. IL-10 however results in M2c macrophages, which induce anti-inflammatory reactions[103,225,226]. M2c HBCs are known to express CD14[228]. Other markers include major histocompatibility complex class II DR (HLA-DR), which is found in M2a/M2b HBCs, and CD206 which is found in M2a/M2c HBCs[103,228,229]. HBCs may also play a role in infection during pregnancy, as ZIKV[230,231] and HIV-1[232] viral particles have been detected in HBCs. HBCs isolated from first trimester placentae are also able to replicate ZIKV[233], however, this these *in vitro* cell cultures do not model the villous stromal environment occurring *in vivo*[210].

The contribution of the immune and inflammatory system in the pathogenesis of diabetes, including GDM, has been increasingly studied[234–237]. Maternal hyperglycaemia has been attributed to systemic inflammation and immune dysfunction in GDM, potentially through aberrant adaptation of the maternal immune system in pregnancy[238]. Although varied findings, circulating cytokine and chemokine levels have been found to be altered in women with GDM[216,239,248,249,240–247]. The production of inflammatory mediators by the placenta is thought to be responsible for elevated levels in the circulation in GDM, as *in vitro* studies using a perfusion model have observed that Tumour Necrosis Factor α (TNF-α) produced by the placenta is released primarily to the maternal side[250]. Several conflicting studies have also investigated HBC polarisation in pregnancies complicated by maternal diabetes, reporting either an increase in M1/pro-inflammatory markers[251,252], or that HBCs maintain their anti-inflammatory M2 profile[224,253].

Maternal BMI, which is associated with GDM, has been linked to activation of placental inflammatory pathways, such as p38 Mitogen-activated protein kinase (MAPK) and Signal transducer and activator of transcription 3 (STAT3), which are activated by inflammatory receptors, without changes in fetal cytokine levels (although women with GDM were not included in this study). Placental p38 MAPK phosphorylation was also correlated with birthweight[254]. This signalling pathway activates several transcription factors, which regulate pro-inflammatory gene expression. Moreover, this pathway has

been associated with glucose and amino acid transport regulation in other systems[255–257]. Cytokines have also been linked to nutrient transport. In primary trophoblasts, IL-6 has been shown to upregulate STAT3 system A amino acid transport, by increasing SNAT2[258]. Whereas IL-1β downregulates system A but activates system L[259]. In other systems and diseases, IL-1β has been associated with increasing *SLC2A1* (GLUT1) mRNA expression, GLUT3 and GLUT4 translocation, hexokinase 2 expression (involved in glucose metabolism and glycolysis) and glucose uptake (Reviewed by [260]). Moreover, IL-6 treatment in neuronal cells increased the translocation of GLUT4 to the membrane, via AMPK phosphorylation and subsequently increased cellular glucose uptake[261]. Overall, there appears to be an association between placental inflammation and nutrient transport, which could ultimately be linked to pathological fetal growth.

1.2.10 The impact of hyperglycaemia on placental function

Glycaemic control can be variable between individuals with maternal diabetes, and several studies have associated this with altered placental vascularisation. For example, Calderon *et al*. (2007) observed placental hypervascularisation in mild hyperglycaemic cases and hypovascularisation in GDM and overt diabetic cases[132]. Similarly, Higgins *et al*. (2011) reported increased capillary volume with poor glycaemic control in T1DM and T2DM pregnancies[133].

In *in vitro* studies, high glucose has been attributed to endothelial dysfunction. HUVECs treated with 25 mM glucose, had increased protein levels of VEGF and several components of the L-arginine/NO signalling pathway, involved in vasodilation, including phosphorylated Ser1177-eNOS and hCAT-1 at the protein and mRNA level[262]. ICAM-1 expression is increased in ECs in response to high glucose, with an additional increase in soluble ICAM-1 (sICAM-1), suggesting dysfunctional endothelial activation. Glucose can also influence the release of angiogenic factors from trophoblast cells[93]. Glucose was found to downregulate pro-angiogenic factors, VEGF and PlGF and upregulate anti-angiogenic factors, sFlt1 and soluble endoglin (sEng) in trophoblast cell lines[263–265]. In addition to inflammatory cytokines and chemokines[265]. Several studies have shown that glucose modulates vascular genes in other cells, such as increased expression of VEGF, VCAM-1 in bovine aortic and human microvascular ECs[266] and VEGF in human and porcine VSMCs[267,268], suggesting glucose may also regulate placental vascular genes. Hulme *et al.* (2018) observed over 5,000 differentially expressed genes between human trophoblast cells (BeWo) exposed to either high concentrations or normal concentrations of glucose[269].

A limitation, however, of many *in vitro* studies is that they model hyperglycaemia at supraphysiological levels (~25 mM). As previously discussed, diabetes in pregnancy is well treated, however adverse outcomes, including LGA, still occur[62]. Given that Law *et al*. (2019) reported that GDM LGA mothers have an average glucose of 6.2 mM, using CGM[62], the impact of physiological concentrations needs to be further investigated.

In *in vivo* rodent models, streptozotocin (STZ) has been used to model hyperglycaemia. STZ destroys the insulin-producing β-cells of the pancreatic islets, therefore more accurately models T1DM[270]. In mice, STZ-induced hyperglycaemia alters the placental transcriptome. Differentially expressed genes were found to be associated with chemotaxis, ossification, negative regulation of cell development, and positive regulation of vascular development[271]. STZ also increased the glycogen content of the spongiotrophoblast, and increased apoptosis and proliferation in the junctional zone[271]. Impaired spiral artery remodelling has also been reported in STZ mice, which can result in preeclampsia, of which diabetes is a major risk factor. This study showed reduced apoptosis surrounding the spiral arteries and increased expression of VSMCs, labelled with α-SMA[272]. The interhemal membrane (IHM) was also thicker in STZ-treated mice, consistent with the thickening of the basement membrane in human GDM placentae[273,274]. In rats, STZ increased umbilical artery pulsatility index, and increased placental area, width and thickness was observed. Thrombosis in the peripheral sinus veins was also more common with hyperglycaemia[275]. Placental gene expression was also altered, including increased expression of GLUT3 (*Slc2a3*), and decreased expression of placental growth-related genes, epidermal growth factor receptor *(Egfr)*, platelet derived growth factor receptor β (*Pdgfrb)* and insulin like growth factor binding protein 6 (*Igfbp6)* and inflammatory genes, prostaglandin-endoperoxide synthase 2 (*Ptgs2)* and hydroxyprostaglandin dehydrogenase *(Pgdh)*. Protein levels of IL-2 and IL-4 were also reduced and IL-1β increased[275].

In contrast, maternal hypoglycaemia can occur in pregnancies complicated by maternal diabetes, particularly in the first trimester in women with insulin treated T1DM[276,277]. This can result in pregnancy complications, such as placental insufficiency and pathological fetal growth[277,278]. Circulating factors, such as VCAM-1, ICAM-1, E-selectin, P-selectin, IL-6 and VEGF, are elevated during acute hypoglycaemia (2 hours) of those with T1DM, when compared to normoglycaemic healthy subjects[279]. In non-diabetic males, pro-inflammatory cytokines, including IL-8 and TNF-α are elevated in insulin-induced hypoglycaemia[280]. These elevated circulating factors may contribute to

endothelial and vascular dysfunction[281], although the impact of hypoglycaemia in pregnancy on placental function needs to be directly studied.

1.2.11 Other contributing factors to placental dysfunction in pregnancies complicated by maternal diabetes

In addition to glucose, the diabetic milieu is comprised of altered insulin, adipokines, lipids and oxidative stress, which may contribute to placental dysfunction. Oxidative stress has also been reported in diabetic pregnancies, as well as a reduction in antioxidant activity, which usually protects against oxidative stress. Poor glycaemic control has been linked to ischemic changes in peripheral villi, which can lead to hypoxia, and increase angiogenesis and chorangiosis of the chorionic villi[282]. Hypoxia can also regulate the transcription, translation and stability of angiogenic factors, such as VEGF[283].

Insulin receptors are primarily expressed on the MVM in early pregnancy, and on the fetal endothelium, in contact with the fetal circulation at term. Thus, fetal hyperinsulinemia in pregnancies complicated by maternal diabetes could influence insulin signalling in the placenta[284]. Moreover, many components of the insulin/insulin-like growth factor (IGF) system are dysregulated in diabetic pregnancies, such as IGF-I, IGF-II, and IGF-binding proteins (IGFBPs)[285–287]. This has also been linked to placental vascular dysfunction, as IGF-I has been correlated with IVS, villous trophoblast volume, and capillary volume in placentae from T1DM pregnancies[288]. IGF-1 and IGFBP3 have also been associated with fetal growth, with increased levels in the maternal and cord serum in GDM LGA pregnancies[289]. Maternal obesity, a common risk factor for development of diabetes in pregnancy, and LGA outcomes, results in the overexpression of adipokines, such as leptin and adiponectin[290,291]. Adipokines are produced by the placenta and adipose tissue[292], and can regulate many functions of placental cells, including proliferation, invasion, apoptosis and endothelial function [293–295]. Studies have also shown that physiological levels of insulin can upregulate system A nutrient transporters and activity in primary trophoblast cells. Full length adiponectin abolished the insulin-induced increase in system A activity and SNAT2 expression, suggesting a crosstalk between insulin and adiponectin can influence nutrient transport in the placenta[296].

The placenta also produces short regulatory RNA molecules, termed microRNAs (miRNAs), which regulate mRNA degradation and protein translation, and are therefore important for many biological processes including placental development[297]. Altered miRNA expression in both the circulation and placenta have been reported in pre-

gestational diabetes and GDM[298–300], including several miRNAs with known roles in placental vascular development (e.g. miR-16, miR-125 and miR-517)[301–306]. miRNAs can also be secreted from cells into lipid bilayer-bound particles known as extracellular vesicles (EVs)[307–309], where they can travel to other tissues and regulate gene expression[310]. In GDM, higher concentrations of circulating EVs have been reported, compared to normal pregnancies[311], as well as altered miRNA cargo[312]. Several altered circulating miRNAs include those with roles in vascular development, such as miR-122 and miR-342[313,314].

Overall, there are a myriad of factors that may contribute to placental dysfunction, and specifically altered placental vascular development. This may also explain why many studies report conflicting findings in placental vascularisation. Individuals may have varying levels of these associated factors, which could lead to a different clinical phenotype. Nonetheless, it is important to understand the impact of physiological levels of hyperglycaemia associated with GDM and altered fetal growth on the placenta.

1.2.12 Current models for investigating placental function

To study the placenta and its altered function in complications of pregnancy, such as maternal diabetes, several models have been developed, including models of the trophoblast barrier (including those to assess maternal-fetal exchange), placental vascular development, as well as *ex vivo* placental explants and *in vivo* animal models.

1.2.12.1 *In vivo* animal models

Mice are widely used as an *in vivo* model for placentation, as they have a haemochorial placenta with the trophoblast in direct contact with the maternal blood, similar to humans[315]. However, the structure of the placenta is completed halfway through gestation and trophoblast invasion occurs late in gestation, all of which occurs much earlier in pregnancy in humans. The endocrine function also differs, to maintain pregnancy in mice, the corpus luteum is responsible for progesterone production throughout gestation, and in humans from 8 weeks of gestation placental progesterone is produced by the syncytiotrophoblast[315]. Many studies have also used sheep to investigate the fetal-maternal vasculature, as catheters can be placed and maintained in both the maternal and fetal vasculature for repeated sampling. This has provided insight into placental oxygen and nutrient transfer and utilisation in pregnant sheep[316]. However, there are differences in the rate of angiogenesis, physiological structure, and glucose transfer. They also have a long gestation period (~65 days), and require greater resources, both of which can be a financial constraint[317]. Non-human primate

pregnancy closely relates to humans in terms of the length of gestation, process of placentation and uterine contractions. The rhesus placenta also has a villous structure and pattern of circulation in the IVS similar to that in humans[318]. Placental *in vivo* models have been widely used to study pregnancy pathologies, such as FGR[319] and diabetes[320].

1.2.12.2 *Ex vivo* placental villous explants

Placental villous explants can be generated from human placental tissue to study placental transfer, metabolism, syncytialisation and endocrine function. This is a widely used technique, likely due to the easy accessibility of human placentae (given that most are discarded after birth). Explants can also be generated from first trimester and term placental tissue, as well as from complicated pregnancies (e.g. FGR, diabetes and pre-eclampsia)[317]. They also contain of multiple cell types, including the trophoblast, stromal cells and endothelium[321]. However, explants have some limitations. During culture the sycytium sheds, and regenerates after ~4 days[322]. Explants can only be cultured for up to 10 days[322] as long-term culture of placental explants results in the collapsing of vessels, as they are no longer perfused as *in vivo*[115], which is a major limitation for assessing placental vasculature. Explants also have reduced steroidogenic enzyme activities, and are therefore not appropriate for studying sex steroids[323].

1.2.12.3 Trophoblast cells

Trophoblast cells are widely used, which have been derived from choriocarcinoma, such as BeWo cells[324], or immortalised cell line trophoblasts, such as HTR/SvNeo[325]. BeWo cells have hormonal secretion abilities and have many characteristics of third trimester trophoblasts. The ability of cultured trophoblast cells to syncytialise is important for investigating the placental barrier. BeWo cells are not able to spontaneously differentiate into syncytiotrophoblasts, but can be stimulated to do so with forskolin treatment[326], however this can cause cellular aggregates to form, and disrupt monolayers[327]. Undifferentiated BeWo cells have close cell apposition in monolayers and exhibit microvilli projections on the apical surface[328] and are therefore widely used to assess transplacental transport of nutrients and compounds, such as glucose, folic acid, and fatty acids[327]. Other trophoblast cells derived from choriocarcinoma include JEG-3 cells, which were derived from serial cloning of BeWo cells, which also release placental hormones[329], and JAR cells which were also derived from a trophoblastic tumour[330].

The HTR/SvNeo cell line was generated from EVTs derived from first trimester placentae, which were transfected with a plasmid containing the simian virus 40 large T antigen (SV40). Transfected cells are known to release hCG[325]. However, some studies have shown that this cell line contains populations of stromal/mesenchymal cells in addition to trophoblast. Clusters of HTR/SvNeo cells were found to express Vimentin, a mesenchymal marker. Whereas BeWo, JAR and JEG-3 cells expressed the trophoblast markers cytokeratin 7 and E-cadherin, without any Vimentin expression[331]. This mixed population cells are therefore a limitation when using HTR/SvNeo to investigate trophoblast.

Primary cytotrophoblasts can also be isolated from the placenta[332]. However, these can be difficult to culture as they do not proliferate, and can be contaminated with other highly proliferative cells, such as fibroblasts[333]. This often limits the lifespan of these cultures to 7-10 days[334]. Although, a recent study by Nursalim *et al.* (2021) cultured primary trophoblasts for 30 days by using medium containing lower FBS and adhering cells to Matrigel, which have previously been shown to reduce fibroblast growth[333]. Term primary cytotrophoblasts are known to spontaneously differentiate into syncytiotrophoblast multi-nucleated cells *in vitro*[332]. However, all cytotrophoblasts do not appear to syncytialise, and some fail to do so even after the addition of forskolin[332–334].

Monolayers of various trophoblast cell types have been used to investigate the placental barrier. For example, investigating the transplacental transfer of glucose, hormone secretion[335] or the susceptibility to infection with parasites[336].

1.2.12.3.1 Trophoblast organoids

Placental organoids, or trophoblast organoids have been used to model maternal-fetal interactions in early pregnancy and placentation. These are generated from first trimester placentae, which are enzymatically digested to enrich for clusters of cells, which express a marker of proliferative trophoblast (Epithelial cell adhesion molecule; EPCAM). These cell clusters are then seeded onto Matrigel drops and grown in trophoblast organoid medium, which contains growth factors such as epidermal growth factor (EGF), FGF2, hepatocyte growth factor (HGF) and prostaglandin E2 (PGE2)[337,338].

Trophoblast organoids are also able to secrete pregnancy hormones and proteins, including hCG, KISS1 and Chorionic Somatomammotropin Hormone 1 (CSH1). The structure of trophoblast organoids differs from the *in vivo* situation, with the syncytiotrophoblast detected inside the organoids, with their multi-nucleated structure,

microvilli, and expression of CD46 and CD71. Whereas the outer layer is the villous cytotrophoblast expressing EPCAM and E-cadherin, with the basement membrane being in contact with the Matrigel[337,338]. Trophoblast organoids can also be differentiated into EVTs using EVT differentiation medium for 7-10 days, as described previously[339]. EVTs migrate from the organoids and digest Matrigel, similar to the migratory and invasive properties of EVTs *in vivo*[337,338]. Trophoblast organoids have been derived from individual patients[337,338] and also from pooled patient samples[340].

Models using single monolayers of trophoblast, or trophoblast organoids lack the complexity of the several cell types associated with the maternal-fetal interface *in vivo*, such as immune cells and blood vessels. Moreover, the 'inside-out' structure of trophoblast organoids limits their use for assessing the syncytium as an outer barrier for transplacental transport of molecules, nutrients, and drugs. Therefore, other researchers have implemented other cell types into these *in vitro* models, using transwells or 'on-a-chip' methods[341].

1.2.12.4 Placental transwell models

Nishiguchi *et al*. (2019) developed a 3D first trimester placental model using a collagen (type IV) and laminin ECM scaffold on transwell inserts and seeded primary cytotrophoblasts or BeWo cells. Primary cytotrophoblasts spontaneously syncytialised overtime and released hCG. They then incorporated capillary networks below the transwell, which were comprised of human dermal fibroblasts and HUVECs, which formed capillary-like structures with lumens. This model was used to investigate cell damage to embryonic cortical neurons across the placental barrier. Conditioned medium from vascularised primary cytotrophoblast barriers which were subjected to hypoxia reoxygenation caused a reduction in dendrite length of cortical neurons, whereas conditioned medium from non-vascularised barriers caused minimal reductions in dendrite length. These vessels were not perfusable but demonstrate an interaction between the trophoblast and vascular network[342]. Another transwell model was developed by Kreuder *et al*. (2020). In this model, a methacrylated gelatin membrane (GelMA) was bio-printed to mimic the ECM, and human villous mesenchymal fibroblasts were integrated into this membrane. BeWo cells were seeded onto the apical side of the membrane, and human placental villous ECs (HPVECs) onto the basolateral side. Permeability assays were performed to measure the barrier properties. Paracellular permeation of low molecular weight lucifer yellow was decreased in both single cultures and co-culture models, and transepithelial electrical resistance (TEER) values were increased with co-culture, suggesting a reduced

permeability (leakiness of the barrier) when the stromal compartment is incorporated[343] (Figure 1.5).

1.2.12.5 Placenta-on-a-chip models

In recent years, microfluidic devices have been utilised for the culture of cells, particularly to mimic the *in vivo* microenvironment of cells. These devices utilise small volumes of fluids (10^{-9} to 10^{-18} L) in channels with tens of micrometre dimensions[344]. The use of microfluidics extends into the development of 'Organ-on-chip' devices, which can allow the co-culture of multiple cell types, to reproduce tissue and organ functions, *in vitro*[345]. These models also allow for exposure to fluid flow, to mimic the shear stress in the placenta, as static culture conditions fail to represent the dynamic flow milieu in the placenta[127].

Therefore, several groups have developed 'Placenta-on-a-chip' models, with trophoblast and endothelial cell compartments, which have provided platforms to model the structure and function of the placenta *in vitro*[127,346]. These models primarily use trophoblast cell lines (BeWos, HTR8/SvNeo and JEG-3) with HUVECs. However, some have used primary HPVECs isolated from term placentae[127,347]. Most of these models utilise a two-channel device, usually made from PDMS separated by a porous membrane. In these models, the endothelial cell type is usually seeded into the bottom channel and then the device is inverted to allow these cells to adhere to the lower side of the membrane. Following this, the trophoblast cell type is seeded into the top channel onto the top surface of the membrane to adhere (Figure 1.5). The formation of the placental barrier is widely assessed in these studies, primarily though permeability assays (FITC-Dextran and TEER measurements) and formation of intercellular junctions. Some studies also investigated microvilli formation on the apical surface of the trophoblast by staining for F-actin. The flow rates used in these placenta-on-a-chip models vary between 0.01-2.5 µL/min. Shear stress is rarely reported in the studies, but where detailed is lower than the shear stress in fetoplacental capillaries, likely due to the size and shape of the microfluidic devices. As there are several studies that have developed 'Placenta-on-a-chip' models, with various characteristics, these have been outlined in Table 1.1.

Transwell Models

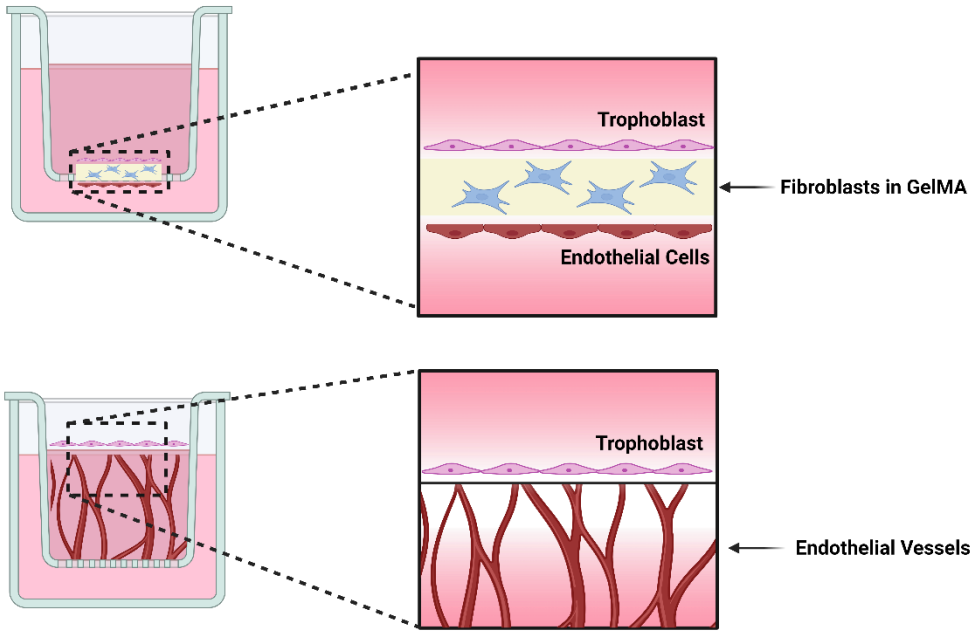

Placenta-On-A-Chip

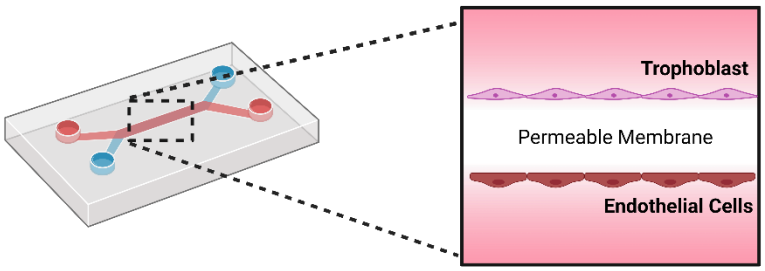

Placental Microvasculature

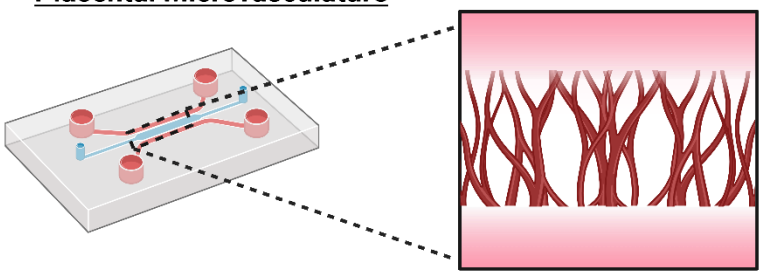

Figure 1.5 - Schematic representing different placental models depicting the trophoblast barrier and endothelium. For the transwell models, the top panel shows that developed by developed by Kreuder *et al*. (2020)[343]**,** which contains a bioprinted layer of fibroblasts, between the trophoblast and endothelium. The lower panel represents the transwell model developed by Nishiguchi *et al*. (2019)[342], which includes a layer of trophoblast and vasculature in a 3D matrix. Many placenta-on-a-chip models incorporate trophoblasts and endothelial cells on either side of a permeable membrane in a PDMS device. Placental microvasculature models, such as those developed by Haase *et al*. (2019)[348], incorporate endothelial cells and stromal cells (e.g. pericytes and fibroblasts) into a gel matrix to generate perfusable microvessels. Image created with Biorender.com.

1.2.12.6 Placental microvasculature models

Placental microvasculature models have also been developed which model placental blood vessels. These have been developed from general models of microvasculature, which include ECs and supporting perivascular cells (e.g. fibroblasts and pericytes)[349]. Like several placenta-on-a-chip models, these utilise a PDMS device, with a central channel and two side channels. The central channel is filled with HUVECs and fibroblasts, mixed with hydrogel precursors (fibrinogen and thrombin). The fibrin then polymerises and suspends the cells in a 3D matrix. The side channels are then filled with medium (e.g. endothelial growth medium), which causes the ECs to make connections, branch, and anastomose, mimicking vasculogenesis and forming connected lumens after 5-7 days. The lumens can be perfused from the side channel and allow the investigation of different molecules[349] (Figure 1.5). Haase *et al.* (2019) further expanded on this model. Similar to co-cultures with fibroblasts. HUVEC co-cultures with human placental pericytes (HPPs) also generated connected vascular structures, and HPPs were found within the EC basement membrane. However, the total vascular area for HUVEC-pericyte co-cultures was significantly lower than HUVEC-fibroblast co-cultures. While HPPs did proliferate throughout culture, could be recruited by HUVECs and were found to wrap around the HUVECs, the HPP-HUVEC co-cultures were found to have many disconnected vessels.

Therefore, a perfusable triculture mode was generated with HUVECS, fibroblasts (from lung fibroblasts, as placental fibroblasts were not available at the time of study) and HPPs. In these triculture models, pericytes and fibroblasts proliferated at a similar level, much more than HUVECs, which is similar to increased proliferation of stromal cells observed in pre-eclamptic placentae[350]. The presence of HPPs also resulted in reduced vessel lumen diameters compared to HUVEC-fibroblast co-cultures, further confirming the role of pericytes in restricting the diameter of the microvessels. This triculture model was able to generate generates perfusable vessels, and could recapitulate vasculopathies, such as those seen in pre-eclampsia[348]. In further work, these researchers have generated a triculture model using human placental fibroblasts (HPFs) as opposed to lung fibroblasts, where the seeding density is 10:1 (ECs: stromal cells), which models normal placental vasculature[341].

Table 1.1 - Methods of previously published placenta-on-a-chip studies. The device specifications, including the type of device, material, pore size, coating and cell types used are outlined. The type of flow, the rate and shear stress levels (if reported) are also shown. The methods used by each study to determine placental barrier formation, including cell junctions, permeability and microvilli are also outlined.

Reference	Type of device	Material	Pore Size	Cell Types	Coating	Flow Rate and Shear Stress	Formation of placental barrier
Blundell (2016)[127]	PDMS device with two channels (Height 135 µm; Width: 1 mm; Length: 1.5 cm) separated by membrane.	Poly-carbonate	1 µm	BeWos and HPVECs (from term placentae)	Fibronectin (0.1 mg/mL)	• Laminar flow all compartments • Flow rate: 100 µL/hr (1.67 µL/min)	• Forskolin treatment for syncytialisation • Cell junctions: E-cadherin and VE-cadherin showed intercellular junctions formed. • Permeability: FITC-dextran assay and glucose transfer experiment showed semi-permeable membrane. FITC-dextran permeability was reduced as syncytialisation occurred. • Endocrine function: Only forskolin treated trophoblast released hCG. • Microvilli: F-actin staining showed microvilli formation observed on the apical surface.
Blundell (2018)[347]	PDMS device with two channels (Height 135 µm; Width: 1 mm; Length: 1.5 cm) separated by membrane.	Poly-carbonate	1 µm	BeWos and HPVECs (from term placentae)	Fibronectin (0.1 mg/mL)	• Laminar flow all compartments • Flow rate: 100 µL/hr (1.67 µL/min)	• Forskolin treatment for syncytialisation • Cell junctions: E-cadherin (BeWo) and VE-cadherin (HPVECs) showed intercellular junctions formed. • Permeability: TEER measurements increased rapidly over time and FITC-inulin assay which showed negligible transport of FITC-inulin across the barrier. • Microvilli: F-actin staining showed microvilli formation observed on the apical surface.

Lee (2015)[346]	PDMS device with two channels (Height: 200 µm; Width: 500 µm)	Vitrified collagen	N/A	JEG-3 and HUVECs	Fibronectin in HUVEC channel (40 µg/mL) and gelatin (1.5%) in JEG-3 channel	• Laminar flow all compartments • Flow rate: 30 µL/hr (0.5 µL/min)	• Cell junctions: GFP (HUVECs) and CellTracker Red (JEG-3) showed monolayers formed. • Permeability: Glucose transfer experiment showed a semi-permeable membrane.
Lermant (2023)[351]	Mimetas OrganoPlate 3-lane 40 (Height: 220 µm; Side Channels Width: 300 µm; Middle Channel Width: µm)	ECM scaffold (HEPES, $NaHCO_3$ and rat collagen I)	N/A	ChiPS4 (human iPSC cell line) differentiated into trophoblast	0.2 mg/mL Geltrex in DMEM	• Mimetas OrganoFlow interval rocker platform set at a 7-degree inclination and 8 minute cycle time	• Cell junctions: E-Cadherin • Endocrine function: b-hCG release, with high levels in a region with loss of E-cadherin, suggesting fusion and formation of syncytium • Peremeability: Leak-tight barrier formed by dday 4 (FITC- and TRITC-Dextran assays)
Mandt (2018)[352]	PEGdma X shaped device, split into two channels, separated by membrane.	Gelatin hydrogel (GelMOD)	N/A	BeWos and HUVECs	Fibronectin (50 µL/mL)	• Flow rate: 50-70 µL/hr (0.83-1.167 µL/min)	• Cell junctions: Calcien-AM shows cell layers formed. • Permeability: FITC-dextran assay, showed a semi-permeable membrane. Riboflavin transfer experiment showed it is permeable to small molecules (350 Da).
Mosavati (2020)[353]	PDMS device with two channels (Height: 200 µm; Width: 1 mm) separated by membrane.	Poly-carbonate	400 nm	BeWos and HUVECs	Type I collagen	• Peristaltic pump • Flow rates of 10-150 µL/hr (0.16-2.5 µL/min) [Optimal: 50 µL/hr]	• Cell junctions: Calcien-AM (HUVECs) and CellTracker Orange (BeWo) showed intercellular junctions formed. • Permeability: Co-culture of cells in device reduced glucose transfer compared to single cell type or no cells.
Pemathilaka (2019)[354]	PDMS device with two channels (Height: 100 µm; Width: 400 µm) separated by membrane.	Polyester track etched (PETE)	400 nm	BeWos and HUVECs	Entactin–collagen IV–laminin (E–C–L, 10 µg/mL)	• Laminar flow all compartments • Flow rate: 50 µL/hr (0.83 µL/min)	• Cell junctions: E-cadherin (BeWo) and VE-cadherin (HUVECs) showed intercellular junctions formed. • Permeability: FITC-dextran assay, showed a semi-permeable membrane.

Pu (2021)[355]	PDMS circular device with central compartment connected to two inlet and two outlet ports. Two outer channels (Width: 200 μm) with an inlet and outlet port. Barrier between (Width: 50 μm) composed of pillars.	Pillars	3 μm between pillars	HTR8/SvNeo and HUVECs	Tested gelatin (0.2% w/v), Matrigel (1 mg/mL) or fibronectin (200 μg/mL)	• Laminar flow all compartments • Tested flow rates of 0.01, 0.05 and 0.1 μL/min • Shear stress: 0.0046, 0.0228, and 0.0457 N m−2	• Permeability: FITC-dextran assay, endothelial cells prevented diffusion for 48 hours. Flow-dependent changed in permeability.
Yin (2019)[356]	PDMS device with two channels in parallel (Length: 2 mm; Width, 350 μm; Height, 200 μm) and one middle matrix channel (Length: 2 mm; Width: 300 μm; Height: 50 μm).	Matrigel Matrix Channel	N/A	BeWos and HUVECs	Chitosan (2%) in BeWo compartment	• Laminar flow all compartments • Flow rate: 20 μL/hr (0.33 μL/min) • Shear stress: 0.03 dyn/cm2 (0.003 Pa)	• Cell junctions: E-cadherin (BeWo) and VE-cadherin (HUVECs) showed intercellular junctions formed. • Permeability: FITC-dextran assay, showed a semi-permeable membrane. • Microvilli: F-actin staining showed microvilli formation observed on the apical surface.
Zhu (2018)[357]	PDMS device with two channels (Height: 400 μm; Width: 1.5 mm; Length: 1.5 cm)	N/A	400 nm	BeWos and HUVECs (Plus addition of suspended THP-1 cells)	Type I Collagen (0.1 mg/mL)	• Laminar flow all compartments • Flow rate: 10 μL/hr (0.167 μL/min) to 40 μL/hr when THP-1 cells added	• Cell junctions: Occludin (BeWo) and VE-cadherin (HUVECs) showed intercellular junctions formed. • Microvilli: F-actin staining showed microvilli formation observed on the apical surface.

1.3 Summary

In summary, previous studies have reported that placental vascular dysfunction occurs in pregnancies complicated by GDM, of which maternal hyperglycaemia has been attributed to. As the placenta is responsible for efficient exchange of nutrients and gases between the maternal and fetal circulations, alterations in its structure and function can contribute to pathological fetal growth, including LGA. However, the mechanisms for the development of LGA are unclear and the prevalence of LGA remains high, even when pregnancies are considered well-controlled clinically, using standard methods of monitoring. Recent CGM studies have reported that subtle fluctuations in maternal glucose, with temporal periods of mild hyperglycaemia, are associated with LGA. Taken together with previous *in vitro* and *ex vivo* studies that utilise supraphysiological glucose concentrations to investigate the impact of maternal hyperglycaemia on the placenta, this warrants study into the impact of physiological maternal glucose fluctuations on the placenta in the development of LGA in GDM.

1.4 Hypothesis

Temporal periods of mild hyperglycaemia in GDM can influence placental development and function, resulting in complications of fetal growth, including LGA.

1.5 Aims

1. To develop an *ex vivo* human placental explant model to mimic *in vivo* physiological maternal glucose fluctuations.
2. To determine the impact of physiological maternal glucose fluctuations on the placental transcriptome and determine how this compares to the placental transcriptome in GDM and/or LGA.
3. To investigate the impact of physiological maternal glucose fluctuations on placental vascular development using *in vitro* cell models.

Chapter 2 - Materials and Methods

2.1 Placental Tissue

2.1.1 Patient recruitment and placenta collection

Ethical approval was acquired from the Northwest Greater Manchester Central Research Ethics Committee (08/H1010/55) and London Riverside Research Ethics Committee (18/LO/0067) for collecting term placentae at St. Mary's Hospital in Manchester and at the Leeds Teaching Hospital NHS Trusts, respectively. Written informed consent was given by all mothers prior to delivery and collection of the placenta. Maternal demographic information was collected at booking and pregnancy outcomes were recorded at birth. Placentae were collected within 30 minutes following delivery. The birthweight centile (BWC) was calculated using the Gestation Related Optimal Weight (GROW) calculator[358], which considered maternal BMI, parity, birthweight, ethnicity, fetal sex, and gestational age. These BWCs were used to characterise the pregnancy as LGA ($\geq$ 90th percentile), AGA (< 90th percentile or > 10th percentile) or SGA ($\leq$ 10th percentile).

Placental samples were collected from uncomplicated pregnancies, for placental explants, and control term placental tissue. Placental samples were also collected from pregnancies complicated by GDM (See Section 4.4.4). For these samples, patients were routinely tested for GDM at 24-28 weeks gestation via OGTT, as according to the NICE guidelines. Those diagnosed with GDM were treated to achieve euglycaemia (< 5.3 mM and < 7.8 mM glucose at fasting and post-prandial, respectively)[14].

The maternal demographic and pregnancy outcome information for placentae used for placental villous explant studies (n=14) are outlined in Table 2.1 and control term placental tissue (n=4; used for immunohistochemistry) are outlined in Table 2.2. For RNA sequencing (Section 2.6.5) only placental explants from male infants were used (n=5), due to sample availability at the time, and to control for fetal sex differences.

Table 2.1 – Demographics for placental samples used for explant studies. Data are presented as the mean±SEM. BMI measurements reported are from booking appointments, or later in gestation if booking information was not available. Abbreviations: BMI – body mass index; BWC – birthweight centile; EL LSCS - Elective Lower Segment Caesarean Section; EM LSCS - Emergency Lower Segment Caesarean Section; NVD – Normal Vaginal Delivery.

	n=14
Maternal age (years)	33.07±2.05
BMI at booking (kg/m^2)	25.58±0.79
Gestational age (days)	273.5±0.97
Parity	1.79±0.38
Ethnicity (%)	**White British:** 10 (71%) **Pakistani**: 1 (7.1%) **Asian**: 1 (7.1%) **Mixed White/Black Caribbean**: 1 (7.1%) **Unknown:** 1 (7.1%)
Birthweight (g)	3318.14±81.32
Placental weight (g)	472.97±19.52
Fetal sex (%)	**Male:** 12 (86%) **Female:** 2 (14%)
Mode of delivery (%)	**NVD:** 0 **EM LSCS:** 0 **EL LSCS:** 14 (100%)
Smoked in pregnancy (%)	**Smoked:** 2 (14%) **Non-Smoker:** 11 (79%) **Unknown:** 3 (7%)
BWC	40.19±5.84

Table 2.2 – Demographics for placental samples used for control term placental tissue for immunohistochemistry. Data are presented as the mean±SEM. BMI measurements reported are from booking appointments, or later in gestation if booking information was not available. Abbreviations: BMI – body mass index; BWC – birthweight centile; EL LSCS - Elective Lower Segment Caesarean Section; EM LSCS - Emergency Lower Segment Caesarean Section; NVD – Normal Vaginal Delivery.

	n=4
Maternal age (years)	32±4.14
BMI at booking (kg/m^2)	24.25±1.63
Gestational age (days)	272.25±1.11
Parity	2.5±0.29
Ethnicity (%)	**White British:** 4 (100%)
Birthweight (g)	3377.5±132.99
Placental weight (g)	442.5±28.93
Fetal sex (%)	**Male:** 3 (75%) **Female:** 1 (25%)
Mode of delivery (%)	**NVD:** 0 **EM LSCS:** 0 **EL LSCS:** 4 (100%)
Smoked in pregnancy (%)	**Smoked:** 1 (25%) **Non-Smoker:** 3 (75%)
BWC	43.5±5.79

2.1.2 Placental tissue processing

Following delivery, the fetal membranes and umbilical cord were removed, and the placental weight recorded. The placenta was then transferred to a sterile dissection tray and tissue samples were collected from the centre, middle and edge at 5 cm^3 full thickness, to represent the entire organ. The samples were then washed with sterile phosphate buffered saline (PBS; D8537, Sigma-Aldrich, UK) until the majority of maternal blood was removed. The basal and chorionic plates were then removed using dissection scissors. For histology, a full thickness tissue section from the centre, middle and edge were stored in 10% neutral buffered formalin (NBF; HT501128, Sigma-Aldrich, UK) at 4°C. After 48 hours NBF was removed and replaced with 70% ethanol and stored at 4°C until tissue was processed. For RNA and protein, tissue pieces from the centre, middle and edge were further dissected and small pieces from each area were pooled into collection tubes. RNA samples were placed in RNALater (R0901-500ML; Merck, UK) for 48 hours, before being snap frozen in liquid nitrogen and stored in the -80°C. Protein samples were snap frozen in liquid nitrogen and stored in the -80°C (Figure 2.1).

2.1.3 Placental villous explants

For placental villous explant culture, 2 mm^3 sections from the centre, middle and edge of the placental tissue were placed in each Netwell™ (3477, Costar, UK) in each well of a 12-well plate, containing 2 mL medium (Figure 2.1). Dulbecco's Modified Eagle Medium (DMEM) with Ham's F12 (DMEM-F12) culture medium without glucose (L0091-500, Biowest, France) was used and was supplemented with 10% fetal bovine serum (FBS; 10270-106, Gibco, UK), 1% penicillin, streptomycin and glutamine (PSG; 10378-016, Gibco) and 9.6 µL/mL sterile filtered D-glucose (555 mM, G8644, Sigma-Aldrich, UK) to generate a glucose concentration of 5.5 mM. Explants were then supplemented with additional amounts of glucose for glucose treatment experiments (See Section 2.4.1 on glucose treatments).

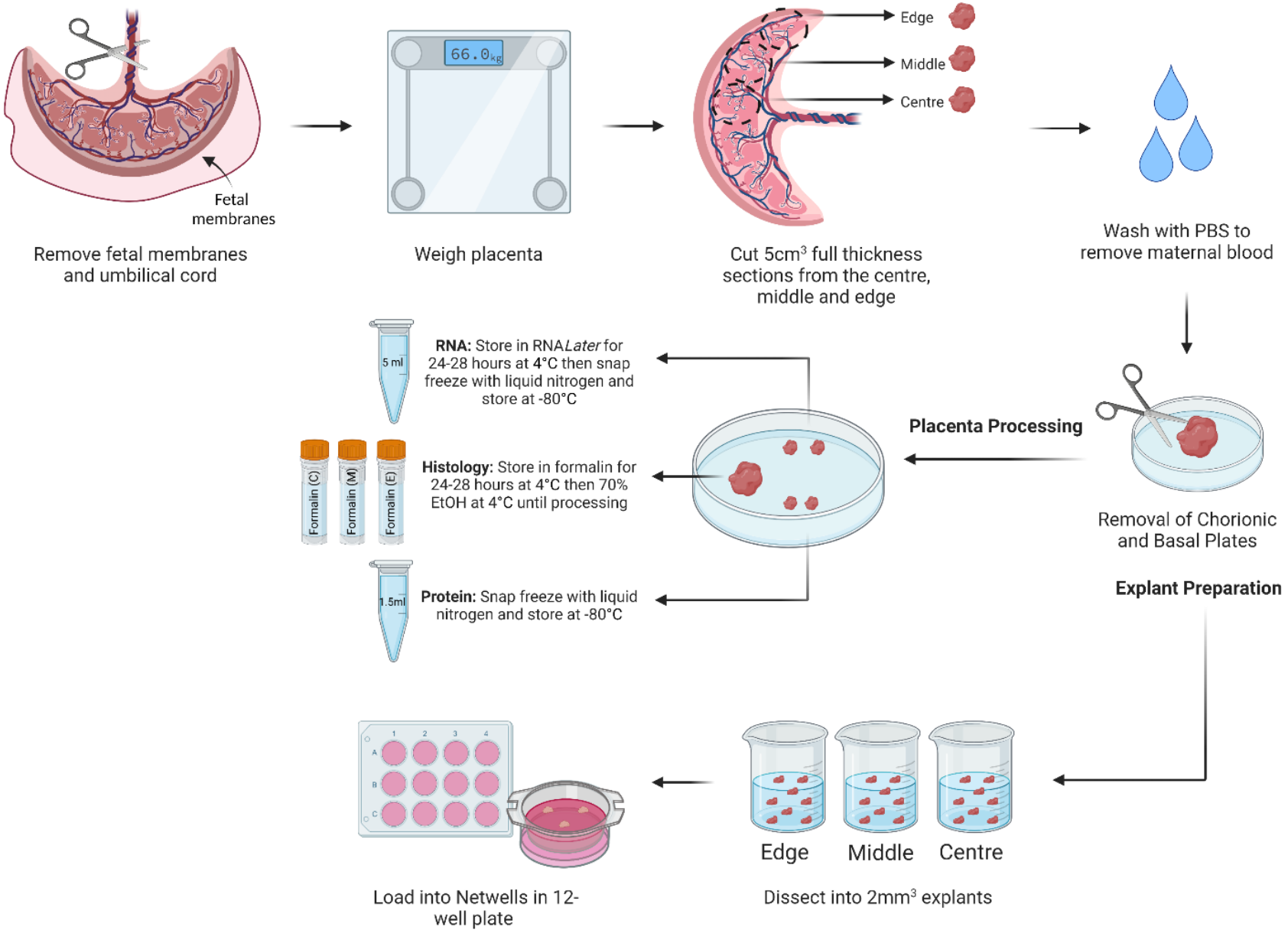
Fetal membranes
Remove fetal membranes and umbilical cord
66.0kg
Weigh placenta
Edge
Middle
Centre
Cut 5cm³ full thickness sections from the centre, middle and edge
Wash with PBS to remove maternal blood
Removal of Chorionic and Basal Plates
Placenta Processing
Explant Preparation
5 ml
RNA: Store in RNALater for 24-28 hours at 4°C then snap freeze with liquid nitrogen and store at -80°C
Formalin (C)
Formalin (M)
Formalin (E)
Histology: Store in formalin for 24-28 hours at 4°C then 70% EtOH at 4°C until processing
1.5ml
Protein: Snap freeze with liquid nitrogen and store at -80°C
Edge
Middle
Centre
Dissect into 2mm³ explants
Load into Netwells in 12-well plate

Figure 2.1 - Placental tissue collection, processing and placental villous explant preparation. Full thickness sections were collected from the centre, middle and edge of the placenta and were washed with sterile PBS. The chorionic and basal plates were removed, and samples were collected for RNA, histology and protein. For explant culture, 2 mm^3 sections from the centre, middle and edge sections of placental tissue were collected and placed in sterile PBS. Three explants, one centre, middle and edge piece, were placed in each Netwell in 12-well plates. Explants were cultured in DMEM-F12 medium, supplemented with 1% penicillin, streptomycin, and glutamine (PSG) and 10% fetal bovine serum (FBS). Figure created with Biorender.com.

2.2 Placental explant viability assays

2.2.1 Lactate dehydrogenase (LDH) colourimetric assay

To assess placental explant viability and necrosis[115], a lactate dehydrogenase (LDH) assay was performed on placental explant culture medium using a cytotoxicity detection kit (11644793001, Roche, Switzerland), according to manufacturer's instructions. For the standards, LDH from rabbit muscle (10127876001, Roche, Switzerland) was diluted DMEM-F12 containing no glucose or FBS to a concentration of 1 U/mL. Standards of LDH were made by 1:2 serial dilutions of the 1 U/mL stock to the following concentrations: 0.5, 0.25, 0.125, 0.0625, 0.03125, 0.015625 and 0.0078125 U/mL. Following the protocol, 50 µL of 1M HCl (35328, Honeywell, Fluka, UK) was added to each well to stop the enzymatic reaction. The absorbance was measured at 492 nm and 690 nm on a plate reader (Powerwave HT, Biotek, USA) with Gen5 Microplate Reader software. Final absorbance values were calculated as the absorbance at 492-690 nm. Concentrations of samples were determined from a linear standard curve (Figure 2.2A).

2.2.2 hCG ELISA

To assess tissue viability, hCG levels (α- and β-hCG) in the placental explant culture medium were determined using a hCG enzyme-linked immunosorbent assay (ELISA; EIA-1469, DRG Diagnostics, Germany), as per the manufacturer's instructions and using a linear standard curve with concentrations of 5, 25, 50, 75, 100, 200, 350, 500, 750 and 1000 mIU/mL. The absorbance was measured at 450 nm on a plate reader (Powerwave HT, BioTek, USA) with Gen5 Microplate Reader software. Concentrations of samples were determined from a linear standard curve (Figure 2.2B).

To assess levels of hCG in placental villous explants that were cultured for 4 days to allow for syncytial regeneration and 96 hours of glucose treatments, we used a more sensitive β-hCG ELISA (EIA-1911, DRG Diagnostics, Germany) on medium that was concentrated. To concentrate medium, Amicon Ultra-0.5 centrifugal filters were used (UFC500396, Millipore, USA). To remove glycine from the filters, 500 µL of PBS was added to the filter and centrifuged at 4,000 RCF for 10 minutes. All remaining PBS was then removed from the filters and 500 µL of medium sample added. The sample was then centrifuged at 14,000 RCF for 15 minutes. The filter, containing the concentrated medium, was then inverted into a new tube, and centrifuged at 1000 RCF for 2 minutes. The β-hCG ELISA was then performed according to manufacturer's instructions, and using a standard curve with concentrations of 5, 25, 50,100 and 200

mIU/mL. Where necessary, conditioned medium samples were diluted 1:10 with the sample diluent provided in the kit. The absorbance was measured at 450 nm on a plate reader (51119300, ThermoFisher) using SkanIt RE 4.1 software. Final concentrations of β-hCG were determined from a Four Parameter Logistic (4PL) curve of the standards (Figure 2.3).

A 4PL is a regression model which follows a sigmodal curve, as the standard concentrations are only linear across a specific range of concentrations and can plateau. The 4PL model follows the below equation (Equation 2.1).

$$y = d + \frac{a - d}{1 + (\frac{x}{c})^b}$$

Equation 2.1 – Four Parameter Logistic (4PL) regression model equation. Here, *a* is the minimum value that can be obtained, *d* is the maximum value, *c* is the point of inflection (the point where the curvature of the response line changes) and *b* is the Hill's slope of the curve (the steepness of the curve at point *c*).

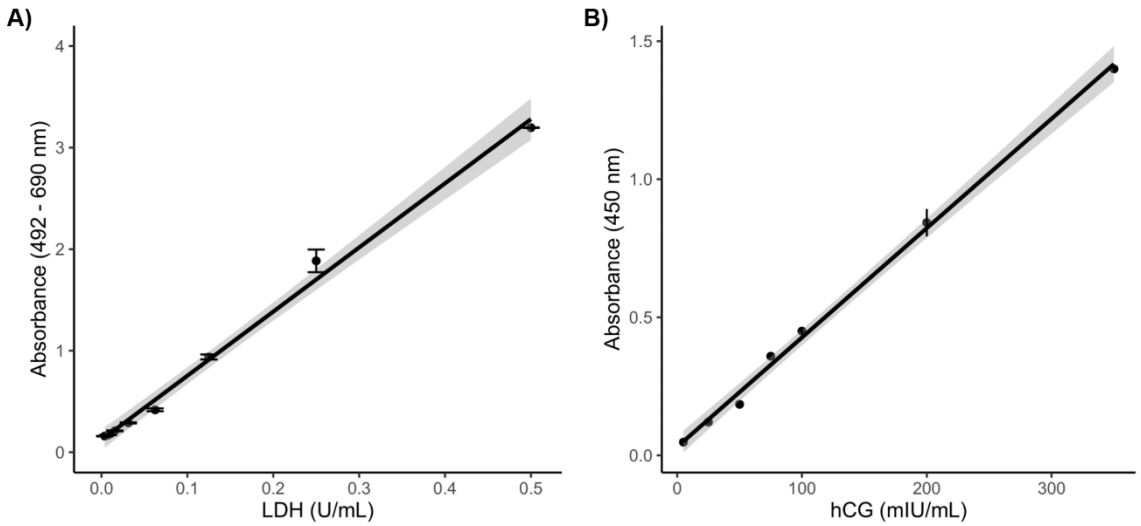

Figure 2.2 - Example of an LDH and hCG assay standard curve. An LDH and hCG assay was performed to calculate the levels of LDH and hCG in placental explant conditioned medium. A) The absorbance was measured at 590 nm and subtracted from the absorbance at 492 nm from known concentrations of LDH (U/mL). The equation for this curve is y=6.32x+0.12, with an R^2 of 0.99. B) The absorbance was measured at 495 nm from known concentrations of hCG (mIU/mL). The equation for this curve is y=0.00396x+0.031, with an R^2 of 0.99.

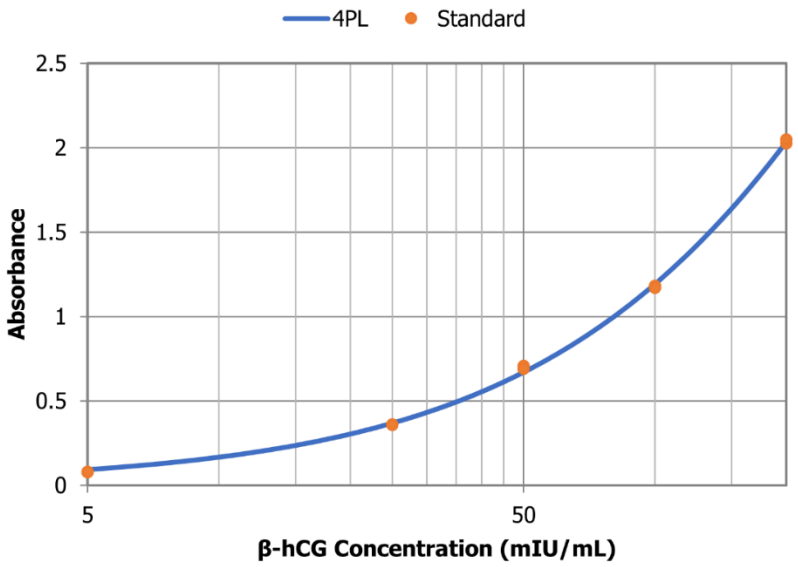

Figure 2.3 - Example of a β-hCG 4PL standard curve. A β-hCG assay was performed to calculate the levels of β-hCG in placental explant conditioned medium. The absorbance was measured at 450 nm from known concentrations of β-hCG (mIU/mL). The standard curve was plotted as a 4-parameter logistic regression (4PL) curve. The R^2 of this curve was 0.99.

2.3 Cell culture

2.3.1 Primary human placental mesenchymal stromal cells (pMSCs)

2.3.1.1 Placental Tissue Collection and Dissection

Placentae from uncomplicated (n=7) pregnancies and GDM pregnancies (n=4) were collected within 30 minutes following elective C-section delivery at the Leeds Teaching Hospital NHS trust (Section 2.1.1). For GDM samples, placentae were collected from patients that had been diagnosed with GDM, during routine tests at 24 – 28 weeks' gestation via OGTT, according to the NICE guidelines[14]. The maternal demographic and pregnancy outcome information for placentae used for pMSC isolations are outlined in Table 2.3.

The protocol for pMSC isolation was adapted by Margeurite Kennedy, a previous PhD student in our research group[359], from the Pelekanos *et al.* (2016) method[360]. Following delivery, the fetal membranes and umbilical cord were removed, and the placental weight recorded. The placenta was then transferred to a sterile dissection tray. Sections of ~0.5 cm in depth were collected from the maternal decidua, chorionic plate and chorionic villi and placed in separate petri dishes containing 1x Hanks Balanced Salt Solution (HBSS; 14185052, Gibco, UK) to be washed, before being transferred into 50 mL falcons. To access the chorionic plate and chorionic villi, the amniotic membrane was then removed from the fetal side of the placenta using two forceps. Approximately 10g of tissue was collected for each placental region. Tissue was then washed by adding 30 mL HBSS to each falcon tube and inverting several times, this washing procedure was repeated three times.

2.3.1.2 Placental Tissue Digestion

Tissue was then transferred into fresh petri dishes, one for each region (decidua, chorionic plate and chorionic villous) and minced into 1-5 mm^3 sections using scissors and forceps. Digestion solution was prepared containing 3 mL 100U/ml collagenase (17100-17) in HBSS, 3 mL 2.4U/ml dispase (17105-041) in PBS, 75 µL 40mg/ml DNase I in NaCl (D5025-150KU) and 24 mL serum free low glucose DMEM (11885-092, Gibco, UK). Minced tissue was transferred into fresh 50 mL falcon tubes and 10 mL of digestion solution was added to each tube and incubated at 37°C on a shaker for 90 minutes. The digestion was then deactivated by adding 30 mL of low glucose DMEM with 10% FBS (10270-106, Gibco, UK).

Table 2.3 - Demographics for GDM and non-GDM placentae used for pMSC isolations. pMSCs were isolated from non-GDM (n=7) or GDM (n=4) placentae. BMI measurements reported are from booking appointments, or later in gestation if booking information was not available. Continuous variables are summarised by the mean±SEM and statistical analysis was performed using either a T-Test or Mann-Whitney U Test, for normally distributed or non-normally distributed variables, respectively. Categorical variables are reported as a number (%) and statistical analysis was performed using a Chi-Squared test. Abbreviations: BMI – body mass index; BWC – birthweight centile; EL LSCS - Elective Lower Segment Caesarean Section; EM LSCS - Emergency Lower Segment Caesarean Section; NVD – Normal Vaginal Delivery.

	Non-GDM (n=7)	GDM (n=4)	Significance
Maternal age (years)	35.86±1.96	33±3.24	p=0.4829 NS (T-Test)
BMI at booking (kg/m^2)	23.83±1.49	31.98±5.45	p=0.1636 NS (Mann-Whitney)
Gestational age (days)	274.14±1.07	272±1.35	p=0.2575 NS (T-Test)
Parity	1.57±0.37	1.50±0.65	p=0.9272 NS (T-Test)
Ethnicity (%)	**White British:** 7 (100%)	**White British:** 2 (50%) **Asian:** 1 (25%) **Other:** 1 (25%)	p=0.1178 NS (Chi-Squared)
Birthweight (g)	3232±167.64	3401.25±190.28	p=0.5251 NS (T-Test)
Placental weight (g)	421.71±52.10	485±28.31	p=0.317 NS (T-Test)
Fetal sex (%)	**Male:** 4 (57.10%) **Female:** 3 (42.86%)	**Male:** 1 (25%) **Female:** 3 (75%)	p=0.6888 NS (Chi-Squared)
Mode of delivery (%)	**NVD:** 0 **EM LSCS:** 0 **EL LSCS:** 7 (100%)	**NVD:** 0 **EM LSCS:** 0 **EL LSCS:** 4 (100%)	p=0.3657 NS (Chi-Squared)
BWC	33±10.18	57.58±19.30	p=0.4121 NS (Mann-Whitney)
Smoked in pregnancy (%)	**Smoked:** 1 (14.3%) **Non-Smoker:** 5 (71.4%) **Unknown:** 1 (14.3%)	**Smoked:** 0 **Non-Smoker:** 4 (100%)	p=0.4974 NS (Chi-Squared

2.3.1.3 Isolation of Placental Cells and Removal of Debris

Digested tissue was then centrifuged for 5 seconds at 340 RCF to bring unwanted tissue debris to the bottom of the tube. The supernatant, containing the mononuclear cells, was transferred to a new 50 mL falcon tube. An additional 30 mL of low glucose DMEM was added to the tissue debris, with vigorous shaking for 15 seconds to liberate any remaining cells, followed by a second centrifugation step. The collected supernatant was centrifuged at 340 RCF for 5 minutes to pellet the mononuclear cells.

The supernatant was then discarded, and each pellet (decidua, chorionic plate and chorionic villous) was resuspended in 15 mL of low glucose DMEM supplemented with 10% FBS (10270-106, Gibco, UK), 1% Antibiotic and Antimitotic (15240-062, Gibco, UK) and 1% Non-Essential Amino Acids (NEAA; 11140035, Gibco, UK), which will be referred to as pMSC culture medium. This medium contained 5.5 mM glucose. The cell suspensions from each of the placental regions were passed through a 100 µm cell strainer (352340, Fisher Scientific, UK) into a fresh falcon, which was then divided into three T75 flasks and incubated at 37°C in 5% CO_2/20% O_2 (Figure 2.4; Figure 2.5). Half of the media was replaced at 72 hours, and then after a further 24 hours. All the media was replaced after a further 24 hours. At approximately 2 weeks, dense MSC-like colonies had formed. These cells were then sub-cultivated (Section 2.3.1.4) once they had reached ~80% confluency to prevent contact inhibition.

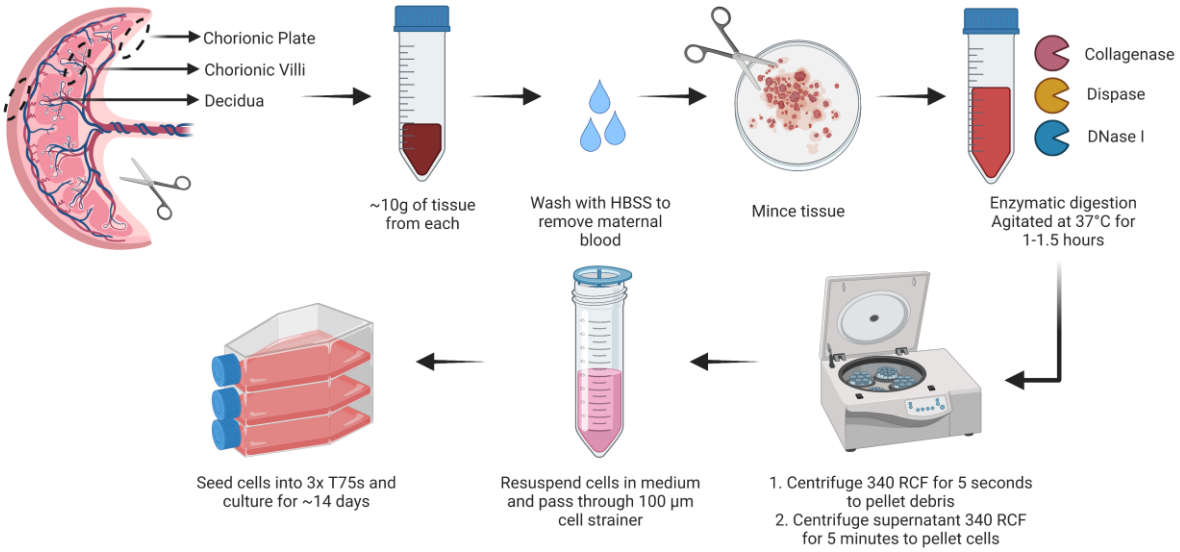

Figure 2.4 - Isolation of placental mesenchymal stromal cells (pMSCs) from human term placentae. Around 10g of placental tissue was collected from the chorionic plate, chorionic villous and decidua. Tissue was washed to remove maternal blood using HBSS, and then minced. An enzymatic digestion was performed at 37°C for 1-1.5 hours using collagenase, dispase and DNase I. Centrifugation steps were then performed to remove debris and pellet the cells. Cells were passed through a 100 µm cell strainer before seeding into T75s. Figure created with Biorender.com.

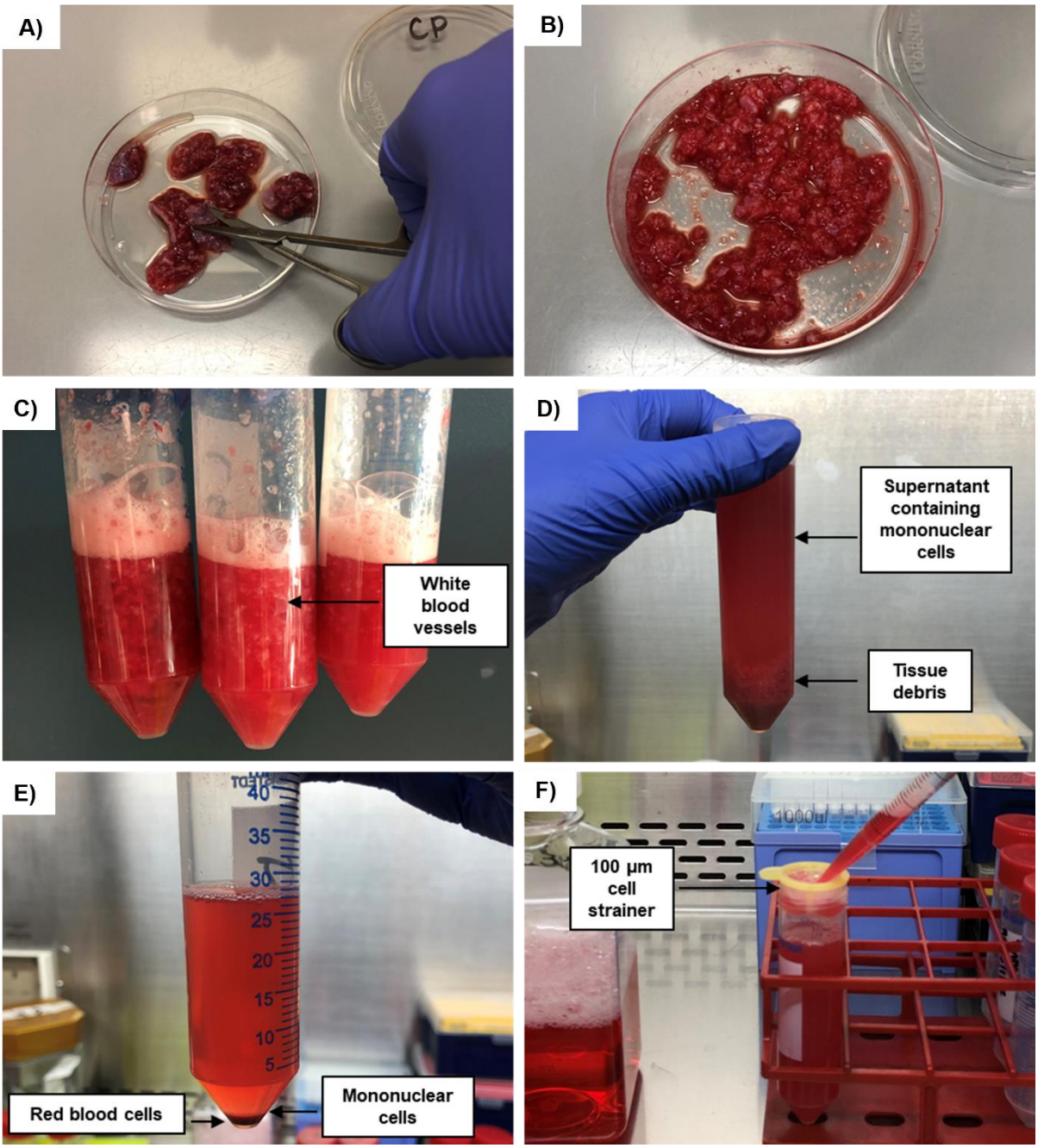

Figure 2.5 - Images showing several steps of the placental mesenchymal stromal cell (pMSC) isolation protocol from human term placentae. A) Mincing of placental tissue. B) Minced placental tissue. C) Tissue following enzymatic digestion D) Pelleting of tissue debris. E) Pelleting of mononuclear cells. F) Passing cells through cell strainer.

2.3.1.4 Primary pMSC cell culture

The primary pMSCs were cultured in pMSC medium, as described above. They were cultured in a humidified incubator at 37°C in 5% CO_2/20% O_2 for the duration of the culture. Cells were seeded into flasks at a density of 1,000-5,000 cells/cm^2. For the sub-cultivation procedure, cells were first washed with sterile PBS and detached from the flasks with 1-2 mLs of TrypLE express (12563-029, Gibco, UK) and incubated at 37°C for 5 minutes. TrypLE was inactivated with 3x pMSC medium. Cells were counted with a haemocytometer and seeded into flasks at the appropriate density described above. To exclude dead cells from cell counts, the cell suspension was mixed 1:2 with trypan blue (TB154, Sigma-Aldrich) before counting, and cells labelled with trypan blue were excluded from counts.

2.3.1.5 Cryopreservation of pMSCs

From passage two (P2), pMSCs were routinely frozen down at ~2x10^6 cells/mL. Cell suspensions were centrifuged at 350 RCF for 5 minutes, and the pellet was resuspended in dimethylsulfoxide (DMSO) Cell Freezing Medium (12648010, Sigma-Aldrich, USA). Cells were placed in a Cell Freezing Container (Corning, USA) cooled by 1°C per min to -80°C over 24 hours. Cells were then transferred to a liquid nitrogen storage vessel and stored in the vapour phase.

2.3.2 Commercial human umbilical vein endothelial cells (HUVECs)

HUVECs from pooled donors (C-12203, Promocell, Germany) were used as positive controls for pMSC endothelial lineage differentiation experiments. HUVECs were cultured in Endothelial Growth Medium 2 (EGM-2; C-22011, Promocell) supplemented with a supplement mix (**Appendix 1**). The culture medium contained 5.6 mM glucose.

HUVECs were cultured in a humidified incubator at 37°C in 5% CO_2/20% O_2 for the duration of the culture. Cells were seeded into flasks at a density of 5,000-10,000 cells/cm^2. For the sub-cultivation procedure, cells were first washed with sterile PBS and detached from the flasks by addition of 3-5 mLs of Accutase (C-4130, Promocell) prior to incubation at 37°C for 5-15 minutes. Cells were then transferred to 15 mL Falcon tubes and centrifuged for 3 minutes at 220 RCF. The supernatant was removed, and cells were resuspended in 5 mLs of EGM-2 media before being counted with a haemocytometer and seeded into flasks at the appropriate density described above. To exclude dead cells from cell counts, the cell suspension was mixed 1:2 with trypan blue (TB154, Sigma-Aldrich) before counting, and cells labelled with trypan blue were excluded from counts.

2.3.3 Placental microvascular cells

For the triculture placental microvascular model, HUVECs, placental pericytes (HPPs) and placental fibroblasts (HPFs) were used. HUVECs were transduced to stably express cytoplasmic red fluorescent protein (RFP) (17-10409 LentiBrite RFP Control Lentiviral Biosensor, Millipore Sigma Aldrich) and cultured in VascuLife® VEGF Endothelial Medium containing supplements (LL-0003, LifeLine Cell Technologies, USA; **Appendix 2**).

HPPs (cAP-0029, Angioproteomie) were cultured in pericyte growth medium (PB-MH-031-4000, PELOBiotech, medium composition not available from manufacturers).

HPFs (CRL-7526, ATCC) were cultured in FibroLife S2 Fibroblast Medium containing supplements (LL-0011, LifeLine Cell Technologies, USA; **Appendix 3**).

2.3.4 Cell culture in microfluidic devices

2.3.4.1 Culture of HUVECs and pMSCs in PDMS fabricated devices

Microfluidic devices were fabricated and provided by Dr Virginia Pensabene and Elena Mancinelli (School of Electronic and Electrical Engineering, University of Leeds). Microfluidic devices were fabricated by soft lithography in polydimethylsiloxane (PDMS). The specification of the devices used are outlined in Figure 2.6 and Figure 2.7[361].

pMSCs (n=3) or HUVECs (n=3) were cultured in microfluidic devices. Firstly, each microfluidic device was sterilised by UV light exposure for 30 minutes and loaded with sterile water, to prevent the device from drying out. This was then incubated at 37°C for 1 hour. Excess water was then removed from the reservoirs. Medium (EGM-2 or pMSC medium, for HUVECs and pMSCs, respectively) was pre-warmed to 37°C and ~500 µL loaded into a 1 mL syringe and gentle pressure was applied on the inlet port to fill the chamber with medium. Excess medium was then removed from the reservoirs and 3% Matrigel (356230, Corning, USA) in medium (EGM-2/pMSC) was loaded into the device using a 1 mL Luer slip syringe (15489199, BD, USA). Following removal of excess Matrigel solution, 15 µL of fresh medium was added at each port and devices were incubated at 37°C for 2-3 hours. Following this, the devices were washed 3x with PBS and once with medium.

The sub-cultivation procedure (Section 2.3.2 for HUVECs and Section 2.3.1.4 for pMSCs) up to and including the cell counting step was performed on confluent cells (~90%). Once the cell count was determined, 1 million or 500,000 cells were resuspended in 1 mL of medium for HUVECs and pMSCs, respectively. Following this, 100 µL of the cell suspension was loaded into a 1 mL syringe and gentle pressure was applied on the inlet port within the reservoir to fill the chamber with cells. The device was then observed under the microscope to ensure cells were entering the device. Once the cells had travelled through the channels, any excess cell suspension was removed from the reservoirs and 15 µL of fresh medium was added at each port (to prevent the ports from drying out). Cells were left to attach at 37°C for 2 hours. After this time, ~500 µL medium was added to the inlet port.

For flow culture, a 6-Channel Syringe Pump (AL-1600, World Precision Instruments, UK) was used. Cells were allowed to adhere to the microfluidic devices for 72 hours under static conditions before exposure to flow. To eliminate bubbles, 10 mL Luer lock syringes (15544835, BD, USA) with 24G sterile blunt needles (SAI Infusion Technologies, USA) were loaded with medium the day prior to flow culture and warmed to 37°C overnight. On the day of flow culture, the syringe pump was placed inside the tissue culture hood. Bubbles were then expelled from the syringes, which were then loaded into the syringe pump. Tygon tubing with an internal diameter of 0.020” and outer diameter of 0.060” (Cole Parmer, USA) was attached to the blunt needles and medium manually pushed through the syringes until a droplet had formed at the end of the tubing. The inlet and outlet reservoirs were then removed from the devices and the tubing was inserted into the inlet using forceps. Tubing was also attached to the outlet into a bijou to collect spent medium (Figure 2.8). The syringe pump was incubated at 37°C in 20% O_2/5% CO_2. Unidirectional flow was initiated for 72 hours at a flow rate of 1 µL/min. One device per experiment was left under static conditions for comparison (1-2 devices per flow/static condition).

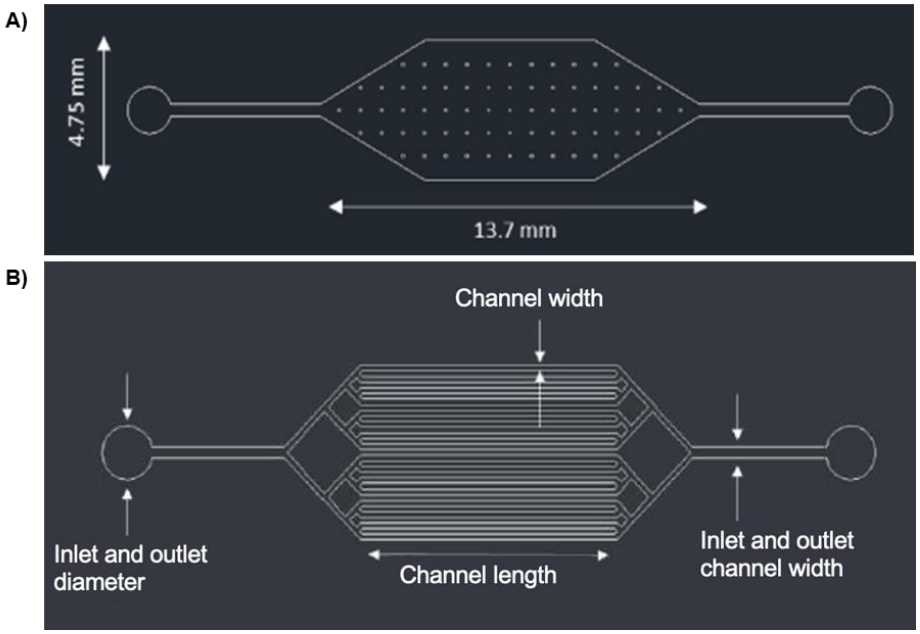

Figure 2.6 - Specifications of the PDMS microfluidic device designs. A) Rhomboidal device with one channel. Height: 150 µm, Area 48.85 mm^2, Volume of 7.33 µL. B) Rhomboidal device with 16 channels. Height: 100 µm, Channel width: 400 µm, Channel length: 20 mm, Single channel area 2 mm^2, Total area: 48 mm^2, Single channel volume: 0.2 µL, Total volume: 4.8 µL, Inlet and outlet diameter: 2 mm, Inlet and outlet channel width: 400 µm (Adapted from Mancini, 2020).

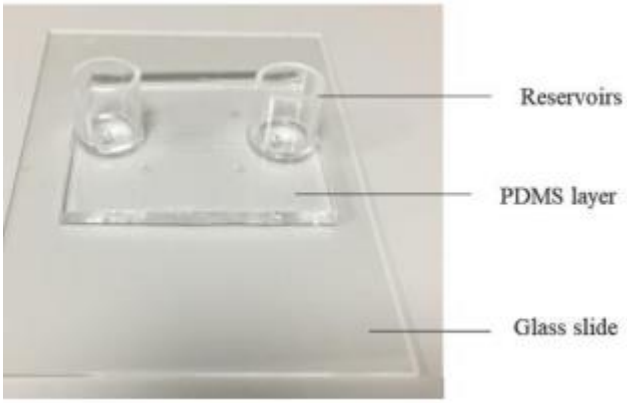

Figure 2.7 - Example image of a PDMS microfluidic device with reservoirs. The PDMS device is plasma bonded to a glass slide and inlet and outlet medium reservoirs are added[361].

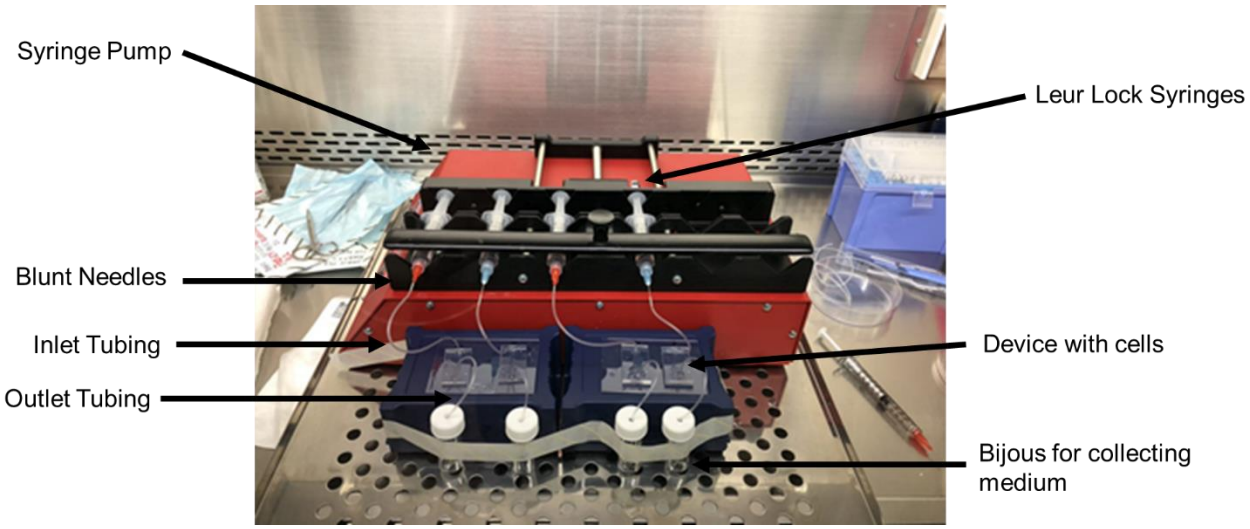

Figure 2.8 – PDMS Device Experimental set up. Devices were connected to the syringe pump using blunt needles and inlet Tygon tubing. Outlet tubing and bijou tubes were also used to collect spent media for assays.

2.3.4.2 Culture of pMSCs in Ibidi Microfluidic Devices

Use of commercial devices were also optimised for flow culture of pMSCs (n=2). The µ-Slide VI 0.4 (IbiTreat; IB-80606, Ibidi, Thistle Scientific, UK) was used which contains 6 individual channels. The specification of the devices used are outlined in Figure 2.9.

The device was incubated 37°C for 1 hour. The sub-cultivation procedure (Section 2.3.1.4) up to and including the cell counting step was performed on confluent cells (~90%). To determine appropriate cell concentrations, once the cell count was determined, 500,000 or 250,000 cells were resuspended in 1 mL of medium and 30 µL of cell suspension at 250,000 cells/mL was loaded into the top three channels and 30 µL of cell suspension at 500,000 cells/mL was loaded into the lower three channels. Cells were left to attach before the addition of fresh medium.

For flow culture, a 6-Channel Syringe Pump (World Precision Instruments, UK) was used. Cells were allowed to adhere to the microfluidic devices for 24 hours under static conditions before exposure to flow. To eliminate bubbles, 10 mL Luer lock syringes (305959, BD, USA) with 24G sterile blunt needles (B24-50, SAI Infusion Technologies, USA) were loaded with medium the day prior to flow culture and warmed to 37°C overnight. On the day of flow culture, the syringe pump was placed inside the tissue culture hood. Bubbles were then expelled from the syringes, which were then loaded into the syringe pump. Needles were removed and female Luer connectors (IB-10825, Ibidi) were attached to the syringes. Silicon tubing 0.8 mm (IB-10841, Ibidi) was then attached to the female Luer connectors, with elbow connectors (IB-10802, Ibidi) attached to the opposite end. Medium was manually pushed through the syringes until a droplet had formed at the end of the elbow connectors. The elbow connectors were then placed into the inlet reservoirs. Tubing was also attached to the outlets using elbow connectors and placed into a bijou to collect spent medium (Figure 2.10). The syringe pump was incubated at 37°C in 5% CO_2. Unidirectional flow was initiated for 72 hours at a flow rate of 1 µL/min. One channel per cell seeding density was left under static conditions for comparison.

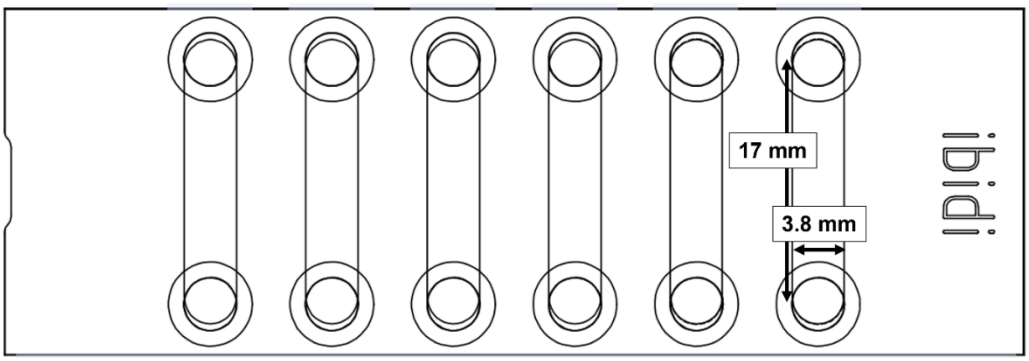

Figure 2.9 - Specifications of the Ibidi µ-Slide VI 0.4 (IbiTreat) devices. Channel Height: 0.4 mm, Channel Area: 0.6 cm^2, Channel Volume: 30 µL, Reservoir volume: 60 µL.

Figure 2.10 - Ibidi Device Experimental set up. Devices were connected to the syringe pump using female Luer connectors, inlet silicon tubing and elbow connectors. Elbow connectors were placed in the outlet and connected to silicone tubing in bijou tubes to collect spent media for assays.

2.3.4.3 Triculture model of placental microvasculature

This work was conducted in collaboration with Dr Kristina Haase's laboratory (EMBL, Barcelona), based on their triculture model of placental microvasculature, incorporating HUVECs, HPPs and HPFs, described in Cherubini *et al.* (2023)[362]. Microfluidic devices were provided by Dr Kristina Haase and Dr Marta Cherubini. Devices were fabricated from PDMS using a 0.5 mm cast Clarex (polymethylmethacrylate) mould and were plasma bonded onto glass slides as described in Cherubini and Haase (2023)[363]. The specification of the device is outlined in Figure 2.11; Figure 2.12A). Each microfluidic device was sterilised by UV light exposure for 30 minutes.

Cells were washed with PBS and detached from the flask using 3-5 mL of TrypLE express (12563-029, Gibco, UK) and incubated at 37°C for 3-5 minutes. Cells were resuspended in their appropriate medium (15-50 mL) and then counted. Resuspended cells were centrifuged for 5 minutes at 1200 RPM. For seeding into devices, a ratio of 10:1 ECs to stromal cells (pericytes and fibroblasts) were needed. Therefore, cell pellets were resuspended in VascuLife medium (LL-0003, LifeLine Cell Technologies, USA) containing thrombin (4 U/mL; T4648-1KU, Sigma-Aldrich, UK) at a concentration of 24 x 10^6 cells/mL for HUVECs and 2.4 x 10^6 cells/mL for HPPs and for HPFs and placed on ice immediately. For each device 20 µL of cell mixture, containing 10 µL of HUVECs (~240,000 cells), 5 µL of HPPs (~12,000 cells) and 5 µL HPFs (~12,000 cells) was required and therefore a master mix was prepared. Before seeding into the device, the 20 µL of cell mixture was mixed with 20 µL of fibrinogen (6 mg/mL; F8630-5G, Sigma-Aldrich, UK). This was done immediately prior to seeding to prevent the thrombin and fibrinogen from polymerising too early. The mixture containing cells and fibrinogen (40 µL) was then loaded into the central channel. Devices were incubated at 37°C for 15-20 minutes to allow the thrombin and fibrinogen to polymerise (final concentration 2 U/mL and 3 mg/mL, respectively). Following this, 75 µL of VascuLife (LL-0003, LifeLine Cell Technologies, USA), containing the appropriate glucose concentration was added to each side channel (See Section 2.4.3 on glucose treatments).

After 48 hours, reservoirs were added to initiate gravitational fluid flow. Firstly, the medium was collected from the side channels and refreshed with 40 µL of medium of the appropriate glucose concentration. The ports of the central channel were then plugged with PDMS tips to prevent any medium leaking from these ports when the reservoir was added (Figure 2.12B). The reservoirs were then added by pushing them into the ports of the side channels (Figure 2.12C). Any bubbles were then removed from the side channels by washing with medium. To initiate flow, 840 µL of medium

with the appropriate glucose concentration was added to one side of the reservoir (inlet reservoir), which generates a pressure of 7 mmH_2O (ΔP). Two independent experiments were performed (n=2), with 6-9 devices per condition.

2.3.4.4 Shear stress calculations in microfluidic devices

The level of shear stress within microfluidic devices was calculated using the following formula (Equation 2.2)[364,365].

$$Shear\ Stress = \frac{6\eta Q}{h^2 w}$$

Equation 2.2 – Shear Stress Formula.

This is derived by solving the Navier-Stokes equation, assuming an incompressible liquid, no gravity, dominance of viscous force, laminar flow in a rectangular channel of with height<width<<length.

To calculate the shear stress (in Pa), using equation 2.2, Q is the flow rate (in μm^3/min, where μL/min=0.017*10^9 μm^3/s), η is the dynamic viscosity (assuming the culture medium viscosity equals to the viscosity of the water; in Pa*s, where dyne*s/c^2=Pose=0.1 Pa*s), h is the channel height (in μm) and w the channel width (in μm).

For the two PDMS fabricated devices (channel and rhomboidal), the parameters used, and the respective shear stress values are as outlined in Table 2.4. The calculations were made assuming not including the hydraulic resistance and the dimensions (length = 10 cm, ID=0.20") of the connecting tubes and considering negligible the contribution of the short inlet channels in the two configurations. The parameters and respective shear stress values for the Ibidi μ-Slide VI 0.4 devices are also outlined in Table 2.4.

As the PDMS devices used for the placental microvasculature triculture model did not use a a rectangular channel, and generated a microvessel network as opposed to a monolayer of cells, the above equation could not be used. Therefore, this has been investigated by the collaborators in Cherubini *et al*. (2023)[362], using computational fluid dynamics software. A laminar flow physics module for flow through porous media was utilised, with microvessel networks treated as open pores filled with cell culture medium (density = 998.2 kg/m^3, viscosity = 9.4*10^{-4} Pa*s). The extravascular gel matrix (EVM) was treated as a porous domain with fibrin gel (density = 985 kg/m^3, viscosity = 1*10^{-2} Pa*s) having a porosity of 0.3 and hydraulic permeability k=1e^{-13} m^2. A simulated pressure gradient of 70 Pa (7 mmH_2O) was applied across the gel region, to model the pressure generated by flow through the microvessels (Section 2.3.4.3). From these

simulations, the shear stress for flow-conditioned vessels and in the EVM were predicted to be 0.32 Pa (3.2 dyne/cm^2) and 0.001 Pa (0.01 dyne/cm^2), respectively.

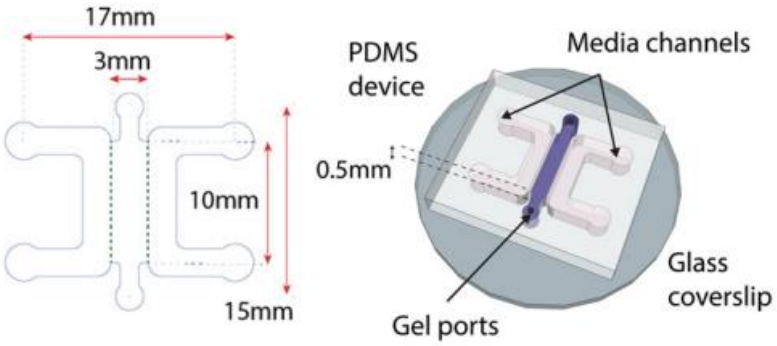

Figure 2.11 - Specifications of the PDMS device used for the placental microvasculature triculture model. The device contained two side channels for medium, each with two ports and a inner channel where the cells are seeded, with two ports. The height of the device was 0.5 mm. Central channel width: 3 mm; height (excluding ports: 10 mm)[363].

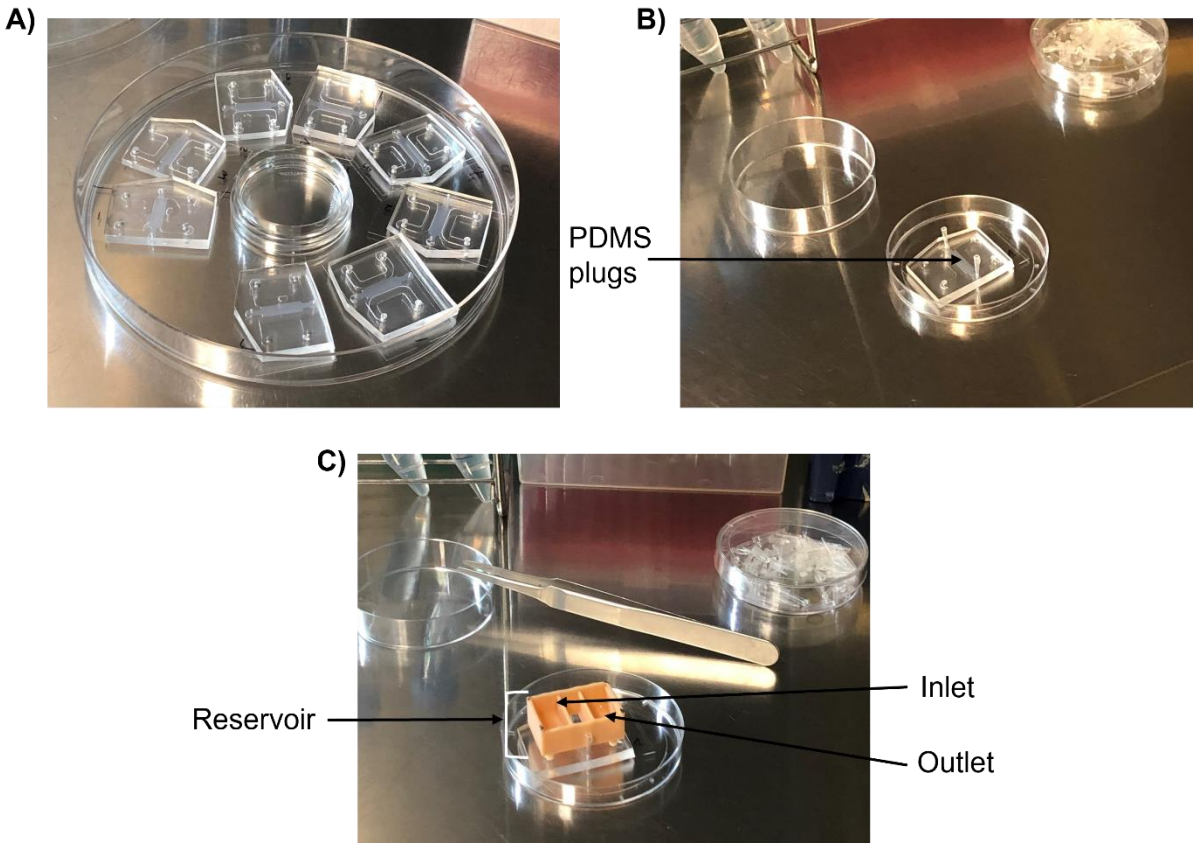

Figure 2.12 - PDMS device used for the placental microvasculature triculture model and the addition of reservoirs. A) Devices prior to the addition of reservoirs. B) PDMS plugs added to the central channel ports to prevent leaking. C) Addition of reservoirs containing an inlet and outlet to the side channel ports.

Table 2.4 - Shear stress calculations for microfluidic devices used. The dynamic viscosity of water was used as an assumption. The Shear stress was calculated using a derivative of the Navier-Stokes equation.

Device	Flow rate (Q, μL/min)	Dynamic viscosity (η, dyne.s/cm²)	Chamber height (μm)	Chamber width (μm)	Chamber length (μm)	Shear stress (Pa)	Shear stress (dyne/cm²)
Rhomboidal	1 (10^9 μm^3/ 60s)	(Water) 0.01 (0.001 Pa*s)	150	4750	13740	$5.6*10^{-2}$	0.56
Parallel channels	0.0625	0.01	100	400	20000	$9.4*10^{-2}$	0.94
Ibidi channel (μ-Slide VI 0.4)	1	0.01	400	3800	17000	$9.9*10^{-3}$	0.099

2.3.5 Differentiation of pMSCs into endothelial cells

2.3.5.1 Static Differentiation

pMSCs (passage 3, n=7 and n=4 from uncomplicated and GDM placentae, respectively) were seeded into flasks at a density of 1,000 cells/cm^2 in pMSC medium. After 24 hours medium was refreshed to either pMSC medium (controls) or EGM-2 with an additional 50 ng/mL recombinant Human VEGF-165 (VEGF-A; 583704, BioLegend) (Differentiation Medium; Table 2.5). Medium was refreshed thereafter every 3-4 days. Cells were passaged at day 7, 14 and 21 and used for flow cytometry, or seeded onto coverslips and 6-well plates at a density of 4,000 cells/cm^2 and cultured for a further 4 days. Cells were either fixed with 4% paraformaldehyde (PFA) (See Section 2.3.7.2) or processed for RNA extraction (See Section 2.6.1.2) after 11, 18 and 25 days culture in differentiation or control medium. For functional assays, at 21 days cells were also seeded onto an extracellular matrix for the tube formation assay (Section 2.3.8.1) or coated onto beads for the bead assay (Section 2.3.8.2).

2.3.5.2 Differentiation under low flow/shear stress

pMSCs (n=5) were seeded into Ibidi µ-Slide VI 0.4 devices at a concentration of 250,000 cells/mL (IbiTreat; IB-80606, Ibidi, Thistle Scientific, UK) in normal pMSC medium. The cells were left to attach for 24 hours, and the medium was then refreshed to either pMSC medium (controls) or differentiation medium (Table 2.5, EGM-2 with 50 ng/mL VEGF-A). The device was then connected to a 6-channel syringe pump (as described in Section 2.3.4.2). Three syringes contained control medium, and three syringes contained EGM-2 (Figure 2.13). The flow was initiated at a rate of 1 µL/min for 72 hours. As flow is known to initiate differentiation alone[366], cells were also seeded into a second device and cultured under static conditions for the total time of the experiment.

2.3.6 Cell morphology imaging

Morphological images of cells cultured in plates, flasks and microfluidic devices were taken with phase contrast either using the Olympus fluorescence microscope, using the Cell F software (Olympus, Japan) or the Incucyte ZOOM (software v.2016; Essen Bioscience, USA).

2.3.7 Fixing and characterisation of cells by immuno- and cyto-chemical staining

2.3.7.1 Seeding cells onto coverslips

Round 13 mm diameter, size 1, coverslips (631-1578, VWR) were dipped in methanol and dried in the tissue culture hood before placing in 24-well plates. Once cells were passaged, they were seeded onto the coverslips in a total 1 mL of medium. pMSCs and HUVECs were seeded at a density of 4,000 cells/cm^2 and 6,000 cells/cm^2, respectively. To promote adhesion of HUVECs to the coverslips, the coverslips were coated with 10 µg/mL fibronectin (F0895-2MG, Merck) for 45 minutes at room temperature. The coverslips were then washed with PBS three times before seeding the cells.

2.3.7.2 Fixing cells with paraformaldehyde

A solution of 4% PFA was made up in sterile PBS by dissolving the powder on a heated stirrer at 50°C. Cells grown on coverslips were washed with 1 mL sterile PBS. PBS was then removed and 1 mL of 4% PFA was added to each coverslip. This was placed on ice for 20 minutes. PFA was then removed, and coverslips were washed with 1 mL PBS three times. Coverslips were stored in 2 mL PBS at 4°C until immunocytochemistry was performed.

2.3.7.3 Immunocytochemistry

Coverslips were placed onto microscope slides (cells facing upwards) and circled with a PAP pen (H-4000, 2B Scientific, UK). For intracellular markers, coverslips were incubated with PBS containing 0.1% Triton-X100 (X100-500ML, Sigma-Aldrich, USA) for 30 minutes. Coverslips were then washed 3 times with PBS and blocked with 5% bovine serum albumin (BSA; Sigma-Aldrich, USA) for 1 hour. Primary antibodies (Table 2.6) were then diluted in 5% BSA and applied to the coverslips overnight at 4°C or for 1 hour at room temperature. IgG controls, at the same concentration as the primary antibody were used as controls. Some coverslips were incubated with PBS, to determine if any positive staining has occurred from non-specific binding of the secondary antibody. The primary antibodies were washed off 3 times with PBS. Appropriate secondary antibodies (Table 2.7) were diluted in 5% BSA and applied to the coverslips for 1 hour at room temperature. The secondary antibodies were washed off 3 times with PBS and coverslips were mounted onto fresh microscope slides using Fluoromount-G with 4′,6-diamidino-2-phenylindole (DAPI) (0100-20, Southern Biotech, USA). Coverslips were sealed with clear nail varnish. Slides were stored in the dark at 4°C.

Table 2.5 – Final concentrations of supplements in differentiation medium. Endothelial differentiation medium 2 (EGM-2) with 50 ng/mL additional VEGF-A.

Media Supplement	Final Supplement Concentration
Fetal Calf Serum (FCS)	0.02 mL/mL
Ascorbic Acid	1 µg/mL
Hydrocortisone	0.2 µg/mL
Long R3 Insulin-like Growth Factor 1 (IGF-1)	20 ng/mL
Heparin	22.5 µg/mL
Epidermal Growth Factor (EGF; recombinant human)	5 ng/mL
Basic Fibroblast Growth Factor (FGF; recombinant human)	10 ng/mL
VEGF-A (recombinant human)	50.5 ng/mL

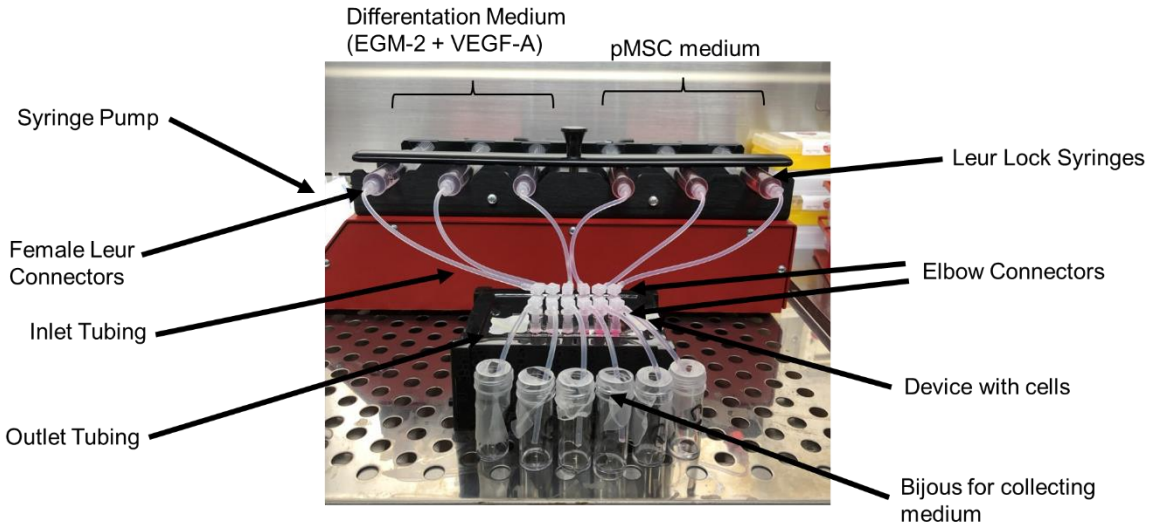

Figure 2.13 - Ibidi device experimental set up for pMSC differentiation experiments. Devices were connected to the syringe pump using female Luer connectors, inlet silicon tubing and elbow connectors. Three syringes were filled with differentiation medium (EGM-2 + VEGF-A) or control pMSC medium. Elbow connectors were placed in the outlet and connected to silicone tubing in bijou tubes to collect spent media for assays.

.

Table 2.6 – Primary antibodies used for immunocytochemistry and/or immunohistochemistry. The primary antibodies used throughout the study are shown, including their host species, dilution's, final concentrations, manufacturers and product codes.

Protein	Labels	Host Species	Stock Concentration	Dilution	Final Concentration	Manufacturer	Product Code
CCR7	M1 Marker	Rabbit	300 µg/mL	1:100	3 µg/mL	Protein Tech	25898-1-AP
CD105	MSC/Endothelial	Rabbit	550 µg/mL	1:100	5.5 µg/mL	Protein Tech	10862-1-AP
CD14	Macrophage Marker	Mouse	1000 µg/mL	1:500	2 µg/mL	Merk	Part of SCR067
CD163	M2 Marker	Rabbit	771 µg/mL	1:200	3.855 µg/mL	Abcam	ab182422
CD19	Lymphocytes	Mouse	1000 µg/mL	1:500	2 µg/mL	Merk	Part of SCR067
CD206	M2 Marker	Mouse	1000 µg/mL	1:10,000	0.1 µg/mL	Protein Tech	60143-1-Ig
CD31	Endothelial Cells	Mouse	201 µg/mL	1:100	2.01 µg/mL	Dako	M0823
CD34	Endothelial/Hematopoietic	Rabbit	550 µg/mL	1:250	2.2 µg/mL	Protein Tech	14486-1-AP
CD44	MSC	Mouse	1000 µg/mL	1:500	2 µg/mL	Merk	Part of SCR067
CD73	MSC	Mouse	1000 µg/mL	1:250	4 µg/mL	Protein Tech	67789-1-Ig
Cytokeratin 7	Syncytiotrophoblast	Mouse	96 µg/mL	1:500	0.192 µg/mL	Dako	M7018
F-Actin 488 (Phalloidin Ready Probe)	Fillamentous Actin	N/A	N/A	N/A	2 drops / mL	ThermoFisher	A12379
FLT1	VEGFR Endothelial	Rabbit	1000 µg/mL	1:500	2 µg/mL	Bio Techne	NB100-527
IL1β	Interleukin/Chemokine	Rabbit	700 µg/mL	1:250	2.8 µg/mL	Protein Tech	16806-1-AP
IL6	Interleukin/Chemokine	Rabbit	500 µg/mL	1:500	1 µg/mL	Protein Tech	21865-1-AP
KDR	VEGFR Endothelial	Mouse	500 µg/mL	1:25	20 µg/mL	Bio Techne	MAB3571
Ki67	Proliferation	Mouse	46 µg/mL	1:100	0.46 µg/mL	Dako	M7240
M30	Apoptosis	Mouse	6.6 µg/mL	1:100	0.066 µg/mL	Roche	12140322001
vWF	Endothelial	Mouse	140 µg/mL	1:200	0.7 µg/mL	Agilient	M061601-2
Mouse IgG	IgG	Mouse	2000 µg/mL	Various	Various	Vector Labs	I-2000-1
Rabbit IgG	IgG	Rabbit	5000 µg/mL	Various	Various	Vector Labs	I-1000-5

Table 2.7 - Secondary antibodies used for immunocytochemistry and/or immunohistochemistry. The secondary antibodies used throughout the study are shown, including their host species, dilution's, final concentrations, manufacturers and product codes.

Protein	Host Species	Stock Concentration	Dilution	Final Concentration	Manufacturer	Product Code
Anti-Mouse Biotin	Goat	1000 µg/mL	1:200	5 µg/mL	AAT BioQuest	16729
Anti-Rabbit Biotin	Swine	500 µg/mL	1:200	2.5 µg/mL	Dako	E0353
Anti-Mouse 488	Goat	2000 µg/mL	1:2000	1 µg/mL	Invitrogen	A11001
Anti-Rabbit 488	Goat	2000 µg/mL	1:2000	1 µg/mL	Invitrogen	A11008
Anti-Mouse 568	Goat	2000 µg/mL	1:1500	1.3 µg/mL	Invitrogen	A11031
Anti-Rabbit 568	Goat	2000 µg/mL	1:1500	1.3 µg/mL	Invitrogen	A11011

2.3.7.4 Microscopy

Coverslips were imaged using the Axio Scope.A1 Fluorescent Microscope, and the following fluorophores were used: DAPI (Excitation: 353 nm, Emission: 465 nm), Alexa 488 (Excitation: 493 nm, Emission: 517 nm) and Alexa 568 (Excitation: 577, Emission: 603 nm). For imaging of whole coverslips, the Axioscan Z1 Slide Scanner (Zeiss, Germany) was used in the Bioimaging Core Facility (Faculty of Biological Sciences, University of Leeds). For the slide scanner the following fluorophores were used: DAPI (Excitation: 353 nm, Emission: 465 nm), Alexa 488 (Excitation: 488 nm, Emission: 509 nm) and Alexa 568 (Excitation: 545, Emission: 572 nm). Zen Blue software was used with both microscopes (Zeiss, Germany).

2.3.7.5 Image analysis using Qupath

Immunocytochemistry images were analysed using QuPath (v0.3.2). In coverslips, four regions of interest (ROI) were selected from each coverslip. In Ibidi devices, five images were taken, with an image at the top, bottom, middle, inlet, and outlet of the device. A pixel classifier threshold was set to detect the cells in the ROI. The fluorescence intensity was then determined using the intensity features tool. The intensity was calculated per pixel, to account for differing numbers and sizes of cells in each ROI/image.

2.3.7.6 Flow Cytometry

pMSCs undergoing endothelial lineage differentiation were characterised by flow cytometry (n=3). pMSCs were cultured in T75 flasks in either control or differentiation medium. Once cells had reached 90-100% confluency they were passaged and centrifuged at 350 RCF for 5 minutes to pellet the cells. The pellet was resuspended in 1 mL staining buffer (R&D systems, USA). Cells were then counted by taking a 1:5 dilution of cells in trypan blue and cells labelled with trypan blue were excluded from counts. A 1.5 mL Eppendorf was prepared for each combination of antibodies (Table 2.8) containing 200,000 cells in 80 µL of staining buffer. Following this, 20 µL of Fc receptor (FcR) blocking reagent (Miltenyi Biotech, Germany) was added to each tube and incubated for 10 minutes at 4°C. The primary antibodies were then added to the tubes. FLT1-PE (FAB321P, R&D Biosystems, USA) and KDR-APC (FAB357A-025, R&D Biosystems) were used at a 1:10 dilution (10 µL in 100 µL of cell suspension) and incubated for 30 minutes at 4°C. CD31-FITC (130-110-806, Miltenyi Biotech, Germany) was at a 1:50 dilution (2 µL in 100 µL of cell suspension), and was added after 20 minutes, and incubated at 4°C for the final 10 minutes. Appropriate IgG controls for

each antibody were also used. Cells were then centrifuged at 350 RCF and the pellet was resuspended in 1 mL of staining buffer, to wash the cells. Cells were centrifuged for a further 5 minutes at 350 RCF and the pellet was resuspended in 200 µL of staining buffer. Flow cytometry was performed using the Cytoflex S Flow Cytometer (Beckman, USA). HUVECs (n=3) were used as a positive control. The following fluorophores were used: FITC (Laser: 488 nm, Emission Filter: 525/30), APC (Laser: 561 nm, Emission Filter: 660/20) and PE (Laser: 640 nm, Emission Filter: 585/42).

To characterise GDM pMSCs (n=4) using MSC markers, the above protocol was performed using antibodies from the Human MSC Verification Multi-Colour Flow Cytometry Kit (FMC020, R&D systems, USA). Appropriate IgG controls for each antibody were also included. A 1:10 dilution of each antibody was used (10 µL in 100 µL of cell suspension) and incubated at 4°C for 30 minutes. Additionally, CD31-FITC (130-110-806, Miltenyi Biotech, Germany) was used (as above) as an additional negative marker. The Eppendorf tubes prepared for each combination of antibodies is outlined in Table 2.9. The following fluorophores were used: CFS/FITC (Laser: 488 nm, Emission Filter: 525/30), PerCP (Laser: 488 nm, Emission Filter: 690/50), APC (Laser: 561 nm, Emission Filter: 660/20) and PE (Laser: 640 nm, Emission Filter: 585/42).

Prior to quantification, the antibodies were also added separately to individual tubes of cells to generate a compensation matrix on the CytExpert Software (Beckman, USA). This process corrects spectral overlap when multiple fluorophore emissions are recorded for each cell[367]. This compensation matrix was applied to all further experiments. The cellular debris was gated by plotting the forward scatter area (FSC-A) and the side scatter area (SSC-A) (Figure 2.14A). The FSC indicates the relative size of the cell, and the SSC indicates the complexity or granularity of the cell[368]. Dead and fragmented cells, which have a low FSC and SSC were excluded (Figure 2.14A). From this population generated, the single cells were gated by plotting the FSC-height (FSC-H) and FSC-A and gating the cells with a similar FSC-H and -A. This is because cell doublets have increased FSC-A at the same FSC-H[369] (Figure 2.14B). The unstained cells (no staining control) were first gated by plotting the FSC-A against fluorescent intensity for each fluorophore (Figure 2.14C). These gates were then applied to the stained samples to determine the percentage of cells positive for each marker (Figure 2.14D).

Table 2.8 - Antibodies used for flow cytometry characterisation of pMSCs treated in control and differentiation medium. Details of each antibody and their catalogue numbers are shown.

Tube No.	Name	Antibodies	Cat No.
1	No staining control	None	
2	Endothelial Markers	○ CD31-FITC Recombinant Human IgG_1 Clone REA730	130-110-806
		○ KDR-APC Monoclonal Mouse IgG_1 Clone # 89106	FAB357A-025
		○ FLT1-PE Monoclonal Mouse IgG_1 Clone # 49560	FAB321P
3	IgG controls	○ REA Control Antibody (S), Human IgG_1, FITC, REAfinity™	130-113-437
		○ Mouse IgG1 APC-conjugated Antibody	IC002A
		○ Mouse IgG1 PE-conjugated Antibody	IC002P

Table 2.9 - Antibodies used for flow cytometry characterisation of GDM pMSCs. Details of each antibody and their catalog numbers are shown. Details of each antibody and their catalogue numbers are shown.

Tube No.	Name	Antibodies	Cat No.
1	No staining control	None	
2	Positive and negative markers	Positive markers: ○ CD90-APC Mouse IgG_{2A}; Clone Thy-1A1 ○ CD73-CFS Mouse IgG_{2B}; Clone 606112 ○ CD105-PerCP Mouse IgG_1; Clone 166707 Negative marker cocktail containing: ○ CD45-PE Mouse IgG_1; Clone 2D1 ○ CD34-PE Mouse IgG_1; Clone QBEnd10 ○ CD11b-PE Mouse IgG_{2B}; Clone 238446 ○ CD79A-PE Mouse IgG_1; Clone 706931 ○ HLA-DR-PE Mouse IgG_1; Clone L203	FMC020
3	IgG controls for positive markers	○ Mouse IgG_{2A}-APC Isotype Control; Clone 20102 ○ Mouse IgG_{2B}-CFS Isotype Control; Clone 133303 ○ Mouse IgG_1-PerCP Isotype Control; Clone 11711	FMC020
4	IgG controls for negative markers	Negative isotype cocktail containing: ○ Mouse IgG_1-PE Isotype Control; Clone 11711 ○ Mouse IgG_{2B}-PE Isotype Control; Clone 133303	FMC020
5	CD31-FITC	○ CD31-FITC Human Recombinant IgG_1; Clone REA730	130-110-806
6	IgG control for CD31	○ Human Recombinant IgG1-FITC, REAfinity™; Clone REA293	130-113-437

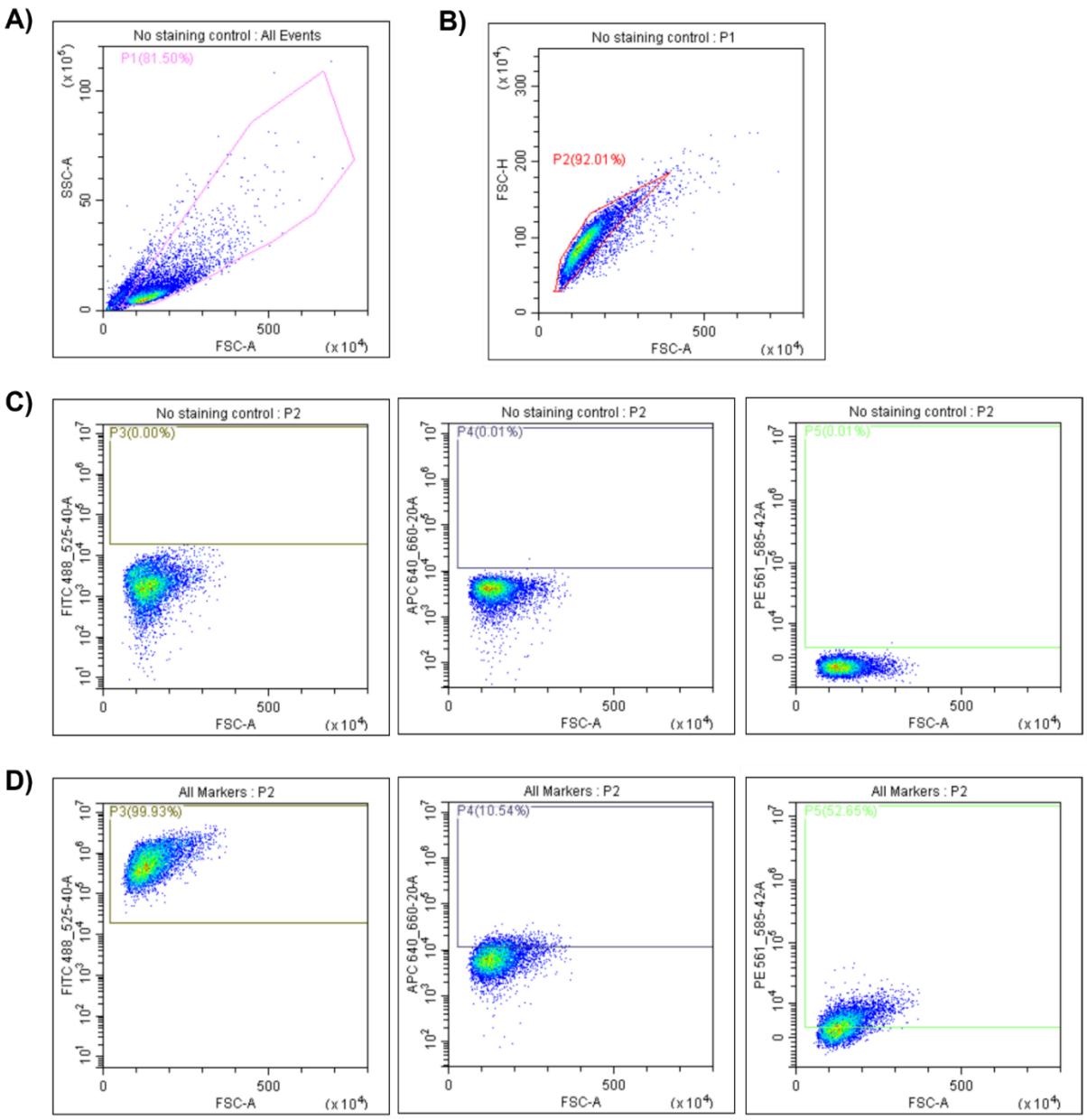

Figure 2.14 - Gating strategy for flow cytometry. Example of the gating strategy for detection of endothelial cell markers in pMSCs and HUVECs. The positive control of HUVECs was used here to demonstrate positive staining. A) Cell debris is removed based on the intensity of the forward scatter (FSC) and side scatter (SSC) of light. B) Identification of single cells based on a FSC area at a similar height (FSC-A and -H). C) Unstained cell control to gate for positively stained cells for each fluorescence channel used. D) Example of gating a stained sample detected in each fluorescence channel.

2.3.8 Functional cell assays

2.3.8.1 Endothelial tube formation assay

Endothelial tube formation was assessed in pMSCs undergoing endothelial lineage differentiation using an angiogenesis assay kit (ab204726, Abcam, UK). The ECM was thawed on ice at 4°C overnight, to prevent it from solidifying. Pipette tips, and a 96-well plate was also pre-chilled. Once thawed, 50 µL of ECM was added to each well of the 96-well plate on ice, with care not to cause bubbles. The plate was then placed at 37°C to allow the ECM to form a gel. Cells were loaded onto the ECM at a concentration of 10,000 cells per well, in 50 µL of medium. Each condition was performed in duplicate (except for cells cultured in devices, as the small number of cells only allowed one replicate). As a negative control, 50 µM of suramin was also used, as this is anti-angiogenic, and wells without ECM, and therefore no endothelial tubes should be formed. To ensure that tubes were not forming solely due to the presence of VEGF-A in the endothelial differentiation medium during the assay, the same concentration of VEGF-A (50.5 ng/mL) was added to extra wells containing cells grown in the control medium. The plate was then placed at 37°C for 2 hours. Phase contrast images were then taken using the Incucyte ZOOM (software v.2016; Essen Bioscience, USA) in 4 regions of each well, at 10x magnification. This assay was also performed on HUVECs (n=3), as a positive control for static differentiation experiments. While the use of the angiogenesis analyser plugin on ImageJ was attempted to determine the number of endothelial tubes, branch points and branching length, false positives meant that manual counting was performed. An endothelial tube was only counted if all the boundaries were observed in the image. An example of manually counted tubes can be seen in Figure 2.15. The average number of endothelial tubes for each condition was taken.

2.3.8.2 Endothelial sprouting bead assay

Angiogenic sprouting was assessed in pMSCs undergoing endothelial lineage differentiation using the fibrin bead assay (n=3). This assay involves the coating of endothelial cells to Cytodex microcarriers, and embedding into a fibrin gel containing necessary growth factors that lead to endothelial sprouting[370,371]. Firstly, 21 µL of Cytodex-3 Beads (C3275, Sigma-Aldrich, UK) and 50 µL of sterile PBS were placed in a 1.5 mL Eppendorf. The beads were left to settle for 5 minutes, and the PBS removed. Beads were then resuspended in the appropriate medium (control medium or differentiation medium) and allowed to settle again for 5 minutes. A cell suspension of 500,000 cells/mL was added to the beads and then transferred to a FACs tube

(352058, Corning, USA). A further 500 µL of medium was used to wash remaining beads from the Eppendorf and added to the FACs tube. FACs tubes containing the cell/bead mixture was then placed at 37°C for 4 hours, with agitation (manual flicking of tubes) every 30 minutes, to prevent the beads from clumping together. The cell/bead mixture was then transferred into a T25 and made up to a total of 5 mLs with medium and incubated at 37°C overnight. The following day, a 2 mg/mL solution of fibrinogen (F-8630, Sigma-Aldrich, UK) was prepared. To prevent the fibrinogen clotting, this was prepared by pouring 7 mL of warm sterile PBS onto 14 mg of fibrinogen and incubating at 37°C for 30 minutes. Following this, the fibrinogen was filter sterilised using a 20 mL syringe (300629, BD, USA) and a 200 µm filter (SLGP033R, Sigma-Aldrich, UK). The flasks were observed to ensure that cells were attached to the beads and were gently tapped to dislodge the beads from the flask. The cell/bead mixture was then transferred to a falcon tube, and an extra 4 mL of medium was added to the flask to wash any remaining cells/beads from the flask. The falcon tube of cells/beads was left for 15 minutes to allow the coated beads to pellet. During this time, a fibrinogen master mix was prepared (Table 2.10)

The medium was then removed from the settled cells/beads and were washed 3x for 5 minutes with fresh medium. After the final wash, the cells/beads were resuspended in the fibrinogen master mix. In a 24-well plate 12.5 µL of thrombin (T-3399, Sigma-Aldrich, UK) was reverse pipetted into the centre of each well. Following this, 500 µL of the cells/beads was mixed into the thrombin by pipetting up and down in circular motions. This forms a clot with the thrombin and fibrinogen; therefore, this was done within 5 seconds before the clot hardens. Care was taken not to introduce bubbles or scratches. For each condition, 4 wells were used. The plate was left undisturbed for 5 minutes, before being transferred to 37°C for 15 minutes to allow the clot to harden. Before leaving overnight at 37°C, 1 mL of medium was added dropwise to the clot, to prevent dislodging. After 24 hours, phase contrast images were then taken using the Incucyte ZOOM (software v.2016; Essen Bioscience, USA) of the whole well at 4x and 10x magnification. This assay was also performed on HUVECs (n=3), as a positive control.

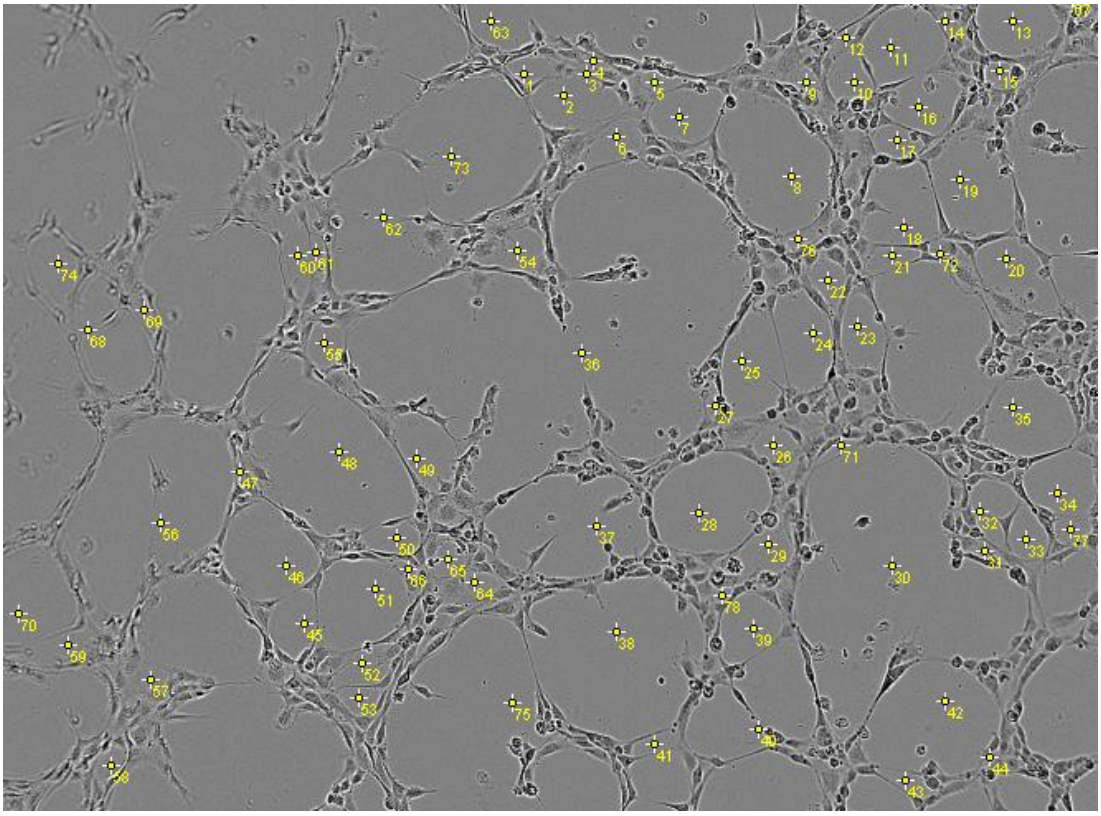

Figure 2.15 - Example of endothelial tubes counted using ImageJ in pMSCs and HUVECs. The positive control of HUVECs was used here to demonstrate the formation of endothelial tubes.

Table 2.10 - Components in the fibrinogen master mix for the endothelial sprouting bead assay.

Master Mix Component	Stock Concentration	Volume	Final Concentration	Cat No.
Fibrinogen	N/A	2.5 mL	2 mg/mL	F-8630
Aprotinin	4 U/mL	93.75 µL	0.15U/mL	A-1153
VEGF	5 µg/mL	2.5 µL	5 ng/mL	C-64423
FGF	5 µg/mL	2.5 µL	5 ng/mL	450-33

2.4 Glucose treatments in placental models

2.4.1 Glucose treatments in placental explants

2.4.1.1 Acute glucose fluctuations for 48 hours

DMEM-F12 was supplemented with 9 µL/mL, 9.6 µL/mL or 12.6 µL/mL sterile filtered D-glucose (555 mM, G8644, Sigma-Aldrich, UK) to generate concentrations of 5-, 5.5- and 7-mM glucose, respectively. Following overnight culture in 5.5 mM glucose, medium was replenished with the different glucose treatments. Glucose treatments were either fluctuating 5 and 5.5 mM glucose every 18 and 6 hours, respectively (replenished to 5.5 mM at 0 and 24 hours and 5 mM at 18 and 42 hours) or constant 5, 5.5 or 7 mM glucose, replenished at 0, 18, 24 and 42 hours. Explants were cultured for a total of 48 hours in glucose treatments (Figure 2.16A).

2.4.1.2 Longer-term glucose fluctuations for 96 hours following syncytial degeneration and regeneration

DMEM-F12 was prepared supplemented with glucose (Section 2.4.1.1). Explants were cultured in 5.5 mM glucose for 4 days, with daily medium refreshments to allow for the syncytium to degenerate and regenerate. Following this, medium was replenished with the different glucose treatments. Glucose treatments were either constant 7 mM glucose, replenished at 0, 18, 24, 42, 48, 66, 72 and 90 hours, or fluctuating 5 and 5.5 mM glucose every 18 and 6 hours, respectively (replenished to 5.5 mM at 0, 24, 48 and 72 hours and 5 mM at 18, 42, 66 and 90 hours) (Figure 2.16A).

2.4.1.3 Collection of medium and samples

Conditioned medium was collected during each medium refreshment and stored at -80°C. Following treatments, explants for protein and RNA were snap frozen in liquid nitrogen and stored in the -80°C. Where possible, samples for RNA were stored in RNALater for approximately 24 hours at 4°C before being snap frozen in liquid nitrogen and stored in the -80°C. Explants for histology were stored in 10% NBF at 4°C. After around 24 hours formalin was removed and replaced with 70% ethanol and stored at 4°C until tissue was processed.

2.4.2 Glucose treatments in the static pMSC differentiation model

EGM-2 (5.6 mM glucose) was supplemented with 2.52 µL/mL or 6.13 µL/mL sterile filtered D-glucose (555 mM, G8644, Sigma-Aldrich, UK) to generate concentrations of 7 and 9 mM glucose, respectively. For the hyperosmolar control, a 500 mM solution of

D-mannitol (M4125, Sigma-Aldrich, UK) was prepared in ultrapure water (91.1 mg/mL) and sterile filtered, and the EGM-2 was supplemented with 6.8 µL/mL of the 500 mM D-mannitol to generate a 3.4 mM mannitol control.

pMSCs (passage 3, n=6) were seeded into flasks at a density of 1,000 cells/cm^2 in pMSC medium. After 24 hours medium was refreshed to either control medium (5.5 mM glucose) or differentiation medium with 5.6, 7, 9 mM glucose or 5.6 mM glucose with 3.4 mM D-mannitol (hyperosmolar control). After 7 days in culture, cells were passaged and were seeded into 6-well plates at a density of 4,000 cells/cm^2 and cultured in different glucose conditions for a further 4 days. Medium was refreshed daily throughout entire culture to maintain glucose levels. Conditioned medium was collected during each medium refreshment and stored at -80°C. RNA was extracted after 11 days in differentiation or control medium. For functional assays, at 7 days cells were also seeded onto an ECM for the tube formation assay (Section 2.3.8.1). Conditioned medium was collected during each medium refreshment and stored at -80°C.

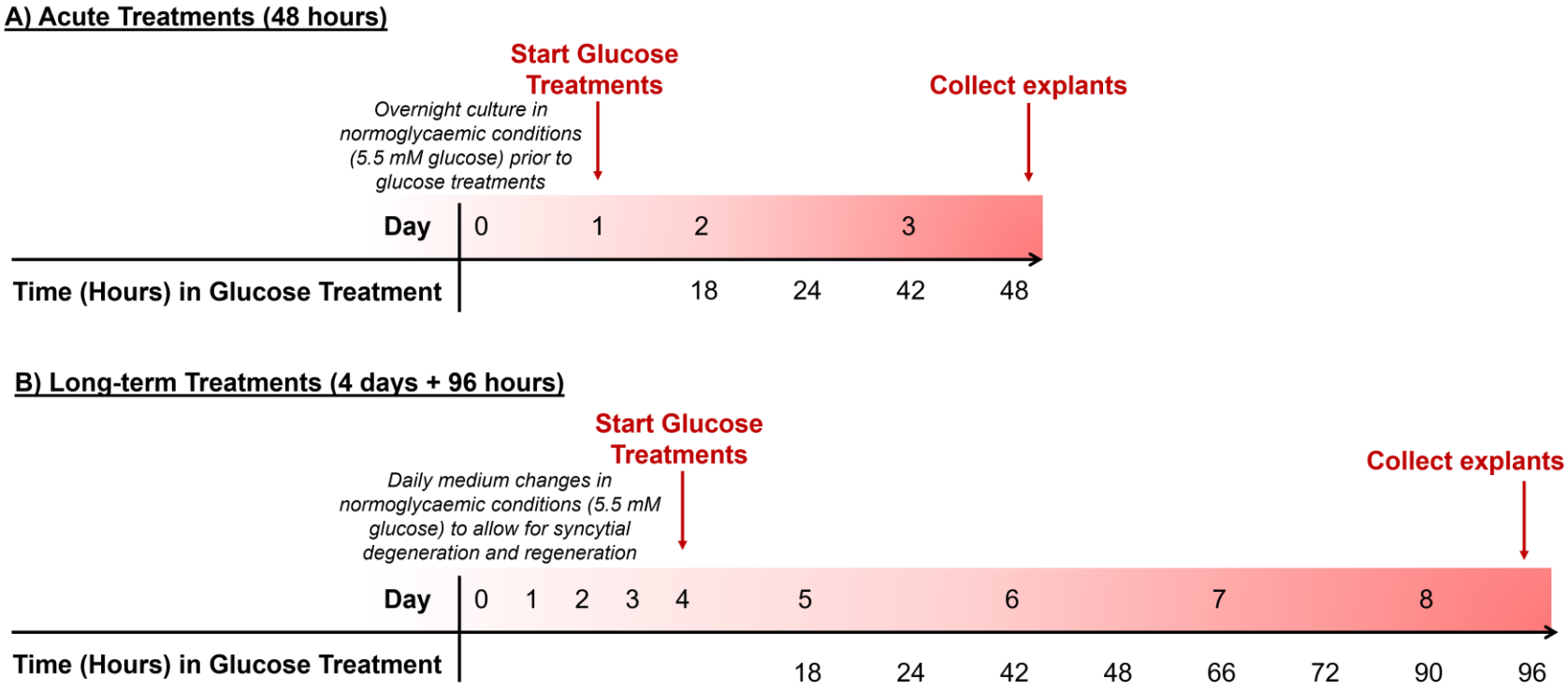

Figure 2.16 - Acute and longer-term glucose treatments in placental explants. A) For acute treatments, explants were cultured overnight in 5.5 mM glucose and medium was replenished with either fluctuating 5 and 5.5 mM glucose every 18 and 6 hours, respectively (replenished to 5.5 mM at 0 and 24 hours and 5 mM at 18 and 42 hours) or constant 5, 5.5 or 7 mM glucose, replenished at 0, 18, 24 and 42 hours. After 48 hours of glucose treatments explants were collected. B) For longer-term treatments, explants were cultured in 5.5 mM glucose for 4 days, with daily medium refreshments to allow for the syncytium to degenerate and regenerate. Following this, medium was replenished with either constant 7 mM glucose, replenished at 0, 18, 24, 42, 48, 66, 72 and 90 hours, or fluctuating 5 and 5.5 mM glucose every 18 and 6 hours, respectively (replenished to 5.5 mM at 0, 24, 48 and 72 hours and 5 mM at 18, 42, 66 and 90 hours). After 96 hours of glucose treatments, explants were collected.

2.4.3 Glucose treatments in the placental microvasculature triculture model

Firstly, 500 mM solutions of D-glucose (G8270, Sigma-Aldrich, UK) and D-mannitol (M4125, Sigma-Aldrich, UK) were prepared in ultrapure water (90.1 and 91.1 mg/mL) and sterile filtered. VascuLife (5.6 mM glucose) was supplemented with 2.8 µL/mL, 6.8 µL/mL or 38.8 µL/mL 500 mM D-glucose to generate concentrations of 7, 9 and 25 mM glucose, respectively. For the hyperosmolar control, VascuLife was supplemented with 38.8 µL/mL 500 mM D-mannitol to generate a 19.4 mM mannitol control.

Following cell seeding in the triculture device, 75 µL of VascuLife, containing either 5.6, 7, 9, 25 mM D-glucose or 5.6 mM glucose + 19.4 mM D-mannitol was added to each side channel. The following day medium was collected from the side channels and refreshed. On the following day, reservoirs were added to initiate flow and 840 µL of medium with the appropriate glucose/mannitol concentration was added to the inlet reservoir. Medium was refreshed daily by removing medium from the outlet reservoir and adding 840 µL of medium with the appropriate glucose/mannitol concentration to the inlet reservoir.

2.4.3.1.1 Medium collection, imaging, and measurements

Medium was collected on days 1-7, with glucose and osmolality measurements performed on days 1, 4 and 7. Z-stack images of the RFP (HUVEC) channel were acquired daily on days 2-7 using a Leica confocal microscope (DMi8, Leica, Germany) with LAS X Navigator Software (Leica). Images were taken from three regions of the central channel, which consisted of a 5 µm step size and ~20–25 slices (beyond which intensity diminishes). For microvessel morphology quantification, acquired confocal images were analysed using ImageJ. Morphological parameters included area (%), diameter of vessels (µm) and branch length (µm). A maximum projection of each Z-stack image (RFP HUVEC channel) was generated and a macro, which generates a binarized image and creates a ‘skeleton’ of the vessels to determine vessel branch parameters, was used, as provided by and described in Cherubini and Haase (2023)[363], this analysis was conducted by Dr Marta Cherubini in the collaborating lab.

On the seventh day devices were used to assess permeability or to extract cells for RNA isolation. For all of these, the reservoir was removed from each device and medium was then removed from the side channels. Washes were performed with PBS by adding 150 µL into the inlet side channel and waiting for it to move across the inner compartment (containing the vessels) and into the outlet side channel.

2.4.3.1.2 FITC-Dextran permeability assay

All PBS was removed from the side channels and 40 µL of FITC-Dextran 70 kDa (100 µg/mL, 46945-100MG-F, Merck) in Vasculife (LL-0003, LifeLine Cell Technologies, USA) was added to the inlet side channel, and after 5-10 seconds, once the FITC-Dextran has moved across the inner compartment (containing the vessels), another 40 µL of FITC-Dextran was added to the outlet side channel. Z-stack images were taken as described above (Section 2.4.3.1.1) at 0, 3 and 6 minutes following perfusion with FITC-Dextran. A maximum projection of each Z-stack image (FITC-Dextran channel) at the first time point (time t = 0 minutes) was used to generate a binary outline of the vessel perimeter (P_V) and extravascular tissue area (A_T) in ImageJ. Assuming that the intensity (I) is linearly related to the fluorophore concentration, flux across the imaging boundary is negligible, and transendothelial flux is constant, the permeability (P in cm/s) of the microvessels to solutes can be approximated, using the equation previously described[348,372] (Equation 2.3).

$$P = \left(\frac{A_T}{P_v}\left(I_{fT} - I_{0T}\right)\right)/t \times \left(I_{0v} - I_{0T}\right)$$

Equation 2.3 – Equation used to calculate permeability of microvessels using a FITC-dextran permeability assay. A_T is the extravascular tissue area, P_v is the perimeter of the vessels, I_{fT} is the intensity at the final time point in the extravascular space, I_{0T} is the intensity at the first time point (0 minutes) in the extravascular space, t is the time interval and I_{0V} is the intensity at the first time point (0 minutes) inside the vessels.

2.4.4 Assessment of glucose and osmolality in conditioned medium

2.4.4.1 Assessing the accuracy of the GlucCell glucose monitoring system

To confirm the accuracy of the GlucCell® Glucose Monitoring System, a serial dilution of D-Glucose (G8644, Sigma-Aldrich, UK) was performed in DMEM-F12 medium (L0091-500, Biowest, France). This generated concentrations of 20, 10, 5 and 2.5 mM, which were measured using the monitor, in triplicate. Observed glucose concentrations were similar to the expected concentrations. As the manufacturer's instructions suggest measuring samples at 37°C, glucose standards were tested at both room temperature

and 37°C. Both yielded similar results, with 37°C being the most in line with expected values (Figure 2.17).

2.4.4.2 Glucose concentrations in conditioned medium

To assess glucose concentrations in the conditioned medium of cells and placental explants, the GlucCell® Glucose Monitoring System (CLS-1322-02, GPE Scientific, UK) was used. Medium samples were warmed to 37°C and 3 µL were loaded onto a GlucCell® test strip (CLS-1324-01, GPE Scientific) in triplicate.

2.4.4.3 Osmolality in conditioned medium

To assess osmolality in the conditioned medium of cells and placental explants, a Single-Sample Micro Osmometer (Model 3320, Advanced Instruments, USA) was used. Samples were warmed to room temperature and 20 µL was loaded into the osmometer. Osmolality was recorded in mOsm/kg.

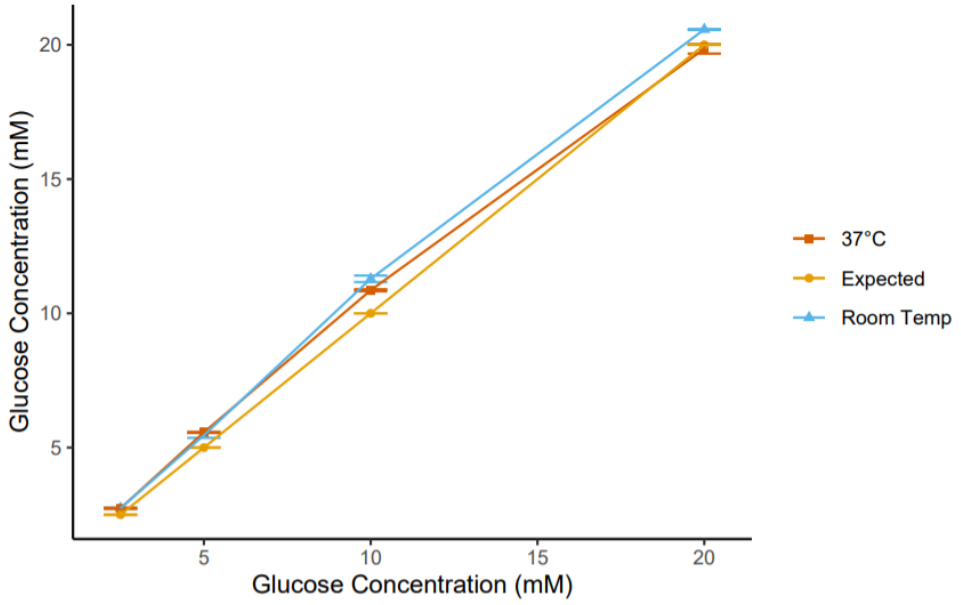

Figure 2.17 - Accuracy of the GlucCell Glucose Monitoring System. Known concentrations of D-glucose (2.5-20 mM) were added to DMEM-F12 medium and assayed using the GlucCell glucose monitoring system. Data is presented as the mean±SEM (n=3).

2.5 Histology

2.5.1 Tissue processing, embedding and sectioning

Following tissue fixation in NBF, term placental tissue and placental explants were placed in histological cassettes (EBG-0304-12A, CellPath, ProMarc and 720-1627, VWR, USA for term tissue and explants, respectively) and then into a beaker containing 70% ethanol. Cassettes were then placed into the tissue processor (TP1020, Leica) and dehydrated and embedded on a specific program. For term placental tissue the program ran for 19 hours and 12 minutes and for explants the program ran for 14 hours and 27 minutes (**Appendix 4**). Cassettes were then placed into hot paraffin wax and explants were removed from one cassette at a time and placed in hot paraffin wax in a mould (HIS0225 and HIS0221, SLS, USA for term tissue and explants, respectively). The cassette lid was then placed on top. The wax was then set on a 4°C plate. Once set, the formalin fixed paraffin embedded tissue (FFPE) was taken out of each mould and excess wax was removed.

FFPE tissue was then sectioned into 5 µm slices using a microtome (RM2125RTF, Leica, Germany). Ribbons of tissue sections were cut and placed into a beaker of cold water. Bubbles were removed using a paint brush and tissue sections were transferred onto Poly-L-Lysine coated slides (631-0107, VWR, USA) in a water bath at 37°C. Slides were left to dry at room temperature overnight.

2.5.2 Haematoxylin and Eosin in FFPE tissue

For haematoxylin and eosin (H&E) staining, slides were first placed in an oven at 55°C for 15-20 minutes to remove wax. Slides were then rehydrated by placing them in three HistoClear solutions (HS-200, National Diagnostics, USA), each for 5 minutes, followed by two 100% ethanol solutions, two 95% ethanol solutions and a 70% ethanol solution for 1 minute each. Slides were then placed in filtered haematoxylin (HHS16, Sigma-Aldrich) for 1 minute and transferred to cold tap water. To remove cytoplasmic staining, slides were placed in Acid Alcohol (0.25% HCl in Ethanol) for a few seconds and then transferred again to cold tap water. Staining of nuclei was confirmed using a light microscope and then haematoxylin was ‘blued’ using hot tap water for 2 minutes, before being transferred to cold tap water. Slides were then placed in eosin (HT110116, Sigma-Aldrich, UK) for 1 minute and transferred to cold tap water. Slides were then dehydrated by placing them in 70% ethanol, two 95% ethanol solutions and then two 100% ethanol solutions for 3 minutes each. Slides were then placed in two HistoClear solutions, each for 10 minutes (or overnight if needed). Slides were

mounted using Dibutylphthalate Polystyrene Xylene (DPX; LAMB/DPX, ThermoFisher, UK).

2.5.3 Immunohistochemistry in FFPE tissue

To remove wax, slides were placed in an oven at 55°C for 15-20 minutes. Slides were then rehydrated by placing them in three HistoClear solutions, each for 10 minutes, followed by two 100% ethanol solutions and a 70% ethanol solution for 3 minutes each. Slides were then placed in cold tap water for at least 3-5 minutes. Heat-activated antigen retrieval was then performed by placing the slides in a microwavable container with ~500 mL 1X sodium citrate buffer (0.1 M, pH 6.0; Table 2.11). The tissue was boiled in the microwave for 5 minutes twice, with a short break in between. Slides were then cooled for 20 minutes. Slides were then dried with a tissue and placed in a humidity chamber. A PAP pen (H-4000, 2B Scientific, UK) was used to draw around each section of tissue on the slide. Endogenous peroxidase was quenched by incubating tissue with 3% hydrogen peroxide in dH_2O (31642, Sigma-Aldrich, UK) for 10 minutes, followed by two washes with 1X Tris Buffered Saline (TBS; Table 2.11). Tissue sections were then blocked with 5% BSA in TBS (BSAV-RO, Sigma-Aldrich, UK) for 30 minutes to 1 hour. Primary antibodies (Table 2.6) were diluted to appropriate concentrations in 1X TBS. Mouse/Rabbit IgGs were used as controls, at the same concentration as the primary antibody (Table 2.6). Blocking buffer was removed from tissue. Primary antibodies were applied and stored at 4°C overnight. Tissue sections were then washed with 1X TBS three times. The appropriate biotinylated secondary antibody (Table 2.7) was then diluted and applied for 30 minutes to 1 hour. Tissue sections were then washed again with 1X TBS three times. An avidin peroxidase solution was then prepared by diluting avidin peroxidase (A3151, Merck, UK) to a concentration of 100 ug/mL in 1X high salt TBS (Table 2.11). Tissue sections were then washed again with 1X TBS three times. 3,3′-Diaminobenzidine (DAB; ImmPACT DAB EqV, SK41-3, Vector Laboratories, USA) was then prepared according to manufacturer's instructions. DAB was applied to the tissue and visualised under a light microscope to determine appropriate timings for incubation. Tissue sections were then washed with dH_2O for 5 minutes. Slides were then counterstained in filtered haematoxylin (HHS16, Sigma-Aldrich, UK) for a few seconds and transferred to cold tap water. To remove cytoplasmic staining, slides were placed in Acid Alcohol (0.25% HCl in Ethanol) for a few seconds and then transferred again to cold tap water. Staining of nuclei was confirmed using a light microscope and then haematoxylin was 'blued' using hot tap water for 2 minutes, before being transferred to cold tap water. Slides were then dehydrated by placing them in 70% ethanol, 95% ethanol and then 100%

ethanol for 3 minutes each. Finally, slides were placed in two HistoClear solutions, each for 10 minutes (or overnight if needed) and mounted using DPX (LAMB/DPX, ThermoFisher, UK).

All buffers used for immunohistochemistry are outlined in Table 2.11.

2.5.4 Immunofluorescence in FFPE tissue

Sudan Black B was dissolved in 70% Ethanol overnight in the dark to make a concentration of 0.1% w/v. The solution was then filtered using Whatman 595½ filter paper.

Dewaxing, rehydration, and heat-activated antigen retrieval were performed as outlined above (Section 2.5.3). Slides were then dried with a tissue and placed in a humidity chamber. A PAP pen (H-4000, 2B Scientific) was used to draw around each section of tissue on the slide. Tissue sections were then blocked with 5% BSA (in TBS) for 1 hour. Primary antibodies (Table 2.6) were applied and stored at 4°C overnight. Mouse/Rabbit IgGs were used as controls, at the same concentration as the primary antibody (Table 2.6). Tissue sections were then washed with 1X TBS three times. The appropriate fluorescent-conjugated secondary antibody (Table 2.7) was then diluted and applied for 1 hour. To reduce autofluorescence, slides were then incubated in Sudan Black B for 30 minutes in the dark, as described in Holder *et al.* (2012)[373]. Slides were then placed in 70% ethanol for 1 minute, and then washed with 1X TBS. Slides were mounted using Fluoromount-G™ with DAPI (0100-20, Southern Biotech, USA).

2.5.5 Microscopy

H&E and immunohistochemistry in FFPE tissue were imaged using the Axioscan Z1 Slide Scanner (Zeiss, Germany) in the Bioimaging Core Facility (Faculty of Biological Sciences, University of Leeds). Immunofluorescence in FFPE tissue was imaged using the Zeiss Axio Scope.A1 and the following fluorophores were used: DAPI (Excitation: 353 nm, Emission: 465 nm), Alexa 488 (Excitation: 493 nm, Emission: 517 nm) and Alexa 568 (Excitation: 577, Emission: 603 nm). Zen Blue software was used with both microscopes (Zeiss, Germany).

2.5.6 Image analysis using QuPath

Images from placental explants were analysed using QuPath (v0.3.2). A pixel classifier threshold was set to detect the tissue in the images. Tissue was initially drawn around manually to remove any artefacts or unfocused regions. The tissue detection pixel classifier was then used to annotate the tissue, excluding any membranous tissue

(Figure 2.18A). This detected tissue was used to calculate total villous area (μm^2). For CD31 DAB area analysis, a previously published script was used[374]. The area of CD31 (μm^2) was normalised to total villous area (μm^2) (Figure 2.18B). For other markers, the positive cell detection tool was used to identify the number of DAB positive cells. A threshold was set to determine 'positive' cells and were adjusted depending on the antigen. The number of positive cells were then normalised to total villous area (μm^2) or reported as a percentage of total (haematoxylin labelled) cells (Figure 2.18C).

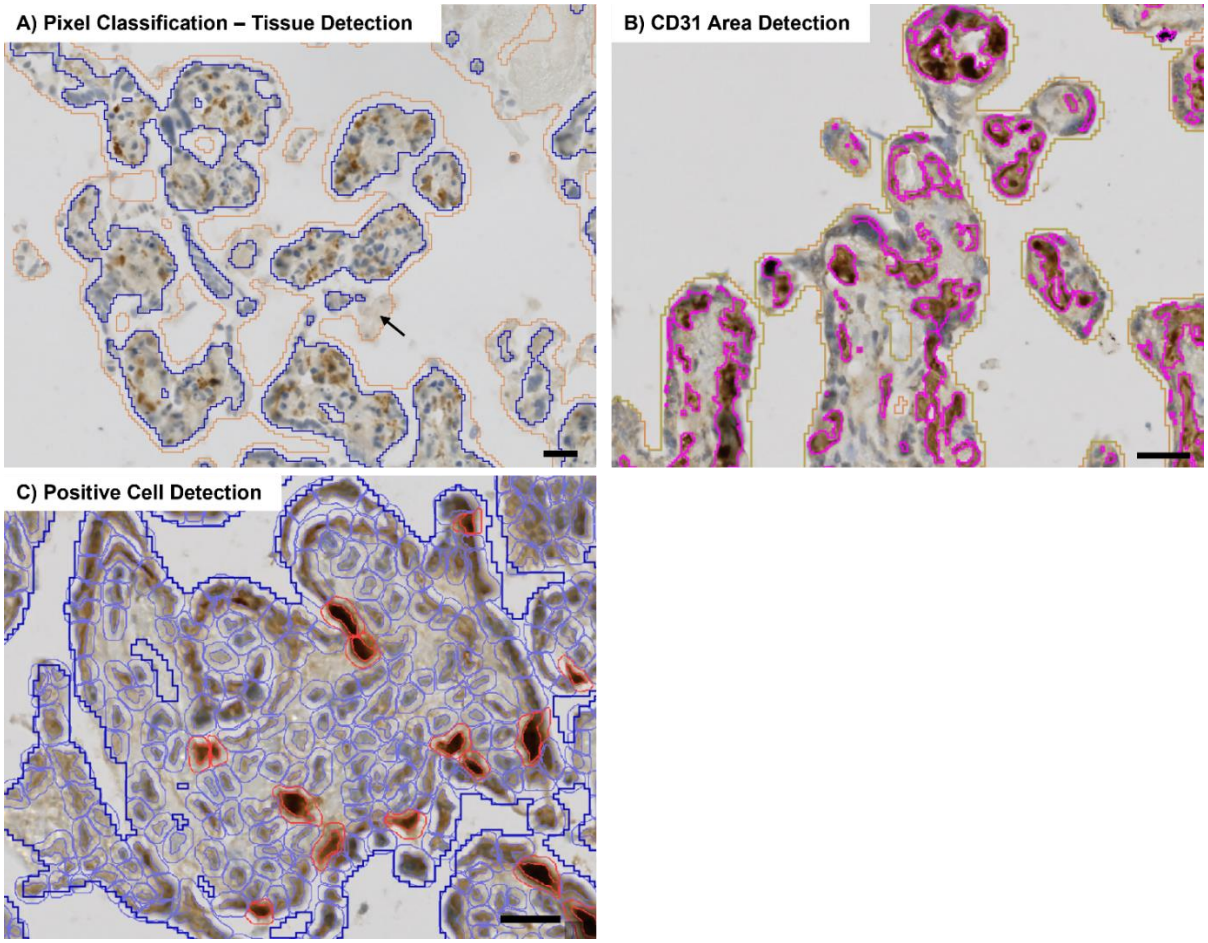

Figure 2.18 - Methods for quantification of immunohistochemistry of placental explants using QuPath (v0.3.2). A) Pixel classification used to detect placental tissue. B) CD31 area was determined using a previously published script[374]. The area of CD31 (μm^2) was normalised to total villous area (μm^2). C) Positive cell detection was used for other markers. The number of positive cells (red outline) were normalised to total villous area (μm^2) or reported as a percentage of total cells (red and blue outline). Scale bars = 20 µm.

Table 2.11 - Buffers used for immunohistochemistry. Abbreviations: TBS – Tris buffered saline, NaCl – Sodium chloride.

Buffer	Constituents
10X TBS High Salt	0.05 M Trizma base, 3 M NaCl, pH 7.6 in dH_2O
10X TBS	0.2 M Trizma base, 1.5 M NaCl, pH 7.4 in dH_2O
10X Citrate Buffer	0.1 M Sodium Citrate Tribasic Dihydrate, pH 6.0 in dH_2O

2.6 Analysis of mRNA expression

2.6.1 RNA extraction

2.6.1.1 Placental explant tissue

To extract RNA from placental explants (~15-30 mg), 500 µL of lysis/binding buffer was added to nuclease-free Eppendorf's containing the explants and a 5 mm metal ball (69989, Qiagen, Germany). The tissue was homogenised using the Tissue Lyser II (Qiagen) for 2 minutes, at a frequency of 27/s. Following this, the mirVana^{TM} miRNA isolation kit (AM1561, Invitrogen, UK) was used to isolate total RNA, including small RNAs, according to manufacturer's instructions. All centrifugation steps were performed at 10,000 RCF, except for elution which was performed at maximum speed. For the phase separation, 500 µL of Acid-Phenol:Chlorophorm (AM9720, Invitrogen, UK) was added to the tubes, which were vortexed and centrifuged and the aqueous upper phase collected. The remainder of the mirVana protocol was followed, including several wash steps to remove impurities prior to elution with 100 µL of pre-heated elution solution (95°C). The RNA eluate was stored at -80°C.

2.6.1.2 Cells cultured in plates

Cells were first washed with sterile PBS. Total RNA, including small RNAs was extracted using the miRNeasy Advanced Mini kit for tissues and cells (217604, Qiagen, UK), according to manufacturer's instructions. Cells were scraped into 260 µL of RLT lysis buffer using sterile cell scrapers (83.3950, Sarstedt, Germany) and the remainder of the miRNeasy protocol followed. All centrifugation steps were performed at 12,000 RCF, except for those where maximum speed was required. This kit also included genomic DNA (gDNA) eliminator spin columns, to remove contaminating gDNA. RNA was eluted in 40 µL of nuclease-free water and stored at -80°C.

2.6.1.3 Cells cultured in Ibidi microfluidic devices

Medium was removed from the outlet and inlet reservoirs and 120 µL of sterile PBS was added to the inlet to wash the cells. Excess PBS was removed from the reservoirs and 120 µL of TrypLE express (12563-029, Gibco, UK) was added to the inlet reservoir. The device was then incubated at 37°C for 5 minutes. Detached cells in TrypLE were collected into a nuclease-free Eppendorf. Appropriate culture medium was added into the inlet reservoir and removed from the outlet reservoir to collect remaining cells. Cells were centrifuged at 350 RCF for 5 minutes and the supernatant was removed from the pellet. Total RNA, including small RNAs were extracted using

the miRNeasy micro kit for tissues and cells (217684, Qiagen, UK), according to manufacturer's instructions. All centrifugation steps were performed at 10-12,000 RCF, except for those where maximum speed was required. A DNase step was included to remove any contaminating gDNA. RNA was eluted in 14 µL of nuclease free water and stored at -80°C.

2.6.1.4 Cells cultured in the triculture microvasculature model devices

To extract the cells from the triculture devices, the gels were resected and digested in a solution of PBS containing Accutase (SCR005, Millipore, UK) and 50 FU/ml Nattokinase (TFSBE-20 Japan Bioscience Ltd, Japan) for 15-20 min at 37°C. All PBS was removed from the side channels and the PDMS plugs were removed from the inner compartment. A scalpel was then used to cut away the central channel from the glass slide. The end of a p200 pipette tip was used to peel the gel containing the cells away from the PDMS and then to place it in a well of a 24-well plate containing 500 µL of the gel digestion solution. Samples were pooled from 3 devices for each condition. The plate was then placed at 37°C for 15-20 minutes. The solution was then mixed well by pipetting to digest the gel, and cells were checked under the microscope. The solution was then transferred to a 15 mL tube, and a further 9 mLs of gel digestion solution was then added to the tube. This was then centrifuged at 1200 RPM for 5 minutes to pellet the cells. The supernatant was then removed, and the pellet was resuspended in 650 µL of RLT plus lysis buffer (a part of 74134, Qiagen, UK) and stored at -80°C until the following day. RNA was isolated using the RNeasy Plus Mini Kit (74134, Qiagen, UK) according to manufacturer's instructions. All centrifugation steps were performed at maximum speed. This kit also included gDNA eliminator spin columns, to remove contaminating gDNA. RNA was eluted in 25 µL nuclease-free water and stored at -80°C.

2.6.2 RNA quantification

The concentration of RNA (ng/µL) was recorded using the Nanodrop-1000 or -2000 (ThermoFisher Scientific, UK) by loading 1.5 µL of the RNA sample. The nanodrop also recorded the 260:280 and 260:230 ratios assess for common contaminants, such as gDNA and phenol, respectively[375]. An example nanodrop trace can be seen in Figure 2.19**.**

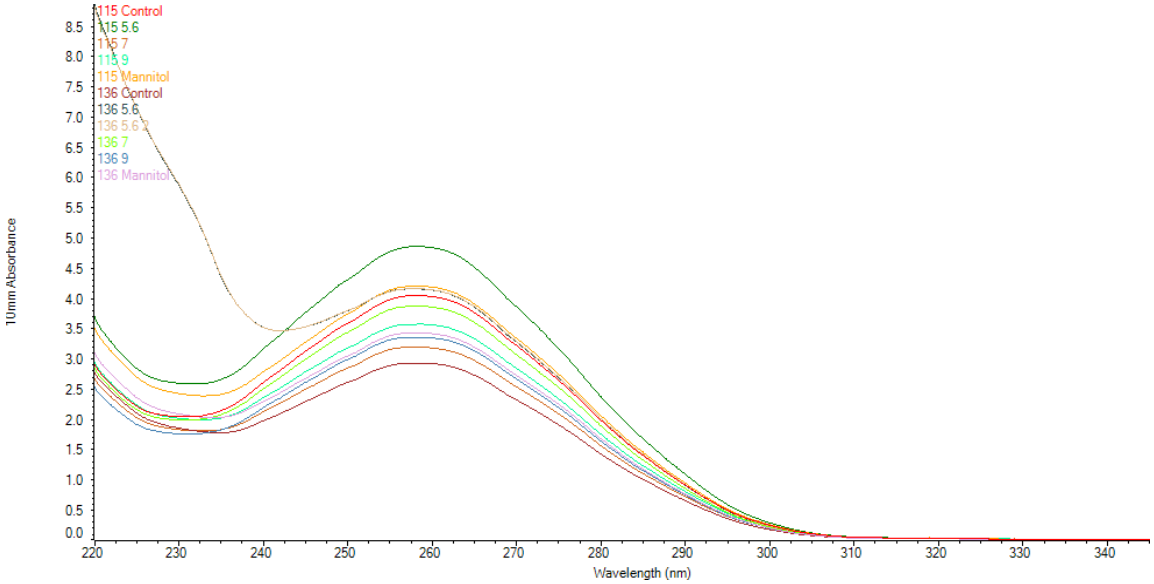

Figure 2.19 - Example nanodrop traces for RNA samples. The concentration and purity of RNA samples were measured using the NanoDrop-1000 or -2000 Spectrophotometer. The nanodrop traces in this example were generated using the NanoDrop-2000. The 10 mm absorbance is plotted against the absorbance wavelength (nm) to allow the RNA concentration (ng/µL), 260:280 and 260:230 absorbance ratios to be calculated.

2.6.3 RT-qPCR

For reverse transcription the Affinity Script kit (200436, Agilent, USA) was used, according to the manufacturer's instructions. Samples were prepared by adding 100 ng RNA to nuclease-free water in a total volume of 12.5 µL. No template (NTC) and no reverse transcriptase controls (NRT) were also prepared, with nuclease-free water to replace the RNA or the reverse transcriptase enzyme, respectively. Complementary DNA (cDNA) synthesis was performed using a thermal cycler (Applied Biosystems Venti 96 Well, ThermoFisher) and samples were heated to 25°C for 10 minutes, 42°C for 60 minutes and 70°C for 15 minutes, with a final indefinite hold at 4°C. Samples were then stored in the -20°C.

For the qPCR, the Brilliant III Ultra-Fast SYBER Green Master Mix kit was used (600882, Agilent), according to manufacturer's instructions. cDNA samples were diluted 1:10 with nuclease-free water. The passive reference dye, 5-carboxy-X-rhodamine (ROX) was also diluted 1:500 with nuclease-free water. PCR primers were used at a final concentration of 0.36 µM. Following the loading of the master mix and cDNA samples into a 96-well PCR plate, qPCR was performed using the LightCycler 96 Instrument (Roche). The plate was preincubated at 95°C for 3 minutes, followed by 40 cycles of 2 step amplification: 95°C for 20 seconds, followed by an annealing step for 20 seconds. The temperature of the annealing step varied depending on the primer melting temperature (T_m). This was followed by a final cycle of 95°C for 1 minute, 55°C for 30 seconds and 95°C for 1 second to perform melt curve analysis and determine specificity of the primers. The data was then analysed using the LightCycler 96 1.1 software (Roche; Figure 2.20). Results were acquired as an amplification curve and raw cycle threshold (Ct) values which were used to calculate the relative gene expression via the $2^{(-Ct)}$x100 method, normalising against the appropriate housekeeping genes (see results). Appropriate housekeeping genes for each experiment were determined using RefFinder (Figure 2.21). This is a web-based tool which incorporates the currently available major computational programs (geNorm, Normfinder, BestKeeper, and the comparative Delta-Ct method) to compare and rank the tested candidate reference genes (https://blooge.cn/RefFinder/).

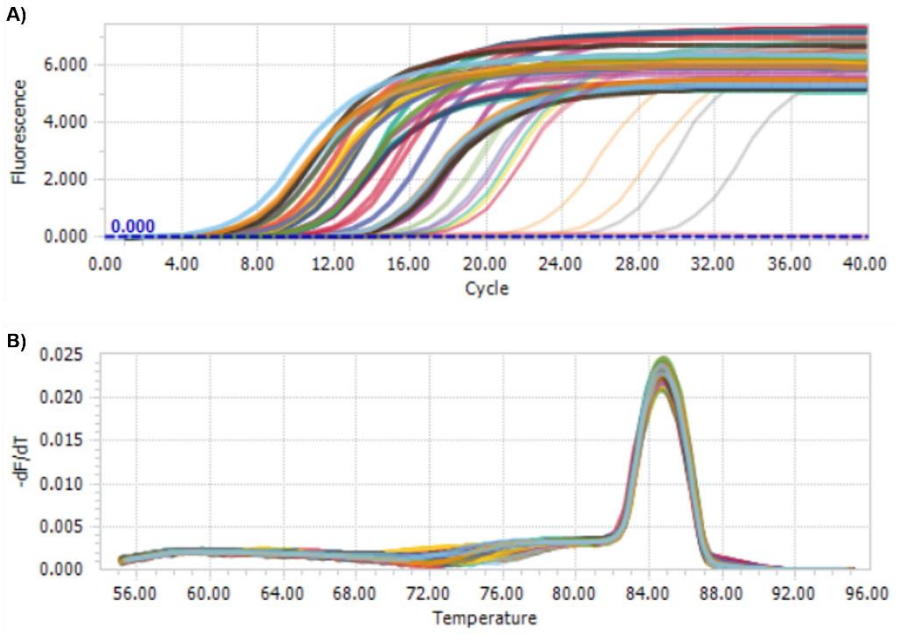

Figure 2.20 - Example of an mRNA RT-qPCR output. A) Amplification plot from an RT-qPCR reaction monitoring the amplification of an mRNA transcript from an RNA sample, to determine its relative abundance. B) The melt curve generated after the 40 cycles of 2-step qPCR to determine the specificity of primer binding.

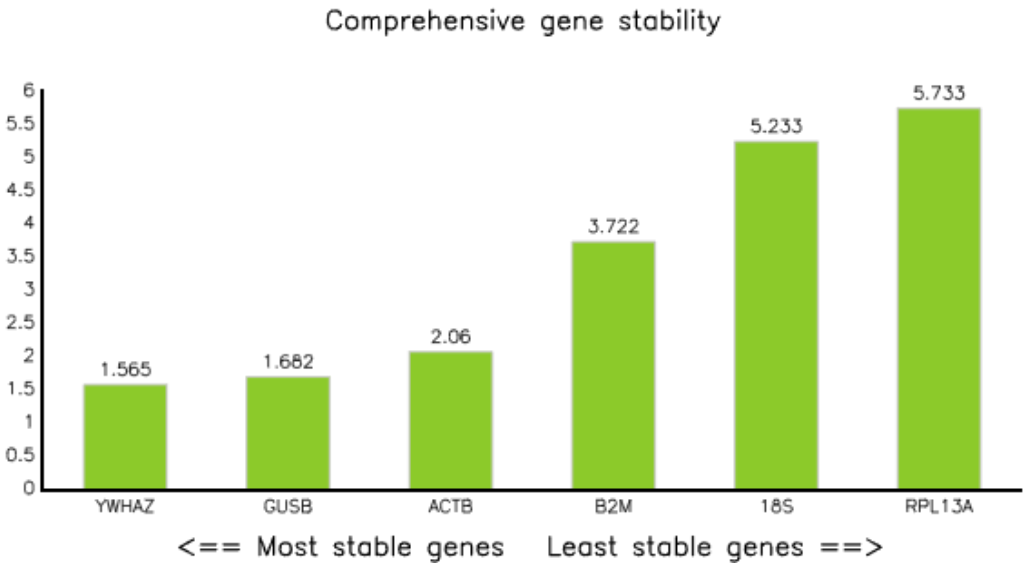

Figure 2.21 - Example of RefFinder results used to determine the most stable housekeeping genes. Ct values for selected housekeeping genes for each sample were inputted into RefFinder. This is a web-based tool which incorporates the currently available major computational programs (geNorm, Normfinder, BestKeeper, and the comparative Delta-Ct method) to compare and rank the tested candidate reference genes (https://blooge.cn/RefFinder/).

2.6.3.1 Primers

Primers were either identified from previous studies or designed using the Primer Designing tool on NCBI (Primer-BLAST)[376]. If a gene had multiple transcripts, the FASTA sequences for each transcript were inputted into the EMBL-EBI Multiple Sequence Alignment tool[377] to identify which regions of the sequences overlapped. Primers were then designed within this region. Primers were selected with a GC content between 40-60%, a product size between 90-300, at least 4 base mismatches from off-target transcripts and spanning an exon-exon junction, where possible. The sequences of primers and their annealing temperatures are outlined in Table 2.12 (Housekeeping genes) and Table 2.13 (Target genes). Custom oligonucleotides were ordered from IDT (USA).

Table 2.12 - RT-qPCR primers for housekeeping genes. Custom oligonucleotides were ordered for each housekeeping (IDT, USA). The forward and reverse primer sequences are shown, with their appropriate annealing temperatures, product lengths and references.

Gene	Primer	Sequence (5'->3')	Annealing Temperature	Product Length	Reference
***18S* (rRNA)** (XR_007086113.1)	**Forward primer**	GCTGGAATTACCGCGGCT	52	187	Designed
	Reverse primer	CGGCTACCACATCCAAGGA			
ACTB (NM_001101.5)	**Forward primer**	CATGTACGTTGCTATCCAGGC	50	250	Designed
	Reverse primer	CTCCTTAATGTCACGCACGAT			
B2M (NM_004048.4)	**Forward primer**	TGACTTTGTCACAGCCCAAGATA	55	75	[378]
	Reverse primer	CGGCATCTTCAAACCTCCA			
GAPDH (NM_002046.7)	**Forward primer**	CTGGGCTACACTGAGCACC	60	101	Designed
	Reverse primer	AAGTGGTCGTTGAGGGCAATG			
GUSB (NM_000181.4)	**Forward primer**	GTCTGCGGCATTTTGTCGG	55	127	[378]
	Reverse primer	CACACGATGGCATAGGAATGG			
HPRT1 (NM_000194.3)	**Forward primer**	TGACACTGGCAAAACAATGCA	55	94	[378]
	Reverse primer	GGTCCTTTTCACCAGCAAGCT			
RPL13A (NM_012423.4)	**Forward primer**	GCCATCGTGGCTAAACAGGTA	55	135	[378]
	Reverse primer	GTTGGTGTTCATCCGCTTGC			
RPLP0 (NM_001002.4)	**Forward primer**	AGCCCAGAACACTGGTCTC	55	97	[378]
	Reverse primer	ACTCAGGATTTCAATGGTGCC			
YWHAZ (NM_003406.4)	**Forward primer**	ACTTTTGGTACATTGTGGCTTCAA	55	94	Designed
	Reverse primer	CCGCCAGGACAAACCAGTAT			

Table 2.13 - RT-qPCR primers for target genes. Custom oligonucleotides were ordered for each target gene (IDT, USA). The forward and reverse primer sequences are shown, with their appropriate annealing temperatures, product lengths and references.

Gene	Primer	Sequence (5'->3')	Annealing Temperature (°C)	Product Length	Reference
CD44 (NM_000610.4)	**Forward primer**	CAGAGGAGTAGGAGAGAGGAAACA	60	219	Designed
	Reverse primer	ACCAGAGGAAGGGTGTGCTC			
CXCL2 (NM_002089.4)	**Forward primer**	TGGGCAGAAAGCTTGTCTCAA	60	90	Designed
	Reverse primer	TCTGGTCAGTTGGATTTGCCATTTT			
EGF (NM_001963.6)	**Forward primer**	ACTGCACGTGCCCTGTAGGA	60	193	Designed
	Reverse primer	TCGGGTGAGGAACAACCGCT			
FABP4 (NM_001442.3)	**Forward primer**	GAATGCGTCATGAAAGGCG	60	87	[379]
	Reverse primer	CAATGCGAACTTCAGTCCAGG			
***FLT1* (VEGFR1)** (NM_002019.4)	**Forward primer**	CCCAGTTTCTGCCATTCCAG	60	90	[380]
	Reverse primer	CGCGATTTTCCTTTCCAGCT			
IL1B (NM_000576.3)	**Forward primer**	CACCAATGCCCAACTGCCTGC	60	219	Designed
	Reverse primer	TGCTCATCAGAATGTGGGAGCGA			
IL6 (NM_000600.5)	**Forward primer**	GGTACATCCTCGACGGCATCT	60	81	[381]
	Reverse primer	GTGCCTCTTTGCTGCTTTCAC			
JCAD (NM_020848.4)	**Forward primer**	AGACCCTGGATTGGAACCTC	60	117	[382]
	Reverse primer	TGACCGCCACACACATTTAT			
***KDR* (VEGFR2)** (NM_002253.4)	**Forward primer**	CTCACAGTCCTAGAGCGTGT	60	85	[380]
	Reverse primer	AGACTTCGATGCTTTCCCCA			
NAMPT (NM_005746.3)	**Forward primer**	TCCAGCAGCAGAACACAGTACCA	60	111	Designed
	Reverse primer	TCGCTGACCACAGATACAGGCAC			
***NT5E* (CD73)** (NM_002526.4)	**Forward primer**	CTAGCGCAACCACAAACCATAC	65	79	Designed
	Reverse primer	CTGGGTCCTCTCTGAGTCTCG			
PDGFD (NM_025208.5)	**Forward primer**	TTGTACCGAAGAGATGAGACCA	60	133	[383]
	Reverse primer	GCTGTATCCGTGTATTCTCCTGA			

Gene	Primer	Sequence (5'->3')	Annealing Temperature (°C)	Product Length	Reference
***PECAM1* (CD31)** (NM_000442.5)	**Forward primer**	GCTGAGTCTCACAAAGATCTAGGA	57	91	[384]
	Reverse primer	ATCTGCTTTCCACGGCATCA			
PIEZO1 (NM_001142864.4)	**Forward primer**	CAGGCCTATGAGGAGCTGTC	60	170	[385]
	Reverse primer	TTGTAGAGCTCCCGCTTCAT			
PINK1 (NM_032409.3)	**Forward primer**	TACGTGGATCGGGGCGGAAA	60	294	Designed
	Reverse primer	TCGGGCAGATGGTCTCTTGCT			
PTGS2 (NM_000963.4)	**Forward primer**	CAAATTGCTGGCAGGGTTGCTGG	60	236	Designed
	Reverse primer	AGGGCAGGATACAGCTCCACAG			
RAMP2 (NM_005854.3)	**Forward primer**	GGCCATGATTAGCAGGCCTTA	60	292	Designed
	Reverse primer	TGTTGAGAAGCTCGTGGCCC			
***SLC2A1* (GLUT1)** (NM_006516.4)	**Forward primer**	AACCACTGCAACGGCTTAGA	57	199	Designed
	Reverse primer	TCACGGCTGGCACAAAACTA			
***SLC2A3* (GLUT3)** (NM_006931.3)	**Forward primer**	TGCAACTTCATGTCAACTTCTGG	57	72	Designed
	Reverse primer	TCAGTGAGAAATGGGACCCTG			
***SLC2A4* (GLUT4)** (NM_001042.3)	**Forward primer**	AGAGCCAGCTCTCTCTACCC	57	165	Designed
	Reverse primer	TCACACGAGGGGAATGAGG			
***SLC2A8* (GLUT8)** (NM_014580.5)	**Forward primer**	CTAGTGGCCCCGGTCTACAT	57	89	Designed
	Reverse primer	CCGACGACGACCATTAGCTG			
***SLC2A9* (GLUT9)** (NM_020041.3)	**Forward primer**	CAATAGACCCAGACACTCTGACT	57	90	Designed
	Reverse primer	TCTTCACAATTAACGTCCCCAC			
***SLC2A10* (GLUT10)** (NM_030777.4)	**Forward primer**	CTTGCTGTATCTACGTGTCAGAG	57	124	Designed
	Reverse primer	CCAGCCAGTGCATAGTTGAGG			
***SLC2A12* (GLUT12)** (NM_145176.3)	**Forward primer**	CTTGCCTCACTCACCGGAG	57	138	Designed
	Reverse primer	GCGTCCCACTATAAGAACCGTG			
***THY1* (CD90)** (NM_006288.5)	**Forward primer**	AGGGCCATCAGCTCTCTTCTGCT	60	240	Designed
	Reverse primer	TCCTGGTGCAGAGCCACACTT			
VWF (NM_000552.5)	**Forward primer**	CCCATTTGCTGAGCCTTGT	57	141	[386]
	Reverse primer	GGATGACCACCGCCTTTG			

2.6.4 qPCR sign arrays

To further identify endothelial and mesenchymal genes in endothelial lineage differentiated pMSCs (n=4), an Endothelial-to-Mesenchymal transition (EndMT) qPCR SignArray (EndMT1H1, AnyGenes, France) was performed. Samples were prepared by adding 400 ng RNA to nuclease-free water in a total volume of 10 µL. RNA was converted to cDNA using the Applied Systems High-Capacity cDNA Reverse Transcription Kit (4368814, ThermoFisher Scientific, UK). This kit was recommended by the manufacturers of the qPCR array. Each qPCR sign array plate was first centrifuged at 1000 RCF for 60 seconds at room temperature, to bring contents to the bottom of each well. cDNA was diluted 1:6 in nuclease-free water. A master mix was then prepared for each sample containing 575 µL SYBR green (600882, Agilent, USA), 460 µL nuclease-free water and 115 µL diluted cDNA. A master mix was also prepared for the QC wells of the plate containing 90 µL SYBR green and 90 µL nuclease-free water. The master mix for each sample was then vortexed and centrifuged briefly before loading 10 µL into each well, according to the plate layout. The plate was centrifuged at 1000 RCF for 60 seconds at room temperature before loading into the Light Cycler 384 Instrument (Roche, Switzerland).

The plate was preincubated at 95°C for 10 minutes, followed by 40 cycles of 2 step amplification: 95°C for 10 seconds, followed by an annealing step at 60°C for 30 seconds. This was followed by a final cycle of 95°C for 10 seconds, 65°C for 30 seconds and 95°C for 1 second to perform melt curve analysis and determine specificity of the primers. The plate contained 83 genes of interest and 8 housekeeping genes (Table 2.14). Positive controls and negative controls were also included in the plate. The cycle Ct values were inputted into an analysis spreadsheet provided by AnyGenes and carried out according to manufacturer's instructions. The analysis used in the spreadsheet is based on the delta-delta Ct (ΔΔCt) method, which compares the experimental condition to the control condition, and included a student's T-Test to determine statistical significance ($p<0.05$ considered statistically significant). A positive or negative gene expression variation was used to determine whether a gene was up- or down-regulated, respectively based on a fold change in pMSCs cultured in differentiation medium compared to control medium.

Table 2.14 - List of primers included in the endothelial to mesenchymal transition (EndMT) qPCR sign array. Genes shaded in grey are the housekeeping genes, at the end of the list.

RefSeq ID	Symbol
NM_014795.3	*ZEB2*
NM_001128128.2	*ZEB1*
NM_003068.4	*SNAI2*
NM_005985.3	*SNAI1*
NM_000602.4	*SERPINE1*
NM_006162.3	*NFATC1*
NM_003392.4	*WNT5A*
NM_000638.3	*VTN*
NM_003380.3	*VIM*
NM_001001522.1	*TAGLN*
NM_001792.3	*CDH2*
NM_001299.4	*CNN1*
NM_000088.3	*COL1A1*
NM_212482.1	*FN1*
NM_004612.2	*TGFBR1*
NM_001024847.2	*TGFBR2*
NM_000660.4	*TGFB1*
NM_001135599.2	*TGFB2*
NM_003239.2	*TGFB3*
NM_005359.5	*SMAD4*
NM_005902.3	*SMAD3*
NM_005901.4	*SMAD2*
NM_016269.4	*LEF1*
NM_001200.2	*BMP2*
NM_024408.3	*NOTCH2*
NM_000474.3	*TWIST1*
NM_003200.3	*TCF3*
NM_001243226.1	*TCF4*
NM_005163.2	*AKT1*
NM_002746.2	*MAPK3*
NM_004530.4	*MMP2*
NM_002422.3	*MMP3*
NM_002448.3	*MSX1*
NM_000603.4	*NOS3*
NM_181523.2	*PIK3R1*
NM_006254.3	*PRKCD*
NM_000552.3	*VWF*
NM_000450.2	*SELE*
NM_001025109.1	*CD34*
NM_001795.3	*CDH5*
NM_001130861.1	*CLDN5*
NM_000132.3	*F8*
NM_001099786.1	*ICAM2*
NM_002210.3	*ITGAV*
NM_000212.2	*ITGB3*

NM_017617.3	*NOTCH1*
NM_006218.2	*PIK3CA*
NM_002093.3	*GSK3B*
NM_000601.4	*HGF*
NM_001530.3	*HIF1A*
NM_002449.4	*MSX2*
NM_000214.2	*JAG1*
NM_002226.4	*JAG2*
NM_002253.2	*KDR*
NM_000435.2	*NOTCH3*
NM_004626.2	*WNT11*
NM_001904.3	*CTNNB1*
NM_173849.2	*GSC*
NM_001315.2	*MAPK14*
NM_002019.4	*FLT1*
NM_138957.2	*MAPK1*
NM_000576.2	*IL1B*
NM_001025366.2	*VEGFA*
NM_001719.2	*BMP7*
NM_001014796.1	*DDR2*
NM_002006.4	*FGF2*
NM_002205.2	*ITGA5*
NM_133376.2	*ITGB1*
NM_004557.3	*NOTCH4*
NM_000442.4	*PECAM1*
NM_000594.2	*TNF*
NM_005424.2	*TIE1*
NM_002052.3	*GATA4*
NM_005157.4	*ABL1*
NM_001141945.1	*ACTA2*
NM_001105.4	*ACVR1*
NM_001202.3	*BMP4*
NM_001901.2	*CTGF*
NM_001955.4	*EDN1*
NM_001127598.1	*IGF2*
NM_001429.3	*EP300*
NM_003998.3	*NFKB1*
NM_004994.2	*MMP9*
NM_001146312.1	*MYOCD*
NM_021130	*PPIA*
NM_001101	*ACTB*
NM_001172085	*TBP*
NM_004048	*B2M*
NM_053275	*RPLP0*
NM_000194	*HPRT1*
NM_001128148	*TFRC*
NM_000181.3	*GUSB*

2.6.5 RNA sequencing

2.6.5.1 Preparation of samples

Following glucose treatments (Section 2.4.1), placental explant RNA samples (n=5) were prepared into 20 µL aliquots in nuclease-free Eppendorf's and sent to Novogene (Cambridge, UK).

2.6.5.2 mRNA sequencing

RNA sample purity was determined using agarose gel electrophoresis and the Agilent 2100. All samples passed the required criteria. For mRNA-sequencing, the library prep was conducted using the Novogene next generation sequencing (NGS) RNA Library Prep Set (PT042). mRNA was enriched with oligo(dT) beads and fragmented by adding fragmentation buffer. The cDNA synthesis was the performed with an mRNA template, random hexamers primer, and an Ilumina custom second-strand synthesis buffer. The second-strand synthesis was instigated by the addition of dNTPs, DNA polymerase I and RNase H. Ligation and sequence adapter ligation was then performed. The cDNA library was then finalised by determining the library concentration (using the Qubit 2.0), the insert size (using the Agilent 2100), followed by qPCR to quantify the precise library concentration. The cDNA library was then loaded into Ilumina sequencers for mRNA-sequencing (Illumina Novaseq 6000, S4 flow cell, PE150 sequencing; Figure 2.22). Raw reads of FASTQ format were processed through fastp to remove reads containing adapter sequences, poly-N and low quality reads. Error scores, such as Q20 and Q30, which represent an error rate of 1 in 100 and 1 in 1000 base pairs, respectively, were also calculated[387]. These were used as a cut off so that all downstream analyses were based on clean data with high quality. Reads were then mapped to a reference genome (Homo Sapiens, GRCh38/hg38) and aligned using STAR[388]. FeatureCounts was used to count the read numbers mapped to each gene[389].

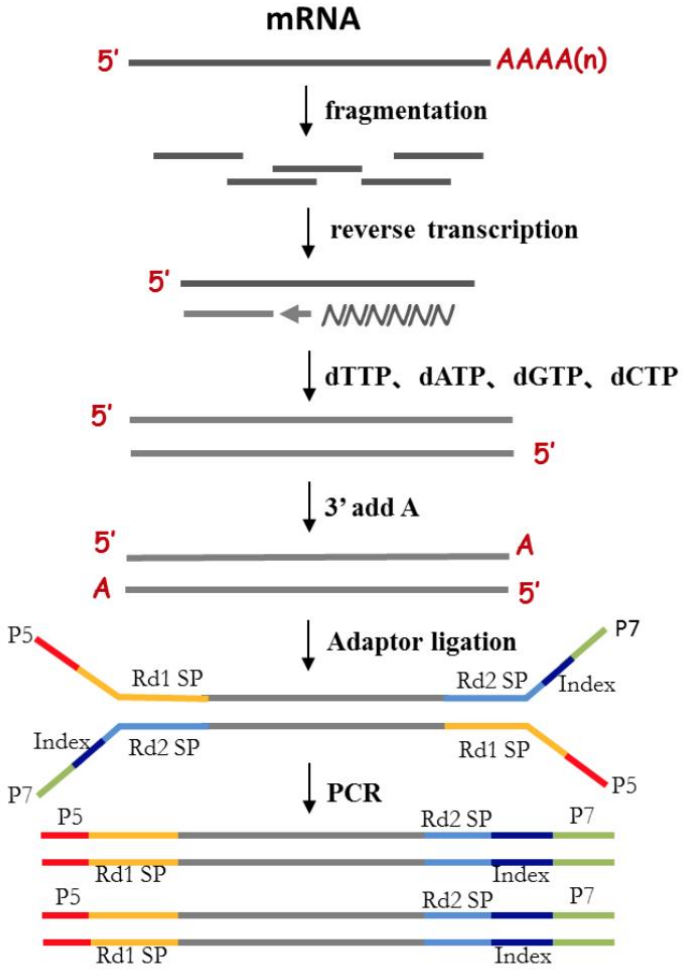

Figure 2.22 - mRNA-sequencing cDNA library preparation workflow. mRNA is fragmented and reverse transcribed to produce cDNA. Second-strand synthesis is initiated with the addition of dNTPs (dTTP, dATP, dGTP, dCTP). Adapter ligation is then performed and subsequent PCR to determine the precise library concentration (Novogene, UK).

2.6.5.3 Differential gene expression analysis

Differential gene expression analysis was performed by Dr Dapeng Wang (LeedsOMICs). Only genes that had at least 10 read counts in total across all samples examined were retained. DESeq2 was used to perform the differential expression analysis on raw read counts[390]. Due to variation between individual patient samples, the patient variable was added to the design formula to enable matched sample analysis[390,391]. Significantly differentially expressed genes (DEGs) were determined based on the cut-offs $p<0.05$ and Log_2 Fold Change (Log_2FC) >0.5 or < -0.5.

2.6.6 Functional enrichment analysis

Functional predictions of DEGs were performed using WebGestalt for Over Representation Analysis (ORA), Ingenuity Pathway analysis (IPA; Qiagen) and the ClusterOne algorithm on Cytoscape.

2.6.6.1 Overrepresentation Analysis

Ensembl IDs for DEGs ($p<0.05$ and Log_2FC >0.5 or < -0.5) were inputted into WebGestalt (http://www.webgestalt.org/) and ORA was performed[392]. This produced a list of enriched gene ontology (GO) annotations (biological processes, cellular components, and molecular functions)[393,394] and Kyoto Encyclopaedia of Genes and Genomes (KEGG)[395–397], Panther[398] and Reactome[399] pathways. For GO annotations, redundant terms were excluded. For identified pathways and GO terms, a false discovery rate (FDR) value of <0.05 was used as threshold. Enrichment ratios (ER) were also reported which is the number of observed genes divided by the number of expected genes in each GO/pathway category.

2.6.6.2 Ingenuity Pathway Analysis

ORA is routinely used to predict functional consequences but is unable to predict the direction of change, whilst IPA takes into consideration the direction of Log_2FC of the genes, and therefore can predict whether a function or pathway appears to be activated and deactivated based on a Z-score[400]. The Ensembl IDs for DEGs ($p<0.05$ and Log2FC >0.5 or < -0.5), and the associated Log_2FC's were inputted into IPA (QIAGEN Inc., https://digitalinsights.qiagen.com/IPA)[401] for core analysis. This included canonical pathway analysis, disease and function, regulator effects, upstream regulators, causal networks, and molecular networks. For identified canonical pathways and diseases and functions $p<0.01$ (-log (p value) > 2) was used as threshold.

2.6.6.3 Cluster analysis using CytoScape and ClusterOne

The Ensembl IDs for DEGs ($p<0.05$ and Log2FC >0.5 or < -0.5) were inputted into STRING (v11.3, https://string-db.org/), an online database that integrates and scores all publicly available sources of protein–protein interaction[402]. This generated a protein-protein interaction network of the proteins associated with the DEGs. This network was loaded into Cytoscape (v3.8.2), a software for integrated models of biomolecular interaction networks[403]. ClusterOne (v1.0) was used which detects densely connected regions (clusters) in large protein-protein interaction networks[404,405]. ClusterOne identified significant clusters ($p<0.05$), which contained 'nodes', which are the proteins, and 'edges' that show interactions between different proteins. The minimum node number for ClusterOne was set to 3. To determine their biological significance, these clusters were then inputted into Reactome (https://reactome.org/), the online pathway analysis tool, which provides molecular details on biological processes in humans[399].

2.6.6.4 Computational methods to predict localisation of altered inflammatory mediators within the placenta

Inflammatory mediators (cytokines and chemokines) were identified within the DEG list, based on those found within the associated immune/inflammatory pathways. The maternal-fetal interface atlas (https://maternal-fetal-interface.cellgeni.sanger.ac.uk/) was used, which is an online tool, developed from single-cell RNA sequencing data of the placenta and decidua[406]. To determine which cell types within the placenta express/produce these inflammatory mediators, the tool was subset to placental cell types (excluding decidual cell types), and each inflammatory mediator gene was inputted individually. Results were displayed as a Uniform Manifold Approximation and Projection (uMAP) plot of single cell RNA sequencing data, with a colour scale to show the level of expression in various placental cell types.

2.6.6.5 Comparison of DEGs to Hofbauer cell proteomics data

To further confirm whether differentially expressed inflammatory mediators are produced by HBCs, the DEGs altered by 7 mM glucose in placental explants were compared to HBC proteomics data by Pantazi *et al*. (2022)[407], using Venny (https://bioinfogp.cnb.csic.es/tools/venny/). In this study, placentae were collected from uncomplicated pregnancies and HBCs were isolated using a previously published protocol[408]. Tandem Mass Tagging (TMT) proteomics was then conducted on isolated HBCs (n=6), as described in Pantazi *et al*. (2022)[407].

2.6.6.6 Comparison of DEGs to M1/M2 macrophage polarisation transcriptomic data

To determine whether differentially expressed genes were associated with M1 or M2 polarised HBCs, the DEGs altered by 7 mM glucose in placental explants were compared to genes differentially expressed in M1/M2 macrophages using Venny (https://bioinfogp.cnb.csic.es/tools/venny/). The M1/M2 transcriptomic data was taken from a previous RNA sequencing study that investigated the gene expression profiles of monocyte-to-macrophage transition and polarisation to either M1 or M2 macrophages, using monocytes from human blood[409]. Additionally, these genes were also compared with the HBC proteomics data, to determine which of these M1/M2 markers are associated with HBCs.

2.6.7 Analysis of publicly available transcriptomic data on GDM and/or LGA

The gene expression omnibus (GEO) and ArrayExpress were searched (2020)[410,411] to identify publicly available transcriptomic datasets of human placentae, which included samples from women with GDM and/or contained information on birthweight or BWCs to determine whether samples were LGA or AGA. For GEO datasets, GEO2R was used to identify DEGs between the groups in the identified studies. This is an interactive web tool that allows users to compare two or more groups of samples in a GEO Series[412]. GenomeStudio (v1.0)[413] was used to assess DEGs in ArrayExpress datasets, which was conducted by Dr Dapeng Wang (LeedsOMICs). DEGs in each study were defined as those with $p<0.05$ and a Log_2FC of <-0.5 or >0.5, to apply the same cut offs as those used for the transcriptome analysis of glucose fluctuations in placental explants. The DEG lists ($p<0.05$ and Log_2FC of <-0.5 and >0.5) were then inputted into WebGestalt for ORA to identify significant overrepresented GO terms and KEGG, Reactome and Panther pathways (Section 2.6.6.1). The DEG lists were then compared to DEGs altered by 7 mM glucose in placental explants using Venny (https://bioinfogp.cnb.csic.es/tools/venny/).

2.7 Analysis of proteins

2.7.1 Protein extraction from placental villous explant tissue

To extract protein from placental explant tissue (~15-30 mg), radioimmunoprecipitation assay (RIPA) buffer was prepared with appropriate inhibitors. A 10x RIPA buffer (20-188, Merck, UK) was diluted to 1x with nuclease free water and phosphatase inhibitors (1% phosphatase inhibitor cocktail 2, P5726, Scientific Laboratory Supplies, UK; 1% phosphatase inhibitor cocktail 3, P0044, Sigma-Aldrich, UK) and a protease inhibitor (1%, protease inhibitor cocktail tablet, 04693124001, Roche, Switzerland) were added.

Following this, 500 µL of 1x RIPA buffer containing the inhibitors was added to nuclease free tubes containing the explants and a 5 mm Qiagen metal ball. The tissue was then homogenised using the Tissue Lyser II (Qiagen, UK) at a frequency of 27/s at 30 second intervals until the tissue appeared fully lysed. The samples were then kept on ice for 30 minutes with occasional vortexing. Finally, the samples were centrifuged at 18,928 RCF, to remove cellular debris, for 10 minutes at 4°C and the supernatant containing protein transferred and aliquoted into fresh tubes.

2.7.2 Protein assay

To quantify the concentration of protein isolated from placental explants, the BioRad protein assay was performed. An initial protein standard was made with BSA at a concentration of 1 mg/mL in distilled water. Serial dilutions were then performed at 1:2 to make the following concentrations: 0.5, 0.25, 0.125, 0.0625, 0.03125, 0.015625 and 0.0078125 mg/mL. Protein samples were also diluted 1:10. In a 96-well plate, 10 µL of standard or samples were loaded into the wells in duplicate, followed by 100 µL of the 1x Quick Start Bradford Dye Reagent (5000205, Bio-Rad, USA). The plate was incubated at room temperature for 15 minutes, protected from light. The absorbance was then measured at 595 nm on a plate reader (BioTek Powerwave HT, Agilent, USA) with Gen5 Microplate Reader and Imager software. Protein concentrations in the samples were determined using the linear standard curve (Figure 2.23).

2.7.3 Interleukin protein ELISAs

To assess levels of IL-1β and IL-6 in placental villous explant protein, human uncoated IL-1β (88-7261-22, ThermoFisher Scientific) and IL-6 ELISAs (88-7066-22, ThermoFisher Scientific) were used according to manufacturer's instructions. Explant protein was diluted (1:10-1:100) in 1x ELISA diluent. For IL1-β ELISAs, a standard curve with concentrations of 1.17, 2.34, 4.69, 9.38, 18.75, 37.5, 75, 150 pg/mL was used. For IL-6 ELISAs, a standard curve with concentrations of 1.56, 3.13, 6.25, 12.5, 25, 50, 100, 200 pg/mL was used. The absorbance was measured at 450 nm and 570 nm on a plate reader (Powerwave HT, Biotek) with Gen5 Microplate Reader software. Final absorbance values were calculated as the absorbance at 450-570 nm. Concentrations in explant samples were determined from a 4PL curve of the standards (Figure 2.24, See Section 2.2.2). Concentrations were normalised to total explant protein (mg). A 1x RIPA buffer, used in the protein extractions, was spiked into and IL1-β and IL-6 standard to ensure the RIPA buffer was not interfering with ELISA results.

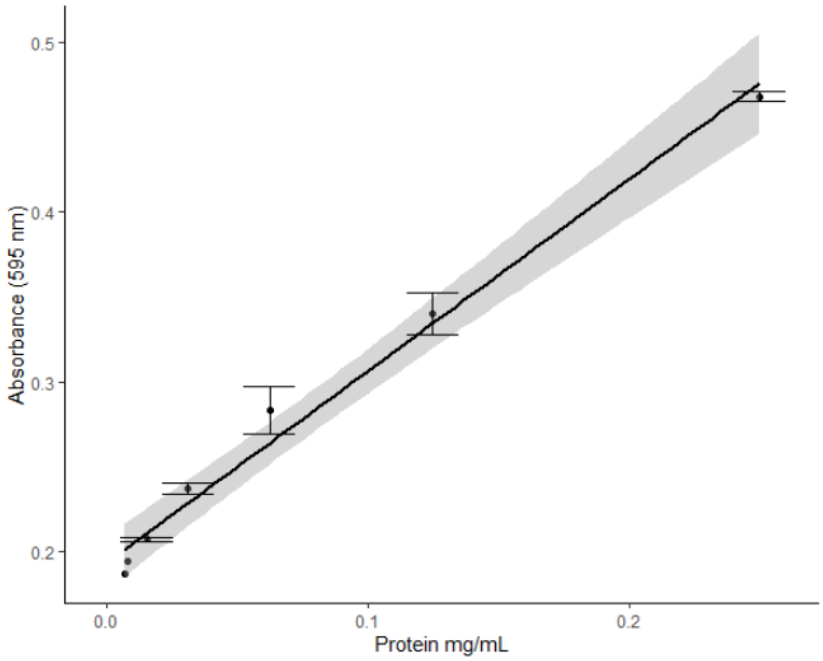

Figure 2.23 - Example of a protein assay standard curve. The Bio-Rad colourimetric protein assay was performed to calculate the concentration of protein in placental explants. The absorbance was measured at 595 nm of known concentrations of bovine serum albumin (BSA). The equation for this curve was y=1.11x+0.196, with an R^2 of 0.98.

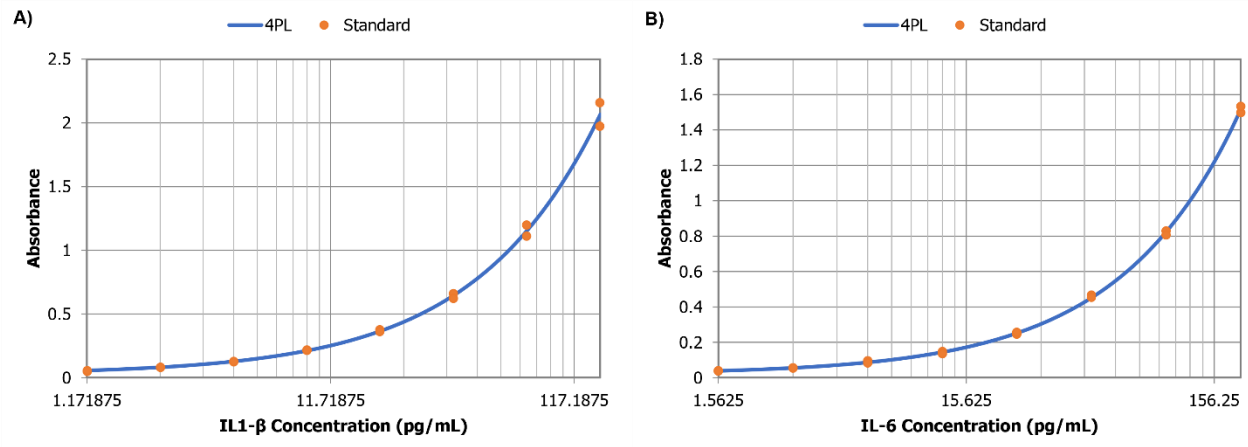

Figure 2.24 - Example of an interleukin ELISA 4PL standard curve. ELISAs for IL1-β (A) and IL-6 (B) in placental explant protein were performed. The absorbance at 570 nm was subtracted from the absorbance at 450 nm from known concentrations of IL1-β and IL-6 (pg/mL). The standard curve was plotted as a 4 parameter logistic regression (4PL) curve. The R^2 for both curves are 0.99.

2.7.4 Western blots

To assess levels of HBC markers in placental explant protein, a Western blot was performed. Firstly, placental explant protein was concentrated using Amicon Ultra-0.5 centrifugal filters (UFC500396, Millipore, USA). To remove glycine from the filters, 500 µL of PBS was added to the filter and centrifuged at 4,000 RCF for 10 minutes. All remaining PBS was then removed from the filters and up to 500 µL of the protein sample was added. The sample was then centrifuged at 14,000 RCF for 15 minutes. The filter, containing the concentrated protein, was then inverted into a new tube, and centrifuged at 1000 RCF for 2 minutes. For each gel, 30 µg of concentrated protein was made up in a total of 13 µL of dH_2O. A 9:1 master mix of NuPAGE lithium dodecyl sulfate (LDS) 4x sample buffer (NP0007, ThermoFisher, USA) and 10x reducing agent (NP0009, ThermoFisher, USA) was prepared and 5 µL added to each sample. The samples were then heated at 70°C for 10 minutes. Pre-cast Mini-PROTEAN 4-15% polyacrylamide gels (4561086, Bio-Rad, USA) were loaded into the cassette, which was filled with 1x running buffer (Table 2.16). Samples were briefly centrifuged for 20 seconds. In the first well, 5 µL of PageRuler Plus Pre-Stained Protein Ladder (26619, ThermoFisher, USA) was loaded, and subsequent wells were loaded with 15 µL of sample. The samples were then electrophoresed at 50V for 5 minutes followed by 100V for ~90 minutes. A polyvinylidene fluoride (PVDF) membrane (88585, ThermoFisher, USA) was first activated in methanol for 2 minutes, followed by washes in dH_2O. Protein bands from the gel were transferred to the PVDF membrane in a transfer tank and cassette. The transfer tank was filled with 1x transfer buffer (Table 2.16) and an ice block and ran at 100V for 1 hour. Blots were then blocked in 3% BSA in TBS with 0.3% Tween-20 (TBST) for 1 hour (Table 2.16), to prevent non-specific binding of the antibody. Blots were then incubated overnight at 4°C with primary antibodies (Table 2.15) in 3% BSA in TBST, and then washed 8 times with TBST. Blots were then incubated with the appropriate secondary antibody for 1 hour at room temperature in 3% BSA in TBST (Table 2.15; Table 2.6), and then washed 8 times with TBST. The SuperSignal West Femto Maximum Sensitivity Substrate (34094, ThermoFisher, USA) was added to detect the secondary antibody. Finally, blots were photographed using the G:Box imager (Syngene, India). Following detection of target proteins, the blots were stripped using a Glycine strip buffer (Table 2.16) for 30 minutes and then washed with TBST before applying the primary antibody for the loading control (β-actin, Table 2.15) in 3% BSA in TBST overnight at 4°C. The blot was washed, secondary antibody applied and visualised as above. Densitometry measurements were taken of the target protein bands using ImageJ. A background

reading was taken for each band and subtracted. Measurements were normalised to densitometry measurements of β-actin protein bands. The buffers used for Western blots are outlined in Table 2.16.

2.8 Statistical analysis

All data analysis, statistical analysis and data visualisation were performed using R (v4.04) and R studio (v1.3.959). R packages used for data visualisation included, ggplot2, Enhanced Volcano[414], ggbreak[415] and ggsignif. Normality of data was assessed using quantile-quantile (QQ) plots (Figure 2.25) and Shapiro-Wilk tests. For Shapiro-Wilk tests $p>0.05$ was considered normally distributed.

Data that was not normally distributed was presented as the median, and statistical analysis was performed using a Mann Whitney U test or a Kruskal-Wallis with Dunn's post-hoc test for two, or more than two groups, respectively. Data that was normally distributed was presented as the mean, and statistical analysis was performed using a T-Test, one-way analysis of variance (ANOVA) or two-way ANOVA (with Tukey's post-hoc test) for two, more than two groups (1 independent variable) or more than two groups (2 independent variables). For fold change data, statistical analysis was performed using a Wilcoxon Signed-Rank test. For categorical variables, statistical analysis was performed using a Chi-Squared test.

Table 2.15 - Antibodies used for Western blots. The primary and secondary antibodies used for Western blots, including their host species, dilution's, final concentrations, manufacturers, and product codes. Abbreviations: HRP – Horseradish Peroxidase.

Protein	Labels	Host Species	Stock Concentration	Dilution	Final Concentration	Manufacturer	Product Code
CD163	Hofbauer Cell Marker	Rabbit	771 µg/mL	1:1000	0.771 µg/mL	Abcam	ab182422
CD206	Hofbauer Cell Marker	Mouse	1000 µg/mL	1:2000	0.5 µg/mL	Protein Tech	60143-1-Ig
β-Actin	Loading Control	Rabbit	11 µg/mL	1:1000	0.011 µg/mL	Cell Signalling Tech	4967S
Anti-Rabbit HRP	Secondary	Goat	µg/mL	1:1250	µg/mL	Dako	P0448
Anti-Mouse HRP	Secondary	Goat	µg/mL	1:1250	µg/mL	Dako	P0447

Table 2.16 - Buffers used for Western blots. Abbreviations: TBS – Tris buffered saline, TBST – Tris buffered saline with Tween-20, NaCl – Sodium chloride.

Buffer	Constituents
10X TBS	0.2 M Trizma base, 1.5 M NaCl, pH 7.4 in dH_2O
10X Running Buffer	0.25 M Trizma base, 1.92 M Glycine and 0.03 M SDS in dH_2O
10X Transfer Buffer	0.25 M Trizma base and 1.92 M Glycine in dH_2O
1X Transfer Buffer with Methanol	20% Methanol in 1X Transfer Buffer in dH_2O
TBST	0.03% Tween-20 in 1X TBS in dH_2O
Glycine Strip Buffer	0.1 M Glycine, pH 2.5 in dH_2O

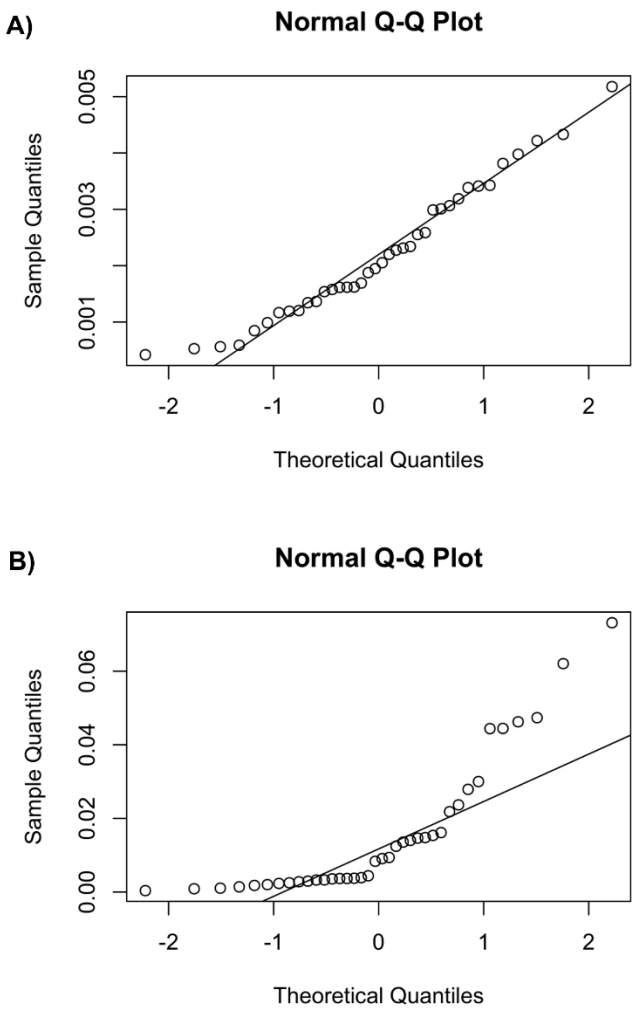

Figure 2.25 - Example Q-Q Plots for assessing normality of data. A) Example of a Q-Q plot that shows data points are along the normal distribution. B) Example of a Q-Q plot that shows data points are not along normal distribution.

Chapter 3 - The impact of physiological maternal glucose fluctuations on the human placenta

3.1 Introduction

Despite treatment of GDM to normalise maternal glucose levels to those within the normoglycaemic range, infants can still be born LGA, however the mechanism behind this is unclear. Recent work from our group and others have used CGM to show that this may be explained by subtle fluctuations in glucose levels over the 24-hour day that are undetectable by other measures[36,56,60–62]. In the study by Law *et al.* (2019) glycaemic profiles were assessed in women with GDM who wore masked-CGM for 7 days between 30-32 weeks' gestation, and pregnancy outcomes were reported. While mean maternal glucose levels did not differ between women with GDM that delivered LGA or AGA infants, and were considered 'normoglycemic', women that went on to deliver LGA infants had temporal periods of mild hyperglycaemia. For example, women with GDM that delivered LGA infants had a higher nocturnal glucose (6.0 ± 1.0 mM) for 6-hours overnight (00:30-06:30), compared to mothers of AGA infants (5.5 ± 0.8 mM; p=0.005)[62]. It is unclear how this small change in glucose impacts on fetal weight, however many *in vivo* and *in vitro* studies have shown that maternal hyperglycaemia alters placental development and function[93,262–265,416–420], contributing to LGA and poor pregnancy outcomes in GDM. However, many current *ex vivo* and *in vitro* studies are limited as they utilise supraphysiological concentrations of glucose (≥ 25 mM)[262,282,420]. The impact of subtle fluctuations in glucose, within a normoglycaemic range over time (as observed by CGM), have not been investigated. Although not at physiological levels, several studies have demonstrated that fluctuating glucose levels (cycling between ~5 mM and ~20-50 mM) can influence cellular function and gene expression in other tissues[421–423].

Therefore, an *ex vivo* placental explant model was employed to mimic *in vivo* maternal glucose fluctuations in women with GDM who had LGA and AGA infants and determine the effect on the placental transcriptome and function.

3.2 Hypothesis

Temporal periods of mild hyperglycaemia in GDM alters placental development and function, which could lead to LGA.

3.3 Aims

1. To develop an *ex vivo* human placental explant model to mimic physiological *in vivo* maternal glucose fluctuations in women with GDM LGA and GDM AGA pregnancies.
2. To assess the impact of physiological glucose fluctuations on the placental transcriptome.

3.4 Results

3.4.1 *In vivo* glucose fluctuations associated with LGA in GDM pregnancies can be modelled in *ex vivo* placental villous explants

An *ex vivo* placental villous explant model was utilised to mimic *in vivo* maternal glucose fluctuations evident in CGM profiles of women with GDM. For acute treatments (48 hours), explants were cultured in normoglycaemic conditions (5.5 mM) for the first day of culture. Explants were then exposed to fluctuating 5- and 5.5-mM glucose (5/5.5 mM) or constant 5, 5.5 or 7 mM glucose. For the 5/5.5 mM fluctuating condition, medium was replenished to 5 mM glucose at 18 and 42 hours, and 5.5 mM glucose at 24 hours. For the constant conditions, medium was replenished to 5, 5.5 or 7 mM glucose at 18, 24 and 42 hours.

To determine if the concentration of glucose in the medium and the frequency of medium changes were suitable for modelling physiological glucose levels in placental explants glucose was measured at each time point (n=5-9). Input concentrations of 7 mM glucose decreased to within normoglycemic levels of 5.36±0.36 mM at 18 hours and 5.77±0.40 mM at 42 hours and mild hyperglycaemic levels of 6.74±0.16 mM at 24 hours and 6.9±0.16 mM at 48 hours (Figure 3.1). cInput concentrations of constant 5.5 mM glucose and fluctuating 5/5.5 mM glucose were at normoglycaemic levels. For the 5.5 mM condition, glucose levels were 3.96±0.10, 5.40±0.17, 4.10±0.22 and 5.39±0.16 mM at 18, 24, 42 and 48 hours, respectively (Figure 3.1). For the 5/5.5 mM condition, glucose levels remained more stable throughout culture, with levels of 4.38±0.27, 4.97±0.12, 4.62±0.25 and 4.99±0.10 mM at 18, 24, 42 and 48 hours, respectively (Figure 3.1). This glucose profile (5/5.5 mM) best represented women with GDM that have appropriate control of glycaemia (normoglycaemia), likely to go onto develop AGA infants[62]. Input concentrations of 5 mM glucose decreased to near hypoglycaemic levels of 3.31±0.07 mM at 18 hours and 3.51±0.10 mM at 42 hours and normoglycaemic levels of 4.71±0.11 mM at 24 hours and 4.85±0.08 mM at 48 hours (Figure 3.1). This glucose profile (5 mM) best represented women with periods of

hypoglycaemia, with glucose below the recommended time in range for CGM (3.5-7.8 mM)[55]. Occurrences of maternal hypoglycaemia in pregnancy have been reported, particularly during the first trimester of pregnancy, in pregnant women with T1DM treated with insulin therapy[276,277]. Due to the current focus on GDM, this was therefore not within the scope of this study.

The 5/5.5 mM (normoglycaemia) and 7 mM (mild hyperglycaemia) conditions were therefore selected for further study as they best represented *in vivo* conditions in GDM AGA and GDM LGA pregnancies, respectively. Furthermore, the suitability of these concentrations for longer-term exposure was also assessed. For longer-term treatments (4 days + 96 hours) explants were cultured in normoglycaemic conditions (5.5 mM) glucose for 4 days to allow for the syncytium to degenerate and regenerate and then exposed to either fluctuating 5/5.5 mM glucose or constant 7 mM glucose for 96 hours. Similar glucose profiles were observed in longer-term treatments, with input concentrations of 5/5.5 mM glucose remaining stable and within normoglycaemic levels. Input concentrations of 7 mM glucose remained mildly hyperglycaemic at all time points, with levels between 6.49±0.14 – 6.93±0.22 mM at 18, 42, 66 and 90 hours and levels between 7.23±0.05 – 7.63±0.11 mM at 24, 48, 72 and 96 hours (n=4, Figure 3.2).

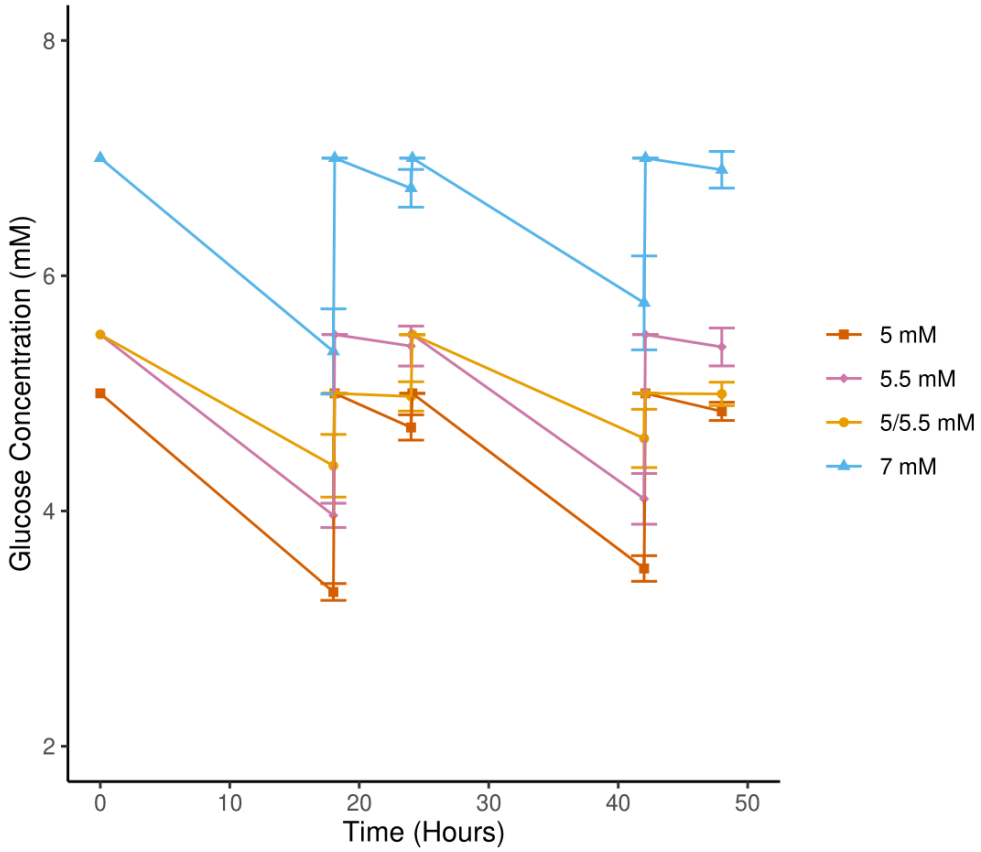

Figure 3.1 – Acute glucose treatments in placental explants for 48 hours. Glucose concentrations (mM) were assessed in culture medium of placental explants exposed to either constant 5, 5.5 or 7 mM glucose or fluctuating 5/5.5 mM glucose. Data is presented as the mean±SEM (n=5-9).

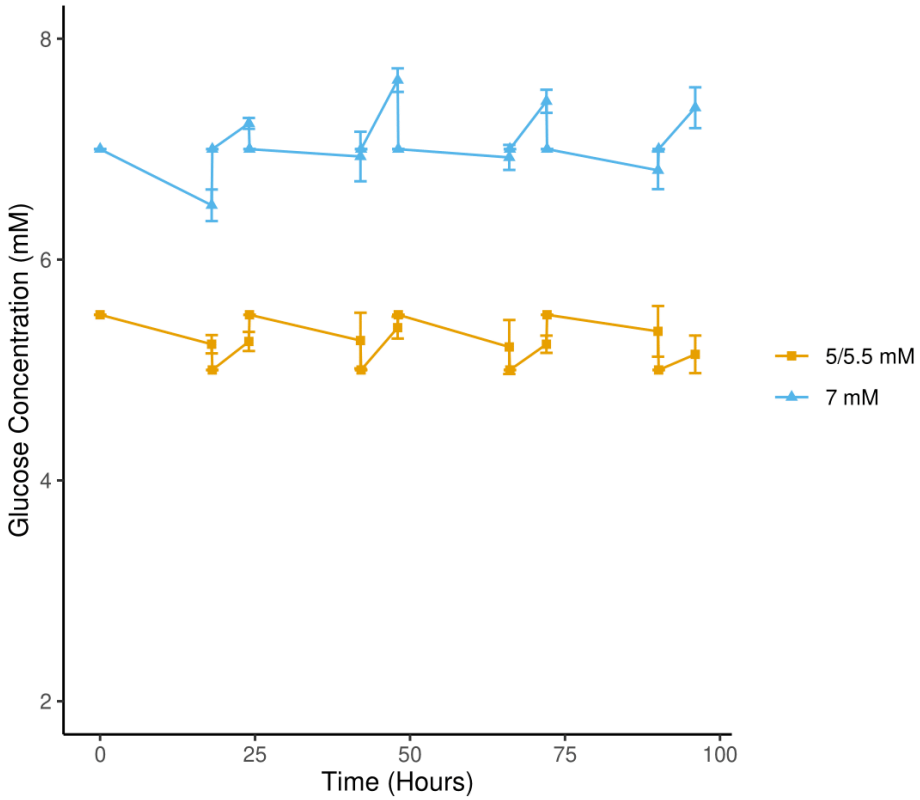

Figure 3.2 – Longer-term glucose treatments in placental explants for 96 hours. Glucose concentrations (mM) were assessed in culture medium of placental explants exposed to either constant 7 mM glucose or fluctuating 5/5.5 mM glucose. Data is presented as the mean±SEM (n=4).

The osmolality of conditioned medium was also assessed at each time point using an Osmometer. The osmolality of explant medium containing 5.5 mM glucose and 7 mM glucose was 293.60±4.70 and 294.20±5.08 mOsm/kg, respectively. In acute treatments, this increased in the first 18 hours of culture (307.11±7.41 and 317.00±5.35 mOsm/kg for 5/5.5 mM and 7 mM, respectively) and then returned to levels between 296 and 301 mOsm/kg at further timepoints (Figure 3.3A). A similar pattern was observed in longer-term treatments (Figure 3.3B). Osmolality was not altered by 7 mM glucose in acute treatments ($p>0.05$, n=9) or longer-term treatments ($p>0.05$, n=4).

3.4.2 Impact of glucose fluctuations on hCG secretion in explants

To assess syncytial regeneration and the ability of placental explants to secrete placental hormones, hCG levels were assessed in conditioned medium of acute glucose treatments using a hCG ELISA (α- and β- isoforms) (Figure 3.4A, n=9). Where explant weights were available, hCG secretion levels were normalised to explant weight (mg, n=4; Figure 3.4B). At 18 hours, hCG levels were 0.52±0.32 and 0.52±0.35 mIU/mL/mg in 5/5.5 mM and 7 mM, respectively. At further time points hCG levels were below the detection level for the ELISA (Figure 3.4B), however, this is expected as the syncytium degenerates after the first few days of culture, resulting in a decrease in hCG secretion[322]. hCG levels were not altered by 7 mM glucose ($p>0.05$, n=4).

In longer-term treatments, hCG secretion was assessed in conditioned medium using a hCG ELISA. However, after two days of explant culture, hCG levels were below the detection level for the ELISA for the remaining 8 days (data not shown). Therefore, conditioned medium was concentrated using Amicon Ultra-0.5 centrifugal filters to ensure the hCG was not being diluted by the 2 mLs of culture medium used in each well. A more sensitive, β-hCG ELISA was then performed, which detects levels within a smaller range (0-200 mIU/mL). Figure 3.5 shows that the hCG secretion was initially high at the beginning of culture (day 1 [D1]) prior to glucose treatments. However, hCG levels after the second day of culture were between 0.43±0.33 and 1.33±0.77 mIU/mL/mg for 5/5.5 mM and 2.19±1.58 and 0.78±0.69 mIU/mL/mg for 7 mM, respectively. This suggests that hCG secretion was minimal in these samples during glucose treatments between day 5 (D5) and day 8 (D8), despite trying a more sensitive ELISA.

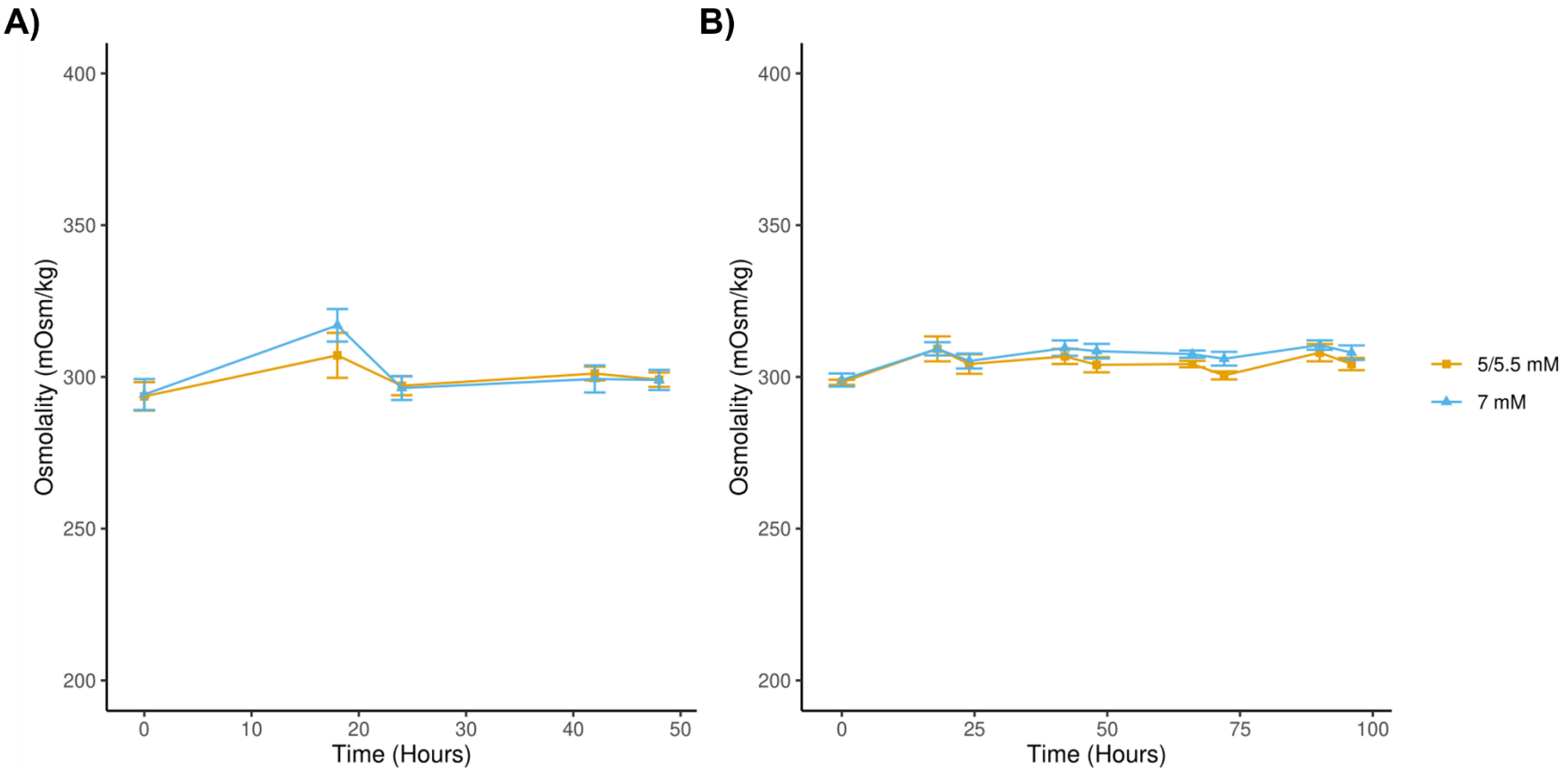

Figure 3.3 – Osmolality of culture medium during acute and longer-term glucose treatments in placental explants. Osmolality (mOsm/kg) was assessed in culture medium of placental explants cultured in fluctuating 5/5.5 or constant 7 mM glucose for 48 hours (acute treatments; A) and 4 days + 96 hours (longer-term treatments; B) at each time point using an Osmometer. Data is presented as the mean±SEM (n=9 for acute treatments; n=4 for longer-term treatments) and statistical analysis was performed using a Two-Way ANOVA on log transformed data.

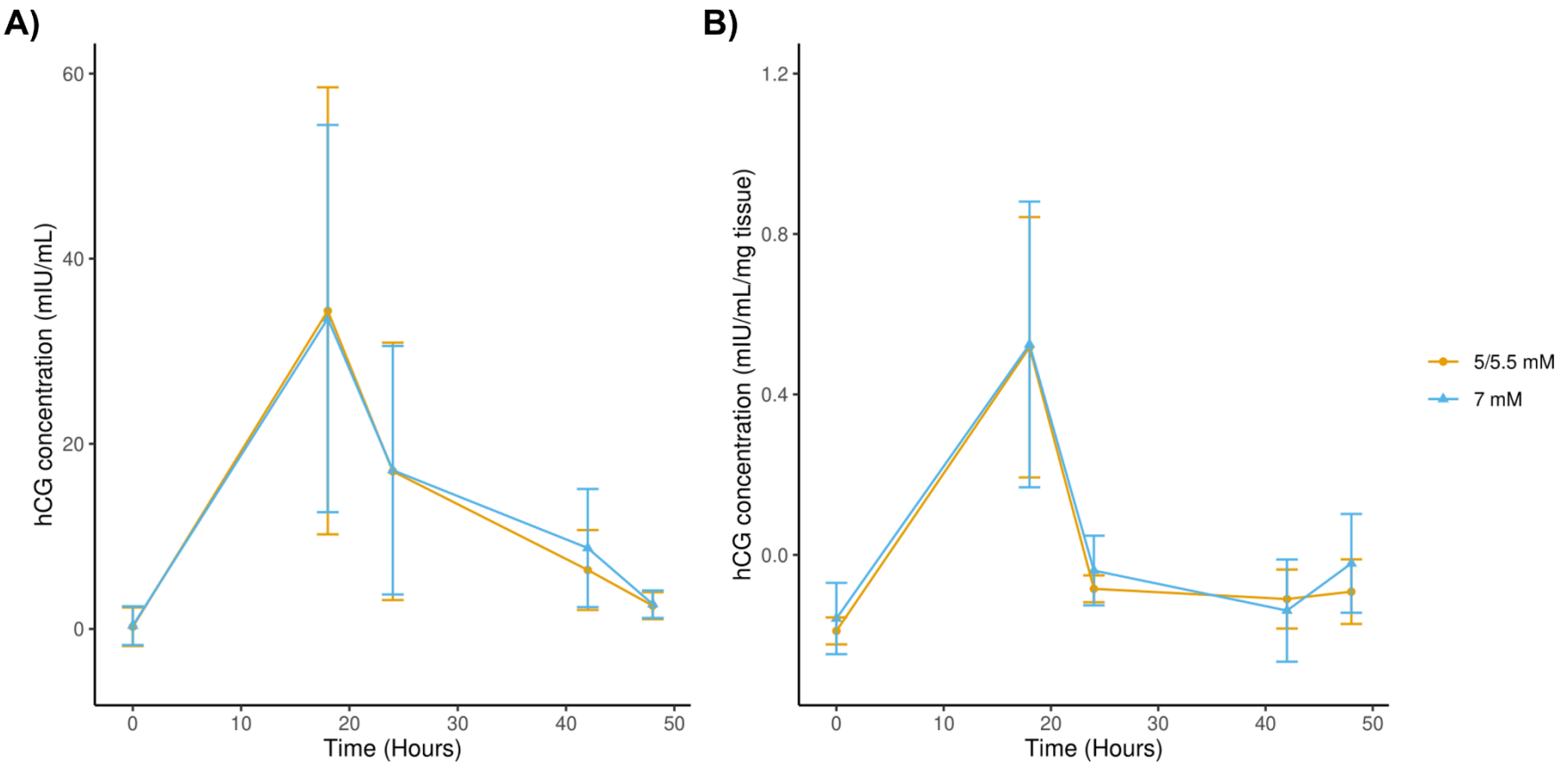

Figure 3.4 - hCG secretion from placental explants following acute glucose treatments. An α- and β-hCG ELISA was performed on conditioned medium from placental explants cultured in either fluctuating 5/5.5 mM or constant 7 mM glucose for 48 hours to assess hCG release (mIU/mL). A) Data is presented as the mean±SEM (n=9). B) Data is normalised to explant tissue weight (mg) and is presented as the mean±SEM (n=4). Statistical analysis was performed using a Two-Way ANOVA on log transformed data.

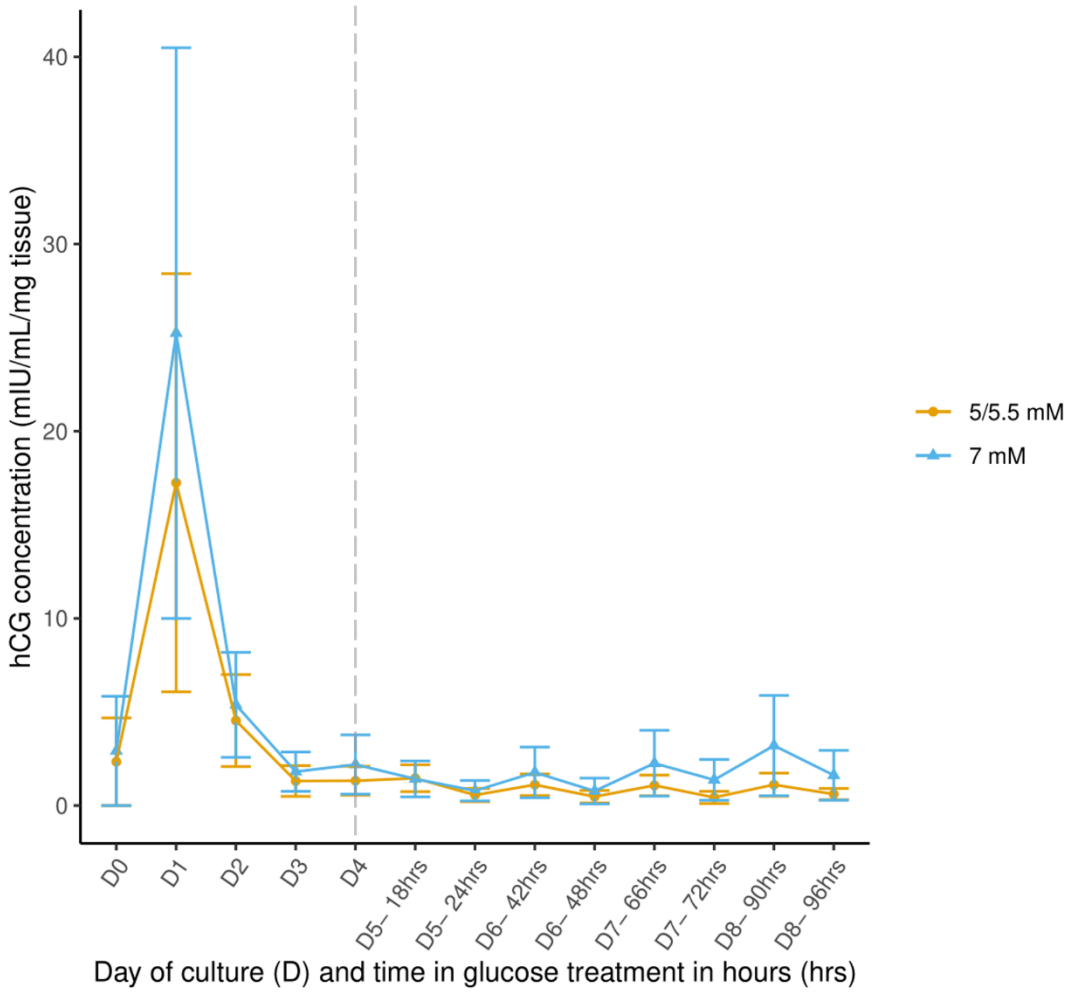

Figure 3.5 - hCG secretion from placental explants following longer-term glucose treatments for 96 hours. A more sensitive β-hCG ELISA was performed on conditioned medium from placental explants cultured in either fluctuating 5/5.5 mM glucose or constant 7 mM glucose for 96 hours that was concentrated prior to performing the assay to assess hCG release (mIU/mL). Data is normalised to explant tissue weight (mg) and is presented as the mean±SEM (n=4). Explants were cultured in normoglycaemic conditions (5.5 mM glucose) for the first 4 days of culture (D0-D4) before starting glucose fluctuations, to allow for syncytial degeneration and regeneration. The dotted line represents the point at which the explants were exposed to glucose treatments at day 4 (D4), and therefore the x axis labels denote the day of culture (D), and the cumulative time the explants have been exposed to the glucose treatment in hours (Hrs).

3.4.3 Impact of glucose fluctuations on placental morphology

As there were issues with the detection range of the hCG ELISA in longer-term cultures, despite trying alternative methods, explant morphology was examined using H&E staining and immunohistochemistry for cytokeratin-7. Cytokeratin-7 is an epithelial cell marker which is used in placental tissue to detect trophoblast[115]. These histological methods can be applied to determine if the syncytium is regenerating during culture.

In acute glucose treatments for 48 hours, the syncytiotrophoblast layer had started to lift away from the villi, which has previously been reported in the first 48 hours[115,322] (Figure 3.6A-D). Fetal blood vessels remained intact, with the fetal endothelium present (Figure 3.6A-B). Consistent with previous studies[322], in longer-term experiments where explants were cultured for a total of 8 days, syncytial regeneration was starting to occur, as multinucleated trophoblast could be observed below layers of detached syncytium (Figure 3.6E-H). Fetal blood vessels and their fetal endothelium were more difficult to distinguish at this timepoint, suggesting that the structural integrity of vessels may have been lost over time in culture (Figure 3.6E-F). This was further confirmed by immunohistochemical staining for the endothelial marker CD31. In acute glucose treatments for 48 hours, CD31 labelled the endothelium surrounding open blood vessel lumens (Figure 3.7A-B). To quantify retention of existing placental vessels following acute glucose treatments, the total area of CD31 staining (μm^2) was detected in the tissue using a previously published script[374] and was normalised to the total villous area (μm^2). The CD31 area was not altered by 7 mM glucose (median fold change of 0.91 [0.71-1.13]; p=0.589, n=4; Figure 3.7G), suggesting glucose fluctuations do not impact the number of existing vascular structures. However, in longer-term glucose treatments for 96 hours, while CD31 positive staning was observed, it was more difficult to distinguish open blood vessel lumens (Figure 3.7C-D). This is likely because collapsing of fetal vessels can occur during prolonged explant culture, as the vessels are no longer perfused as *in vivo*[115]. This is in line with findings from previous studies[115], and demonstrates that explants are not an ideal model for assessing placental vasculature.

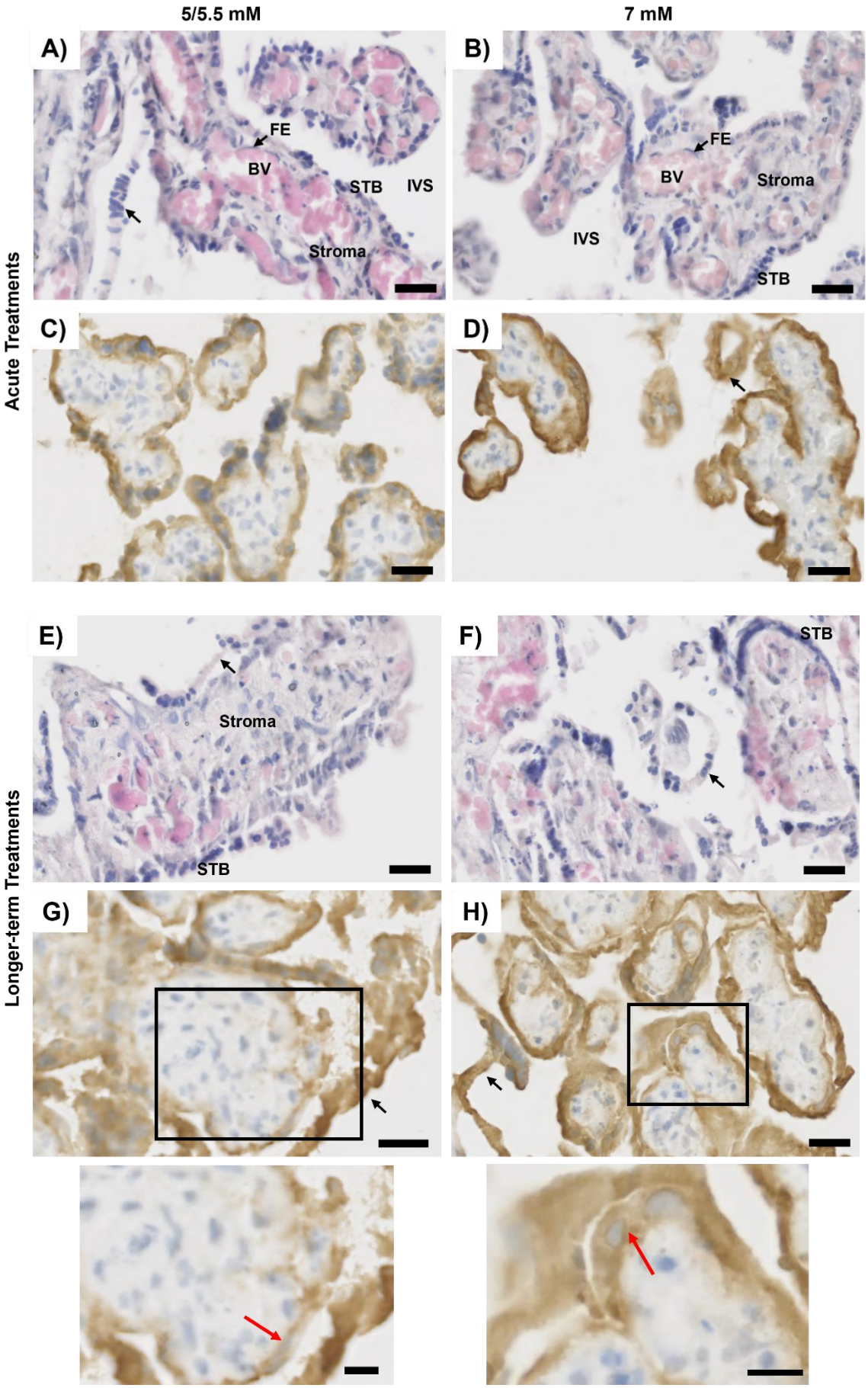
5/5.5 mM
7 mM
Acute Treatments
Longer-term Treatments
A)
B)
C)
D)
E)
F)
G)
H)
FE
BV
STB
IVS
Stroma

Figure 3.6 - Placental explant morphology and syncytial integrity following acute glucose treatments for 48 hours and longer-term glucose treatments for 96 hours. Haematoxylin and Eosin staining was used to assess morphology of placental explants cultured in either fluctuating 5/5.5 mM glucose or constant 7 mM glucose for 48 hours (A-B) or cultured for 4 days in 5.5 mM glucose to allow for syncytial degeneration and regeneration before starting glucose treatments (E-F). Immunohistochemical staining for the trophoblast marker, Cytokeratin-7 was used to assess the presence of the syncytium in placental explants cultured in either fluctuating 5/5.5 mM glucose or constant 7 mM glucose for 48 hours (C-D) or cultured for 4 days in 5.5 mM glucose to allow for syncytial degeneration and regeneration before starting glucose treatments (G-H). Black arrows show the detached syncytium. Scale Bars: 20 µm. Insets: Higher magnification images of explants with longer-term treatments. Red arrows show multinucleated trophoblast below layers of detached syncytium, suggesting syncytial regeneration was starting to occur. Scale Bars: 10 µm. Abbreviations: BV- Blood Vessel; FE – Fetal Endothelium; IVS- Intervillous Space; STB- Syncytiotrophoblast.

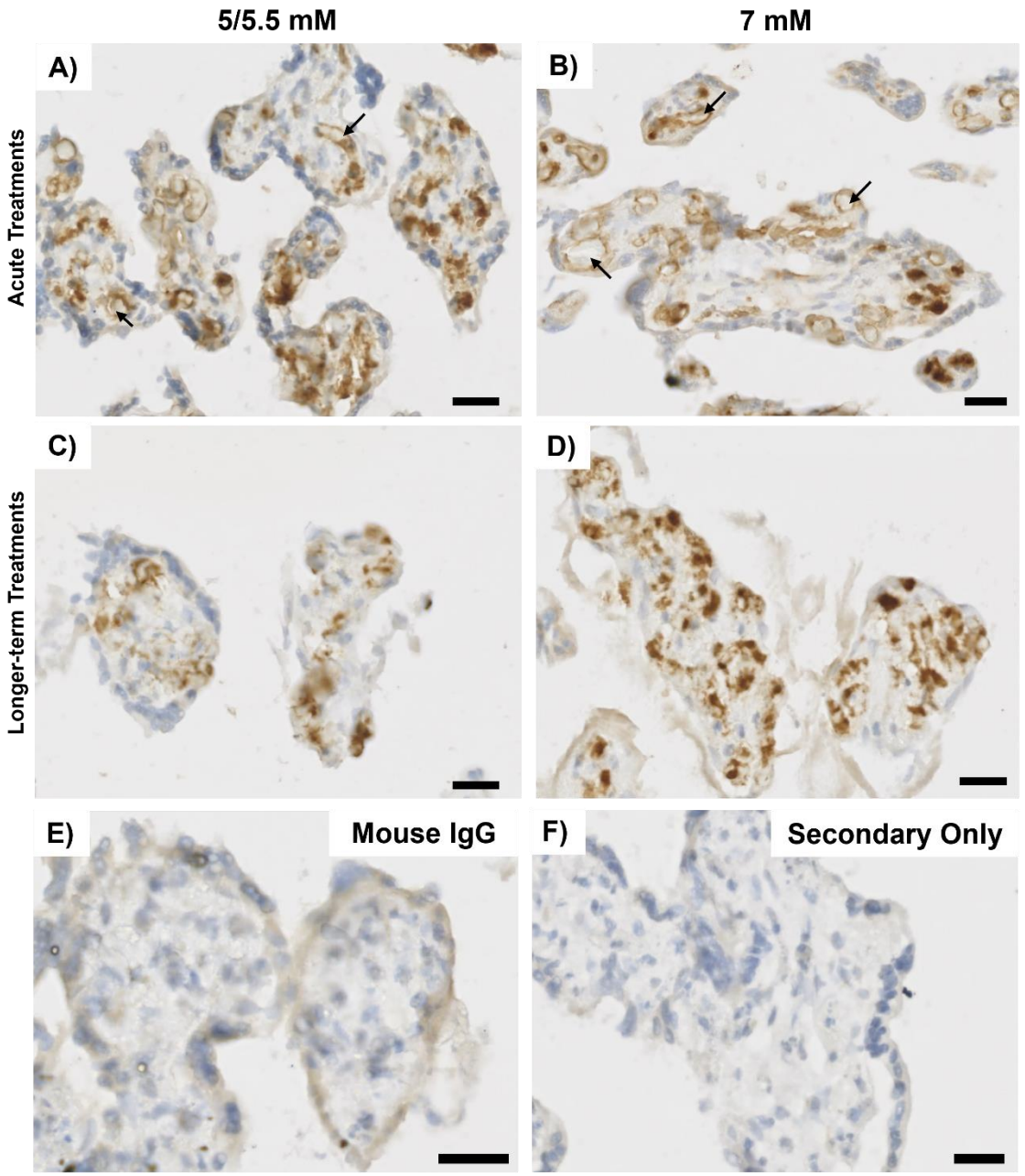
5/5.5 mM
7 mM
A)
B)
C)
D)
E)
Mouse IgG
F)
Secondary Only
Acute Treatments
Longer-term Treatments

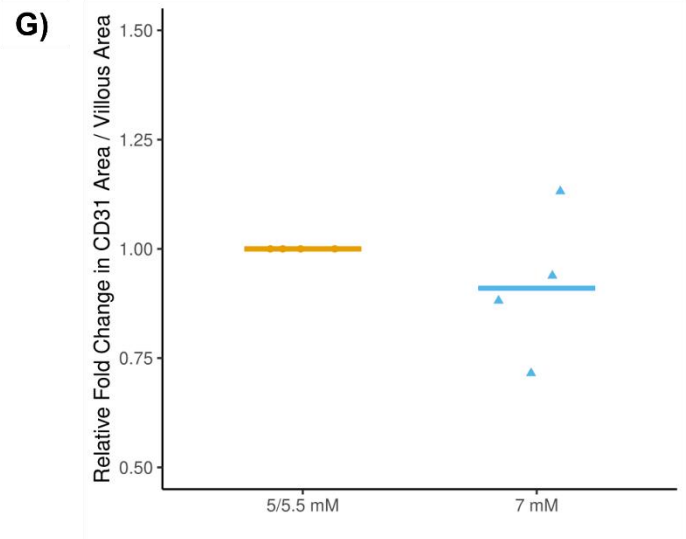
G)
Relative Fold Change in CD31 Area / Villous Area
1.50
1.25
1.00
0.75
0.50
5/5.5 mM
7 mM

Figure 3.7 - Placental blood vessel integrity following acute glucose treatments for 48 hours and longer-term glucose treatments for 96 hours.
Immunohistochemical staining for the endothelial marker, CD31 was used to assess the presence of the fetal endothelium in placental explants cultured in either fluctuating 5/5.5 mM glucose or constant 7 mM glucose for 48 hours (A-B) or cultured for 4 days in 5.5 mM glucose to allow for syncytial degeneration and regeneration before starting glucose treatments (C-D). Arrowheads show the open blood vessel lumens surrounded by CD31 stained fetal endothelium. Controls are also shown, including the non-immune mouse IgG (C) and secondary antibody only control (D). Scale Bars: 20 µm. G) Quantification of the total CD31 area (vascular area; μm^2) normalised to total villous area (μm^2). Data is presented as the median fold change (compared to 5/5.5 mM) and statistical analysis was performed using a Wilcoxon-Signed Rank Test (as data was not normally distributed). Individual points represent individual patient placentae. n=4.

3.4.4 Impact of glucose fluctuations on LDH secretion in explants

As a further assessment of explant viability, levels of LDH release (tissue necrosis) were measured in conditioned medium of acute glucose treatments throughout the culture period (Figure 3.8). There are minimal amounts of LDH in explant medium containing 5.5 mM glucose and 7 mM glucose (0.11±0.037 and 0.10±0.035, respectively; Figure 3.8A), which is likely due to the presence of LDH in FBS used in the medium[424]. Where explant weights (mg) were available, LDH levels were normalised to this (mg, n=4; Figure 3.8B). At 18 hours there was a small increase in LDH, levels were 0.019±0.0021 and 0.016±0.0022 U/mL/mg in 5/5.5 mM and 7 mM treatments, respectively. LDH levels plateaued after this timepoint, and at 48 hours LDH levels were 0.017±0.0024 and 0.014±0.0025 U/mL/mg (5/5.5 mM and 7 mM, respectively; Figure 3.8B). This pattern of release is in line with previous studies[322]. As there was no further increase in LDH across the culture period, this suggests that the tissue was viable and minimal levels of cell death were occurring. In longer-term glucose treatments for 96 hours a similar pattern was observed (Figure 3.9). Overall, lower levels of LDH were observed with 7 mM glucose, compared to 5/5.5 mM glucose in acute and longer-term treatments, however this was not significant ($p>0.05$, n=4).

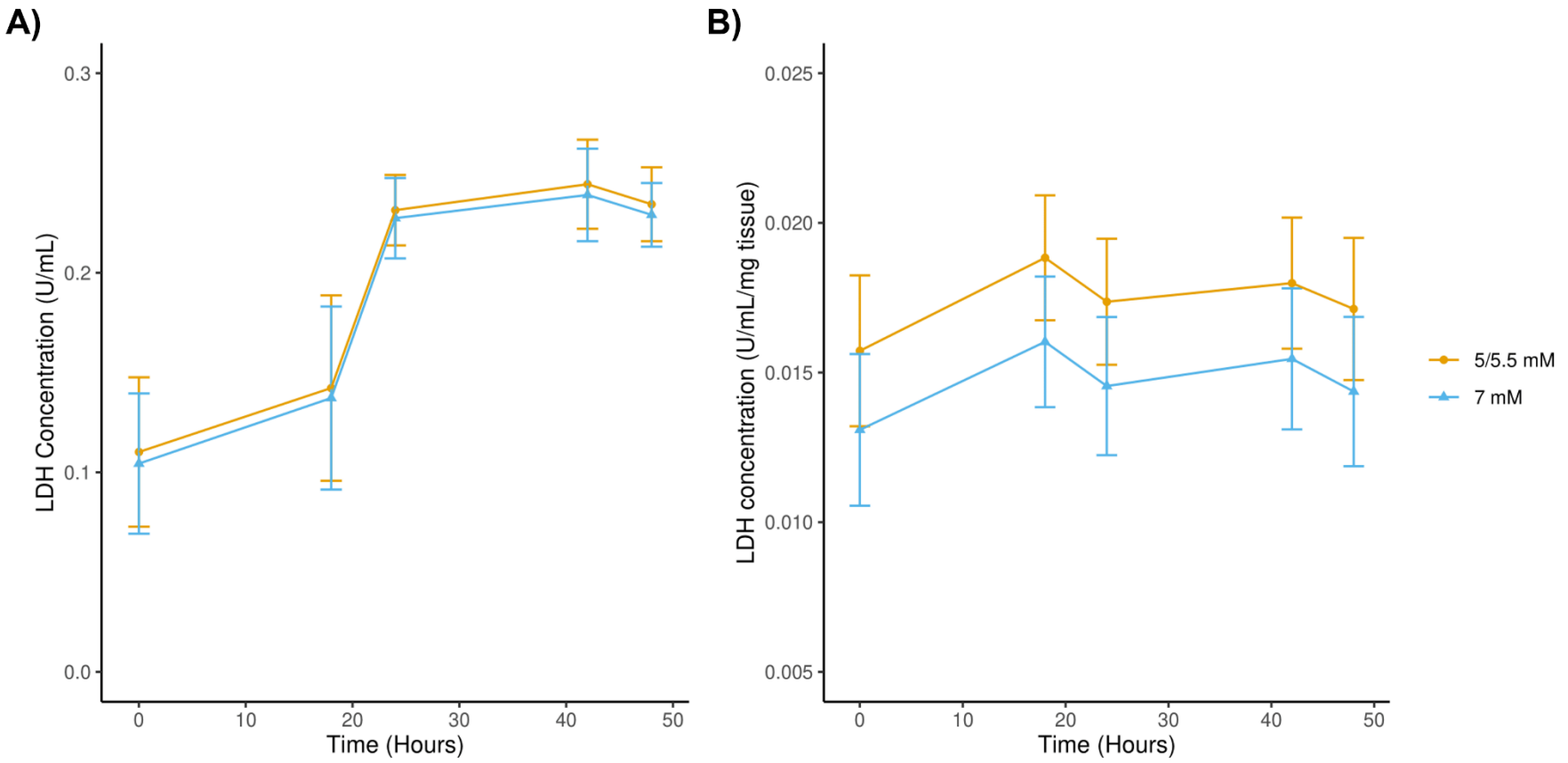

Figure 3.8 - LDH release from placental explants following acute glucose treatments for 48 hours. An LDH assay was performed conditioned medium from placental explants cultured in either fluctuating 5/5.5 mM or constant 7 mM glucose for 48 hours to assess LDH release (U/mL). A) Data is presented as the mean±SEM (n=9). B) Data is normalised to explant tissue weight (mg) and is presented as the mean±SEM (n=4). Statistical analysis was performed using a Two-Way ANOVA.

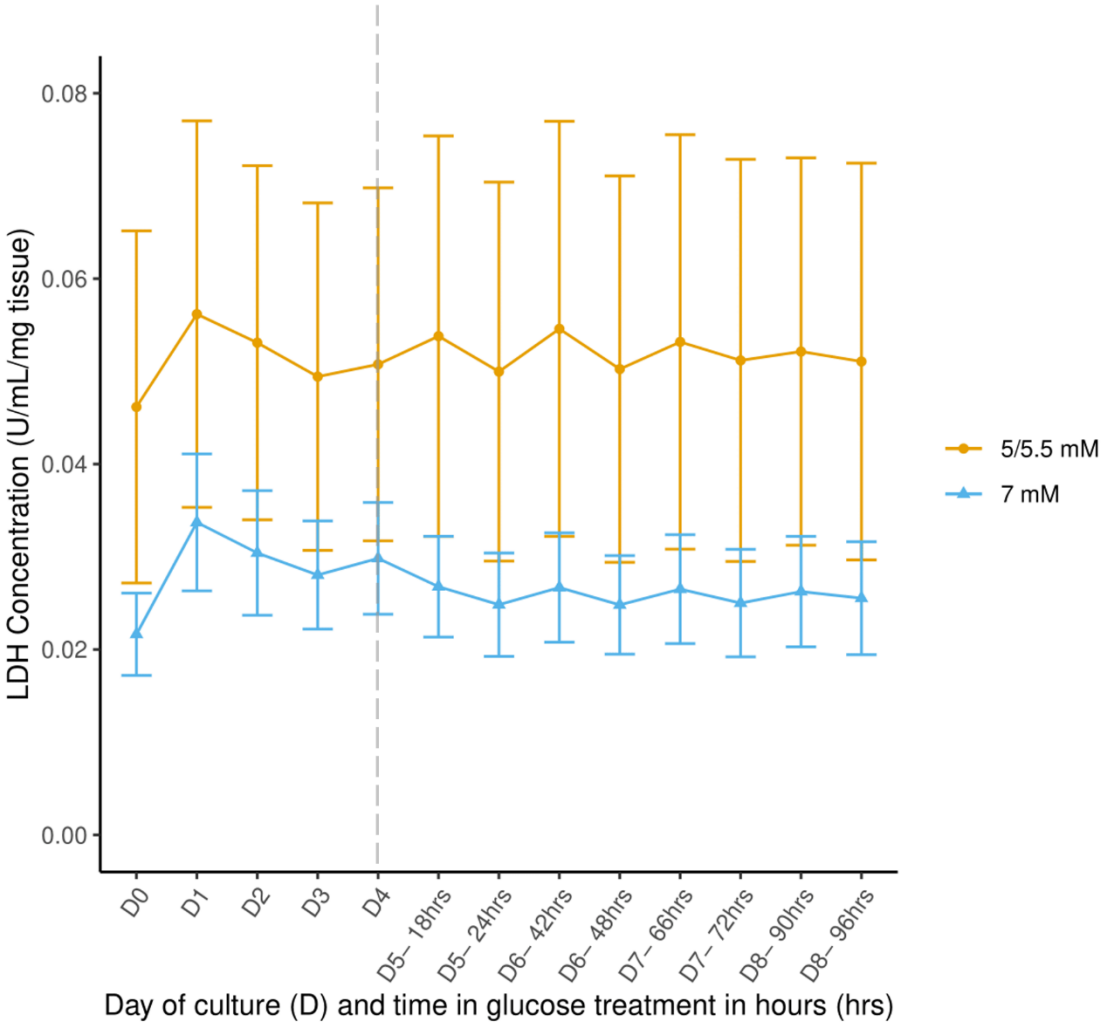

Figure 3.9 - LDH release from placental explants following longer-term glucose treatments for 96 hours. An LDH assay was performed conditioned medium from placental explants cultured in either fluctuating 5/5.5 mM glucose or constant 7 mM glucose for 96 hours assess LDH release (U/mL). Data is normalised to explant tissue weight (mg) and is presented as the mean±SEM (n=4). Explants were cultured in normoglycaemic conditions (5.5 mM glucose) for the first 4 days of culture (D0-D4) before starting glucose fluctuations, to allow for syncytial degeneration and regeneration. The dotted line represents the point at which the explants were exposed to glucose treatments at day 4 (D4), and therefore the x axis labels denote the day of culture (D), and the cumulative time the explants have been exposed to the glucose treatment in hours (Hrs). Statistical analysis was performed using a Two-Way ANOVA on log transformed data.

For further experiments the impact of glucose treatments for 48 hours on placental function were investigated. This was to assess the acute impact of maternal glucose fluctuations in GDM on the placenta. Moreover, glucose profiles of acute treatments showed that input concentrations of 7 mM glucose best represented women with GDM that have suboptimal control of glycaemia, with temporal periods of mild hyperglycaemia, likely to go on to develop LGA infants (Section 3.4.1). Whereas, glucose profiles of longer-term treatments, showed that input concentrations of 7 mM glucose were mildly hyperglycaemic throughout culture, and less representative of physiological glucose fluctuations in GDM LGA (Section 3.4.1).

3.4.5 Impact of glucose fluctuations on placental cell turnover

Placental cell turnover is a key marker of placental development and function and has been linked to altered fetal growth[425–427]. To assess placental cell proliferation in explants treated with glucose, immunohistochemistry was performed for Ki67, which labels cells that are in the proliferative cycle[428] (Figure 3.10). The number of Ki67 positive cells were calculated as a percentage of total cells. There was a trend towards a decrease in Ki67 positive cells in 7 mM glucose (1.16 [0.34-5.41] %) compared to 5/5.5 mM glucose (2.91 [0.89-12.9] %), however this was not significant (p=0.886, n=4).

To assess placental cell apoptosis in explants treated with glucose fluctuations for 48 hours, immunohistochemistry was performed for M30 (cytokeratin 18), as caspases cleave cytokeratin 18 in the early apoptotic stages[429] (Figure 3.11). The number of M30 positive cells were calculated as a percentage of total cells. The number of M30 positive cells was not altered by 7 mM glucose (4.81 [0.50-8.80] % and 4.30 [3.02-8.85] % in 7 mM and 5/5.5 mM glucose, respectively; p=1, n=3).

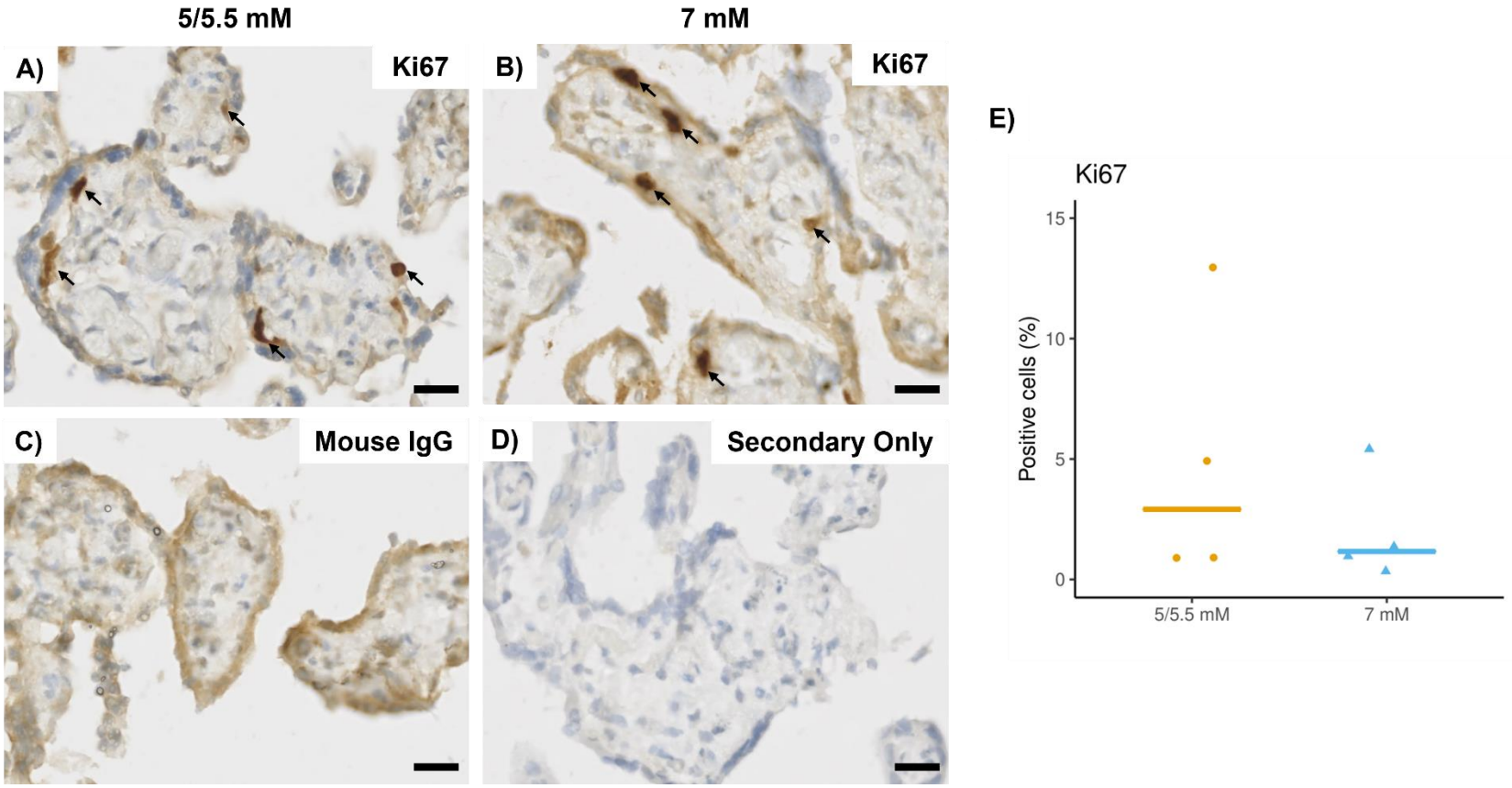

Figure 3.10 - Proliferation (Ki67 expression) in placental explants following acute glucose treatments for 48 hours, measured by immunohistochemistry. A-D) Representative images of Ki67 staining in placental explants are shown in samples treated with fluctuating 5/5.5 mM glucose (A), constant 7 mM glucose (B) and for controls: non-immune IgG (C) and secondary antibody only (D). Scale bars = 20 µm. Arrow heads depict examples of positively stained cells. E) The total number of Ki67 positive cells were calculated as a percentage of total cells. Data is presented as the median and statistical analysis was performed using a Mann-Whitney U test (as data was not normally distributed). Individual points represent individual patient placentae. n=4.

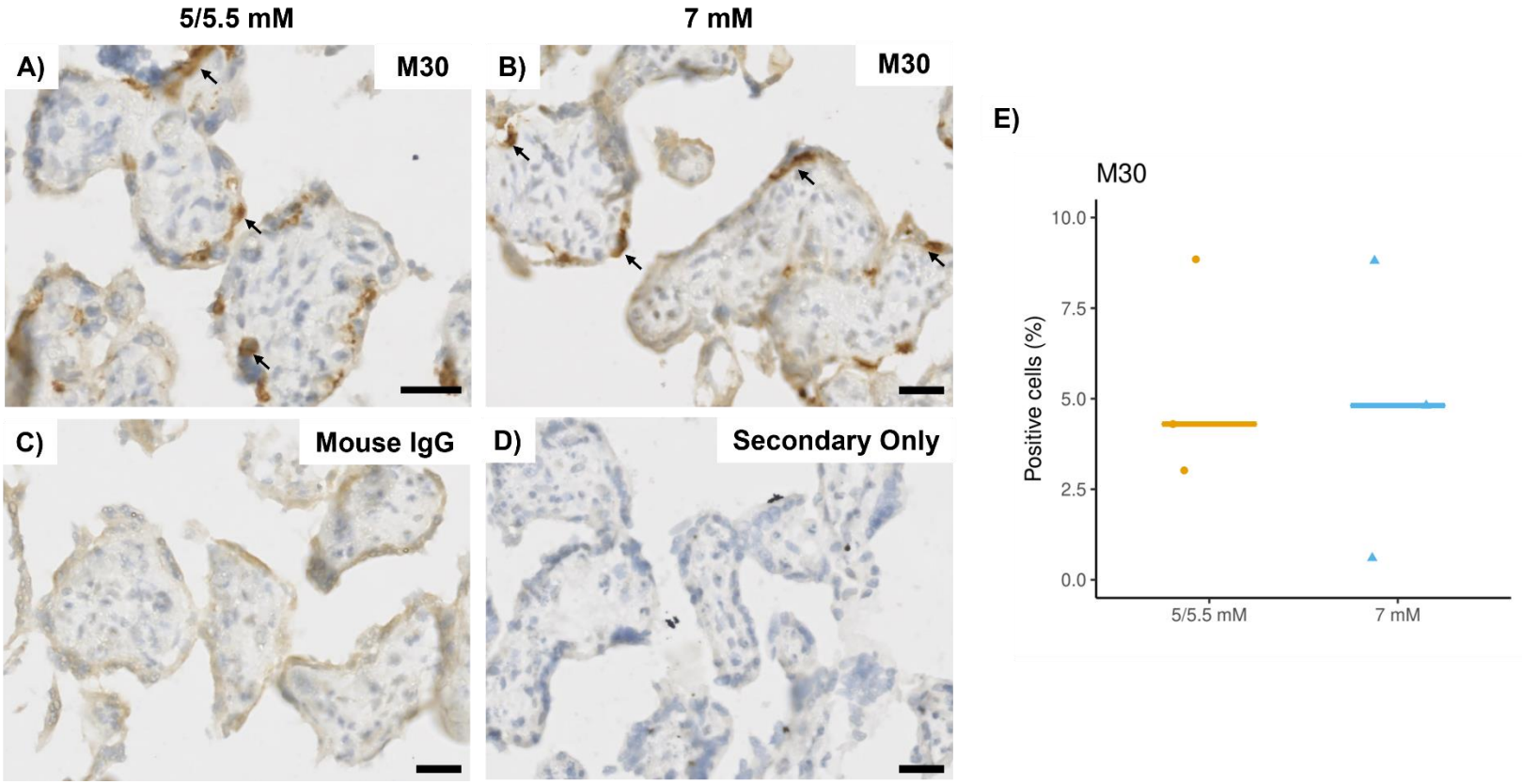

Figure 3.11 – Apoptosis (M30 expression) in placental explants following glucose treatments for 48 hours, measured by immunohistochemistry. A-D) Representative images of M30 staining in placental explants are shown in samples treated with fluctuating 5/5.5 mM glucose (A), constant 7 mM glucose (B) and for controls: non-immune IgG (C) and secondary antibody only (D). Scale bars = 20 µm. Arrow heads depict examples of positively stained cells. E) The total number of M30 positive cells were calculated as a percentage of total cells. Data is presented as the median and statistical analysis was performed using a Mann-Whitney U test (as data was not normally distributed). Individual points represent individual patient placentae. n=3.

3.4.6 Impact of glucose fluctuations on the placental transcriptome

As glucose fluctuations did not impact placental cell turnover or hCG secretion, the potential functional impact of glucose fluctuations was predicted by performing RNA sequencing on placental explants treated with acute glucose fluctuations for 48 hours (n=5), followed by functional enrichment analysis. A principal component analysis (PCA) plot was generated to show clusters of samples based on their similarity. Points that are clustered near each other are biologically similar[430]. The PCA plot of placental explant RNA samples shows that clustering was based on each patient, not by glucose treatment (Figure 3.12). This demonstrates the inherent variability between placental samples from different patients. Therefore, all analyses to assess differential gene expression between 5/5.5 mM and 7 mM glucose, were designed to incorporate the patient variable into the design formula and to enable matched sample analysis[390,391].

A total of 34,386 transcripts were detected in placental explants. Treatment with 7 mM glucose altered 584 transcripts ($p<0.05$ and a Log_2FC of <-0.5 and >0.5); of these, 128 were upregulated and 456 were downregulated (Figure 3.13). Additionally, 30 of the altered transcripts were long non-coding RNAs (lncRNAs; 7 upregulated and 23 downregulated). All differentially expressed genes and lncRNAs, their associated Log_2FC and p values can be seen in **Appendix 5** and **Appendix 6**, respectively.

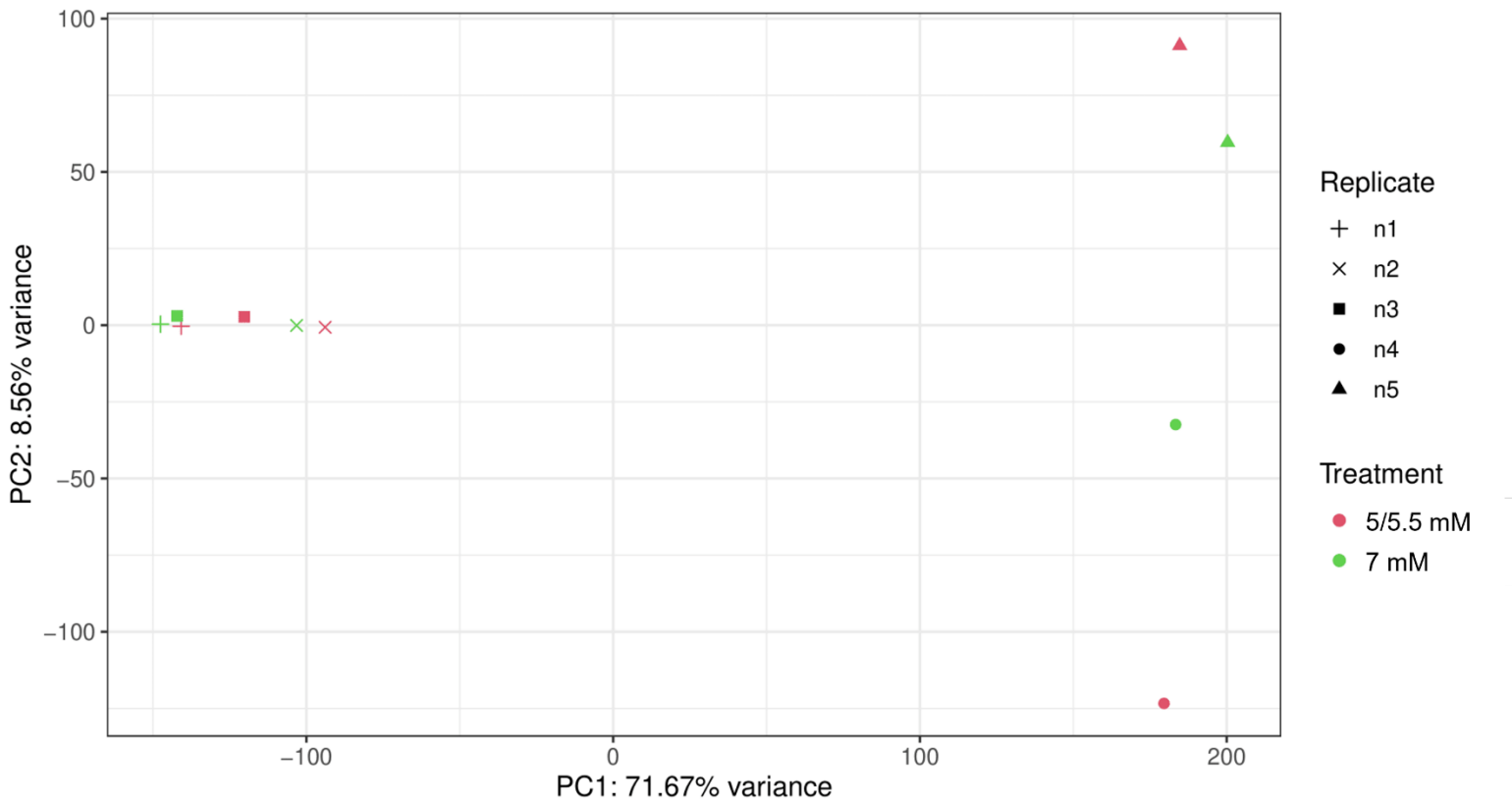

Figure 3.12 - PCA plot of sequenced placental explants following acute glucose treatments for 48 hours. Colour indicates treatment with either fluctuating 5/5.5 mM glucose (**red**) or constant 7 mM glucose (**green**). Different shapes represent individual patient placentae (n=5).

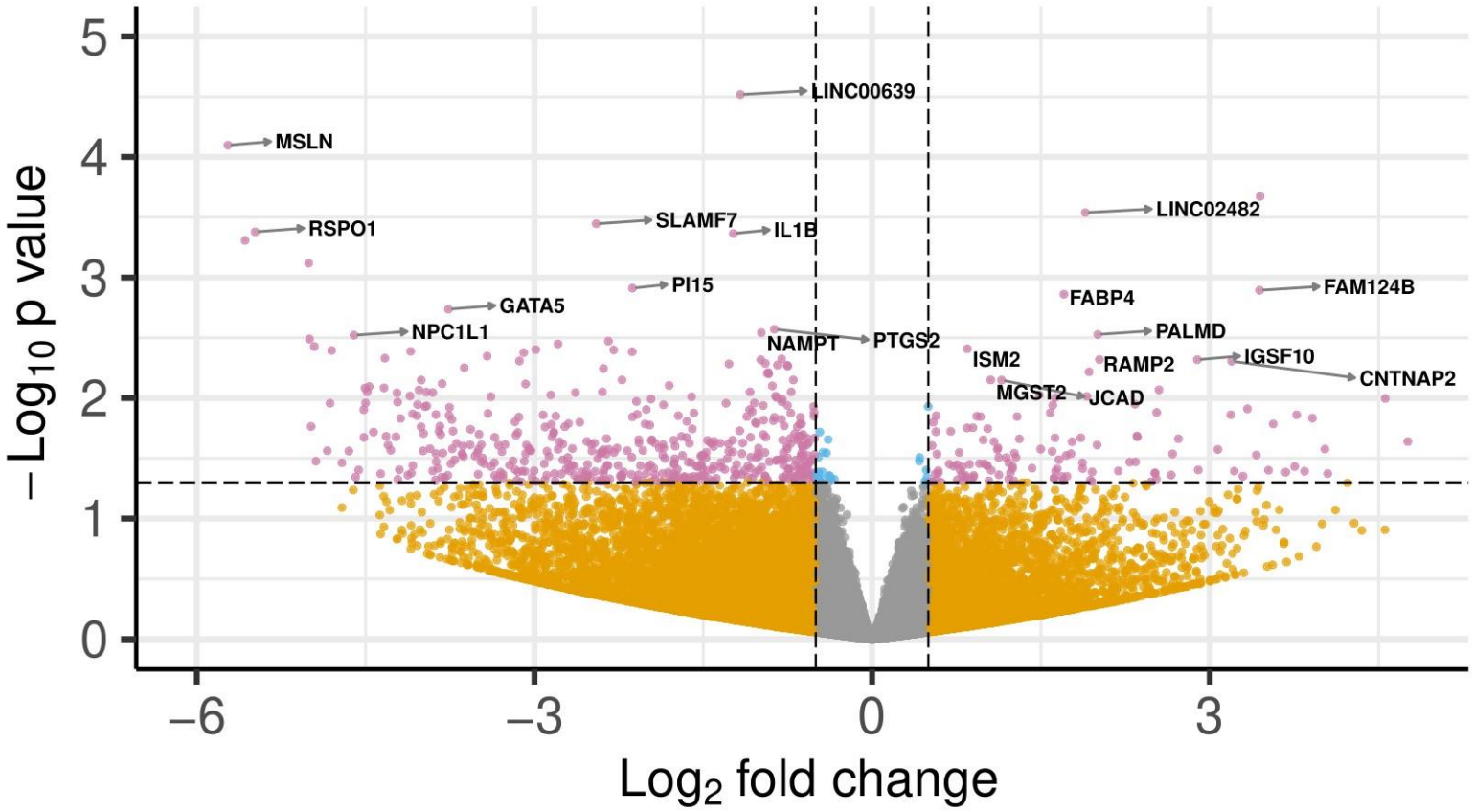

Figure 3.13 – Volcano plot representing differentially expressed genes altered by 7 mM glucose in placental explants following acute glucose treatments for 48 hours. Genes significantly upregulated or downregulated in placental explants cultured for fluctuating 5/5.5 mM glucose or constant 7 mM glucose for 48 hours. Horizontal dashed line represents p=0.05, the vertical dashed lines represent a Log2FC of ± 0.5 equivalent to a fold change of 1.4 and -0.71. NS = grey, significant p value = blue, significant Log2FC = orange, significant p value and Log2FC = pink. The top 10 upregulated and downregulated annotated genes are labelled. Volcano plot generated using EnhancedVolcano in R.

3.4.6.1 Predicted functional impact of genes altered by glucose fluctuations on placental function

To determine the functional impact of gene expression changes elicited by 7 mM glucose treatments, functional enrichment analyses were performed. Both over representation analysis (ORA) and ingenuity pathway analysis (IPA) were utilised to predict functional roles of altered genes, since ORA can predict functional consequences but is unable to predict the direction of change, whilst IPA takes into consideration the direction of Log_2FC of the genes, and therefore can predict whether a function or pathway appears to be activated and deactivated based on a Z-score[400]. Cytoscape and ClusterOne were also used to predict interactions between the protein counterparts of DEGs and identify highly connected regions[404,405].

3.4.6.1.1 Predicted functions

ORA revealed GO terms associated with DEGs, including response to chemokine (FDR: 7.70E-04, Enrichment Ratio [ER]: 3.84), interleukin-1 production (FDR: 0.006, ER: 5.07), response to interleukin-1 (FDR: 0.0051, ER: 4.01), regulation of vascular development (FDR: 0.0011, ER: 3.21) and angiogenesis (FDR: 0.0090, ER: 2.37). A summary of the overrepresented GO terms can be seen in Figure 3.14. Similarly, IPA predicted roles for DEGs including, the inflammatory response (p=3.8E-13-7.79E-06), endocrine system disorders (p=3.92E-12-5.08E-06), cardiovascular system development and function (p=1.28E-11-7.39E-06) and cardiovascular disease (p=1.57E-11-7.73E-06) (Figure 3.14).

Further analysis using IPA revealed that DEGs were predicted to reduce the inflammatory response (p=1.38E-12, Z-score=-3.530) and activation of macrophages (p=1.94E-07, Z-score=-2.017), and inhibit the development of vasculature (p=1.28E-11, Z-score=-3.386), angiogenesis (p=1.44E-10, Z-score=-3.386), vasculogenesis (p=5.88E-10, Z-Score=-3.465), endothelial cell development (p=5.40E-08, Z-score=-3.044) and proliferation of endothelial cells (p=1.62E-07, Z-score=-2.790). A summary of IPA predicted functions can be seen in Figure 3.15.

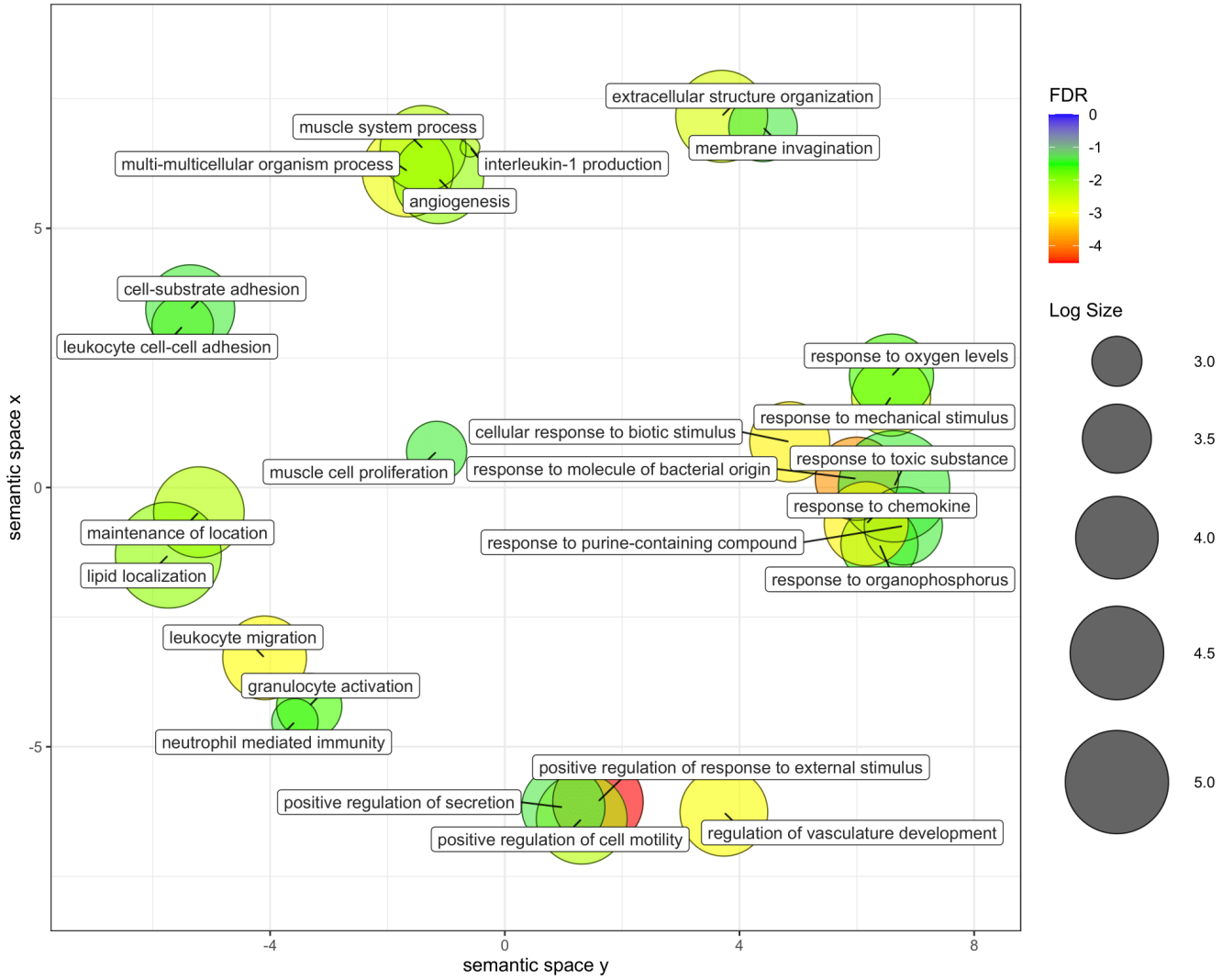

Figure 3.14 - Gene ontology (GO) terms associated with 7 mM glucose in placental explants determined by over representation analysis (ORA). DEGs (p<0.05, Log2FC -0.5< or >0.5) that were altered in placental explants treated with constant 7 mM glucose compared to fluctuating 5/5.5 mM glucose were inputted into WebGestalt for GO analysis. Bubble plot with colour representing the FDR value, where red is the most significant. Size of bubbles represent the generality of the GO terms, where smaller bubbles indicate more specific terms, and larger bubbles represent more general terms. Plot generated using REVIGO.

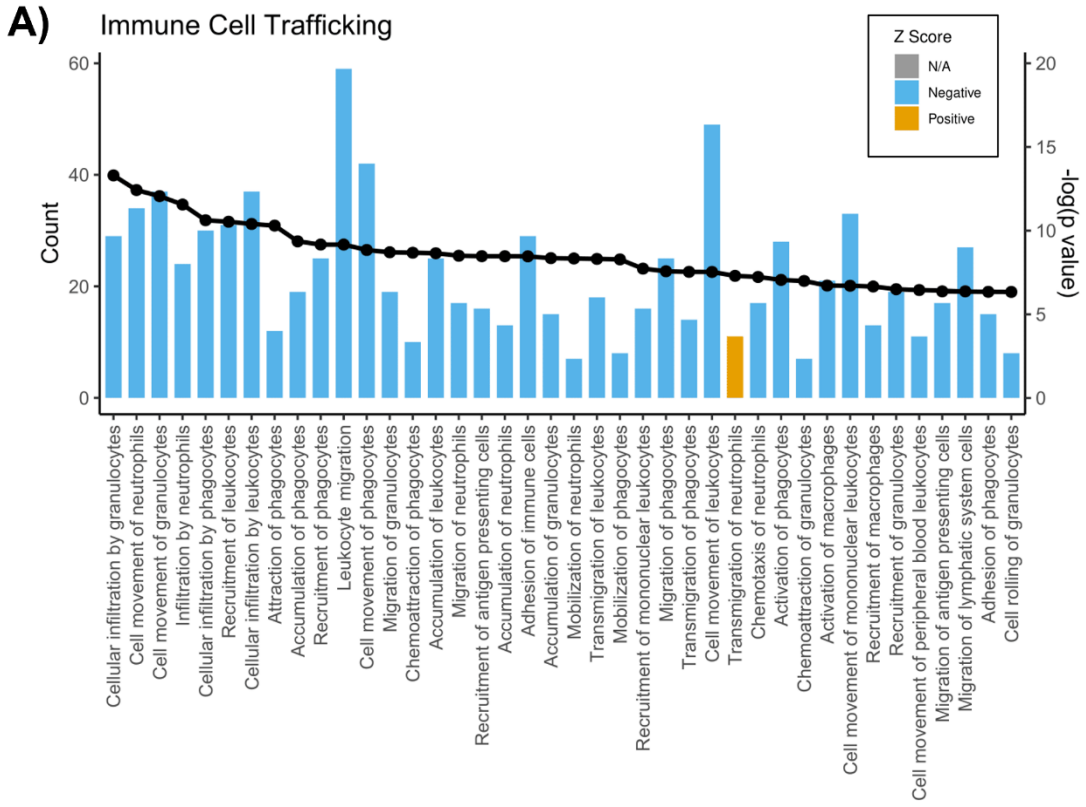
A)
Immune Cell Trafficking
Z Score
N/A
Negative
Positive
Count
-log(p value)
Cellular infiltration by granulocytes
Cell movement of neutrophils
Cell movement of granulocytes
Infiltration by neutrophils
Cellular infiltration by phagocytes
Recruitment of leukocytes
Cellular infiltration by leukocytes
Attraction of phagocytes
Accumulation of phagocytes
Recruitment of phagocytes
Leukocyte migration
Cell movement of phagocytes
Migration of granulocytes
Chemoattraction of phagocytes
Accumulation of leukocytes
Migration of neutrophils
Recruitment of antigen presenting cells
Accumulation of neutrophils
Adhesion of immune cells
Accumulation of granulocytes
Mobilization of neutrophils
Transmigration of leukocytes
Mobilization of phagocytes
Recruitment of mononuclear leukocytes
Migration of phagocytes
Transmigration of phagocytes
Cell movement of leukocytes
Transmigration of neutrophils
Chemotaxis of neutrophils
Activation of phagocytes
Chemoattraction of granulocytes
Activation of macrophages
Cell movement of mononuclear leukocytes
Recruitment of macrophages
Recruitment of granulocytes
Cell movement of peripheral blood leukocytes
Migration of antigen presenting cells
Migration of lymphatic system cells
Adhesion of phagocytes
Cell rolling of granulocytes

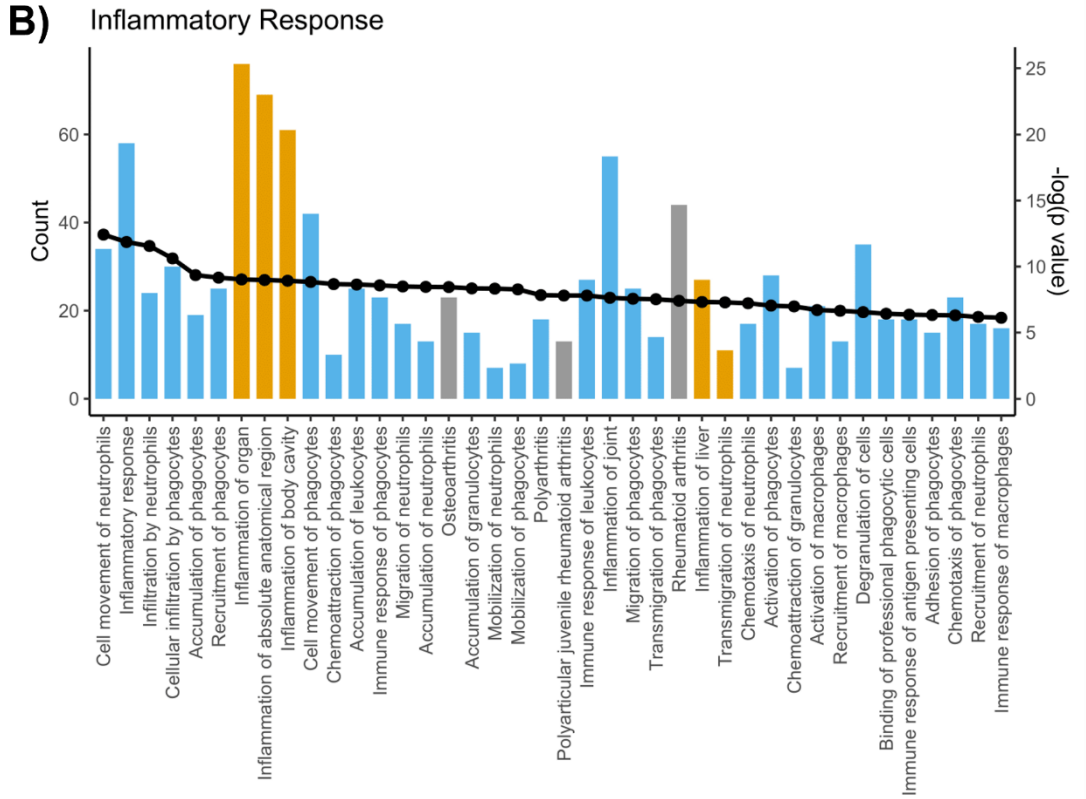
B)
Inflammatory Response
Count
-log(p value)
Cell movement of neutrophils
Inflammatory response
Infiltration by neutrophils
Cellular infiltration by phagocytes
Accumulation of phagocytes
Recruitment of phagocytes
Inflammation of organ
Inflammation of absolute anatomical region
Inflammation of body cavity
Cell movement of phagocytes
Chemoattraction of phagocytes
Accumulation of leukocytes
Immune response of phagocytes
Migration of neutrophils
Accumulation of neutrophils
Osteoarthritis
Accumulation of granulocytes
Mobilization of neutrophils
Mobilization of phagocytes
Polyarthritis
Polyarticular juvenile rheumatoid arthritis
Immune response of leukocytes
Inflammation of joint
Migration of phagocytes
Transmigration of phagocytes
Rheumatoid arthritis
Inflammation of liver
Transmigration of neutrophils
Chemotaxis of neutrophils
Activation of phagocytes
Chemoattraction of granulocytes
Activation of macrophages
Recruitment of macrophages
Degranulation of cells
Binding of professional phagocytic cells
Immune response of antigen presenting cells
Adhesion of phagocytes
Chemotaxis of phagocytes
Recruitment of neutrophils
Immune response of macrophages

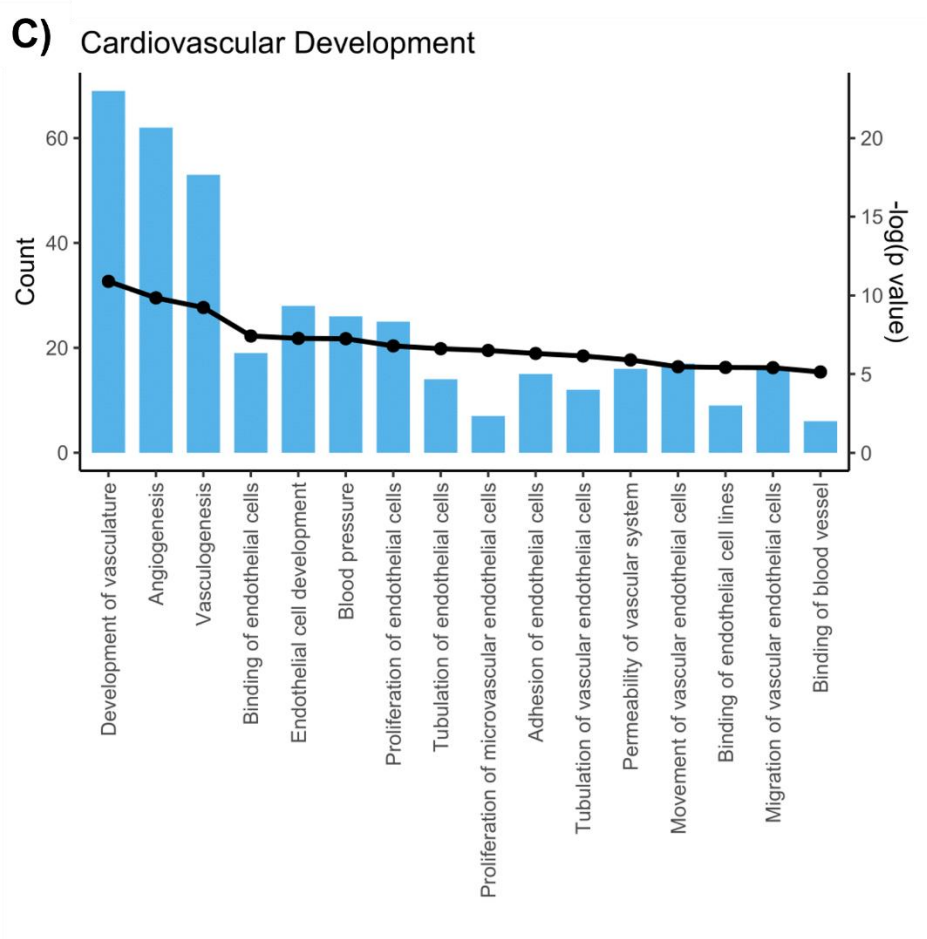

Figure 3.15 - Diseases and functions associated with 7 mM glucose in placental explants determined by ingenuity pathway analysis (IPA). DEGs ($p<0.05$, Log2FC -0.5< or >0.5) that were altered in placental explants treated constant 7 mM glucose compared to fluctuating 5/5.5 mM glucose were inputted into ingenuity pathway analysis (IPA). Possible functions of mild hyperglycaemia in immune cell trafficking (A), inflammatory response (B) and cardiovascular system development (C). The left y-axis represents the number of genes counted for each of the represented functions, indicated by the bars. The colour of the bars represents a **positive**, **negative**, or **unknown z-score** (key). The right y-axis represents the -log(p value), indicated by the black line plot. Up to 40 functions are included in the plots.

3.4.6.1.2 Predicted pathways

To assess the key signalling pathways that may be responsible for any functional effects of the DEGs ORA and IPA were utilised. Pathways which were overrepresented (Figure 3.16) included IL-10 signalling (FDR: 2.10E-07, ER: 12.65), IL-17 signalling pathway (FDR: 5.06E-07, ER: 7.99), chemokine receptors bind chemokines (FDR: 0.009, ER: 2.45), IL-4 and IL-13 signalling (FDR: 9.20E-04, ER: 5.50) and regulation of IGF transport and uptake by IGFBPs (FDR: 0.009, ER: 4.36) (Figure 3.16). Similar canonical pathways were identified by IPA including signalling by interleukins, such as, IL-17 (p=2.45E-04; Z-Score=-3.317), IL-6 (p=1.15E-03; Z-Score=-2.121), IL-8 (p=2.40E-03; Z-Score=-2.121), which had negative Z-scores, and therefore are predicted to be deactivated by 7 mM glucose. In addition to, signalling by IL-10 (p=1.10E-03) and IL-23 (p=6.46E-03). Other identified pathways included atherosclerosis signalling (p=8.91E-06) and inhibition of MMPs (p=3.55E-03) (Figure 3.17).

3.4.6.1.3 Identification of significant protein-protein interaction clusters

A network of protein-protein interactions was generated of DEGs using STRING (v11.5). ClusterOne (v1.0) in Cytoscape (v3.8.2) was then used to identify highly connected regions that were central to the network. This method identified 7 significant clusters ($p<0.05$). The biological functions of these clusters were assessed using Reactome (Figure 3.18; Table 3.1). Cluster 1 had the greatest number of interconnecting DEGs (39) and was found to be associated with interleukin signalling. Central to this cluster were many cytokines and chemokines, including *IL1B* and *IL6* (Figure 3.18; Table 3.1).

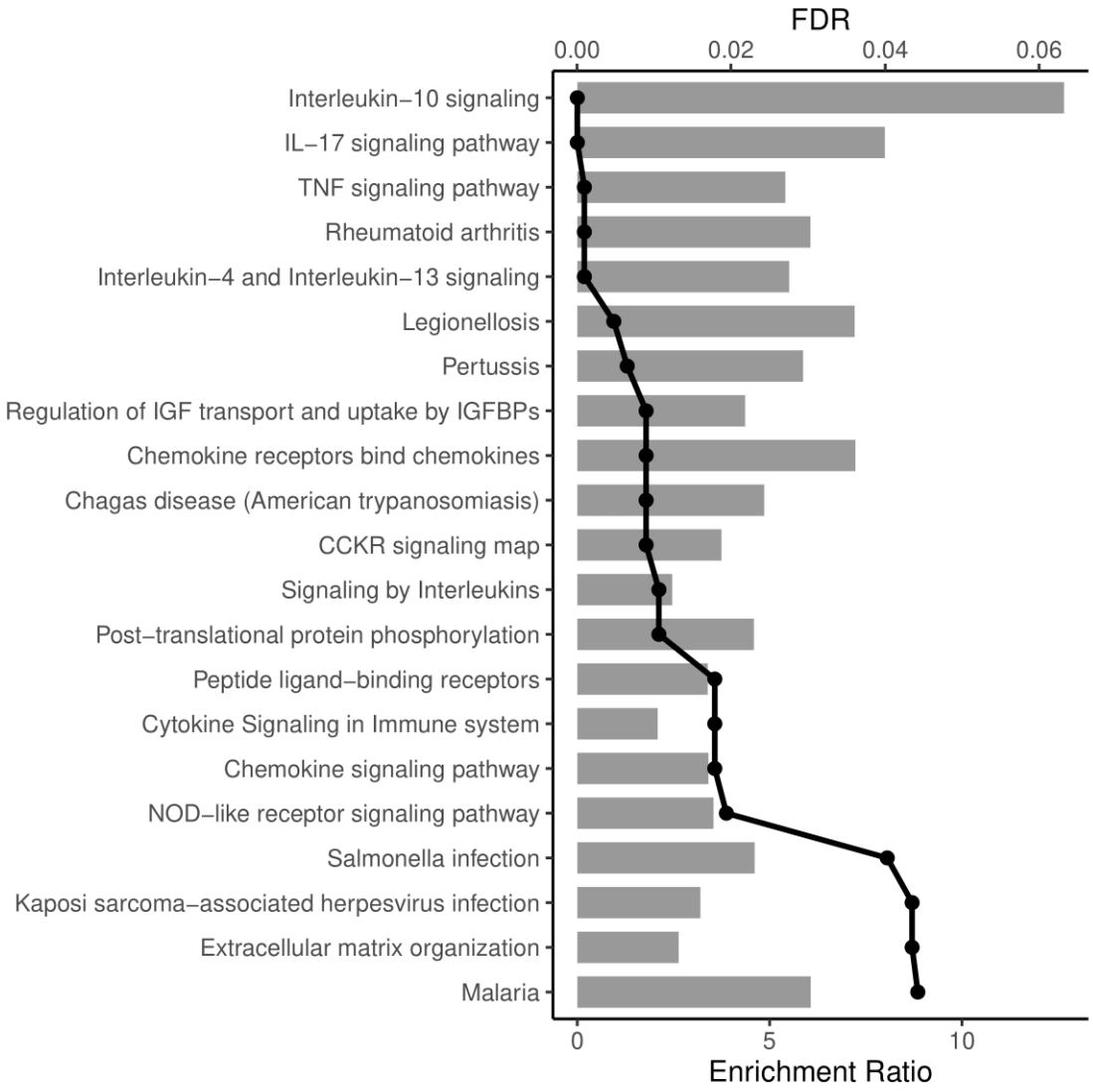

Figure 3.16 - KEGG, reactome and panther pathways associated with 7 mM glucose in placental explants determined by over representation analysis (ORA). DEGs ($p<0.05$, Log2FC -0.5< or >0.5) that were altered in placental explants treated with constant 7 mM glucose compared to fluctuating 5/5.5 mM glucose were inputted into WebGestalt for pathway analysis. The top y-axis represents the FDR value indicated by the black line plot, and the lower y-axis represents the enrichment ratio (number of observed genes divided by the number of expected genes in each pathway) for each of the represented pathways, indicated by the bars. Pathways are ordered by most significant FDR value.

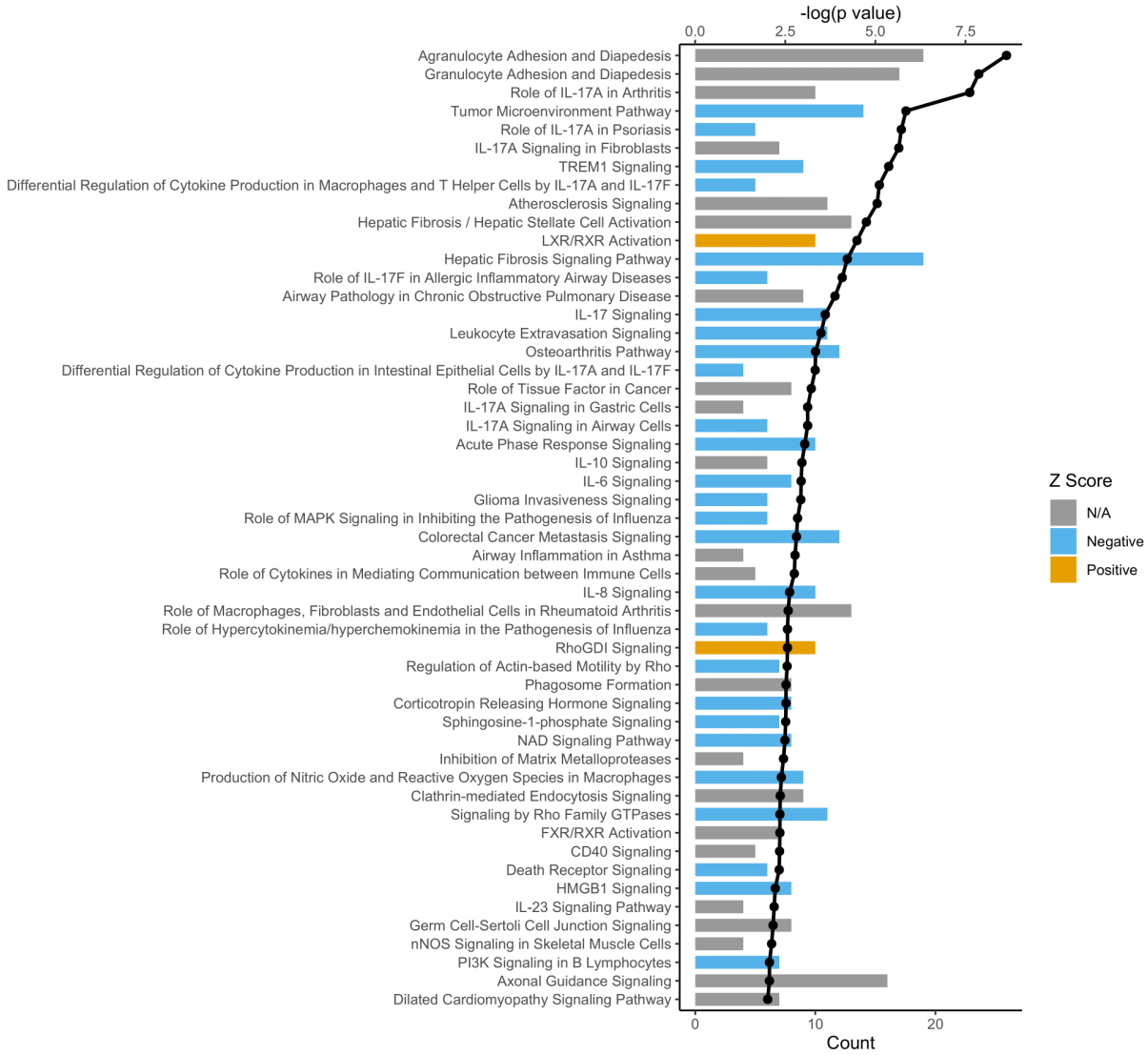

Figure 3.17 - Canonical pathways associated with 7 mM glucose in placental explants determined by ingenuity pathway analysis (IPA). DEGs ($p<0.05$, Log2FC -0.5< or >0.5) that were altered in placental explants treated with constant 7 mM glucose compared to fluctuating 5/5.5 mM glucose were inputted into ingenuity pathway analysis (IPA). Canonical pathways shown are those with a –log(p value) >2). The top y-axis represents the -log(p value), indicated by the black line plot, and the lower y-axis represents the number of genes counted for each of the represented canonical pathways, indicated by the bars. colour of the bars represents a **positive**, **negative**, or **unknown z-score** (key). Pathways are ordered by most significant p-value.

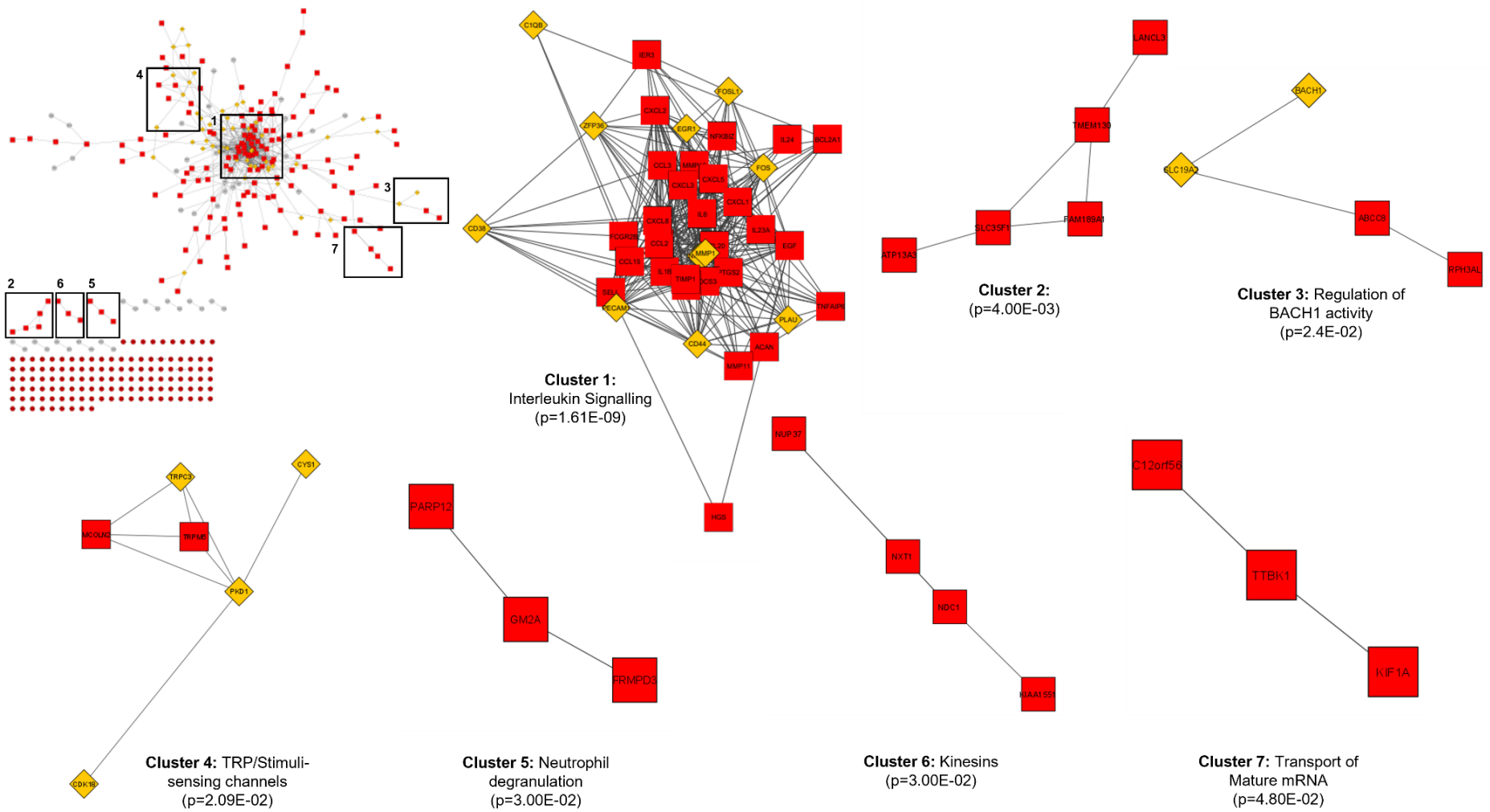

Figure 3.18 - Significant clusters identified from the network of protein-protein interactions for DEGs associated with 7 mM glucose in placental explants. Significant clusters identified using the ClusterOne algorithm on Cytoscape. A protein-protein interaction

network was generated using STRING from DEGs associated with 7 mM glucose. Within this network, the significant clusters are outlined (**Yellow** = associated with multiple clusters within the network, **Red square** = associated with only one cluster within the network, **Red circle** = no interactions with other genes/proteins, **Grey** = not associated with a cluster). The p-value is based on the connectivity of the cluster. Reactome was used to determine the biological functions associated with each cluster, the top biological function is labelled.

Table 3.1 - Significant clusters identified using the ClusterOne algorithm from the network of protein-protein interactions for DEGs associated with 7 mM glucose in placental explants and their accompanying biological functions. The number of nodes refers to the number of proteins within the cluster. The p-value is based on the connectivity of the cluster. Reactome was used to determine the functional significance of each cluster. The top 5 biological functions for each cluster are shown.

Cluster	Nodes	Density	Quality	P-Value	Biological Functions
1	39	0.452	0.625	1.61E-09	Interleukin-10 signaling, Signaling by Interleukins, Interleukin-4 and Interleukin-13 signaling, Cytokine Signaling in Immune system, Immune System
2	5	0.5	1	4.00E-03	None Identified
3	4	0.5	0.75	2.40E-02	Regulation of BACH1 activity, KEAP1-NFE2L2 pathway, Defective ABCC8 can cause hypo- and hyper-glycemias, ATP sensitive Potassium channels, Regulation of HMOX1 expression and activity
4	6	0.533	0.571	2.09E-02	TRP channels, Stimuli-sensing channels, MECP2 regulates neuronal receptors and channels, Ion channel transport, Cargo trafficking to the periciliary membrane
5	3	0.667	1	3.00E-02	Neutrophil degranulation, Glycosphingolipid metabolism, Sphingolipid metabolism, Innate Immune System, Immune System
6	3	0.667	1	3.00E-02	Kinesins, COPI-dependent Golgi-to-ER retrograde traffic, Golgi-to-ER retrograde transport, Factors involved in megakaryocyte development and platelet production, Intra-Golgi and retrograde Golgi-to-ER traffic
7	4	0.667	0.667	4.80E-02	Transport of Mature mRNA derived from an Intron-Containing Transcript, Transport of Mature Transcript to Cytoplasm, Postmitotic nuclear pore complex (NPC) reformation, Processing of Capped Intron-Containing Pre-mRNA, Defective TPR may confer susceptibility towards thyroid papillary carcinoma (TPC)

3.4.6.2 RT-qPCR validation of DEGs

The findings from the functional enrichment analysis and further literature searches revealed key DEGs associated with the inflammatory/immune response in diabetes (e.g. *IL1B, IL6, CXCL8* and *PTGS2*)[431–440], placental fatty acid transport and lipid metabolism (e.g. *FABP3, FABP4, SLC27A6, CD36* and *NPC1L1*)[205,441–443], and vascularisation (e.g. *PECAM1, JCAD, EGF* and *RAMP2*)[444–452]. To confirm altered expression of DEGs in acute glucose treatments, RT-qPCR was performed for a panel of DEGs. These DEGs were selected based on their role in the placenta or diabetes or regulation by glucose in other systems, which is outlined in Table 3.2.

Firstly, RT-qPCR was performed to identify stable housekeeping genes between the conditions for normalisation purposes. Expression levels of *18S* (18s ribosomal RNA), *ACTB* (β-actin) and *YWHAZ* (14-3-3 protein zeta/delta) were assessed in explants exposed to acute glucose treatments (Figure 3.19). Each housekeeping gene was stable across conditions, ($p>0.05$, $n=10$). A geometric mean of these three housekeeping genes was used for normalisation of target genes.

There were trends showing decreases in nicotinamide phosphoribosyltransferase (*NAMPT*; median fold change of 0.89 [0.71-0.97]; $p=0.126$, $n=10$) and platelet derived growth factor D (*PDGFD;* median fold change of 0.74 [0.010-1.52]; $p=0.221$, $n=10$) expression with 7 mM glucose, and an increase in platelet endothelial cell adhesion molecule (*PECAM1;* median fold change of 1.2 [0.66-2.56]; $p=0.123$, $n=10$), however there were no significant differences (Figure 3.20).

3.4.6.3 Impact of glucose fluctuations on glucose transporter expression

Functional enrichment analysis and literature searching revealed that several DEGs were associated with glucose homeostasis and metabolism (e.g. *ECSCR, GHRL, IL6* and *HK2*)[434,453–457]. As glucose uptake and transport across the placenta is mediated by glucose transporters (GLUTs) and GLUT (*SLC2A)* -1, -3, -4, -8, -9, -10 and –12 have previously been shown to be expressed in the placenta[192], the impact of acute glucose treatments on these were assessed using RT-qPCR. All GLUT isoforms assessed were detected in placental explants (Figure 3.21). The expression of *SLC2A4* (GLUT4) was significantly downregulated by 7 mM glucose (median fold change of 0.60 [0.017-1.21]; $p<0.05$, $n=10$). Expression of *SLC2A8* (GLUT8) was also significantly downregulated by 7 mM glucose (median fold change of 0.83 [0.021-0.98]; $p<0.01$, $n=10$) (Figure 3.21). Although these genes were not significantly altered in the RNA sequencing data, they were both detected, with negative Log2FC values (*SLC2A4:* -0.32; *SLC2A8:* -0.26), suggesting downregulation.

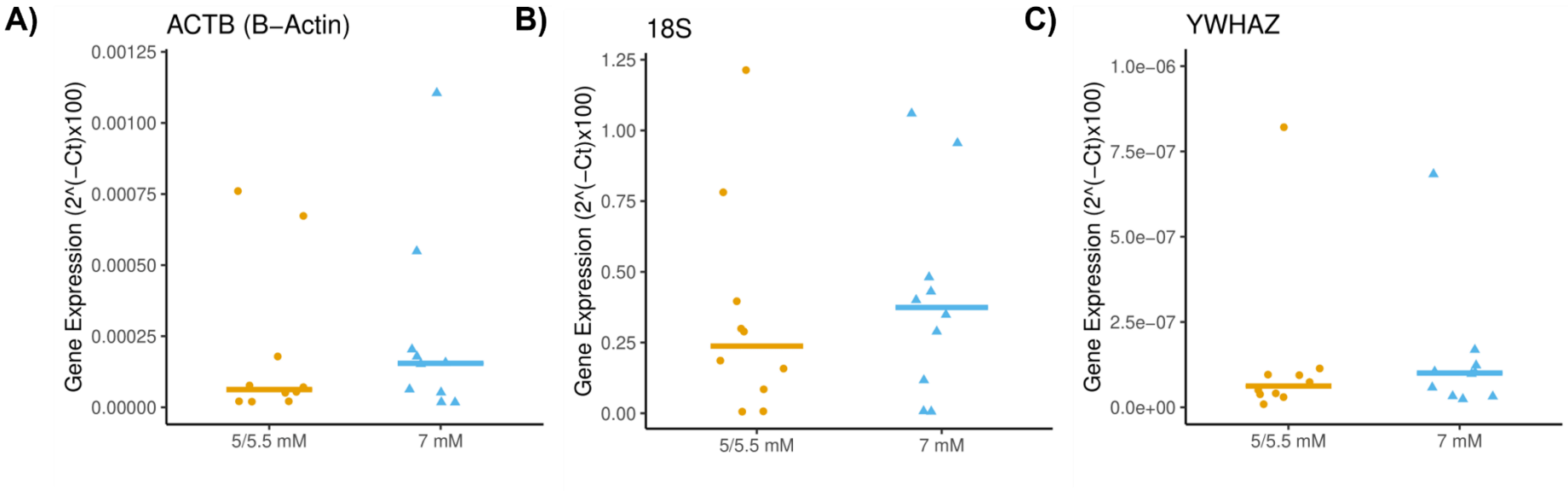

Figure 3.19 - Expression of housekeeping genes placental villous explants following acute glucose treatments. RNA was extracted from placental explants treated with glucose for 48 hours, and RT-qPCRs for housekeeping genes were performed. Data is presented as the median (as the data was not normally distributed) and statistical analysis was performed using a Mann-Whitney U test. Individual points represent individual patient placentae. n=10.

Table 3.2 - Differentially expressed genes altered by mild hyperglycaemia in placental villous explants following glucose treatments for 48 hours and their roles in the placenta, diabetes, or regulation by glucose in other systems. The associated Log2FC and p values are shown. **Blue** = Downregulated by mild hyperglycaemia; **orange** = upregulated by mild hyperglycaemia.

Gene	Log_2FC	P Value	Description	Role in the placenta	Role in diabetes/regulation by glucose in other systems
EGF	-3.57205	0.024	• Epidermal growth factor (EGF) binds to its receptor (EGFR) to increase cell proliferation[458]. • Regulator of angiogenesis[451].	• Important for fetal growth and development. EGFR signalling has been reported to be reduced in placentae from fetal growth restricted (FGR) pregnancies[458]. • Embryos lacking EGFR have impaired placental development and are growth restricted[459].	• Produced in the pancreas, and circulating levels are known to be reduced in diabetic mice[460–462]. • Increases insulin secretion from pancreatic islets, and increases plasma insulin and lowers blood glucose in normal and diabetic mice[463].
FABP4	1.70414	0.0014	• Fatty acid binding protein 4 (FABP4) plays an important role in regulation of glucose and lipid homeostasis as well as inflammation through actions in adipocytes and macrophages[464].	• Increased in the placentae of women with GDM, compared to controls[465]. • FABP4 knockout in HUVECs was associated with an increased susceptibility to apoptosis, reduced migration and reduced tube formation[464]. • FABP4 expression increased in maternal serum and placenta of pre-eclamptic pregnancies, thought to contribute to the pathogenesis of PE. The maternal serum FABP4 levels significantly positively correlated with placental FABP4[466]. • FABP4 siRNA reduced the proliferation of trophoblastic cells (Swan-71 and Jar), as well as migration and invasion[467]	• Glucose treatment (25 mM) stimulated the expression of FABP4 in HTR8/SVneo cells, thought to be associated the increase in fatty acid uptake under high glucose conditions[468]. • Umbilical cord serum FABP4 levels were found to be higher in offspring of women with GDM, which was directly associated with maternal serum FABP4, and leptin, and negatively correlated with birthweight[469]. • FABP4 has been shown to be significantly increased in the serum of women with GDM compared to controls[469–472].
JCAD	1.15042	0.0071	• Junction cadherin 5 associated (JCAD) is a junctional and coronary artery disease risk protein which promotes endothelial dysfunction[446]. • Regulates angiogenesis *in vitro* and *in vivo*[447,473].	• Expression reduced in placentae from pregnancies complicated by Placenta accreta spectrum (PAS)[474].	• Associated with obesity and increased expression in high fat diet fed mice (containing high glucose)[382].

NAMPT (Visfatin)	-0.98446	0.0028	• Visfatin is an adipokine, which is found in fat tissue. It has intrinsic enzymatic activity as a nicotinamide phosphoribosyltransferase (Nampt), which catalyses the rate-limiting step in the salvage pathway leading to NAD+ synthesis in cellular redox reactions[475]. • Longevity protein, which extends the lifespan of human cells by activating sirtuin 1 (SIRT1)[476].	• In a study with 78 pregnant women (26 lean, 24 overweight, and 28 obese) NAMPT was significantly and linearly increased in the syncytiotrophoblast with increasing maternal BMI. No differences in those with/without GDM. Suggested that visfatin/Nampt in the syncytiotrophoblast is acting as the rate-limiting component in the NAD biosynthesis pathway, is a potential biological mechanism by which the placenta is protected against the cellular stress of obesity[476]. • Decreased in pre-term HELLP placentas compared to term HELLP placentas (small sample size, NS 0.07 5 vs 3). • Increased in the placentae of women with GDM, compared to controls[465].	• Reported to exhibit insulin mimetic properties in mice. Enhanced levels in the circulation have been reported in metabolic diseases, such as obesity and T2DM, as well as correlating with markers of systemic inflammation, cardiovascular diseases, atherosclerosis, endothelial dysfunction, and vascular damage[475]. • Altered circulating levels in serum of women with GDM [476–480].
PDGFD	-2.52819	0.036	• Platelet derived growth factor D (PDGFD) is a member of the PDGF family that binds the PDGFRβ[481].	• Levels of PDGFD are increased in HELLP placentae and serum of women with HELLP syndrome. Knockdown of PDGFD in rats with HELLP syndrome reduces inflammation and levels of plasma cytokines[482].	• PDGFD has been implicated in diabetic wound healing. PDGFD can recruit macrophages and decrease vascular permeability in the angiogenic response of wound healing[483].
PECAM1 (CD31)	1.02209	0.036	• Platelet endothelial cell adhesion molecule (PECAM1) is a junctional protein[445]. • Important in mediating endothelial integrity, vascular permeability, regulation of bioavailability of nitric oxide (NO), and angiogenesis[445].	• Used as a marker of placental vasculature[445]. • CD31 immunohistochemical staining has shown reduction in microvessels of pre-eclamptic placentae[484]. • Increased CD31 positive area and number of CD31 positive cells in the labyrinth zone of rat placentae from high fat diet fed mice[485].	• Increased CD31 expression in the placenta has been observed in GDM and was associated with pre-gestational BMI and gestational weight gain[486].
PINK1	1.24814	0.038	• PTEN induced putative kinase 1 (PINK1) initiates the ubiquitin-mediated mitophagy pathway (mitochondrial degradation)[487].	• Protein levels reduced in BeWo cells (trophoblast) following exposure to hypoxia[487].	• In T2DM skeletal muscle, all transcripts from the PINK1 locus were reduced and gene expression levels were correlated with diabetes status[488].
RAMP2	2.01969	0.0048	• RAMP2 is a single-pass transmembrane protein that heterodimerizes with GPCRs (family B), its association with the calcitonin receptor-like receptor (CLR) has been well documented, this forms a	• In the mouse placenta, RAMP2 is expressed in the fetal labyrinth layer, and knockout mice have a thinner labyrinth layer with significantly fewer trophoblast cells due to a reduction in trophoblast proliferation.	• In HEK-293 cells, RAMP2 alters the signalling of all ligands of the glucagon receptor (GCGR). Insulin release is stimulated by activation of the glucagon-like-peptide (GLP-1), in this study ligands of the GLP-1 were shown to act at the GCGR but they were blocked by RAMP2, suggesting a

			receptor complex for the endocrine peptide adrenomedullin (ADM)[489]. • Also known to interact with the glucagon receptor (GCGR). Glucagon is released from pancreatic alpha cells and acts as a counterregulatory hormone to insulin, causing release of glucose release from the liver into the blood. Increased blood glucose in T2DM is associated with an imbalance of insulin and glucagon levels[490].	• In RAMP2 knockout mice, spiral artery remodelling is also impaired, and this was not due to changes in uterine NK cells[489]. • Expressed in bovine placenta throughout gestation. mRNA expression was observed in the trophoblast cells, fetal membrane, luminal epithelium, stroma under the epithelium, endothelial lineage of blood vessels and glandular epithelium[491]. • In the rat, thought to play a role in the differentiation of trophoblast stem cells to trophoblast giant cells, as an ADM inhibitor which blocks the receptors consisting of CALCRL and RAMP2 inhibited stem cell differentiation[492]. • RAMP2 and other components of the adrenomedullin system have increased expression later in pregnancy in pregnant rats[493]. • Expression reduced in the umbilical artery and uterus of patients with pregnancy-induced hypertension, however it was increased in the fetal membranes of patients with pregnancy-induced hypertension. A significant negative correlation was also observed between RAMP2 mRNA levels in the umbilical artery and uterine muscle and blood pressure[494].	role for RAMP2 in the signalling of this receptor[490]. • Levels of RAMP2 (and other components of the ADM system) were increased in the aortic media of fructose-induced insulin-resistant rats[495]. • mRNA expression in the kidney of RAMP2 and AM are increased in STZ-induced diabetic rats[496].

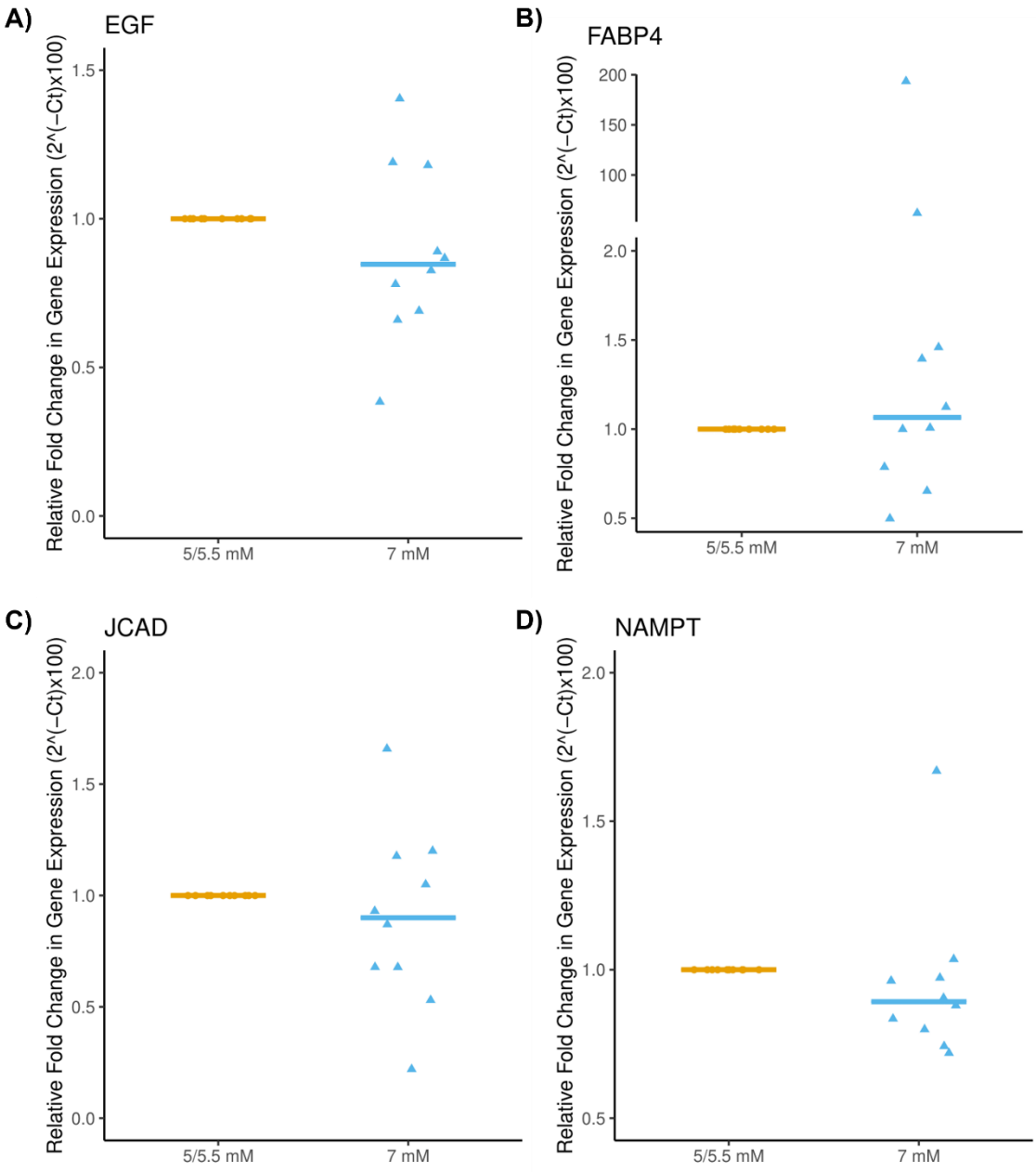
A)
EGF
Relative Fold Change in Gene Expression (2^(−Ct)x100)
1.5
1.0
0.5
0.0
5/5.5 mM
7 mM
B)
FABP4
Relative Fold Change in Gene Expression (2^(−Ct)x100)
200
150
100
2.0
1.5
1.0
0.5
5/5.5 mM
7 mM
C)
JCAD
Relative Fold Change in Gene Expression (2^(−Ct)x100)
2.0
1.5
1.0
0.5
0.0
5/5.5 mM
7 mM
D)
NAMPT
Relative Fold Change in Gene Expression (2^(−Ct)x100)
2.0
1.5
1.0
0.5
5/5.5 mM
7 mM

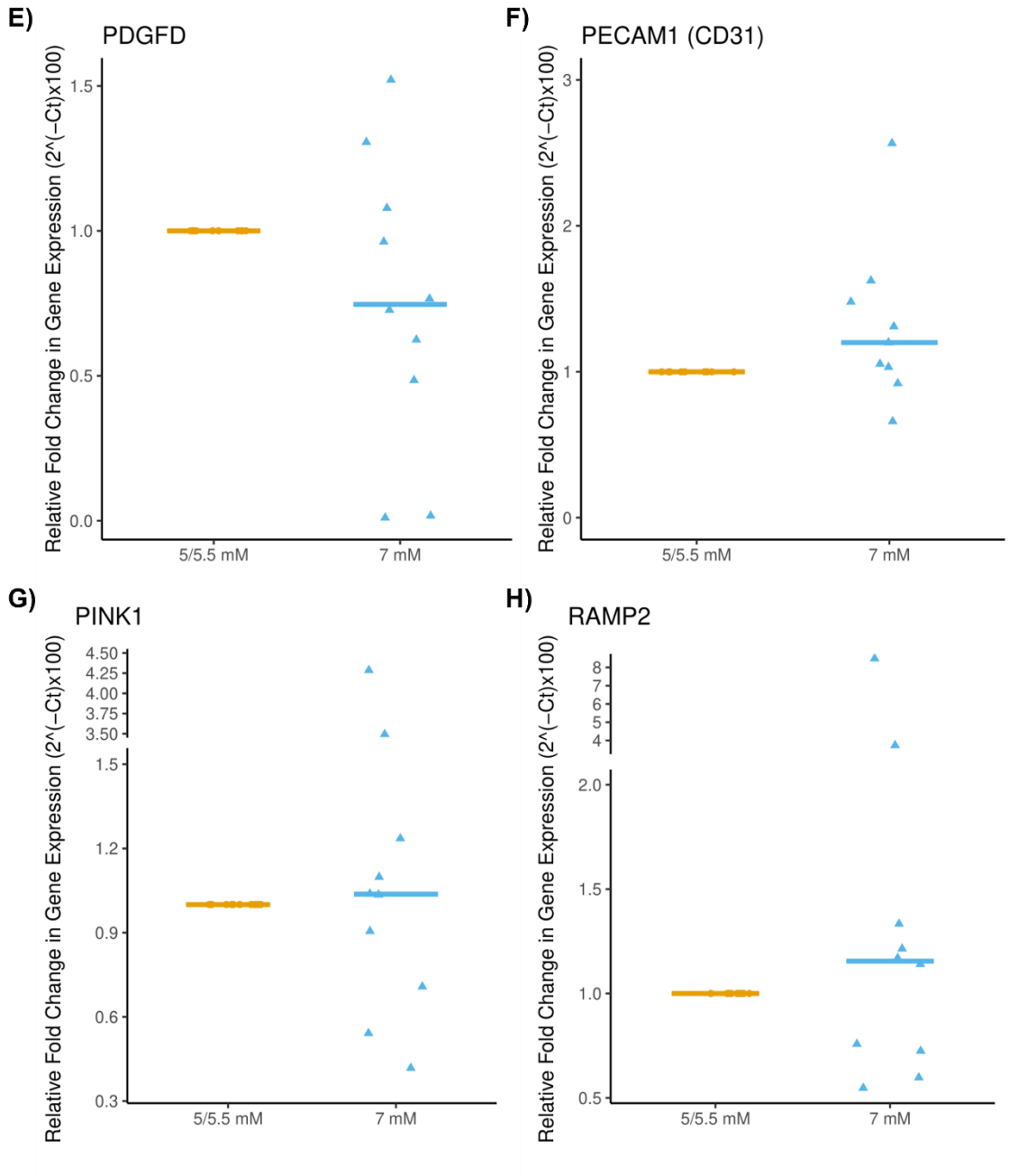

Figure 3.20 - Expression of selected DEGs in placental explants following acute glucose treatments, measured by RT-qPCR. Selected DEGs were measured in placental explants cultured in either fluctuating 5/5.5 mM glucose or constant 7 mM glucose for 48 hours by RT-qPCR. The expression of each target gene was normalised to a geometric mean of *18S, ACTB* and *YWHAZ* housekeeping gene expression. Data is presented as the median fold change compared to 5/5.5 mM glucose (as the data was not normally distributed) and statistical analysis was performed using a Wilcoxon Signed-Rank Test. Individual points represent individual patient placentae. n=10.

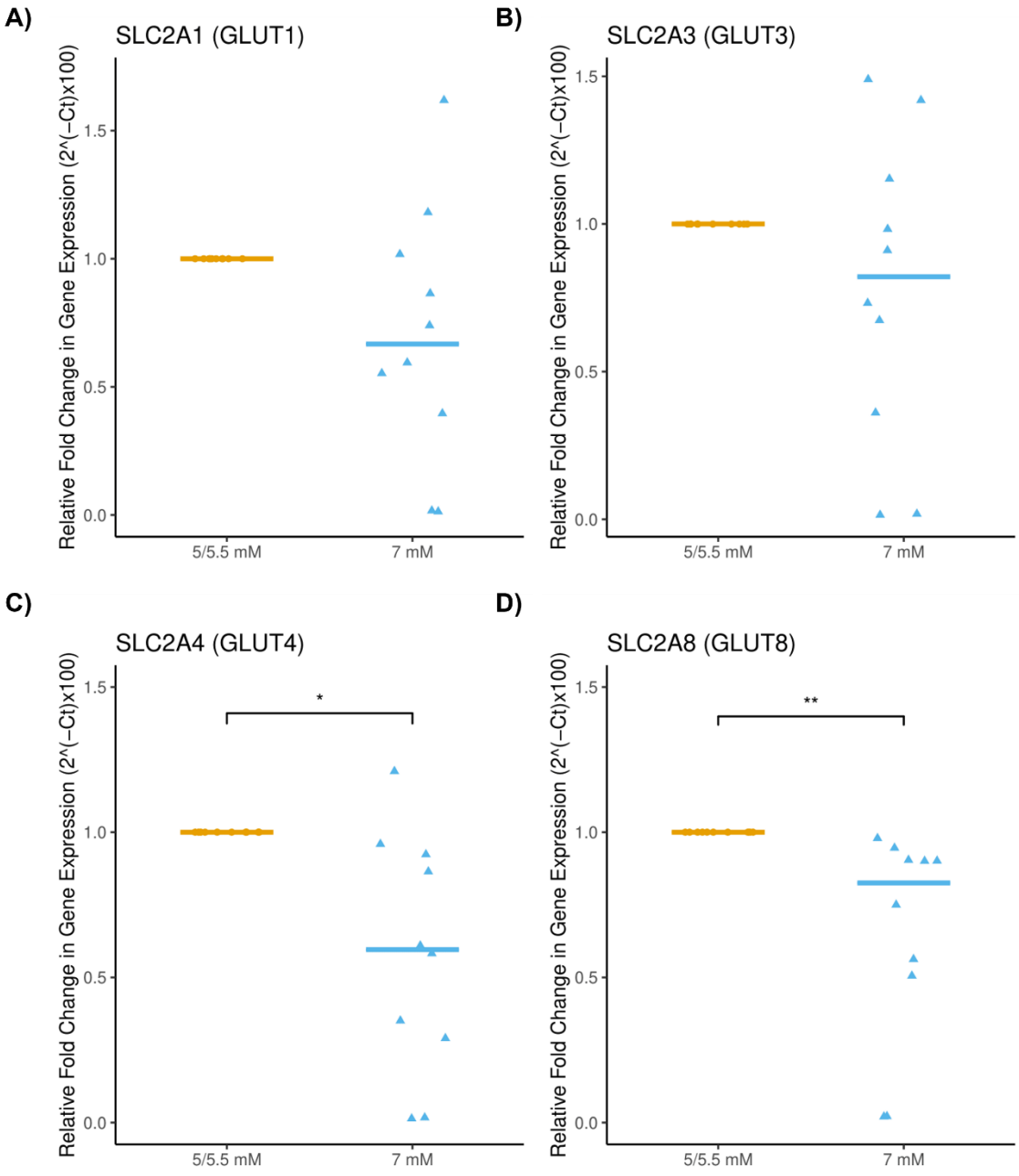
A)
SLC2A1 (GLUT1)
Relative Fold Change in Gene Expression (2^(−Ct)x100)
1.5
1.0
0.5
0.0
5/5.5 mM
7 mM
B)
SLC2A3 (GLUT3)
Relative Fold Change in Gene Expression (2^(−Ct)x100)
1.5
1.0
0.5
0.0
5/5.5 mM
7 mM
C)
SLC2A4 (GLUT4)
*
Relative Fold Change in Gene Expression (2^(−Ct)x100)
1.5
1.0
0.5
0.0
5/5.5 mM
7 mM
D)
SLC2A8 (GLUT8)
**
Relative Fold Change in Gene Expression (2^(−Ct)x100)
1.5
1.0
0.5
0.0
5/5.5 mM
7 mM

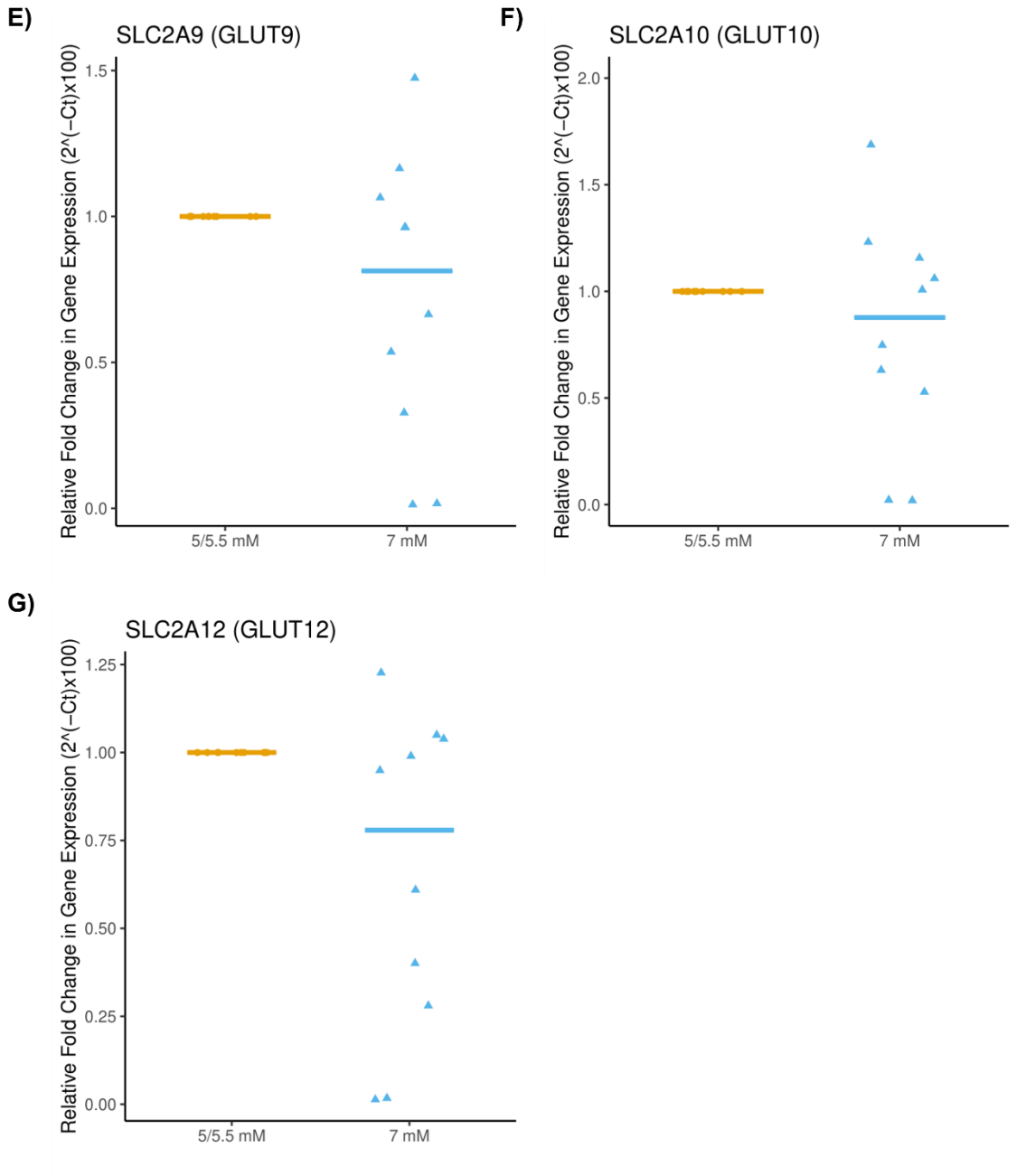

Figure 3.21 - Expression of glucose transporters (GLUTs) in placental explants following acute glucose treatments for 48 hours, measured by RT-qPCR. GLUTs were measured in placental explant RNA cultured in either fluctuating 5/5.5 mM glucose or constant 7 mM glucose for 48 hours by RT-qPCR. The expression of each target gene was normalised to a geometric mean of *18S, ACTB* and *YWHAZ* housekeeping gene expression. Data is presented as the median fold change compared to 5/5.5 mM glucose (as the data was not normally distributed) and statistical analysis was performed using a Wilcoxon Signed-Rank Test. Individual points represent individual patient placentae. n=10. * $p<0.05$, ** $p<0.01$.

3.5 Discussion

The aim of this chapter was to investigate the impact of physiological levels of maternal glucose associated with GDM LGA and GDM AGA pregnancies on the placenta. To achieve this, an *ex vivo* placental explant model was developed which allowed placental tissue to be cultured in, and exposed to, glucose concentrations that mimic levels observed *in vivo* in maternal circulation. Culture of tissue in 5/5.5 or 7 mM conditions did not affect tissue viability or rates of trophoblast proliferation/apoptosis. In the explant model, mild hyperglycaemia (7 mM glucose) altered the placental transcriptome and functional enrichment analysis predicted that altered genes were associated with immune/inflammatory and vascular development pathways and functions.

3.5.1 An *ex vivo* model to study the impact of maternal hyperglycaemia on the placenta

A placental villous explant model was employed to mimic physiological *in vivo* maternal glucose fluctuations in GDM LGA (7 mM) and GDM AGA (5/5.5 mM) pregnancies. Glucose concentrations utilised in this model were selected based CGM profiles of women with GDM LGA and GDM AGA pregnancies identified by Law *et al*. (2019)[62].

Studies in other tissues have shown that fluctuating glucose levels (cycling between ~5 mM and ~20-50 mM) can influence cellular function[421–423]. In placental cells, Risso *et al*. (2001) revealed that apoptosis was increased in HUVECs exposed to daily fluctuations in glucose (5-20 mM), compared to constant 20 mM glucose, accompanied by an increase in expression of the pro-apoptotic protein, Bax[422]. This suggests that glycaemic variability is more damaging to ECs than a constantly high glucose concentration. Moreover, *in vitro* studies of the placenta have shown that high levels of glucose impact the function of HUVECs, trophoblast cells, and placental tissue. Specifically, Caywer *et al*. (2016) investigated a range of glucose concentrations on cultured cytotrophoblast cells (Sw. 71), including 150 mg/dL (~8.3 mM), which increased secretion of anti-angiogenic factors, sFLT1 and sEng, and reduced secretion of pro-angiogenic factors, PlGF and VEGF, in addition to increased apoptotic markers, compared to 100 mg/dL (~5.6 mM)[264]. Similarly, Han *et al*. (2015) observed an increase in sFLT1 and sEng secretion in Sw.71 cells with 10 mM glucose, compared to 5 mM glucose[497]. Overall, these studies suggest that a subtle increase in glucose can impact placental function.

However, a limitation of many previous studies is that they utilise supraphysiological concentrations of glucose (≥25 mM)[262,282,420]. Despite treatment of GDM to achieve normoglycaemia, infants can still be born LGA[62]. Thus, taken with the findings and methodologies of the previous studies this highlights the importance of developing a placental model of physiological maternal glucose fluctuations.

As expected, glucose was rapidly consumed by placental explants in the present study and medium was replenished every 6-18 hours. Further assessment of glucose concentrations in the conditioned medium revealed that the model was able to recapitulate fluctuations in maternal glucose, observed in CGM profiles of women with GDM LGA and GDM AGA pregnancies[62], using 7 mM and 5/5.5 mM glucose, respectively. The previous studies discussed do not assess the levels of glucose in the culture medium[262,264,282,420,497], and therefore it is unclear what concentrations the cells or tissue are exposed to during culture.

In addition to glucose, osmolality measurements of conditioned medium were also conducted. *In vitro* and *ex vivo* culture in excessive glucose can increase the osmolality of the culture medium. Hyperosmolarity has been studied in cultured cells and has been shown to alter cell proliferation and growth, as well as nutrient transport[498]. Thus, increased osmolality could contribute to observed functional changes. Hyperosmolar controls can be used in the culture medium, including D-mannitol, a sugar alcohol, or L-glucose, the enantiomer of D-glucose. These compounds will increase the osmolality of the medium, similarly to glucose, however, are devoid of metabolic activities[499,500]. In the present study, osmolality was not significantly altered by subtle fluctuations in glucose, and thus is not the cause of functional changes in placental explants. Similarly to glucose measurements, previous studies also do not assess osmolality, and while some utilise hyperosmolar controls[264,497], many do not[262,282,420].

Overall, the model developed in the present study is superior to previous studies, in that it recapitulates physiological fluctuations in glucose levels and assesses the profiles of glucose and osmolality overtime in culture.

3.5.1.1 Viability of placental explants treated with glucose fluctuations

The viability of placental explants was assessed using H&E, immunohistological staining and measurements of hCG and LDH secretion.

The placental syncytium is also known to degenerate during placental explant cultures[322,501], but is then replenished by the underlying cytotrophoblast, by proliferation and fusion[502]. Secretion of hCG from placental explants is indicative of a viable

syncytiotrophoblast. Patterns of hCG release from explants with acute glucose treatments were in line with profiles described by Siman *et al.* (2001)[322]. Lower levels of hCG were measured in explants with longer-term glucose treatments, between days 2 and 8, despite trying a more sensitive ELISA. Thus, the presence of the syncytium was assessed using H&E staining and immunohistochemistry for cytokeratin-7, which labels all trophoblast, including the syncytiotrophoblast and villous cytotrophoblast[115]. As expected, the syncytiotrophoblast layer had started to lift away from the villi in explants with acute glucose treatments, however, many syncytial layers remained intact. This is also reflected by the decline of hCG release between 42-48 hours in these explants. In longer-term glucose treatments, remnants of shedded syncytium were observed. Some underlying regions of trophoblast appeared to be multinucleated , suggesting these underlying cytotrophoblast cells were fusing to regenerate the syncytial layer. These findings are all in line with previous studies[115,322].

To further confirm viability, an LDH assay was used as a measure of necrosis. Between days 2 and 7 of explant culture, LDH levels are known to decline, suggesting less tissue necrosis during this time, and then rise again around 11 days of culture, due to loss of tissue integrity in prolonged cultures[503,504]. The pattern of LDH release from placental explants was in line with this, as levels increased in the first day of culture, and then plateaued, suggesting minimal cell death was occurring in the explants. There was a trend towards a decrease in LDH with 7 mM glucose, which is interesting given that LDH is known to regulate glucose metabolism, as it converts pyruvate into lactate during glycolysis[505]. Diabetes has been associated with elevated serum LDH[505], and overexpression of LDH in insulin-producing cells reduces glucose oxidation and increases lactate production[506]. This suggests that mild hyperglycaemia may reduce LDH, altering glucose metabolism in the placenta (See Section 3.5.2 on glucose metabolism).

Overall, the presence of a regenerating syncytium and the minimal levels of cell death in placental explants exposed to glucose treatments suggests that the model was viable.

A limitation of the model is that placental explants are not ideal for assessing placental vasculature over longer periods of culture. H&E and immunohistochemical staining for CD31 to label the fetal endothelium revealed that fetal blood vessels were intact, with open blood vessel lumens surrounded by an endothelial layer, in acute glucose treatments. In longer-term treated explants, fetal blood vessels were more difficult to distinguish and the endothelium was less visible. This is likely due to the collapsing of vessels throughout culture, as they are no longer perfused as *in vivo,* and thus is a

limitation of longer-term placental explant cultures[115]. Utilising a placental-perfusion model is known to best preserve the structural integrity of placental vasculature, although it is incredibly difficult and reduces viability[507,508]. In recent studies, exposure of placental explants to shear stress has been employed to mimic the dynamic flow environment *in vivo* in the placenta. Explants exposed to flow conditions had a better structural integrity, with more preserved villi observed in H&E staining and less damaged and disrupted vessels compared to static explants[115]. Other models include the culture of placental vascular cells, such as HUVECs[509], however these exhibit a mature EC phenotype and do not model the early development of placental blood vessels, which involves the differentiation of pMSCs. Overall, greater *in vitro* and *ex vivo* models are needed to study the development of placental vasculature.

3.5.1.2 Placental cell turnover in placental explants treated with glucose fluctuations

Aberrant trophoblast cell turnover, including proliferation and apoptosis, can influence the size and integrity of the placental barrier, which may impact nutrient and oxygen transfer to the developing fetus, thus impacting fetal growth[427]. To assess placental cell turnover, Ki67 and M30 staining was performed to measure proliferation and apoptosis, respectively. Treatment with 7 mM glucose did not significantly alter levels of proliferation or apoptosis.

Complications of pregnancy have been linked to altered trophoblast turnover, such as FGR (decreased proliferation[426] and increased apoptosis[425]), preeclampsia (increased proliferation and apoptosis[428,510]), GDM (decreased apoptosis[511]) and maternal obesity (decreased proliferation and apoptosis)[427]. In the latter study, obese pregnant women that delivered LGA infants had the lowest apoptotic indices, suggesting that lower rates of apoptosis in LGA placentas may be linked to an increase in placental and fetal growth. Additionally, placentas of GDM pregnancies are usually larger than controls, which is a predictor of birthweight[512]. Thus, increased placental cell turnover, or decreased apoptosis would be expected in GDM and/or LGA. In contrast, there was a trend towards a decrease in proliferation in explants treated with 7 mM glucose. Interestingly, Zhang *et al.* (2021) found that Ki67 expression was downregulated in GDM placentae, and the number of TUNEL positive (apoptotic) cells were increased. This study also employed a GDM mouse model, which involved mating $LepR^{db}$ mice, which lack the functional full-length Ob-Rb leptin receptor and are characteristic of T2DM, to generate mice which have impaired glucose tolerance at gestational day 16.5. In GDM mice, Ki67 protein levels were also reduced[513]. Moreover, some studies

have shown that high glucose can impact trophoblast proliferation, however the levels utilised (≥25 mM) are not physiological[514]. In the study by Zhang *et al.* (2021) protein expression of Ki67 was reduced with high glucose (30 mM) in HTR8/SVneo trophoblast cells in Western blots[513], although 7 mM glucose was used as the control condition, which is the experimental condition in the present study.

However, in addition to increased trophoblast turnover, increased placental size in GDM and LGA may also be linked to increased ECs, fibroblasts, HBCs and increased vascularisation[515]. While Ki67 and M30 staining was primarily localised to the trophoblast, identification of positive cells was assessed across the placental villi. To specifically assess trophoblast cell turnover, dual staining with E-cadherin, a trophoblast cell-cell adhesion molecule, should be performed[516].

Overall, subtle fluctuations in glucose did not significantly impact cell turnover in placental explants, however, this further confirms the viability of the *ex vivo* model.

3.5.2 Glucose transport and metabolism in placental explants treated with glucose fluctuations

As glucose transport across the placenta is essential for meeting the demands of the fetus, and is dependent on GLUTs for facilitated diffusion, the expression of GLUT isoforms known to be expressed in the placenta were assessed in explants by RT-qPCR[192]. mRNA expression of GLUT4 and GLUT8 (*SCL2A4* and *SLC2A8*, respectively) were significantly downregulated by 7 mM glucose.

GLUT4 primarily transports glucose but can also transport glucosamine and DHA[192,517] and is regulated by insulin[195]. It is one of the most studied transporters as it contributes to the rate-limiting step in insulin-stimulated glucose uptake of skeletal, cardiac muscle and brown and white adipose tissue. Thus, impaired translocation or a reduction in this transporter is linked to insulin resistance in diabetes[518,519]. In the placenta, James-Allan *et al.* (2021) found that GLUT4, expressed in the BM of the syncytiotrophoblast and GLUT1, in the MVM, were reduced in obese women that delivered macrosomic infants, compared to obese women that delivered AGA infants and compared to controls[520]. Similarly, Colomiere *et al*. (2009) also reported a decrease in placental *GLUT4* mRNA in women with insulin controlled GDM (obese and non-obese) compared to controls, which was compensated by an increase in *GLUT1*[521]. These studies suggest that placental *GLUT4* expression is reduced in GDM and in LGA (macrosomia), which is likely localised to the BM, impairing glucose transport from the placenta to the fetus. Given that 7 mM glucose in placental explants also reduced the mRNA expression of this transporter, this may be attributed to mild hyperglycaemia in GDM/LGA. In

contrast, Stanirowski *et al*. (2017) observed increased protein expression of GLUT4 and GLUT9 in women with GDM and pre-gestational diabetes treated with insulin. Macrosomia was also more common in the women with insulin-dependent diabetes, suggesting this may be linked to increased glucose transfer to the fetus, although this is an assumption[196].

GLUT8 has a high affinity for glucose and can also transport fructose and galactose[192,517]. GLUT8 has been reported to be expressed in the syncytiotrophoblast and cytotrophoblast in term placentae, as well as in EVTs and the HTR8/SVneo cell line, and ECs. Its expression is primarily observed in the cytosol, and thus it is thought to be involved in glucose delivery to intracellular organelles[192]. However, in mice blastocysts, GLUT8 has been found to be responsible for insulin-stimulated glucose uptake[522]. Moreover, GLUT4 and GLUT8 were translocated to the cell surface in atrial myocytes following insulin stimulation[523]. However, in atrial myocytes from diabetic rodents, cell surface GLUT4 and GLUT8 were reduced, which could be rescued with insulin treatment[523]. In the study by Stanirowski *et al*. (2021), GLUT8 protein expression, assessed by immunohistochemistry, was not altered in macrosomic fetuses (GDM excluded) but was found to be decreased in placentae of SGA fetuses, suggesting a link to fetal growth[524]. Moreover, in an ovine placental insufficiency model of IUGR, GLUT8 placental expression was reduced[525]. Similarly, in a GLUT8 knockout mouse model (*slc2a8*-null mice), decidualisation is impaired, which leads to altered placentation and reduced fetal growth[526]. In contrast, another study observed an increased expression of GLUT8 in the maternal compartment of the placenta in pregnancies complicated by FGR[527]. Taken together, these findings demonstrate an association between GLUT8 expression and pathological fetal growth.

Some studies have also assessed the effects of glucose on the expression of glucose transporters in trophoblast cell lines. In one study, GLUT1 mRNA was found to be increased and GLUT3 reduced with 25 mM glucose in JAR choriocarcinoma cells, but this was not observed with JEG-3 cells[528]. JEG-3 cells have previously been shown to exhibit a lower transport of glucose, than JAR cells (and other trophoblast cell lines), and the mechanism for transport in this cell line may differ to that *in vivo*[335]. In contrast, other studies have shown suppression of GLUT1 expression in primary term trophoblasts[529]. In the study by Zhang *et al.* (2021), when HTR8/SVneo cells were exposed to high glucose (30 mM), the plasma membrane expression of GLUT3 was significantly reduced, as was glucose uptake.

Overall, it appears that GLUT expression may be linked to complications of fetal growth, and high glucose may play a role in regulating this. The reduced gene

expression of GLUT4 and GLUT8 with 7 mM glucose in placental explants may be a compensatory mechanism following exposure to mild hyperglycaemia, to protect the fetus from excessive glucose, which is in line with studies that have shown a decrease in GLUT4 in LGA infants[520,521]. In contrast, GLUT1 was unaltered by 7 mM glucose, which is ubiquitously expressed in the placenta, with high expression on the syncytiotrophoblast, primarily responsible for glucose transport into the placenta[192,521]. This suggests that in mild hyperglycaemia in GDM, glucose is still transported across the placenta and subsequently to the fetus, via GLUT1.

Several genes associated with glucose metabolism and homeostasis were downregulated by 7 mM glucose, including ghrelin-obestatin prepropeptide (*GHRL*) and hexokinase 2 (*HK2*). GHRL deletion in obese mice reduces hyperglycaemia and improves insulin sensitivity by enhancing glucose-stimulated insulin secretion[530]. Hexokinase 2 catalyses the phosphorylation of glucose, the first and rate-limiting step of glycolysis, HK2 is the isoform predominantly found in insulin-sensitive tissues[455]. Moreover, HK2 protein expression has been reported to be increased, along with GLUT1 expression in the placentae of women with GDM[531]. The downregulation of these genes by 7 mM glucose may indicate reduced placental glucose metabolism. Given that placental glucose consumption is thought to regulate glucose transfer to the fetus[175], a reduction in placental glucose metabolism may increase the transfer of glucose to the fetus and accelerate fetal growth. Additionally, Endothelial Cell Surface Expressed Chemotaxis and Apoptosis Regulator (*ECSCR*) was upregulated by 7 mM glucose, which is known to be expressed highly in the placenta, particularly in the trophoblast[452]. ECSCR is known to regulate glucose homeostasis and energy metabolism via EC function, as deletion of ECSCR enhances the insulin mediated Akt/eNOS activation in ECs and subsequent insulin delivery into the skeletal muscle. Whereas, targeted activation of ECSCR in ECs impairs glucose tolerance in mice, and pre-disposes them to diet-induced obesity[453]. As exposure to mild hyperglycaemia (7 mM glucose) appears to alter glucose transporters, and genes associated with glucose metabolism, it would be interesting to assess glucose uptake across the placental explants. For example, utilising an assay that incorporates 2-deoxyglucose (2DG), which can be transported into cells and metabolised to 2-deoxyglucose-6-phosphate (2DG6P) that can be detected in the cells[532].

3.5.3 Altered vascular regulatory genes in placental explants treated with glucose fluctuations

Functional enrichment analysis revealed that 7 mM glucose altered genes associated with vascular development, including angiogenesis, vasculogenesis, and EC functions. DEGs included EC junctional molecules (*PECAM1* and *JCAD*)[444,446], which were upregulated by 7 mM glucose. Platelet endothelial cell adhesion molecule (*PECAM1*), also known as CD31 is expressed on all cells in the vascular compartment, including ECs and is known to play roles in angiogenesis, platelet function and mechanosensing of ECs in response to shear stress[444]. CD31 is often used as a marker of vasculature in the placenta[445]. Moreover, junctional cadherin 5 associated (*JCAD*) is a coronary artery disease risk protein which promotes endothelial dysfunction[446]. Knockdown of JCAD in HUVECs leads to decreased proliferation and migration, increased apoptosis, and reduced tube formation[447]. It is also known to regulate angiogenesis *in vivo*[473]. Similarly, nuclear receptor subfamily 4 group A member 1 (*NR4A1*), which was downregulated by 7 mM glucose is a key regulator of VEGF-induced vascular leakage, which destabilises endothelial junctions by increasing NO synthase expression and downregulation of EC junction proteins[533,534]. In line with this, endothelial barrier function is thought to be impaired in GDM placentae[535,536], in addition to altered placental vascularisation[122,125,130]. Taken together, alterations in these vascular genes suggests that mild hyperglycaemia in GDM may alter levels of vascular markers, and endothelial junction proteins, which may regulate vascular permeability.

Other vascular regulatory DEGs are associated with embryonic and placental vascular development, including Receptor Activity Modifying Protein 2 (*RAMP2*) and epidermal growth factor (*EGF*), which were upregulated and downregulated by 7 mM glucose, respectively. For example, RAMP2 knockout mice die *in utero* due to blood vessel abnormalities[449] and specific knockout of RAMP2 in the vascular endothelium of mice leads to death in the perinatal period due to endothelial abnormalities and vascular leakage[450]. Additionally, EGF is known to be a key regulator of placental and fetal growth. EGF binds to the EGF receptor (EGFR) and leads to increased cell proliferation. Embryos lacking EGFR have impaired placental development and are growth restricted[459] and EGFR signalling has been reported to be reduced in placentae from FGR pregnancies[458]. EGF is also known to play roles in angiogenesis and proliferation of ECs[451], suggesting its crucial role in embryonic development may be associated with development of placental vasculature. While studies have not assessed levels of EGF in diabetic placentae, circulating levels of EGF are known to be reduced in diabetic mice[460,462]. Moreover, glucose injections in mice increased EGF in plasma[463], suggesting that glucose can regulate EGF levels. Overall, altered levels of these genes in response to mild hyperglycaemia in GDM, as observed in the present

ex vivo model, may contribute to impaired placental vascular development. In turn, this will impair blood flow to the fetus, and the exchange of nutrients and gases, resulting in altered fetal growth. The impact of maternal glucose fluctuations on placental vascular development will be investigated further in Chapter 7.

3.5.4 Altered placental lipid transport and metabolism genes in placental explants treated with glucose fluctuations

Genes encoding several fatty acid transport proteins were altered by 7 mM glucose. NEFAs cross the placenta by diffusion or facilitated diffusion by fatty acid carriers, such as CD36 (FAT) and FATPs and bind to FABPs in the cytoplasm[205]. *CD36, FABP4* and *SLC27A6* (FATP6) were upregulated and *FABP3* was downregulated by 7 mM glucose. In previous studies, FABP4 and FABP5 were increased in placentas from obese women with diabetes, compared to those without diabetes. Additionally, FABP4 has been shown to be significantly increased in the serum of women with GDM compared to controls[469–472]. Other studies have found that umbilical cord serum FABP4 levels were higher in offspring of women with GDM, which was directly associated with maternal serum FABP4, and leptin, and negatively correlated with birthweight[469]. In line with this, Ciborowski *et al.* (2014) also reported that FABP levels in healthy pregnant women are correlated with lipids and birthweight[537]. In the placenta, several factors were found to be increased in women with GDM compared to controls, including visfatin (NAMPT), NF-κB, EL, FABP1, FABP3, FABP4, FATP4, FATP5 and lipoprotein lipase, in ELISAs of protein[465]. The levels of CD36 in diabetic placentas has not been widely studied, however its expression was found to be augmented in syncytiotrophoblast isolated from GDM placentas[418], and in placentas from obese[538] and overweight women[539]. LPL and EL have also been reported to be increased in placentas from women insulin-dependent diabetes, and from obese women with GDM[64,206]. EL mRNA expression (*LIPG*) is also increased in T1DM pregnancies, particularly in those with poor metabolic control[207].

Supraphysiological concentrations of glucose promote placental triglyceride accumulation in placental explants, however no differences in expression or localisation of LPL, EL, FATP2, FATP4 or FAT (CD36) were observed in immunohistochemistry[420]. Similarly, *CD36* gene expression was not altered by supraphysiological glucose in GDM and non-GDM syncytio- and cyto-trophoblasts[418]. This is contrary to our findings using physiological glucose concentrations, where 7 mM glucose increased *CD36* expression, demonstrating differences between supraphysiological and physiological glucose. Visiedo *et al*. utilised a more

physiological level of glucose (11 mM) in placental explants and showed that it reduced mitochondrial fatty acid oxidation, increased esterification, which lead to an accumulation of placental triglycerides[540]. This study further suggests a role for maternal hyperglycaemia in placental triglyceride accumulation.

These findings suggest that lipid transport proteins are altered in diabetic pregnancies, by supraphysiological levels of glucose and in the present study, by physiological increases in glucose. Alterations in these transport proteins can dysregulate levels of circulating lipids in pregnancy, which can lead to maternal dyslipidaemia, altered fetal growth (including LGA) and increased risk of offspring metabolic disease later in life[541]. Thus, the findings suggest a role for mild hyperglycaemia in GDM in regulating placental lipid transport and fetal growth. It would therefore be interesting to investigate lipid metabolism in the placental explants further, by assessing triglyceride accumulation, protein levels of the transporters or metabolomics[269,420].

3.5.5 Altered immune and inflammatory genes in placental explants treated with glucose fluctuations

Functional enrichment analysis also predicted that glucose altered genes associated with the inflammatory/immune response, interleukin signalling, and reduced recruitment/activation of macrophages. Key DEGs within these pathways included several cytokines and chemokines (*CXCL- 1, 2, 3, 5, 8; CCL- 2, 3, 19, 20 and IL- 1B, 6, 23A, 24*), which were downregulated by 7 mM glucose. Cytokines and chemokines are proteins that act as immune mediators and regulators[214], and are expressed at the maternal-fetal interface[215,216]. The immune imbalance between pro-inflammatory and anti-inflammatory mediators are thought to contribute to insulin resistance, glucose intolerance, and increase the risk of adverse pregnancy outcomes[236,246]. Circulating cytokine and chemokine levels have been found to be altered in women with GDM, however these findings are varied across studies[216,239,248,249,240–247].

Predicted functional pathways included, signalling by IL- 4, 13, 10 and 17. IL-17 is pro-inflammatory, and known to promote the production of pro-inflammatory cytokines and chemokines, including *CXCL1, CXCL2, CXCL5, CXCL8, CCL2, CCL20, IL6, IL1B* and prostaglandin-endoperoxide synthase 2 (*PTGS2*)[542], all of which were downregulated by 7 mM glucose. In contrast, IL-10 and IL-4/13 are anti-inflammatory and are known to inhibit production of several pro-inflammatory mediators which were found to be downregulated by 7 mM glucose, including *IL1B, IL6, CCL2, CCL3, CCL19, CXCL8, CXCL1, CXCL2, PTGS2*[543,544]. Further Cytoscape analysis revealed a cluster of genes associated with interleukin signalling, with IL genes, *IL1B* and *IL6*, being central

mediators. Additionally, extracellular NAMPT, which was downregulated by 7 mM glucose, has been linked with an activation of the inflammatory response, mainly in macrophages[545]. NAMPT treatment can upregulate inflammatory mediators, such as IL-1β and IL-6, in addition to MMPs[545], which were also downregulated by 7 mM glucose. Taken together, these findings suggest an anti-inflammatory response to 7 mM glucose in placental explants.

These findings suggest that mild hyperglycaemia in pregnancies complicated by GDM and LGA may result in altered activation of immune and inflammatory pathways. The contribution of the immune and inflammatory system in the pathogenesis of diabetes mellitus, including GDM, has been increasingly studied[234–237]. Maternal hyperglycaemia has been attributed to systemic inflammation and immune dysfunction in GDM, potentially through aberrant adaptation of the maternal immune system in pregnancy[238]. Interestingly, many of the altered inflammatory mediators are also known to contribute to placental development and vascularisation. Placental cytokines and chemokines are thought to contribute to trophoblast invasion, differentiation and apoptosis and placental proliferation, villous formation and angiogenesis[218,236,546–549]. Moreover, inflammatory mediators, such as IL-6 and TNF-α have been shown to stimulate, and IL-1β to inhibit, system A activity (a placental amino acid nutrient transporter[550]) in the trophoblast[551]. IL-1β has also been associated with increasing expression *HK2* expression[260]. This suggests that inflammatory mediators altered by mild hyperglycaemia in GDM may influence placental nutrient transport, glucose metabolism and thus fetal growth. The impact of mild hyperglycaemia on the immune/inflammatory response in the placenta will be investigated further in Chapter 5.

3.6 Summary

- Maternal glucose fluctuations evident *in vivo* in CGM analyses of women with GDM that deliver LGA and AGA offspring could be modelled using an *ex vivo* placental explant model.
- Culture of tissue in 5/5.5 or 7 mM conditions did not affect tissue viability or rates of trophoblast proliferation/apoptosis.
- Gene expression of glucose transporters, GLUT4 and GLUT8, were significantly downregulated by 7 mM glucose.
- Treatment with 7 mM glucose (mild hyperglycaemia) altered the placental transcriptome, including genes associated with placental vascular development, glucose homeostasis and metabolism, fatty acid transport and metabolism and inflammation and the immune response.

- Functional enrichment analyses, through multiple methods, revealed that altered genes are known to play roles in vascular development and the immune/inflammatory response, and key DEGs within these pathways are inflammatory mediators, including cytokines and chemokines.
- Findings from this chapter revealed that subtle and physiological fluctuations in maternal glucose can impact the placental transcriptome, which may lead to functional consequences in the placenta.

Chapter 4 - The human placental transcriptome in pregnancies complicated by GDM and/or LGA

4.1 Introduction

In Chapter 3, physiological maternal glucose fluctuations associated with GDM LGA pregnancies, were found to alter the placental transcriptome. This impact on gene expression may be linked to changes in the placenta in pregnancies complicated by GDM that deliver LGA infants. Therefore, it is important to determine if the placental explant model induced transcriptomic changes similar to placentas from GDM and/or LGA pregnancies. Previous studies have shown through bulk RNA sequencing and single-cell RNA sequencing that GDM alters the placental transcriptome[552–554]. Others have investigated a selected number of genes and reported some alterations in expression in either GDM-LGA compared to uncomplicated pregnancies[555], or non-GDM LGA compared to non-GDM AGA/SGA pregnancies[556]. However, to date, there are no known publications describing the placental transcriptome in pregnancies complicated by both GDM and LGA. The aim of this chapter was to identify publicly available data sets that could be analysed to determine if there are transcriptomic changes in the human placenta in GDM and/or LGA and to use these to assess whether these are linked to the placental transcriptome changes observed in placental explants treated with glucose fluctuations. Thus, establishing whether any changes in GDM and/or LGA placentae are likely attributed to glucose fluctuations.

4.2 Hypothesis

Alterations in the placental transcriptome in pregnancies complicated by GDM and/or LGA will be attributed to physiological maternal glucose fluctuations.

4.3 Aims

1. To identify publicly available placental transcriptomic datasets and determine differentially expressed genes associated with GDM and/or LGA.
2. To compare alterations in the transcriptome induced by physiological maternal glucose fluctuations in placental explants and in GDM and/or LGA pregnancies.

4.4 Results

4.4.1 Identification of publicly available data on the GDM and/or LGA transcriptome

GEO[410] and ArrayExpress[411] were searched (2020) to identify publicly available transcriptomic datasets of human placentae, which included samples from women with GDM and/or contained information on birthweight or BWCs to determine whether samples were LGA or AGA. All identified studies are outlined in Table 4.1.

Two suitable studies were identified that contained placental transcriptomic data from GDM compared to non-GDM pregnancies. One study, from Binder *et al*. (Accession No. GSE70493)[553], contained placental samples from 41 GDM cases and 41 matched controls matched for maternal age, BMI, gestational age, gravidity/parity, ethnicity, birthweight, fetal sex, and smoking. A limitation of this dataset is that information on the BWC were not reported, so although the samples could be classified as GDM or non-GDM, it was not possible to separate based on birthweight category and it is unclear if and how many of the samples were LGA, AGA or SGA. Furthermore, since demographic information for individual samples was not available for this study, I was unable to conduct my own statistical analyses on the demographics and it was therefore assumed that the reported data were correct. These demographics are outlined in Table 4.2 as reported in the published paper[553].

The second study was by Cox *et al.* (Accession No. GSE128381)[557], which contained placental samples from lean, overweight, and obese mothers, which included 6 GDM cases, all of which were AGA. The BWCs, and classifications (AGA or LGA) were calculated using the world health organisation (WHO) growth charts[558], based on the available demographic information. Here, 6 ‘Normal’ matched controls were selected for the GDM cases, based on maternal BMI, fetal sex, parity, and ethnicity, where possible. Samples with gestational hypertension were excluded. Demographic information was provided for each sample, and averages for each group were calculated in the present study and analysed for any differences between the groups (Table 4.3). Similarly, to the previous study, there were no significant differences in maternal age, BMI, gestational age, parity, ethnicity, birthweight, fetal sex, or smoking. All 6 GDM samples in this data set were AGA, therefore the matched non-GDM controls were also AGA.

For analysis of the placental transcriptome in GDM LGA compared to GDM AGA pregnancies, one suitable study was identified (E-MTAB-6418)[559], from the Effect of Metformin on Maternal and Fetal Outcomes in Pregnant Obese Women (EMPOWaR) trial which had a primary outcome of determining whether exposure to metformin could affect the offspring BWC in obese pregnancies[559]. GDM women were not excluded from the study and the data set included 6 GDM LGA samples and 23 GDM AGA samples. This study also included samples from 12 non-GDM LGA and 51 non-GDM

AGA pregnancies, which were also compared. Some demographic information was provided for each sample that allowed BWCs and classifications (AGA or LGA) to be calculated using the WHO growth charts[558]. It was then possible to categorise the samples into four groups: non-GDM AGA, non-GDM LGA, GDM AGA and GDM LGA (Table 4.4). All categories were matched for maternal age, gestational age, fetal sex, metformin treatment, or smoking, however there was a significant difference in mode of delivery ($p<0.05$), which is likely associated with earlier delivery in women with GDM/LGA by caesarean section, to reduce the risk of complications, such as shoulder dystocia, with vaginal delivery[27,28,560]. BMI was not provided, but as part of the study inclusion criteria, all samples were from obese pregnancies. Birthweight and BWCs were significantly higher in groups with LGA infants, as expected based on the grouping of samples by AGA and LGA ($p<0.0001$).

For further analysis of the placental transcriptome in non-GDM LGA compared to non-GDM AGA pregnancies (non-GDM) two suitable published datasets were identified. This included again the study by Cox *et al.* (2019)[557] (GSE128381), which included 15 placental samples from LGA pregnancies (non-GDM). Here, 15 matched AGA placental samples from non-GDM pregnancies were selected based on maternal BMI, parity, and ethnicity, where possible. Samples with gestational hypertension were excluded. Demographic information was provided for each sample, and statistical analysis was performed to determine how well matched the groups were (Table 4.5). Samples were all matched for maternal age, BMI, gestational age, parity, ethnicity, fetal sex, and smoking status. The absolute birthweight was higher in the LGA group, although this was not significant ($p=0.06$). However, when BWC were calculated using WHO criteria, as expected, there was a significant difference in the BWC ($p<0.0001$) in the LGA group. The second dataset was by Turan and Sapienza (Unpublished; GSE32868). This contained 12 placental samples from LGA pregnancies (non-GDM) and 36 placental samples from AGA pregnancies (non-GDM). The 12 LGA samples could not be matched to 12 AGA samples as limited demographic information was provided. Therefore, all 12 LGA samples were compared to all 36 AGA samples. The demographic information that was provided included gestational age, birthweight and BWCs. The averages for each group were calculated in the present study and analysed for any differences between the groups (Table 4.6). As expected, there was a significant increase in birthweight ($p<0.0001$) and BWC ($p<0.0001$) in the LGA group. No significant differences were observed in gestational age.

Table 4.1 - Transcriptomic datasets on placentae identified on the Gene Expression Omnibus (GEO) or Array Express. The dataset IDs for GEO (GSE) and Array Express (E-MTAB-), the number of GDM samples (if applicable) and demographic information for the calculation of birthweight centiles (BWC) are shown. The final column details whether the dataset was included in the analysis and reasons for inclusion/exclusion.

Dataset	Array Type	Tissue	GDM Samples	Sample Number	Birthweight	Gestational Age	Fetal Sex	BMI	Other info	Included or excluded from analysis
GSE128381	Agilent-039494 SurePrint G3 Human GE v2 8x60K Microarray 039381	Term Placenta	6 with GDM	183	✓	✓ (Weeks)	✓	✓		**Included** – GDM samples and some demographic information to calculate BWC provided.
GSE70493	Affymetrix Human transcriptome array v2.0	Term Placenta	41 with GDM	82	×	×	×	×		**Included –** GDM samples.
E-MTAB-4541	RNA Sequencing	Term Placenta	GDM excluded	10	×	×	×	No but class (lean/overweight/ obese)		**Excluded** – No GDM and demographic information to calculate BWC not provided.
E-MTAB-6418	Illumina HumanHT-12 v4.0 expression beadchip	Term Placenta	All GDM	108	✓ (adjusted for gestational age)	✓ (Days)	✓	All obese BMI greater or equal to 30	Metformin and Non-Metformin Samples	**Included** – GDM samples and some demographic information to calculate BWC provided.
GSE36828	Illumina HumanHT-12 v3.0 expression beadchip	Term Placenta (+Cord blood)	GDM excluded	48 (Placenta)	✓ (and BWC)	✓ (Weeks)	×	×		**Included** – No GDM but BWC provided.
GSE27272	Illumina HumanRef-8 v3.0 expression beadchip	Term Placenta (+Maternal and Cord Blood)	GDM excluded	54 (Placenta)	✓	✓ (Weeks)	×	✓	Smokers and non-smokers	**Excluded** – Demographic information to calculate BWC not provided.
GSE100415	Affymetrix Human Gene 1.0 ST Array	Term Placenta	GDM excluded	20	× (All samples SGA)	✓ (Weeks)	✓	✓		**Excluded** – All samples SGA

Table 4.2 - Demographic information for GDM and Non-GDM samples from the GSE70493 study. Demographic information for individual samples was not available for this study, and therefore the patient demographics are as reported in the published paper. Continuous variables are summarised by the mean±SD and categorical variables are reported as a number (%). The statistical methods used were not reported in this study.

	GDM (n=41)	Non-GDM (n=41)	Significance
Maternal age (years)	33.17±4.65	33.49±4.85	p=0.7635 NS
BMI at booking (kg/m^2)	26.65±5.73	26.41±5.42	p=0.7635 NS
Gestational age (weeks)	39.08±0.93	39.21±1.05	p=0.5576 NS
Gravidity	1: 8 (19.51%) 2: 11 (26.83%) 3: 13 (31.71%) >4: 8 (19.51%)	1: 4 (9.76%) 2: 16 (39.02%) 3: 10 (24.39%) >4: 11 (26.83%)	
Ethnicity	Non-Hispanic White: 23 (56.098%) Hispanic or Latino: 5 (12.195%) Asian/Pacific Islander: 7 (17.073%) Black/African American: 6 (14.634%)	Non-Hispanic White: 23 (56.098%) Hispanic or Latino: 4 (9.756%) Asian/Pacific Islander: 6 (14.634%) Black/African American: 8 (19.512%)	p=0.9437 NS
Birthweight (g)	3540±54	3921±50	p=0.7590 NS
Male infant (%)	20 (48.78%)	21 (51.22%)	p=1 NS
Smoked in Pregnancy (%)	3 (7.32%)	3 (7.32%)	p=1 NS

Table 4.3 - Demographics for GDM and non-GDM samples in the GSE128381 study. Continuous variables are summarised by the mean±SEM and statistical analysis was performed using either an unpaired T-Test or a Mann-Whitney U test, for normally distributed or non-normally distributed variables, respectively. Categorical variables are reported as a number (%) and statistical analysis was performed using a Chi-Squared test.

	GDM (n=6)	Non-GDM (n=6)	Significance
Maternal age (years)	30.17±1.40	27.16±1.45	p=0.1672 (T-Test)
BMI at booking (kg/m^2)	26.58±2.32	20.08±2.22	p=0.8795 (T-Test)
Gestational age (weeks)	38.83±0.79	39.33±0.49	p=0.6063 (T-Test)
Parity	2±0.26	1.83±0.31	p=0.718 (Mann-Whitney)
European (%)	4 (66%)	4 (66%)	p=1 (Chi-Squared)
Birthweight (g)	3279.17±229.89	3400.83±116.80	p=0.6506 (T-Test)
Male infant (%)	3 (50%)	3 (50%)	p=1 (Chi-Squared)
AGA (%)	100%	100%	p=1 (Chi-Squared)
BWC	45.67±11.61	43.67±11.11	p=0.9043 (T-Test)
Smoked in Pregnancy (%)	0 (0%)	0 (0%)	p=1 (Chi-Squared)

Table 4.4 - Demographics for Non-GDM AGA, Non-GDM LGA, GDM AGA and GDM LGA samples in the E-MTAB-6418 study. Continuous variables are summarised by the mean±SEM and statistical analysis was performed using either a One-way ANOVA with Tukey's post-hoc test or a Kruskal-Wallis with Dunn's post-hoc test, for normally distributed or non-normally distributed variables, respectively. Categorical variables are reported as a number (%) and statistical analysis was performed using a Chi-Squared test. Abbreviations: BWC – birthweight centile.

	Non-GDM AGA (n=51)	Non-GDM LGA (n=12)	GDM AGA (n=23)	GDM LGA (n=6)	Significance
Maternal age (years)	29.5±0.75	30.42±1.40	29.17±1.13	34.17±2.10	NS (One-Way ANOVA)
Gestational age (days)	279.78±1.31	281.25±2.83	274.74±1.32	279.50±5.44	NS (One-Way ANOVA)
Birthweight (Adjusted for gestational age) (g)	3459.76±48.84	4203.33±53.29	3402.522±68.12	4533.67±153.21	Non-GDM AGA vs GDM LGA p<0.00000001**** Non-GDM LGA vs GDM AGA p<0.00000001**** Non-GDM AGA vs Non-GDM LGA p<0.00000001**** GDM AGA vs GDM LGA p<0.00000001**** (One-Way ANOVA)
Metformin (%)	**Metformin:** 27 (53%) **No Metformin:** 24 (47%)	**Metformin:** 8 (67%) **No Metformin:** 4 (33%)	**Metformin:** 11 (48%) **No Metformin:** 12 (52%)	**Metformin:** 1 (17%) **No Metformin:** 5 (83%)	p=0.24 NS (Chi-Squared)
Fetal Sex (%)	**Male:** 26 (51%) **Female:** 25 (49%)	**Male:** 5 (42%) **Female:** 7 (58%)	**Male:** 16 (70%) **Female:** 7 (30%)	**Male:** 5 (83%) **Female: 1** (17%)	p=0.17 NS (Chi-Squared)
Mode of delivery (%)	**Labour:** 44 (86%) **No Labour:** 7 (14%)	**Labour:** 7 (58%) **No Labour:** 5 (42%)	**Labour:** 19 (83%) **No Labour:** 4 (17%)	**Labour:** 3 (50%) **No Labour:** 3 (50%)	P=0.045 * (Chi-Squared)

Smoked in pregnancy (%)	**Smoked:** 8 (16%) **Non-Smoker:** 43 (84%)	**Smoked:** 0 **Non-Smoker:** 12 (100%)	**Smoked:** 1 (4%) **Non-Smoker:** 22 (96%)	**Smoked:** 0 **Non-Smoker:** 6 (100%)	p=0.19 NS (Chi-Squared)
BWC	48.98±3.55	93.83±0.84	45.65±5.12	96.43±1.28	Non-GDM AGA vs GDM LGA p=0.000027 **** Non-GDM LGA vs GDM AGA p=0.000001 **** Non-GDM AGA vs Non-GDM LGA p=0.00000041 **** GDM AGA vs GDM LGA p=0.000026 **** (Kruskal-Wallis)

Table 4.5 - Demographics for non-GDM LGA and non-GDM AGA samples in the GSE128381 study. Continuous variables are summarised by the mean±SEM and statistical analysis was performed using either an unpaired T-Test or a Mann-Whitney U test, for normally distributed or non-normally distributed variables, respectively. Categorical variables are reported as a number (%) and statistical analysis was performed using a Fisher's Exact test.

	LGA (n=15)	AGA (n=15)	Significance
Maternal age (years)	30.5±1.18	32.71±1.40	p=0.3167 NS (T-Test)
BMI at booking (kg/m^2)	26.61±1.88	26.32±1.66	p=0.8845 NS (Mann-Whitney)
Gestational age (weeks)	38.5±0.85	38.9±0.52	p=0.398 NS (Mann-Whitney)
Parity	1.5±0.17	1.64±0.19	p=0.6557 NS (Mann-Whitney)
European (%)	14 (93%)	15 (100%)	p=1 NS (Chi-Squared)
Birthweight (g)	3719.64±201.84	3277.5±93.71	p=0.06 NS (T-Test)
Male infant (%)	6 (40%)	6 (40%)	p=1 NS (Chi-Squared)
BWC	92.57±0.61	51.5±6.49	p=0.00000325 **** (Mann-Whitney)
Smoked in Pregnancy (%)	0 (0%)	1 (6.7%)	p=1 (Chi-Squared)

Table 4.6 - Demographics for non-GDM LGA and non-GDM AGA samples in the GSE36828 study. Continuous variables are summarised by the mean±SEM and statistical analysis was performed using either an unpaired T-Test or a Mann-Whitney U test, for normally distributed or non-normally distributed variables, respectively.

	LGA (n=12)	AGA (n=36)	Significance
Gestational age (weeks)	39.35±0.31	39.61±0.19	p=0.4688 NS (T-Test)
Birthweight (g)	4279.83±74.32	3543.44±50.31	p=0.000000285 **** (Mann-Whitney)
BWC	95.17±0.85	56.25±3.87	p=0.000000039 **** (T-Test)

4.4.2 The placental transcriptome in pregnancies complicated by GDM

GEO2R was used to identify DEGs ($p<0.05$ and Log_2FC of <-0.5 and >0.5) between GDM and matched non-GDM placental samples in the Cox *et al.* (2019)[557] (GSE128381) and Binder *et al.* (2015)[553] (GSE70493) studies.

In the analysis of the GSE128381 data 14,040 transcripts were detected and 575 were differentially expressed, with 104 upregulated and 471 downregulated in GDM placentae (Figure 4.1). ORA did not identify any significant pathways associated with DEGs; however, two significant GO terms were identified which were related to peptidase regulator activity in apoptotic processes (FDR: 0.030). DEGs within these GO terms included several immune and inflammatory-related genes, such as, NLR family pyrin domain containing 1 (*NLRP1*)[561], Tumour necrosis factor-α–induced protein 8 (*TNFAIP8*)[562] and apoptosis-related genes Caspase 3 (*CASP3*)[563] and X-linked inhibitor of apoptosis protein (*XIAP*)[564].

In the analysis of the GSE70493 data 70,523 transcripts were detected and 40 were differentially expressed, with 36 upregulated and 4 downregulated in GDM placentae (Figure 4.2A). The top upregulated genes in GDM included IGF binding protein 1 (*IGFBP1*), which has previously been linked to fetal growth and placental development[565–567], in addition to inflammatory genes interleukin-1 receptor-like 1 (*ILRL1*)[568], *CXCL9* and *CXCL10*[569]. There were also several differentially expressed transcripts that were unannotated, including pseudogenes or unnamed lncRNAs.

DEGs were associated with pathways related to autoimmune diseases (T1DM, thyroid disease) and immune responses (allograft rejection) (FDR: 1.18E-06- 1.07E-05) (Figure 4.2B). However, the DEGs associated with all these pathways were primarily altered human leukocyte antigen (HLA) genes: *HLA-DRB5, HLA-DRB1, HLA-DQA1* and *HLA-DRA*. These DEGs were also enriched in GO terms associated with MHC major histocompatibility complex (MHC) protein complexes and antigen presentation (FDR: 4.63E-07-1.48E-03) (Figure 4.2C). In addition to HLA genes, other key genes in these GO terms were *CXCL9* and *CXCL10*.

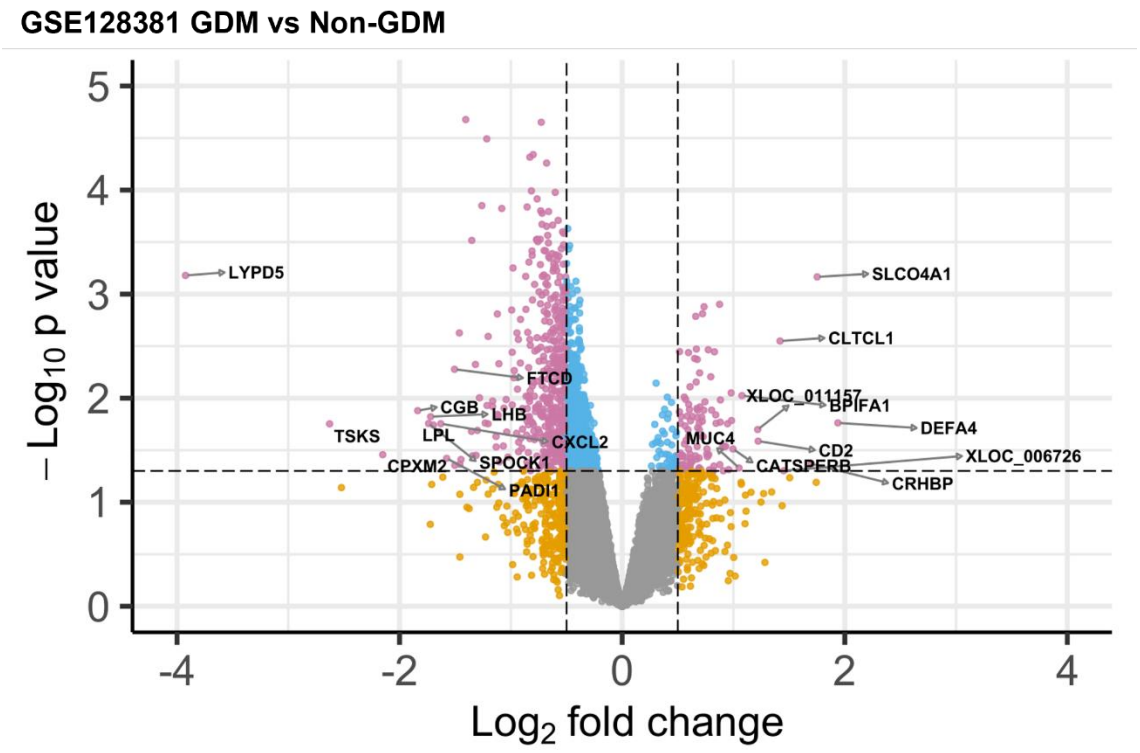

Figure 4.1 - Alterations in the placental transcriptome in GDM in the GSE128381 study. Volcano plot representing differentially expressed genes (DEGs) in GDM compared to non-GDM placentae identified in transcriptomic data from the Cox *et al.* (GSE128381) study[557]. Horizontal dashed line represents p=0.05, the vertical dashed lines represent a Log2FC of ± 0.5 equivalent to a fold change of 1.4 and -0.71. NS = grey, significant p value = blue, significant Log_2FC = orange, significant p value and Log_2FC = pink. The top 10 upregulated and downregulated annotated genes are labelled. Volcano plot generated using EnhancedVolcano in R.

A) GSE70493 GDM vs Non-GDM

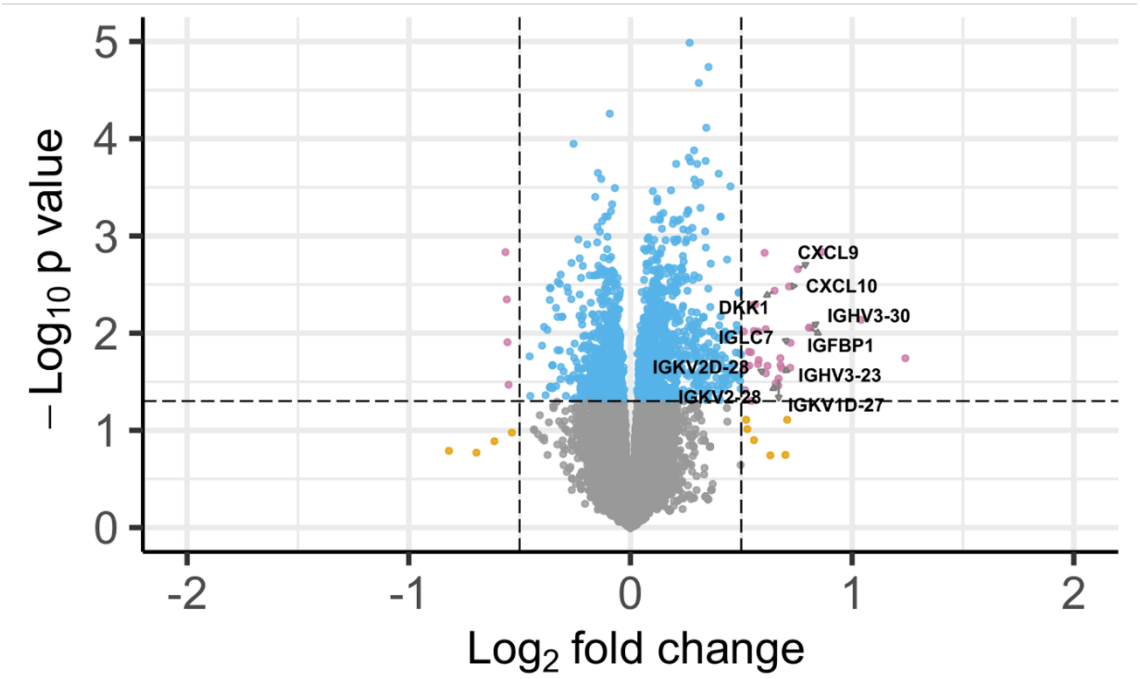

B)

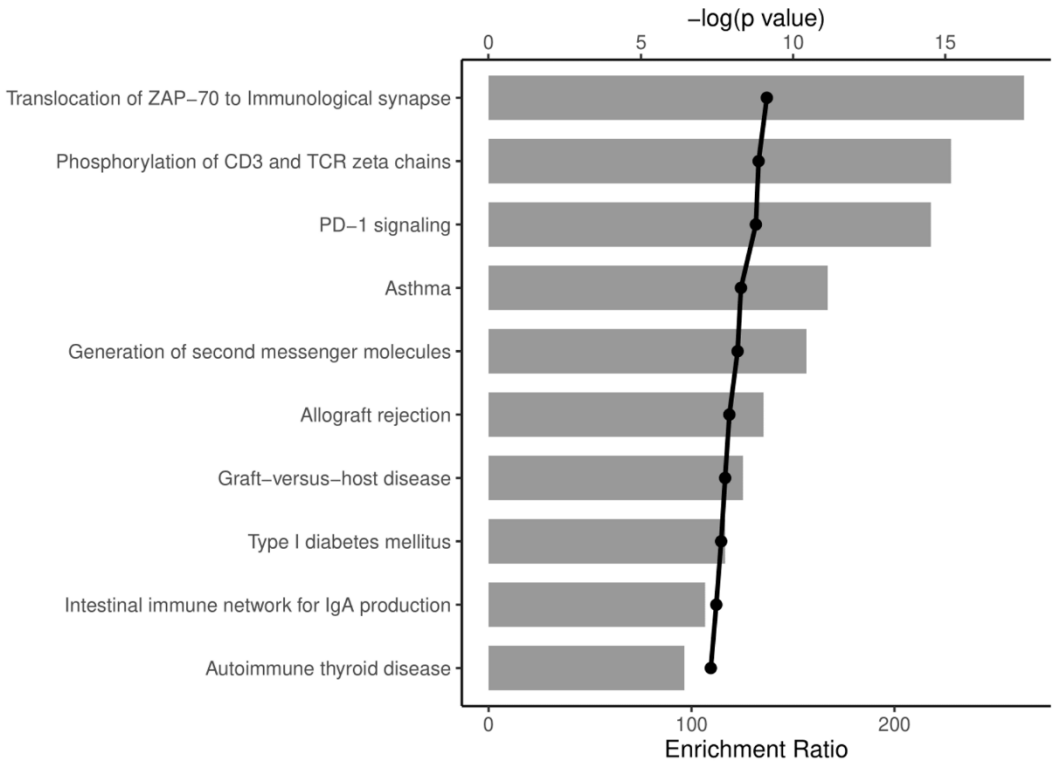

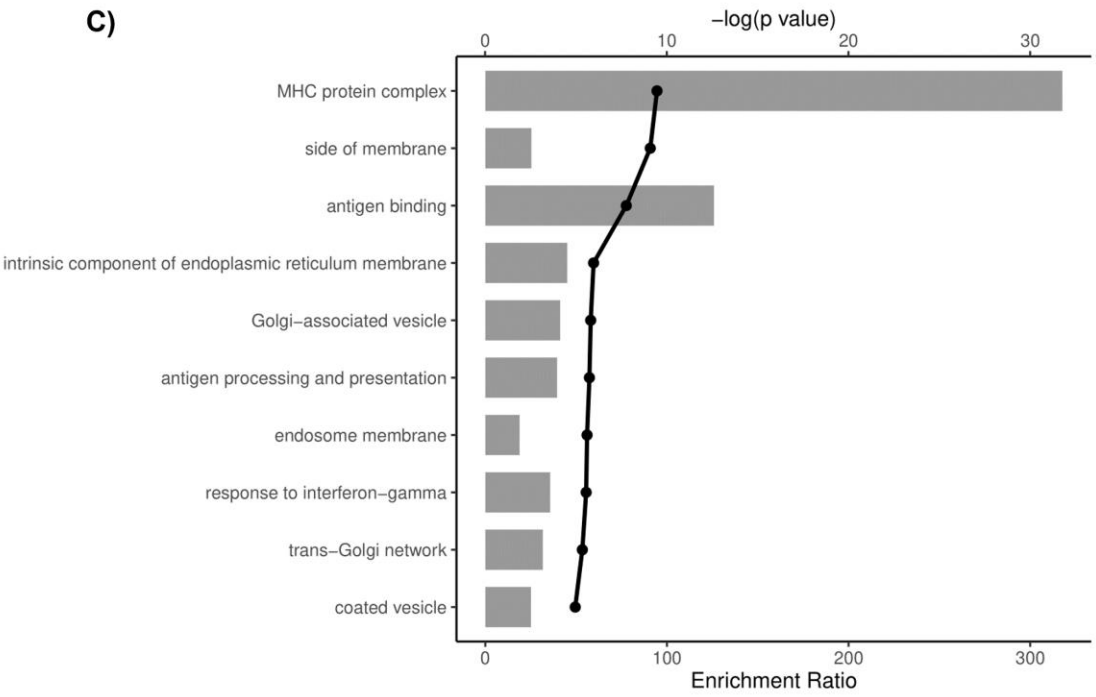

Figure 4.2 – Alterations in the placental transcriptome in GDM in the GSE70493 study. A) Volcano plot representing differentially expressed genes (DEGs) in GDM compared to non-GDM placentae identified in transcriptomic data from the Binder *et al.* (GSE70493) study. Horizontal dashed line represents p=0.05, the vertical dashed lines represent a Log2FC of ± 0.5 equivalent to a fold change of 1.4 and -0.71. NS = grey, significant p value = blue, significant Log_2FC = orange, significant p value and Log_2FC = pink. The top 10 upregulated and downregulated annotated genes are labelled. Volcano plot generated using EnhancedVolcano in R. B) DEGs ($p<0.05$, Log2FC -0.5< or >0.5) that were altered in GDM compared to non-GDM placentae from the GSE70493 study were inputted into WebGestalt for GO and pathway analysis. The top y-axis represents the -log(p value) indicated by the black line plot, and the lower y-axis represents the enrichment ratio (number of observed genes divided by the number of expected genes in each GO term/pathway) for each of the represented GO terms/pathways, indicated by the bars. Pathways are ordered by most significant p value.

4.4.2.1 A comparison of genes altered by glucose fluctuations and genes associated with GDM

The annotated DEGs altered in GDM placentae from both studies were then compared to the DEGs altered by 7 mM glucose in placental explants. When comparing to the GSE128381 DEGs, 7 genes overlapped (Figure 4.3). Interestingly, *CXCL2,* L-Selectin *(SELL), TIPARP,* Serrate RNA effector molecule homolog *(SRRT),* Topoisomerase 1 *(TOP1)* and Hyaluronan and Proteoglycan Link Protein 2 *(HAPLN2)* were downregulated in GDM placentae and by 7 mM glucose in explants. The one overlapping gene that was upregulated in GDM placentae was the Fc gamma receptor IIb *(FCGR2B)* gene, which was also upregulated by 7 mM glucose. The overlapping genes, their functions, and associated p values/Log_2FC's are summarised in Table 4.7.

No DEGs altered by 7 mM glucose overlapped with the GSE70493 DEGs. Additionally, GO terms and pathways identified through ORA did not overlap with those associated with glucose fluctuations in placental explants. However, DEGs altered in GDM placentae included chemokines *CXCL2, CXCL9* and *CXCL10* and other inflammatory-related genes, *FCGR2B, SELL, NLRP1* and *TNFAIP8*[561,562], in line with the immune and inflammatory genes associated with glucose fluctuations in explants. Interestingly, there were no overlapping genes between the two studies on the GDM placentae, likely due to differences between these cohorts.

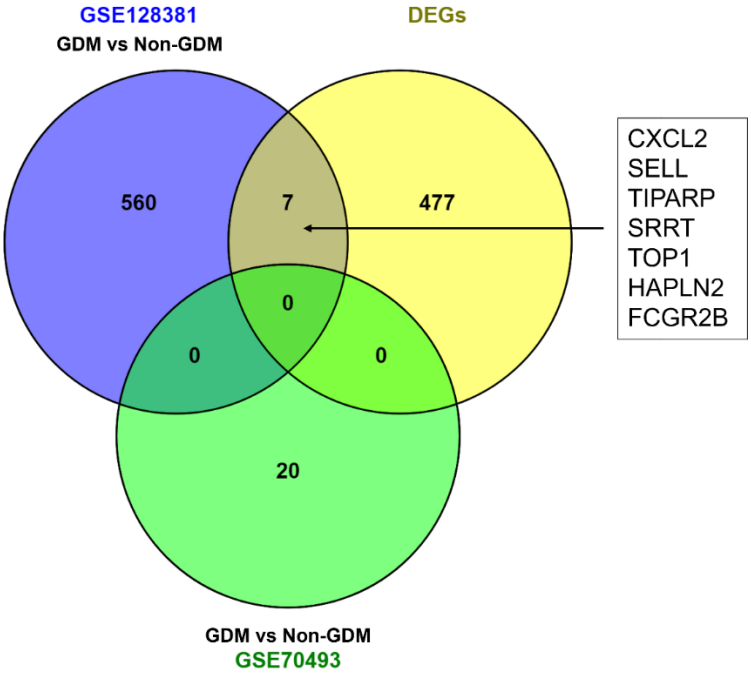

Figure 4.3 - Genes altered by 7 mM glucose in placental explants that are also altered in GDM placentae. GEO2R was used to identify DEGs in the Binder *et al.* (GSE70493) and the Cox *et al.* (GSE128381) studies comparing the transcriptome of GDM compared to non-GDM placentae. Venn diagrams were used to identify genes which were altered in GDM placentae and by 7 mM glucose in placental explants.

Table 4.7 - Genes altered by 7 mM glucose in placental explants that are also altered in GDM placentae. The genes altered by 7 mM glucose in placental explants that were also altered by GDM in the Cox *et al.* (GSE128381) study are shown, with their known functions and associated p values/Log_2FC values.

Gene	Function	Genes altered by 7 mM glucose in placental explants		Genes altered by GDM (GSE128381)	
		Log_2FC	P Value	Log_2FC	P Value
CXCL2	• Chemokine (C-X-C motif) ligand 2 (CXCL2) is a chemokine, which recruits leukocytes in areas of inflammation[570].	-0.6289	0.02069	-1.6298	0.0176
SELL	• L-Selectin (SELL) is a cell adhesion molecule found leukocytes and facilitates cell adhesion between leukocytes and endothelial cells, important for recruiting monocytes in trans-endothelial migration[571].	-2.7768	0.0231	-0.7888	0.00958
TIPARP	• TCDD-inducible poly [ADP-ribose] polymerase (TIPARP) which catalyses mono-ADP-ribosylation[572].	-1.6492	0.02124	-0.686	0.00254
SRRT	• Serrate RNA effector molecule homolog (SRRT), also known as also known as arsenite-resistance protein 2 (ARS2) contributes to miRNA biogenesis and cellular proliferation[573].	-0.5306	0.04396	-0.6853	0.00816
TOP1	• DNA topoisomerase 1 (TOP1) is an enzyme that removes torsional stress in DNA which is generated during DNA unwinding[574].	-0.6043	0.04518	-0.67	0.00128
HAPLN2	• Hyaluronan and proteoglycan link protein 2 (HAPLN2) is important for the formation of the extracellular matrix, by the binding of chondroitin sulphate proteoglycans to hyaluronan[575].	-1.3495	0.02367	-0.5429	0.02074
FCGR2B	• Fc gamma receptor IIb (FCGR2B) is a member of the immune receptor IgG Fc gamma family. It is expressed in a variety of immune cells and are involved in the clearance of immune complexes by binding to the Fc region of IgGs for the effective control of inflammation and infection[576].	1.6276	0.00994	0.58446	0.0404

4.4.3 The placental transcriptome in pregnancies complicated by LGA

To assess whether the placental transcriptome is altered in GDM LGA pregnancies compared to GDM AGA pregnancies, GenomeStudio (v1.0) was used to assess DEGs in the E-MTAB-6418 study. This study also included non-GDM LGA and non-GDM AGA samples, which were also compared. This method was different to that used in the other analyses based on the format of the available data. No significant DEGs were identified in GDM LGA compared to GDM AGA pregnancies, or non-GDM LGA compared to non-GDM AGA pregnancies.

To further assess whether the placental transcriptome is altered in LGA pregnancies (non-GDM), GEO2R was used to identify placental DEGs ($p<0.05$ and Log_2FC of <-0.5 and >0.5) between non-GDM LGA and non-GDM AGA in the Cox *et al.* (2019)[557] (GSE128381) and Turan and Sapienza (Unpublished; GSE36828) studies.

In the analysis of the GSE128381 data, 14,040 transcripts were detected, and 48 were differentially expressed, with 23 upregulated and 25 downregulated (Figure 4.4). DEGs included the inflammatory gene, interleukin 36 receptor antagonist (*IL36RN*)[577], *FABP4* and genes associated with gas transport, including erythroid-specific 5-aminolevulinate synthase (*ALAS2*) and haemoglobin subunit alpha 2 (*HBA2*)[578].

In the analysis of the GSE36828 data, 48,803 transcripts were detected, and 7 were differentially expressed, with 3 upregulated and 5 downregulated (Figure 4.5). DEGs included the adipokine, leptin (*LEP*)[579], which has previously been linked to fetal growth[580]. A top upregulated gene in LGA identified in both studies was carbamoyl phosphate synthetase 1 (*CPS1*), which is a mitochondrial enzyme involved in urea production[581]. ORA did not identify any significant pathways or GO terms associated with DEGs in either study.

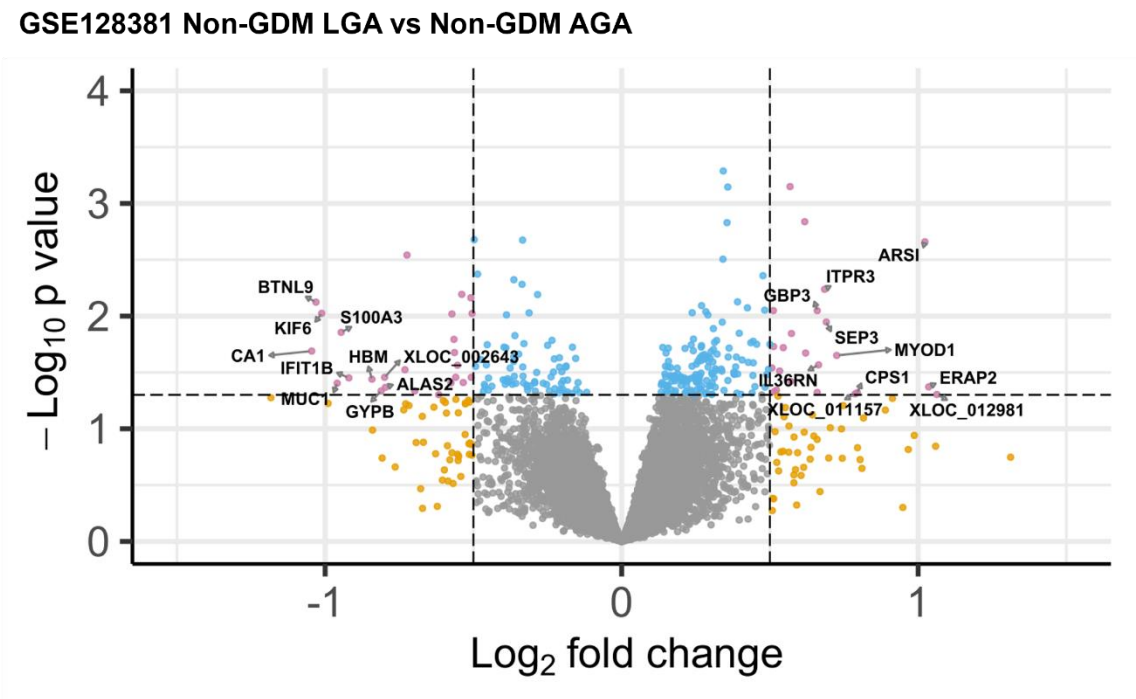

Figure 4.4 – Alterations in the placental transcriptome in non-GDM LGA pregnancies in the GSE128381 study. Volcano plot representing differentially expressed genes in non-GDM LGA compared to non-GDM LGA placentae identified in transcriptomic data from the Cox *et al.* (GSE128381) study[557]. Horizontal dashed line represents p=0.05, the vertical dashed lines represent a Log2FC of ± 0.5 equivalent to a fold change of 1.4 and -0.71. NS = grey, significant p value = blue, significant Log_2FC = orange, significant p value and Log_2FC = pink. The top 10 upregulated and downregulated annotated genes are labelled. Volcano plot generated using EnhancedVolcano in R.

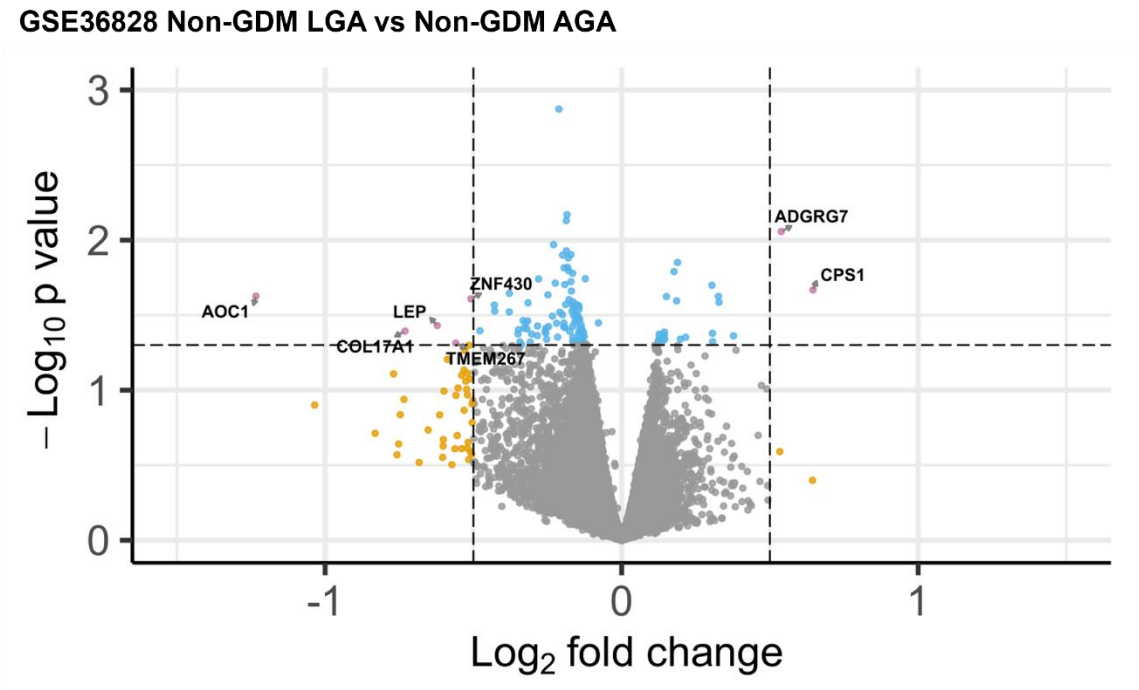

Figure 4.5 – Alterations in the placental transcriptome in non-GDM LGA pregnancies in the GSE36828 study. Volcano plot representing differentially expressed genes in non-GDM LGA compared to non-GDM LGA placentae identified in transcriptomic data from the Turan and Sapienza (Unpublished; GSE36828). Horizontal dashed line represents p=0.05, the vertical dashed lines represent a Log2FC of ± 0.5 equivalent to a fold change of 1.4 and -0.71. NS = grey, significant p value = blue, significant Log_2FC = orange, significant p value and Log_2FC = pink. The top 10 upregulated and downregulated annotated genes are labelled. Volcano plot generated using EnhancedVolcano in R.

4.4.3.1 A comparison of genes altered by glucose fluctuations and genes associated with LGA

The annotated DEGs between non-GDM LGA and non-GDM AGA in the Cox *et al.* (2019)[557] (GSE128381) and Turan and Sapienza (Unpublished; GSE36828) studies were then compared to the DEGs altered by 7 mM glucose in placental explants. When comparing to the GSE128381 data, three genes that were altered by 7 mM glucose were also altered in LGA placentae (Figure 4.6). Of these, two genes, *PDGFD* and *ALAS2*, were downregulated 7 mM glucose and downregulated in LGA placentae. However, *FABP4* was upregulated by 7 mM glucose and downregulated in LGA placentae (Table 4.8). No genes altered by 7 mM glucose overlapped with the GSE36828 DEGs. One gene, *CPS1* was upregulated in LGA in both previously published data sets.

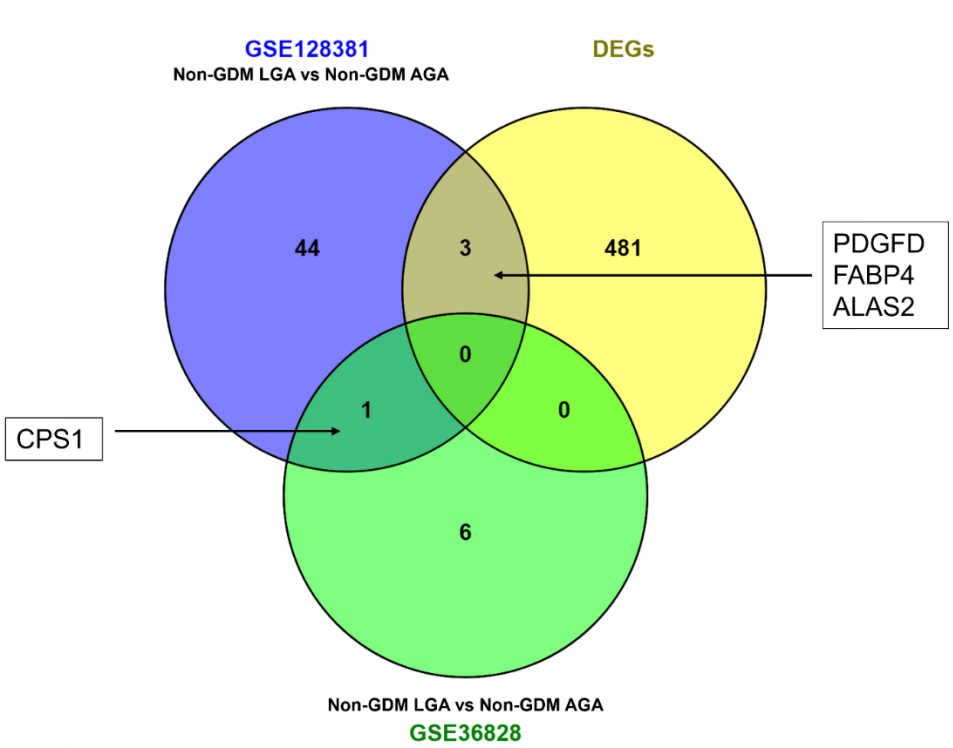

Figure 4.6 - Genes altered by 7 mM glucose in placental explants that are also altered in non-GDM LGA compared to non-GDM AGA placentae. GEO2R was used to identify DEGs in the Cox *et al.* (GSE128381) and Turan and Sapienza (Unpublished; GSE36828) studies comparing the transcriptome of non-GDM LGA compared to non-GDM AGA placentae. Venn diagrams were used to identify genes which were altered in LGA placentae and by 7 mM glucose in placental explants.

Table 4.8 - Genes altered by 7 mM glucose in placental explants that are also altered in non-GDM LGA compared to non-GDM AGA placentae. The genes altered by 7 mM glucose in placental explants that were also altered by LGA in the Cox *et al.* (GSE128381) study are shown, with their known functions and associated p values/Log_2FC values.

Gene ID	Function	Genes altered by 7 mM glucose in placental explants		Genes altered by LGA (GSE128381)	
		Log_2FC	P Value	Log_2FC	P Value
PDGFD	• Platelet derived growth factor D (PDGFD) is a member of the PDGF family that binds the PDGFRβ[481] and promotes cell growth and angiogenesis[582].	-2.52819	0.035585	-0.61684	0.049828
ALAS2	• Erythroid-specific 5-aminolevulinate synthase (ALAS2) is the rate-limiting enzyme for haem biosynthesis in erythroid cells[583]	-2.85152	0.016554	-0.79686	0.04290
FABP4	• Fatty acid binding protein 4 (FABP4) is an intracellular lipid chaperone, which regulates lipid trafficking and responses in cells[584]. In the placenta It binds fatty acids following their transport across the placental barrier[205].	1.704141	0.001375	-0.72401	0.002871

4.4.4 DEG expression in a further cohort of GDM/non-GDM and LGA/AGA placental RNA samples

To further assess whether any genes altered by 7 mM glucose in placental explants were also altered by GDM and/or LGA, a panel of DEGs were assessed in a separate cohort of samples of human term placental RNA using RT-qPCR.

Firstly, the samples were divided into GDM (n=26) and non-GDM (n=24). The demographic information for each group is outlined in Table 4.9. The samples were then further divided into non-GDM AGA (n=13), non-GDM LGA (n=11), GDM AGA (n=15) and GDM LGA (n=11). The demographic information for each group is outlined in Table 4.10.

Maternal age was higher in GDM LGA (33.36±1.36) and AGA groups (33.60±1.15) than non-GDM AGA (26.92±1.69; $p<0.05$), but not compared to non-GDM LGA (30±1.32). This likely because there is an increased risk of developing GDM and/or LGA infants with increasing maternal age[585,586]. Gestational age was also significantly lower in the GDM AGA (269.93±1.87) group compared to non-GDM AGA (276.62±1.91; $p<0.01$), and there was also a significant difference in mode of delivery ($p<0.01$). As previously discussed, both findings are likely associated with earlier delivery in women with GDM by caesarean section, to reduce the risk of complications[27,28,560]. Birthweight and placental weight were significantly higher in groups with LGA infants ($p<0.05$), as expected based on the grouping of samples by AGA and LGA. BWCs were also significantly higher in LGA groups ($p<0.0001$). In line with this, when samples were divided into GDM and non-GDM, maternal age was significantly higher in the GDM group ($p<0.001$) and gestational age was significantly lower ($p<0.05$).

Table 4.9 - Demographics for GDM and non-GDM RNA placental samples used in the present study. Patients were grouped into either GDM (n=26) or non-GDM (n=24). Continuous variables are summarised by the mean±SEM and statistical analysis was performed using either a T-Test or Mann-Whitney U Test, for normally distributed or non-normally distributed variables, respectively. Categorical variables are reported as a number (%) and statistical analysis was performed using a Chi-Squared test. Abbreviations: BMI – body mass index; BWC – birthweight centile; EL LSCS - Elective Lower Segment Caesarean Section; EM LSCS - Emergency Lower Segment Caesarean Section; NVD – Normal Vaginal Delivery.

	GDM (n=26)	Non-GDM (n=24)	Significance
Maternal age (years)	33.50±0.86	28.33±0.89	p=0.00068 *** (T-Test)
BMI at booking (kg/m^2)	31.03±1.24	30.14±2.10	p=0.689 NS (T-Test)
Gestational age (days)	270.43±1.28	275.63±1.46	p=0.0146 * (Mann Whitney)
Parity	2.12±0.38	1.08±0.18	p=0.02716 * (Mann Whitney)
Ethnicity (%)	**Arab:** 3 (12%) **Asian:** 9 (35%) **Black:** 3 (12%) **White:** 11 (42%)	**Arab:** 0 **Asian:** 5 (21%) **Black:** 2 (8%) **White:** 17 (71%)	p=0.1352 NS (Chi-Squared)
Birthweight (g)	3640.15±119.09	3776.46±86.27	p=0.3688 NS (T-Test)
Placental weight (g)	637.99±44.52	617.74±25.27	p=0.7046 NS (T-Test)
Fetal sex (%)	**Male:** 12 (46%) **Female:** 12 (46%) **Unknown:** 2 (8%)	**Male:** 11 (46%) **Female:** 13 (54%)	p=0.3667 NS (Chi-Squared)
Birthweight Class (%)	**AGA:** 15 (58%) **LGA:** 11 (42%)	**AGA:** 13 (54%) **LGA:** 11 (46%)	p=1 NS (Chi-Squared)
BWC	70.69±5.82	69.08±5.09	p=0.7411 NS (Mann Whitney)
Smoked in Pregnancy (%)	**Smoked:** 0 **Non-Smoker:** 26 (100%)	**Smoked:** 4 (17%) **Non-Smoker:** 20 (83%)	p=0.09923 NS (Chi-Squared)
Mode of delivery (%)	**NVD:** 9 (35%) **EM LSCS:** 5 (19%) **EL LSCS:** 10 (38%) **Unknown:** 2 (8%)	**NVD:** 9 (38%) **EM LSCS:** 0 **EL LSCS:** 14 (58%) **Unknown:** 1 (4%)	p=0.1151 NS (Chi-Squared)

Table 4.10 – Demographics for non-GDM/GDM and AGA/LGA samples RNA used in the present study. Patients were grouped into four categories based on their GDM diagnosis and BWC: Non-GDM AGA (n=13), Non-GDM LGA (n=11), GDM AGA (n=15) and GDM LGA (n=11). Continuous variables are summarised by the mean±SEM and statistical analysis was performed using either a One-way ANOVA with Tukey's post-hoc test or a Kruskal-Wallis with Dunn's post-hoc test, for normally distributed or non-normally distributed variables, respectively. Categorical variables are reported as a number (%) and statistical analysis was performed using a Chi-Squared test. Abbreviations: BMI – body mass index; BWC – birthweight centile; EL LSCS - Elective Lower Segment Caesarean Section; EM LSCS - Emergency Lower Segment Caesarean Section; NVD – Normal Vaginal Delivery.

	Non-GDM AGA (n=13)	Non-GDM LGA (n=11)	GDM AGA (n=15)	GDM LGA (n=11)	Significance
Maternal age (years)	26.92±1.69	30±1.32	33.60±1.15	33.36±1.36	Non-GDM AGA vs GDM AGA p=0.0046 ** No-GDM AGA vs GDM LGA p=0.013 * (One-Way ANOVA)
BMI at booking (kg/m^2)	29.98±2.18	30.34±3.11	30.37±1.67	32.02±1.91	p=0.92-0.99 NS (One-Way ANOVA)
Gestational age (Days)	276.62±1.91	274.45±2.58	269.93±1.87	271.38±1.61	Non-GDM AGA vs GDM AGA p=0.0085 ** (Kruskal-Wallis)
Parity	1.23±0.28	0.91±0.25	1.87±0.29	2.45±0.81	Non-GDM LGA vs GDM AGA p=0.038 * (Kruskal-Wallis)
Ethnicity (%)	**Arab:** 0 **Asian:** 2 (15%) **Black:** 1 (8%) **White:** 10 (77%)	**Arab:** 0 **Asian:** 3 (27%) **Black:** 1 (9%) **White:** 7 (64%)	**Arab:** 1 (7%) **Asian:** 6 (40%) **Black:** 3 (20%) **White:** 5 (33%)	**Arab:** 2 (18%) **Asian:** 3 (27%) **Black:** 0 **White:** 6 (55%)	p=0.28 NS (Chi-Squared)
Birthweight (g)	3457.69±67.43	4153.18±96.80	3262±91.93	4155.82±146.87	Non-GDM AGA vs GDM LGA p=0.00012 ***

					Non-GDM LGA vs GDM AGA p=0.0000007 **** Non-GDM AGA vs Non-GDM LGA p=0.00012 *** GDM AGA vs GDM LGA p=0.0000006 **** (One-Way ANOVA)
Placental weight (g)	552.75±28.68	688.64±37.62	548.50±32.27	772.22±85.15	Non-GDM LGA vs GDM AGA p=0.018 * GDM AGA vs GDM LGA p=0.0098 ** (One-Way ANOVA)
Fetal Sex (%)	**Male:** 5 (38%) **Female:** 8 (62%)	**Male:** 6 (55%) **Female:** 5 (45%)	**Male:** 8 (53%) **Female:** 7 (47%)	**Male:** 4 (36%) **Female:** 5 (45%) **Unknown:** 2 (18%)	p=0.217 NS (Chi-Squared)
Mode of delivery (%)	**NVD:** 4 (30%) **EM LSCS:** 0 **EL LSCS:** 8 (62%) **Unknown:** 1 (8%)	**NVD:** 5 (45%) **EM LSCS:** 0 **EL LSCS:** 6 (55%) **Unknown:** 0	**NVD:** 9 (60%) **EM LSCS:** 1 (7%) **EL LSCS:** 5 (33%) **Unknown:** 0	**NVD:** 0 **EM LSCS:** 4 (36%) **EL LSCS:** 5 (45%) **Unknown:** 2 (18%)	P=0.0072 ** (Chi-Squared)
Smoked in pregnancy (%)	**Smoked:** 3 (23%) **Non-Smoker:** 10 (77%)	**Smoked:** 1 (9%) **Non-Smoker:** 10 (91%)	**Smoked:** 0 **Non-Smoker:** 15 (100%)	**Smoked:** 0 **Non-Smoker:** 11 (100%)	p=0.090 NS (Chi-Squared)
BWC	46.92±3.69	95.27±0.71	52.04±6.72	96.13±1.28	Non-GDM AGA vs GDM LGA p=0.0000047 **** Non-GDM LGA vs GDM AGA p=0.000082 **** Non-GDM AGA vs Non-GDM LGA p=0.000024 **** GDM AGA vs GDM LGA p=0.000016 **** (Kruskal-Wallis)

DEGs to be tested in this cohort were selected based on their reported roles in the placenta and/or diabetes and/or glucose (Chapter 3; Table 3.2) and included *CXCL2*, which was found to be downregulated in GDM placentae (Figure 4.3) and *PDGFD* and *FABP4*, which were found to be downregulated and upregulated in LGA placentae, respectively (Figure 4.6).

Firstly, the expression of DEGs in the placentae of non-GDM (n=24) and GDM (n=26) pregnancies were compared (Figure 4.7). These results showed that *PECAM1* (135.07 [49.69-800.63] vs 253.0 [160.34-736.73]; p<0.001) and *RAMP2* (10.09 [1.18-35.14] vs 15.95 [0.76-100.78]; p<0.05) were downregulated in GDM placentae. In GDM placentae, there was also a trend towards a decrease in *NAMPT* (31.075 [5.28-81.01] vs 36.47 [8.03-110.28]; p=0.256) and *IL1B* (0.51 [0.18-40.36] vs 0.83 [0.24-6.00]; p=0.255). Interestingly, there was also a trend towards a decrease in *CXCL2* in GDM placentae (0.36 [0.066-44.94] vs 0.63 [0.097-14.27]; p=0.519), which is in line with findings in the transcriptomic analysis of publicly available data (Figure 4.3). Similarly, *NAMPT, IL1B* and *CXCL2* were all downregulated by 7 mM glucose in placental explants.

Secondly, the expression of DEGs in the placenta of non-GDM AGA (n=13), non-GDM LGA (n=11), GDM AGA (n=15) and GDM LGA (n=11) pregnancies were compared (Figure 4.8). *NAMPT*, was upregulated in non-GDM LGA compared to non-GDM AGA placentae (43.56 [25.90-110.28] vs 21.41 [8.03-92.09]; p<0.05). Similarly, *PECAM1*, was downregulated in GDM AGA, compared to non-GDM AGA (119.84 [49.69-800.63] vs 246.42 [160.34-736.73]; p<0.01) and non-GDM LGA placentae (119.84 [49.69-800.63] vs 259.57 [170.07-445.72]; p<0.01). Interestingly, *NAMPT* was downregulated and *PECAM1* was upregulated by 7 mM glucose in placental explants.

RAMP2 was upregulated in non-GDM LGA (28.05 [11.59-50.39]) compared to non-GDM AGA (11.39 [0.76-100.78]; p<0.05) and GDM LGA placentae (12.86 [1.18-35.14]; p<0.05). There was also a trend towards an increase in *FABP4* in the non-GDM LGA (53.82 [27.47-129.34]) and GDM LGA (78.79 [28.44-207.94]) groups compared to the non-GDM AGA (38.72 [17.69-444.18]) and GDM AGA (39.67 [15.78-215.27]) groups (p=0.172-0.316). *FABP4* was also upregulated with 7 mM glucose in placental explants.

The expression changes of these DEGs in placental explants with glucose fluctuations, transcriptomic analysis of publicly available data and RT-qPCRs of term placental GDM/non-GDM LGA/AGA samples is summarised in Table 4.11.

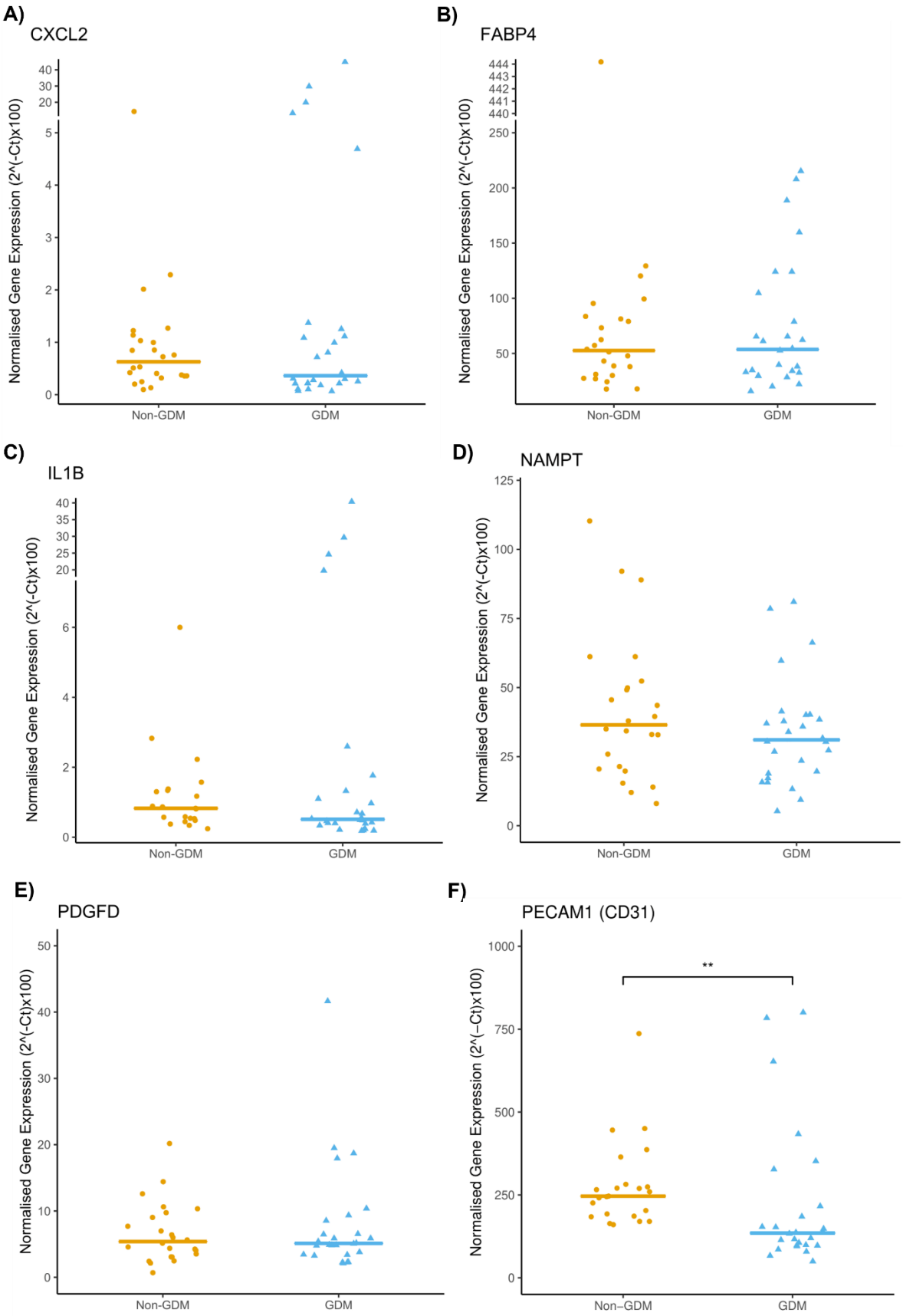
A)
CXCL2
Normalised Gene Expression (2^(-Ct)x100)
Non-GDM
GDM
B)
FABP4
Normalised Gene Expression (2^(-Ct)x100)
Non-GDM
GDM
C)
IL1B
Normalised Gene Expression (2^(-Ct)x100)
Non-GDM
GDM
D)
NAMPT
Normalised Gene Expression (2^(-Ct)x100)
Non-GDM
GDM
E)
PDGFD
Normalised Gene Expression (2^(-Ct)x100)
Non-GDM
GDM
F)
PECAM1 (CD31)
Normalised Gene Expression (2^(-Ct)x100)
**
Non-GDM
GDM

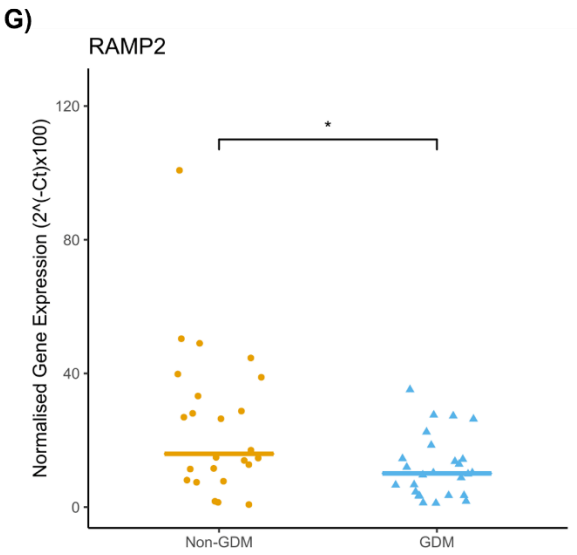

Figure 4.7 - Selected DEGs altered by 7 mM glucose in placental explants in human placentae from GDM and non-GDM pregnancies. Selected DEGs were measured in term placental RNA from non-GDM (n=24) and GDM (n=26) pregnancies by RT-qPCR. The expression of each target gene was normalised to *YWHAZ* housekeeping gene expression, which was unaltered between groups. Data are presented as the median (as data was not normally distributed) and statistical analysis was performed using a Mann-Whitney U Test. Individual points represent individual patient placentae. * $p<0.05$, ** $p<0.01$.

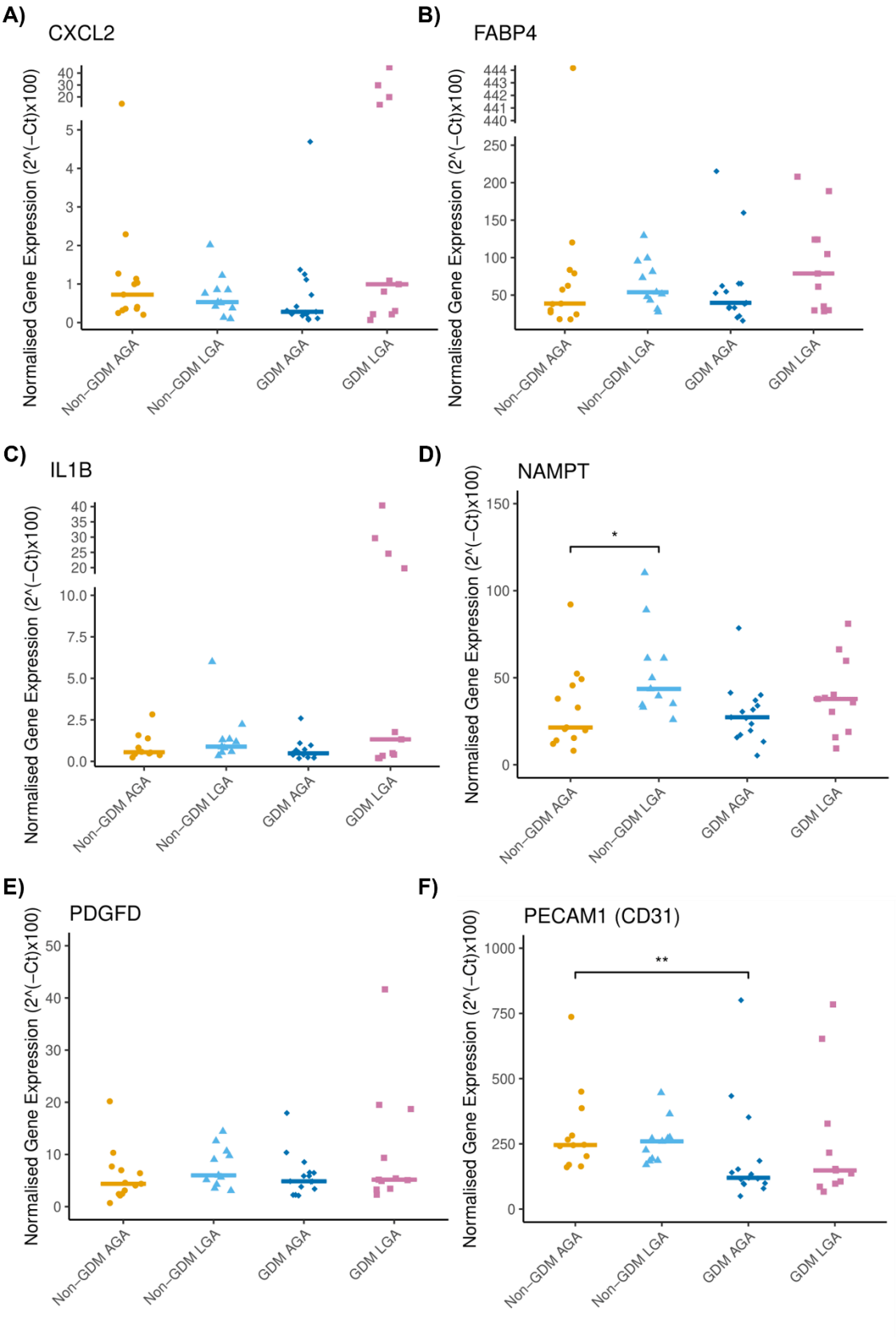
A)
CXCL2
B)
FABP4
C)
IL1B
D)
NAMPT
E)
PDGFD
F)
PECAM1 (CD31)
Normalised Gene Expression (2^(−Ct)x100)
Non−GDM AGA
Non−GDM LGA
GDM AGA
GDM LGA
*
**

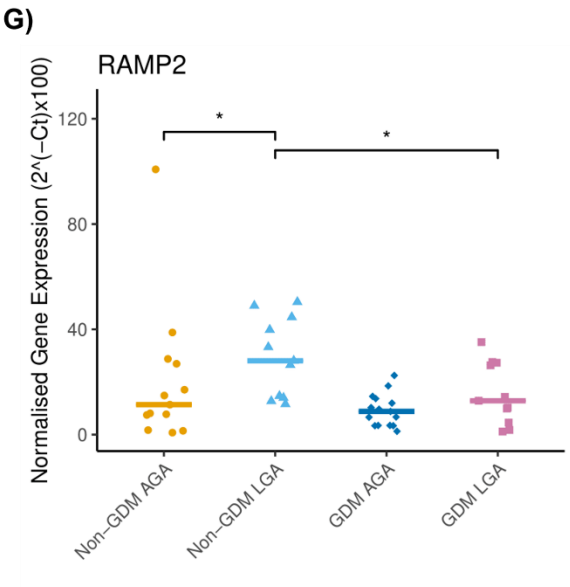

Figure 4.8 - Selected DEGs altered by 7 mM glucose in placental explants in human placentae from non-GDM AGA, non-GDM LGA, GDM AGA and GDM LGA pregnancies. Selected DEGs were measured in term placental RNA from non-GDM AGA (n=13), non-GDM LGA (n=11), GDM AGA (n=15) and GDM LGA (n=11) pregnancies by RT-qPCR. The expression of each target gene was normalised to *YWHAZ* housekeeping gene expression, which was unaltered between groups. Data are presented as the median (as data was not normally distributed) and statistical analysis was performed using a Kruskal-Wallis with a Dunn's post-hoc test. Individual points represent individual patient placentae. * $p<0.05$, ** $p<0.01$, *** $p<0.001$.

Table 4.11 - A summary of expression changes of selected DEGs in placental explants with glucose fluctuations, transcriptomic analysis of publicly available data and RT-qPCRs of term placental GDM/non-GDM LGA/AGA samples. ↑ = increased expression, ↓ = decreased expression, ~ = no change in expression.

Gene	Placental explants with glucose fluctuations	Publicly available transcriptomic data analysis	RT-qPCRs of term placental GDM/non-GDM LGA/AGA samples
CXCL2	↓ in 7 mM glucose	↓ in GDM compared to non-GDM	Trend showing ↓ in GDM compared to non-GDM
FABP4	↑ in 7 mM glucose	↓ in non-GDM LGA compared to non-GDM AGA	Trend showing ↑ in non-GDM LGA and GDM LGA compared to non-GDM AGA and GDM AGA
IL1B	↓ in 7 mM glucose	~	Trend showing ↓ in GDM compared to non-GDM
NAMPT	↓ in 7 mM glucose	~	↑ in non-GDM LGA compared to non-GDM AGA * Trend showing ↓ in GDM compared to non-GDM
PDGFD	↓ in 7 mM glucose	↓ in non-GDM LGA compared to non-GDM AGA	~
PECAM1	↑ in 7 mM glucose	~	↓ in GDM compared to non-GDM ** ↓ in GDM AGA compared to non-GDM AGA **
RAMP2	↑ in 7 mM glucose	~	↓ in GDM compared to non-GDM * ↑ in non-GDM LGA compared to non-GDM AGA * and GDM LGA *

4.5 Discussion

The aim of this chapter was to determine whether alterations in the transcriptome induced by physiological maternal glucose fluctuations in placental explants are linked to placental transcriptomic changes in GDM and/or LGA. Using publicly available placental transcriptomic data, the placental transcriptome was found to be altered in GDM (compared to non-GDM) and in non-GDM LGA (compared to non-GDM AGA). Several DEGs found in the publicly available data sets were also altered by 7 mM glucose in placental explants, linking these gene expression changes to maternal glucose fluctuations. Selected genes were also assessed by RT-qPCR in human placental RNA from a separate cohort of samples, some of which were found to be associated with GDM and/or LGA. However, the discrepancies between gene expression changes in placental explants, transcriptomic analysis of publicly available datasets and RT-qPCRs are likely explained by differences in the cohorts, their demographics and *in vivo* glucose profiles.

4.5.1 The placental transcriptome in GDM

To investigate alterations in the placental transcriptome in pregnancies complicated by GDM, two previously published datasets were used, including the study by Cox *et al.* (2019) (GSE128381)[557] and Binder *et al.* (2015) (GSE70493)[553]. GDM samples were compared to matched non-GDM controls.

In the original study by Cox *et al.* (2019), genes associated with maternal BMI and birthweight were identified, which were found to be enriched in angiogenesis, blood vessel morphogenesis and ECM-related functions. These researchers did not assess differences between GDM and non-GDM placentae. In the present analysis, GDM altered 575 genes, including inflammatory genes, *CXCL2, FCGR2B* and *SELL*[570,571,576] and apoptosis-related genes, *CASP3* and *XIAP*[563,564]. In the original study by Binder *et al*. (2015), GDM was associated with reduced expression of MHC class I and class II genes, which have been implicated in T1DM[553]. These findings were also observed in the present analysis, where DEGs were associated with pathways related to autoimmune diseases, including T1DM, and MHC protein complexes. Several altered genes were HLA genes, as well as inflammatory related genes, *ILRL1, CXCL9* and *CXCL10*[568,569]. Similar to these findings, previous studies have linked altered placental genes in GDM to apoptotic processes[554], using whole placental transcriptomic sequencing, as well as antigen processing/presentation and IL-17 signalling in GDM trophoblasts using single-cell RNA sequencing[552].

A major limitation of the GSE70493 dataset is that is that information on BWCs or individual sample information to calculate this was not included. Although the samples could be classified as GDM or non-GDM, it's unclear how many of these samples were LGA, AGA or SGA. Thus, this could explain why there was no overlap between DEGs in the analysis of this study and the GSE128381 study. However, both studies did show alterations in genes associated IGF-signalling (*IGFBP1* and *IGBP2* were altered by GDM in the GSE70493 and GSE128381 studies, respectively), which have been linked to altered fetal growth and placental development[565–567]. As well as the immune/inflammatory response (e.g. chemokines), which are similar to findings in placental explants exposed to glucose fluctuations.

The GSE70483 placental samples were taken from the maternal side, and therefore will contain maternal tissue of the decidua. Whereas the placental samples in the GSE128381 study were taken from the fetal side, which may also explain differences between the findings in these two studies. Moreover, the decidual membrane was removed from the placental explants treated with glucose fluctuations. Therefore, the samples isolated from the fetal side of the placenta in the GSE128381 study more closely resemble tissue in placental explants and could explain why a greater overlap was found between DEGs in this study and DEGs associated with 7 mM glucose in placental explants.

4.5.2 The placental transcriptome in LGA

Previous studies have investigated a small number of genes in GDM-LGA placentae. Uusküla *et al.* (2012) identified several genes, *STC1, CCNG2, LYPD6, GATM* and *GPR183,* which were significantly increased in GDM LGA compared to uncomplicated pregnancies[555]. In functional enrichment analyses, *STC1, GPR183, GATM* and *LYPD6*, were found to be associated with embryonic development and growth, and *CCNG2* was found to be involved in cell cycle regulation, proliferation, and RNA metabolism. Other researchers assessed a panel of 17 genes, previously reported to be associated with placental function in the placentae of women with LGA, AGA and SGA pregnancies. *ABCG2, CEBPB, CRH, GCM1, GPC3, INSL4, PGF* (PlGF) and *PLAC1* were inversely associated with LGA, whereas *NR3C1* was positively associated with LGA[556]. However, no studies have assessed the whole GDM LGA transcriptome.

Additionally, limited publicly available datasets included samples from GDM LGA and GDM AGA pregnancies. One dataset (E-MTAB-6418) was used to compare the placental transcriptome in GDM LGA pregnancies compared to GDM AGA pregnancies and non-GDM LGA to non-GDM LGA pregnancies. However, no significant DEGs were

identified in GDM LGA compared to GDM AGA pregnancies, or non-GDM LGA compared to non-GDM AGA pregnancies. These samples were taken from the EMPOWaR study[559]. Therefore, a limitation of this dataset is that it contained samples only from obese pregnancies and did not consider non-obese pregnant women. As the transcriptomic analysis of this study has not been published, it is also unclear what regions of placental tissue were used. Demographic information provided did not include parity, ethnicity, maternal height/weight, and birthweight (that wasn't already adjusted for gestational age), therefore BWC's calculated will be less accurate than if all this information was provided. Collectively, these limitations could explain the lack of findings. An original aim of the present study was to perform RNA sequencing on placental tissue from GDM AGA and GDM LGA pregnancies, however given that the available sample numbers and demographics were similar to those from the EMPOWaR study, it was deemed unlikely that any changes would be observed.

To investigate alterations in the placental transcriptome in pregnancies complicated by LGA, transcriptomic data of placental samples from uncomplicated pregnancies (non-GDM) that had LGA outcomes were compared to AGA outcomes (also non-GDM) from two publicly available datasets. This included again the study by Cox *et al.* (2019)[557] (GSE128381), where samples from LGA pregnancies (non-GDM) were compared to matched AGA (non-GDM) controls. DEGs associated with LGA included the inflammatory gene, *IL36RN*[577], the fatty acid binding protein, *FABP4*[205] and genes associated with gas transport, including *ALAS2* and *HBA2*[578]. Similarly to the E-MTAB-6148 dataset, a limitation of this study however is that information provided did not include detailed ethnicity and maternal height/weight, therefore BWC's calculated will be less accurate than if all this information was provided.

The second dataset was by Turan and Sapienza (Unpublished; GSE32868). This contained 12 placental samples from LGA pregnancies (non-GDM) and 36 placental samples from AGA pregnancies (non-GDM). The 12 LGA samples could not be matched to 12 AGA samples as limited demographic information was provided, thus all 12 LGA samples were compared to all 36 AGA samples. This is a major limitation of this dataset, as the limited demographic information means that other confounding variables could be influencing the transcriptome, such as maternal BMI, age, fetal sex etc. This may also explain why there were no overlapping DEGs between this study and with DEGs associated with 7 mM glucose in placental explants, and only one overlapping gene with the GSE128381 DEGs. However, DEGs associated with LGA in this dataset included leptin (*LEP)*, which was downregulated. Increased circulating leptin has been reported in GDM[587]. Leptin has also been found to be upregulated in

IUGR[565,580,588] and increased in cord serum in LGA infants, suggesting that leptin is linked to fetal growth[589]. A positive correlation between leptin concentration in cord serum and birthweight has also been reported, which was also correlated with IGF-1 levels[590]. Moreover, a study by White *et al*. (2006) reported that leptin decreased levels of triglycerides and cholesterol in the placenta, suggesting that it regulates lipid metabolism in the placenta. Thus, a decrease in this in LGA pregnancies could increase lipid availability to the fetus[591].

4.5.3 Genes associated with GDM and LGA and glucose fluctuations in placental explants

Of the DEGs altered by 7 mM glucose in placental explants, 7 were also altered in GDM placentae (*CXCL2, SELL, TIPARP, SRRT, TOP1, HAPLN2* and *FCGR2B*) and 3 were altered in LGA placentae (*FABP4, PDGFD* and *ALAS2*) in the analysis of the GSE128381 study.

Similar to functional enrichment analysis of placental explants, many of these overlapping genes are associated with the immune and inflammatory response, including *FCGR2B* (upregulated in GDM placentae and with 7 mM glucose) and *CXCL2* (downregulated in GDM placentae and with 7 mM glucose). FCGR2B is a member of the immune receptor IgG Fc gamma family. In the placenta, FCGR2B is present in the villous stroma on HBCs where it binds and can clear immune complexes, for the effective control of inflammation and infection[576]. CXCL2 is a chemokine, which recruits leukocytes in areas of inflammation[570]. Hyperglycaemia in diabetes is known to contribute to inflammation and immune dysfunction and subsequent failure to control invading pathogens, resulting in infections and comorbidities[238]. In line with this, *Fcgr2b* knock out in diabetic mice has been linked to renal injury, a secondary complication of diabetes[576]. Knockout of *Fcgr2b* in high fat diet fed mice, increased deposition of oxidative LDLs, which are immunogenic and cause production of autoantibodies. This results in pro-inflammatory and pro-fibrotic consequences, leading to the progression of renal lipotoxicity[576]. Thus, the increase in *FCGR2B* and decrease in *CXCL2* in GDM placentae and with 7 mM glucose in placental explants could be associated with immune dysfunction and potentially be acting as a compensatory mechanism to control inflammation and infection in response to the diabetic insult and mild hyperglycaemia. In line with this, studies utilising mouse models showed that levels of FCGR2B are increased in the liver of high fat diet-fed pre-diabetic mice at the mRNA and protein level. Interestingly, mRNA expression of *Fcgr2b* was significantly decreased in ob/ob

and db/db mice compared to lean mice, suggesting that this increase is only associated with pre-diabetes[592].

PDGFD, which was downregulated in LGA placentae and with 7 mM glucose, and *CXCL2,* have been linked to vascular development. CXCL2 acts as a proangiogenic factor, binding to its receptor CXCR2[593]. Studies have also shown that treatment with CXCL2 increases the proliferation, migration and angiogenic sprouting of HUVECs, and human brain microvascular ECs[593]. Similarly, PDGFD is a member of the PDGF family that binds the PDGF receptor β, and has been associated with proliferation, migration and tube formation of endothelial progenitor cells[481]. In studies from the cancer research field, PDGFD promotes cell growth, angiogenesis and endothelial to mesenchymal transition (EndMT)[582]. EndMT is a process whereby ECs lose their characteristics and acquire mesenchymal traits[594]. Dysregulation of EndMT could therefore result in vascular regression and placental hypovascularisation[595]. Moreover, altered placental vascularisation is well-documented in GDM, including villous immaturity and hypovascularisation[122,132]. In accordance with this, functional enrichment analysis in placental explants with glucose fluctuations revealed that 7 mM glucose was associated with reductions in vasculogenesis and angiogenesis, suggesting immature vascular development. Thus, gene expression changes in *PDGFD* and *CXCL2* could be contributing to placental hypovascularisation in GDM and/or LGA. In turn, this would influence the delivery of nutrients and gases to the placenta.

Erythroid-specific 5-aminolevulinate synthase (*ALAS2*) is the rate-limiting enzyme for haem biosynthesis in erythroid cells[583], which was downregulated by 7 mM glucose in placental explants and in LGA placentae, along with *HBA2*, which was also altered in LGA placentae, have been identified as placental 'hub' genes associated with gas transport and the essential role of the placenta in gas exchange[578]. Although their role in the placenta has yet to be further established, this may also be linked to impaired gas exchange in the placenta, which can impact the growth and development of the fetus.

To further assess whether any genes altered by 7 mM glucose in placental explants were also altered by GDM and/or LGA, selected DEGs were assessed in a separate cohort of samples of human term placental RNA. The samples were divided into GDM and non-GDM and then non-GDM AGA, non-GDM LGA, GDM AGA and GDM LGA to assess gene expression changes in GDM and across all groups, respectively. The available demographics for these samples enabled the BWCs to be calculated more accurately than publicly available data, using the GROW centile calculator. Several

genes were altered between birthweight categories, that were not detected when comparing GDM and non-GDM alone, such as *NAMPT* and *IL1B*.

Although 5/5.5 mM and 7 mM glucose in placental explants were used to mimic GDM AGA and GDM LGA pregnancies, respectively, no DEGs were found to be altered between GDM LGA and GDM AGA placentae. However, *RAMP2*, which was increased by 7 mM glucose, is increased in non-GDM LGA placentae compared to non-GDM AGA. Moreover, there was a trend towards an increase in *FABP4* in non-GDM LGA and GDM LGA, compared to AGA groups, which was also found to be upregulated by 7 mM glucose in placental explants. Given that LGA also occurs in women without a diagnosis of GDM, which is thought to be linked to glucose dysregulation[596], it is possible that the 7 mM glucose used in placental explants mimicked mild hyperglycaemia in non-GDM LGA pregnancies, and the 5/5.5 mM glucose mimicked normoglycaemic levels in non-GDM AGA pregnancies.

4.5.4 The impact of *in vivo* maternal glucose fluctuations in GDM/LGA pregnancies on the placenta

The discrepancies between genes altered by 7 mM glucose in placental explants and LGA/GDM in the transcriptomic analyses and in the RT-qPCRs of term placental samples is likely due to the glucose profiles of these samples being unknown. The most appropriate way to investigate the impact of *in vivo* maternal glucose fluctuations on placental function and fetal growth would be to use samples from women that have received CGM in pregnancy. A current study in our research group is the Maternal Glucose in Pregnancy Study (MAGiC). In this study, pregnant women were recruited in the first trimester who had at least one risk factor for developing GDM (e.g. BMI over 30 kg/m^2, relative with diabetes, ethnic minority or previous unexplained still birth or baby weighing over 4.5 kg) and were given routine CGM throughout pregnancy[596]. Using samples from this study would enable *in vivo* glucose fluctuations (from CGM data), in women with and without GDM, to be linked to placental gene expression and fetal growth outcomes. Unfortunately, due to the MAGiC study being delayed by Covid-19 these samples could not be assessed in the present study. However, future research should aim to investigate placentae exposed to *in vivo* maternal glucose fluctuations.

Other contributing factors include fetal sex, as a recent study by Kedziora *et al*. (2022) revealed that placental gene expression changes were primarily driven by fetal sex rather than clinical diagnosis of GDM, T1DM or T2DM[597] and previous studies have also linked fetal sex to placental transcriptomic changes, even in early pregnancy[268].

Therefore, it would be important to further subcategorise analysis in the present study by fetal sex with larger sample sizes. Finally, GDM is a complex condition, that is not only linked to maternal hyperglycaemia and glycaemic control but also hyperlipidaemia, altered adipokines, oxidative stress, in addition to circulating miRNAs EVs)[298–300,541,598–600]. Thus, the placental transcriptomic changes observed with mild hyperglycaemia are only investigating the impact of glycaemic control on the placenta, and not all factors associated with GDM.

4.6 Summary

- Publicly available transcriptomic datasets were identified that enabled comparisons of placentae from GDM and non-GDM, GDM LGA and GDM AGA, and non-GDM LGA and non-GDM AGA pregnancies.
- The placental transcriptome was altered in GDM compared to non-GDM pregnancies, and non-GDM LGA compared to non-GDM AGA pregnancies.
- Several of these DEGs were also altered by 7 mM glucose in placental explants, linking these gene expression changes in GDM/LGA to maternal glucose fluctuations.
- Selected genes were also assessed by RT-qPCR in human placental RNA from a separate cohort of samples, some of which were found to be associated with GDM and/or LGA.
- The discrepancies between gene expression changes in placental explants, transcriptomic analysis of publicly available datasets and RT-qPCRs are likely explained by differences in the cohorts, their demographics and glucose profiles.
- Further study, utilising placental samples from women with CGM in pregnancy would reveal how *in vivo* maternal glucose fluctuations are associated with placental function.

Chapter 5 - The impact of physiological maternal glucose fluctuations on the placental immune and inflammatory response

5.1 Introduction

In Chapter 3, physiological maternal glucose fluctuations associated with GDM LGA pregnancies (7 mM glucose), were found to alter the placental transcriptome. Functional enrichment analyses demonstrated that many genes differentially expressed by 7 mM glucose were inflammatory mediators, including cytokines and chemokines, that are associated with inflammatory and immune pathways. Additionally in Chapter 4, although there were limitations in the publicly available data sets, several chemokines (*CXCL2, CXCL9* and *CXCL10*) and inflammatory-related genes (*FCGR2B, SELL, NLRP1* and *TNFAIP8)* were found to be altered in GDM placentae and several of these genes were also linked to glucose fluctuations in placental explants.

In normal pregnancy, the balance between pro- and anti- inflammatory mediators regulates many processes, including implantation, trophoblast invasion and labour. Cytotrophoblast, syncytiotrophoblast and placental macrophages (HBCs) are known to secrete cytokines to regulate these processes[236]. Similarly, several chemokines are also known to be detected within the villous stroma in HBCs, placental fibroblasts[601], and EVTs[602,603].

GDM is thought to be associated with a state of chronic, low grade inflammation, and maternal hyperglycaemia has been attributed to this[238]. Although varied findings, circulating cytokine and chemokine levels have been found to be altered in women with GDM[216,239,248,249,240–247], which are thought to be produced by the placenta[604]. However, 7 mM glucose was shown to downregulate pro-inflammatory mediators in the placenta, suggesting that mild hyperglycaemia in GDM LGA pregnancies induces an anti-inflammatory state. One possibility is that the polarisation or abundance of HBCs, the only immune cells present within the placental villous stroma[605], are altered by mild hyperglycaemia. HBCs are known to primarily possess an M2 macrophage phenotype[103,221–223], which are associated with the production of anti-inflammatory cytokines[606,607], whereas M1 polarised macrophages are known to release pro-inflammatory cytokines[606,607]. Functional enrichment analysis also predicted that 7 mM glucose was associated with a reduced activation of macrophages. It is therefore hypothesised temporal periods of mild hyperglycaemia in GDM could be reducing pro-inflammatory mediators in the placenta by increasing the levels of M2 HBCs. The aim

of this chapter is to establish the mechanisms of the altered placental inflammatory profile in response to glucose fluctuations.

5.2 Hypothesis

Temporal periods of mild hyperglycaemia in GDM alters the release of inflammatory mediators in the placenta.

5.3 Aims

To determine the mechanisms through which physiological maternal glucose fluctuations impact placental inflammatory mediators.

5.4 Results

5.4.1 Validation of inflammatory mediators altered by glucose fluctuations

Functional enrichment analysis demonstrated that many genes differentially expressed by 7 mM glucose were inflammatory cytokines and chemokines. Of these, *IL1B* and *IL6* were central mediators of the inflammatory signalling pathways and were investigated further. Consistent with RNA sequencing data, RT-qPCR revealed significantly reduced levels of *IL1B* gene expression in explants treated with constant 7 mM glucose compared to fluctuating 5/5.5 mM glucose (median fold change of 0.78 [0.54-1.02]; $p<0.05$). *IL6* gene expression was also reduced with 7 mM glucose, although this did not reach significance (median fold change of 0.90 [0.53-2.64]; $p=0.919$; $n=10$) (Figure 5.1).

At the protein level, there was a decrease in IL-1β in explants treated with 7 mM glucose compared to 5/5.5 mM (median fold change of 0.55 [0.16-0.98]), which was approaching significance ($p=0.059$, $n=5$). There was also a trend towards a decrease in IL-6 protein (median fold change of 0.76 [0.49-1.22], $p=0.201$, $n=4$) (Figure 5.2).

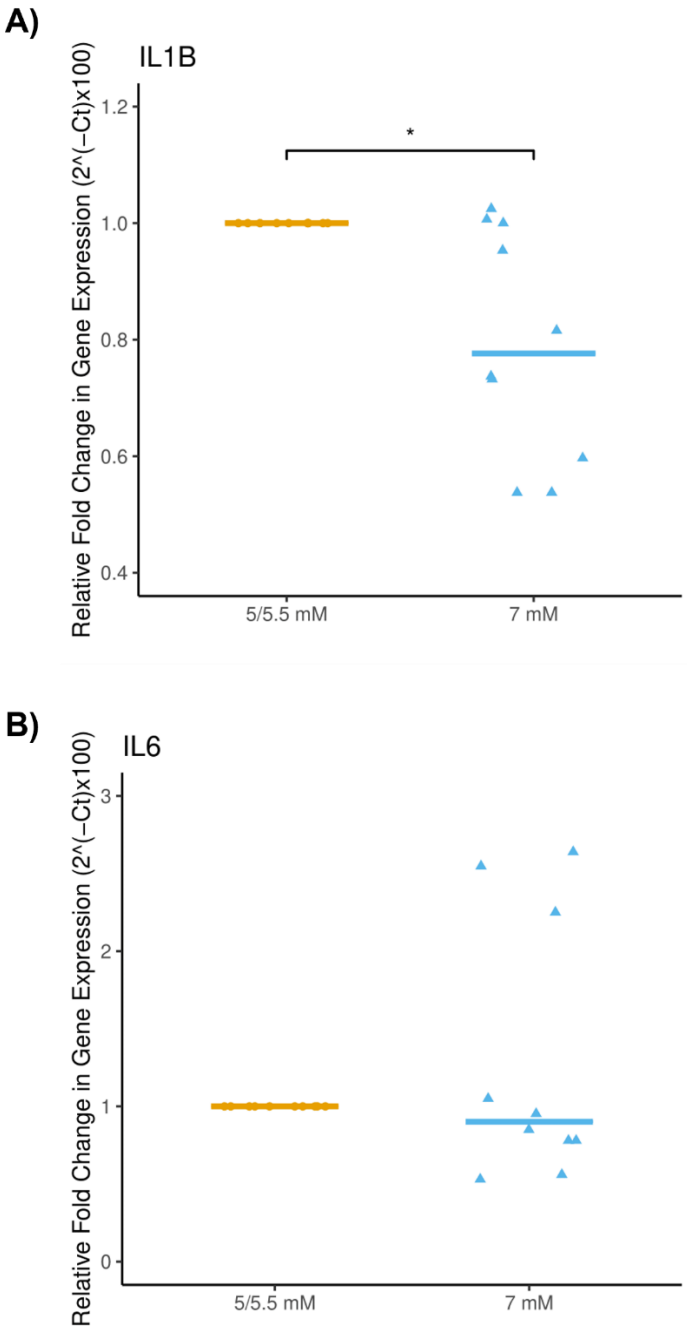

Figure 5.1 – Gene expression of *IL1B* and *IL6* in placental explants following glucose treatments for 48 hours, measured by RT-qPCR. *IL1B* and *IL6* were measured in placental explants cultured in either fluctuating 5/5.5 mM or constant 7 mM glucose for 48 hours by RT-qPCR. The expression of each target gene was normalised to a geometric mean of *18S*, *ACTB* and *YWHAZ* housekeeping gene expression. Data are presented as the median fold change (compared to 5/5.5 mM) and statistical analysis was performed using a Wilcoxon Signed-Rank Test (as the data was not normally distributed). n=10. * $p<0.05$.

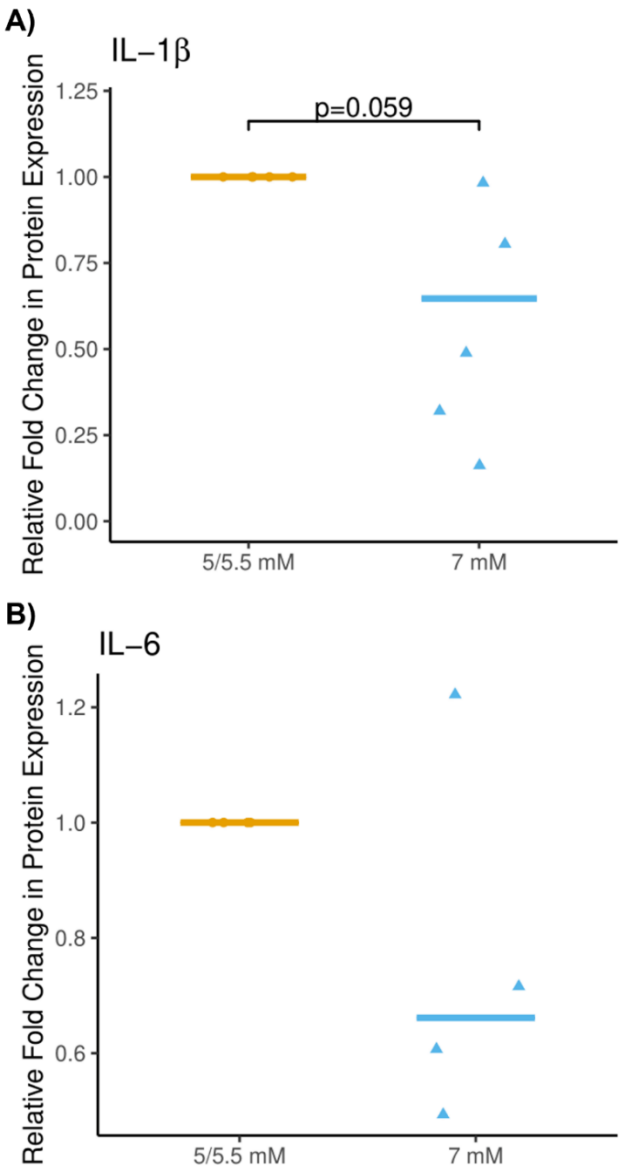

Figure 5.2 - Protein levels of IL-1β and IL-6 in placental explants following glucose treatments for 48 hours, measured by ELISA. IL-1β and IL-6 were measured in placental explant protein cultured in either fluctuating 5/5.5 mM or constant 7 mM glucose for 48 hours by ELISA. The concentration of IL-1β and IL-6 (pg/mL) were normalised to total explant protein (mg). Data are presented as the median fold change (compared to 5/5.5 mM) and statistical analysis was performed using a Wilcoxon Signed-Rank Test (as the data was not normally distributed). n=4-5.

5.4.2 Source of altered inflammatory mediators in the placenta

To assess which cells in the placenta were producing or expressing IL-1β and IL-6, immunohistochemistry was performed in term placental tissue from uncomplicated pregnancies (Figure 5.3). In line with previous studies[608–610], IL-1β and IL-6 were primarily expressed in the syncytiotrophoblast and within the stroma, where HBCs reside[102]. IL-6 was also found to be expressed highly within the fetal endothelium, surrounding the fetal blood vessels. Overall, this suggests that the trophoblast and HBCs may be the source of IL-1β and IL-6 in the placenta.

To further investigate the source of other altered inflammatory mediators, the 'maternal-fetal interface atlas' was used, which is an online tool, developed from single-cell RNA sequencing data of the placenta and decidua[406]. The tool was subset to placental cell types (excluding decidual cell types) to assess expression levels in various placental cells. Several chemokines had high expression in HBCs, including, *CCL2, CCL3, CXCL2* and *CXCL8*. Other chemokines, *CXCL1* and *CXCL3*, were found to be lowly expressed in HBCs. Similarly, interleukins, *IL1B* and *IL6*, had some expression in HBCs. There was also some low expression of these inflammatory mediators in the syncytiotrophoblast and villous cytotrophoblast. Low/minimal expression was observed for *CCL19, CXCL5, IL23A* and *IL24* in placental cells. An example of the inflammatory mediators with high expression in HBCs are shown in Figure 5.4.

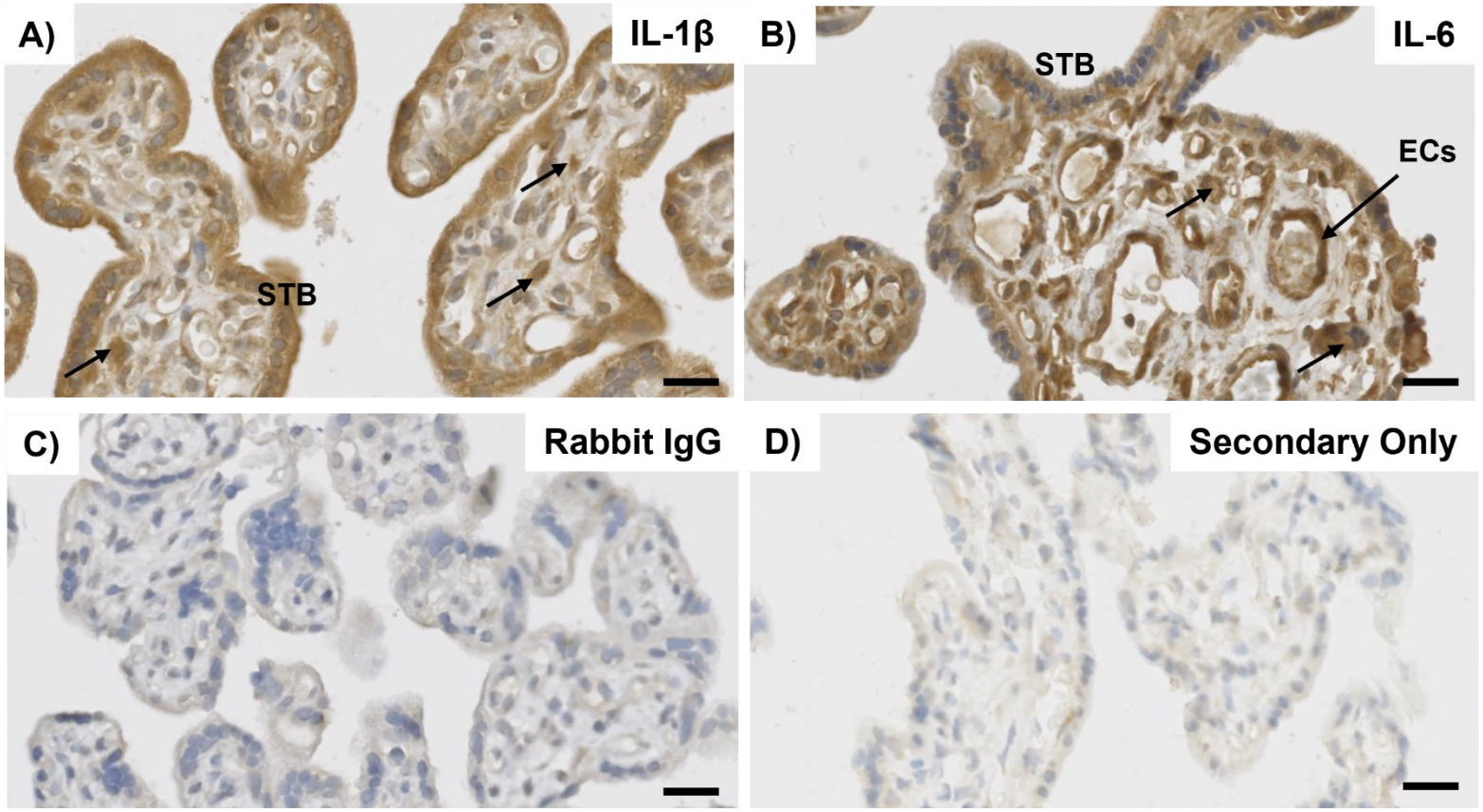

Figure 5.3 - Localisation of IL-1β and IL-6 in human term placental tissue from uncomplicated pregnancies. Immunohistochemistry for IL-1β (A) and IL-6 (B) was performed using DAB and haematoxylin in term placental tissue. C) IgGs for the same species and concentration as the primary antibody were used. The most concentrated IgG is shown. D) Secondary antibody only control. Scale bars = 20 µm. Abbreviations = ECs: Endothelial Cells; STB: syncytiotrophoblast. n=4.

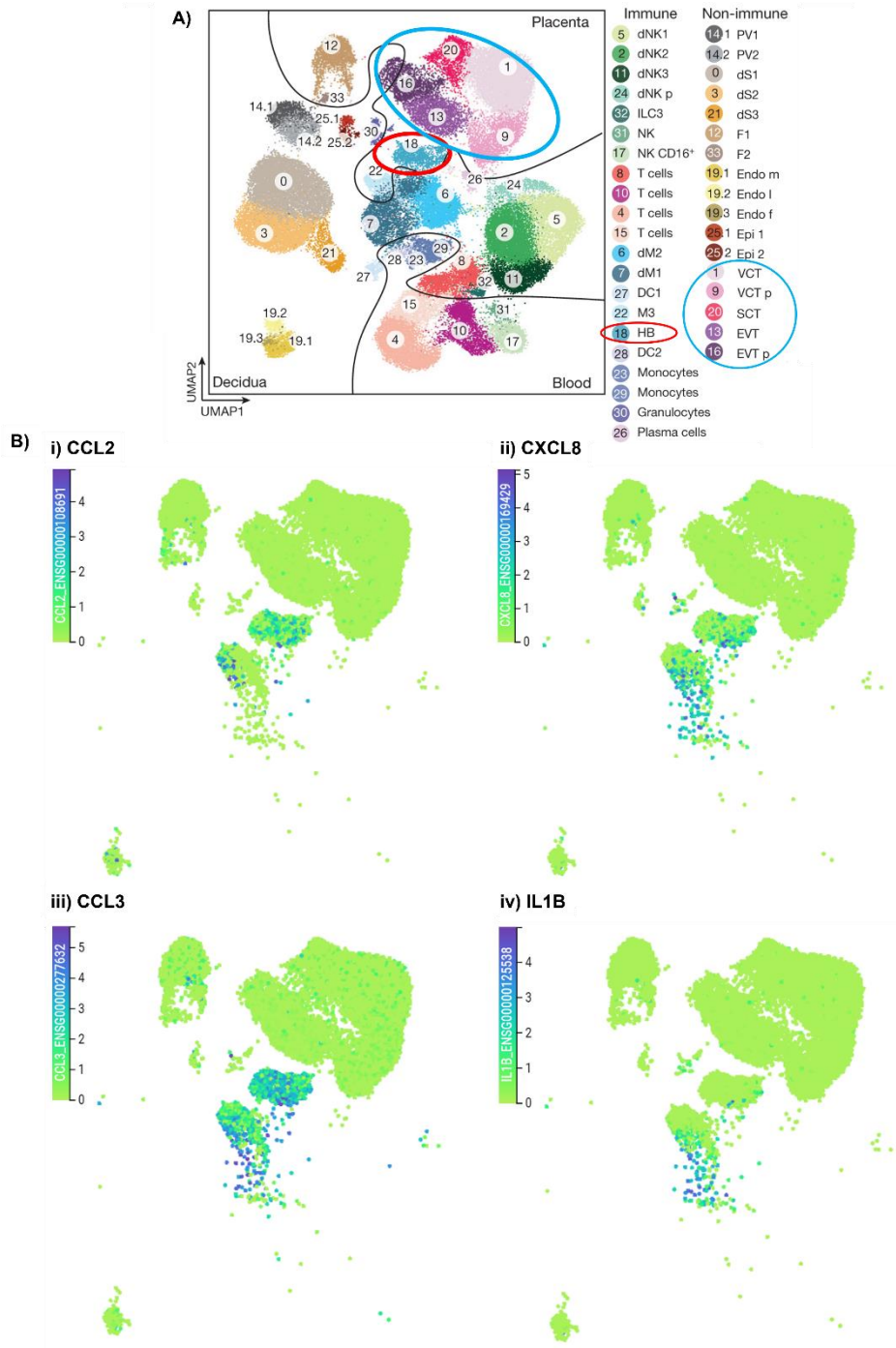

Figure 5.4 – Expression of inflammatory mediators altered by 7 mM glucose in placental cell types. A) Clusters of placental, decidual and blood cell types from single cell RNA sequencing data by Vento-Tormo *et al.* 2018[406]. The red circle shows the Hofbauer cells (HBCs), and the blue circle shows the trophoblast cells. B) Examples of expression profiles of inflammatory mediators, *CCL2* (i), *CXCL8* (ii), *CCL3* (iii) and *IL1B* (iv), which were altered by 7 mM glucose. The cell types were subset to only display placental cells. The level of expression in each cell type is represented by the colour scale (**green** – low expression, **blue/purple** – high expression).

5.4.3 Effects of glucose fluctuations on placental Hofbauer cells (HBCs)

5.4.3.1 Expression of DEGs in HBCs

To further confirm whether differentially expressed inflammatory mediators are produced by HBCs, the DEGs altered by 7 mM glucose in placental explants were compared to HBC proteomics data by Pantazi *et al*. (2022)[407] (Figure 5.5). The protein expression of 87 DEGs were found in HBCs. This included interleukins (*IL1B, IL6*), chemokines (*CXCL-1, 2, 3, 5, 8* and *CCL-2, 3, 20*) and other inflammatory mediators (*PTGS2, NAMPT*)[545,611]. This further suggests that altered inflammatory mediators are produced/expressed in HBCs. Moreover, several DEGs also found in HBCs were macrophage markers, including *VSIG4* (V-set and immunoglobulin domain containing 4)[104] and *CD36*[103] and therefore glucose fluctuations may influence levels of HBCs.

5.4.3.2 M1 and M2 macrophage markers

HBCs are known to primarily possess an M2 macrophage phenotype[103,221–223], which are associated with the production of anti-inflammatory cytokines[606,607], whereas M1 polarised macrophages are known to release pro-inflammatory cytokines[606,607]. Given that 7 mM glucose in placental explants resulted in a downregulation of pro-inflammatory cytokines, it would be expected that there would be an increase in M2 polarised HBCs. Therefore, the DEGs altered by 7 mM glucose in placental explants were compared to genes differentially expressed between M1 and M2 macrophages (taken from a previously published RNA sequencing study of human blood monocytes differentiating into macrophages)[409].

Of the M1/M2 DEGs, 7 were also altered by 7 mM glucose in placental explants. This included *BCL2A1* (Bcl-2-related protein A1)*, IL6, CCL20, CCL19, SPHK1* (Sphingosine kinase 1), which were decreased in M2 macrophages and by 7 mM glucose. Moreover, 1 gene, *CD36*, which was increased in M2 macrophages, was increased by 7 mM glucose. This suggests that placental explants treated with mild hyperglycaemia (7 mM glucose), express markers associated with an M2 polarisation of macrophages. Additionally, these genes were also compared with the HBC proteomics data, to determine which of these M1/M2 markers are associated with HBCs. Of these genes, the protein expression of *IL6, CCL20* and *CD36* were also found to be expressed in HBCs (Figure 5.6; Table 5.1).

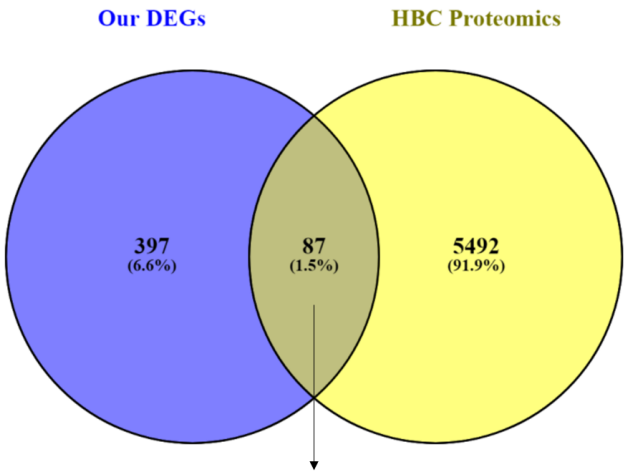

SLAMF7	TNFAIP6	ARHGAP6	MT2A	CLPTM1L	CD83
IL1B	KRT19	TRIM36	PECAM1	LSM4	WDR18
FABP4	MRPL13	PDXP	NDUFAF8	MANBA	DOCK8
PTGS2	ST3GAL1	C1QB	EFL1	FPR1	NUP37
NAMPT	CXCL8	PLAU	FABP3	GM2A	SCARF1
CXCL5	IL6	HIVEP2	CSGALNACT2	MAPKAPK2	RNF214
CD44	CCL20	NBEAL2	NBN	RHOT2	ZNF800
CXCL3	DES	CD38	PARP12	DENND5A	
CXCL1	CCL2	CDK18	PALD1	CMAS	
MGST2	CMC1	NDC1	CYBA	TBC1D2	
ZFP36	CD36	DNAJA4	RHBDF2	SRRT	
SERPINA1	HK2	PON2	HGS	PAXBP1	
UAP1L1	MROH1	GLS	EDC4	MIS12	
NFKBIZ	CXCL2	PUM1	TIMP1	CCL3	
ITGB1	TANK	ARHGAP45	DAPP1	TOP1	
VSIG4	C3	PLCH1	PLEKHJ1	BACH1	

Figure 5.5 - Comparison of genes altered by 7 mM glucose and proteins found to be expressed within placental Hofbauer cells (HBCs). Venn diagrams were used to identify genes altered by 7 mM glucose in placental explants which were also known to be expressed in HBCs at the protein level, based on proteomics data (Pantazi *et al*. (2022)[407]).

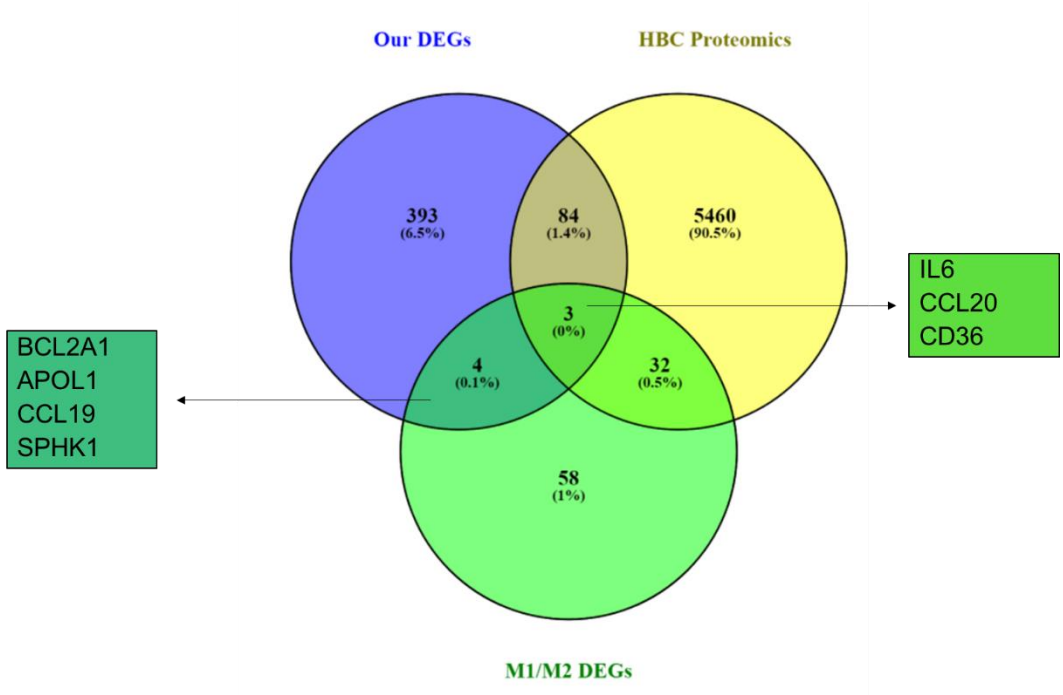

Figure 5.6 - Comparison of genes altered in M1/M2 macrophages to genes altered by 7 mM glucose and proteins expressed in Hofbauer cells (HBCs). Venn diagrams were used to identify altered genes in M1 and M2 macrophages, based on RNAseq data by Martinez et al. (2006)[409], which were also altered by 7 mM glucose in placental explants. The Venn diagram also compares to proteins expressed by HBCs.

Table 5.1 - Genes differentially expressed in M2 vs M1 macrophages and their change in expression in placental explants treated with 7 mM glucose.

Gene	M2 vs M1	Placental explants treated with 7 mM glucose (compared to 5/.5 mM)		
			Log_2FC	P Value
BCL2A1	↓	↓	-2.12992	0.014348
IL6	↓	↓	-0.86841	0.014429
CCL20	↓	↓	-1.02854	0.01627
CD36	↑	↑	0.844584	0.017715
APOL1	↓	↑	0.56667	0.019023
CCL19	↓	↓	-4.30014	0.024535
SPHK1	↓	↓	-0.62807	0.028826

5.4.3.3 Expression and localisation of HBC markers in the placenta

Given that HBCs have characteristics of M2 macrophages[103,221–223], the HBC polarisation in term placentae from uncomplicated pregnancies (n=4) was assessed using immunohistochemistry for the M2 marker, CD163, the M2a/M2c (M2 subtypes) marker, CD206, and the M1 marker, C-C chemokine receptor type 7 (CCR7). CCR7 was assessed as an additional M1 marker, as it was found to be the most differentially expressed gene between M1 and M2 macrophages in the RNA sequencing study by Martinez *et al.* (2006)[409]. CCR7 was not specific to HBCs and was observed throughout the placental villous tissue, including in the stroma, endothelium and the syncytiotrophoblast. Other M1 markers, including CD80, CD86 and CD11c have previously been reported not to have specific expression in the placenta[253], thus this makes it difficult to assess M1 polarisation in the placenta. Specific expression was observed for M2 markers, CD206 and CD163, which were localised to the stroma of the placental villi, where HBCs reside (Figure 5.7).

5.4.3.4 M2 HBC marker expression in placental explants treated with glucose fluctuations

As CD163 and CD206 appeared to be the most specific markers of HBCs in immunohistochemistry of term tissue, their levels in placental explants exposed to glucose fluctuations were assessed (Figure 5.8; Figure 5.9). The number of CD163 and CD206 positive cells (normalised to total villous area μm^2) were slightly increased by 7 mM glucose (median fold change of 1.56 [1.07-3.06], and median fold change of 1.79 [0.72-4.62], for CD163 and CD206, respectively), which suggests that M2 HBCs may be increased with mild hyperglycaemia. However, these differences did not reach significance (p=0.10 and p=0.361 for CD163 and CD206, respectively, n=4).

To further investigate this, Western blots for CD163 (Figure 5.10) and CD206 (Figure 5.11) were performed on protein samples from placental explants treated with glucose fluctuations. The total protein level of CD163 and CD206 were not significantly altered by 7 mM glucose. However, there was a small trend towards increased levels of CD163 with 7 mM glucose (median fold change of 1.14 [0.82-1.60]; p=0.281, n=5), in line with immunohistochemical findings.

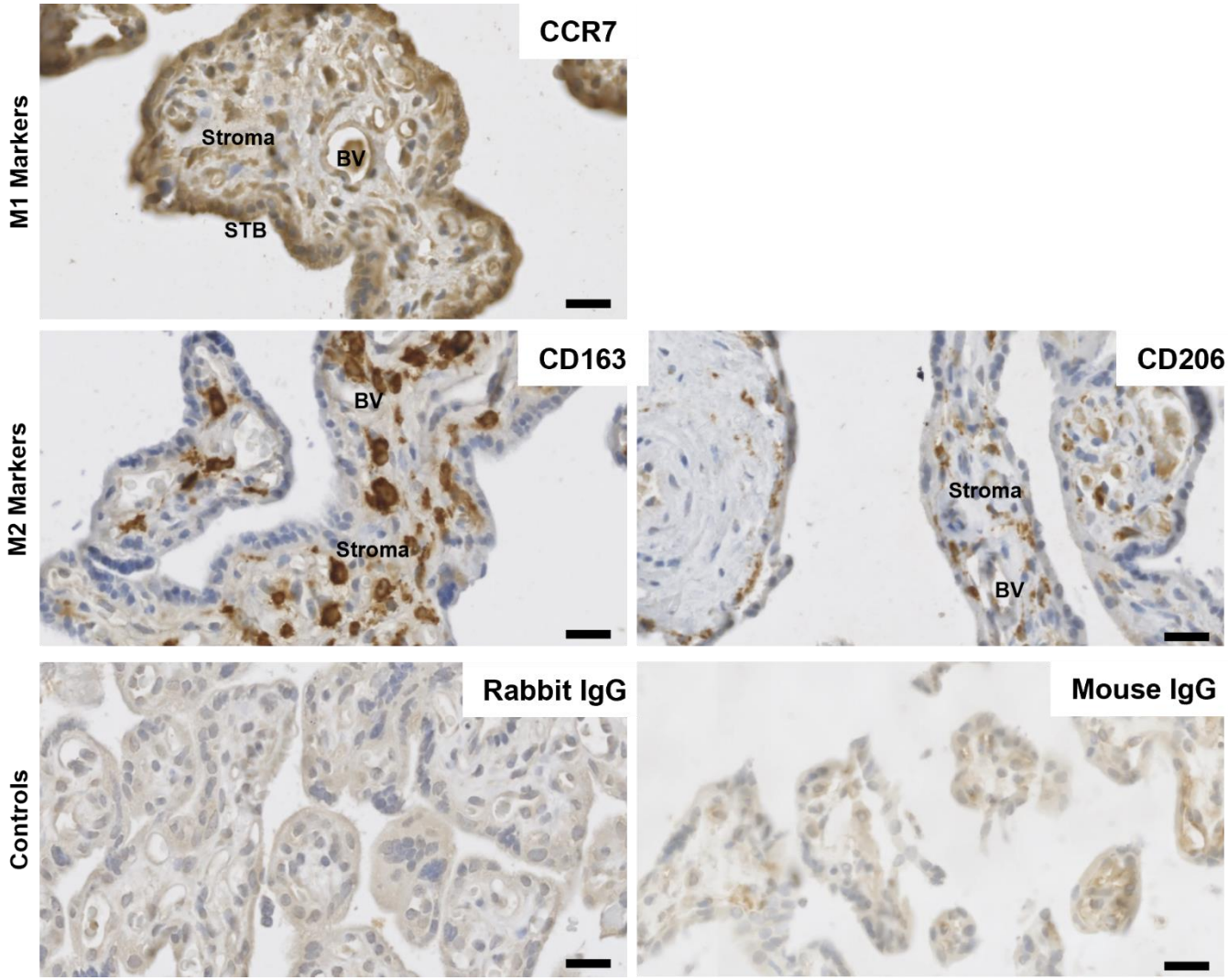

Figure 5.7 – Localisation of Hofbauer cell markers in term placental tissue from uncomplicated pregnancies. Immunohistochemistry of the M1 Hofbauer cell marker (CCR7) and M2 Hofbauer cell markers (CD163 and CD206) using DAB and haematoxylin in term placental tissue. IgGs for the same species and concentration as the primary antibody were used. The most concentrated IgG is shown. Scale bars = 20 µm. Abbreviations = BV: blood vessel; STB: syncytiotrophoblast. n=4.

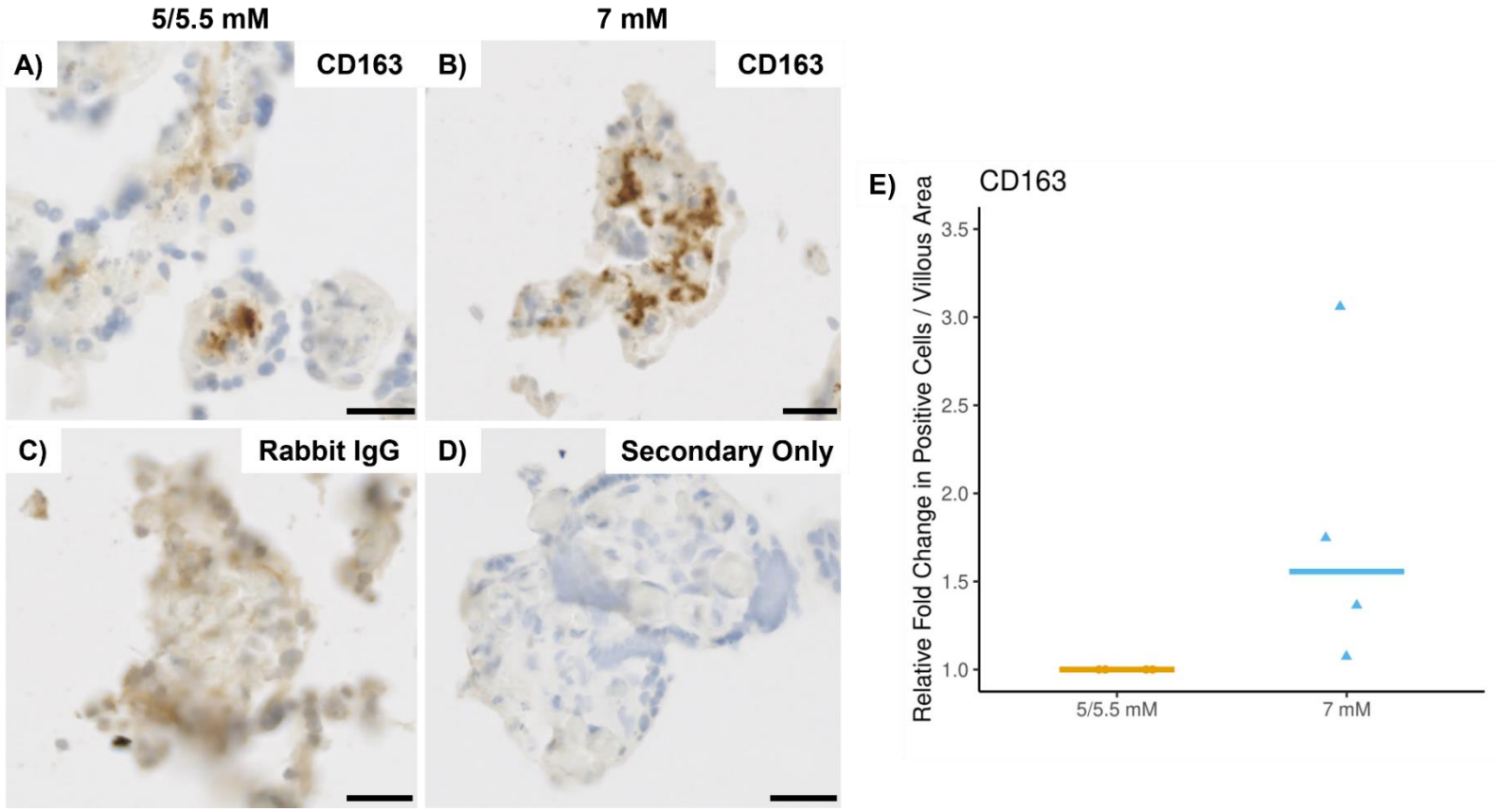

Figure 5.8 - CD163 protein expression in placental explants following glucose treatments for 48 hours, measured by immunohistochemistry. A-D) Representative images of CD163 staining in placental explants are shown in samples treated with fluctuating 5/5.5 mM glucose (A) or constant 7 mM glucose (B) and for controls: non-immune IgG used at the same concentration as the primary antibody (C) and secondary antibody only control (D). Scale bars = 20 µm. E) Quantification of the total number of CD163 positive cells normalised to total villous area (μm^2). Data is presented as the median fold change (compared to 5/5.5 mM) and statistical analysis was performed using a Wilcoxon Signed-Rank Test (as the data was not normally distributed). n=4.

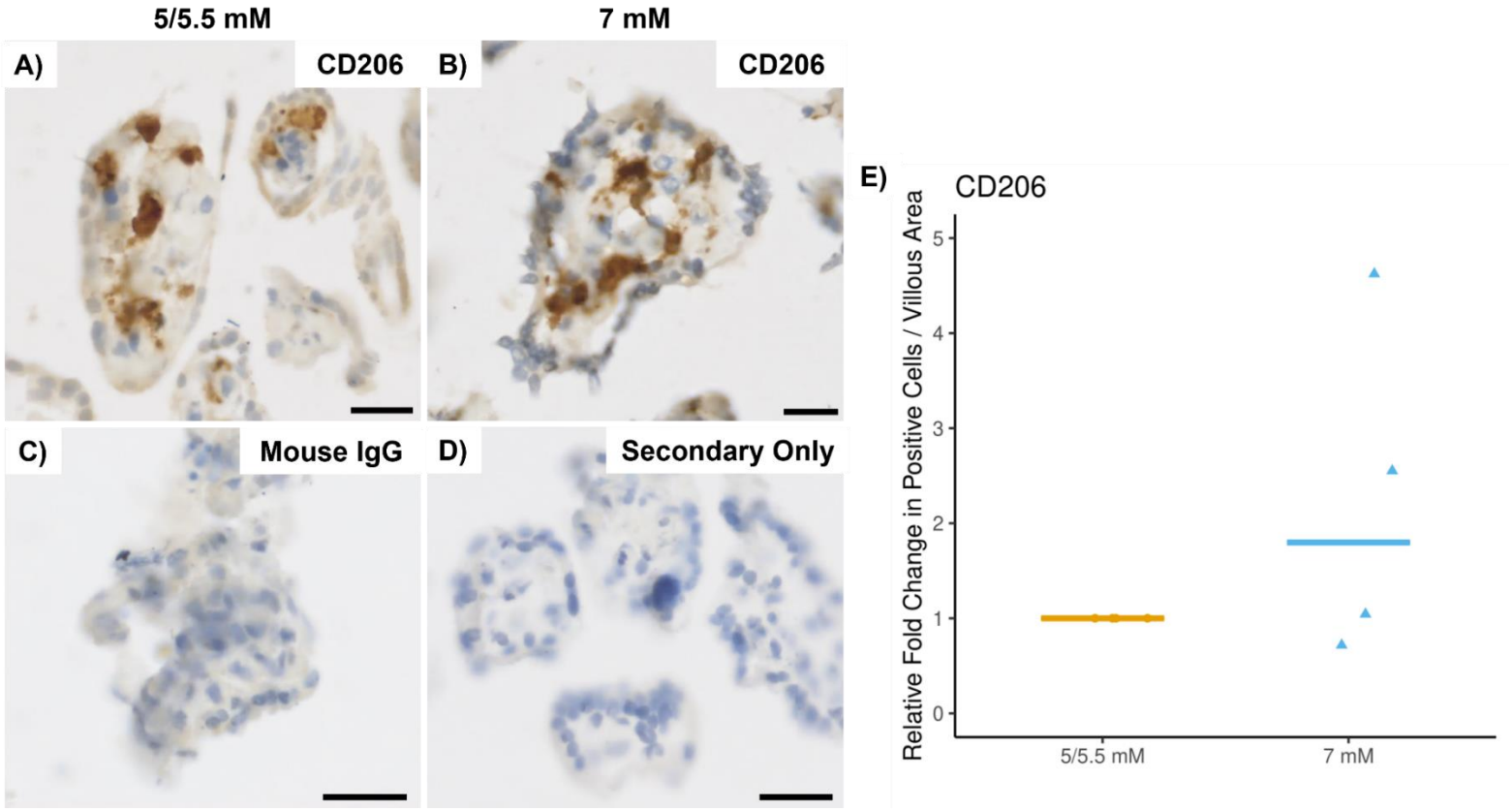

Figure 5.9 - CD206 protein expression in placental explants following glucose treatments for 48 hours, measured by immunohistochemistry. A-D) Representative images of CD206 staining in placental explants are shown in samples treated with fluctuating 5/5.5 mM glucose (A) or constant 7 mM glucose (B) and for controls: non-immune IgG used at the same concentration as the primary antibody (C) and secondary antibody only control (D). Scale bars = 20 µm. E) Quantification of the total number of CD206 positive cells normalised to total villous area (μm^2). Data is presented as the median fold change (compared to 5/5.5 mM) and statistical analysis was performed using a Wilcoxon Signed-Rank Test (as the data was not normally distributed). n=4.

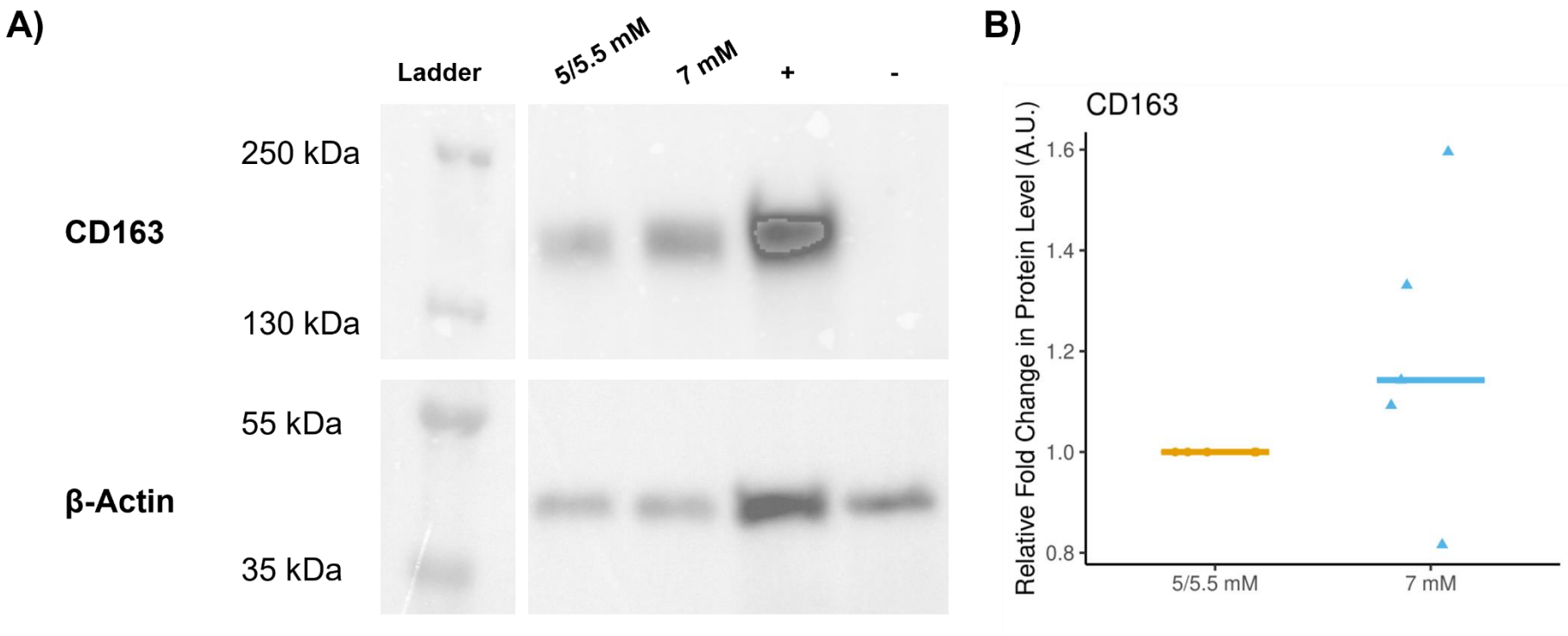

Figure 5.10 – CD163 protein expression in placental explants following glucose treatments for 48 hours, measured by Western Blot. A) Representative image of Western Blot. Levels of CD163 are shown in samples treated with fluctuating 5/5.5 mM glucose or constant 7 mM glucose, and in a positive control (+; Hofbauer cell lysate) and negative control (-; BeWo/Trophoblast cell lysate). The loading control β-actin is also shown. B) Quantification of CD163 protein level, normalised to β-actin. Data is presented as the median fold change (compared to 5/5.5 mM) and statistical analysis was performed using a Wilcoxon Signed-Rank Test (as the data was not normally distributed). n=5.

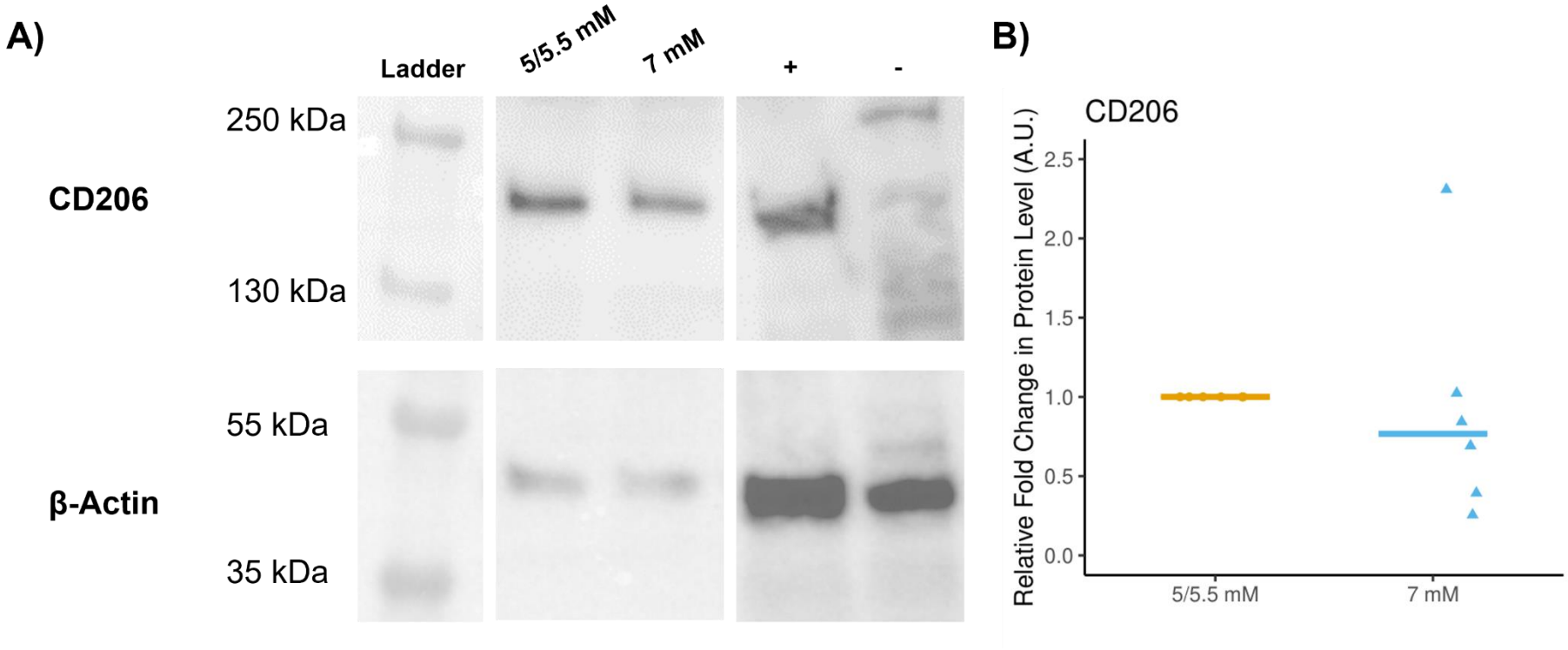

Figure 5.11 - CD206 protein expression in placental explants following glucose treatments for 48 hours, measured by Western Blot. A) Representative image of Western Blot. Levels of CD206 are shown in samples treated with fluctuating 5/5.5 mM glucose or constant 7 mM glucose, and in a positive control (+; Hofbauer cell lysate) and negative control (-; BeWo/Trophoblast cell lysate). The loading control β-actin is also shown. B) Quantification of CD206 protein level, normalised to β-actin. Data is presented as the median fold change (compared to 5/5.5 mM) and statistical analysis was performed using a Wilcoxon Signed-Rank Test (as the data was not normally distributed). n=6.

5.4.3.5 Localisation of M2 HBCs to fetal blood vessels

As M2 HBCs are known to promote tissue remodelling and angiogenesis[606], the proximity of M2 HBCs to fetal blood vessels in term placental tissue from uncomplicated pregnancies was assessed. Immunofluorescent dual staining of CD163 and CD31 to label M2 HBCs and the fetal endothelium, respectively, was performed. CD163 positive HBCs were found in close proximity to the fetal endothelium (Figure 5.12). Taken with the ability of HBCs to secrete angiogenic factors, including inflammatory mediators, paracrine signalling by these cells may contribute to placental vascular development[93,94].

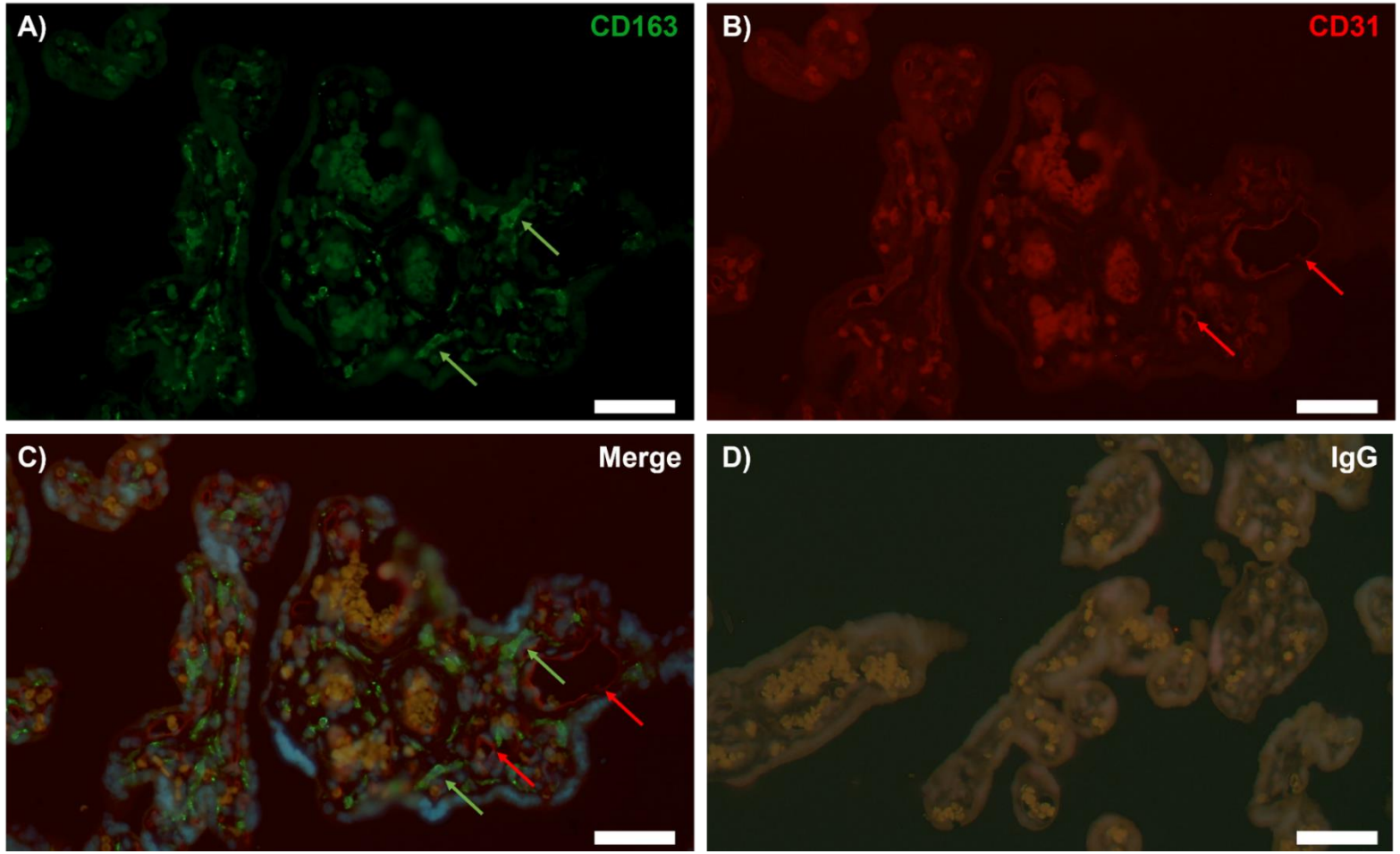

Figure 5.12 – Localisation of M2 Hofbauer cells and their proximity to fetal blood vessels in term placental tissue from uncomplicated pregnancies. Immunofluorescence was performed to dual label the fetal endothelium with CD31 (**Red** and **Red Arrows**) and M2 Hofbauer cells using CD163 (**Green** and **Green Arrows**), followed by mounting in media containing DAPI (**blue**) Scale bars = 50 µm. n=4.

5.5 Discussion

The aim of this chapter was to identify the source of inflammatory mediators altered by 7 mM glucose in placental explants. The pro-inflammatory mediator, IL-1β was validated in RT-qPCRs and ELISAs and was shown to be decreased by 7 mM glucose. Using computational methods and immunohistochemistry HBCs were found to express these inflammatory mediators, and 87 of the DEGs altered by 7 mM glucose overlapped with the HBC proteome. Given that HBCs are known to predominantly be M2 polarised (and hence anti-inflammatory) and that the profile of inflammatory mediators in RNA sequencing data suggests an anti-inflammatory response to 7 mM glucose (Chapter 3), the location of HBC markers in term placental tissue and levels in placental explants treated with glucose were assessed using immunohistochemistry. There was a trend towards an increase in the number of M2 HBCs ($CD163^+$) with 7 mM glucose.

5.5.1 Inflammatory mediators in the placenta altered by glucose fluctuations

Functional enrichment analysis demonstrated that many genes differentially expressed by 7 mM glucose were inflammatory cytokines and chemokines. These pro-inflammatory mediators were downregulated by 7 mM glucose in placental explants, which suggests an anti-inflammatory response to mild hyperglycaemia in the placenta in GDM. Of these, *IL1B* and *IL6* were central mediators of the inflammatory signalling pathways. Trends towards decreases in IL-1β and IL-6 protein levels were observed with 7 mM glucose in ELISAs, and *IL1B* gene expression was significantly downregulated in 7 mM glucose in an RT-qPCR.

Many circulating cytokines and chemokines have been found to be altered in women with GDM, however these findings are varied[216,239,248,249,240–247]. Some studies have also assessed levels of inflammatory mediators within the placenta. In one study, mRNA expression levels of *IL6* and *TNFA* were increased in placentae of women with GDM[252]. In another study by Mrizak *et al.* (2014) comparing women with GDM that deliver macrosomic infants to healthy controls, placental mRNA expression levels of *IL6* and *TGFB* were not significantly altered, whereas *CCL2* was significantly increased in women with GDM that delivered macrosomic infants[612], suggesting altered levels of cytokines/chemokines in the placentae may be associated with GDM and/or LGA. In contrast, Kleiblova *et al*. (2010) found no significant differences in the gene expression levels of *IL6, IL8, TNFA* and *CD68* (a HBC marker) in placentae from women with GDM

compared to controls[613]. Previous studies have not investigated the expression of IL-1β in placentae from women with GDM. However, Schulze *et al.* (2020) utilised a GDM mouse model (high fat diet-induced obese with impaired glucose tolerance) and found that IL-1β levels is increased in pregnancy (circulating and in the placenta and uterus), but levels were not altered in GDM mice[431]. Moreover, in further experiments, a neutralising anti-IL-1β antibody (anti-IL-1β) was injected on day 7.5 of pregnancy, which improved glucose tolerance, without impacting insulin secretion, suggesting increased insulin sensitivity. However, this murine model is limited, as there were no differences in fetal weight in normal lean mice compared to GDM mice (with or without the neutralising antibody), suggesting this is not the best model to investigate GDM and LGA, as the offspring do not develop complications of fetal growth.

Other studies have shown that IL-1β protein expression is not altered in the placentae of women with preeclampsia or pre-term births, however, in *ex vivo* placental explants, IL-1β (along with IL-1α and TNFα) secretion was increased under hypoxic conditions (2.1% O_2)[614]. Generally, pre-term labour is associated with an increase in inflammatory cytokines and chemokines, including IL-1, IL-6, CCL2, IL-8 and TNFα, which leads to leukocyte activation, further increases in pro-inflammatory mediators, and uterine activation. IL-1 is also increased in term deliveries, without infection, and is known to induce muscle contraction[615,616]. An RNA sequencing study also observed a decrease in inflammatory mediators, *IL1B*, *CXCL8* and *PTGS2* in placentae from spontaneous pre-term compared to term births[617], all of which were decreased by 7 mM glucose in placental explants. Although these researchers excluded diabetic pregnancies, and did not collect any glycaemic measurements, this could be linked to maternal hyperglycaemia, as spontaneous pre-term birth has been found to be increased with increasing levels of glycaemia in pregnancy, including abnormal glucose tolerance (but not diabetes) and GDM[618].

Immunohistochemistry of term placental tissue from uncomplicated pregnancies was performed for IL-1β and IL-6, to determine which cells in the placenta were producing or expressing these interleukins. In line with previous studies, IL-1β was expressed in the syncytiotrophoblast and villous stroma[608,609], which was also observed in our immunohistochemistry. IL-6 expression was found in the syncytiotrophoblast, villous stroma, and fetal endothelium, surrounding fetal blood vessels. In previous studies, IL-6 expression has also been reported in STB and cytotrophoblast[609,610], as well as the villous stroma[609]. No studies have reported expression of IL-6 in endothelial cells in immunohistochemical analysis of placental tissue, however the human protein atlas results also show that IL-6 is expressed in placental endothelial cells. To further

investigate the source of other inflammatory mediators altered by 7 mM glucose, the 'maternal-fetal interface atlas' was used[406]. Several chemokines had high expression in HBCs, including, *CCL2, CCL3, CXCL2* and *CXCL8*. *IL1B* and *IL6*, also displayed some expression in HBCs. Taken together with the immunohistochemical findings demonstrating that IL-1β and IL-6 are expressed in the villous stroma, where HBCs reside, this data suggests that the inflammatory mediators altered by 7 mM glucose in placental explants are produced/expressed in HBCs.

To further confirm this, the DEGs altered by 7 mM glucose were compared to HBC proteomics data by Pantazi *et al*. (2022)[407]. The protein expression of 87 DEGs was found in HBCs, including several cytokines and chemokines. Although previous studies have shown that placental levels of pro-inflammatory cytokines are increased in GDM and altered fetal growth (discussed above), the anti-inflammatory profile of inflammatory mediators in response to 7 mM glucose may be linked to HBCs, given that HBCs are known to be predominantly M2 polarised (hence anti-inflammatory)[103,221–223].

In line with this, glucose has been shown to regulate the levels of inflammatory mediators in macrophages from other tissues, primarily IL-1. In RAW 264.7 murine macrophage cells, 20 mM glucose increased mRNA expression of *IL1B* and decreased expression of *IL12*[619]. However, the control used here was 0.5 mM, which is hypoglycaemic. Similarly, Pavlou *et al*. (2018) investigated high glucose (25 mM) compared to control (5.5 mM) in bone marrow-derived murine macrophages for 24 hours or 7 days. High glucose increased *IL1B* mRNA after both 24 hours and 7 days. In M1 polarised bone marrow macrophages, *TNFA* mRNA was increased and *IL12* was decreased after 7 days. In M2 polarised macrophages, *IL10* was increased with long-term treatment. For all conditions, *IL6* was unaltered. Although these studies suggest increases in inflammatory mediators, whereas 7 mM glucose induced decreases, these studies are based on macrophages from other tissues and species and utilise supraphysiological glucose concentrations. Interestingly, in an earlier study, Hill *et al.* (1997) found that 10-20 mM glucose inhibited the release of IL-1 from RAW 264.7 murine macrophage cells, measured in the conditioned medium. However, the intracellular levels of IL-1 were unaltered, suggesting that high glucose reduced the secretion of IL-1 but not the production[620].

Collectively, the findings from these studies suggest that glucose can modulate the expression of and/or release of inflammatory mediators, such as IL-1β, in macrophages. Therefore, this further suggests that the decrease in inflammatory

mediators with 7 mM glucose in placental explants could be specifically linked to a decreased release from HBCs.

5.5.2 HBC levels in response to glucose fluctuations

As HBCs are known to have characteristics of M2 macrophages[103,221–223], HBC marker expression was assessed in term placentae from uncomplicated pregnancies using immunohistochemistry. The M2 markers, CD163 and CD206, were found to have specific expression in the stroma of placental villi, where HBCs reside. While pan-macrophage markers, such as CD68 have also been investigated, CD163 is more abundant in the placenta[253]. Young *et al.* (2015) also found that 99% of isolated HBCs express CD163[621]. This further confirms that HBCs are predominantly M2 polarised and CD163 may be a better pan-macrophage marker in the placenta for assessing 'total' HBCs. In contrast, CD206, also known as C-type mannose receptor 1 (MRC1) is a marker of M2a and M2c subtypes, which have which have tissue repair/immunoregulatory properties[103,225,226] and anti-inflammatory roles[103,225,226], respectively. CD206 has been reported to be expressed in several types of tissue-resident macrophages, including HBCs[103,622], and is known to promote the expression of several anti-inflammatory cytokines, including TGF-β, IL-10 and CCL18[225].

The M1 marker, CCR7, was selected as it was found to be the most differentially expressed gene between M1 and M2 macrophages in the RNA sequencing study in macrophages from human blood[409]. In the present study, CCR7 was expressed throughout the placenta, and was not specific to HBCs, in immunohistochemistry. Other M1 markers, including CD80 and CD11c were also assessed, but there were issues with antibody specificity (data not shown). In line with this, previous studies have also reported that M1 markers, CD80, CD11c and CD86, do not have specific expression in the placenta[253], which makes it difficult to assess levels of M1 polarised HBCs.

Given that CD163 is thought to label all HBCs, and that CD163 and CD206 immunohistochemistry specifically labelled cells in the villous stroma, where HBCs reside, their levels were assessed in placental explants treated with glucose fluctuations via immunohistochemistry and Western blotting. In immunohistochemistry, a trend towards an increase in the levels of CD163 positive cells was observed in placental explants treated with 7 mM glucose. This suggests that the level of M2 polarised HBCs were increased with mild hyperglycaemia. Western blotting also demonstrated increased levels of CD163 protein in placental explants treated with 7 mM glucose, although this did not reach significance. As discussed, CD163 is a marker

of M2 HBCs, but is generally used as a pan-HBC marker[253,621]. Levels of CD206, which labels specific subtypes of M2 HBCs, M2a and M2c[103,622], also showed trends towards an increase with 7 mM glucose in immunohistochemistry. A limitation of this is the low sample numbers used for immunohistochemistry (n=4), an increase in samples would allow confirmation of whether glucose fluctuations alter levels of M2 HBCs in the placenta.

It would also be interesting to assess the levels of each individual M2 subtype in these explants. For example, M2a HBCs are known to express CD209 and secrete IL1RN[103,225,226]. M2b HBCs express CD86 and secrete TNF-α and IL-6, and therefore interestingly exhibit similar properties to M1 macrophages[103,225–227]. M2c HBCs are known to express CD14[228]. To further investigate the phenotype and abundance of HBCs in response to glucose fluctuations, it would be ideal to perform dual staining for subtype markers, with CD163, or other pan-macrophage markers, such as CD68, to assess their levels as a ratio of total HBCs.

In addition to downregulation of pro-inflammatory mediators, several other DEGs altered by 7 mM glucose in placental explants also indicated an increase in M2 HBCs. M2 macrophages are also known to reduce their expression of tissue inhibitor of metalloproteinases-1 (TIMP1), which results in the production of an angiogenic, TIMP-deficient MMP-9 zymogen (proMMP-9)[623]. *TIMP1* was found to be downregulated by 7 mM glucose, in addition to *MMP1*, *MMP10* and an upregulation in *MMP11*. When comparing the DEGs to M1/M2 macrophage transcriptomics, other DEGs were found to be consistent with M2 macrophage polarisation, including the M2 marker, *CD36*, which was upregulated[103]. CD36 is a scavenger receptor for the endocytosis of lipoproteins, such as low-density lipoproteins (LDLs) and very low-density lipoproteins (VLDLs). Peroxisome proliferator-activated receptor γ (PPARγ) activation in macrophages enhances CD36 expression, increasing uptake of LDLs, which is observed in M2 macrophage function. The uptake of acetylated LDL (ac-LDL) has been used in HBCs isolated from placentae to indicate the presence of the M2 marker CD36[103]. However, when localising and assessing abundance in term placental tissue, CD36 expression is not specific to HBCs, and is expressed in the trophoblast, endothelium, and fetal vessels[624,625]. This limits the use of CD36 as a marker in immunohistochemistry to assess levels of M2 HBCs, and therefore was not performed in the present study. Moreover, *CD38* has also been reported to be specific to M1 macrophages and was downregulated by 7 mM glucose[626].

Hyperglycaemia has also been shown to influence macrophage polarisation from other sources. In RAW 264.7 murine macrophage cells, 25 mM glucose decreased mRNA

and protein expression of CD206 compared to 5.5 mM glucose, when M2 polarisation was stimulated with IL-4. When LPS was used to induce M1 polarisation, 25 mM glucose increased the mRNA expression of M1 associated inflammatory mediators, *IL6* and *TNFA*[627]. In contrast, in J774A.1 murine macrophages from ascites, high glucose (83.3 and 138.8 mM) increased the percentage of M2 polarised cells ($CD206^+$), compared to 5.6 mM, dose-dependently, in flow cytometry. There were also some increases in M1 polarised cells ($CCR7^+$) with 138.8 mM glucose. These studies suggest that the impact of glucose on macrophage polarisation is dependent on the type/origin of the macrophages[628]. A limitation of these studies is that again the glucose concentrations utilised are supraphysiological.

The polarisation of HBCs in diabetic pregnancies is unclear. Several conflicting studies have assessed the phenotype of macrophages in diabetic placentae compared to placentae from uncomplicated pregnancies. In a study on T1DM pregnancies, a decrease in placental gene expression of M2 markers, *CD163, CD209, IL10* and an increase in of M1 markers, *CD68* (although often referred to as a pan-macrophage marker), *CCR7* and *IL1B* were observed. This was confirmed at the protein level for CD163 and CD68. Further experiments in STZ-induced diabetic rats also showed a reduction in *CD163* and an increase in *CD68* mRNA[251]. Similarly, levels of CD14 and CD68 were increased in placentae of women with GDM compared to healthy controls in immunohistochemistry and mRNA expression of *CD68* was also increased[252]. In contrast, other studies in GDM pregnancies have shown that the number of $CD163^+$ cells within the chorion and decidua were increased, suggesting M2 polarisation in GDM[224]. Moreover, Schliefsteiner *et al.* (2017) found similar levels of CD163 in immunohistochemistry of GDM and control placentae, which was used to account for the overall number of HBCs. When assessing M2 markers, CD209 and CD206, these were increased in GDM placentae relative to CD163, with CD209 being significantly increased[253]. Flow cytometry also revealed increased levels of CD206 and CD209 in HBCs isolated from GDM placentae compared to normal placentae. Moreover, HBCs from normal placentae were also treated with 25 mM glucose, which did not alter the expression of CD163, CD209 or CD86. However, the levels utilised are supraphysiological concentrations in glucose, and do not reflect physiological levels used in the present study.

These studies did not consider birthweight, BWCs or glycaemic control, and could explain these contrasting results. Therefore, further study is needed into the polarisation of HBCs in GDM with varying levels of glycaemic control, and/or GDM LGA/GDM AGA pregnancies. Limited studies have further characterised glycaemia or

investigated fetal overgrowth specifically. In the Mrizak *et al.* (2014) study, there was a significant increase in the mRNA expression of macrophage markers *CD68* and *CD14* in the placenta of women with GDM that delivered macrosomic infants, compared to healthy controls[612]. Bhattacharjee *et al*. (2017), compared placentae of women who were normoglycaemic, had GDM, were mild hyperglycaemic or had overt diabetes. In overt diabetic placentae HBC hyperplasia/proliferation occurred in 44.4% of cases, which was not observed in the normoglycaemic, GDM or mild hyperglycaemic groups, however it is not clear how they identified the HBCs or their levels[123]. Based on these limited studies, if more time was available, it would be interesting to assess the levels of HBC markers using immunohistochemistry in placental tissue from GDM and non-GDM pregnancies with various birthweight outcomes used in Chapter 4.

5.5.3 M2 HBCs and placental vascular development

Given that 7 mM glucose increased the levels of M2 HBCs, which are known to promote tissue remodelling and angiogenesis[606], the proximity of M2 HBCs to fetal blood vessels in term placental tissue from uncomplicated pregnancies was assessed. Dual immunofluorescent staining showed that CD163 positive HBCs were in close proximity to the CD31 labelled fetal endothelium. Paracrine signalling by HBCs is known to contribute to vascular development, based on this close proximity, and their ability to release angiogenic factors[93,94]. HBC levels have been correlated with the number of vasculogenic structures[94], and VEGF is strongly expressed in HBCs during the very early stages of pregnancy[105]. *In vitro,* HBC conditioned medium has been reported to increase tubular formation in primary fetoplacental endothelial cells[103].

HBCs isolated from first trimester and term placentae have been found to secrete VEGF-A and FGF-2[103,104]. Loegl *et al.* (2016) also showed that isolated HBCs from term placentae possess an M2 phenotype and when conditioned medium from these HBCs was applied to fetoplacental ECs, angiogenesis was stimulated, in a tube formation assay[103]. This angiogenic role of M2 macrophages has also been observed in other systems. Matrigel supplemented with macrophage subsets (M1, M2a or M2c) injected subcutaneously into C57BL/6 mice increased tubular structures and CD31-labelled endothelial cells in M2-matrigel compared to control and M1 subsets. Induced gene expression of angiogenic factors, *Fgf2, Igf1, Ccl2* and *Plgf* were observed in M2 macrophages[629].

As demonstrated in the present study, HBCs are also known to release inflammatory mediators, many of which also have vascular regulatory roles, and were downregulated by 7 mM glucose in placental explants. For example, IL-1β has been shown to increase

mRNA expression and secretion of VEGF in several cell types, including cardiomyocytes, cardiac microvascular ECs and human airway smooth muscle cells[630,631]. IL-1β is known to simultaneously regulate inflammation and angiogenesis, and there are several overlaps between the pathways and functions of IL-1β and VEGF[632]. IL-8 is also known to increase endothelial permeability in early stages of angiogenesis and phosphorylate VEGFR2 in a VEGF-dependent manner, in primary human microvascular ECs, and murine ECs[106,107]. CCL2 has been reported to upregulate angiogenic factors, including *KDR* (VEGFR2), angiopoietins, *PECAM1* and *VCAM1* in brain ECs[108]. Other immune and inflammatory DEGs included *PTGS2* (COX-2), which is also known to be a mediator of angiogenesis and thought to act via increased VEGF production. COX-2 inhibitors reduce angiogenesis, and in HUVECs this has also been shown to cause reduced endothelial cell migration[633].

In further studies, isolation of HBCs and further exposure to glucose fluctuations could confirm whether the altered inflammatory mediators in response to 7 mM glucose were being released by HBCs, by assessing their secretory profile. Conditioned medium could also be applied to placental endothelial cells to assess their function (i.e. in a endothelial tube formation assay). Although HBCs are present throughout gestation, their levels are higher in the first trimester (~50%), compared to the third trimester (~20%)[209]. The high level of HBCs in early pregnancy correlates with the process of vasculogenesis in the first trimester and the development of primitive capillary network[80,81]. Therefore, it would also be interesting to assess the impact of glucose fluctuations on HBCs isolated from early pregnancy, and how this influences placental vasculogenesis. Although GDM is diagnosed at ~28 weeks, there is a potential for maternal glucose fluctuations to be present earlier in pregnancy[596], prior to diagnosis, and thus could impair normal placental development at an earlier timepoint.

It would also be interesting to assess whether the proximity of HBCs to fetal blood vessels is altered by glucose fluctuations, or in placentae from GDM LGA compared to GDM AGA pregnancies, using dual staining (as in Section 5.4.3.5). However, in early pregnancy HBCs are present in villi with ‘loose’ stroma, primarily immature intermediate villi, occupying stromal channels, that are lined with MSCs. These HBCs are mobile and can rapidly migrate in the loose stroma. However, at term, there are lower numbers of HBCs, and a much lower percentage of ‘loose’ stromal types due to the development of mature intermediate and terminal villi, suggesting that the HBCs are less mobile[634]. Therefore, it is important to take this into account if assessing whether the localisation is altered by glucose (or GDM/LGA) if looking in term placental tissue, where HBCs are more ‘fixed’ within the villous stroma.

Overall, given that M2 macrophages and HBCs are known to regulate vascular development, this data suggests the reduced levels of angiogenic inflammatory mediators in response to 7 mM glucose may be associated with HBCs, and contribute to placental vascular dysfunction in pregnancies complicated by GDM and LGA.

5.6 Summary

- RNA sequencing showed that gene expression of inflammatory mediators, including cytokines and chemokines were altered by 7 mM glucose in placental explants.
- Many pro-inflammatory cytokines and chemokines were downregulated by 7 mM glucose, including *IL1B*, which was validated by RT-qPCR.
- Placental macrophages (HBCs) were found to express many of these inflammatory mediators altered by 7 mM glucose.
- HBCs are known to be primarily M2 polarised (anti-inflammatory) and play roles in vascular development. Although not significant, the number of HBCs in placental explants were found to be slightly increased by 7 mM glucose, determined by CD163 staining in immunohistochemistry.
- Findings from this chapter therefore show that mild hyperglycaemia in GDM (7 mM glucose) reduces the levels of pro-inflammatory mediators in the placenta, and increases the levels of M2 HBCs, which in turn may contribute to altered placental vascular development and angiogenesis, resulting in altered fetal growth and LGA.

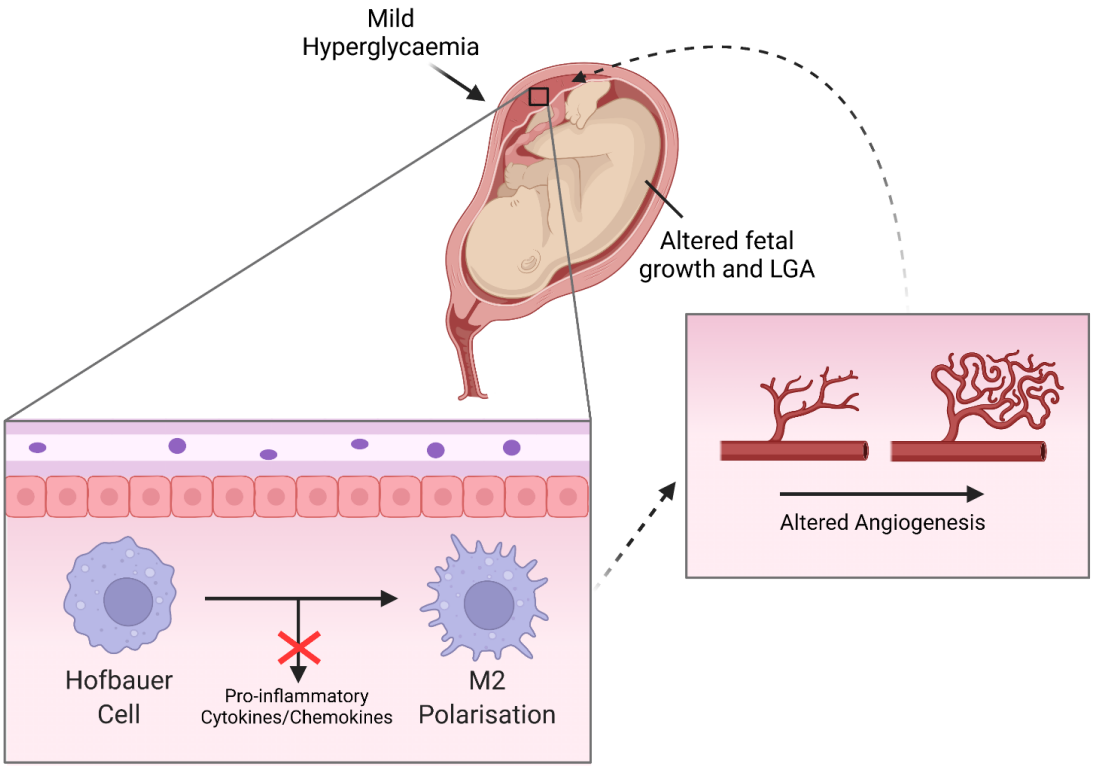
Mild
Hyperglycaemia
Altered fetal
growth and LGA
Altered Angiogenesis
Hofbauer
Cell
Pro-inflammatory
Cytokines/Chemokines
M2
Polarisation

Chapter 6 – Generating models to assess endothelial differentiation in placental vascular development

6.1 Introduction

6.1.1 Models of placental vascular development

The findings from Chapter 3 showed that physiological maternal glucose fluctuations associated with GDM LGA pregnancies (7 mM glucose) altered genes associated with vascular development, including EC development, proliferation and tubulation, as well as blood vessel permeability, vasculogenesis and angiogenesis. Moreover, many altered genes were found to be downregulated angiogenic inflammatory mediators, which were thought to be associated with an increase in vascular regulatory M2 polarised HBCs (Chapter 5). Placental vascular development involves the differentiation of placental mesenchymal stromal cells (pMSCs) into EC and haematopoietic cell progenitors[80]. These cells form cell cords and intercellular clefts, creating the primitive capillary network[81]. This network is then expanded through angiogenesis, the sprouting or elongation of existing vessels[65,81]. Mature vessels are then formed once perivascular cells are recruited, such as pericytes and VSMCs[65,81]. To further investigate the impact of glucose fluctuations on placental vascularisation, it was important to consider available models of placental vascular development.

Current *in vitro* models to study placental vasculature utilise ECs, such as HUVECs and human placental microvascular ECs[635]. Mono-cultures of placental ECs provide a low-cost, high-throughput method to assess endothelial function, although they lack the physiological complexity of the multiple cell types within the placental villi[635]. Therefore, recent studies have incorporated placental ECs into co-culture models, such as transwells[342,343], or placenta-on-a-chip[127,346,347], to improve the physiological relevance.

Widely used placental ECs in mono- and co-culture models include HUVECs, which are macrovascular ECs, derived from the umbilical vein[509,636]. HUVECs can form a confluent monolayer, and are widely used to assess angiogenesis, and endothelial function[635]. However, umbilical cord vessels are known to differ in their structure from placental blood vessels[637], and *in vitro* HUVECs have differences in morphology and response to endothelial growth factors, compared to placental microvascular ECs[638]. Moreover, the secretion of vasoactive mediators differed between placental microvascular ECs and HUVECs, as HUVECs secreted more endothelin-1 and -2 and placental microvascular ECs secreted more angiotensin-II[636]. Given these differences, HUVECs may not be the best model to study the function of ECs within the placental

villi. In line with this, Lang *et al.* (2008) compared the phenotype of human placental arterial ECs (HPAECs) and human placental venous ECs (HPVECs) isolated from chorionic plate vessels. While HPAECs formed confluent monolayers, with typical EC cobblestone morphology, HPVECs formed monolayers with a whirlpool morphology, a characteristic of mesenchymal cells[360]. Moreover, HPAECs exhibit a mature EC phenotype; whereas HPVECs overexpress developmental associated genes, and have enhanced differentiation potential into osteoblasts and adipocytes, compared to HPAECs. This plasticity suggests a role for HPVECs as endothelial progenitors in vascular development[637]. Placental microvascular ECs, such as fetoplacental ECs (FpECs), can be isolated from digested placental cotyledons or small blood vessels within the cotyledons[636,639]. FpECs express common EC markers and exhibit functional properties, such as the formation of endothelial tubes when cultured on an ECM, and alignment in the direction of fluid flow[639]. Through production of vasoactive mediators, FpECs regulate of angiogenesis and vasomotor tone[639], making them an appropriate model for angiogenesis and endothelial function.

Given that many of these placental/umbilical ECs exhibit a mature EC phenotype, they do not model the early development of placental blood vessels, which involves the differentiation of pMSCs.

6.1.1.1 Placental mesenchymal stromal cells

pMSCs (sometimes referred to as placental mesenchymal stem cells) are known to reside in the perivascular niche throughout pregnancy[640]. pMSCs are thought to contribute to placental vasculogenesis by differentiating into EC and haematopoietic cell progenitors[80,641]. Additionally, pMSCs release paracrine factors, such as VEGF, IGF-1 and angiopoietin-1, which influence vessel development and the expansion of vascular networks in the placenta[80,642]. The release of these paracrine factors has been shown to influence angiogenesis *in vitro* and *in vivo* as conditioned medium from pMSCs increased EC proliferation and tube formation[643] and transplanted pMSCs into mice increased neovascularisation[644].

Furthermore, pMSCs isolated from GDM placentae have decreased gene expression of angiogenic factors *VEGFA* and *FGF*. Interestingly, this decrease in angiogenic factors was also observed when non-GDM pMSCs were treated with 25 mM glucose[645]. Similarly, co-culture of GDM pMSCs with HUVECs resulted in reduced proliferation, migration, and tube formation of HUVECs in further functional assays, compared to non-GDM pMSCs[646]. pMSCs isolated from FGR pregnancies have an altered transcriptome, including upregulation of *ADAMSTS1* and downregulation of

HAS2, both known to regulate angiogenesis and *FBLN2*, which regulates vascular elasticity[647]. Umapathy *et al*. (2020) also showed that exposure to pMSC conditioned medium, isolated from FGR pregnancies, inhibited tube formation of ECs, compared to conditioned medium of pMSCs from normal pregnancies. Macrophages exposed to conditioned medium from FGR pMSCs also had a lesser effect on stimulating EC tube formation[648]. Thus, suggesting a role for altered pMSC function in complications of pregnancy.

In vitro, pMSCs are known to differentiate into perivascular cell types, such as pericytes and VSMCs by upregulating contractile proteins, expressed in these cells[359,649]. Boss *et al*. (2020) showed that first trimester pMSCs cultured in DMEM/F12 have increased expression of the early smooth-muscle marker αSMA and the late smooth muscle marker calponin. In term pMSCs, culture in DMEM/F12 increased expression of αSMA[649]. Moreover, Kennedy (2023) demonstrated that term pMSCs could adopt a VSMC phenotype, with increased expression of VSMC markers Myosin 11 (*MYH11)* and Caldesmon *(CALD1)* with TGF-β1 and ascorbic acid induced differentiation and collagen support[359]. This ability of pMSCs to differentiate into key vascular cell types associated with blood vessel development in the placenta, makes them a potential model for investigating endothelial differentiation during placental vascular development. The use of term pMSCs is also relevant to investigate the impact of maternal glucose fluctuations in GDM, given that these fluctuations were observed in CGM between 30-32 weeks' gestation[62] and that GDM is diagnosed later in pregnancy (between 24-28 weeks' gestation)[13].

6.1.1.1.1 Differentiation of mesenchymal stromal cells into endothelial cells

Several studies have investigated the differentiation potential of MSCs, from other tissues, into ECs, including, human bone marrow stem cells (BMSCs). The microenvironment of vascular cells contains biochemical factors that influence differentiation into ECs[366], therefore these studies use either endothelial growth medium (EGM) and/or medium that contains additional VEGF (25-50 ng/mL). The findings of these studies have been outlined in Table 6.1.

To determine whether the cells have differentiated, various methods are utilised. Firstly, any morphological differences are usually observed, as MSCs display a characteristic whirlpool morphology[360], and ECs a cobblestone morphology[650]. Expression of EC markers are also assessed, either by RT-qPCR, flow cytometry and/or immunocytochemistry. Finally, functional assays are performed, including the endothelial tube formation assay and the ac-LDL uptake assay. The tube formation

assay involves seeding cells onto an ECM. ECs will then form tube-like structures, which contain a lumen surrounded by ECs linked together through junctional complexes[651]. The ac-LDL assay involves assessing the uptake of a labelled, ac-LDL into the cells, as the uptake of ac-LDL is specific to ECs and macrophages, via the scavenger cell pathway of LDL metabolism[652]. A limitation of these studies, however, is that they do not investigate the impact on mesenchymal markers, which would be expected to be decreased during endothelial lineage differentiation.

A few studies have investigated the differentiation of MSC isolated from the placenta. Wu *et al.* (2008) cultured pMSCs in EGM-2 with additional VEGF-A under static conditions for 24 hours and observed increases in VEGF receptors (VEGFRs), fms related receptor tyrosine kinase (*FLT1*) and kinase insert domain receptor (*KDR*) in RT-qPCRs, but observed no differences in mature EC markers[653]. Periods longer than 24 hours were not assessed. Chen *et al*. (2015) cultured pMSCs in EGM-2 with 50 ng/mL VEGF-A, and reported that the EC marker, von willebrand factor (vWF), was observed in immunocytochemistry, however this was the only marker investigated[654].

6.1.1.1.2 Differentiation of mesenchymal stromal cells into endothelial cells using shear stress

In vivo, vascular cells are exposed to hemodynamic forces caused by blood flow, including flow shear stress and cyclic stretch[655]. Shear stress is known to influence the morphology, orientation, and differentiation of ECs. In addition to biochemical factors, shear stress can also influence the differentiation of MSCs into cells of the endothelial lineage[366]. The findings of these studies have been outlined in Table 6.2. Of these studies, Wu *et al.* (2008) cultured pMSCs in EGM-2 with additional VEGF-A under static conditions or in a parallel plate flow chamber with 6 or 12 dyn/cm^2 [653]. Cells cultured under flow conditions aligned in the direction of flow, and at 12 dyn/cm^2, cells expressed mature endothelial markers, CD31 and vWF in immunocytochemistry, Western blots, and RT-qPCR. These cells were also able to uptake ac-LDL and form tube-like structures.

Therefore, the aim of this chapter was to determine the potential of pMSCs to differentiate towards an endothelial lineage. Given that previous studies assessed the impact of endothelial growth factors on pMSCs for short time periods (~24 hours) and did not investigate mesenchymal marker expression, differentiation medium was used for up to 25 days, and the phenotype of differentiating cells were fully characterised by assessing endothelial, as well as mesenchymal markers via RT-qPCR and immunocytochemistry, in addition to endothelial function using a tube formation assay

and a fibrin bead assay. The impact of shear stress was also investigated, using a low flow/shear stress of 1 µL/min in microfluidic devices, as used in most placenta-on-a-chip studies[127,347,352,354].

Table 6.1 - Key findings of studies investigating the potential differentiation of mesenchymal stromal cells from different sources, into endothelial cells. Abbreviations: BMSCs – Bone Marrow MSCs; pMSCs – Placental MSCs; av-MSCs – Amnion Avascular MSCs; CMSCs – Chorionic (Plate) MSCs; UMSCs - Umbilical Cord MSCs; AMSCs – Adipose Tissue MSCs; bv-MSCs - Placental Chorionic Blood Vessel MSCs. ↑ Increased expression, ↓ decreased expression, ~ no change in expression.

Reference	Cell Type	Differentiation Medium	Timepoints	Morphology	Flow Cytometry	Immunocytochemistry	PCRS	Functional Assays
Chen 2015[654]	Primary Human pMSCs	EGM-2 (Promo Cell) with 50 ng/mL VEGF-A	· 14 and 21 days · Medium refreshed every 3 days	N/A	N/A	· VWF	N/A	N/A
Du 2016[643]	Human Primary BMSCs, AMSCs, UMSCs and PMSCs	Cells on Matrigel with EGM2-MV with 50 ng/mL VEGF	· 14 days · Medium refreshed twice a week	N/A	N/A	*Weak expression of CD31 and vWF*	~CD31 ~CD34 ~FLT1 (VEGFR1) ~VWF ~CDH5 (VE-Cadherin) ~TIE2	· Endothelial tubes (Primarily in BMSCs and pMSCs) · Uptake of acLDL · Produce eNOS
Konig 2011[656]	Primary Human Av-MSCs	EGM-2 (Lonza)	N/A	Cobblestone after 5 days	N/A	*No expression of VWF or VE-Cadherin, even at 100 ng/mL VEGF*	↓TIE2 ↓VEGFA ↓CD146 ↓FGF2 ↑SERPINF1 ↑SPRY1 ↑ARP1 (Angioarrestin)	· Endothelial tubes · Uptake of acLDL
Konig 2015[657]	Primary Human Bv-MSCs	EGM-2 (Lonza)	N/A	Cobblestone at passage 6	N/A	*No expression of VWF*	N/A	· Endothelial tubes

Reference	Cell Type	Differentiation Medium	Timepoints	Morphology	Flow Cytometry	Immunocytochemistry	PCRS	Functional Assays
Oswald 2004[658]	Primary Human BMSCs	Medium with 2% FCS and 50 ng/mL VEGF.	· 7 days · Medium refreshed every 2 days	No morphological differences	· VEGFR1 · VEGFR2 · VE-Cadherin · VCAM1 *Laser scanning cytometry*	· VWF	N/A	· Endothelial tubes
Panakajakshan 2013[659]	Primary porcine BMSCs	EGM-2 (Lonza) with additional 50 ng/mL VEGF-A	· 10 days · Medium refreshed every 3 days	Cobblestone morphology	↑VWF ↑CD31 ↑CDH5 (VE-Cadherin)	↑ VWF	↑VWF ↑PECAM1 ↑CDH5 (VE-Cadherin) ↑FLT1 ↑KDR	· Uptake of acLDL · Endothelial tubes
Wang 2018[386]	Primary Human BMSCs	Medium with 50 ng/mL VEGF, 10 ng/mL bFGF, 20 ng/mL IGF, 5 ng/mL EGF, ascorbic acid, heparin and 2% FBS.	· 3, 7 and 14 days · Medium refreshed daily	Shorter spindle shapes	· CD31 · CD34 *In 60% of cells by day 14*	· CD31 · CD34	↑VWF ↑CDH5 (VE-Cadherin) ↑KDR (VEGFR2) *By day 14*	· Endothelial tubes *By day 7 and 14 (tubes labelled with CD31 and CD34)*
Yu 2021[660]	Primary human CMSCs (First and third trimester)	MCDB 131 medium with 5% FBS, 50 ng/mL VEGF and 20 ng/mL IGF-1	· 14 days · Medium refreshed every 2 days	First trimester differentiated CMSCs has a morphology more similar to ECs	· VWF · CD31 *More in first trimester CMSCs*	· VWF · CD31 *More in first trimester CMSCs*	↑PDGFD ↑VEGFA ↑TNC ↓SPRY1 ↓ANGPTL1	· Endothelial tubes (More in first trimester CMSCs) · Improved cardiac function when first trimester CMSCs were transplanted into a rat myocardial infarction model

Table 6.2 - Key findings of studies investigating the potential differentiation of mesenchymal stromal cells from different sources into endothelial cells under shear stress conditions. Abbreviations: AMSCs – amnion MSCs; BMSCs – Bone Marrow MSCs; pMSCs – Placental MSCs; SHEDs - Stem cells from human exfoliated deciduous teeth. ↑ Increased expression, ↓ decreased expression, ~ no change in expression.

Reference	Cell Type	Differentiation Medium	Shear Stress	Timepoints	Morphology	Protein Expression	PCRs	Functional Assays
Bai (2010)[661]	Rat primary BMSCs	DMEM with 10% FBS and 50 ng/mL VEGF	Parallel plate flow chamber at 15 dyn/cm^2 (1.5 Pa). In further experiments assessed 10, 20 and 25 dyn/cm^2.	· Static experiments: VEGF treatment for up to 7 days · Shear stress experiments: VEGF treatment for 7 days then shear stress for up to 24 hours.	Alignment and elongation in the direction of flow. Cytoskeletal reorganisation (Phalloidin staining). *Following 24 hours shear stress. At 48 hours cells detached.*	↑CD31 ↑Factor VIII *With VEGF and shear stress (Immuno-cytochemistry)*	↑t-PA ↑KDR *With VEGF and shear stress KDR expression decreased when shear stress was applied for 48 hours and at higher levels (20 and 25 dyn/cm^2)*	N/A
Fischer (2009)[662]	Primary human AMSCs	Endothelial cell growth supplement (ECGS; 50 ug/mL) added to medium	Orbital shaker at 12 dyn/cm^2 (1.2 Pa – 210 cycles/min)	· Static experiments: ECGS treatment for 3 weeks. · Shear stress experiments: ECGS treatment for 2 weeks then shear stress for up to 8 days	Alignment in the direction of flow *After 2 weeks static with ECGS followed by 2 days with 12 dyn/cm^2*	↑CD31 *After 2 weeks static with ECGS followed by 4 days with 12 dyn/cm^2 (IF and WB)*	↑CD31 ~VWF ~eNOS *After 2 weeks static with ECGS followed by 2 days with 12 dyn/cm^2*	· Uptake of acLDL *After 2 weeks static with ECGS followed by 4 days with 12 dyn/cm^2* · Endothelial tubes *In 7 days static treatment with ECGS*

Reference	Cell Type	Differentiation Medium	Shear Stress	Timepoints	Morphology	Protein Expression	PCRs	Functional Assays
Janeczek Portalska (2012)[663]	Human primary BMSCs	EGM-2 then seeded onto Matrigel for 24 hours.	Shaker shear stress at 20 RPM.	· 10 days in EGM-2 with shear stress then seeded onto Matrigel for 24 hours.	Cell circularity increased (F-Actin Staining)	↑CD31 ↑VEGFR2 (KDR) *(Immuno-cytochemistry)*	↑PECAM1 ↑VWF ↑KDR	· Uptake of acLDL
Shojaei (2013)[664]	Primary human adipose AMSCs	Static condition was treated with 50 ng/mL VEGF	Bioreactor with either cyclic stretch of 10% (1 Hz), cyclic shear stress of 0 to 2.5 dyn/cm^2 (1 Hz) or concurrent cyclic and shear stresses both with the same characteristics.	· Static experiments: VEGF treatment for 1, 2 or 7 days · Shear stress experiments: 24 hours shear stress		N/A	↑KDR ↑VWF *With cyclic shear stress* ↑CDH5 (VE-Cadherin) *With all types of mechanical stimuli (Combination of cyclic and shear caused greatest increase)* ↑KDR ↑VWF ↑CDH5 (VE-Cadherin) *In static VEGF experiments after 2 days, greatest effect after 7 days.*	N/A
Wang et al. (2005)[665]	Murine embryonic mesenchymal progenitor cell line (C3H/10T1/2)	N/A	Parallel plate flow chamber with a shear stress of 15 dyn/cm^2 (1.5 Pa)	· Exposed to shear stress for 6 and 12 hours	Cells became a more fusiform shape	↑VWF ↑CD31 *After 12 hours shear stress (Flow cytometry and Immuno-cytochemistry)*	↑VWF ↑PECAM1 *After 6 and 12 hours shear stress* ↑CDH5 *After 12 hours shear stress*	· Uptake of acLDL · Endothelial tubes *After 12 hours shear stress*

Reference	Cell Type	Differentiation Medium	Shear Stress	Timepoints	Morphology	Protein Expression	PCRs	Functional Assays
Wang et al. (2018)[666]	SHEDs	Some cells were exposed to differentiation medium containing: 50 ng/mL VEGF in FBS-free α-MEM following shear stress.	Streamer shear stress Device at 4 and 16 dyn/cm^2.	· Shear stress for 2 hours. Some? cells were then exposed to differentiation medium for 12 hours.	N/A	↑VEGFR2 ↑CD31 ↑DLL4 *With 4 and 16 dyn/cm^2 (Western Blot)* ↑VEGF secretion *With 4 and 16 dyn/cm^2 (ELISA)*	↑VEGF *With 4 dyn/cm^2* ↑KDR ↑DLL4 *With 4 and 16 dyn/cm^2. All increased with shear stress and differentiation medium.*	· Endothelial tubes *With 4 and 16 dyn/cm^2*
Wu (2008)[653]	Primary human pMSCs	EGM containing: M199 medium, 20% FBS, 20% EGM-2 and additional 50 ng/mL VEGF	Parallel plate flow chamber with 6 or 12 dyn/cm^2 (0.6 or 1.2 Pa) or static conditions	· 3 days under static conditions followed by 24 hours of shear stress	Alignment in the direction of flow *In EGM with 12 dyn/cm^2*	↑VWF ↑CD31 *In EGM with 12 dyn/cm^2 (IF and WB)*	↑VWF ↑PECAM1 (CD31) *In EGM with 6 dyn/cm^2, but further with 12 dyn/cm^2* ↑FLT1 ↑KDR *Even in static conditions with EGM for 24 hours.*	· Uptake of acLDL · Endothelial tubes *In EGM with 12 dyn/cm^2*

Reference	Cell Type	Differentiation Medium	Shear Stress	Timepoints	Morphology	Protein Expression	PCRs	Functional Assays
Yuan (2013) [667]	Human BMSCs	N/A	Parallel flow chamber with 0.2 or 2 Pa shear stress.	· Shear stress for 2 days, then static culture for 5 days.	N/A	↑VWF ↑CD31 ↑CDH5 (VE-Cadherin) *After 2 Pa shear stress (Immuno-cytochemistry and Western blot)* ↑VEGF secretion *After 2 Pa shear stress with subsequent static culture for 1, 3 and 5 days (ELISA)*	N/A	N/A
Zhang (2009)[668]	Primary human amniotic fluid MSCs	EGM-2 (Clonetics)	Orbital shaker at 12 dyn/cm^2 (1.2 Pa – 210 cycles/min)	· Static experiments: EGM-2 for 3 weeks · Shear stress experiments: EGM-2 for 2 weeks then shear stress for 48 hours · Medium refreshed every 3 days	Endothelial-like morphology *In static with EGM-2* Alignment in the direction of flow *In EGM-2 with 12 dyn/cm^2*	↑CD31 (18.1%) ↑VWF (24.7%) *In static with EGM-2 after 3 weeks and further increased with shear stress. (Flow cytometry)*	↑VWF ↑PECAM1 (CD31) *In static with EGM-2 after 3 weeks and further increased with 12 dyne/cm^2.*	· Uptake of acLDL *In 2 weeks static with EGM-2. Not assessed with shear stress.* · Endothelial tubes *In 2 weeks static with EGM-2. With 12 dyn/cm^2 tubes formed earlier and had greater tube length.* · eNOS expression *In EGM-2 after 2 weeks of static culture with 50 ng/mL additional VEGF.*

6.2 Hypothesis

Primary pMSCs can be differentiated into cells of the endothelial lineage using endothelial growth factors and/or shear stress conditions.

6.3 Aims

To develop a model of placental vascular development through differentiation of primary pMSCs into cells of endothelial lineage under:

1. Static conditions using growth factors;
2. Low flow/shear stress conditions in microfluidic devices in addition to growth factors.

6.4 Results

6.4.1 Isolation of primary human placental mesenchymal stromal cells (pMSCs)

Primary human pMSCs were isolated using an adapted version of a previously published protocol by Pelekanos *et al.* (2016)[360], developed by Margeurite Kennedy[359]. Within the first few days of seeding into tissue culture flasks, unattached red blood cells and other cellular debris could be observed. By day 10, following several medium refreshments, attached MSC-like cells could be identified. After 15 days of culture, colonies of MSC-like cells had formed in the tissue culture flask, which displayed a spindle-shaped morphology, characteristic of MSCs[360]. Other, smaller, rounder cells were observed in the flasks, which are likely contaminating hematopoietic, trophoblastic, or ECs[360,669]. Once colonies of MSC-like cells were covering 70-80% of the flasks, the MSCs were sub-cultured to passage 1 (P1) and continued to exhibit a spindle-shaped morphology. Less contaminating, non-spindle-shaped cells were observed following subsequent passaging (Figure 6.1).

6.4.1.1 Characterisation of surface marker proteins in pMSCs

The international society of cellular therapy (ISCT) states that MSCs must express cell surface markers CD90, CD73 and CD105, and be negative for CD45, CD34, CD14 or CD11b, CD79α or CD19 and HLA-DR surface molecules[670]. Flow cytometry characterisation of the isolated pMSCs used in the current study was previously carried out by Marguerite Kennedy[359]. This showed that pMSCs expressed high levels of the MSC markers CD90 and CD73 (positive staining in 98.89±0.85% and 98.81±0.38% of

cells, respectively) and expression of CD105 (positive staining in 11.87±10.14% of cells), all of which were a similar level to the BMSC positive control. The flow cytometry characterisation kit also included a negative marker cocktail, which probed for CD45, CD34, CD11b, CD79A and HLA-DR. Positive staining for negative markers were present in 18.68±2.84% of pMSCs, which was lower than BMSCs (54.51±5.94%). The EC marker CD31 was also assessed which was exclusively present in the HUVEC control (99.67±0.45%), with negligible expression in pMSCs and BMSCs.

To further confirm that the primary pMSCs expressed markers characteristic of MSCs, immunocytochemistry was performed. Positive markers included: CD105, CD73 and CD44, as well as negative markers: CD34 (a haematopoietic cell marker), CD14 (a macrophage marker) and CD19 (a lymphocyte marker). pMSCs were positive for CD44, CD105 and CD73. Some expression of the haematopoietic marker, CD34 was observed, however no positive staining for CD14 and CD19 was detected (Figure 6.2).

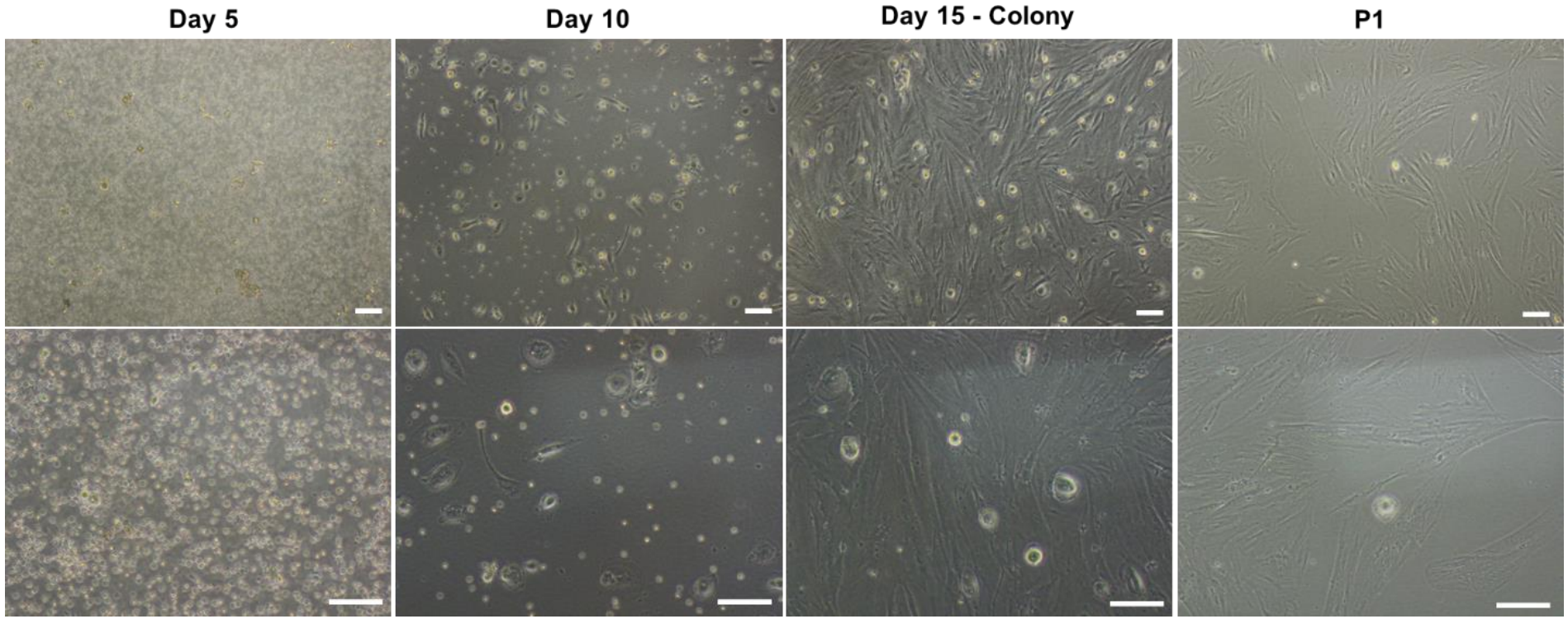

Figure 6.1 - Placental mesenchymal stromal cells (pMSCs) throughout the isolation and culture period. Primary human pMSCs were isolated from placental tissue of healthy pregnancies. Images were taken at 4x (top panel) and 10x (lower panel) magnification, using the Olympus fluorescent microscope with Cell F software. Scale bars = 100 µm. Red blood cells (RBCs) and cellular debris can be observed at day 5. At day 10 MSC-like cells are present, which have formed into colonies by day 15. At passage 1 (P1) spindle shaped MSCs can clearly be observed.

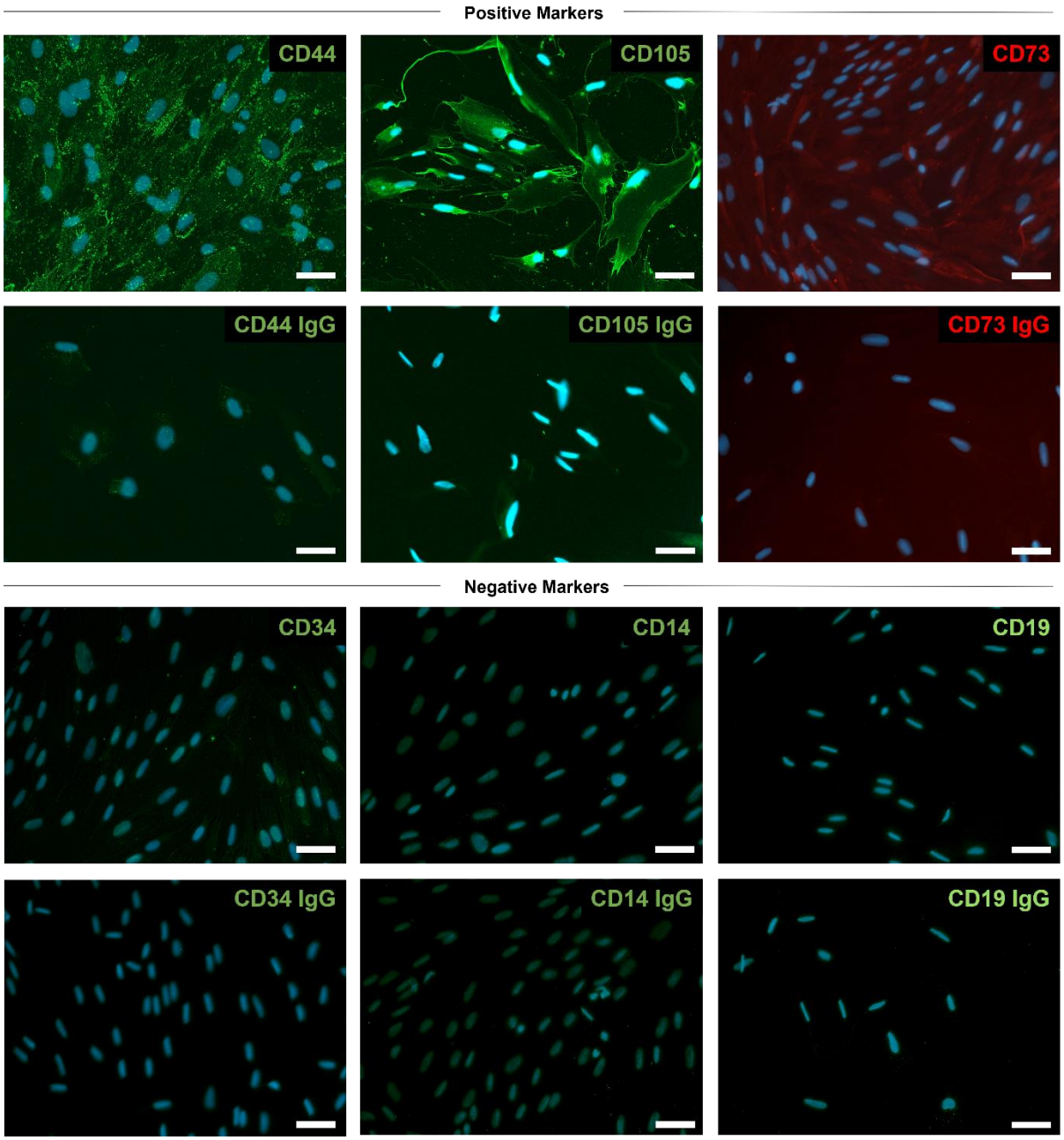

Figure 6.2 - Characterisation of pMSCs by immunocytochemistry. MSCs were isolated from term human placental tissue from uncomplicated pregnancies. Immunocytochemistry was performed on cells at P3-P5 (n=3) using antibodies specific for positive MSC markers, CD44, CD105 and CD73 and negative MSC markers, CD34, CD19 and CD14, followed by mounting in media containing DAPI (blue). Bottom panels show cells incubated with control IgGs for the same species and concentration as the primary antibodies used in the top panel. Images were taken at 20x magnification using the Zeiss Axioscan.A1 microscope. Scale bars = 50 µm.

6.4.2 Differentiation of pMSCs into cells of the endothelial lineage under static conditions

The ability of pMSCs to differentiate into cells of the endothelial lineage was assessed by culturing pMSCs in either control medium or differentiation medium, for up to 25 days (n=7).

6.4.2.1 Morphological changes

Cells were imaged throughout culture to assess morphological differences (n=7). By day 4, pMSCs cultured in differentiation medium had lost their characteristic whirlpool morphology[360] and had a more disorganised pattern. By day 11, clusters of smaller EC-like cells[650] were observed in cells treated with differentiation medium. Cells were imaged before passaging on day 7 and 14 and hence are at a higher confluence, therefore morphological differences were more difficult to distinguish at these timepoints (Figure 6.3).

6.4.2.2 Determining appropriate endothelial and mesenchymal markers

To characterise the phenotype of pMSCs following differentiation, appropriate markers of MSCs and ECs needed to be identified in the literature (Table 6.3). VEGFR1 and VEGFR2 (*FLT1* and *KDR*, respectively) were selected based on their specific expression in ECs[80] and their role in early placental development[85,87,671,672]. CD31 (*PECAM1*) and VWF were also specifically expressed in ECs, and were selected as mature endothelial markers[444,673,674]. Given that most MSC markers also had reported expression in ECs[675–679], CD90 (*THY1;* Thymocyte differentiation antigen 1), CD73 (*NT5E*; Ecto-5′-nucleotidase) and CD44 (also known as Homing cell adhesion molecule, HCAM1) were selected.

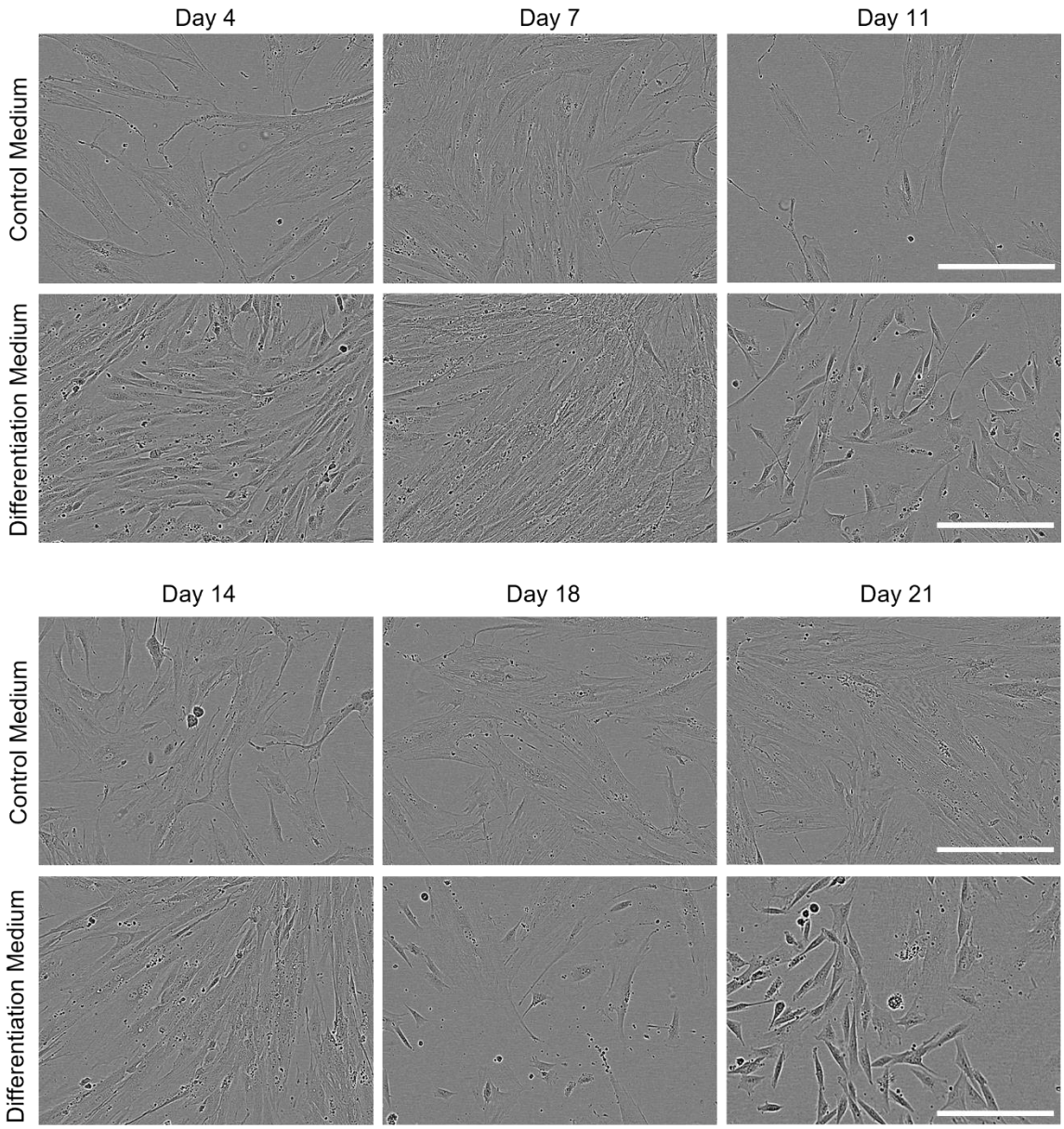

Figure 6.3 - Morphological differences in pMSCs cultured in control or differentiation medium for 25 days. Primary human pMSCs were isolated from placental tissue of healthy pregnancies. At P3 pMSCs were cultured in either control (pMSC medium) or differentiation medium (EGM-2 + VEGF-A) for up to 25 days to induce differentiation towards the endothelial lineage. Cells were imaged at days 4, 7, 11, 14, 18 and 21. Morphological differences can be observed in pMSCs cultured in differentiation medium, where they have lost their whirlpool, spindle-like morphology, and clusters of smaller cells are present. Representative images (n=7). Images were taken on the Incucyte ZOOM at 10x magnification. Scale bars = 300 µm.

Table 6.3 – Widely used MSC and EC markers, their function and reported expression in MSCs and ECs reported in the literature. Abbreviations: ECs – endothelial cells; MSCs – mesenchymal stem cells; VSCs – vascular stem cells.

Marker	Full Name	Description/Function	MSCs	ECs
CD105	Endoglin	Expressed on MSCs and vascular ECs. Type I membrane glycoprotein, which is an accessory receptor for TGF-β ligands. Involved in angiogenesis, neovascularisation and smooth muscle differentiation[673,680].	✓[681,682]	✓[683 684]
CD106 V-CAM1	Vascular cell adhesion molecule 1	Adhesion molecule that mediates the adhesion of immune cells to the vascular endothelium during inflammation[673].	✓[681]	✓(activated ECs[685])
CD144 VE-Cadherin CDH5	Vascular endothelial cadherin	Endothelial cell-cell adherens junctional marker, stabilises vessels and regulates vascular permeability and leukocyte extravasation[673].		✓[686]
CD146 MCAM	Melanoma cell adhesion molecule	Adhesion molecule expressed by pericytes, ECs and smooth muscle cells[687,688]. Regulates vascular permeability, angiogenesis and leukocyte transmigration[688].	✓[681,689]	✓[690]
CD31 PECAM1	Platelet endothelial cell adhesion molecule	Adhesion molecule found at endothelial junctions. In addition to ECs, CD31 is also expressed in platelets, granulocytes, macrophages, dendritic cells (DCs), T- and B-cells and natural killer (NK) cells[691].		✓[444]
CD34	Haematopoietic Progenitor Cell Antigen	Transmembrane phosphoglycoprotein, found in haematopoietic and vascular progenitors, as well as adipose derived MSCs[680,692–694].	✓(in some MSCs and VSCs[680,692])	✓[695]
CD44 HCAM1	Homing cell adhesion molecule	An adhesion molecule which interacts with multiple ligands, such as selectins, collagen, and fibronectin. CD44 is also known to play roles in maintaining a functional vascular barrier and modulating angiogenesis[696].	✓[682] ([681] - in culture)	✓[675,676]
CD73 NT5E	Ecto-5′-nucleotidase	Expressed on MSCs, lymphocytes, ECs, smooth muscle cells, epithelial cells, and fibroblasts. Converts extracellular adenosine monophosphate to adenosine[680].	✓[680,681]	✓[679]
CD90 Thy-1	Thymocyte differentiation antigen 1	Expressed on MSCs, vascular and lymphatic ECs, fibroblasts, and neurons. A glycosylphosphatidylinositol-linked protein involved in cell-cell and cell-matrix interactions[680].	✓[682]	✓[677,678]

Marker	Full Name	Description/Function	MSCs	ECs
VEGFR1 FLT1	Vascular Endothelial Growth Factor Receptor 1/Fms related receptor tyrosine kinase	Expressed on ECs, as well as human peripheral blood monocytes[697]. Important for the organisation of embryonic vasculature[85,672] and is involved in cell survival, vascular permeability and cell migration[698]		✓[80]
VEGFR2 KDR	Vascular Endothelial Growth Factor Receptor 2/Kinase Insert Domain Receptor	Expressed primarily on vascular ECs and endothelial progenitors[673]. Receptor for VEGF, involved in vascular development[87,671].		✓[80]
VWF	Von Willebrand factor	Glycoprotein participating in blood coagulation, released from Weibel-Palade bodies of ECs[673].		✓[673,674]

6.4.2.3 Endothelial and mesenchymal gene expression

6.4.2.3.1 Housekeeping gene expression

To assess the expression levels of MSC and EC genes, housekeeping genes that did not differ between the culture conditions needed to be first identified, for normalisation purposes. Expression levels of widely used housekeeping genes[378,699], *18S, ACTB, B2M* (β2 microglobulin)*, GUSB* (β-glucuronidase), *RPL13A* (60S ribosomal protein L13a) and *YWHAZ* were assessed in pMSCs cultured in control or differentiation medium at 11, 18 and 25 days (Figure 6.4). Expression of *ACTB* was significantly different between the control medium and differentiation medium at both 18 and 25 days ($p<0.001$ and $p<0.01$, respectively), which may indicate changes to the cytoskeleton during differentiation[700,701]. Trends towards altered levels of *B2M* and *18S* over the time course of differentiation were also observed. *YWHAZ*, which was identified as the most stable housekeeping gene using RefFinder (Section 2.6.3) appeared to be the most similar between control and differentiation medium at each timepoint and was used for further normalisation of target genes.

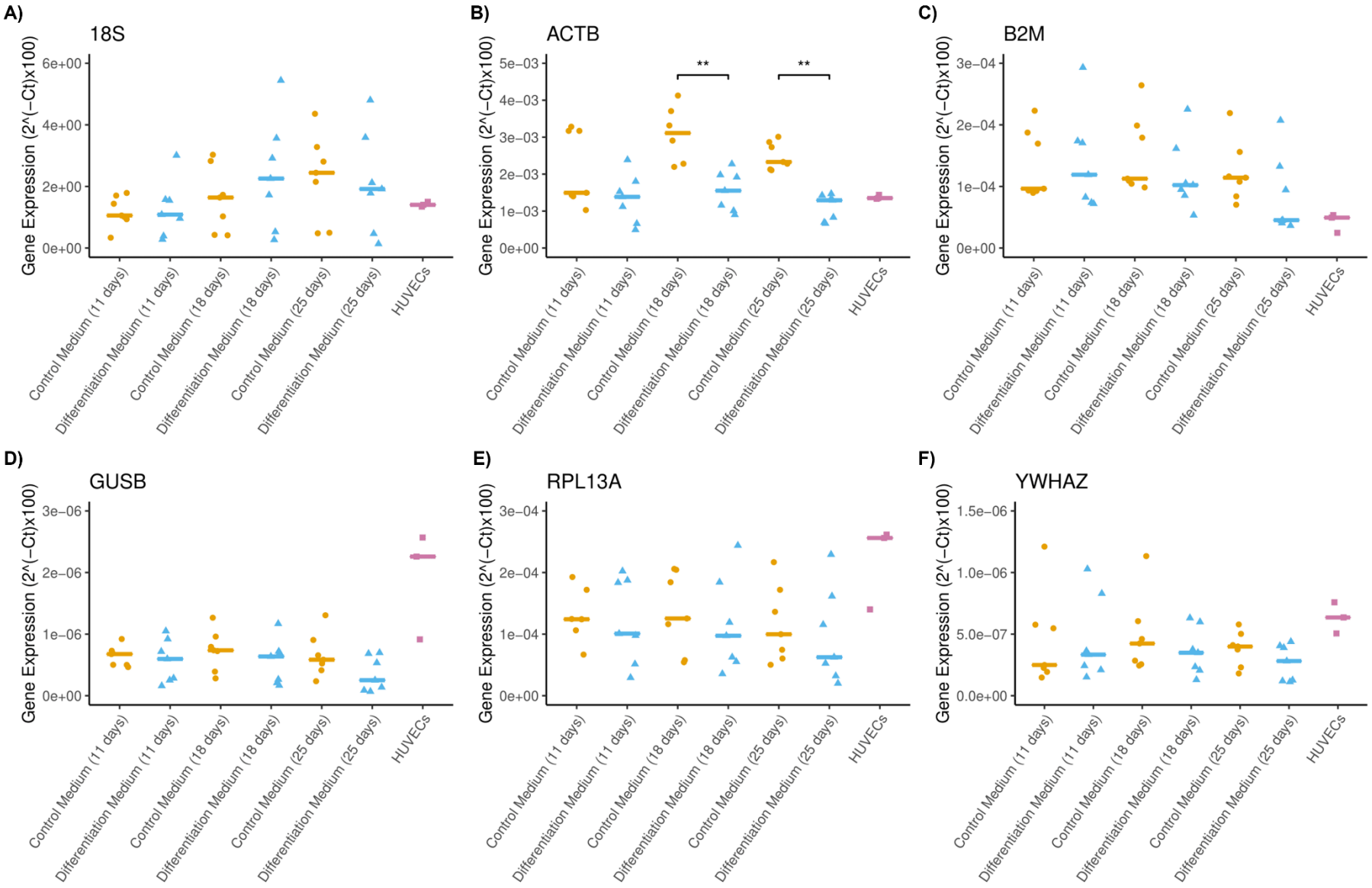
A)
18S
B)
ACTB
C)
B2M
D)
GUSB
E)
RPL13A
F)
YWHAZ
Gene Expression (2^(−Ct)x100)
**
**
Control Medium (11 days)
Differentiation Medium (11 days)
Control Medium (18 days)
Differentiation Medium (18 days)
Control Medium (25 days)
Differentiation Medium (25 days)
HUVECs

Figure 6.4 - Housekeeping gene expression in pMSCs cultured in control or differentiation medium for up to 25 days.
Housekeeping genes were assessed in pMSCs cultured in control or differentiation medium at 11, 18 and 25 days, using RT-qPCR. HUVECs were used as a positive control for endothelial markers. Data is presented as the median and statistical analysis was performed using a Kruskal-Wallis with a Dunn's post-hoc test (as the data was not normally distributed). Significances between pMSCs cultured in control medium and differentiation medium at each time point are shown, ** $p<0.01$. Individual points represent each patient placenta. n=7. HUVECs (n=3) were used as a positive control for endothelial genes.

6.4.2.3.2 Expression of endothelial and mesenchymal genes

Expression of MSC markers, *NT5E* and *THY1* were not significantly altered between pMSCs treated with control or differentiation medium at each timepoint. However, a small decrease in *NT5E* was observed at day 11 (0.23±0.031 vs 0.36±0.075; p=0.408, n=7). Interestingly, the MSC marker *CD44* was significantly increased in pMSCs treated with differentiation medium at 18 days (270.60 [81.57-539.32] vs 111.82 [32.90-196.72]; p<0.05, n=7) and 25 days (326.29 [163.14-724.08] vs 152.74 [50.38-405.91]; p<0.05, n=7) (Figure 6.5).

Expression of EC markers, *KDR* and *PECAM1*, were increased in pMSCs treated with differentiation medium at 11 days (p<0.05, n=7), which were comparable to levels detected in HUVECs, the mature EC cell line. The EC marker *FLT1* was also significantly increased in pMSCs treated with differentiation medium at all timepoints (2.74 [2.15-6.70] vs 0.47 [0.074-0.64] at 11 days, 3.53 [0.66-6.12] vs 0.57 [0.072-0.65] at 18 days, 1.78 [0.63-4.76] vs 0.56 [0.064-1.06] at 25 days; p<0.001-0.05, n=7). There were no differences in the mature EC marker, *VWF,* between pMSCs cultured in control and differentiation medium, and levels in pMSCs cultured in differentiation medium were significantly lower than in HUVECs (p<0.001-0.05, n=3-7) (Figure 6.6).

To confirm the significant increases in EC gene expression observed after 11 days culture in differentiation medium, and to further explore the mechanisms of pMSC to endothelial lineage differentiation, a larger panel of MSC and EC genes were assessed at this time point using a qPCR array (n=4). Of the 84 genes assessed, 17 were significantly altered in pMSCs cultured in differentiation compared to control medium (p<0.05, expression variation [EV] >2 and <-2). In line with the RT-qPCR data, an increase in VEGF receptor genes, *FLT1* (EV=14.63, p=0.0065) and *KDR* (EV=3.77, p=0.047) were observed in pMSCs cultured in differentiation medium. A reduction in several other MSC genes was observed, including *VTN* (Vitronectin; EV=-2.32, p=0.039), *TAGLN* (Transgelin; EV=-2.94, p=0.0019), *CDH2* (Cadherin 2; EV=-16.13, p=0.0011) and *CCN1* (Calponin; EV=-11.26, p=0.00001), suggesting that culture in endothelial differentiation medium leads to a reduction in the mesenchymal phenotype. Genes that are known to regulate endothelial/epithelial-mesenchymal transition were also altered (*MMP2, MMP9, PIK3R1, BMP2* and *WNT11*), which likely also regulate mesenchymal to endothelial differentiation, and hence may contribute to the mechanism of pMSC to endothelial lineage differentiation. The most upregulated gene in pMSCs treated with differentiation medium was *HGF* (Hepatocyte Growth Factor; EV=28.12, p=0.00102), which is known to stimulate branching and tubule formation in ECs[702] (Figure 6.7).

The gene expression variation and p value's for all genes assessed in the qPCR array are reported in **Appendix 7.**

6.4.2.4 Endothelial protein expression

To confirm that changes in EC markers were also apparent at the protein level, immunocytochemistry was performed. VEGFR1 (*FLT1*) and CD34 expression were observed in pMSCs cultured in control medium and differentiation medium, as well as in HUVECs (Figure 6.8A; Figure 6.9A). The fluorescence intensity of VEGFR1 was significantly increased at day 25 in pMSCs cultured in differentiation medium (19.34 [13.56-31.07], n=5), compared to control medium (13.52 [11.17-15.91]; n=6, $p<0.01$) (Figure 6.8C). While CD34 was not significantly altered, fluorescence intensity decreased with time in culture (Figure 6.9C). Although expressed in the HUVEC positive control, minimal expression of VEGFR2 (*KDR*) and no expression of the mature EC markers CD31 (*PECAM1*) and vWF were detected in pMSCs, and therefore were not quantified (Figure 6.8A; Figure 6.9A; Figure 6.10A).

As differences in intensity of EC marker proteins were minimal, flow cytometry was performed to determine the percentage of pMSCs expressing endothelial marker proteins following treatment with control or differentiation medium, albeit slightly different time points and low sample numbers. Levels of VEGFR1 (*FLT1*), VEGFR2 (*KDR*) and CD31 (*PECAM1*) were assessed. Trends towards increases in VEGFR1 was observed in differentiation medium (p=0.68-1, n=3) and VEGFR2 was increased with differentiation medium at 14 days (12.76 [7.83-13.20] % vs 1.41 [0.84-1.95] %; $p<0.05$, n=3) (Figure 6.11). The immunocytochemistry and flow cytometry data suggest that longer time in culture is needed for protein levels to reflect changes in gene expression.

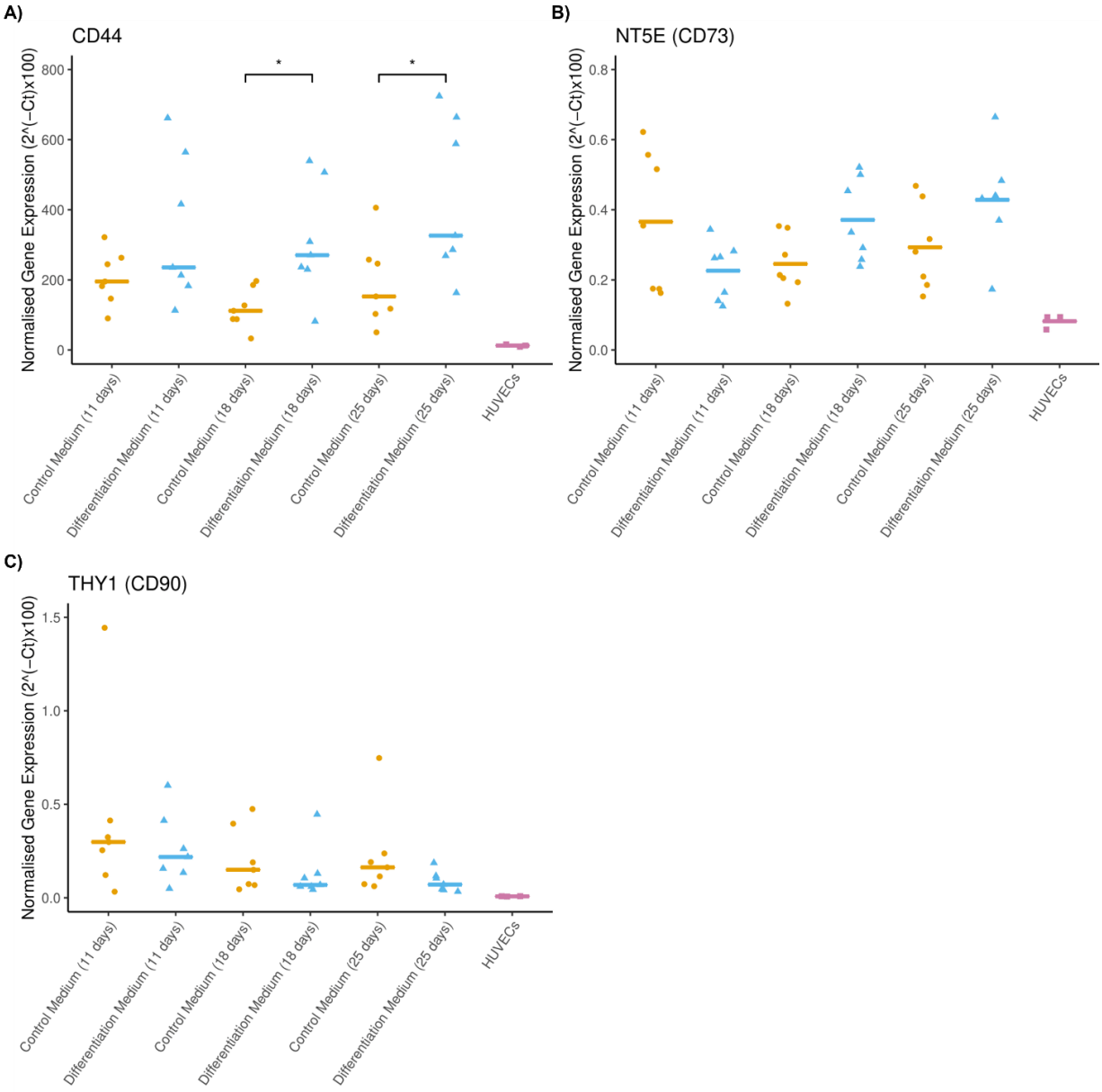

Figure 6.5 - Mesenchymal gene expression in pMSCs cultured in control or differentiation medium for up to 25 days. Mesenchymal genes were assessed in pMSCs cultured in control or differentiation medium at 11, 18 and 25 days, using RT-qPCR. The expression of target genes was normalised to a geometric average of *YWHAZ* housekeeping gene expression. *THY1* is presented as the mean, and statistical analysis was performed using a one-way ANOVA with Tukey's post-hoc test. *NT5E* (CD73) and *CD44* are presented as the median, and statistical analysis was performed using a Kruskal-Wallis with a Dunn's post-hoc test (Based on normal distribution of the data). Individual points represent each patient placenta. n=7. HUVECs (n=3) were used as a positive control for endothelial markers. Significances between pMSCs cultured in control medium and differentiation medium at each time point are shown. * $p<0.05$.

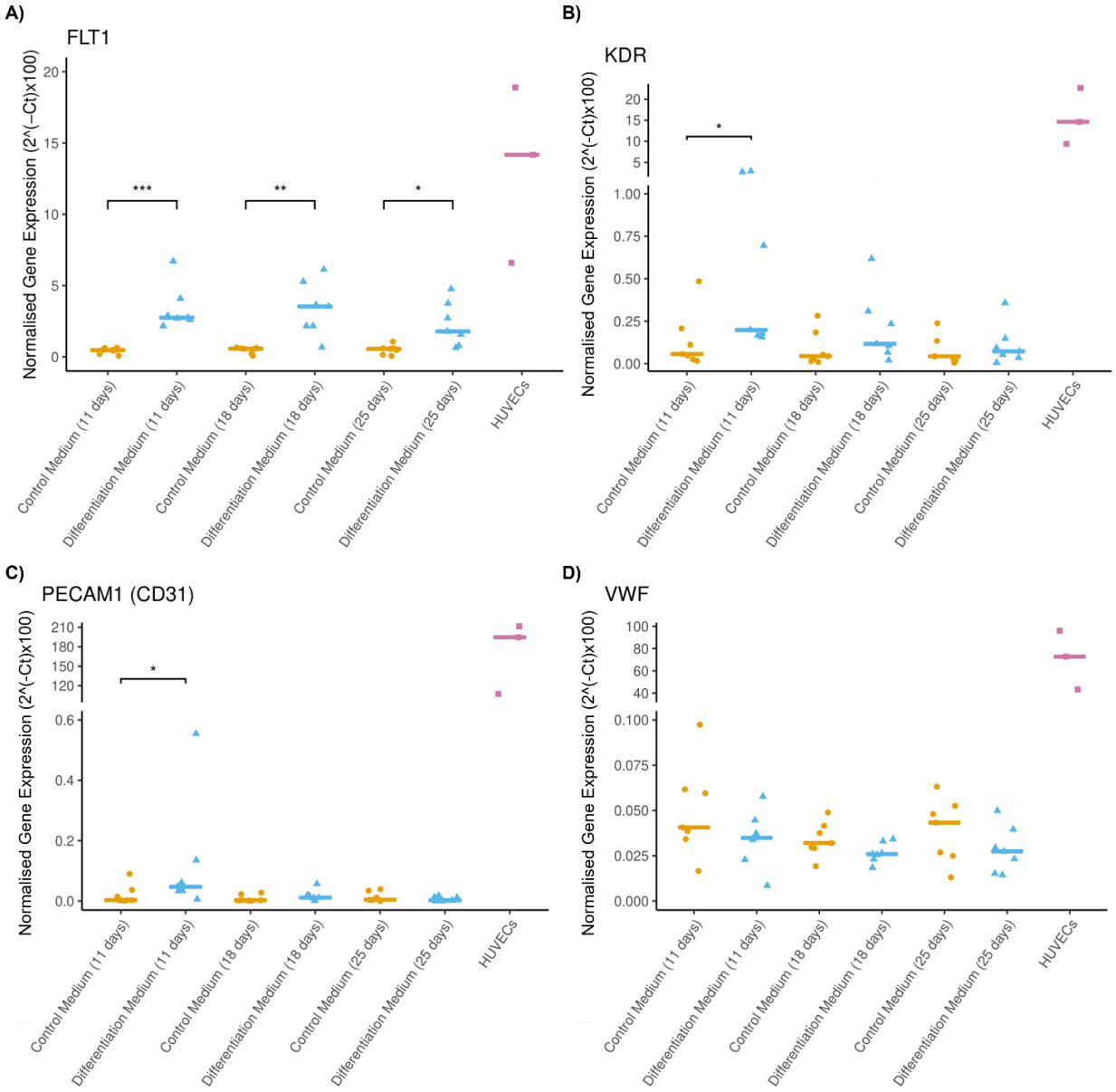

Figure 6.6 - Endothelial gene expression in pMSCs cultured in control or differentiation medium for up to 25 days. Endothelial genes were assessed in pMSCs cultured in control or differentiation medium at 11, 18 and 25 days, using RT-qPCR. HUVECs were used as a positive control for endothelial markers. The expression of target genes was normalised to *YWHAZ* housekeeping gene expression. Data are presented as the median, and statistical analysis was performed using a Kruskal-Wallis with a Dunn's post-hoc test (as data was not normally distributed). Individual points represent each patient placenta. n=7. HUVECs (n=3) were used as a positive control. Significances between pMSCs cultured in control medium and differentiation medium at each time point are shown. * p<0.05, ** p<0.01, ***p<0.001.

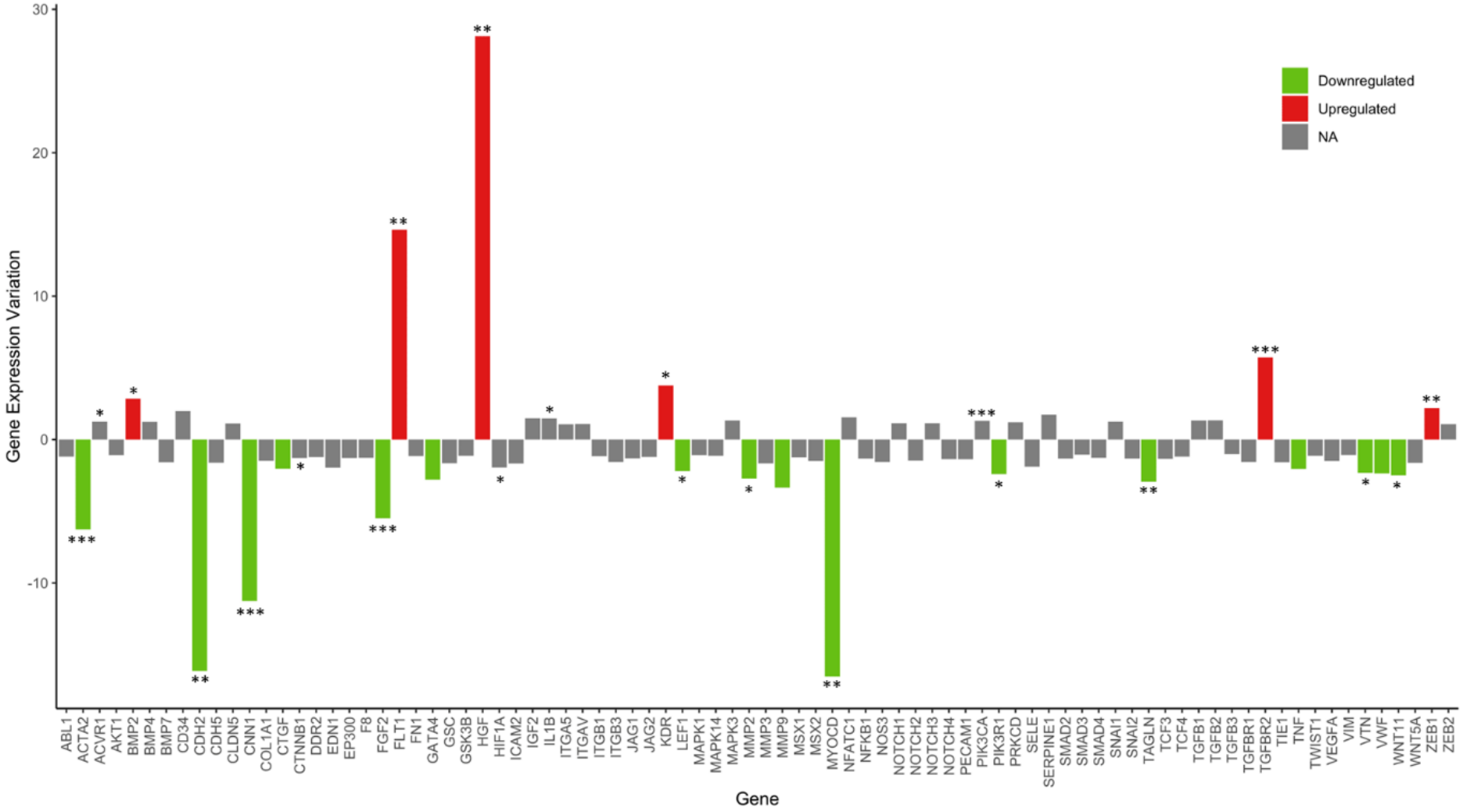
Gene Expression Variation
30
20
10
0
-10
Downregulated
Upregulated
NA
ABL1
ACTA2
ACVR1
AKT1
BMP2
BMP4
BMP7
CD34
CDH2
CDH5
CLDN5
CNN1
COL1A1
CTGF
CTNNB1
DDR2
EDN1
EP300
F8
FGF2
FLT1
FN1
GATA4
GSC
GSK3B
HGF
HIF1A
ICAM2
IGF2
IL1B
ITGA5
ITGAV
ITGB1
ITGB3
JAG1
JAG2
KDR
LEF1
MAPK1
MAPK14
MAPK3
MMP2
MMP3
MMP9
MSX1
MSX2
MYOCD
NFATC1
NFKB1
NOS3
NOTCH1
NOTCH2
NOTCH3
NOTCH4
PECAM1
PIK3CA
PIK3R1
PRKCD
SELE
SERPINE1
SMAD2
SMAD3
SMAD4
SNAI1
SNAI2
TAGLN
TCF3
TCF4
TGFB1
TGFB2
TGFB3
TGFBR1
TGFBR2
TIE1
TNF
TWIST1
VEGFA
VIM
VTN
VWF
WNT11
WNT5A
ZEB1
ZEB2
Gene

Figure 6.7 - Expression of a larger panel of endothelial and mesenchymal genes in pMSCs cultured in control medium or differentiation medium for 11 days. The cycle threshold (Ct) values were inputted into an analysis spreadsheet provided by AnyGenes and carried out according to manufacturer's instructions. The Student's T-Test was used to determine statistical significance ($p<0.05$ considered statistically significant). A positive or negative gene expression variation was used to determine whether a gene was up- or down-regulated, respectively in pMSCs cultured in differentiation medium compared to control medium. **Red** bars indicate genes that are upregulated in pMSCs cultured in differentiation medium (gene expression variation > 2) and **green** bars indicate genes that are downregulated in pMSCs cultured in differentiation medium (gene expression variation < -2). * $p<0.05$, ** $p<0.01$, *** $p<0.001$.

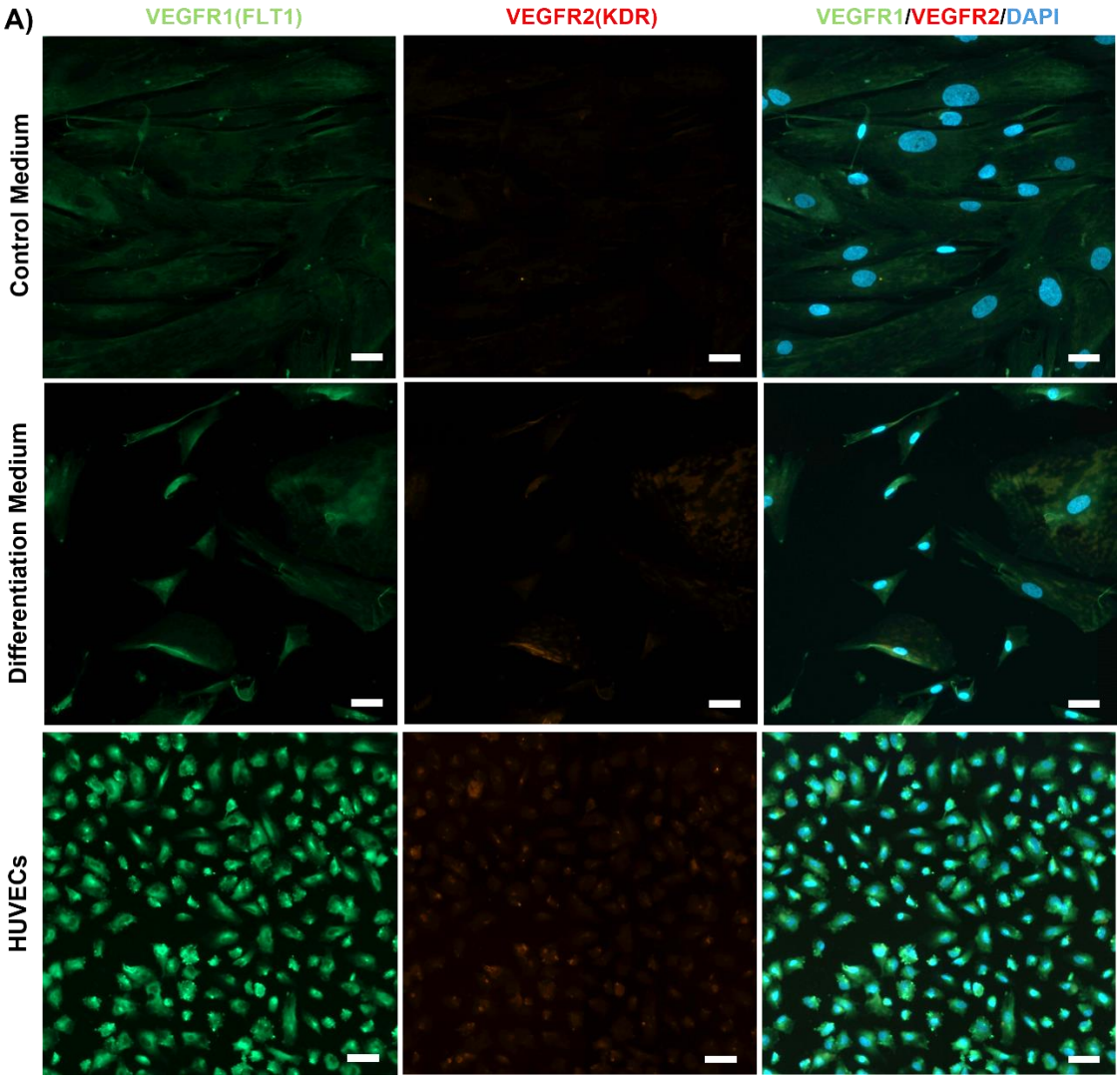
A)
VEGFR1(FLT1)
VEGFR2(KDR)
VEGFR1/VEGFR2/DAPI
Control Medium
Differentiation Medium
HUVECs

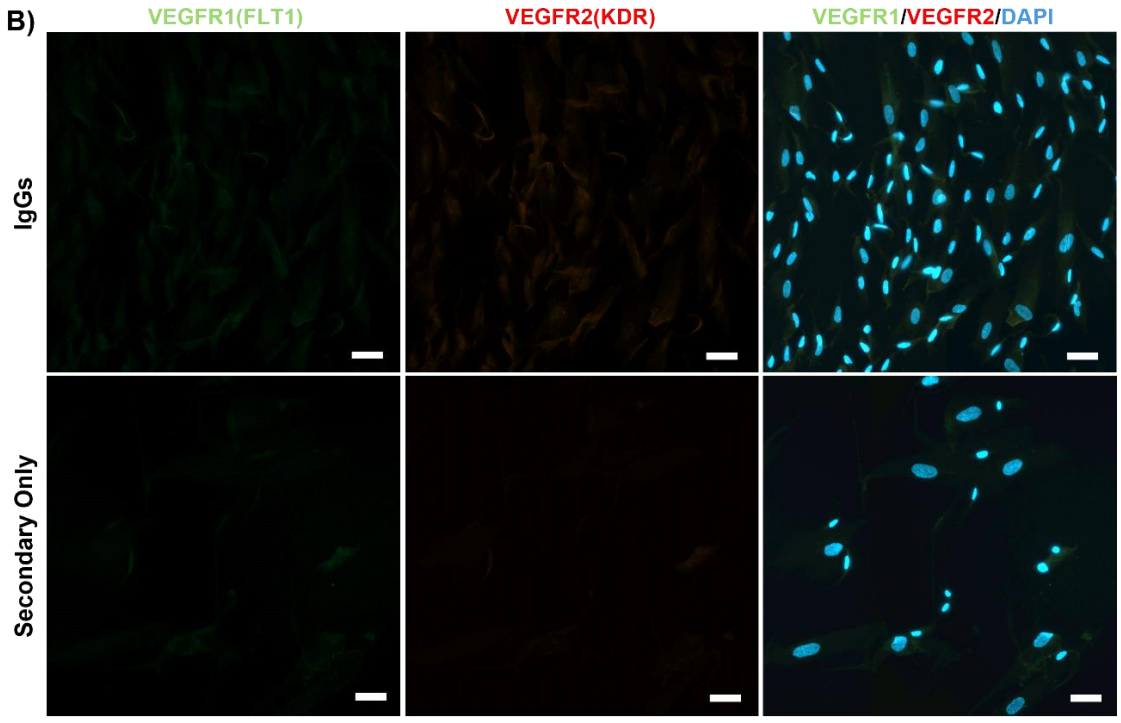
B)
VEGFR1(FLT1)
VEGFR2(KDR)
VEGFR1/VEGFR2/DAPI
IgGs
Secondary Only

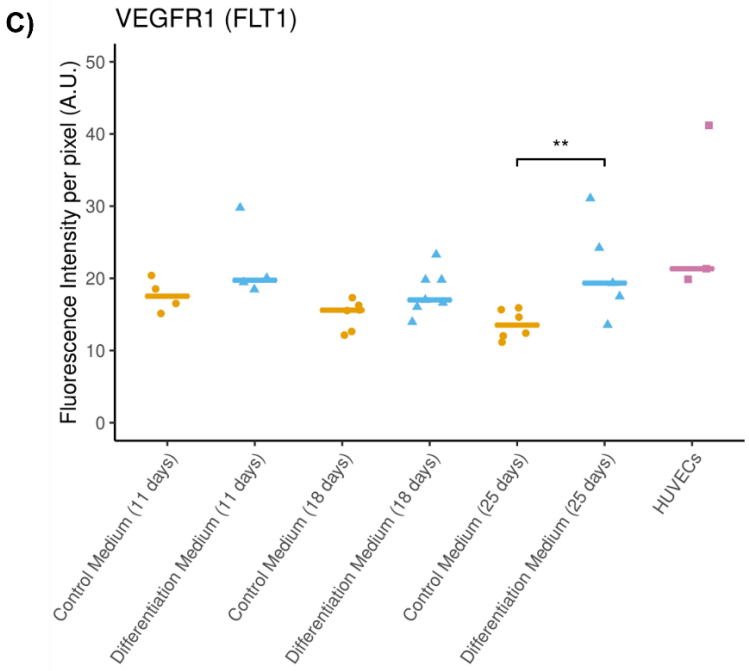

Figure 6.8 - Protein expression of VEGFR1 (FLT1) and VEGFR2 (KDR) in pMSCs cultured in control or differentiation medium for up to 25 days, measured by immunocytochemistry. VEGFRs were assessed in pMSCs cultured in control or differentiation medium at 11, 18 and 25 days, followed by mounting in media containing DAPI (blue). A) Representative images VEGFR1 and VEGFR2 in pMSCs cultured in control or differentiation medium at 25 days. Images were taken with the Zeiss Axio Scan Z1 Slide Scanner. B) IgG controls for the same species and concentration of the primary antibodies and secondary antibody only control. Scale bars = 50 µm. Images were taken with the Zeiss Axio Scan Z1 Slide Scanner. C) Cells were detected using QuPath and fluorescence intensity was quantified per pixel of detected cells (to account for different numbers and sizes of cells). An average fluorescence intensity was taken from four ROIs on each coverslip. Data are presented as the median, and statistical analysis was performed using a Kruskal-Wallis with a Dunn's post-hoc test (as the data was not normally distributed). Individual points represent each patient placenta. n=4-7. HUVECs (n=3) were used as a positive control. Significances between pMSCs cultured in control medium and differentiation medium at each time point are shown. ** $p<0.01$.

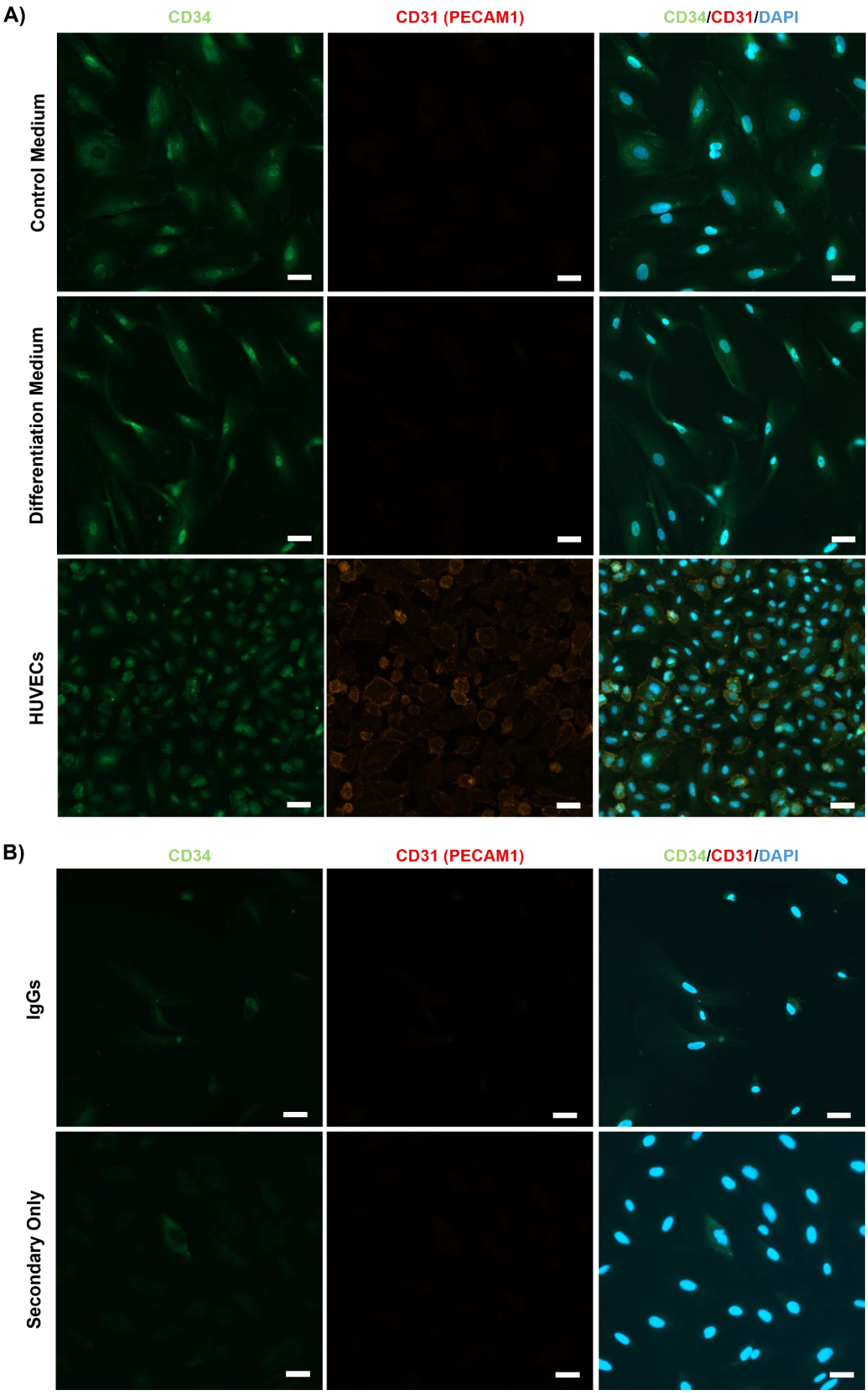
A)
CD34
CD31 (PECAM1)
CD34/CD31/DAPI
Control Medium
Differentiation Medium
HUVECs
B)
CD34
CD31 (PECAM1)
CD34/CD31/DAPI
IgGs
Secondary Only

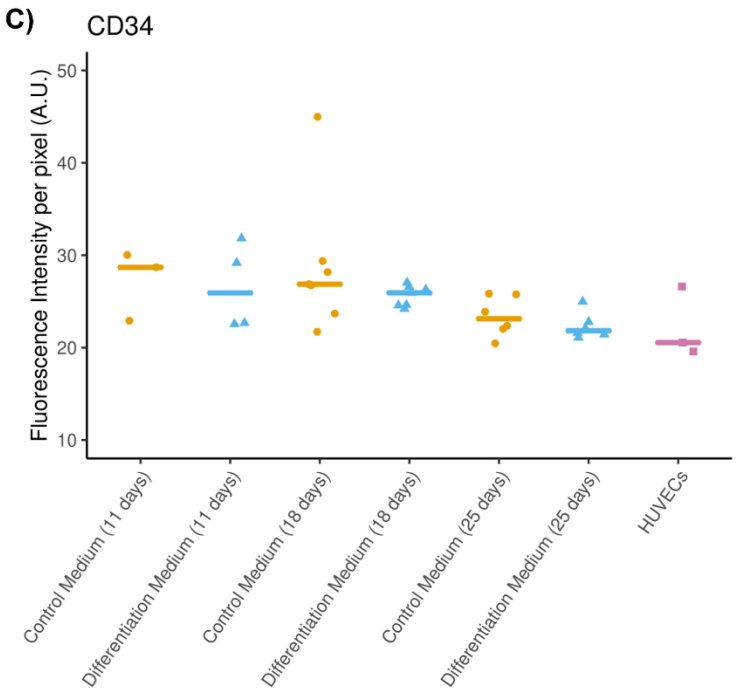

Figure 6.9 - Protein expression of CD34 and CD31 (PECAM1) in pMSCs cultured in control or differentiation medium for up to 25 days, measured by immunocytochemistry. CD34 and CD31 were assessed in pMSCs cultured in control or differentiation medium at 11, 18 and 25 days, followed by mounting in media containing DAPI (blue). A) Representative images CD34 and CD31 in pMSCs cultured in control or differentiation medium at 25 days. HUVECs were used as a positive control. B) IgG controls for the same species and concentration of the primary antibodies and secondary antibody only control. Scale bars = 50 µm. Images were taken with the Zeiss Axio Scan Z1 Slide Scanner. C) Cells were detected using QuPath and fluorescence intensity was quantified per pixel of detected cells (to account for different numbers and sizes of cells). An average fluorescence intensity was taken from four ROIs on each coverslip. Data are presented as the median, and statistical analysis was performed using a Kruskal-Wallis with a Dunn's post-hoc test (as the data was not normally distributed). Individual points represent each patient placenta. n=3-7 . HUVECs (n=3) were used as a positive control.

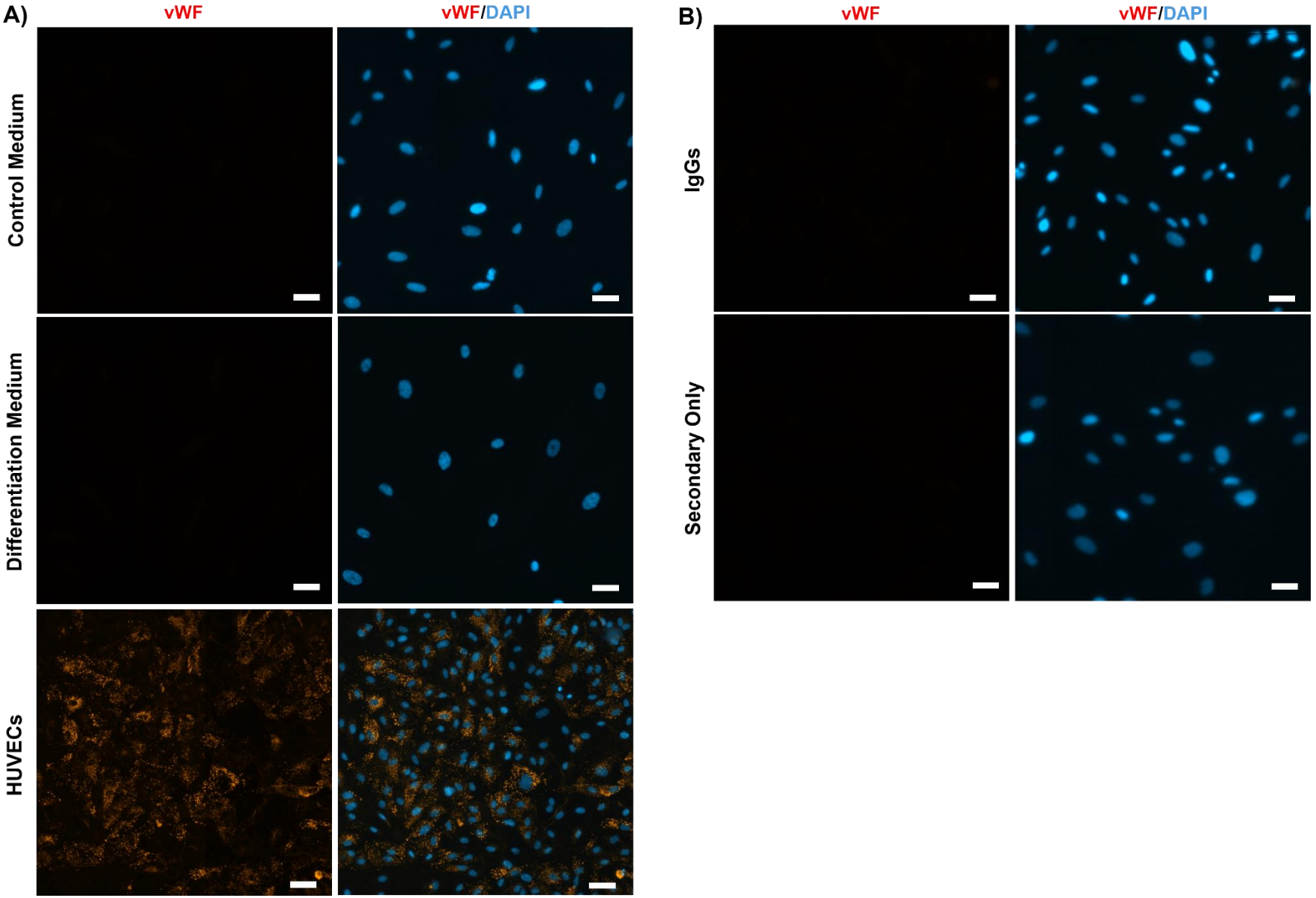
A)
vWF
vWF/DAPI
Control Medium
Differentiation Medium
HUVECs
B)
vWF
vWF/DAPI
IgGs
Secondary Only

Figure 6.10 - Protein expression of vWF in pMSCs cultured in control or differentiation medium for up to 25 days, measured by immunocytochemistry. vWF was assessed in pMSCs cultured in control or differentiation medium at 11, 18 and 25 days, followed by mounting in media containing DAPI (blue). A) Representative images vWF in pMSCs cultured in control or differentiation medium at 25 days n=3-4. HUVECs (n=3) were used as a positive control. B) IgG controls for the same species and concentration of the primary antibody and secondary antibody only control. Scale bars = 50 µm. Images were taken with the Zeiss Axio Scan Z1 Slide Scanner.

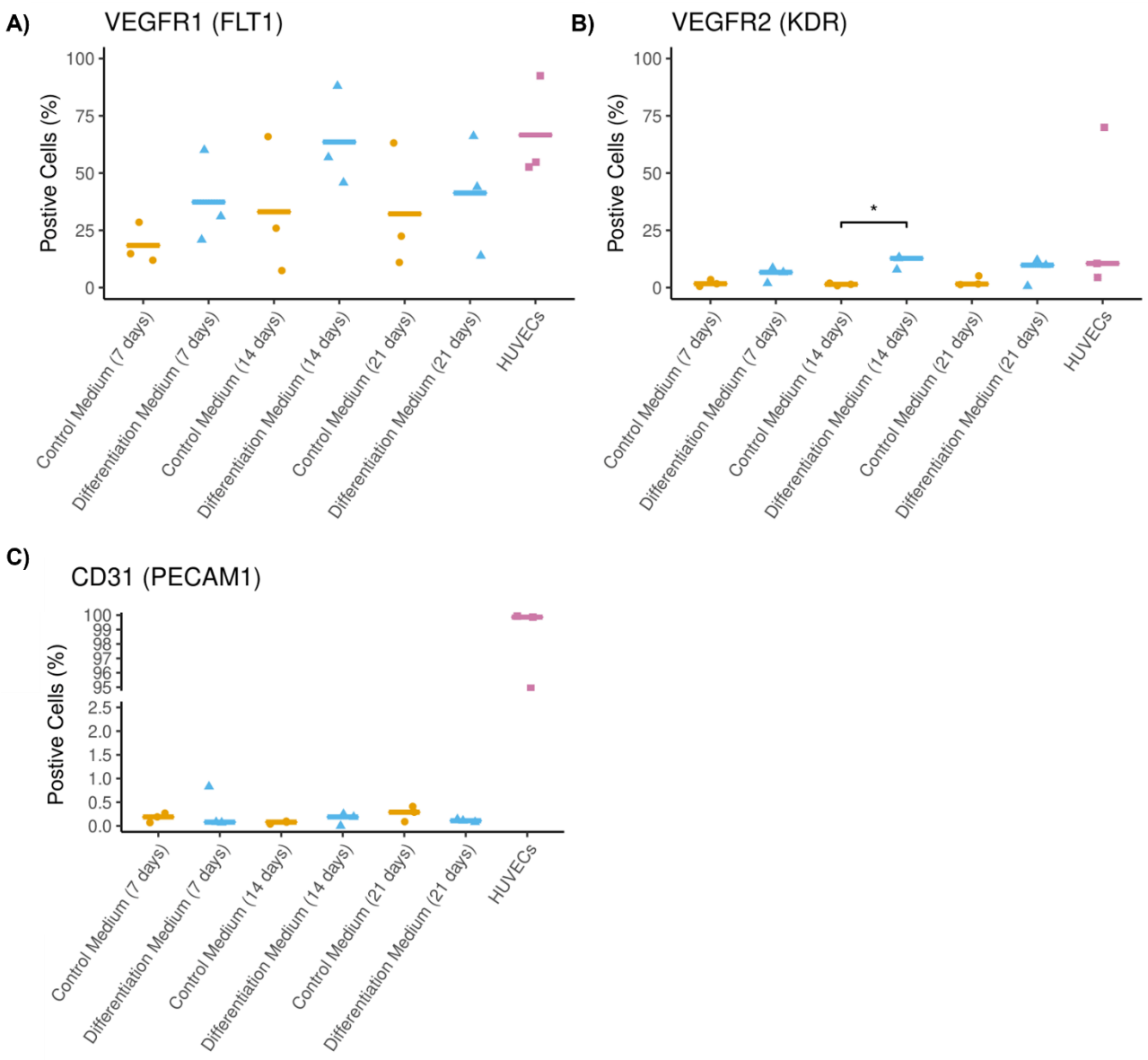

Figure 6.11 - Flow cytometry characterisation of pMSCs cultured in control medium or differentiation medium for up to 21 days. Cell surface expression of VEGFR1 (FLT1), VEGFR2 (KDR) and CD31 (PECAM1) were assessed in pMSCs cultured in control or differentiation medium at 7, 14 and 21 days, using flow cytometry. HUVECs were used as a positive control. VEGFR1 is presented as the mean, and statistical analysis was performed using a one-way ANOVA with a Tukey's post-hoc test. VEGFR2 and CD31 are presented as the median, and statistical analysis was performed using a Kruskal-Wallis with a Dunn's post-hoc test (based on normal distribution of the data). n=3. * $p<0.05$.

6.4.2.5 Endothelial function assays

6.4.2.5.1 Endothelial tube formation

To determine whether differentiated pMSCs behaved like ECs, endothelial tube formation was assessed following culture in differentiation medium or control medium for 21 days (n=7) (Figure 6.12; Figure 6.13). While the use of the angiogenesis analyser plugin on ImageJ was attempted to determine the number of endothelial tubes, branch points and branching length, false positives meant that manual counting was performed.

pMSCs cultured in differentiation medium formed a significantly higher number of endothelial tubes (62.5 [30-155.5]), compared to those cultured in control medium (16.5 [2-37.0]; $p<0.05$, n=7). During quantification, some tubes were counted in the control medium condition, however these were less well-defined, and appeared more like clusters of cells (Figure 6.12). Negative controls were also used, including 50 µM of the anti-angiogenic compound, suramin, and the absence of the ECM. In these negative controls, no endothelial tubes were formed. To ensure that tubes were not forming solely due to the presence of VEGF-A in the endothelial differentiation medium during the assay, the same concentration of VEGF-A (50.5 ng/mL) was added to cells grown in the control medium, however this did not lead to an increase in tube formation (Figure 6.12; Figure 6.13). This suggests that the ability of the cells cultured in differentiation medium to form endothelial tubes is due to their induction towards cells of the endothelial lineage over the 21-day differentiation. As a positive control, HUVECs were also used, which formed the highest number of endothelial tubes (235.5 [74-266], n=3).

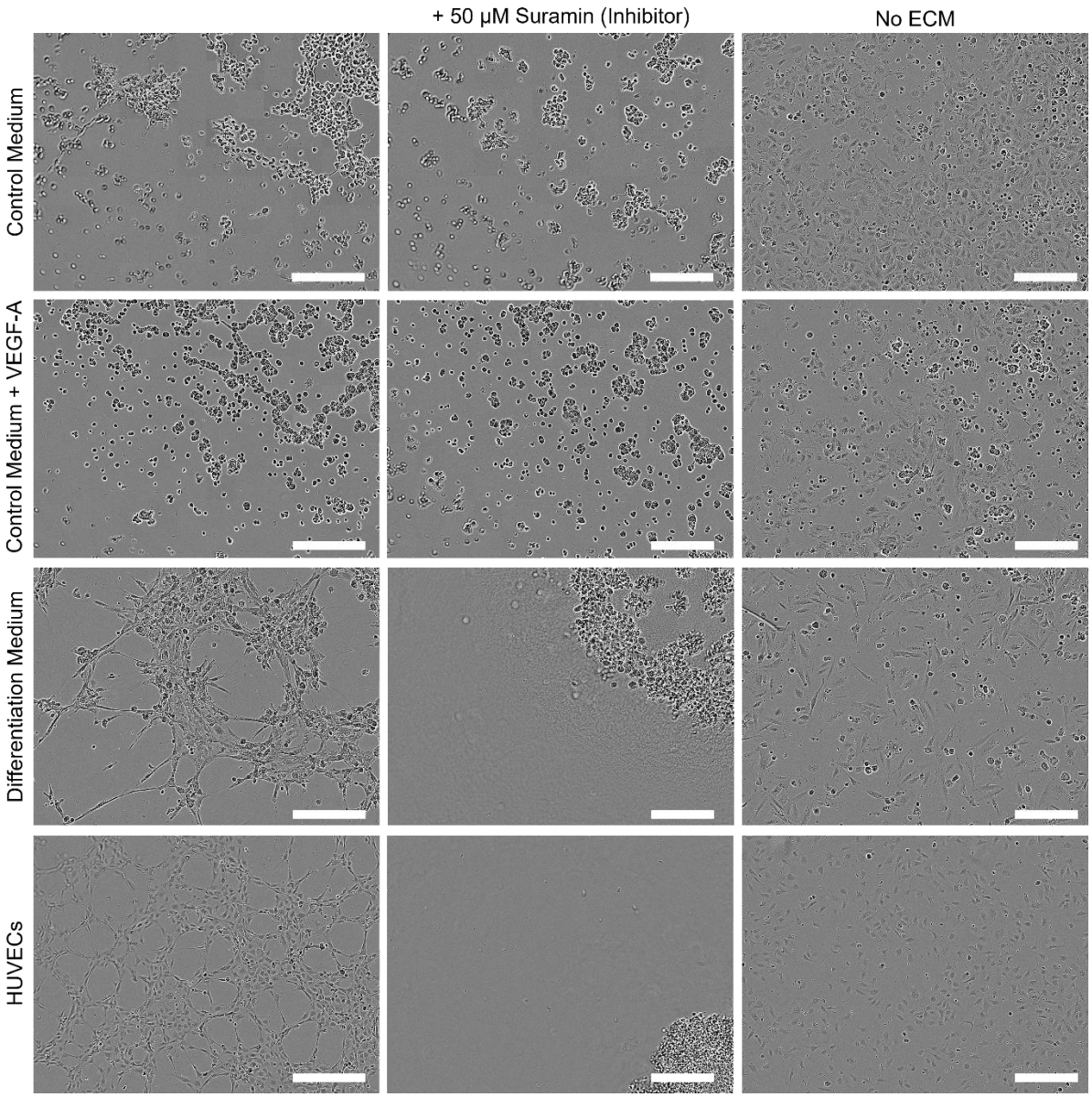

Figure 6.12 - Endothelial tube formation assay of pMSCs treated with either control medium or differentiation medium for 21 days. Cells were seeded onto ECM (10,000 cells per well of 96-well plate) and incubated for 2 hours at 37°C (n=7). Suramin, which inhibits tube formation, and no ECM were used as negative controls. HUVECs were used as a positive control (n=3). Images were taken on the Incucyte ZOOM at 10x magnification. Scale bars = 300 µm.

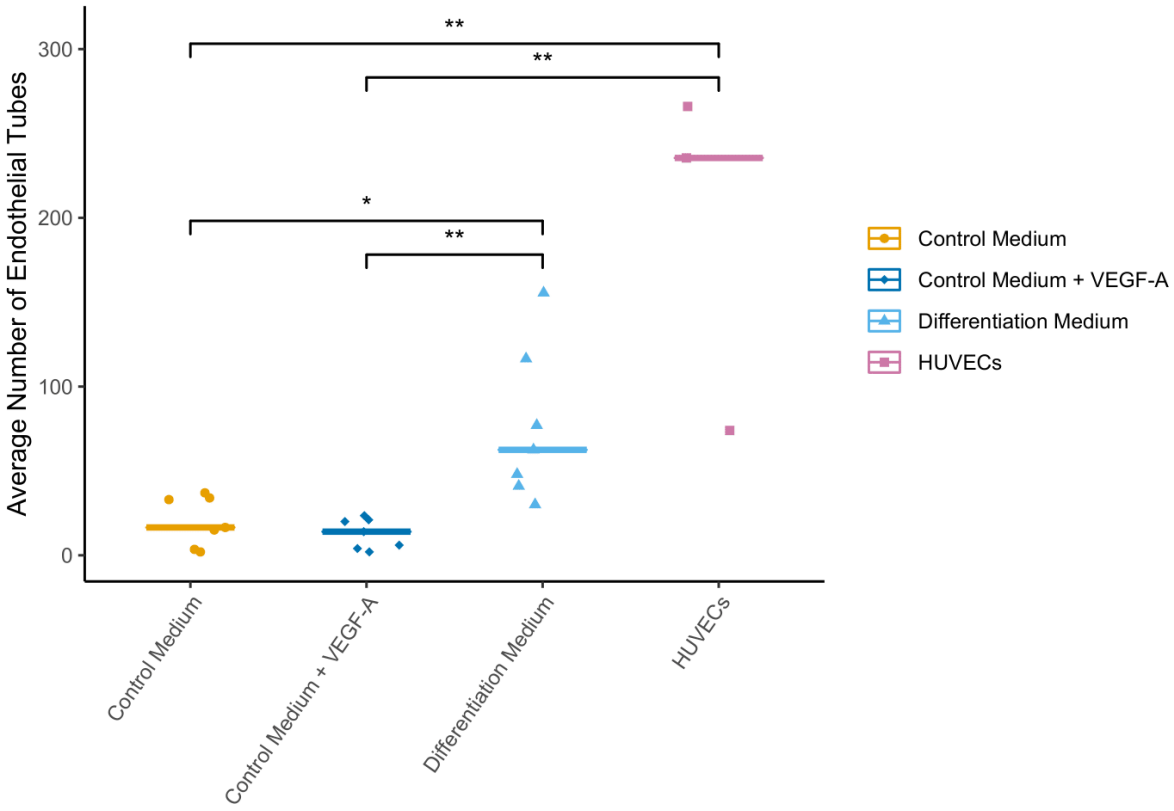

Figure 6.13 - Quantification of endothelial tube formation assay on pMSCs treated in either control medium or differentiation medium for 21 days. Cells were seeded onto ECM (10,000 cells per well of 96-well plate) and incubated for 2 hours at 37°C. The total number of tubes was manually counted using ImageJ. Data is presented as the median and statistical analysis was performed using a Kruskal-Wallis with a Dunn's post-hoc test (as the data was not normally distributed). Individual points represent each patient placenta. n=7. HUVECs were used as a positive control (n=3). * $p<0.05$, ** $p<0.01$.

6.4.2.5.2 Angiogenic sprouting

To further assess endothelial function of pMSCs treated with differentiation medium, angiogenic sprouting was assessed using the fibrin bead assay. This assay involves the coating of ECs to Cytodex microcarriers, and embedding into a fibrin gel containing necessary growth factors (e.g. VEGF, FGF2) that lead to endothelial sprouting[370,371]. Once the cell-coated Cytodex beads were embedded into the fibrin gel, they were incubated at 37°C for 24 hours before imaging. Cells cultured in control medium, either did not stay attached to the beads during the experiment, or did not form angiogenic sprouts, whereas cells cultured in differentiation medium remained attached to the beads and formed several angiogenic sprouts (n=3, Figure 6.14).

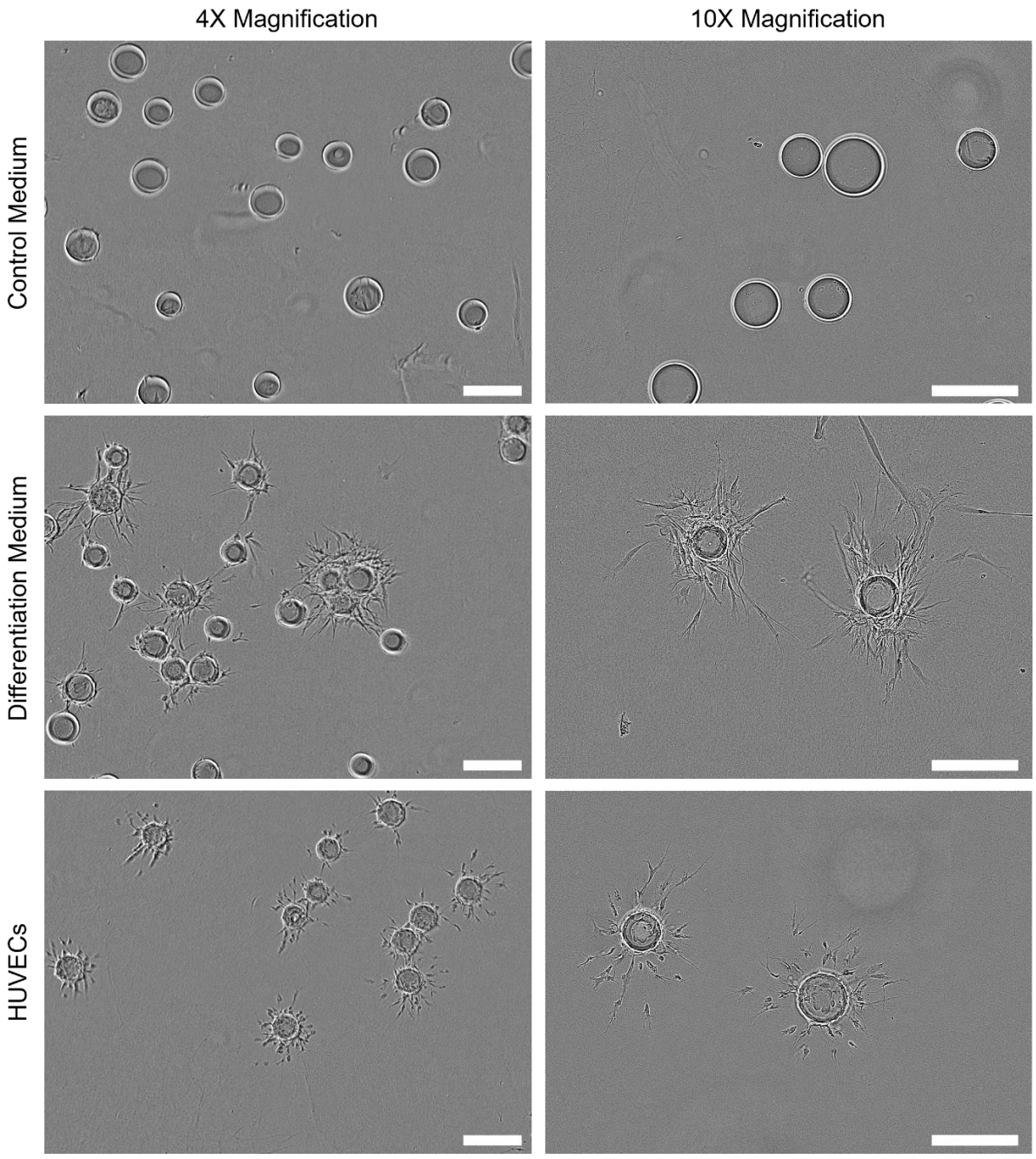

Figure 6.14 - Endothelial sprouting fibrin bead assay of pMSCs treated with either control or differentiation medium for 21 days. Cytodex beads were coated with pMSCs (500,000 cells/mL) that had been treated with control or differentiation medium for 21 days. A clot was formed, and angiogenic sprouts were imaged (n=3). HUVECs were used as a positive control (n=3). Images were taken on the Incucyte ZOOM at 4x and 10x magnification. Scale bars = 300 µm.

6.4.3 Optimising the culture of cells in microfluidic devices

In addition to biochemical factors, shear stress can also influence the differentiation of MSCs into cells of the endothelial lineage[366]. To expose cells to shear stress, orbital shakers can be used with cells cultured in standard cell culture plates, however this results in heterogenous levels of shear stress across the well[703]. Whereas parallel plate flow chambers, and microfluidic devices can be used to apply unidirectional laminar flow to cells[703,704]. Microfluidic devices can be constructed in different shapes and sizes, to precisely control shear stress and model *in vivo* conditions[703]. Here, microfluidic devices were used, and appropriate devices to culture pMSCs needed to be first optimised.

6.4.3.1 Culture of pMSCs or HUVECs in PDMS fabricated devices

pMSCs (n=3) were cultured in PDMS fabricated devices and exposed to 1 µL/min flow. After 72 hours, morphological responses to flow were evident, however, some cell detachment and cell death was observed (Figure 6.15). Cell detachment persisted after trialling lower flow rates (0.1 µL/min) and thicker coating with 30% Matrigel (data not shown).

As flow culture in PDMS fabricated devices resulted in the detachment of pMSCs, the ability to culture HUVECs (n=3) was also assessed. After 24 hours of 1 µL/min flow cell detachment and cell death was observed (Figure 6.16). HUVECs were also seeded into channel devices, to increase the shear stress and mimic their physiological environment in vessels more closely. However, even under static conditions, it was difficult to get an even spread and growth of cells within the channels (Figure 6.17).

6.4.3.2 Culture of pMSCs in Ibidi µ-Slide VI 0.4 Devices

To determine if different microfluidic device was more suitable for the culture of pMSCs (n=2), commercially available, Ibidi µ-Slide VI 0.4 devices were used. After 72 hours of 1 µL/min flow, morphological responses to flow were evident. Cells appeared viable, and little cell detachment was observed (Figure 6.18). These devices were therefore used for all subsequent pMSC differentiation experiments under flow conditions.

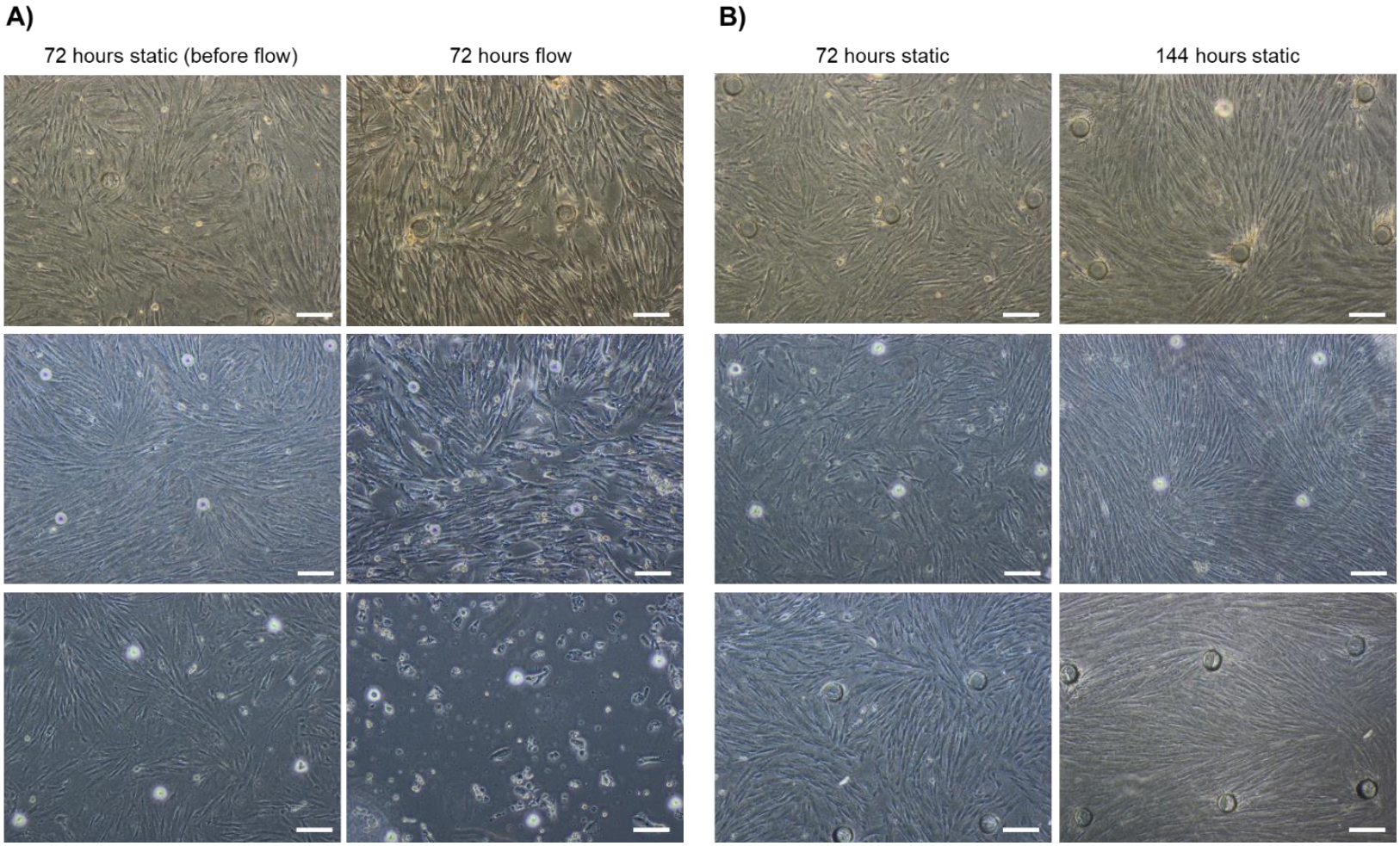

Figure 6.15 – pMSCs cultured in PDMS microfluidic devices under static and flow conditions. Primary human pMSCs were cultured in PDMS microfluidic devices under 1 µL/min flow (A) or static (B) conditions. Representative images (n=3), 1-2 devices per condition. Images were taken on the Olympus fluorescence microscope at 4x magnification. Scale bars = 200 µm.

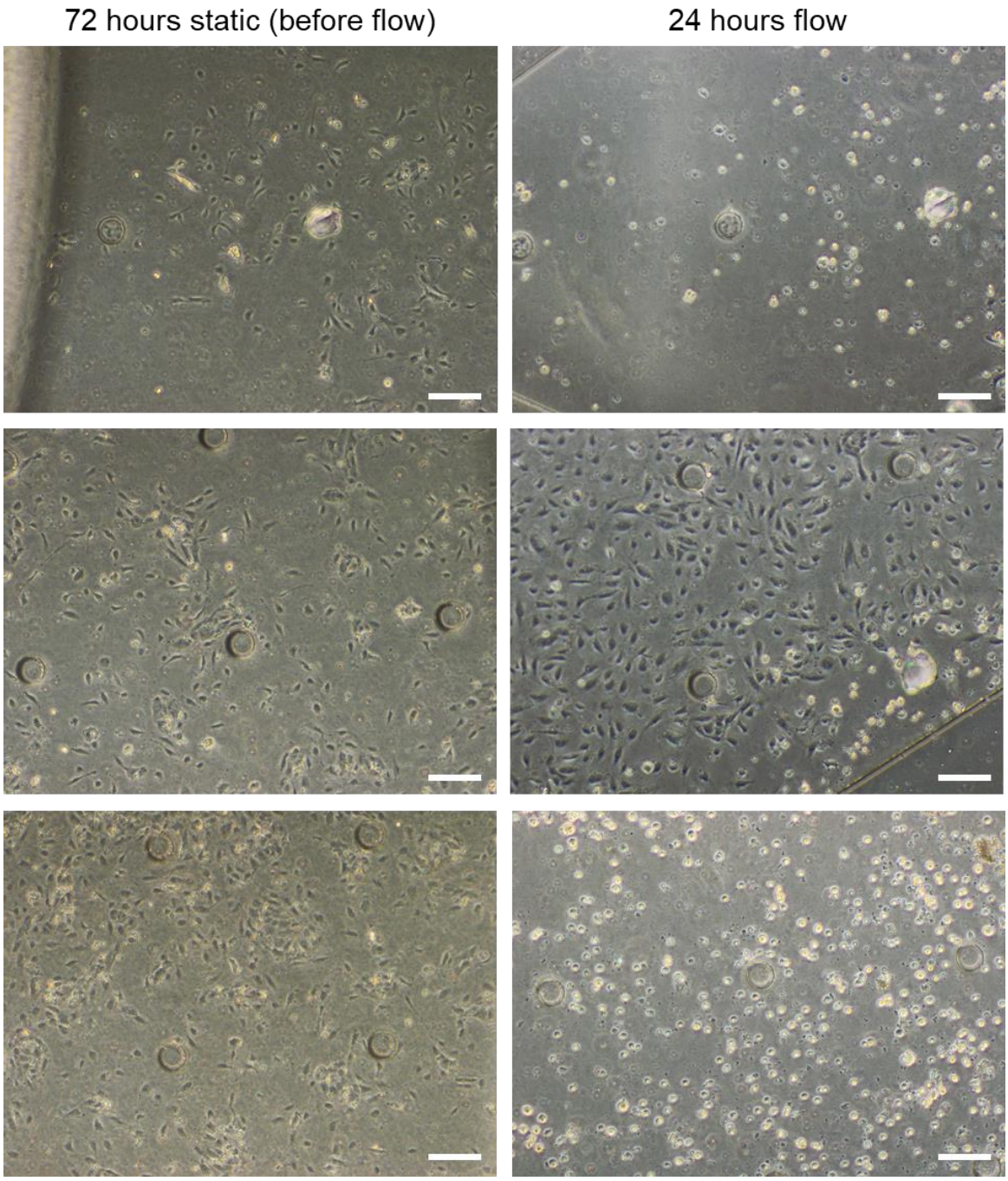

Figure 6.16 - HUVECs cultured in PDMS microfluidic devices under static and flow conditions. HUVECs were cultured in PDMS microfluidic devices under 1 µL/min flow conditions. Cell detachment was observed after exposure to flow for 24 hours. Representative images (n=3). Images were taken on the Olympus fluorescence microscope at 4x magnification. Scale bars = 200 µm.

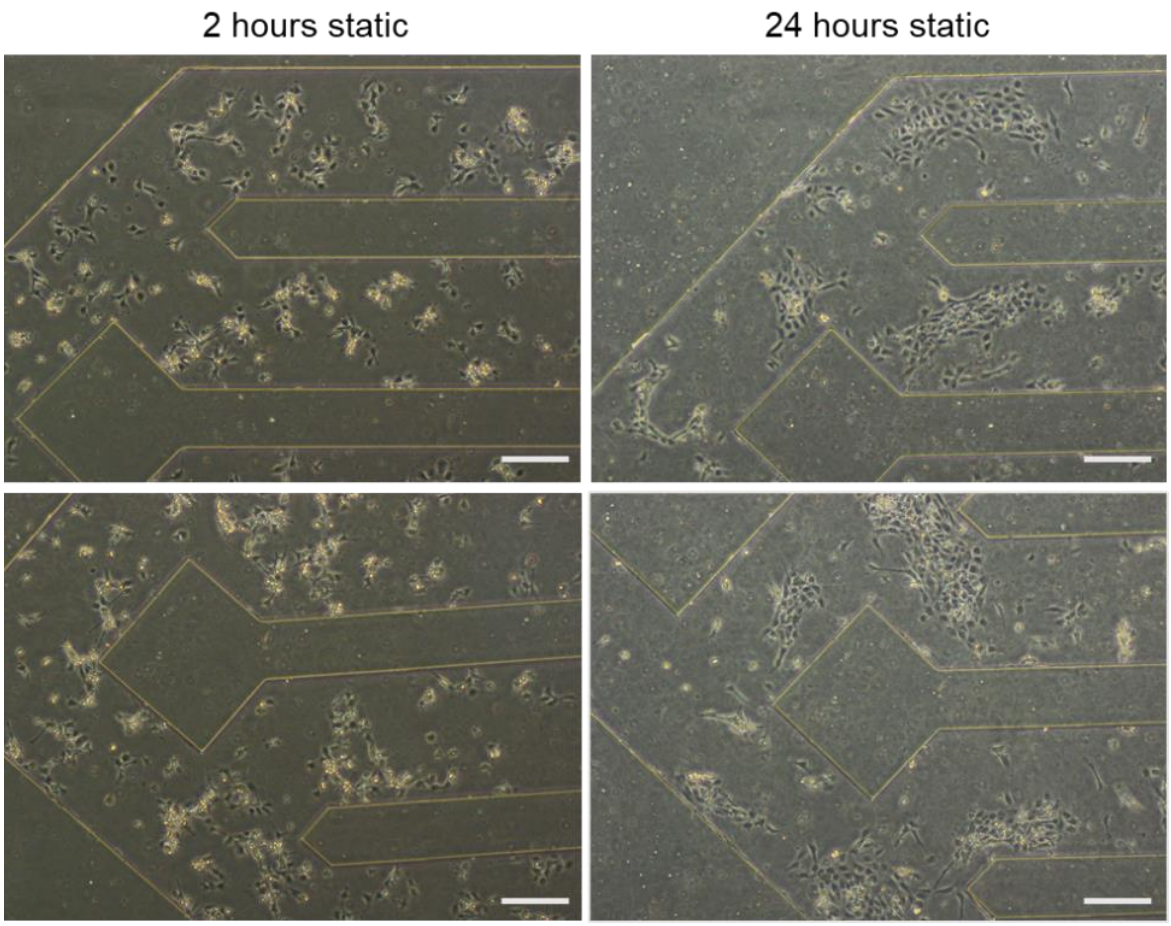

Figure 6.17 - HUVECs cultured in a 16-channel PDMS microfluidic device under static conditions. HUVECs were cultured in 16-channel PDMS microfluidic devices under static conditions. Images were taken on the Olympus fluorescence microscope at 4x magnification. Scale bars = 200 µm.

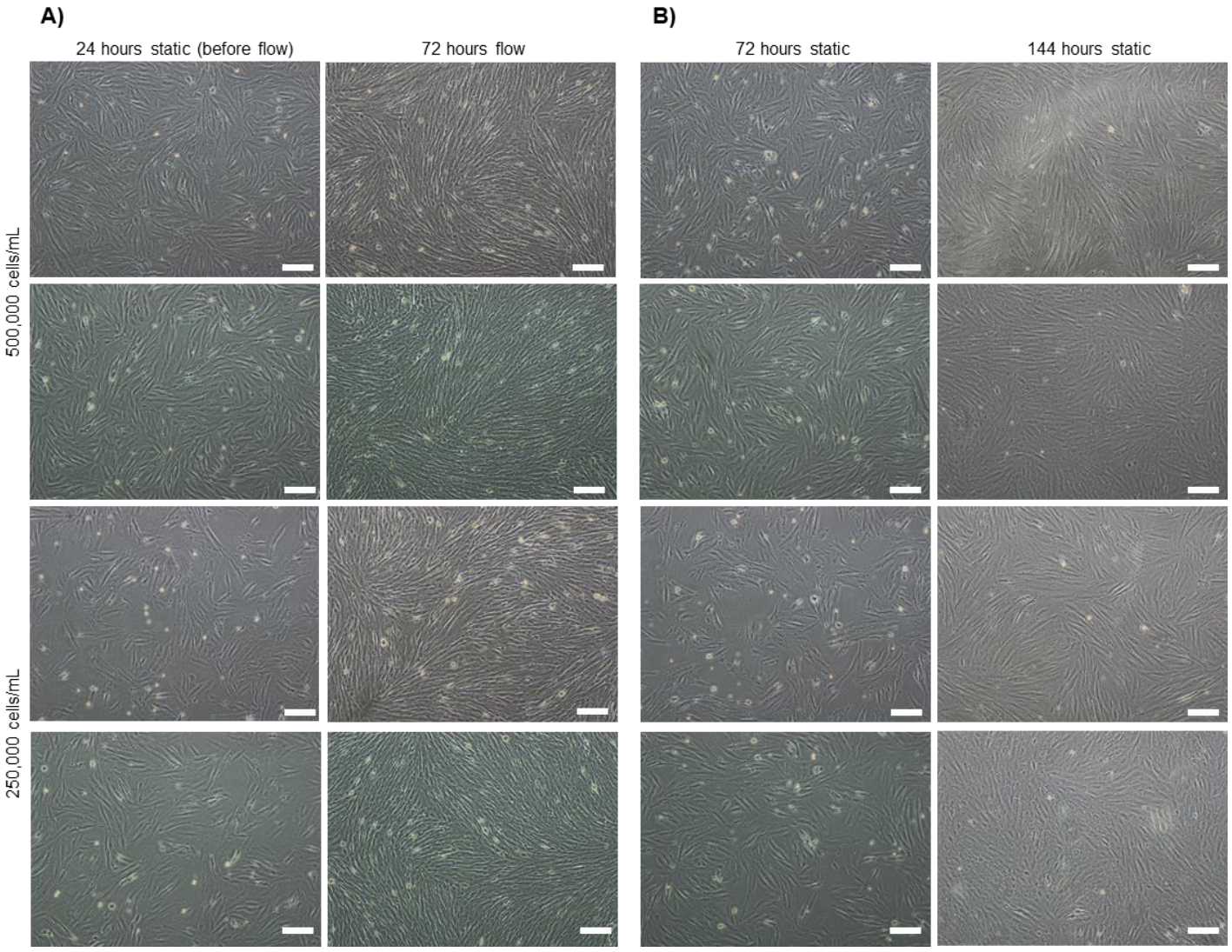

Figure 6.18 – Placental mesenchymal stem cells (pMSCs) cultured in Ibidi microfluidic devices. Primary human pMSCs were cultured in Ibidi microfluidic devices under 1 µL/min flow (A) or static (B) conditions. Representative images (n=2), 1-2 devices per condition. Images were taken on the Olympus fluorescence microscope at 4x magnification. Scale bars = 200 µm

6.4.4 Differentiation of pMSCs into cells of the endothelial lineage under low flow/shear stress conditions

6.4.4.1 Morphological changes

pMSCs (n=5) were cultured in either control or differentiation medium and exposed to low flow/shear stress at a rate of 1 µL/min for 72 hours and then imaged. The time frame of this was much shorter than static experiments, given that it is difficult to recover all cells from microfluidic devices, limiting the ability for passaging and continued culture. pMSCs cultured in differentiation medium with low shear stress had lost their characteristic whirlpool morphology[360] and had formed clusters (Figure 6.19).

6.4.4.2 Endothelial and mesenchymal gene expression

6.4.4.2.1 Housekeeping gene expression

As in Section 6.4.2.3.1, housekeeping genes that did not differ between the culture conditions needed to be first identified. Housekeeping genes were found to be less stable across culture conditions with shear stress compared to static experiments, therefore a larger panel of widely used housekeeping genes were assessed[378,699]. Expression levels of *18S, ACTB, B2M, GAPDH* (Glyceraldehyde 3-phosphate dehydrogenase)*, GUSB, HPRT1* (Hypoxanthine phosphoribosyltransferase 1)*, RPLP0* (60S acidic ribosomal protein P0)*, RPL13A* and *YWHAZ* were assessed in pMSCs cultured in control or differentiation medium under static or low flow/shear stress conditions for 72 hours. All housekeeping genes, except *B2M*, were significantly different between conditions ($p<0.05$-$p<0.0001$), with particularly lower levels of housekeeping genes expressed in the static control medium condition (Figure 6.20). Therefore, as *B2M* was the most stable, this was used for normalisation of target genes.

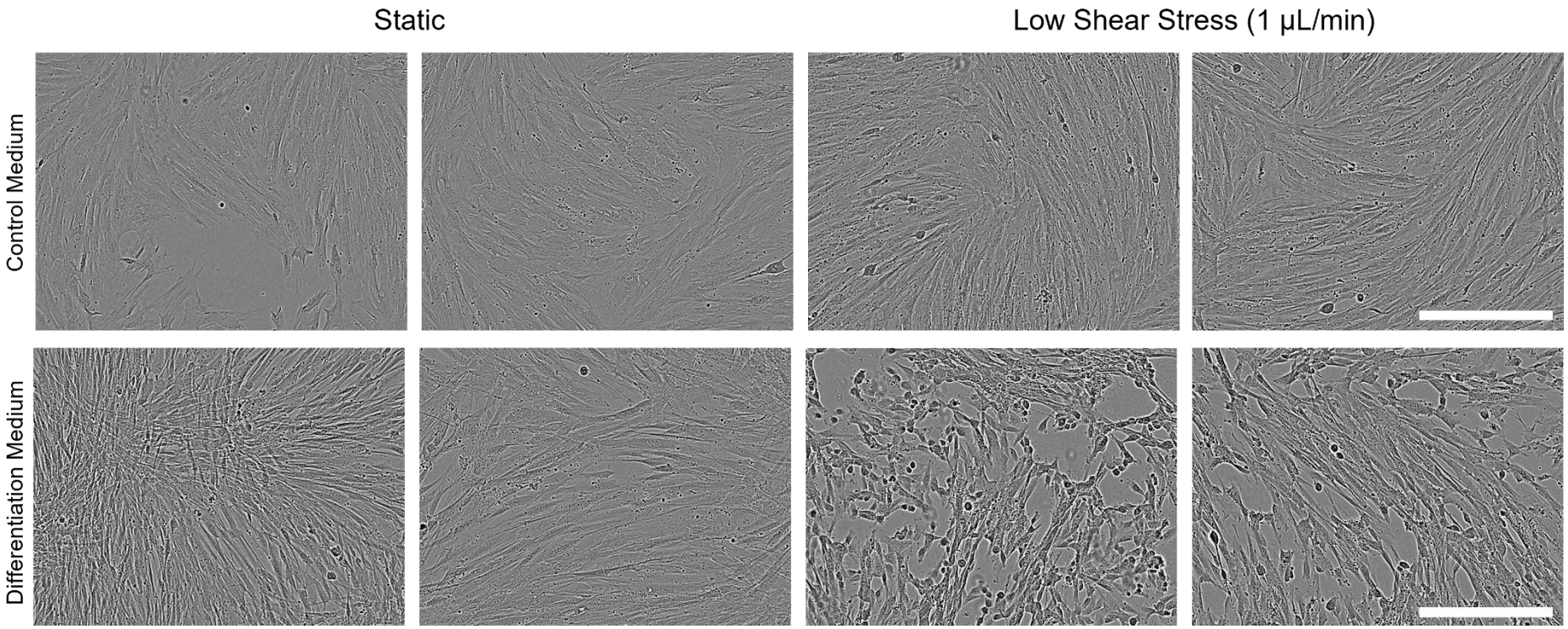

Figure 6.19 - Morphological differences in pMSCs cultured in control or differentiation medium under static or low flow shear stress (1 µL/min flow) conditions. pMSCs were cultured in either control (pMSC medium) or differentiation medium (EGM-2 + VEGF-A) under static or low flow shear stress (1 µL/min flow) conditions to induce differentiation towards the endothelial lineage. Cells were imaged after 72 hours. Morphological differences can be observed in pMSCs cultured in differentiation medium with low flow shear stress. Representative images (n=5). Images were taken on the Incucyte ZOOM at 10x magnification. Scale bars = 300 µm.

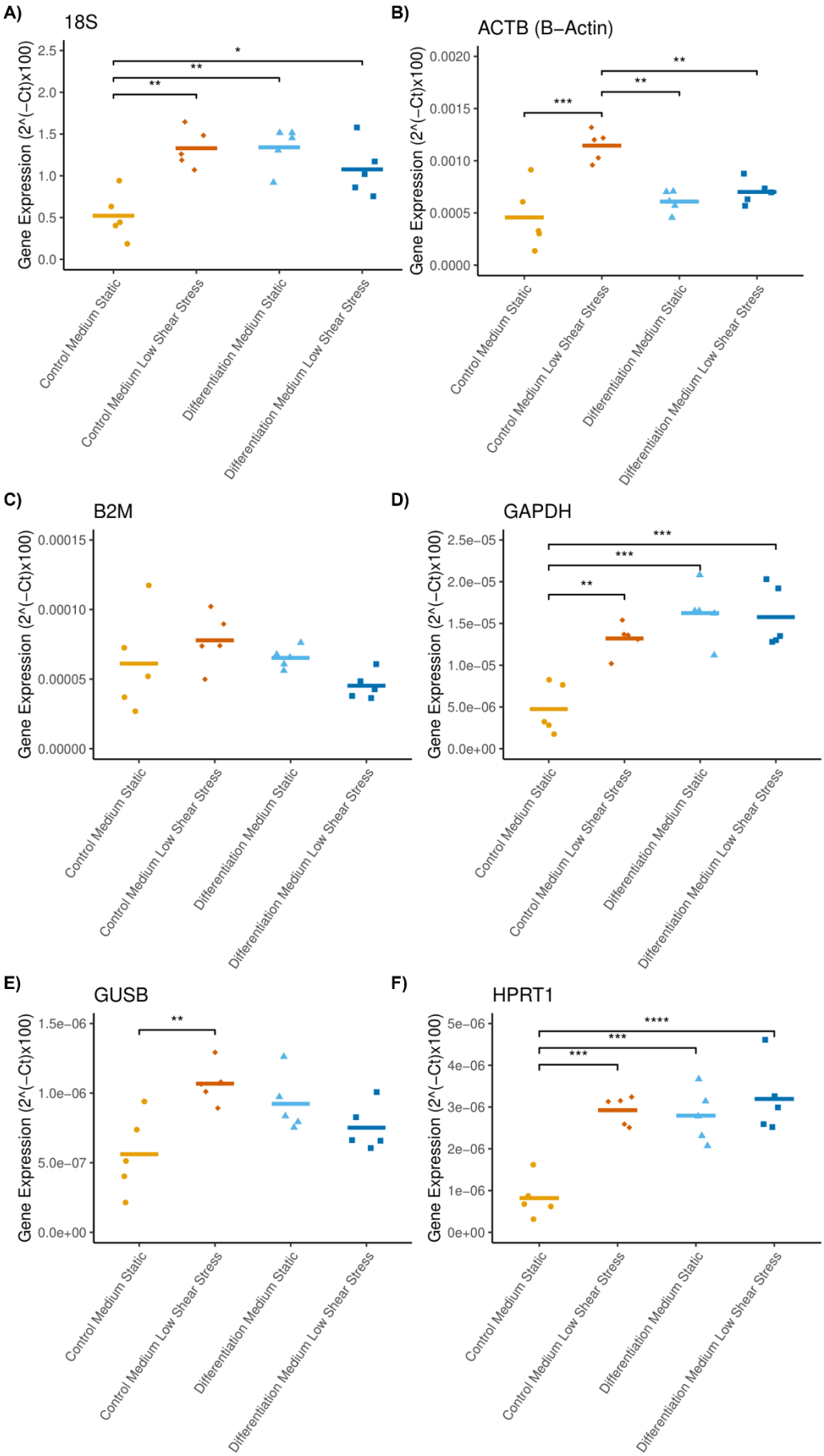
A)
18S
Gene Expression (2^(−Ct)x100)
2.5
2.0
1.5
1.0
0.5
0.0
*
**
**
Control Medium Static
Control Medium Low Shear Stress
Differentiation Medium Static
Differentiation Medium Low Shear Stress
B)
ACTB (B−Actin)
Gene Expression (2^(−Ct)x100)
0.0020
0.0015
0.0010
0.0005
0.0000
**
**
***
Control Medium Static
Control Medium Low Shear Stress
Differentiation Medium Static
Differentiation Medium Low Shear Stress
C)
B2M
Gene Expression (2^(−Ct)x100)
0.00015
0.00010
0.00005
0.00000
Control Medium Static
Control Medium Low Shear Stress
Differentiation Medium Static
Differentiation Medium Low Shear Stress
D)
GAPDH
Gene Expression (2^(−Ct)x100)
2.5e−05
2.0e−05
1.5e−05
1.0e−05
5.0e−06
0.0e+00
***
***
**
Control Medium Static
Control Medium Low Shear Stress
Differentiation Medium Static
Differentiation Medium Low Shear Stress
E)
GUSB
Gene Expression (2^(−Ct)x100)
1.5e−06
1.0e−06
5.0e−07
0.0e+00
**
Control Medium Static
Control Medium Low Shear Stress
Differentiation Medium Static
Differentiation Medium Low Shear Stress
F)
HPRT1
Gene Expression (2^(−Ct)x100)
5e−06
4e−06
3e−06
2e−06
1e−06
0e+00
****
***
***
Control Medium Static
Control Medium Low Shear Stress
Differentiation Medium Static
Differentiation Medium Low Shear Stress

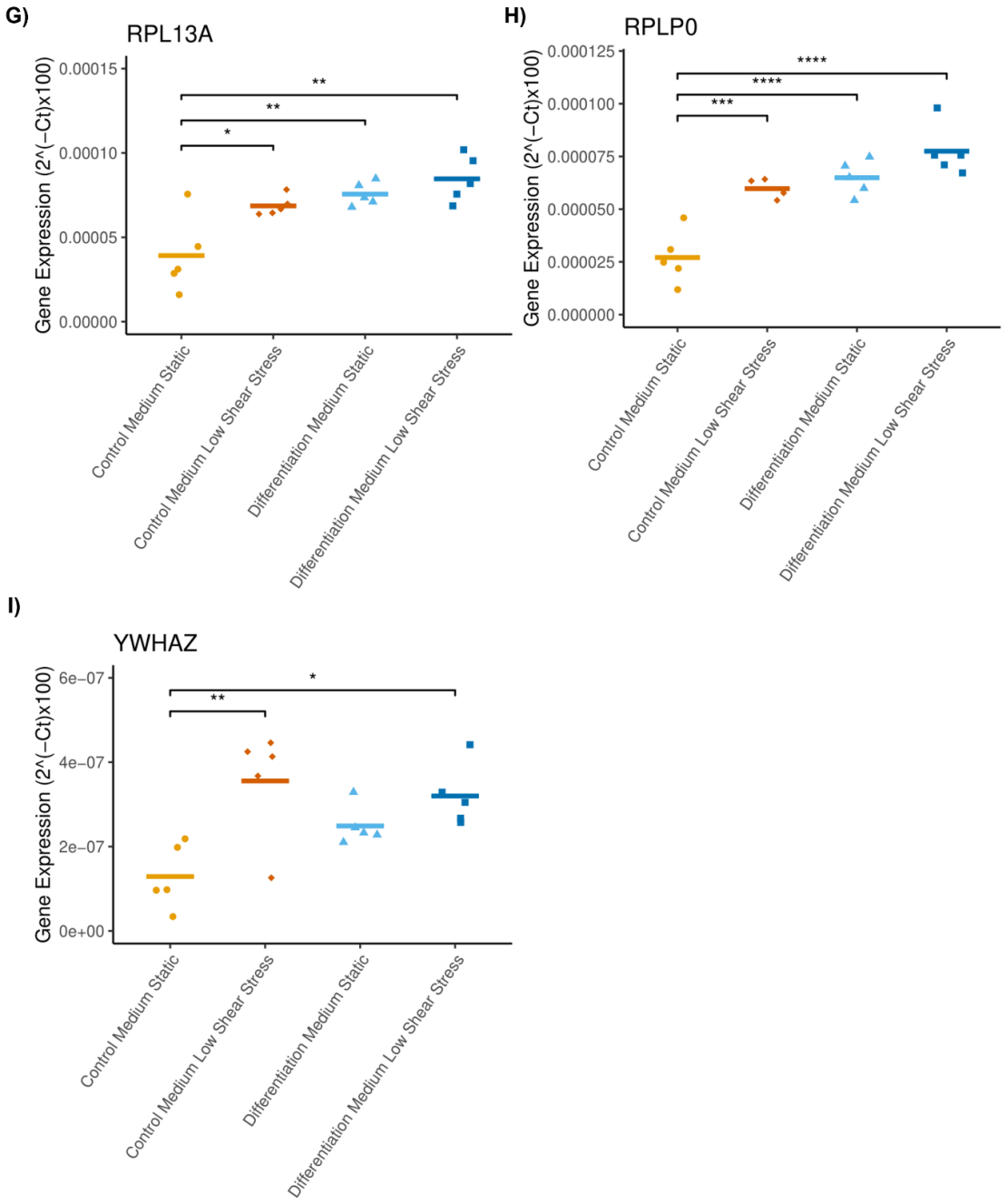

Figure 6.20 - Housekeeping gene expression in pMSCs cultured in control or differentiation medium under static or low flow shear stress (1 µL/min flow) conditions. pMSCs were cultured in either control (pMSC medium) or differentiation medium (EGM-2 + VEGF-A) under static or low flow shear stress (1 µL/min flow) conditions to induce differentiation towards the endothelial lineage. After 72 hours RNA was extracted, and RT-qPCRs for housekeeping genes were performed. Data is presented as the mean, and statistical analysis was performed using a Two-Way ANOVA. Data that was not normally distributed was log transformed. Individual points represent each patient placenta. n=5. * p<0.05, ** p<0.01, *** p<0.001, **** p<0.0001.

6.4.4.2.2 Expression of endothelial and mesenchymal genes

Many changes in EC and MSC gene expression were observed in response to low shear stress. The MSC marker, *NT5E*, was increased in in pMSCs cultured in differentiation medium under low shear stress conditions, compared to control medium under static conditions (0.00032±0.00036 vs 0.00092±0.00020; $p<0.001$, n=5) (Figure 6.21B). Whereas, *CD44* was increased in control and differentiation medium with low shear stress (1.70±0.29; $p<0.01$ and 3.01±0.26; $p<0.0001$, respectively, n=5) and differentiation medium under static conditions (1.54±0.086; $p<0.05$, n=5), compared to control medium under static conditions (0.55±0.081, n=5) (Figure 6.21A).

The mature EC marker, *VWF,* was increased with differentiation medium under static conditions (9.57e-05±1.52e-05; $p<0.05$, n=5) and control medium under shear stress conditions (9.65e-05±2.91e-05; $p=0.060$, n=5) compared to control medium under static conditions (3.24e-05±7.14e-06, n=5) (Figure 6.22D). To determine whether shear stress was impacting the pMSCs, expression of *PIEZO1*, a Ca^{2+}-permeable non-selective cation channel, known to respond to shear stress in ECs[120], was measured. *PIEZO1* was increased in low shear stress conditions with control medium (0.085±0.027; $p=0.067$, n=5) and differentiation medium (0.13±0.018; $p<0.001$, n=5) compared to control medium under static conditions (0.036±0.0054, n=5) (Figure 6.22E).

Consistent with the findings in Section 6.4.2.3.2, increased *FLT1* and *PECAM1* in pMSCs cultured under static conditions in differentiation medium, although this was not significant for *PECAM1* (Figure 6.22A; Figure 6.22C).

6.4.4.3 Endothelial tube formation

While the fibrin bead assay could not be performed on pMSCs cultured in devices as it required a large number of cells (500,000) grown in a T75 flask, endothelial tube formation was assessed in pMSCs cultured in control or differentiation medium under static or low shear stress conditions for 72 hours (n=4, Figure 6.23; Figure 6.24). pMSCs cultured in differentiation medium under low shear stress conditions formed a significantly greater number of endothelial tubes (109.74±13.45) than control medium under static (6.50±4.57; $p<0.001$) and low shear stress conditions (47.00±11.82; $p<0.05$) and differentiation medium under static conditions (30.50±11.86; $p<0.01$). Very few endothelial tubes were observed in control medium under static conditions, whereas some endothelial tubes were observed when low shear stress or differentiation medium was used alone. However, these were less well-defined than

tubes formed when the combination of differentiation medium and shear stress was used (Figure 6.23).

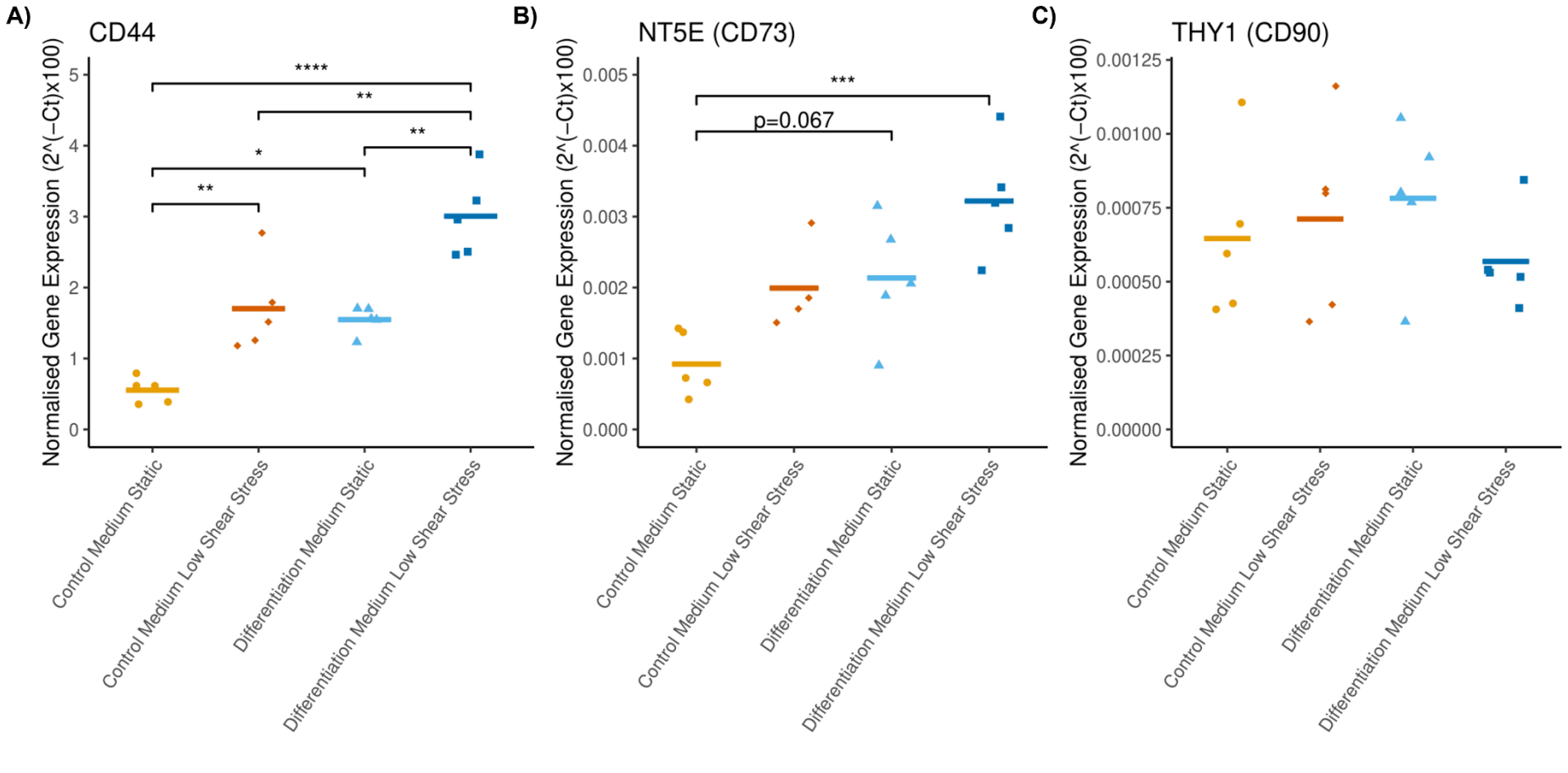

Figure 6.21 - Mesenchymal gene expression in pMSCs cultured in control or differentiation medium under static or low flow shear stress (1 µL/min flow) conditions. Mesenchymal genes were assessed in pMSCs cultured in control or differentiation medium under static or low flow shear stress (1 µL/min flow) for 72 hours using RT-qPCR. The expression of target genes was normalised to *B2M* housekeeping gene. Data is presented as the mean, and statistical analysis was performed using a Two-Way ANOVA with Tukey's post-hoc test. Individual points represent each patient placenta. n=5. * p<0.05, ** p<0.01, ***p<0.001, ****p<0.0001.

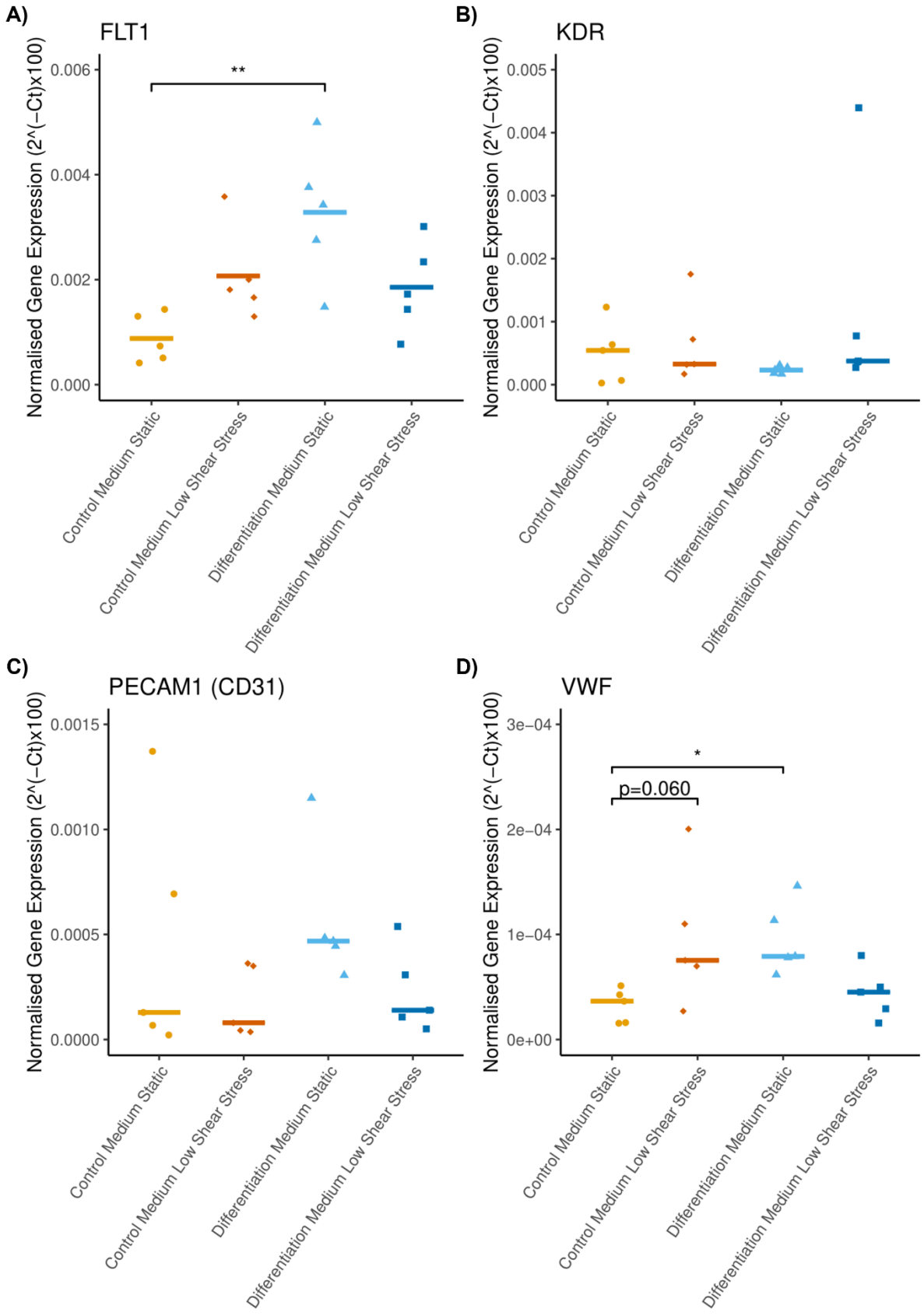
A)
FLT1
Normalised Gene Expression (2^(−Ct)x100)
0.006
0.004
0.002
0.000
**
Control Medium Static
Control Medium Low Shear Stress
Differentiation Medium Static
Differentiation Medium Low Shear Stress
B)
KDR
Normalised Gene Expression (2^(−Ct)x100)
0.005
0.004
0.003
0.002
0.001
0.000
Control Medium Static
Control Medium Low Shear Stress
Differentiation Medium Static
Differentiation Medium Low Shear Stress
C)
PECAM1 (CD31)
Normalised Gene Expression (2^(−Ct)x100)
0.0015
0.0010
0.0005
0.0000
Control Medium Static
Control Medium Low Shear Stress
Differentiation Medium Static
Differentiation Medium Low Shear Stress
D)
VWF
Normalised Gene Expression (2^(−Ct)x100)
3e−04
2e−04
1e−04
0e+00
*
p=0.060
Control Medium Static
Control Medium Low Shear Stress
Differentiation Medium Static
Differentiation Medium Low Shear Stress

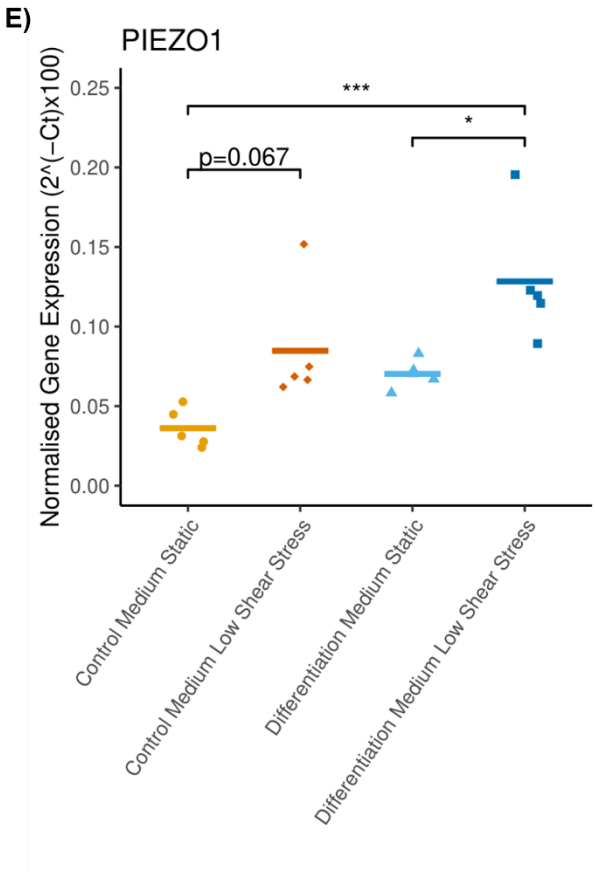

Figure 6.22 - Endothelial gene expression in pMSCs cultured in control or differentiation medium under static or low flow shear stress (1 µL/min flow) conditions. Endothelial genes were assessed in pMSCs cultured in control or differentiation medium under static or low flow shear stress (1 µL/min flow) for 72 hours using RT-qPCR. The expression of target genes was normalised to *B2M* housekeeping gene expression. Data is presented as the mean, and statistical analysis was performed using a Two-Way ANOVA with Tukey's post-hoc test. Data that was not normally distributed was log transformed. Individual points represent each patient placenta. n=5. * $p<0.05$, ** $p<0.01$, ***$p<0.001$.

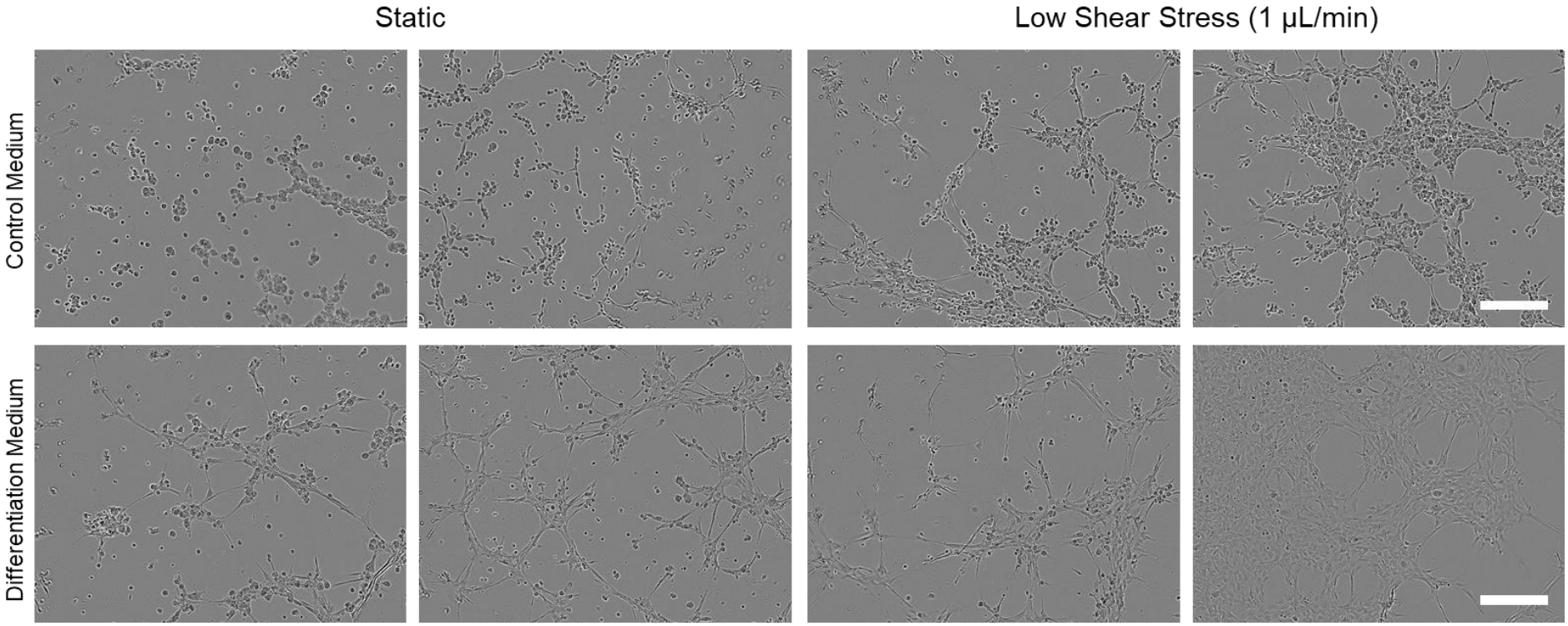

Figure 6.23 - Endothelial tube formation assay of pMSCs treated in control or differentiation medium under static or low flow shear stress (1 µL/min flow) conditions for 72 hours. Cells were seeded onto ECM (10,000 cells per well of 96-well plate) and incubated for 2 hours at 37°C (n=4). Images were taken on the Incucyte ZOOM at 10x magnification. Scale bars = 300 µm.

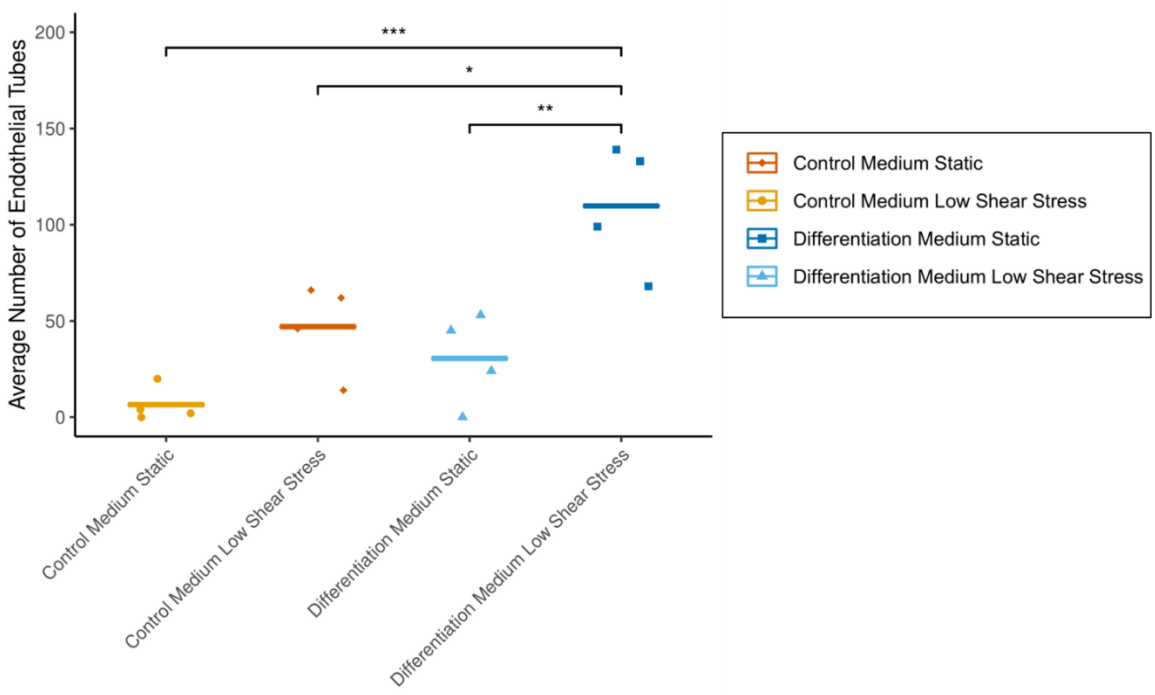

Figure 6.24 - Quantification of endothelial tube formation assay on pMSCs treated in control or differentiation medium under static or low flow shear stress (1 µL/min flow) conditions for 72 hours. Cells were seeded onto ECM (10,000 cells per well of 96-well plate) and incubated for 2 hours at 37°C (n=4). The total number of tubes was manually counted using ImageJ. Data was normally distributed and is presented as the mean. Individual points represent each patient placenta. n=4. Statistical analysis was performed using a Two-Way ANOVA with a Tukey's post-hoc test. * $p<0.05$, ** $p<0.01$.

6.5 Discussion

The aim of this chapter was to determine whether primary pMSCs were a suitable *in vitro* model of placental vascular development. The ability of pMSCs to differentiate into cells of the endothelial lineage was determined using biochemical stimulation with growth factors (differentiation medium containing EGM-2 and VEGF-A) and/or mechanical stimulation by exerting a low shear stress (1 µL/min flow) in microfluidic devices. Biochemical stimulation of pMSCs increased gene expression of EC markers, *FLT1, KDR* and *PECAM1*, as well as protein expression of VEGFR1 (*FLT1*). pMSCs cultured in differentiation medium were also able to form endothelial tubes and angiogenic sprouts. The combination of differentiation medium and low shear stress increased endothelial tube formation of pMSCs but did not further increase EC gene expression. As the most increases in EC marker expression and endothelial function were observed with biochemical stimulation under static conditions, this model will be utilised in Chapter 7 to investigate the impact of physiological maternal glucose fluctuations in GDM LGA pregnancies on placental vascular development.

6.5.1 Isolation and characterisation of pMSCs from term placentae

The ISCT states that MSCs should express markers of MSC identity, CD73, CD90 and CD105 ($\geq$95% positive) and lack expression ($\leq$2% positive) of haematopoietic/endothelial markers (CD34), monocyte/macrophage markers (CD14 or CD11b), B cell markers (CD19 or CD79α), leukocyte markers (CD45) and stimulated MSCs (HLA-DR)[670]. The pMSCs used in this study expressed high levels of CD73 and CD90, at similar levels to BMSCs in flow cytometry[359]. Although only 12% of pMSCs expressed CD105 (at similar levels to BMSCs), which was much lower than the 95% required in the ISCT guidelines. The method for pMSC isolation in the present study was adapted from that by Pelekanos *et al*. (2016). These researchers found that 100% of the pMSCs expressed CD105[360]. Yu *et al*. (2021) also found that around 80% of pMSCs isolated from term placentae expressed CD105[660]. However, in the present study NEAAs were added to the culture medium, which differed from the methods by Pelekanos *et al*. and Yu *et al*. Furthermore, Yu *et al*. included 5 ng/mL of FGF in the medium. These differences in medium composition could explain alterations in CD105 expression. Moreover, adipose tissue derived MSCs have been found to express CD105 at low levels, which increases upon passages[705,706], thus suggesting CD105 expression may be dependent on time in culture. CD105, CD73, in addition to a further MSC marker, CD44, were also observed in immunocytochemical characterisation of pMSCs.

In flow cytometry, the negative marker cocktail, which probed for CD45, CD34, CD11b, CD79A and HLA-DR, was expressed in around 19% of pMSCs[359]. However, the ISCT guidelines are strict due to the use of MSCs in cellular therapies, and therefore need to be regulated to ensure patient safety and standardised protocols for reproducible results. In the present study, the aim was to develop a model of placental vascular development, using pMSCs and differentiating them into cells of the endothelial lineage. Thus, the purity of pMSCs isolated was not vital for the development of this model. Contaminating cell types could have been haematopoietic stem cells (HPCs) or placental macrophages (HBCs). HPCs express the marker CD34[694], of which some expression was observed in immunocytochemistry. Although, these $CD34^+$ cells could contribute to vascular differentiation as $CD34^+$ MSCs, named vascular stem cells (VSCs), are known to reside in the capillaries and adventitia of larger blood vessels, and can differentiate into cell types needed to develop a functional blood vessel[680,707,708]. These cell populations are thought to be adventitial progenitor cells (APCs), which can differentiate into pericytes, VSMCs and ECs[709]. HBCs are known to express CD14[710], as well as HLA-DR at term[711,712]. While CD14 was not observed in pMSCs in immunocytochemistry, a larger panel of HBC markers would be needed to confirm whether HBCs were co-isolated with pMSCs. However, as previously discussed, paracrine signalling by HBCs can contribute to placental vascular development, as they secrete angiogenic molecules, such as VEGF-A and FGF-2[103,104] and inflammatory mediators[104], which are also reported to have angiogenic functions[106–112].

The method to isolate pMSCs in this study included tissue from chorionic plate and chorionic villous, which are a source of fetal MSCs, and the decidua basalis, which is a source of maternal MSCs. In the study by Pelekanos *et al.* (2016), which the current isolation protocol was adapted from, the pMSC cultures were overtaken by maternal pMSCs by P2[360]. To confirm this, HLA typing to detect maternal and fetal alleles[713] or *in situ* hybridisation to detect chromosome X and Y DNA could be used[642,714]. While several studies have reported that maternal and fetal MSCs have comparable phenotypes[642,713,715], and multi-lineage differentiation potential[715], other studies have shown that they have altered angiogenic effects, due to altered release of angiogenic factors[642,716]. As placental vascular dysfunction in GDM occurs within the placenta and the chorionic villi, the most appropriate model would be to utilise fetal pMSCs. However, decidual MSCs are known to reside in the vascular niche of the decidua, and are known to exhibit paracrine effects of vascularisation[714,717].

Overall, the potential contaminating HPCs/VSCs, HBCs or maternally derived MSCs could contribute to vascular differentiation and development in the model.

6.5.2 Primary pMSCs as a model for placental vascular development

6.5.2.1 Mesenchymal Markers

During endothelial lineage differentiation of MSCs, it would be expected that mesenchymal markers would be reduced, however these are not assessed in previous studies (Table 6.1; Table 6.2). In the current study, a trend towards a decrease in *NT5E* (CD73) gene expression with differentiation medium at 11 days was observed, correlating with increases in EC genes (*FLT1, KDR* and *PECAM1*). Moreover, in the PCR array, several mesenchymal genes were downregulated when pMSCs were cultured in differentiation medium for 11 days, including *TAGLN* (Transgelin) and *CCN1* (Calponin), which are known to be enriched in smooth muscle cells and upregulated during myogenic differentiation of MSCs[718–720]. Similarly, *MYOCD* (Myocardin), a regulator of smooth muscle gene expression[721], was also downregulated, which suggests a reduction of smooth muscle markers during endothelial differentiation of pMSCs. The downregulation of *CDH2* (Cadherin 2) in endothelial differentiated pMSCs also demonstrates a reduction in the mesenchymal phenotype, as its expression is increased in EndMT[722] and is also known to regulate cell fate decisions, with altered expression in MSCs undergoing chondrogenic, myogenic, osteogenic or adipogenic differentiation[723].

Unexpectedly, the MSC marker, *CD44* was increased in pMSCs cultured in differentiation medium at 18 and 25 days. After 72 hours, *CD44* was increased with low shear stress, differentiation medium and the combination of both, compared to control medium under static conditions. While CD44 is an MSC marker[681,682], it has also been reported to be found in ECs, in a number of studies[675,676], as well endothelial colony forming cells (ECFCs)[724]. Interestingly however, CD44 expression was low in HUVECs in RT-qPCRs. Previous studies have shown CD44 expression in HUVECs, using immunocytochemistry[725] and flow cytometry[726], although at the protein level.

The increases in *CD44* expression in static and low shear stress experiments also correlate with increased endothelial tube formation, which given that CD44 has been linked to endothelial proliferation, migration, and tube formation[675,676,696], suggests that it may contribute to functional effects. For example, an antibody against CD44 inhibited EC proliferation and migration, as well as capillary formation on a fibrin matrix[676].

Moreover, knockdown of CD44 in foreskin microvascular ECs inhibited their ability to form tubular networks[675]. The mesenchyme-derived mitogen, hepatocyte growth factor (*HGF*) is also known to stimulate cell migration, branching and tubulation of epithelial and ECs[702,716] and has been associated with increased angiogenic potency[642]. *HGF* was the most upregulated gene in pMSCs cultured in differentiation medium for 11 days, in the PCR array. Moreover, *NT5E* expression was increased when pMSCs were exposed to both low shear stress and differentiation medium, which has been linked to MSC migration[727] and increased VEGF signalling and angiogenesis[728,729].

As expected, several mesenchymal genes are downregulated during endothelial lineage differentiation of pMSCs. Other upregulated mesenchymal genes (such as *HGF, CD44* and *NT5E*), with known functions in migration, proliferation, and angiogenesis, may contribute to the endothelial function of differentiated pMSCs.

6.5.2.2 Endothelial Markers and Function

During endothelial differentiation, early endothelial progenitor cells express CD34 and VEGFR2 (*KDR*)[693]. *KDR* (VEGFR2) gene expression was significantly increased with differentiation medium after 11 days. The expression of *FLT1* (VEGFR1), another VEGF receptor, was significantly increased in pMSCs cultured in differentiation medium after 11, 18 and 25 days, via RT-qPCRs. Increased gene expression of *FLT1* in response to differentiation medium occurs even after 72 hours of culture, as observed in the static devices used in the low flow/shear stress experiments. However, the gene expression increases in *KDR*, and to a lesser extent, *FLT1,* are less apparent after 11 days, suggesting dedifferentiation, with the cells reverting to an MSC phenotype. At the protein level, VEGFR1 was increased in pMSCs cultured in differentiation medium after 25 days, in immunocytochemistry. Albeit low sample numbers, trends towards increases in VEGFR1 were observed in flow cytometry, and VEGFR2 was significantly increased in at day 14. Taken with the immunocytochemistry data, this suggests that longer time in culture is needed for protein levels to reflect changes in gene expression. These findings are in line with previous studies that have shown increases in *FLT1* and *KDR* in pMSCs cultured in endothelial differentiation medium after only 24 hours of exposure[653]. In contrast, Du *et al*. (2016) observed trends towards decreases in *FLT1* gene expression in pMSCs cultured in EGM-MV2 with 50 ng/mL VEGF after 14 days[643]. This study seeded the pMSCs onto a coating of Matrigel prior to differentiation, which could explain differences in results. Moreover, the source of pMSCs were supplied by the Cell Products of National Engineering Research Centre, therefore it is unclear how the pMSCs were isolated. In the PCR array, the

early endothelial marker, *CD34*, was not altered in pMSCs cultured in differentiation medium.

As ECs differentiate into mature ECs, the expression of vWF, CD31 (*PECAM1*) and VE-Cadherin (*CDH5*) are increased[693]. A significant increase in *PECAM1* was observed in pMSCs treated in differentiation medium for 11 days, although lower than expression in HUVECs. Increased gene expression of *PECAM1* in response to differentiation medium occurs even after 72 hours of culture (although not significant), as observed in the static devices used in the low flow/shear stress experiments. In contrast, *VWF* gene expression was not altered by differentiation medium at 11, 18 or 25 days. However, in the low 1 µL/min shear stress experiments, VWF was increased in pMSCs cultured in control medium with low shear stress and in differentiation medium under static conditions, compared to control medium under static conditions. This suggests that the differentiation medium could influence *VWF* gene expression following acute exposure (~72 hours), but not longer time periods (~11 days). At the protein level, CD31 and vWF were not detected in pMSCs treated with differentiation medium. *CDH5* was also assessed in the PCR array but was not altered by differentiation medium.

Several studies have reported increased mature EC markers in MSCs exposed to endothelial differentiation medium from other sources, such as BMSCs[386,658,659]. In MSCs from placental tissue, Konig *et al*. (2015)[657] and (2011) [656], observed no expression of vWF in immunocytochemistry in chorionic blood vessel pMSCs and avascular amnion MSCs, respectively, after 10 days of culture in differentiation medium, even when VEGF supplementation was increased to 100 ng/mL[656]. Du *et al.* (2016) assessed endothelial differentiation in pMSCs, BMSCs, Umbilical Cord (UMSCs) and adipose tissue (AMSCs) cultured in endothelial growth medium (EGM2-MV) with 50 ng/mL VEGF for 14 days[643]. There were increases in *PECAM1, CD34, VWF* and *CDH5* in pMSCs, but these did not reach statistical significance. The mRNA levels were also not compared to a positive mature EC control. Similarly, to the present findings, a very weak expression of vWF and CD31 were observed in endothelial-differentiated MSCs from all tissues in immunocytochemistry. Taken with the present findings, this suggests that mature EC markers, CD31 (*PECAM1*) and vWF can be altered at the gene but not protein level in the utilised pMSC models.

A recent study by Yu *et al*. (2021) investigated the endothelial differentiation potential of placental chorionic villous MSCs from both third trimester and term placentae, using medium containing VEGF and IGF-1 (at the same level as the current study). pMSCs from first trimester placentae displayed an endothelial-like morphology, had higher

CD31 and vWF expression (flow cytometry and immunocytochemistry) and had a greater tube formation ability than MSCs from term placentae[660]. Moreover, Boss *et al*. (2020) found that term pMSCs did not express VEGFR2 (*KDR*) but a small population of first trimester pMSCs expressed this marker, which was slightly higher when cultured in EGM-2 than DMEM/F12 (49.6% vs 34.2%)[649]. This is in line with the present findings, where VEGFR2 expression was low in flow cytometry, RT-qPCRs, and immunocytochemistry in pMSCs cultured in control medium but did increase with differentiation medium. These studies suggest that first trimester pMSCs have a greater ability differentiate into ECs and could explain the lack of mature EC markers in the present study. Thus, the use of first trimester pMSCs as a model should be investigated.

6.5.2.2.1 Shear stress

Shear stress may also increase mature EC markers in pMSCs. Wu *et al*. (2008) showed that VWF and CD31 protein expression (immunocytochemistry and Western blots) were only increased when pMSCs were exposed to differentiation medium (containing 20% EGM-2 and 50 ng/mL VEGF) in combination with 12 dyn/cm^2 shear stress[653]. At the gene level, increases in *VWF* and *PECAM1* (CD31) were also observed when cells were treated with differentiation medium and 6 dyn/cm^2 shear stress, however greater increases were observed with 12 dyn/cm^2. Interestingly, the combination of differentiation medium and 1 µL/min low shear stress in the present study, did not further increase *PECAM1* or *VWF* gene expression. The findings by Wu *et al*. suggests that a higher shear stress is needed to elicit these effects and observe changes in protein expression of mature EC markers, as the low shear stress exhibited by the 1 µL/min flow in the devices used is ~0.1 dyn/cm^2. Similar studies have investigated the impact of shear stress in other types of MSCs, such as adipose, amniotic fluid and bone marrow derived. In these studies, shear stress levels between 2.5-20 dyn/cm^2 results in increased EC markers, including CD31, VWF and VE-Cadherin at the protein and/or gene level (Table 6.2).

The greater effect elicited by these higher shear stress levels is likely because this is within the range of physiological shear stress, as ECs are exposed to hemodynamic forces due to the pulsatile characteristics of blood flow and pressure[653]. However, to appropriately model vascular development in the placenta, a shear stress that recapitulates the levels in the placental blood vessels would be needed. Limited studies have assessed the flow rate and shear stress levels in fetoplacental capillaries. Research by Tun *et al.* (2019) developed an anatomically based computational model of the placental vasculature, including macro-level vessels and their interaction with a

capillary structure. This model predicted that the flow rate in the fetoplacental capillaries in normal pregnancies, the flow is ~0.13 µL/min with a shear stress of 0.5 dyn/cm^2 (0.05 Pa)[119]. Therefore, the present model, which elicits a shear stress of ~0.1 dyn/cm^2 more closely recapitulates the shear stress in placental blood vessels than previous studies utilising 2.5-20 dyn/cm^2.

It is also important to note that the culture of cells in microfluidic devices, as utilised in the current study, has limitations. In cells cultured in devices under static conditions medium was only replenished to control or differentiation medium once the cells had attached. Whereas cells cultured in devices under 1 µL/min flow would have had a more constant replenishment of medium, thus a greater supply of nutrients and removal waste products, which may influence cell function[730]. Moreover, the replenishment of medium in the static control conditions will also have induced a gravity flow of medium across the cells, which would elicit some shear stress. Finally, the process of removing the cells from the microfluidic devices, prior to RNA isolation and the endothelial tube formation assay, can be stressful for the cells and could influence gene expression and functional measurements. Although, the static control conditions were also cultured in microfluidic devices, so all conditions would have experienced the same 'stress' when removing from devices.

Overall, the ability for MSCs to differentiate into mature ECs, expressing CD31 and VWF, using endothelial growth factors appears to be dependent on the tissue of origin, or the exposure to high shear stress. In pMSCs specifically, expression of VWF and CD31 appears only to be increased in cells isolated from first trimester placentae or under high shear stress conditions (12 dynes/cm^2).

6.5.2.2.2 Endothelial function

Although endothelial lineage differentiation with biochemical stimulation was observed at early timepoints (72 hours and ~11 days) and dedifferentiation was observed at later timepoints (up to 25 days), increased endothelial tube formation and angiogenic sprouting were observed after 21 days. This is similar to findings by Fischer *et al.* (2009) in human AMSCs, where endothelial growth supplement increased the endothelial-tube formation abilities of the cells, but did not increase expression of *VWF, PECAM1* or *NOS3* (eNOS) in RT-qPCRs[662]. Moreover, Zhang *et al.* (2009) observed increases in endothelial tube formation when amniotic fluid derived MSCs were cultured in EGM-2 for 2 weeks under static conditions[668].

This increase in endothelial tube formation is not observed when pMSCs are exposed to differentiation medium for shorter periods of time, for example when pMSCs were

cultured in devices under static conditions with differentiation medium for 72 hours. However, the combination of differentiation medium and low shear stress significantly increased the number of endothelial tubes. Similarly, Wu *et al*. (2008) observed very few endothelial tube-like structures in pMSCs treated with differentiation medium under static conditions for 4 days, and more distinct tubes were formed when in combination with 12 dyn/cm^2 shear stress[653]. Taken with findings by Zhang *et al.* and Wu *et al*., the current data suggests that under static conditions a longer period of culture in differentiation medium is required for endothelial tube formation, whereas shear stress can elicit these effects after 24-72 hours exposure.

6.5.3 Potential mechanisms of pMSC differentiation

6.5.3.1 Signalling by growth factors (VEGF and IGF-1)

Differentiation medium used included 50 ng/mL VEGF to induce pMSCs down the endothelial lineage. VEGF is one of the main regulators of vasculogenesis and angiogenesis and acts via VEGF receptors (VEGFRs), including VEGFR1 (*FLT1*) and VEGFR2 (*KDR*), which are known to be important for early placental vascular development[85,87,671,672]. VEGFR2 knockout mice models have demonstrated the role of VEGFR2 in the recruitment and differentiation of haemangiogenic stem cells into fetoplacental capillaries[87,671]. Whereas, VEGFR1 knockout in mice results in disorganised vasculature, and abnormal vascular channel formation[672], suggesting VEGFR1 is important for the organisation of embryonic vasculature, where early ECs form endothelial tubes[85,672]. VEGFR1 is thought to activate PI3K-Akt pathways, involved in cell survival, and other pathways associated with vascular permeability and cell migration[698]. VEGFR2 activates several downstream signalling pathways, including P13K-Akt pathways, which influence cell proliferation, survival, migration and permeability, all of which result in the regulation of angiogenesis[731]. VEGFR2 is also known to activate eNOS, which regulates endothelial function by influencing vascular tone, EC permeability and proliferation, as well as being an essential mediator of VEGFA-induced angiogenesis[732]. Similarly, VEGF induced endothelial differentiation of MSCs, is known to increase eNOS[668,733]. The eNOS signalling pathway also contributes to endothelial dysfunction in response to high glucose and in GDM[183,184,262]. Moreover, VEGFR2 mRNA and protein has been reported to be decreased in placentae from women with GDM[124], suggesting that diabetes and glucose may also impact VEGFR/eNOS signalling mechanisms during placental endothelial differentiation.

High levels of shear stress (12 dyn/cm^2) are also thought to induce VEGFR2 tyrosine kinase phosphorylation and clustering of the receptor[653], which was found to be

dependent on integrin activation by shear stress[734]. Integrins here act upstream of VEGFR2, which differs from the biochemical stimulation of VEGFR2 by VEGF, where its subsequently activates integrins[735]. In both cases, the activation of VEGFR2 and integrins would result in tyrosine phosphorylation and cytoskeleton remodelling, which may result in the functional changes observed in the present study[653]. Shear stress can also result in activation of the PI3K-Akt pathway, which phosphorylates eNOS and results in increased NO production. Longer exposure to shear stress can increase eNOS expression in ECs[736].

Differentiation medium used also included 20 ng/mL IGF-1, which binds the IGF-1 receptor (IGF1R). The IGF system regulates cell growth, differentiation, migration, and survival[737]. Interestingly, many components of the IGF system are dysregulated in pregnancies complicated by maternal diabetes[285–287], which have been linked to placental vascular dysfunction[288]. In pMSCs, IGF-1 supplemented into muscle differentiation medium reduced markers of multi-potency, SRY (sex determining region Y)-box 2 (SOX2) and Homeobox protein Nanog (Nanog), and increased Paired box gene (Pax) 3 and 7 levels and the muscle-specific differentiation marker, myoblast determination protein 1 (MyoD), suggesting an increased commitment to pMSCs of the muscle lineage[737]. This suggests that the IGF-1 in the differentiation medium may influence lineage commitment in pMSCs. Moreover, Lin *et al*. utilised co-cultured ECs and adipose derived MSCs which form microvessels and found that IGF-1 exposure promoted angiogenesis in this model, and increased gene expression of angiogenic growth factors, such as VEGF-A and FGF-1 in ECs and adipose derived MSCs. These findings indicate that IGF can regulate angiogenesis and gene expression in ECs and MSCs[738].

To further investigate the mechanisms, expression levels of proteins related to the downstream signalling pathways associated with VEGF signalling (including eNOS) and IGF signalling, could be investigated, such as phosphorylated/total levels of proteins using Western blots.

6.5.3.2 Mechanosensitive signalling via Piezo1

The Ca^{2+}-permeable non-selective cation channel, Piezo1, is known to respond to shear stress in a variety of ECs. Shear stress exerted by blood flow is known to activate Piezo1 and increase NO release, thus regulating vasodilation[120]. Morley *et al*. (2018) showed that Piezo1 is expressed in FpECs and Piezo1 siRNA supressed cell alignment under shear stress conditions[639]. The role of this channel in human embryonic and placental vascular development has also been explored. Li *et al*. (2014)

demonstrated the role of this channel in human embryonic and placental vascular development. In mice with a disrupted endogenous Piezo1 gene, pups that inherited a global or an endothelial-specific knockout were embryonically lethal, mid-gestation and had reduced vascularisation in the yolk sacs[739]. In other tissues, Piezo1 has also been shown to influence the differentiation of stem cells. For example, in human neural stem cells, Piezo1 knockdown by siRNA supressed differentiation into neurons, and increased differentiation into astrocytes[740]. Moreover, loss of Piezo1 in MSCs or osteoblast progenitor cells inhibits osteoblast differentiation[741]. The role of Piezo1 in stem cell differentiation is thought to be associated with its ability to increase Ca^{2+} influx, as Ca^{2+} is an important second messenger in determining cell fate decisions[742]. In the present study, *PIEZO1* was increased in pMSCs cultured under low shear stress conditions. Although, given that the most significant increases in endothelial lineage differentiation were observed in static experiments, and not with the combination of differentiation medium and low shear stress (where *PIEZO1* expression was the highest), signalling by Piezo1 is likely not the mechanism behind endothelial lineage differentiation in pMSCs.

6.5.3.3 Endothelial to mesenchymal transition (EndMT)

In the PCR array, many genes known to regulate endothelial/epithelial-mesenchymal transition were altered (*MMP2, MMP9, PI3KR1, BMP2* and *WNT11*). Given that EndMT is a process where ECs lose their characteristics and acquire mesenchymal traits[594], genes that regulate this process may also regulate endothelial differentiation of MSCs (the reverse process). For example, MMPs are proteolytic enzymes that degrade the ECM[743] and altered ECM composition is known to contribute to EndMT[744]. *PIK3R1* (Phosphatidylinositol 3-kinase regulatory subunit 1) and *WNT11* (Wnt Family Member 11) were downregulated in endothelial differentiated pMSCs, and interestingly, Wnt and PI3K/mTOR signalling pathways initiate mesenchymal transition in EndMT[745]. Additionally, bone morphogenic proteins (BMPs) promote endothelial specification, venous differentiation, angiogenesis and mediating shear and oxidative stress[746]. BMP2 and BMP4 have been shown to induce EndMT[747,748], through activation of the ALK2 receptor[749].

The dysregulation of EndMT in the placenta could result in vascular regression, immaturity and hypovascularisation[595], which has been reported in GDM[122,132]. Moreover, in Chapter 3, mild hyperglycaemia (7 mM glucose) associated with LGA in GDM was predicted to reduce vasculogenesis and angiogenesis, hence vascular immaturity, with alterations in several mesenchymal, endothelial and EndMT genes

(e.g. *CDH2, CD44, PECAM1, MMP1, MMP10* and *MMP11*), which were also explored in the present model. Thus, this further warrants the use of the pMSC to endothelial differentiation model to investigate the impact of maternal glucose fluctuations in GDM and LGA on placental vascular development.

6.6 Summary

- pMSCs were successfully isolated from term placentae. Characterisation of pMSCs showed that they express MSC markers, CD90, CD73, CD105 and CD44.
- pMSCs induced towards cells of the endothelial lineage using biochemical stimulation (differentiation medium containing EGM-2 and VEGF-A) had increased gene expression of VEGFRs (*FLT1* and *KDR*) and *PECAM1* and increased protein expression of VEGFRs.
- pMSCs cultured in differentiation medium were also able to form endothelial tubes and angiogenic sprouts, as observed with the mature EC cell line, HUVECs.
- Low shear stress increased expression of some endothelial markers (e.g. VWF) and increased endothelial tube formation, however the combination of low shear stress and differentiation medium did not further increase endothelial lineage differentiation of pMSCs.
- The ability for pMSCs to adopt an endothelial-lineage phenotype renders them a suitable model for investigating placental vascular development, which will be employed in Chapter 7.

Chapter 7 – The impact of physiological maternal glucose fluctuations on placental vascular development

7.1 Introduction

Reports from previous studies have demonstrated that GDM is associated with placental vascular lesions, villous immaturity, and altered vascularisation, including hyper- and hypo- vascularisation, or a combination of both[122,125,129,130,132]. These alterations in placental vasculature have been linked to glycaemic control, with Calderon *et al*. (2007) reporting hypervascularisation in mild hyperglycaemic placentae and hypovascularisation in GDM and overt diabetic placentae[132], which suggests that the degree of hyperglycaemia could influence how the placental vasculature develops. Placental vascular dysfunction impacts on the organ's ability to transfer nutrients, including glucose, to the fetus, which in turn could influence fetal growth[750]. Hence, the contrasting findings on hyper- and hypo- vascularisation may also explain why some infants are born LGA and some SGA. Moreover, temporal periods of mild hyperglycaemia associated with LGA in GDM, in Chapter 3, altered placental genes associated with vascular development. Thus, it is hypothesised that fluctuations in maternal glucose can impair placental vascular development, leading to pathological growth in GDM. The findings of Chapter 6 revealed that pMSCs can differentiate towards cells of the endothelial lineage, with the greatest increases in EC marker expression and endothelial function elicited using biochemical stimulation under static conditions. This model can therefore be utilised to investigate endothelial differentiation during placental vascular development. Additionally, the triculture placental microvasculature model, developed by Cherubini and Haase *et al.* (2023), incorporates HUVECs, HPPs and HPFs into a microfluidic device and generates perfusable microvessels over 7-days. Thus, the development of the microvessels can be used as a model of placental vasculogenesis[348,362], allowing investigation into vessel morphology and vessel function (i.e. permeability). Therefore, both the pMSC model and the triculture model were employed to investigate the impact of physiological maternal glucose fluctuations in GDM LGA pregnancies on placental vascular development.

7.2 Hypothesis

Physiological maternal glucose fluctuations in GDM alter placental vascular development and function, which could lead to LGA.

7.3 Aims

To determine whether physiological maternal glucose fluctuations impact placental vascular development and function using:

1. pMSCs differentiating into cells of the endothelial lineage under static conditions using growth factors;
2. A triculture model of placental microvasculature.

7.4 Results

7.4.1 Impact of glucose fluctuations on differentiation of pMSC towards cells of the endothelial lineage

7.4.1.1 Modelling maternal glucose fluctuations in the pMSC model

pMSCs (n=6) were cultured in either control medium (~5.5 mM glucose) or endothelial differentiation medium (EGM-2 + 50 ng/mL VEGF-A) containing 5.6, 7 or 9 mM glucose. These physiological concentrations were used to mimic normoglycaemia in GDM AGA, mild hyperglycaemia in GDM LGA and hyperglycaemia in GDM with poor glucose control[14,62,751,752], respectively. Additionally, a hyperosmolar control of 5.6 mM glucose with 3.4 mM D-mannitol was used, referred to as the mannitol control (3.4 mM). Medium was refreshed daily to maintain glucose levels.

To determine if the concentration of glucose in the medium and the frequency of medium changes were suitable for modelling physiological glucose levels in pMSCs, glucose and osmolality were assessed in conditioned medium at days 1, 4, 7 and 11 (n=6; Figure 7.1).

In the differentiation medium, input concentrations of 5.6 mM glucose remained stable within normoglycaemic levels between 5.85±0.17 and 5.0±0.25 mM, during the first 4 days of culture. By day 7 and 11, levels dropped to 2.83±0.52 and 2.89±0.34 mM, respectively. However, medium was refreshed daily to maintain glucose levels, therefore the pMSCs would not have been exposed to low glucose levels for prolonged periods of time. Input concentrations of 7 mM glucose were within mild hyperglycaemic levels between 7.39±0.13 and 6.40±0.28 mM, during the first 4 days of culture. By day 7 and 11, glucose declined to normoglycaemic levels of 4.37±0.68 and 5.88±0.31 mM, respectively. Input concentrations of 9 mM glucose were within hyperglycaemic levels between 8.94±0.36 and 8.29±0.31 mM, during the first 4 days of culture and declined to mild hyperglycaemic levels of 6.49±0.63 and 7.44±0.37 mM at day 7 and 11,

respectively. However, during daily medium refreshments, glucose will have been replenished back to mild hyperglycaemic levels in the 7 mM condition and hyperglycaemic levels in the 9 mM condition (Figure 7.1A).

Glucose concentrations within the control medium (pMSC medium; undifferentiated cells) and in the mannitol control showed very similar patterns to the 5.6 mM condition, with levels between 5.32±0.11- 2.32±0.38 and 5.73±0.15-3.12±0.53 mM, respectively. There was no change in the osmolality across the culture period in cells cultured in differentiation medium (5.6, 7, 9 mM or mannitol control) (Figure 7.1B). Interestingly, the osmolality of the control medium was higher at all timepoints than all other conditions ($p<0.001$-0.05, n=6). This was apparent from day 0, where control medium had a significantly higher osmolality (311.67±1.23 mOsm/kg) than differentiation medium with 5.6 mM glucose (287.0±2.62 mOsm/kg; $p<0.01$), 7 mM glucose (272.50±4.88 mOsm/kg; $p<0.01$), 9 mM glucose (280.50±2.10 mOsm/kg; $p<0.05$) and in the mannitol control (278.33±1.78 mOsm/kg; $p<0.01$, n=6) (Figure 7.1B). The control medium is the standard culture medium for pMSCs (DMEM Low Glucose) and therefore has a different composition to EGM-2 used as the differentiation medium, therefore likely explaining the differences in osmolality.

7.4.1.2 Morphology

Cells were imaged throughout culture to assess morphological differences (n=6). Consistent with data obtained in Chapter 6, pMSCs cultured in differentiation medium had lost their characteristic whirlpool morphology[360] by day 4 and clusters of smaller EC-like cells[650] were observed, which was also evident at day 11 (Figure 7.2). At day 7, prior to passage and further culture, the cells were at a higher confluence, therefore differences between control and differentiation medium were more difficult to distinguish. There were no observable differences in morphology between the glucose treatments. However, fewer cells were observed in pMSCs treated with differentiation medium containing 7 mM and 9 mM glucose compared to 5.6 mM at day 4 and 11 (Figure 7.2).

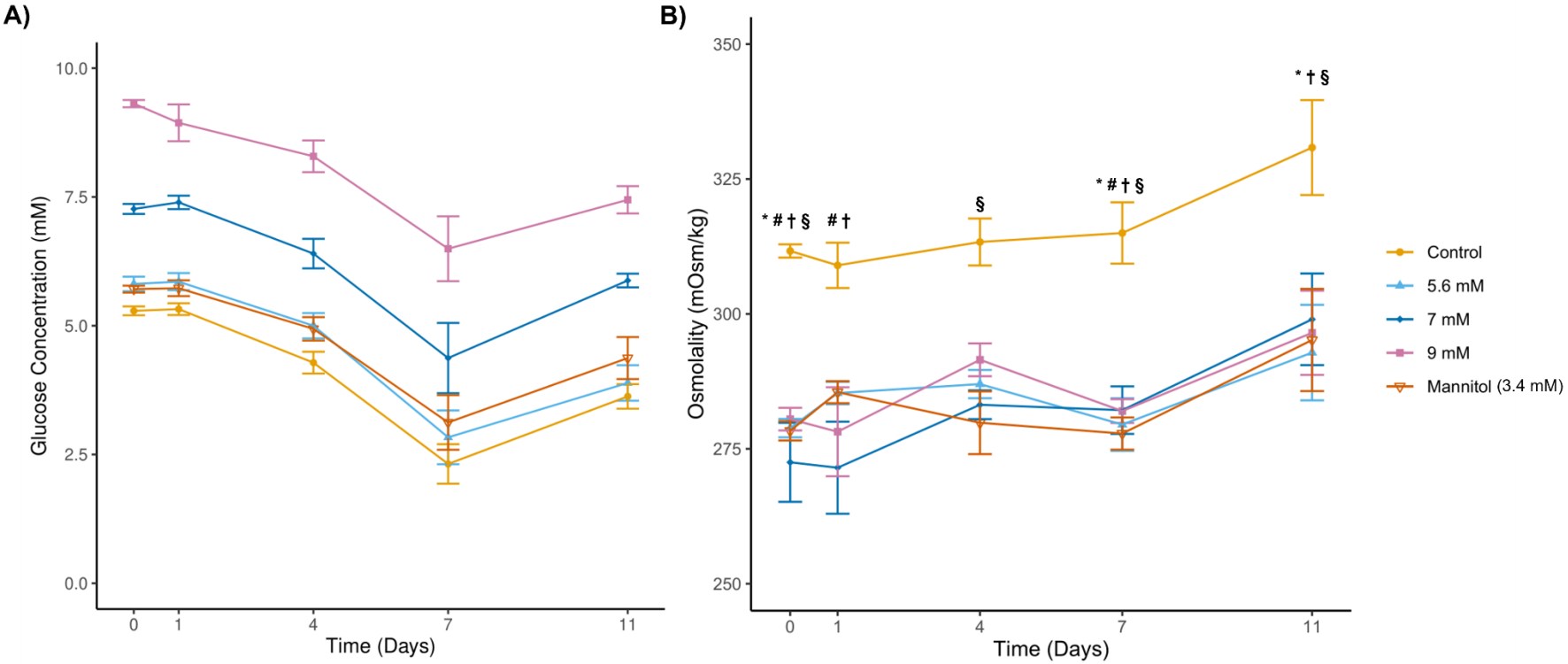

Figure 7.1 - Glucose treatments in pMSCs undergoing differentiation towards cells of the endothelial lineage. A) Glucose (mM) was assessed in culture medium of pMSCs cultured in control medium or differentiation medium (EGM-2 + VEGF-A) with glucose treatments at days 1, 4, 7 and 11 using a GlucCell Meter. Data is presented as the mean ± SEM (n=6). B) Osmolality was assessed in culture medium of pMSCs cultured in control medium or differentiation medium (EGM-2 + VEGF-A) with glucose treatments at days 1, 4, 7 and 11 using an Osmometer. Data is presented as the mean ± SEM (n=6). Differences in osmolality between each glucose concentration were assessed at each time point using a Two-Way ANOVA on log transformed data, * Control vs 5.6 mM, # Control vs 7 mM, † Control vs 9 mM, § Control vs Mannitol (3.4 mM), $p<0.001$-0.05.

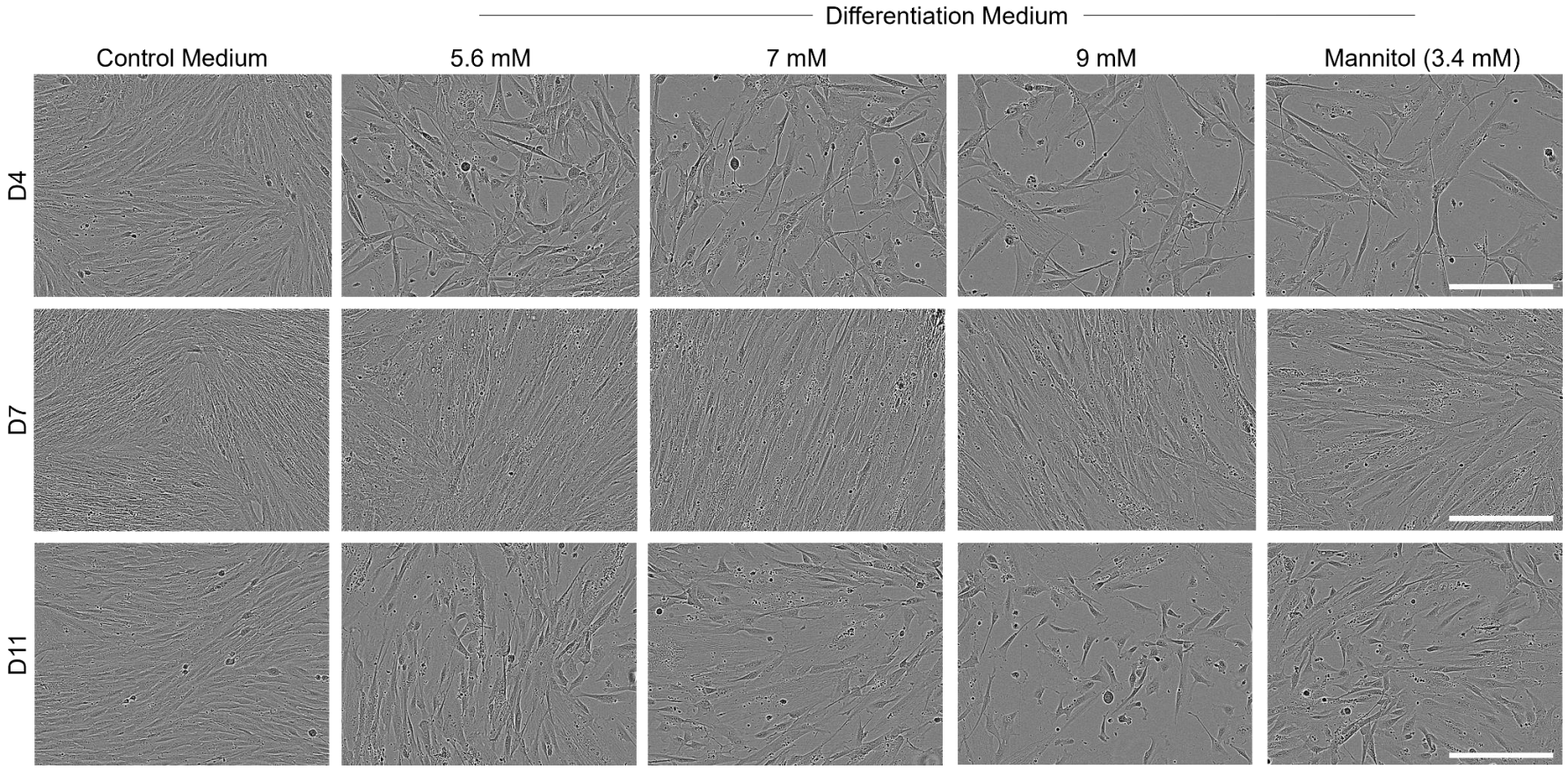

Figure 7.2 - Morphological differences in pMSCs treated with glucose whilst undergoing differentiation towards cells of the endothelial lineage. pMSCs were cultured in control or differentiation medium with glucose treatments for 11 days. Cells were imaged at days 4, 7 and 11. Morphological differences can be observed in pMSCs cultured in differentiation medium, where they have lost their whirlpool, spindle-like morphology, and clusters of smaller cells are present. No differences were observed in morphology between glucose treatments. Representative images (n=6). Images were taken on the Incucyte ZOOM at 10x magnification. Scale bars = 300 µm.

7.4.1.3 Expression of endothelial and mesenchymal genes

Consistent with data presented in Chapter 6, following culture for 11 days, there was an increase in endothelial lineage markers, *FLT1, KDR* and *PECAM1* and MSC markers (with known roles in endothelial function[675,676,696,728,729]) *CD44* and *NT5E*, in cells cultured in differentiation medium with 5.6 mM glucose, compared to control medium (n=6; Figure 7.3; Figure 7.4).

In pMSCs cultured in differentiation medium containing 9 mM glucose, expression of MSC and EC genes were similar to that in differentiation medium containing 5.6 mM glucose (Figure 7.3; Figure 7.4).

However, in pMSCs cultured in differentiation medium containing 7 mM glucose, there was a slight increase in MSC markers *CD44* and *NT5E* compared to those cultured in 5.6 mM glucose (198.81±14.57 vs 184.32±21.67, p=0.973 for *CD44* and 0.22±0.013 vs 0.20±0.010, p=0.923 for *NT5E;* n=6) (Figure 7.3). There was also a small increase in *KDR* and a small decrease in *FLT1* in differentiation medium containing 7 mM glucose compared to 5.6 mM (0.080 [0.035-0.59] vs 0.052 [0.02-0.64], p=0.501 for *KDR* and 0.33±0.044 vs 0.38±0.057, p=0.924 for *FLT1;* n=6) (Figure 7.4). Although these were not approaching significance.

7.4.1.4 Endothelial tube formation

Endothelial tube formation was assessed in pMSCs cultured in control medium or differentiation medium containing various glucose concentrations at day 7. In line with data presented in Chapter 6, there was an increase in endothelial tube formation in cells cultured in differentiation medium with 5.6 mM glucose, compared to control medium (n=6; Figure 7.5). In cells cultured in differentiation medium containing 7 mM glucose, there was a small decrease in the number of endothelial tubes (65.25±14.96) compared to 5.6 mM (72.83±13.70, p=1, n=6). In contrast, in cells cultured in differentiation medium containing 9 mM glucose, there was a small increase in the number of endothelial tubes (76.41±19.51) compared to 5.6 mM (72.83±13.70, p=1, n=6). However, there were no significant differences in tube formation (Figure 7.5B). Additionally, although it wasn't possible to quantify branching due to false positives using the angiogenesis analyser plugin, tubes appeared more well-defined in the 9 mM glucose condition, with greater branching in the 7 mM glucose condition and mannitol control (Figure 7.5A).

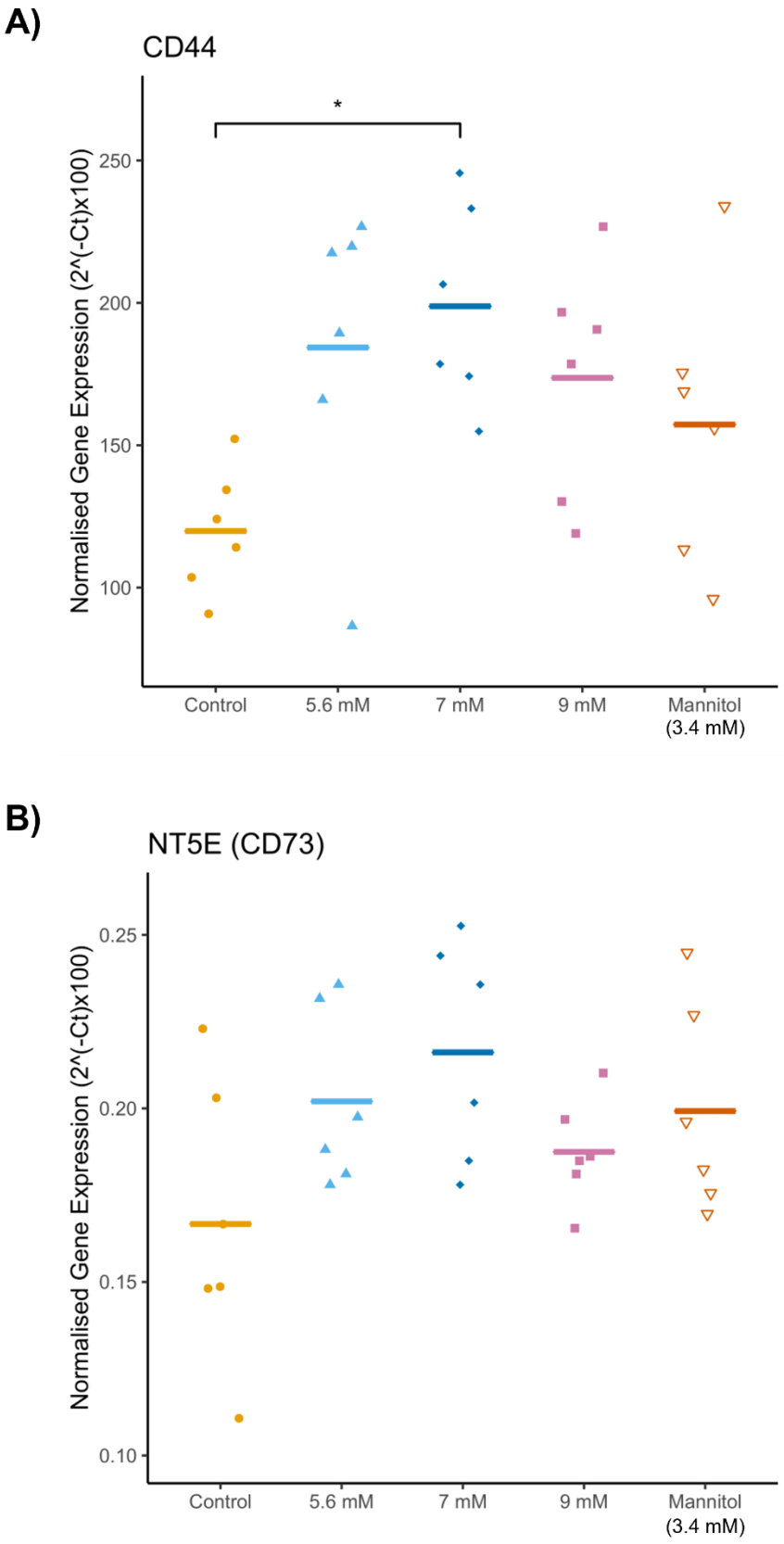
A)
CD44
*
Normalised Gene Expression (2^(-Ct)x100)
250
200
150
100
Control
5.6 mM
7 mM
9 mM
Mannitol
(3.4 mM)
B)
NT5E (CD73)
Normalised Gene Expression (2^(-Ct)x100)
0.25
0.20
0.15
0.10
Control
5.6 mM
7 mM
9 mM
Mannitol
(3.4 mM)

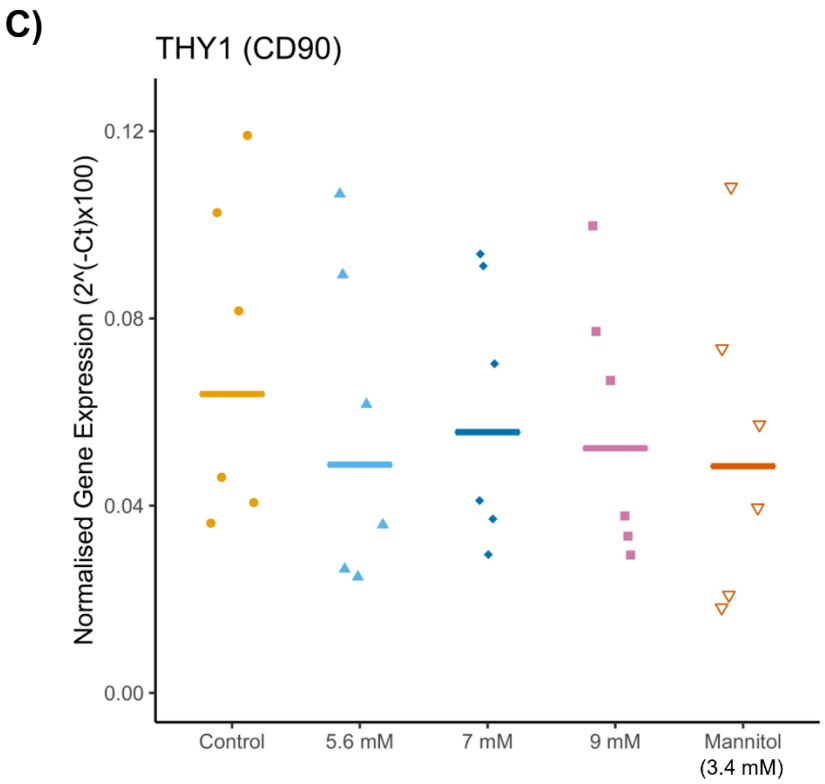

Figure 7.3 - Mesenchymal gene expression in pMSCs treated with glucose whilst undergoing differentiation towards cells of the endothelial lineage. Mesenchymal gene expression was assessed in pMSCs cultured in control or differentiation medium with glucose treatments for 11 days, using RT-qPCR. The expression of target genes was normalised to *YWHAZ* housekeeping gene expression. *THY1* is presented as the median, and statistical analysis was performed using a Kruskal-Wallis with a Dunn's post-hoc test. *CD44* and *NT5E* are presented as the mean, and statistical analysis was performed using a One-Way ANOVA with a Tukey's post-hoc test (Based on normal distribution of the data). Individual points represent each patient placenta. n=6. * $p<0.05$, ** $p<0.01$.

A)

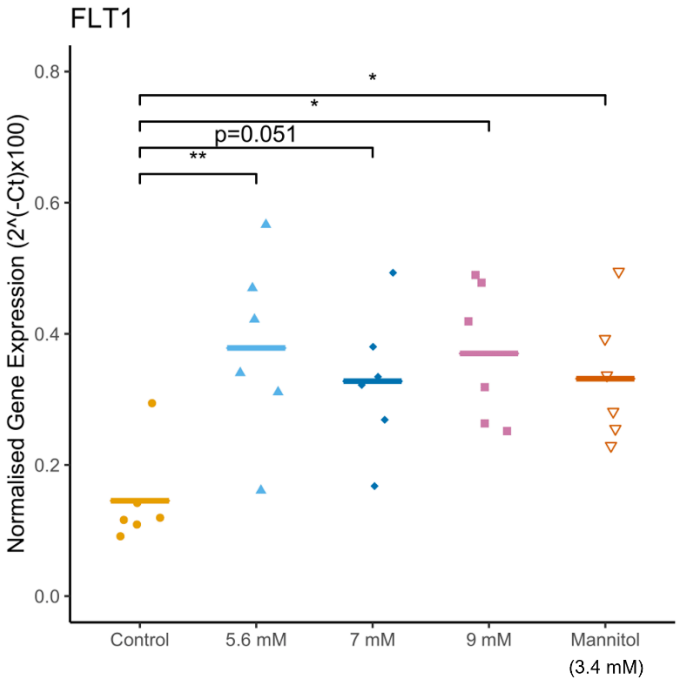
FLT1
Normalised Gene Expression (2^(-Ct)x100)
0.8
0.6
0.4
0.2
0.0
*
*
p=0.051
**
Control
5.6 mM
7 mM
9 mM
Mannitol
(3.4 mM)

B)

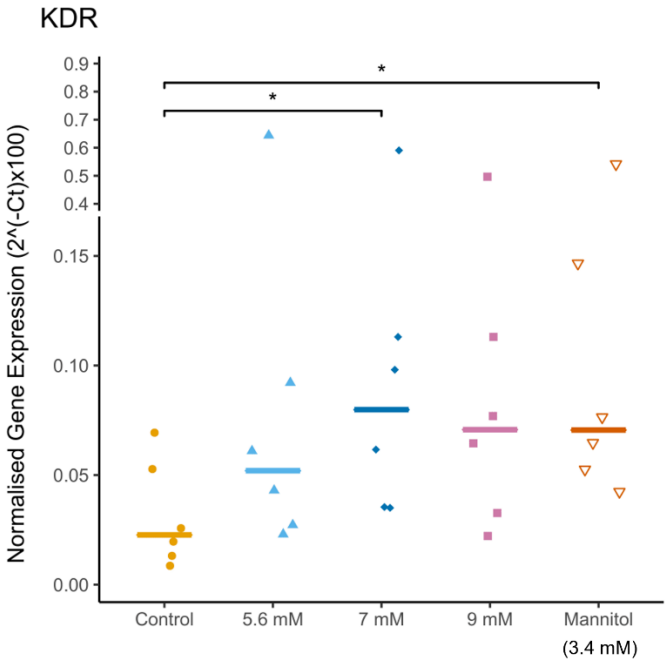
KDR
Normalised Gene Expression (2^(-Ct)x100)
0.9
0.8
0.7
0.6
0.5
0.4
0.15
0.10
0.05
0.00
*
*
Control
5.6 mM
7 mM
9 mM
Mannitol
(3.4 mM)

C)

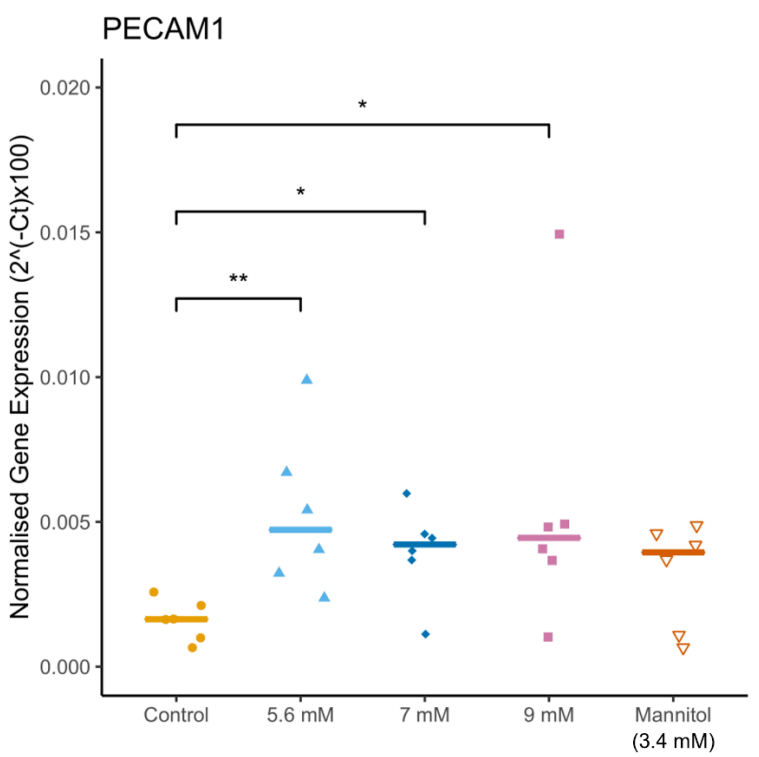
PECAM1
Normalised Gene Expression (2^(-Ct)x100)
0.020
0.015
0.010
0.005
0.000
*
*
**
Control
5.6 mM
7 mM
9 mM
Mannitol
(3.4 mM)

D)

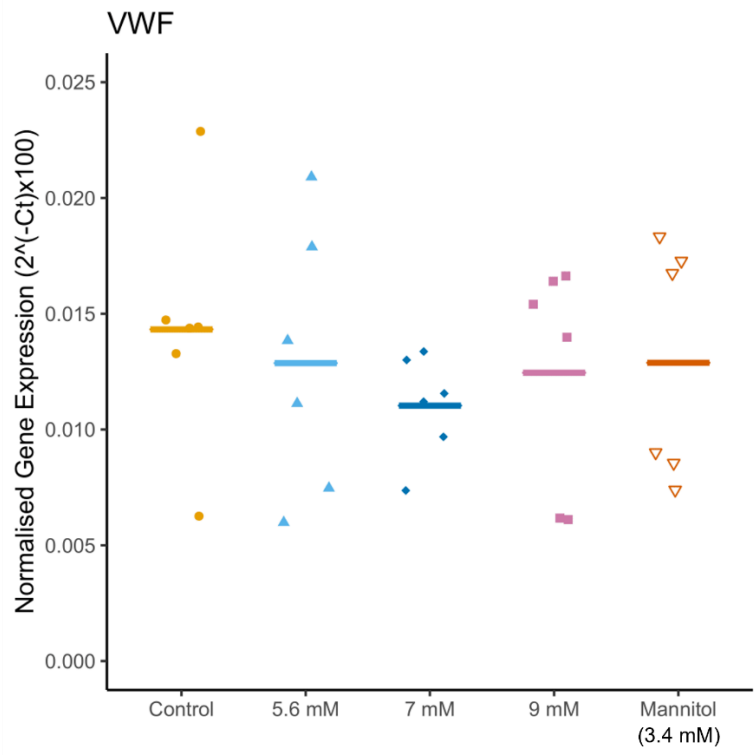
VWF
Normalised Gene Expression (2^(-Ct)x100)
0.025
0.020
0.015
0.010
0.005
0.000
Control
5.6 mM
7 mM
9 mM
Mannitol
(3.4 mM)

Figure 7.4 - Endothelial gene expression in pMSCs treated with glucose whilst undergoing differentiation towards cells of the endothelial lineage. Endothelial gene expression was assessed in pMSCs cultured in control or differentiation medium with glucose treatments for 11 days, using RT-qPCR. The expression of target genes was normalised to *YWHAZ* housekeeping gene expression. *KDR* and *PECAM1* are presented as the median, and statistical analysis was performed using a Kruskal-Wallis with a Dunn's post-hoc test. *FLT1* and *VWF* are presented as the mean, and statistical analysis was performed using a One-Way ANOVA with a Tukey's post-hoc test (Based on normal distribution of the data). Individual points represent each patient placenta. n=6. * $p<0.05$, ** $p<0.01$.

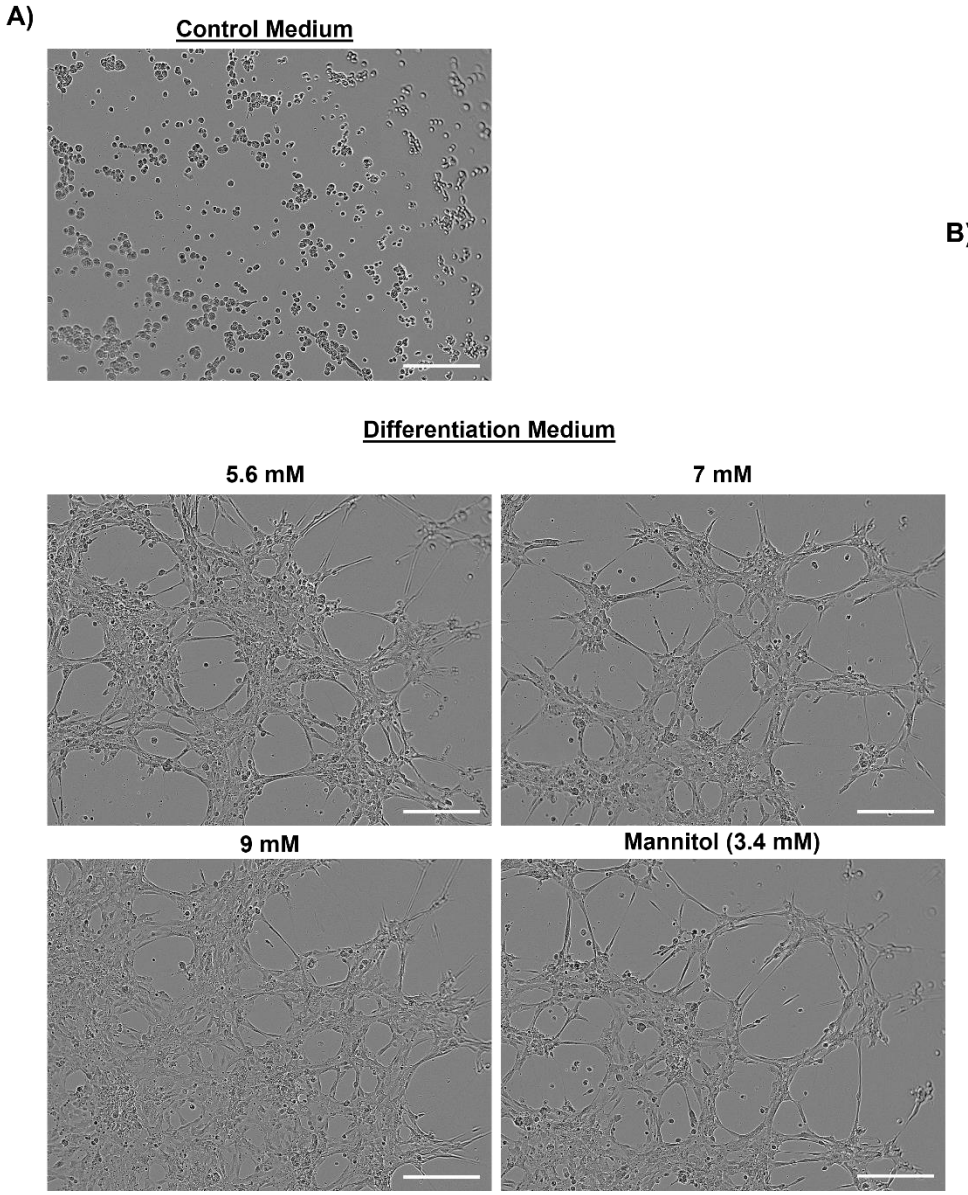
A)
Control Medium
Differentiation Medium
5.6 mM
7 mM
9 mM
Mannitol (3.4 mM)

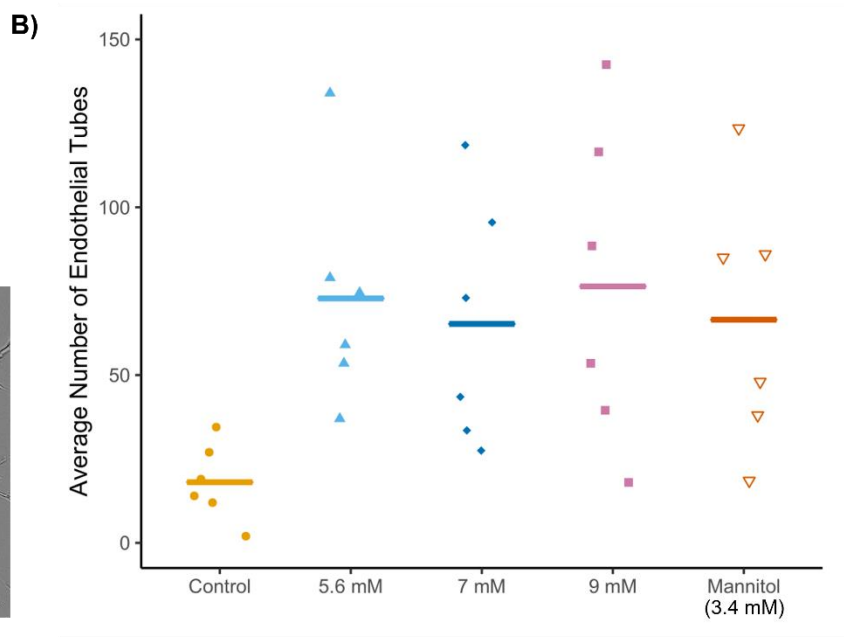
B)
Average Number of Endothelial Tubes
150
100
50
0
Control
5.6 mM
7 mM
9 mM
Mannitol
(3.4 mM)

Figure 7.5 - Endothelial tube formation assay of pMSCs cultured in control or differentiation medium with glucose treatments for 7 days. Cells were seeded onto ECM (10,000 cells per well of 96-well plate) after 7 days in control medium or differentiation medium with glucose treatments and incubated for 2 hours at 37°C. A) Images were taken on the Incucyte ZOOM at 10x magnification. Scale bars = 300 µm. B) The total number of tubes were manually counted using ImageJ. Data was normally distributed and is presented as the mean. Statistical analysis was performed using a One-Way ANOVA with a Tukey's post-hoc test. Individual points represent each patient placenta. n=6.

7.4.2 Ability of pMSCs isolated from patients with GDM to differentiate towards cells of the endothelial lineage

In addition to the impact of glucose on pMSCs differentiating into cells of the endothelial lineage, the impact of GDM was also assessed. pMSCs were isolated from a small number of GDM placentae (n=4) and cultured in control medium or differentiation medium (EGM-2 + 50 ng/mL VEGF-A) for a total of 11 days, with medium refreshments every 3-4 days. Cells were passaged on day 7. Findings were compared to those isolated from non-GDM placentae that were differentiated for 11 days (n=7).

7.4.2.1 Characterisation of GDM pMSCs

Characterisation of pMSCs isolated from GDM placentae, based on the ISCT criteria[670], demonstrated that the isolated cells contained pMSCs (Figure 7.6; Figure 7.7). In summary, in immunocytochemistry, GDM pMSCs expressed MSC markers, CD44, CD105 and CD73. GDM pMSCs also lacked expression of negative markers, CD14 and CD19, but did show some expression of the haematopoietic marker, CD34 (n=3, Figure 7.6). In flow cytometry, pMSCs expressed high levels of CD73 (99.31 [98.65-99.85] %), CD90 (98.115 [95.73-99.23] %) and CD105 91.03 [18.74-93.46]%), and lacked expression of the EC marker, CD31 (0.19 [0.07-1.58] %). The negative marker cocktail, which probed for CD45, CD34, CD11b, CD79A and HLA-DR was expressed in 22.72 [22.68-25.42] % of pMSCs (n=4, Figure 7.7). These immunohistochemical and flow cytometric findings are similar to those observed in pMSCs isolated from normal placentae (Chapter 6).

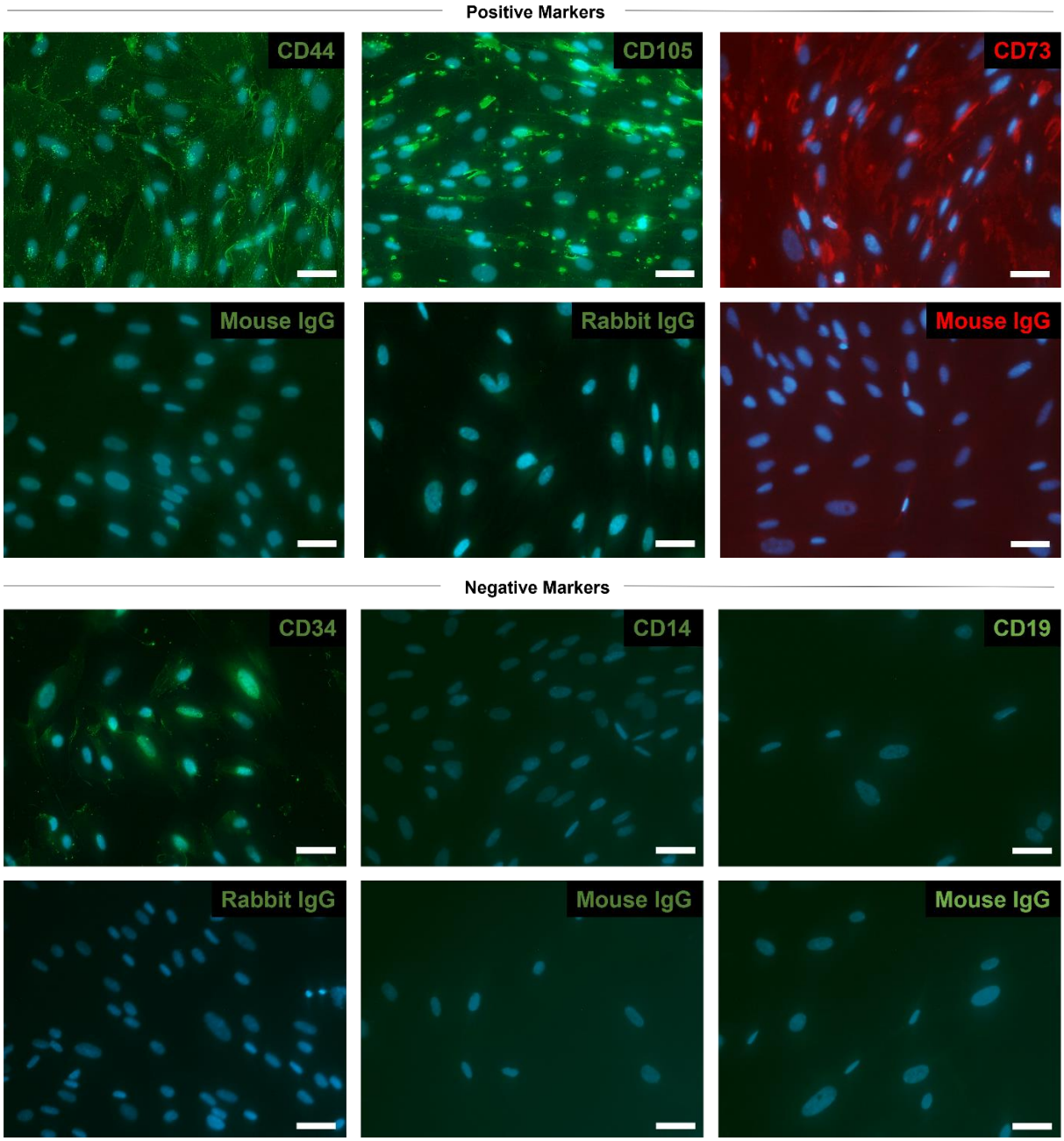

Figure 7.6 – Characterisation of GDM pMSCs by immunocytochemistry. pMSCs were isolated from term human placental tissue from GDM pregnancies. Immunocytochemistry was performed on cells at P3-P5 (n=3) using antibodies specific for positive MSC markers, CD44, CD105 and CD73 and negative MSC markers, CD34, CD19 and CD14, followed by mounting in media containing DAPI (blue). Bottom panels show cells incubated with control IgGs for the same species and concentration as the primary antibodies used in the top panel. Images were taken at 20x magnification using the Zeiss Axioscan.A1 microscope. Scale bars = 50 µm.

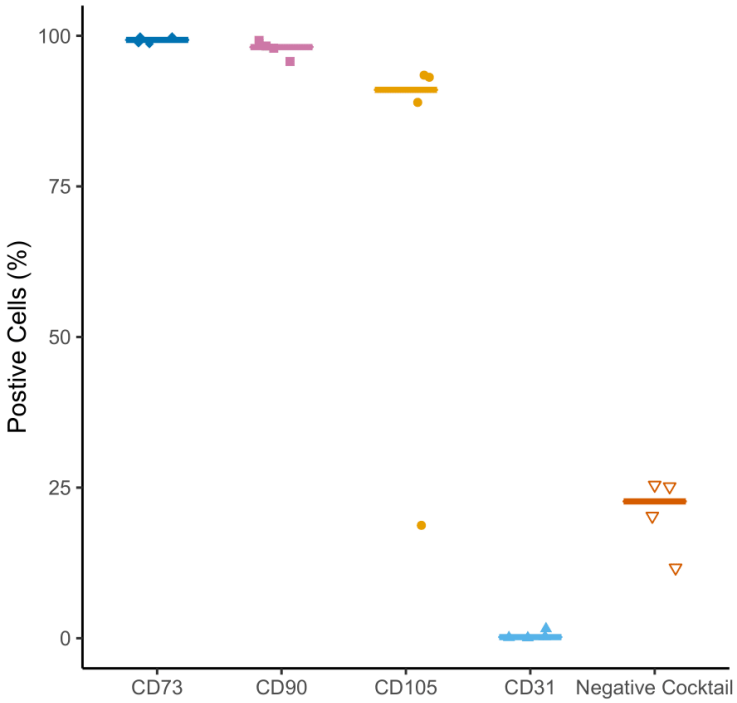

Figure 7.7 - GDM pMSC surface marker flow cytometric characterisation. Primary pMSCs were isolated from term placental tissue of GDM pregnancies, at P3 flow cytometry was used to determine the purity of each isolation by measuring the proportion of cells with surface marker proteins indicative of MSC identity (CD73, CD90, CD105) or contaminating cell types (Negative cocktail and CD31). The negative marker cocktail probed for CD45, CD34, CD11b, CD79A and HLA-DR. The percentage of positive cells for each marker was calculated. Data was not normally distributed and is presented as the median. Individual points represent each patient placenta. n=4.

7.4.2.2 Morphology

Cells were imaged throughout culture to assess morphological differences (n=4-7). As observed in Chapter 6 and in Section 7.4.1.2, pMSCs cultured in differentiation medium had lost their characteristic whirlpool morphology[360] by day 4 and clusters of smaller EC-like cells[650] were observed(Figure 7.8). At day 7 cells were at a higher confluence, therefore differences between control and differentiation medium were more difficult to distinguish. There were no observable differences in morphology between the GDM and non-GDM pMSCs.

7.4.2.3 Endothelial and mesenchymal gene expression

In pMSCs cultured in control medium (undifferentiated), expression levels of MSC markers, *NT5E* and *THY1,* and EC markers, *PECAM1, FLT1* and *KDR* were similar between those isolated from non-GDM and GDM placentae (Figure 7.9; Figure 7.10). The EC marker, *VWF*, however was lower in GDM pMSCs (0.029±0.0045, n=3) compared to non-GDM pMSCs (0.050±0.0098, n=7; Figure 7.10D) and the MSC marker, *CD44* was higher in GDM (343.41±38.91, n=4) compared to non-GDM pMSCs (206.30±29.20, n=7; Figure 7.9A), although these differences were not significant (p=0.376 for *VWF* and p=0.522 for *CD44*).

In pMSCs cultured in differentiation medium (differentiated towards cells of the endothelial lineage), trends showed that expression levels of MSC markers, *CD44* and *NT5E*, were higher in pMSCs isolated from GDM placentae (543.28±104.26 for *CD44* and 0.47±0.10 for *NT5E*, n=4) compared to those isolated from non-GDM placentae (340.89±79.09 for *CD44* and 0.23±0.031 for *NT5E*, n=7), which was approaching significance for *NT5E* (p=0.09) but less so for CD44 (p=0.208) (Figure 7.9A-B). In contrast, there were no differences between GDM and non-GDM differentiated pMSCs in expression of EC markers, except a slight reduction in *VWF* (0.024±0.0028 vs 0.034±0.0059) although this did not reach significance (p=0.803) (Figure 7.10).

7.4.2.4 Endothelial tube formation

Endothelial tube formation was assessed in pMSCs isolated from non-GDM and GDM placentae at 7 days. Both non-GDM and GDM pMSCs cultured in differentiation medium (differentiated towards cells of the endothelial lineage) were able to form endothelial tubes, which appeared more well-defined in GDM differentiated pMSCs (Figure 7.11A). There were a slightly higher number of endothelial tubes formed in differentiated GDM pMSCs (72.88±27.93, n=4) compared to non-GDM differentiated pMSCs (49.75±13.96, n=4) (Figure 7.11B). Although this was not significant (p=1), this

may be due to low n numbers. To further assess this, the relative fold change in the number of endothelial tubes with differentiation medium compared to control medium was calculated. The median fold change for GDM differentiated pMSCs was 41.83 [0.66-91] compared to 2.80 [0.94-40.5] in non-GDM differentiated pMSCs, although not significant (p=0.201), this further suggests increased endothelial tube formation in GDM differentiated pMSCs (Figure 7.11C).

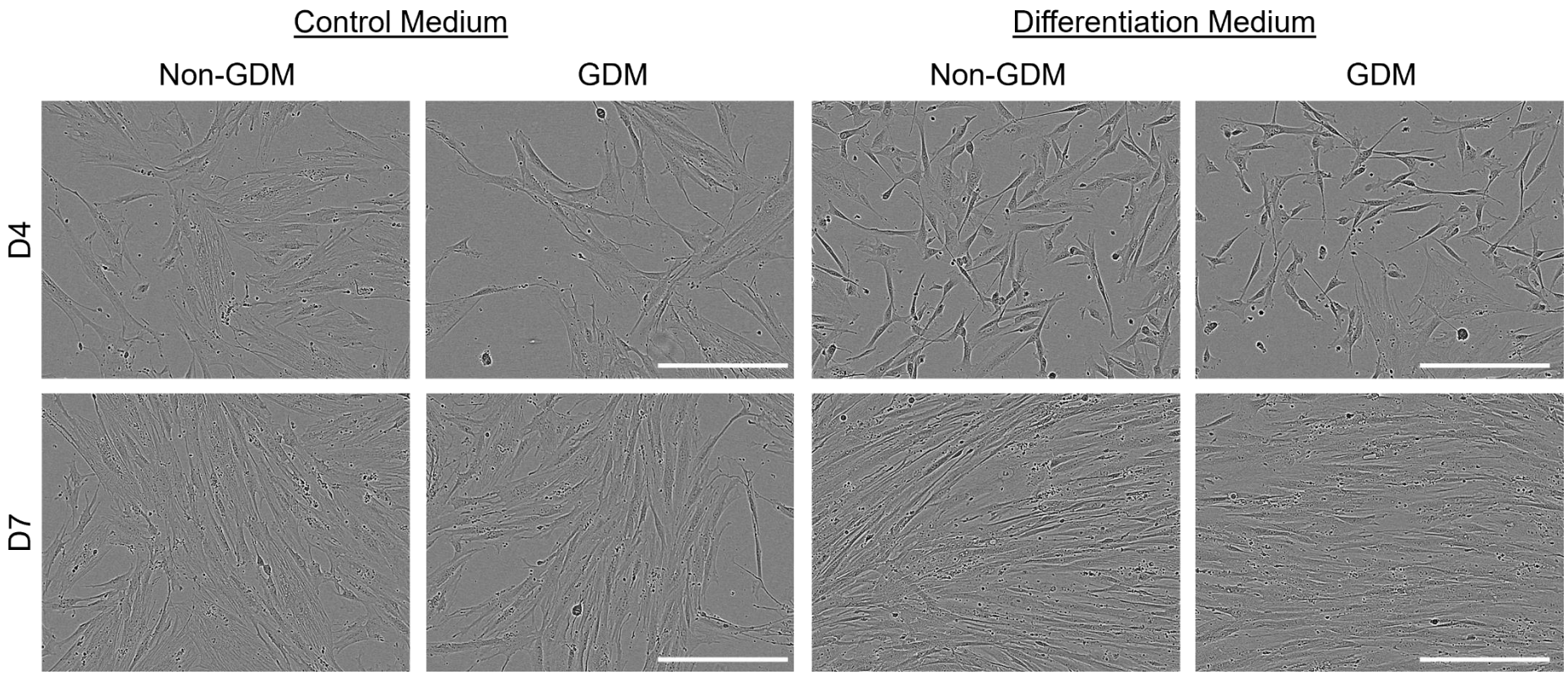

Figure 7.8 - Morphological differences in pMSCs from GDM and non-GDM pregnancies undergoing differentiation towards cells of the endothelial lineage. pMSCs isolated from GDM (n=4) and non-GDM (n=7) placentae were cultured in control or differentiation medium for 11 days. Cells were imaged at days 4 and 7. Morphological differences can be observed in pMSCs cultured in differentiation medium, where they have lost their whirlpool, spindle-like morphology, and clusters of smaller cells are present. No differences were observed in morphology between GDM and non-GDM placentae. Representative images (n=4). Images were taken on the Incucyte ZOOM at 10x magnification. Scale bars = 300 µm.

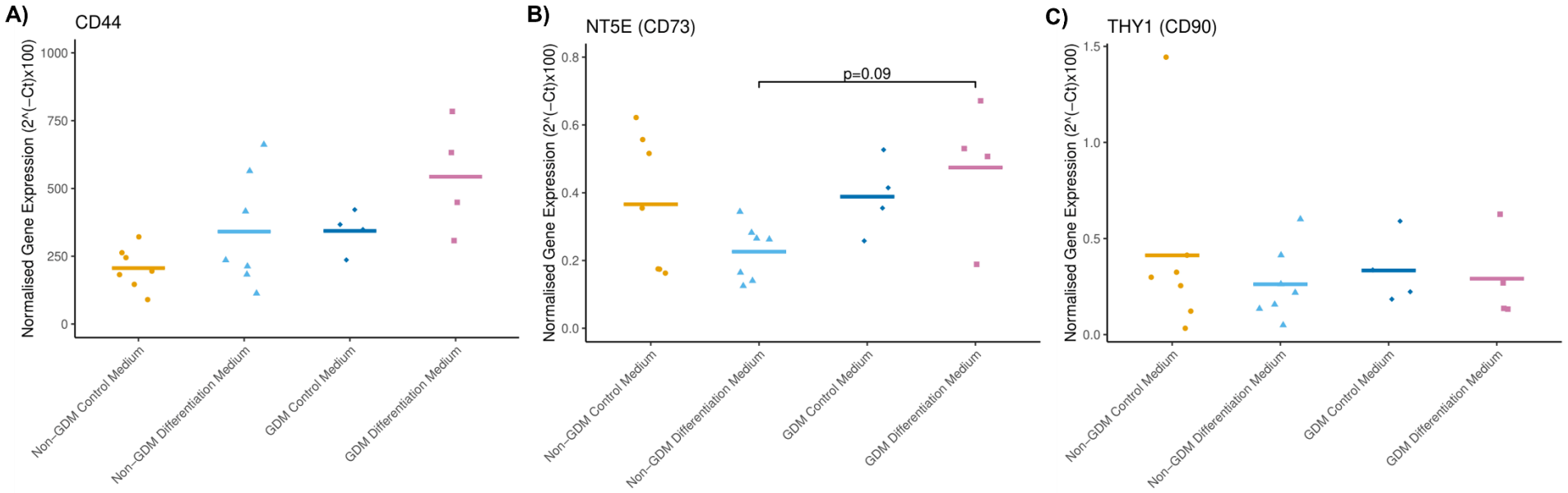

Figure 7.9 – Mesenchymal gene expression in pMSCs from GDM and non-GDM pregnancies undergoing differentiation towards cells of the endothelial lineage. Mesenchymal gene expression was assessed in GDM (n=3-4) and non-GDM (n=7) pMSCs cultured in control or differentiation medium for 11 days, using RT-qPCR. The expression of target genes was normalised to *YWHAZ* housekeeping gene expression. Data is presented as the mean, and statistical analysis was performed using a Two-Way ANOVA, with a Tukey's post-hoc test. Data that was not normally distributed was log transformed. Individual points represent each patient placenta. n=3-7.

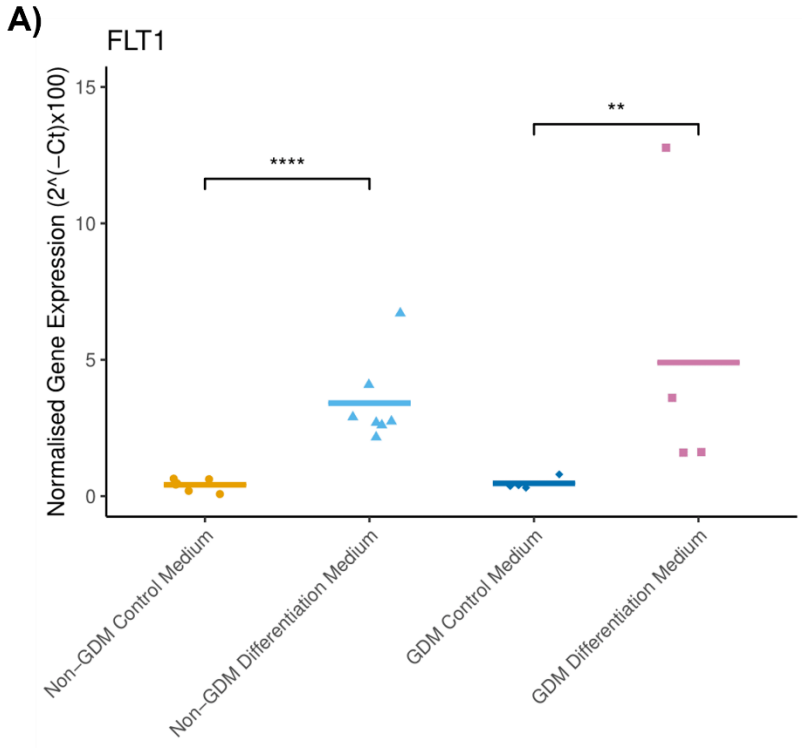
A)
FLT1
Normalised Gene Expression (2^(−Ct)x100)
15
10
5
0
****
**
Non−GDM Control Medium
Non−GDM Differentiation Medium
GDM Control Medium
GDM Differentiation Medium

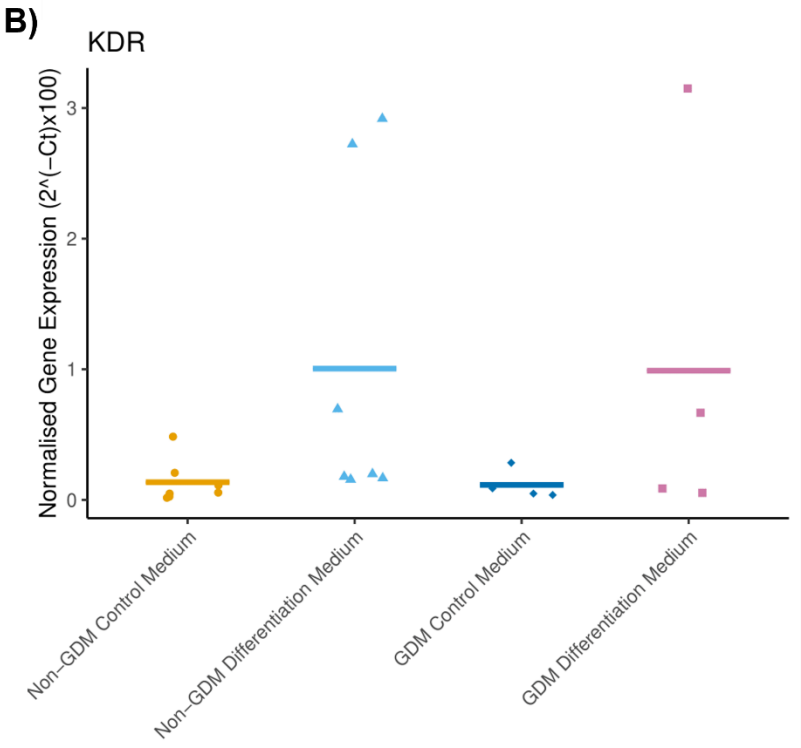
B)
KDR
Normalised Gene Expression (2^(−Ct)x100)
3
2
1
0
Non−GDM Control Medium
Non−GDM Differentiation Medium
GDM Control Medium
GDM Differentiation Medium

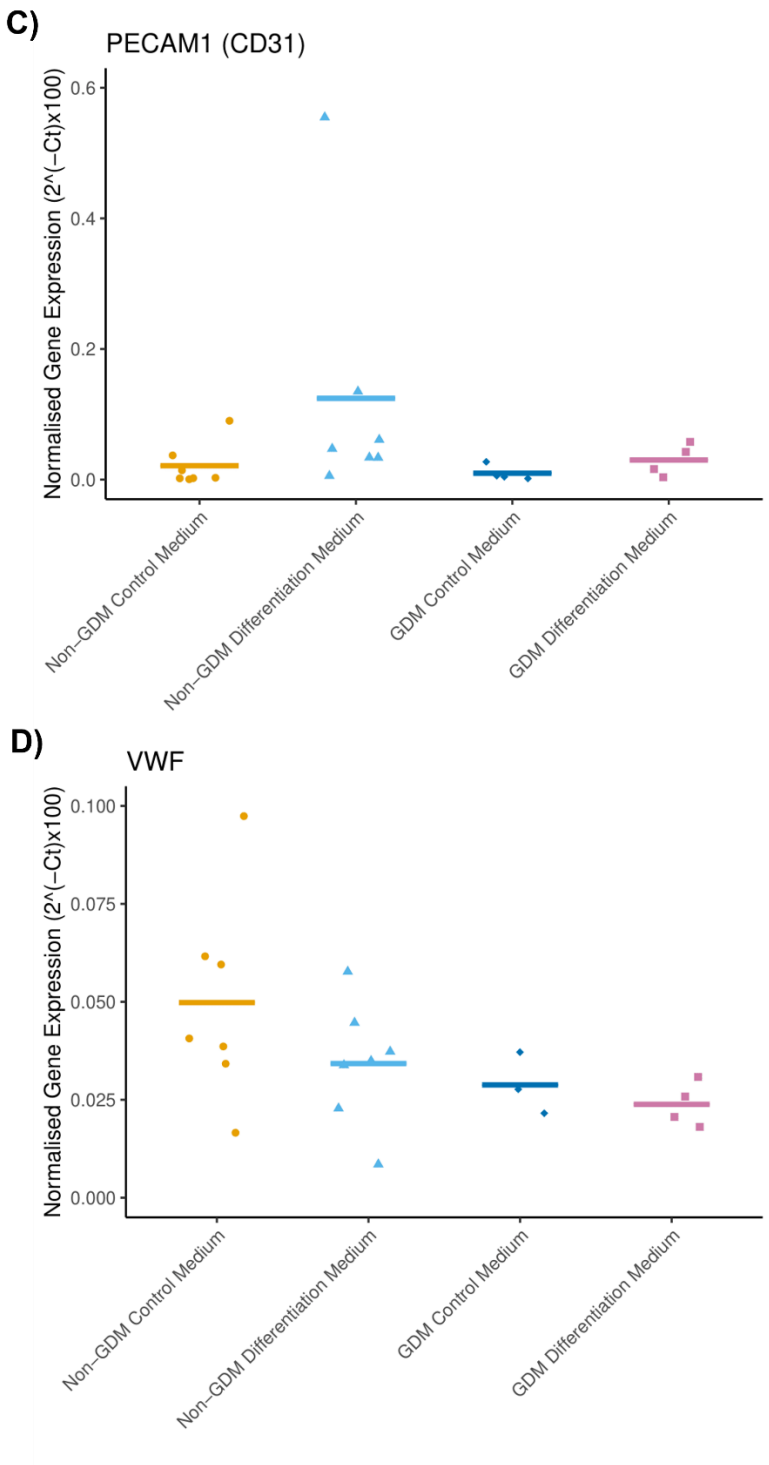

Figure 7.10 - Endothelial gene expression in pMSCs from GDM and non-GDM pregnancies undergoing differentiation towards cells of the endothelial lineage. Endothelial gene expression was assessed in GDM (n=4) and non-GDM (n=7) pMSCs cultured in control or differentiation medium for 11 days, using RT-qPCR. The expression of target genes was normalised to *YWHAZ* housekeeping gene expression. Data is presented as the mean, and statistical analysis was performed using a Two-

Way ANOVA, with a Tukey's post-hoc test. Data that was not normally distributed was log transformed. Individual points represent each patient placenta. n=4-7. ** $p<0.01$, **** $p<0.0001$.

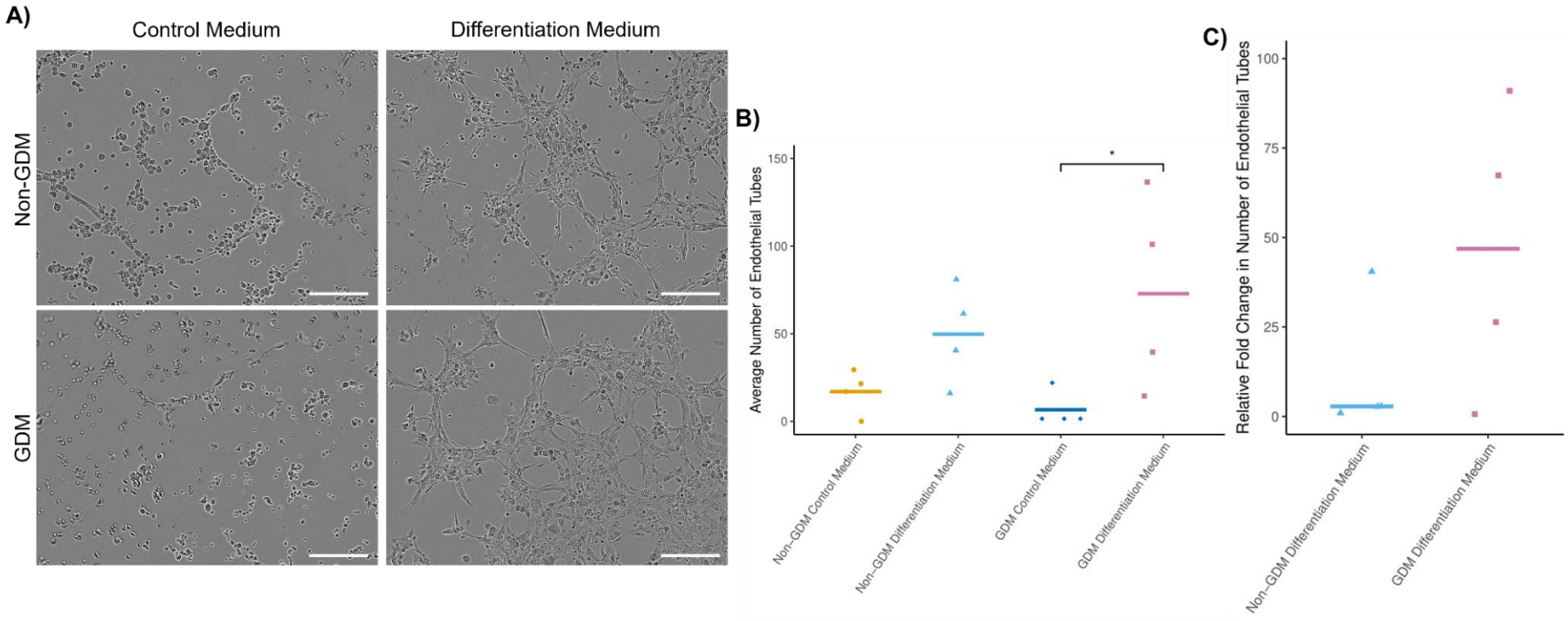

Figure 7.11 - Endothelial tube formation assay of pMSCs from GDM and non-GDM pregnancies cultured in control or differentiation medium for 7 days. pMSCs from GDM (n=4) and non-GDM (n=4) placentae were seeded onto ECM (10,000 cells per well of 96-well plate) after 7 days in differentiation medium or control medium and incubated for 2 hours at 37°C. A) Images were taken on the Incucyte ZOOM at 10x magnification. Scale bars = 300 µm. B) The total number of tubes were manually counted using ImageJ. Data is presented as the mean, and statistical analysis was performed using a Two-Way ANOVA on log transformed data, with a Tukey's post-hoc test. C) The relative fold change in the number of endothelial tubes with differentiation medium compared to control medium was calculated. Data is presented as the median and statistical analysis was performed using a Wilcoxon Signed-Rank Test. Individual points represent each patient placenta. n=4-7. * $p<0.05$.

7.4.3 Impact of glucose on a triculture model of placental microvasculature

As glucose (or GDM) did not appear to induce any changes in the differentiation of pMSCs towards an endothelial lineage, an alternative triculture model of placental microvasculature was used to assess whether glucose impacted on other parameters of placental vascularisation. This model was developed by Dr Kristina Haase's laboratory (EMBL, Barcelona) and I performed these experiments as a visiting researcher in her group.

7.4.3.1 Modelling maternal glucose fluctuations in the triculture model

During microvessel formation, cells were exposed to endothelial medium (VascuLife) containing either 5.6, 7, 9 or 25 mM glucose. Physiological concentrations of 5.6-9 mM glucose were used to mimic levels in GDM pregnancies, with varying degrees of glucose control, as with the pMSC model (Section 7.4.1.1). Additionally, 25 mM was used as supraphysiological level for comparison and a hyperosmolar control of 5.6 mM glucose with 19.4 mM D-mannitol, referred to as the mannitol control (19.4 mM). Medium was refreshed daily to maintain glucose levels.

To determine if the concentration of glucose in the medium and the frequency of medium changes were suitable for modelling physiological glucose levels in the model, glucose and osmolality was assessed in conditioned medium at days 1, 4 and 7 (Figure 7.12).

Input concentrations of 5.6 mM glucose declined to normoglycaemic/mild hypoglycaemic levels of 3.84±0.24, 3.31±0.30 and 3.41±0.65 mM at days 1, 4 and 7, respectively. Medium was refreshed daily to maintain glucose levels and establish flow; therefore, the cells would not have been exposed to low glucose levels for prolonged periods of time. Input concentrations of 7 mM glucose declined to normoglycaemic levels of 4.7±0.37 and 5.58±0.24 mM at days 1 and 4, respectively, and mild hyperglycaemic levels of 6.39±0.11 mM at day 7. Input concentrations of 9 mM glucose declined to mild hyperglycaemic/hyperglycaemic levels of 7.22±0.30, 7.92±0.36 and 8.45±0.17 mM at day 1, 4 and 7, respectively. However, during daily medium refreshments, glucose would have been replenished back to mild hyperglycaemic levels in the 7 mM condition and hyperglycaemic levels in the 9 mM condition. Input concentrations of 25 mM remained at supraphysiological levels of 21.14±0.27, 25.94±0.58 and 23.66±0.43 mM at days 1, 4 and 7, respectively. Glucose concentrations within the mannitol control (5.6 mM glucose + 19.4 mM mannitol)

showed very similar patterns to the 5.6 mM condition, with levels between 3.36±.17 and 4.46±0.13 mM (n=5-6; Figure 7.12A).

The osmolality of VascuLife medium containing 5.6, 7, 9, 25 mM glucose and in the 19.4 mM mannitol control was 201, 175, 181, 193 and 192 mOsm/kg, respectively. Osmolality was not significantly altered by glucose treatment at any timepoint ($p>0.05$). However, when specifically assessing levels at day 7, the osmolality of the mannitol control was higher (324.67±3.33 mOsm/kg) than 5.6 mM (294.50±15.06 mOsm/kg, $p=0.062$), 7 mM (302.40±2.69 mOsm/kg, $p<0.05$) and 9 mM (296±2.92 mOsm/kg, $p<0.01$) but not 25 mM (306.25±4.31, $p=0.112$) (n=3-6; Figure 7.12B).

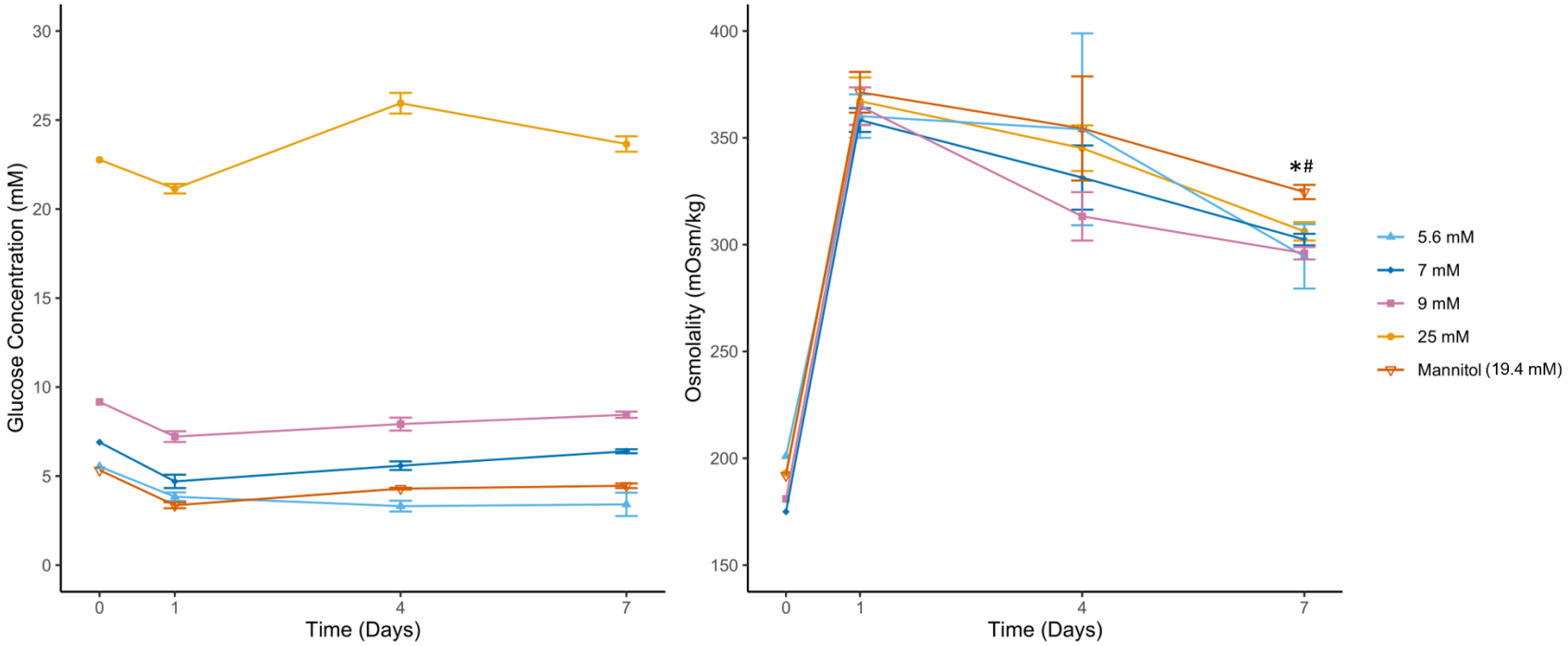

Figure 7.12 - Glucose treatments in the triculture placental microvasculature model. A) Glucose (mM) was assessed in culture medium of the triculture placental microvasculature model with glucose treatments at days 1, 4 and 7 using a GlucCell Meter. Data is presented as the mean ± SEM (n=5-6). B) Osmolality was assessed in culture medium of the triculture placental microvasculature model with glucose treatments at days 1, 4 and 7 using an Osmometer. Data is presented as the mean ± SEM (n=3-6). Differences in osmolality between each glucose concentration were assessed at each time point using a Two-Way ANOVA on log transformed data. Differences in osmolality between glucose concentrations at day 7 were assessed using a Kruskal-Wallis with a Dunn's post-hoc test (as data was not normally distributed), * Mannitol vs 7 mM ($p<0.05$), # Mannitol vs 9 mM ($p<0.01$).

7.4.3.2 Vessel morphology

While the pMSC model enabled investigation into endothelial differentiation during placental vascular development, the triculture model allowed vessel morphology to be assessed during vessel formation. This included percentage area covered by the vessels, vessel diameter and branch length, which is important given that increased growth, branching, length, diameter and surface area of capillaries has been reported in pregnancies complicated by maternal diabetes[134–137].

Images were taken of the microvessels from three regions of the central channel, after 4- and 7-days exposure to glucose treatments (Figure 7.13A). With 7 mM glucose, at day 4, the area of coverage by vessels was increased to 78.64±2.71% compared to 72.29±1.96% with 5.6 mM, although this was not significant ($p=0.412$). By day 7, the area of coverage by vessels was significantly increased to 81.84±2.58% with 7 mM compared to 72.43±1.96% with 5.6 mM ($p<0.05$) (Figure 7.13B). At day 7, there was also an increase in vessel branch length with 7 mM glucose (87.50±3.11 µm) compared to 5.6 mM (75.82±3.37 µm) and vessel diameter (49.28±3.00 µm) compared to 5.6 mM (42.96±2.71 µm), although these differences were not significant ($p=0.186$ for branch length and $p=0.474$ for vessel diameter, n=5-6) (Figure 7.13C-D).

With 9- and 25-mM glucose, at day 7, the area of coverage by vessels was also increased (83.14±2.14% and 82.41±1.46%, respectively) to compared to 5.6 mM (72.43±1.96%) ($p<0.01$, n=5-6) (Figure 7.13B). Vessel branch length was also increased at day 7 with 9- and 25-mM glucose (90.56±3.26 µm and 86.65±2.57 µm, respectively) compared to 5.6 mM (75.82±3.38 µm), which was approaching significance for 9 mM ($p=0.0585$, n=5-6), but less so for 25 mM ($p=0.208$, n=5-6). Vessel diameter was also increased at day 7 with 9- and 25-mM glucose (52.45±2.32 µm and 49.09±1.84 µm, respectively) compared to 5.6 mM (42.96±1.93 µm), although not significant ($p=0.126$ for 9 mM and $p=0.461$ for 25 mM, n=5-6) (Figure 7.13C-D). It is also important to note that the increases in area, diameter, and branch length, with 7 and 9 mM glucose at day 7 were dose-dependent, whereas with 25 mM there was no further increase, and levels were similar to 7 mM.

Unexpectedly, at day 4, the mannitol control had a significantly higher area of coverage by vessels (82.94±0.75%) compared to 5.6 mM (72.29±1.96%; $p<0.05$, n=5-6). This increase was also observed at day 7 (85.55±1.51% with mannitol compared to 72.43±1.96% with 5.6 mM; $p<0.001$, n=5-6) (Figure 7.13B). At day 7, the mannitol control also had a significantly higher diameter of the vessels (57.29±3.29 µm) compared to 5.6 mM (42.96±1.93 µm) and a significantly higher branch length

(97.01±4.81 µm) compared to 5.6 mM (75.82±3.38 µm; $p<0.01$, n=5-6) (Figure 7.13C-D).

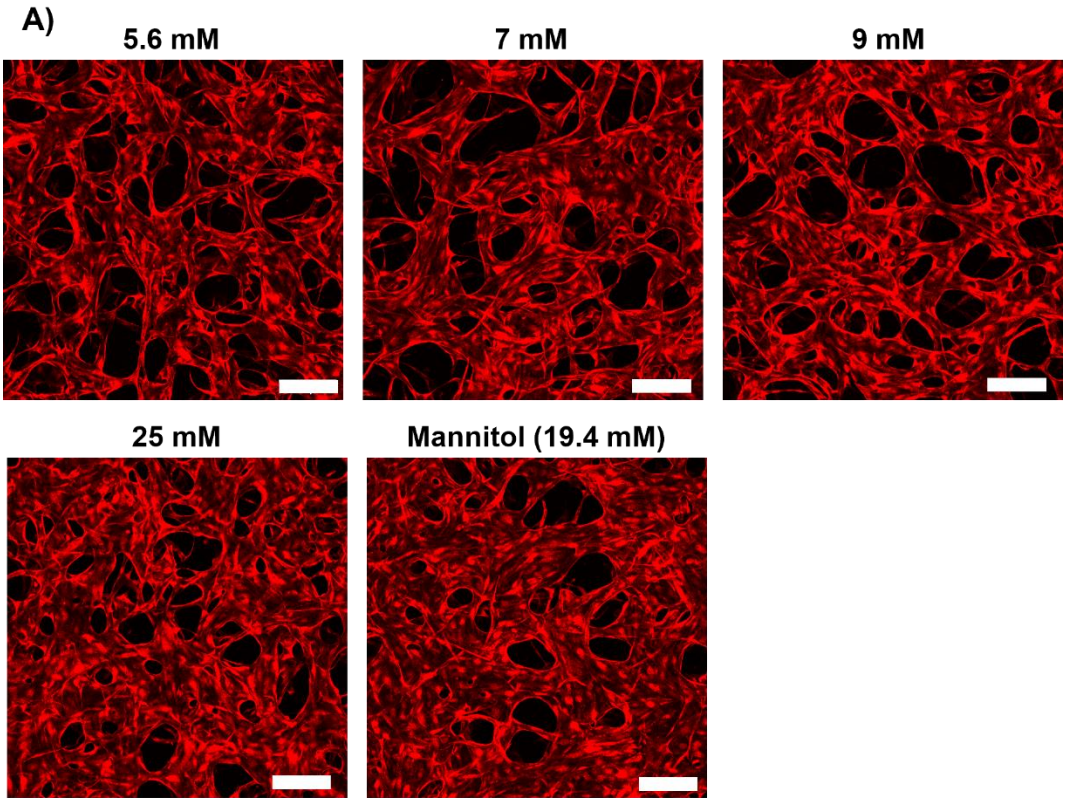
A)
5.6 mM
7 mM
9 mM
25 mM
Mannitol (19.4 mM)

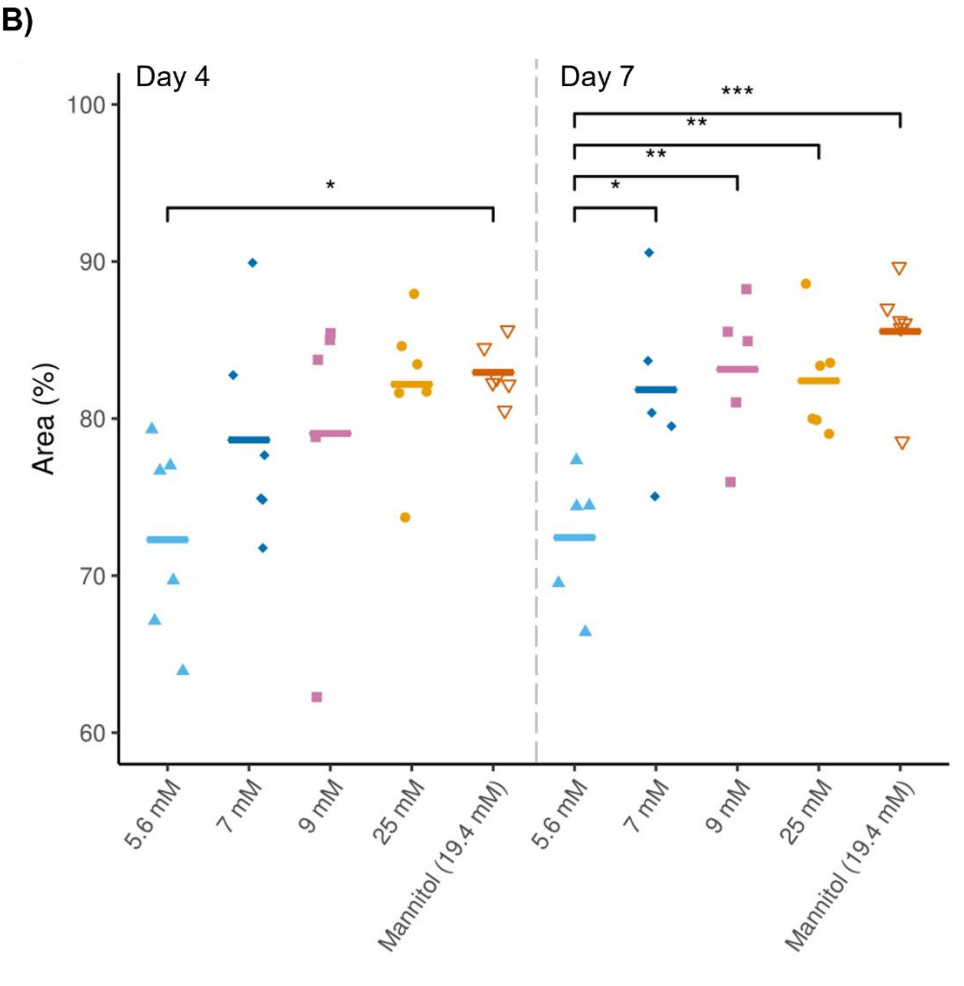
B)
Day 4
Day 7
Area (%)
100
90
80
70
60
*
*
**
**
***
5.6 mM
7 mM
9 mM
25 mM
Mannitol (19.4 mM)
5.6 mM
7 mM
9 mM
25 mM
Mannitol (19.4 mM)

C)

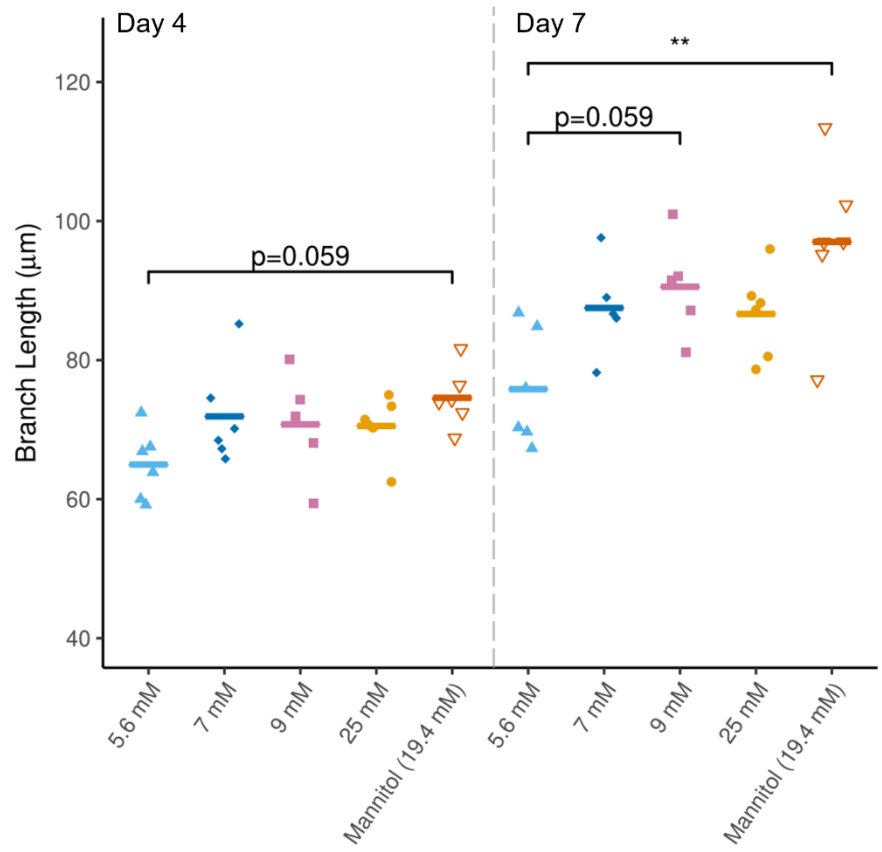
Day 4
Day 7
**
p=0.059
p=0.059
Branch Length (µm)
120
100
80
60
40
5.6 mM
7 mM
9 mM
25 mM
Mannitol (19.4 mM)
5.6 mM
7 mM
9 mM
25 mM
Mannitol (19.4 mM)

D)

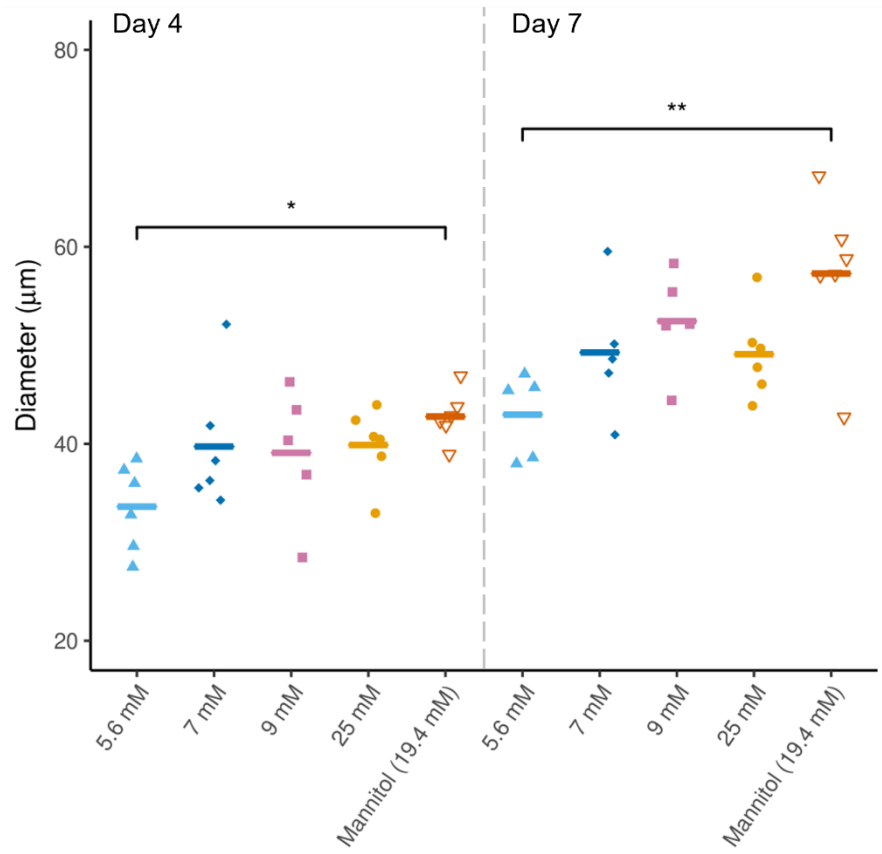
Day 4
Day 7
**
*
Diameter (µm)
80
60
40
20
5.6 mM
7 mM
9 mM
25 mM
Mannitol (19.4 mM)
5.6 mM
7 mM
9 mM
25 mM
Mannitol (19.4 mM)

Figure 7.13 – Morphology of microvessels exposed to glucose in the triculture placental microvasculature model. Images of microvessels were taken on days 4 and 7 of glucose treatments and were quantified for morphological parameters. A) Representative images of microvessels at day 7. Images were taken on the DMi8 Leica Confocal Microscope. Red fluorescence shows the RFP labelled HUVECs. Scale bars = 200 µm. A-D) Quantification of (B) the percentage area of microvessel coverage, (C) branch length (µm) of microvessels and (D) the diameter (µm) of microvessels. Data was not normally distributed and is presented as the median. Statistical analysis was performed using a Kruskal-Wallis with a Dunn's post-hoc test at each time point. Individual points represent each device. n=5-6. * $p<0.05$, ** $p<0.01$ and *** $p<0.001$.

7.4.3.3 Microvessel permeability

Endothelial barrier function is thought to be impaired in GDM and in response to glucose[535,536,753]; therefore, to investigate barrier function, a FITC-dextran assay was performed to assess the permeability of the microvessels, after 7 days exposure to glucose treatments. The intensity of FITC-dextran within the microvessels and in the extravascular space was measured, and the permeability of the microvessels (cm/s) was approximated.

Microvessels of all glucose concentrations were perfusable (Figure 7.14A). The permeability was not altered by 7 mM glucose (6.56E-08 [5.12E-08 – 7.98E-08] cm/s, n=2) compared to 5.6 mM (8.63E-08 [3.48E-08 - 1.051E-07] cm/s, n=5, p=0.647) (Figure 7.14B).

The permeability of the microvessels exposed to 9 mM glucose was increased (9.82E-08 [4.81E-08 - 5.68E-07] cm/s, n=5) compared to 5.6 mM (8.63E-08 [3.48E-08 - 1.051E-07], cm/s, n=5), although this did not reach significance (p=0.709). In contrast, with 25 mM glucose, the permeability of microvessels was decreased (4.57E-08 [2.02E-08 – 9.27E-08], n=6) compared to 5.6 mM (8.63E-08 [3.48E-08 - 1.051E-07] cm/s, n=5), although this was not significant (p=0.149) (Figure 7.14B).

In the mannitol control, the permeability of the microvessels was significantly decreased (2.45E-08 [8.15E-09 - 7.14E-08] cm/s, n=5) compared to 5.6 mM (8.63E-08 [3.48E-08 - 1.051E-07] cm/s; n=5, $p<0.05$) (Figure 7.14B).

7.4.3.4 Expression of vascular-regulatory genes known to be altered by glucose fluctuations

RNA was isolated from the combined cells (HUVECs, HPPs, HPFs) in the central channel of each device. A panel of genes that were altered by 7 mM glucose in placental explants (Chapter 3), that are known to play roles in vasculogenesis and be expressed by ECs and/or perivascular cells, were assessed via RT-qPCR. As there was a very low number of cells within each device, RNA was pooled from 3 devices per glucose concentration. This enabled generation of preliminary data on a small pool of samples (n=2). Consistent with findings in placental explants, 7 mM glucose in the triculture model decreased the gene expression of *CD44, IL6* and *PDGFD* (Figure 7.15), however the limited sample number and variation within groups makes it difficult to draw conclusions. Further experiments are needed to further confirm this data.

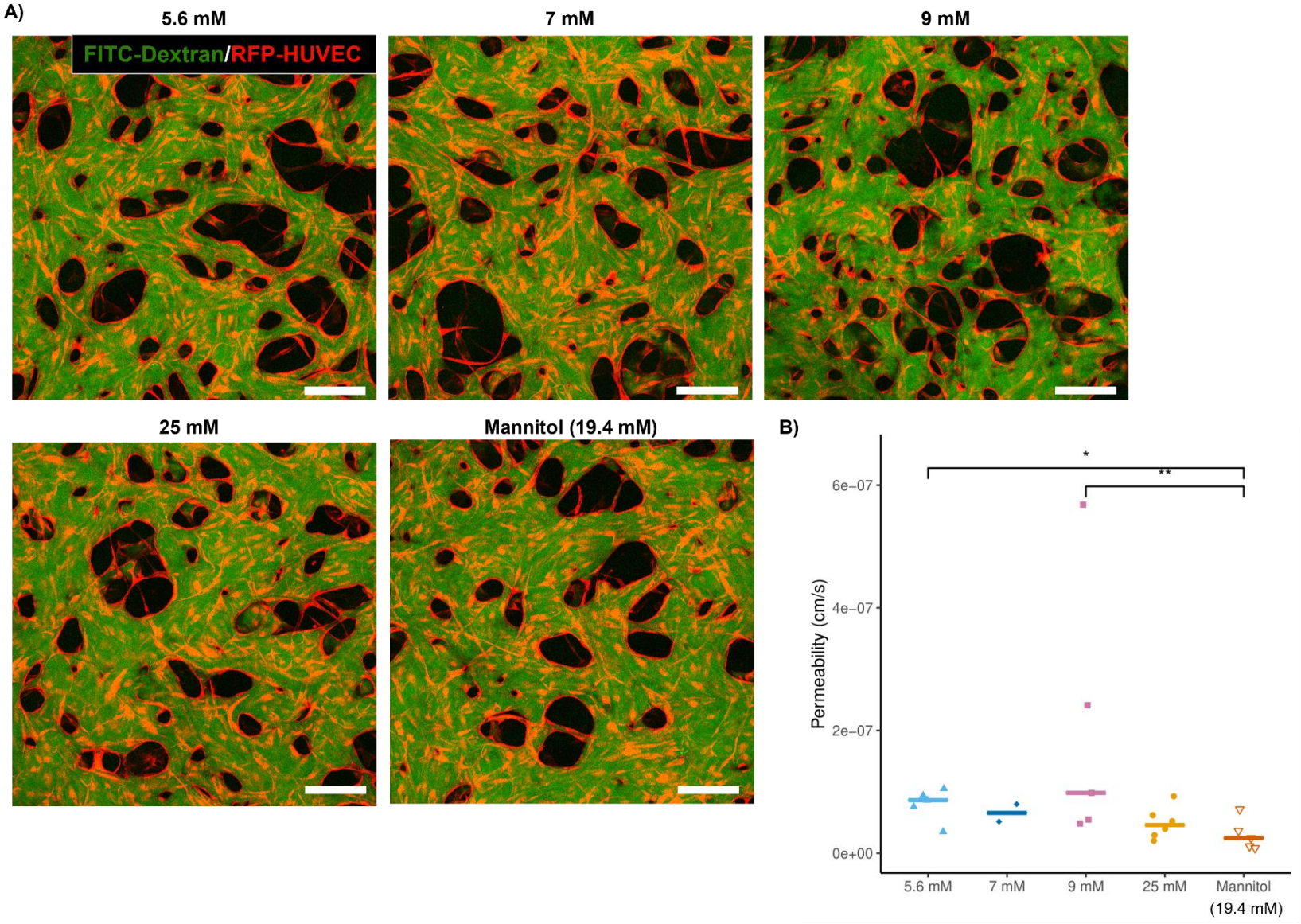
A)
5.6 mM
7 mM
9 mM
FITC-Dextran/RFP-HUVEC
25 mM
Mannitol (19.4 mM)
B)
Permeability (cm/s)
6e−07
4e−07
2e−07
0e+00
*
**
5.6 mM
7 mM
9 mM
25 mM
Mannitol
(19.4 mM)

Figure 7.14 – Permeability of microvessels exposed to glucose in the triculture placental microvasculature model. A FITC-dextran permeability assay was performed after 7 days exposure to glucose treatments. A) Representative images of microvessels at day 7 following infusion of FITC-dextran. Images were taken on the DMi8 Leica Confocal Microscope. Red fluorescence shows the RFP labelled HUVECs. Scale bars = 200 µm. B) Quantification of the permeability (cm/s). Data was not normally distributed and is presented as the median. Statistical analysis was performed using a Kruskal-Wallis with a Dunn's post-hoc test. Individual points represent each device. n=2-6. * $p<0.05$, ** $p<0.01$.

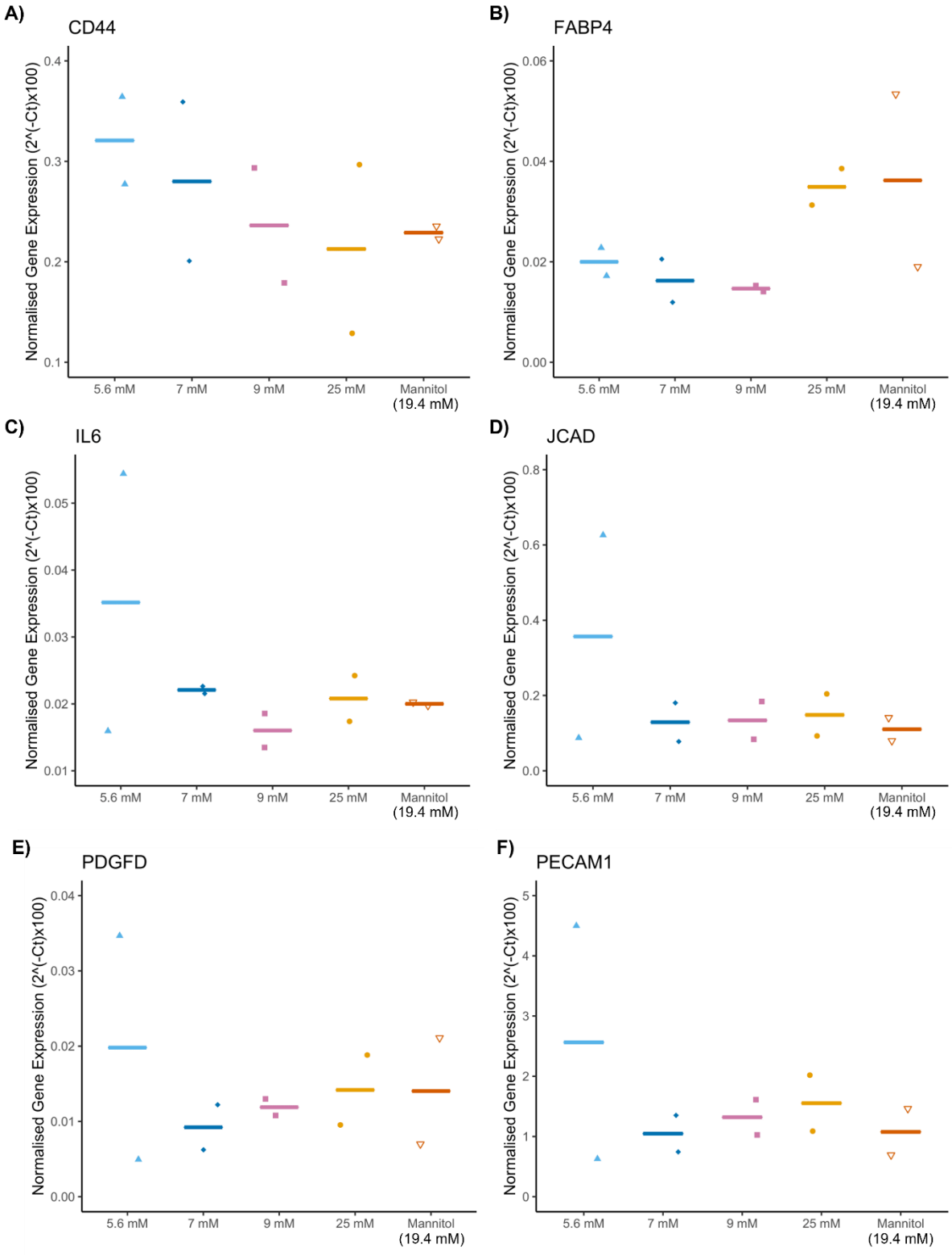
A)
CD44
Normalised Gene Expression (2^(-Ct)x100)
0.4
0.3
0.2
0.1
5.6 mM
7 mM
9 mM
25 mM
Mannitol (19.4 mM)
B)
FABP4
Normalised Gene Expression (2^(-Ct)x100)
0.06
0.04
0.02
0.00
5.6 mM
7 mM
9 mM
25 mM
Mannitol (19.4 mM)
C)
IL6
Normalised Gene Expression (2^(-Ct)x100)
0.05
0.04
0.03
0.02
0.01
5.6 mM
7 mM
9 mM
25 mM
Mannitol (19.4 mM)
D)
JCAD
Normalised Gene Expression (2^(-Ct)x100)
0.8
0.6
0.4
0.2
0.0
5.6 mM
7 mM
9 mM
25 mM
Mannitol (19.4 mM)
E)
PDGFD
Normalised Gene Expression (2^(-Ct)x100)
0.04
0.03
0.02
0.01
0.00
5.6 mM
7 mM
9 mM
25 mM
Mannitol (19.4 mM)
F)
PECAM1
Normalised Gene Expression (2^(-Ct)x100)
5
4
3
2
1
0
5.6 mM
7 mM
9 mM
25 mM
Mannitol (19.4 mM)

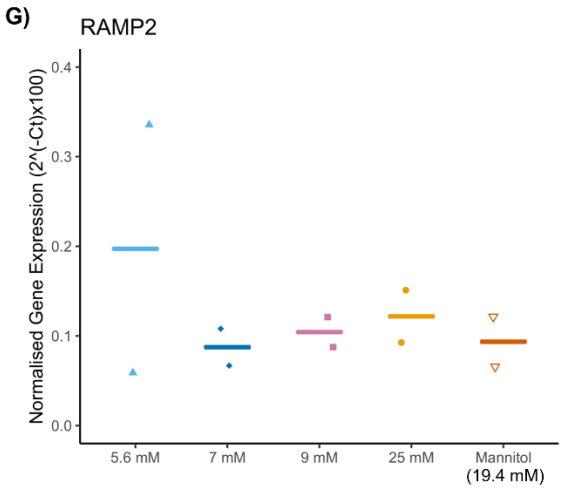

Figure 7.15 - Expression of genes found to be altered by 7 mM glucose in placental explants in microvessels exposed to glucose in the triculture placental microvasculature model. Selected DEGs altered by 7 mM glucose in placental explants were assessed via RT-qPCR in the triculture model. The expression of each target gene was normalised to a geometric mean of *YWHAZ*, *GUSB* and *RPL13A* housekeeping gene expression, which was unaltered between groups. Data are presented as the mean. Individual points represent each device. n=2-6.

7.5 Discussion

The aim of this chapter was to assess the impact of physiological maternal glucose fluctuations associated with LGA pregnancies in GDM on models of placental vascular development. Glucose did not significantly impact the differentiation potential of pMSCs towards the endothelial lineage. Moreover, when pMSCs were also isolated from GDM placentae, there was no difference in their differentiation potential compared to non-GDM pMSCs, suggesting that pMSC to endothelial lineage differentiation may not be affected by hyperglycaemia. Interestingly, when looking at alternative measurements of placental vascularisation and function (using a triculture model of placental microvasculature, containing HUVECs, HPPs and HPFs), it was established that 7 mM glucose increased branch length, and vessel area, compared to 5.6 mM glucose, and may potentially alter genes involved in these processes.

7.5.1 Modelling maternal glucose fluctuations associated with GDM in *in vitro* cell models

Two *in vitro* models were employed to investigate the impact of physiological maternal glucose fluctuations on placental vascular development. Firstly, pMSCs were induced towards cells of the endothelial lineage to model endothelial differentiation. Secondly, a triculture model of placental microvasculature was utilised with HUVECs, HFPs and HPPs, which generate perfusable microvessels to model placental vasculogenesis. As in Chapter 3, glucose concentrations of 5.6 and 7 mM were used in both models, to mimic physiological *in vivo* maternal glucose fluctuations in GDM AGA and GDM LGA, respectively, based on previous CGM studies[62]. Additionally, 9 mM glucose was used in both models, to mimic hyperglycaemia in those with poor glucose control in GDM, given that treatment targets in GDM are to keep glucose below 7 mM[14,751,752]. In the triculture model, 25 mM glucose was also used as a supraphysiological concentration, to compare to mild hyperglycaemic levels. Finally, hyperosmolar controls were included, which reflected the osmolality of the highest glucose concentration. These controls were comprised of 5.6 mM glucose, with an additional 3.4 mM or 19.4 mM D-mannitol, in the pMSC and triculture models, respectively.

Consistent with findings in placental explants (Chapter 3), glucose was rapidly consumed by cells in both *in vitro* models and was replenished daily. Assessment of glucose concentrations in the conditioned medium showed that the models were able to recapitulate fluctuations in maternal glucose observed in women with GDM discussed above. In the pMSC model, the control medium (DMEM Low Glucose; undifferentiated cells) had an increased osmolality compared to the differentiation

medium (EGM-2), which is likely dependent on the different compositions of each medium. However, the aim of these experiments was to determine whether altered glucose in the differentiation medium influenced endothelial lineage differentiation of pMSCs, and osmolality was not significantly altered here, suggesting this was an appropriate model.

7.5.2 Impact of mild hyperglycaemia on placental vascular development

In the pMSC model, exposure to 7 mM glucose (mild hyperglycaemia) caused a trend towards decreased expression of the EC marker, *FLT1*, and increased expression of the MSC markers *CD44* and *NT5E* and the EC marker *KDR*, compared to 5.6 mM glucose. The number of endothelial tubes were also slightly lower with 7 mM glucose compared to 5.6 mM. Although, there were no significant differences in gene expression or endothelial tube formation. This data suggests that 7 mM glucose may reduce endothelial differentiation. This is consistent with RNA sequencing findings in Chapter 3, where functional enrichment analysis revealed that DEGs with 7 mM glucose were associated with inhibition of vascular development, vasculogenesis, EC development and EC proliferation. Moreover, placentae from pregnancies complicated by maternal diabetes are known to have immature villi, such as decreased formation of terminal villi[123], and placental lesions, which indicates villous immaturity[122], and thus could influence nutrient transfer and fetal growth. However, increased sample numbers, in the present model, would be needed to see if these small changes are significant.

In MSCs from other tissues, glucose has been shown to influence their function. For example, in human UMSCs, high glucose (15 mM) reduced metformin-induced apoptosis, which was observed with 5.6 mM glucose, in a AMPK/mTOR dependent manner[754]. Moreover, glucose has been shown to alter the differentiation capacity of MSCs. For example, culture of human BMSCs in high glucose medium (25 mM), prior to differentiation, reduced chondrogenic differentiation, compared to low glucose medium (5.6 mM)[755]. Another study has shown that high glucose (13.9 mM) reduces the osteogenic and chondrogenic potential of AMSCs, compared to 5.6 mM[756]. In contrast, Cheng *et al*. (2016) showed that osteogenic differentiation of AMSCs was comparable between high glucose (25 mM) and low glucose (5.6 mM) conditions, however, ‘stemness’ markers were increased with high glucose, such as Sox-2, Octamer-binding transcription factor 4 (Oct-4) and Nanog[757]. In MSCs isolated from the placenta, culture in 25 mM glucose for 14 days reduced the proliferation of the cells

from day 4 and adipogenic differentiation of the cells was also enhanced. Culture in 25 mM glucose also downregulated some osteogenic genes after 7 days. Similar findings were observed in this study with bone marrow-, chorion- and umbilical- derived MSCs[758].

No studies have assessed the influence of glucose on MSC differentiation into ECs. One study by Mannino *et al.* (2021) assessed the impact of glucose (25 mM) on pericyte-differentiated AMSCs. High glucose increased the proliferation, viability and migration ability of pericyte-differentiated cells; however they did not assess the pericyte phenotype of the MSCs following high glucose[759]. However, these aforementioned studies utilise supraphysiological concentrations of glucose (≥25 mM) and are not comparable to the physiological levels used in the present study and could explain differences in findings.

Given that many of these studies have reported changes in proliferation and viability, and DEGs altered by 7 mM glucose were associated with reduced EC proliferation, it may be interesting to investigate proliferation or apoptosis in the present model. Fewer cells could be observed in morphological images in cells treated with 7 mM glucose compared to 5.6 mM. However, specific markers, such as Ki67 or Terminal deoxynucleotidyl transferase dUTP nick end labelling (TUNEL) staining would be needed to confirm whether glucose was altering proliferation or apoptosis, respectively.

In the triculture model, by day 7, the percentage area covered by the vessels, vessel diameter and branch length were increased with 7 mM glucose compared to 5.6 mM. In line with this, GDM and glucose have been associated with altered tubule formation and branching of ECs. One study showed that HUVECs isolated from GDM placentae have impaired tube formation, proliferation, and migration[760]. Glucose levels of 16.7 and 27.8 mM stimulated tubular elongation in bovine carotid artery ECs, compared to 5.6 mM. In contrast, Lee *et al*. (2014) observed decreased tube formation with 20 and 40 mM glucose, as well as cell viability, compared to 5 mM, in human microvascular ECs[761]. Taken together with the findings of the current study, this is consistent with observations in diabetic placentae, where increased growth, branching, length, diameter and surface area of capillaries has been reported[134–137].

Mild hyperglycaemia may also alter genes involved in these processes, given that many genes altered by 7 mM glucose in placental explants (Chapter 3) were associated with vascular branching, including *CD44*[675,676], *PDGFD*[481], and vascular permeability, including cell-cell junction molecules, *PECAM1* and *JCAD*[445,446], and *RAMP2*, which regulates vascular integrity[49–51]. Preliminary findings also revealed that

mild hyperglycaemia may also alter these genes in the triculture model, however further repeats are needed to confirm this.

7.5.3 Impact of physiological and supraphysiological hyperglycaemia on placental vascular development

In the pMSC model, 9 mM glucose (which mimicked hyperglycaemia in untreated GDM) had little impact on endothelial differentiation, suggesting that subtle fluctuations in maternal glucose (1-1.5 mM) in GDM may have a greater impact on endothelial differentiation during placental vascular development. In contrast, in the triculture model, by day 7, the percentage area covered by the vessels, and vessel diameter and branch length were further increased with 9 mM glucose, compared to 7 and 5.6 mM. These increases in vascular branching, diameter and area were dose-dependent for 7 and 9 mM glucose, however, at 25 mM there was no further increase, and levels were similar to 7 mM. Given that this supraphysiological concentration of glucose does not further increase the response on the vasculature, this further highlights the need for investigating physiological levels of glucose on the placenta.

Moreover, vessel permeability was higher in the 9 mM condition, suggesting that the vessels were ‘leakier’. These findings suggest that while hyperglycaemia induced by 9 mM glucose may have little impact on endothelial differentiation, it may influence the function of mature ECs, by altering the branching and formation of vessels, and the integrity of the endothelial barrier. Consistent with these findings, the function of the endothelial barrier is thought to be impaired in pregnancies complicated by GDM. In a placental perfusion model of placentae from GDM pregnancies, those treated with diet showed increased leakage of dextran, compared to controls, suggesting endothelial barrier dysfunction[535]. Similarly, in fetoplacental arterial ECs isolated from GDM pregnancies, F-actin organisation was altered, and more disorganised (which was not observed in fetoplacental venous ECs). Increased average impedance was observed in these cell monolayers, demonstrating altered barrier function. Alterations in EC function were also detected at the transcriptional level as differential epigenetic programming of genes involved in cell morphology, cell movement and the cell cycle were found in GDM fetoplacental arterial and venous ECs[536]. Moreover, glucose has also been found to alter EC permeability. In porcine endothelial cells, increasing concentrations of glucose caused a dose-dependent increase (10, 20, 30 and 40 mM) in EC permeability. Concentrations above 40 mM did not increase endothelial permeability any further[753].

Given that 9 mM glucose was used to mimic untreated hyperglycaemia in GDM, these findings suggest that treatment to reduce glucose levels might be beneficial, as 5.6 and 7 mM glucose (which modelled treated GDM) did not impact vessel permeability. Interestingly, metformin, which is often used to reduce glucose levels in GDM, has been found to reduce vascular permeability in mice[762], and enhance trans-endothelial resistance of EC monolayers and endothelial barrier integrity, *in vitro*[763,764].

7.5.4 The impact of hyperosmolality on placental vascular development

In the triculture model, the most significant increase in vessel area, diameter and branch length was observed in the mannitol control (5.6 mM glucose + 19.4 mM D-mannitol). Permeability was also significantly decreased in the mannitol control compared to 5.6 mM glucose, suggesting enhanced barrier function. Mannitol, usually around 20% (1100 mOsm/L), is widely used clinically to induce vascular permeability and disrupt the vessel barrier[765,766]. However, on the contrary, hypertonic saline or mannitol has been used to improve barrier function to intervene with serious haemorrhage or traumatic brain injury[767–769]. Therefore, a recent study by Kang *et al*. (2023) assessed hyperosmolarity in another microvasculature model, which incorporated human ECs in a PDMS device with collagen[770]. Hyperosmolarity (600 mOsm/L) was induced by mixing cell culture medium with D-mannitol, D-sorbitol and sodium chloride. Here, hyperosmolality enhanced vascular barrier function as a reduction in permeability was observed (FITC-dextran infusion into the vessel lumen). This was found to be associated with upregulation of VE-Cadherin at cellular junctions, F-actin localisation to cell-cell junctions and junctional tension. This improvement started before the vessels had matured, and until the barrier had matured. This was also observed when range of different human endothelial cell types (HUVECs, human brain ECs and human dermal ECs) were incorporated into the model. This study is consistent with the findings elicited by mannitol in the triculture model and suggests that while mannitol does not exhibit any metabolic effects on cells, its hyperosmolality may induce alterations to the vascular barrier.

In the triculture model, mannitol was used at 19.4 mM with 5.6 mM glucose, which should induce the same osmolality as the 25 mM glucose condition. However, it is interesting that the increased vessel diameter, area, branching, and decreased permeability was observed with the mannitol control, but not 25 mM glucose. This suggests that it may be a mannitol-specific effect. However, the osmolality of the mannitol control was found to be higher on day 7, when these measurements were

made, which suggests this could have influenced the findings. Increased serum osmolality has been reported with an increase in fasting plasma glucose and serum glucose levels in patients with diabetes mellitus[771,772]. In a study by Lemmy *et al*. (2018), blood glucose and plasma osmolarity were significantly higher in db/db mice compared to wild type mice[773]. Given that hyperglycaemia in diabetes has been linked to increased osmolality, this suggests that hyperosmolality in GDM could impact on development of the placental vasculature.

7.5.5 The impact of GDM on placental vascular development

The endothelial lineage differentiation potential was compared between pMSCs isolated from non-GDM and GDM placentae. There were slightly more endothelial tubes formed in GDM differentiated pMSCs than non-GDM differentiated pMSCs and increased expression of MSC genes, *CD44* and *NT5E,* which have known roles in endothelial function[675,676,696,728,729] (discussed in Chapter 6). However, these did not reach significance and increased numbers of GDM samples would be needed to confirm these differences.

Other studies have investigated the impact of diabetes on MSC differentiation. In the study by Kim *et al*. (2015), UMSCs, isolated from GDM pregnancies had a significantly lower adipogenic differentiation capacity and also had reduced cell growth, earlier senescence, and mitochondrial dysfunction (low mitochondrial activity and reduced expression of mitochondrial function genes)[774]. In contrast, when BMSCs were incubated with serum from T2DM patients for 14 days, adipogenic differentiation was increased, with unaltered cell proliferation, apoptosis and osteogenic differentiation[775]. However, this was only observed in serum from post-menopausal women with T2DM, compared to serum from young women with normal glucose tolerance, and post-menopausal women with normal or impaired glucose tolerance, and was not linked to pregnancy, but does suggests that circulating factors in T2DM may influence MSC differentiation. In the study by Cheng *et al*. (2016), AMSCs from diabetic donors also had enhanced expression of pluripotency markers, Sox-2, Oct-4 and Nanog[757]. These adipose-derived MSCs from diabetic donors also show higher levels of senescence and apoptosis than those from non-diabetic donors[756]. Overall, these studies suggest that GDM can influence MSC function, including proliferation/cell death and differentiation.

In comparison, the low sample size may explain the limited findings in the present study. Ideally, pMSCs would have been isolated from GDM placentae with LGA and AGA infants and their differentiation capability assessed, to compare to findings

observed with glucose treatments. However, it was difficult to isolate pMSCs from a large sample size of GDM pregnancies within the time frame of the current study. Thus, increased sample numbers are needed, which should be split into birthweight categories (LGA, AGA and SGA), as this has not previously been studied. Moreover, while it was not possible to collect glucose measurements from the patients used for pMSC isolations, it would be useful to compare endothelial differentiation in pMSCs exposed to glucose fluctuations *in vitro* and those isolated from women with *in vivo* glucose fluctuations (which could be determined by CGM during pregnancy). Additionally, it would also be interesting to utilise primary vascular cells isolated from pregnancies complicated by GDM and altered fetal growth in the triculture model.

7.5.6 Strengths and limitations of the *in vitro* models

The minimal findings in the pMSC model could be because the model is limited. Endothelial lineage differentiation in this model does not result in increases of VWF, or CD31 (*PECAM1*) levels to the same extent of expression found in ECs, suggesting it is not capable of generating mature ECs. Thus this may not be the most appropriate method to model placental vascular development, whereby pMSCs differentiate into hemangiogenic stem cells, becoming angioblast cells (EC progenitors) and eventually forming angioblast cell cords and vessel lumens[80,81,641]. As discussed in Chapter 5, expression of VWF and CD31 appears to be increased in pMSCs isolated from first trimester placentae[660]. Utilising pMSCs from first trimester placentae may more accurately model the development of primitive blood vessels in the placenta in earlier pregnancy. As previously discussed, although GDM is diagnosed at ~28 weeks, there is a potential for maternal glucose fluctuations to be present earlier in pregnancy[596], prior to diagnosis, and thus could impair normal placental development earlier. Thus, first trimester pMSCs may be more useful for assessing the impact of glucose on placental vascular development, in future studies.

Another limitation of this model is that it only incorporates one cell type associated with placental vascular development. Paracrine signalling by other placental cell types, such as trophoblast and HBCs, which release angiogenic factors, can influence vascular development[93,94]. Moreover, glucose has been found to influence the secretion of angiogenic factors from trophoblast[263–265], and in Chapter 5, it is predicted that glucose influenced inflammatory mediator release from HBCs, which also have known angiogenic roles. Therefore, glucose may indirectly affect placental vascular development by acting on other placental cell types. While placental explants were also employed to assess the impact of glucose on all cell types in the placenta, they were

limited in their ability to assess placental vascular development (See Section 3.5.1.1). Therefore, this could be investigated in future studies by incorporating HBCs or trophoblast into a co-culture model with pMSCs, using a multi-layered microfluidic 'placenta-on-chip' style device[127,346] or transwell model[342,343]. Additionally, for maternal glucose to be transported into the placenta and to influence vascularisation directly, it first needs to cross the trophoblast barrier, by facilitated diffusion[192]. Therefore, the physiological levels of glucose utilised in the present study, may not be representative of the levels that would cross the trophoblast, which could further be assessed using a co-culture model with trophoblast.

Based on these limitations, the triculture model of placental microvasculature was used which incorporated multiple placental vascular cell types, including fibroblasts and pericytes which are known to contribute to placental blood vessel formation and maturation[83,101]. This model also enabled further investigation into the function of the endothelial barrier through permeability measurements.

7.6 Summary

- The *in vitro* models utilised in this chapter have enabled several aspects of placental vascular development to be studied.
- While glucose and GDM did not significantly influence the endothelial differentiation of pMSCs, mild hyperglycaemia (7 mM glucose) increased microvessel parameters (area, diameter, and branching) in the triculture model.
- Mild hyperglycaemia may alter genes involved in these processes, given that many genes altered by 7 mM glucose in placental explants were vascular-regulatory. Preliminary data also suggests that these genes are altered by glucose fluctuations in the triculture model.
- Glucose levels of 9 mM (which mimicked poor glucose control in GDM) further increased microvessel parameters and permeability ('leakiness'), however supraphysiological levels of 25 mM did not result in further increases.
- The hyperosmolar mannitol control (5.6 mM glucose + 19.4 mM D-mannitol) resulted in the most significant increases in microvessel parameters, and the most significant decrease in permeability, which suggests increased osmolality in diabetes may influence placental vascular development and endothelial barrier function.
- Overall, the vascular dysfunction that occurs as a result of maternal glucose fluctuations may alter blood flow and nutrient transfer to the fetus, resulting in aberrant fetal growth.

Chapter 8 – General Discussion

8.1 Main findings

LGA is one of the major complications associated with GDM, with high prevalence even when glycaemia is clinically considered well-controlled[35–37]. Although the underlying causes are unclear, LGA has been linked to abnormal placental development and function[64,174,203,776]. Recent CGM studies have reported that subtle fluctuations in maternal glucose, with temporal periods of mild hyperglycaemia, are associated with LGA in GDM[62]. This study is the first to investigate the impact of physiological maternal glucose fluctuations on placental development and function.

In vivo maternal glucose fluctuations, associated with AGA and LGA in GDM were modelled using glucose treatments of 5/5.5 and 7 mM, respectively, in an *ex vivo* placental explant model. The placental transcriptome was altered by 7 mM glucose, and functional enrichment revealed that altered genes were predominantly associated with the immune/inflammatory response and vascular development. Several DEGs were also altered in GDM and LGA (non-GDM) placentae, linking changes in GDM/LGA to maternal glucose fluctuations.

DEGs enriched in inflammatory/immune pathways included many downregulated pro-inflammatory mediators expressed by placental HBCs (suggesting an anti-inflammatory profile). HBCs are known to predominantly be anti-inflammatory M2 polarised macrophages, with roles in placental vascular development, suggesting that they may contribute to placental vascular dysfunction in LGA. Additionally, exposure of placental explants to 7 mM glucose also resulted in small increases in the levels of M2-polarised HBCs, although this was not significant.

pMSCs, successfully isolated from human term placentae, were able to differentiate into cells of the endothelial lineage using biochemical stimulation. This rendered them a suitable model for further investigating early placental vascular development, whereby pMSCs give rise to endothelial progenitors in primitive placental blood vessels[80]. While glucose had minimal impact of pMSC to endothelial lineage differentiation, 7-9 mM glucose altered microvessel development in a model of placental microvasculature.

Overall, the findings from this study support the hypothesis outlined in Chapter 1. Maternal glucose fluctuations can alter the placental transcriptome and contribute to dysfunctional placental vascular development, which may occur directly and/or via HBCs. In turn, this may impact the ability of the placenta to transfer nutrients and gases to the fetus, resulting in aberrant fetal growth and LGA (Figure 8.1).

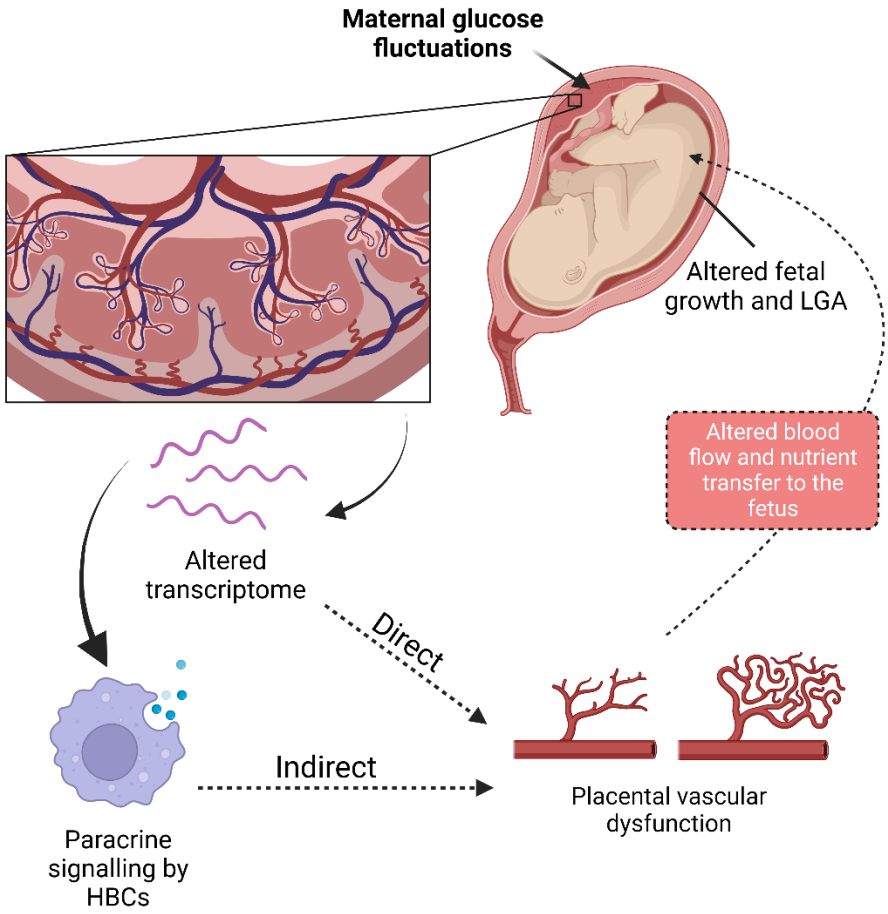

Figure 8.1 - Graphical representation of the main findings from the study and the proposed mechanism for the involvement of maternal glucose fluctuations in the development of LGA in GDM. Physiological maternal glucose fluctuations can alter the placental transcriptome, and either directly alter placental vascular development, or influence paracrine signalling from placental macrophages (Hofbauer Cells, HBCs), which has an indirect impact on placental vascular development. The resulting placental vascular dysfunction then alters blood flow and nutrient transfer to the fetus, leading to altered fetal growth and LGA.

8.2 Clinical relevance

8.2.1 Improving glucose control in pregnancies complicated by maternal diabetes through implementation of CGM

In the present study, physiological fluctuations in maternal glucose associated with LGA in GDM were modelled in placental explants and placental cells. Given that many previous *in vitro and ex vivo* studies utilise supraphysiological glucose concentrations to investigate the impact of maternal hyperglycaemia on the placenta[262,282,420], the present study was more clinically, and physiologically relevant. The findings highlight the need for tighter glucose targets in pregnancy, to improve glucose control, as these small fluctuations can influence placental function and thus may result in pathological fetal growth.

The current glucose targets for diabetes in pregnancy, across all modalities, and the available supporting evidence were recently reviewed (Byford *et al.* 2022)[777]. Here, studies used to define glucose targets, were found to be predominantly based on women with T1DM, with limited research on T2DM and GDM. This is particularly important as the national pregnancy in diabetes (NPID) audit in 2016 revealed that the proportion of diabetic pregnant women that have T2DM has increased to 50%, compared to 27% in 2002-2003[12,778]. Findings from this review revealed that CGM improves pregnancy outcomes and is advantageous over SMBG in that it can prevent maternal hypoglycaemia, through predictions and alerts, allowing women to achieve tighter glucose targets more safely. Unmasked CGM can also immediately inform the patient of their glycaemic control, allowing for self-management of lifestyle and therapy[777]. Additionally, CGM readings can be computed to insulin pumps, to automate insulin doses, via complex algorithms, known as a closed-loop system[779]. The first RCT of closed-loop therapy in T1DM pregnancies (AiDAPT)[779] has recently been carried out and pilot studies have shown that this improves nocturnal TIR and maternal hypoglycaemia in women with T1DM[780,781]. Hence, the implementation of CGM into routine clinical practice could help detect subtle glucose variations, allow treatment modifications, and improve glycaemic control.

In line with this, the NHS in England has recently incorporated diabetes in pregnancy into its ‘saving babies lives’ document, which is implemented in all maternity services[782]. This addition was based on findings from the recent NPID audit, which revealed that independent risk factors for perinatal death included increased HbA1c in the third trimester[783]. The updated saving babies lives document aims to reduce perinatal mortality in pregnancies complicated by both types of pre-gestational

diabetes, by implementing tighter glucose targets and offering wider access to CGM technologies, to improve glucose management[782]. While GDM has not yet been implemented in this, a current multicentre randomised controlled feasibility trial (the RECOGNISE trial) is aiming to establish the use of CGM (compared to SMBG) in women with GDM for reducing fetal macrosomia (LGA) and improving maternal and fetal outcomes[784]. Thus, this may further provide supporting evidence for glucose treatment targets in GDM and for implementation of CGM in this group of patients.

8.2.2 Applications to pre-gestational diabetes in pregnancy and diabetes outside of pregnancy

Although the glucose concentrations utilised in this study were based on CGM profiles of women with GDM[62], these concentrations may also be applicable to other types of diabetes in pregnancy. Analysis of CGM glucose profiles from women with pre-gestational diabetes by Law *et al.* (2015) revealed that LGA was associated with a lower mean glucose in the first trimester (7 vs 7.1 mM) and higher mean glucose in the second and third trimesters (7 vs 6.7 mM and 6.5 vs 6.4 mM, respectively). Using FDA, these subtle differences in glucose were also found to be fluctuating; for example, in the second trimester mothers who delivered LGA infants had higher glucose in the early hours of the morning (3:30 – 6:35 am) and during the afternoon (11:25 am – 17:10 pm). In T1DM pregnancies, Scott *et al*. (2022) revealed that LGA was associated with higher 24-hour CGM profiles from 10 weeks gestation, with higher mean glucose (7.6 mM vs 7.1 mM)[785]. Although only a small increase in glucose (0.5 mM), it was shown to persist throughout pregnancy. The increase in mean glucose from 10 weeks correlates with the development of the fetal pancreas, which can produce insulin to respond to maternal glucose by 12 weeks gestation. This increases fat and protein stores, resulting in fetal adiposity and overgrowth, as proposed by Pedersen[32,33]. Thus, the findings in the present study may also suggest that subtle fluctuations in maternal glucose impact placental function and fetal growth in pregnancies complicated by pre-gestational diabetes. This is important given that LGA is the commonest complication of pre-gestational diabetic pregnancies, affecting 1 in 2 infants[36], and that rates of diabetes in pregnancy are increasing, due to the higher levels of obesity and T2DM associated with unhealthy lifestyles[5,11].

Additionally, the current findings may also be important for researchers investigating diabetes outside of pregnancy. Glycaemic fluctuations are well-documented in T1DM and T2DM, including hypoglycaemic events and postprandial hyperglycaemia. These fluctuations can impact on the patient's quality of life, memory, attention, and mood,

and also may be associated with microvascular complications[786]. This suggests that fluctuating glucose levels should be implemented into *in vitro* studies in diabetes, given that glucose levels are not constant in individuals with diabetes. In line with this, several studies have shown that fluctuating glucose levels can influence cellular function[421–423]. For example, fluctuations in glucose (cycling between 5 and 20 mM), compared to constant high glucose, have been found to impair the viability and function of HUVECs, which are widely used as a model in the diabetes field[422,787]. However, as emphasised throughout, the high glucose concentrations in these fluctuating conditions, are supraphysiological (~20-50 mM). Intensive diabetes management to improve glycaemic control has been implemented, due to the decreased risk of long-term microvascular complications[39,41] and the HbA1c target for diabetes outside of pregnancy is <6.5-7%[788,789], which equates to an average glucose of around 7-8 mM[751]. Thus, blood glucose levels above this would be considered poor glycaemic control. Overall, this suggests that the levels utilised in the present study may be appropriate for investigating diabetes outside of pregnancy, given that they're within a physiological range, and are fluctuating.

8.2.3 The direct and indirect effects of maternal glucose fluctuations on the placenta and fetus

The methods utilised in the present study have assessed the direct impact of maternal glucose fluctuations on the placenta, however, maternal glucose may be acting indirectly, possibly via maternal EVs. In pregnancy, EVs regulate important processes, such as embryo implantation, spiral artery remodelling and metabolism[790]. Research by Holder *et al*. (2016) revealed that maternal macrophage derived EVs could be internalised by the placenta and induce the release of interleukins in placental explants, which suggests that the placenta can endocytose maternal EVs, which may then influence processes in the placenta[791]. In GDM, higher concentrations of circulating EVs have been reported, compared to normal pregnancies[311], as well as altered miRNA cargo[312]. Moreover, unpublished data from our group (Cartland *et al.*), which assessed the miRNA profile of maternal serum EVs in pregnancy using a microarray, identified 20 miRNAs that were differentially expressed in GDM LGA compared to GDM AGA pregnancies[792,793]. These dysregulated miRNAs have known functions in vascular development, including vascular lineage differentiation, EC migration and regulation of angiogenesis[359], suggesting that EVs may contribute to vascular dysfunction in GDM. Thus, given that the miRNA content of EVs is known to be altered in pregnancies complicated by GDM and/or LGA and that impaired glycaemic control has been linked

to LGA, maternal glucose could alter EV content, which could be taken up by and have subsequent effects on the placenta. Additionally, Rice *et al*. (2015) found that glucose (25 mM) increased EV release from first trimester trophoblast cells, *in vitro*. HUVECs were then exposed to these EVs, which led to an increase in IL-4, IL-6 and IL-8 release, suggesting a role for hyperglycaemia in altering EV release and in influencing placental EC function[794]. Therefore, the impact of glucose fluctuations on the content of maternal EVs and subsequent impact on placental function warrants further study.

Additionally, maternal glucose fluctuations could directly impact fetal development, by glucose transfer across the placenta to the fetus. Pedersen hypothesised that high glucose, in maternal hyperglycaemia, can cross the placenta and initiate insulin production in the fetus, resulting in hyperinsulinemia. This increases fat and protein stores and results in fetal adiposity and overgrowth[32,33]. Michelsen *et al*. (2018) assessed fetal and placental glucose consumption and observed that 30% of the glucose was allocated to the placenta and 70% to the fetus. This suggests that while fetal glucose consumption is dependent on the requirements of the placenta, the majority of glucose in the circulation is transferred to the fetus[175].

Interestingly, a secondary analysis of the CONCEPTT study revealed that infants with neonatal hypoglycaemia had higher birthweight and skinfold measures. The link between fetal overgrowth and neonatal hypoglycaemia suggests that this is related to fetal hyperinsulinemia. The mothers of infants with neonatal hypoglycaemia had higher HbA1c (45 vs 48%) and reduced TIR (46 vs 53%), however these were subtle impairments in glycaemic control, suggesting mild hyperglycaemia may directly impact fetal development[795]. Increased glucose in the fetal circulation may also impact the function of fetal pancreatic β-cells, which are known to be irreversibly damaged by long-term exposure to excessive glucose[796]. Rumala *et al.* (2020) found that mild increases in glucose (7 mM compared to 5 mM) can increase mTORC1 in β-cells, which was further increased with 11 mM glucose. Chronic exposure to excess glucose promoted metabolic acceleration of the cells, which further increased mechanistic target of rapamycin complex 1 (mTORC1), ultimately disturbing the metabolism and insulin secretion patterns of β-cells[797]. Thus, this suggests that subtle increases in glucose in GDM, may directly impact pancreatic development and function in the fetus. Hyperglycaemia has also been shown to influence fetal heart development in a mouse model of diabetes. Maternal hyperglycaemia (215 mg/dL, compared to 71 mg/dL in control mice, which equates to ~ 11.9 and 3.4 mM, respectively) increased fetal and neonatal cardiomyocyte proliferation, and increased the thickness of the left and right ventricular free walls[798]. Overall, in addition to impacting placental development,

physiological maternal glucose fluctuations may directly influence fetal organ development.

8.3 Other contributions to the field

Several placental models were employed in the present study to investigate the impact of maternal glucose on the placenta, and the findings have further elucidated the strengths and limitations of these currently available models. For example, the placental explant model allowed investigation into multiple placental cell types, including trophoblast, stromal cells and endothelium[321], and was ideal for assessing viability, trophoblast proliferation/apoptosis and the placental transcriptome. Although, the placental explant model was not ideal for longer-term culture, particularly for assessing placental vascularisation, due to the collapsing of vessels following a loss of perfusion[115].

Therefore, to further investigate placental vasculature, pMSCs were utilised to generate a model of placental vascular development. These findings further contribute to the understanding of the differentiation potential of pMSCs. As discussed in Chapter 6, endothelial lineage differentiation of MSCs from other sources has been established[386,656,658,659]. However, in studies utilising MSCs isolated from the placenta, exposure to endothelial differentiation medium was over short time periods (~24 hours), or the differentiated cells were not fully characterised[653,654]. In contrast, in the present study, pMSCs were exposed to differentiation medium, containing endothelial growth factors, for up to 25 days, and were fully characterised. Differentiated pMSCs had increased gene expression of endothelial markers, *FLT1, KDR* and *PECAM1*, and increased protein expression of VEGFR1 (*FLT1*). Altered levels of mesenchymal markers were also observed, including increased *CD44* gene expression. Differentiated pMSCs also formed endothelial tubes and angiogenic sprouts in functional assays. However, increases in VWF and PECAM1/CD31 were not observed at the same level as ECs, suggesting this model is not capable of generating mature ECs.

A limitation of many placental models is that they use static culture conditions, failing to recapitulate the dynamic flow environment in the placenta[127]. Microfluidic devices utilise fluid flow conditions, more accurately mimicking the *in vivo* microenvironment of cells[344]. In Chapter 6, microfluidic devices were utilised to expose pMSCs to shear stress conditions, which is known to influence the endothelial lineage differentiation potential of MSCs[366]. Low shear stress increased endothelial tube formation and the expression of some endothelial markers (e.g. VWF), although, the combination of low shear stress and differentiation medium did not further increase endothelial lineage

differentiation of pMSCs. Given that paracrine signalling by other placental cell types, such as trophoblasts, pericytes, fibroblasts and HBCs, can influence vascular development[93,94], this model was limited as it included only one cell type. Therefore, a model of placental microvasculature, which included placental ECs (HUVECs), pericytes and fibroblasts, was utilised in Chapter 7. This was an ideal model for assessing placental vasculogenesis by incorporating several cell types important for blood vessel formation and maturation[83,101]. Gravitational fluid flow was established using the addition of reservoirs. This dynamic flow environment has also recently been incorporated into other models, such as placental explants[115], and placenta-on-a-chip[127,347,352,354].

In the diabetes in pregnancy field, previous studies investigating the impact of hyperglycaemia on the placenta, do not assess the levels of glucose in the culture medium[262,264,282,420,497]. Given that glucose is rapidly consumed by tissues and cells, absolute levels overtime in culture will vary and will fail to reflect input concentrations, as demonstrated in the present study. Moreover, cells/tissues could likely be exposed to hypoglycaemic levels between medium changes. This was also highlighted by Torimoto *et al*. (2021) who reported that when vascular cell types from other sources were cultured in standard low glucose medium there was a high risk of hypoglycaemic conditions, which resulted in altered experimental outcomes[799]. *In vitro* and *ex vivo* culture in excessive glucose can also increase the osmolality of the culture medium, which could contribute to functional changes[498]. Measurement of osmolality in the condition medium throughout culture, which is not employed by previous studies[262,264,282,420,497], can reveal any small changes in osmolality between conditions, which was demonstrated in Chapter 7. Thus, the methodologies applied in this study for assessing glucose and osmolality in conditioned medium should be applied to other studies within the field.

Moreover, hyperosmolar controls can be used, including D-mannitol, a sugar alcohol, which will increase the osmolality of the medium, similarly to glucose, but is devoid of metabolic activities[499,500]. While some previous studies utilise hyperosmolar controls[264,497], many do not[262,282,420]. In Chapter 7, the hyperosmolar mannitol control (5.6 mM glucose + 19.4 mM mannitol) was found to have the most significant effect on microvessel morphology and permeability in the placental microvasculature model, which is in line with findings from other studies[770,773,800]. This further highlights the importance of assessing osmolality and/or employing a hyperosmolar control, to establish whether functional changes are a result of increased glucose or increased osmolality.

8.4 Limitations and proposed future study

While the findings of this study have the potential to influence the field, there are also several limitations, which could be addressed in future study. The sample sizes of some experiments were quite small, which increases the risk of false negative conclusions, therefore further experimental replicates would be advantageous. Moreover, RNA sequencing in Chapter 3, revealed that glucose fluctuations downregulated pro-inflammatory mediators. These altered mediators were found to be expressed in the HBC proteome, leading to the hypothesis that glucose fluctuations were influencing levels of inflammatory mediators secreted from HBCs, which could further elicit a paracrine effect on developing placental blood vessels. However, this has not yet been confirmed experimentally. To further investigate this, the secretome of isolated HBCs from human placentae could be assessed following exposure to glucose fluctuations. To elucidate the effect on placental vascular development, conditioned medium from HBCs could be applied to placental ECs during functional assays, such as the tube formation and angiogenic sprouting assay, utilised in Chapter 6. Otherwise, to examine the communication more closely between HBCs and developing blood vessels, a multi-layered microfluidic model could be used to co-culture isolated HBCs with ECs or differentiating pMSCs. As previously discussed, to further confirm whether glucose fluctuations were increasing the levels of M2 HBCs, increased sample numbers for immunohistochemistry would be needed.

HBCs are also known to be present at higher levels in the first trimester of pregnancy[209], therefore it would be interesting to assess the impact of glucose fluctuations on HBCs isolated from early pregnancy, where paracrine signalling may be contributing to the development of early blood vessels and vasculogenesis. Moreover, the pMSC model was limited in that pMSCs were not induced into mature ECs. Expression of mature EC markers, VWF and CD31, are thought to be increased in pMSCs isolated from first trimester placentae[660]. Utilising pMSCs from first trimester placentae may more accurately model the early development of primitive placental blood vessels. Although GDM is diagnosed at ~28 weeks, there is a potential for maternal glucose fluctuations to be present earlier in pregnancy[596], prior to diagnosis, which could impair normal placental development at an earlier timepoint. Therefore, this warrants the use of cells from earlier pregnancy.

To compare to *ex vivo* findings, gene expression was also assessed in placentae of GDM and non-GDM pregnancies, in Chapter 4. Samples were separated for birthweight categories, to allow for comparisons between AGA and LGA placentae, which is not considered in previous studies assessing the placental vasculature in

pregnancies complicated by maternal diabetes[122,125,129–133]. This revealed altered levels of several genes between birthweight categories, that were not detected when comparing GDM and non-GDM alone. This demonstrates the importance of separating samples based on their BWCs. Although, these findings will also be influenced by glycaemic control, and maternal glucose profiles were unknown in these samples. Given that the findings of this study revealed that physiological maternal glucose fluctuations in GDM can impact placental development in *ex vivo* and *in vitro* models, further study should investigate the impact of *in vivo* maternal glucose fluctuations on the placenta, by collecting samples from pregnant women that have received CGM during pregnancy. As discussed in Chapter 4, a current study in our research group is the MAGiC study, which recruited pregnant women in the first trimester who had at least one risk factor for developing GDM and were given routine CGM throughout pregnancy[596]. Given that LGA also occurs in women without a diagnosis of GDM, which is thought to be linked to glucose dysregulation[596], samples from this study would allow investigation into whether *in vivo* glucose fluctuations (from CGM data) in non-GDM pregnancies, as well as GDM pregnancies, can be linked to placental development and fetal growth. Moreover, the use of closed-loop treatment systems, discussed above, also have potential for further studies on the placenta. Given that these systems can customise glucose targets, and provide 'tighter' glycaemic control, it would be important to see if this improves placental vascular function.

Finally, GDM is a complex condition, and there are several components of the diabetic milieu that could potentially be influencing placental development and fetal growth, which have not been explored, such as insulin, hyperlipidaemia, adipokines, oxidative stress and circulating miRNAs (discussed above)[298–300,541,598–600]. However, maternal hyperglycaemia has long been considered the principal determinant of fetal growth complications, and this present study has demonstrated how small, yet significant fluctuations in maternal glucose can influence placental development and function, which may result in LGA.

References

1. Bastaki, S. Diabetes mellitus and its treatment. *Int. J. Diabetes Metab.* **13**, 111–134 (2019).
2. Cnop, M. *et al.* Mechanisms of Pancreatic β-Cell Death in Type 1 and Type 2 Diabetes: Many Differences, Few Similarities. *Diabetes* **54**, S97–S107 (2005).
3. Cerf, M. E. Beta cell dysfunction and insulin resistance. *Front. Endocrinol. (Lausanne).* **4**, 37 (2013).
4. Lin, X. *et al.* Global, regional, and national burden and trend of diabetes in 195 countries and territories: an analysis from 1990 to 2025. *Sci. Rep.* **10**, 14790 (2020).
5. Hart, B. N., Shubrook, J. H. & Mason, T. Pregestational Diabetes and Family Planning. *Clin. Diabetes* **39**, 323–328 (2021).
6. Feleke, B. E. *et al.* Maternal and newborn effects of gestational diabetes mellitus: A prospective cohort study. *Prim. Care Diabetes* **16**, 89–95 (2022).
7. Sonagra, A. D., Biradar, S. M., Dattatreya, K. & Murthy, J. D. S. Normal Pregnancy- A State of Insulin Resistance. *J. Clin. Diagnostic Res.* **8**, 3–5 (2014).
8. Plows, J. F., Stanley, J. L., Baker, P. N., Reynolds, C. M. & Vickers, M. H. The pathophysiology of gestational diabetes mellitus. *Int. J. Mol. Sci.* **19**, 1–21 (2018).
9. Rowan, J. A., Hague, W. M., Gao, W., Battin, M. R. & Moore, M. P. Metformin versus insulin for the treatment of gestational diabetes. *N. Engl. J. Med.* **358**, 2003–2015 (2008).
10. Yuen, L. *et al.* Projections of the prevalence of hyperglycaemia in pregnancy in 2019 and beyond: Results from the International Diabetes Federation Diabetes Atlas, 9th edition. *Diabetes Res. Clin. Pract.* **157**, 107841 (2019).
11. Alfadhli, E. M. Gestational diabetes mellitus. *Saudi Med. J.* **36**, 399–406 (2015).
12. Murphy, H. R., Bell, R., Dornhorst, A., Forde, R. & Lewis-Barned, N. Pregnancy in Diabetes: challenges and opportunities for improving pregnancy outcomes. *Diabet. Med.* **35**, 292–299 (2018).
13. Metzger, B. E. International Association of Diabetes and Pregnancy Study Groups recommendations on the diagnosis and classification of hyperglycemia in pregnancy. *Diabetes Care* **33**, 676–682 (2010).
14. National Institute for Health and Care Excellence. NCC-WCH Diabetes in pregnancy, NG3 Guidelines. 1–681 (2015).
15. Bell, R., Glinianaia, S. V., Tennant, P. W. G., Bilous, R. W. & Rankin, J. Peri-conception hyperglycaemia and nephropathy are associated with risk of congenital anomaly in women with pre-existing diabetes: A population-based cohort study. *Diabetologia* **55**, 936–947 (2012).
16. Tennant, P. W. G., Glinianaia, S. V., Bilous, R. W., Rankin, J. & Bell, R. Pre-existing diabetes, maternal glycated haemoglobin, and the risks of fetal and infant death: A population-based study. *Diabetologia* **57**, 285–294 (2014).
17. Miodovnik, M. *et al.* Elevated maternal glycohemoglobin in early pregnancy and spontaneous abortion among insulin-dependent diabetic women. *Am. J. Obstet. Gynecol.* **153**, 439–442 (1985).
18. Greene, M. F., Hare, J. W., Cloherty, J. P., Benacerraf, B. R. & Soeldner, J. S. First-trimester hemoglobin A1 and risk for major malformation and spontaneous abortion in diabetic pregnancy. *Teratology* **39**, 225–231 (1989).
19. Negrato, C. A., Mattar, R. & Gomes, M. B. Adverse pregnancy outcomes in women with diabetes. *Diabetol. Metab. Syndr.* **4**, (2012).
20. Wu, Y. *et al.* Association of Maternal Prepregnancy Diabetes and Gestational Diabetes Mellitus With Congenital Anomalies of the Newborn. *Diabetes Care* **43**, 2983–2990 (2020).
21. American Diabetes Association. 14. Management of Diabetes in Pregnancy: Standards of Medical Care in Diabetes-2020. *Diabetes Care* **43**, S183–S192

(2020).
22. Lazalde, B., Sánchez-Urbina, R., García de Alba, J. E. & Ramírez-Dueñas, M. L. [Gestational diabetes mellitus and congenital malformations]. *Ginecol. Obstet. Mex.* **69**, 399–405 (2001).
23. Yu, Y. *et al.* Maternal diabetes during pregnancy and early onset of cardiovascular disease in offspring: population based cohort study with 40 years of follow-up. *BMJ* **367**, l6398 (2019).
24. Thirunavukarasu, S. *et al.* Maternal Cardiac Changes in Women With Obesity and Gestational Diabetes Mellitus. *Diabetes Care* **45**, 3007–3015 (2022).
25. Assi, E. *et al.* Placental proteome abnormalities in women with gestational diabetes and large-for-gestational-age newborns. *BMJ open diabetes Res. care* **8**, 1–8 (2020).
26. Chiavaroli, V. *et al.* Incidence of infants born small- and large-for-gestational-age in an Italian cohort over a 20-year period and associated risk factors. *Ital. J. Pediatr.* **42**, 42 (2016).
27. Rezaiee, M. *et al.* Fetal macrosomia: Risk factors, Maternal, and Perinatal outcome. *Ann. Med. Health Sci. Res.* **3**, 546 (2013).
28. Saha, S. & Saha, S. A comparison of the risk of cesarean section in gestational diabetes mellitus patients supplemented antenatally with vitamin d containing supplements versus placebo: A systematic review and meta-analysis of double-blinded randomized controlled trials. *J. Turkish Ger. Gynecol. Assoc.* **21**, 201–212 (2020).
29. Harder, T., Rodekamp, E., Schellong, K., Dudenhausen, J. W. & Plagemann, A. Birth weight and subsequent risk of type 2 diabetes: A meta-analysis. *Am. J. Epidemiol.* **165**, 849–857 (2007).
30. Yan, J. & Yang, H. Gestational diabetes mellitus, programing and epigenetics. *J. Matern. neonatal Med. Off. J. Eur. Assoc. Perinat. Med. Fed. Asia Ocean. Perinat. Soc. Int. Soc. Perinat. Obstet.* **27**, 1266–1269 (2014).
31. Simeoni, U., Yzydorczyk, C., Siddeek, B. & Benahmed, M. Epigenetics and neonatal nutrition. *Early Hum. Dev.* **90**, S23–S24 (2014).
32. Metzger, B. E. *et al.* Hyperglycemia and adverse pregnancy outcomes. *N. Engl. J. Med.* **358**, 1991–2002 (2008).
33. Catalano, P. M. & Hauguel-De Mouzon, S. Is it time to revisit the Pedersen hypothesis in the face of the obesity epidemic? *Am. J. Obstet. Gynecol.* **204**, 479–487 (2011).
34. Nahavandi, S., Seah, J.-M., Shub, A., Houlihan, C. & Ekinci, E. I. Biomarkers for Macrosomia Prediction in Pregnancies Affected by Diabetes. *Front. Endocrinol. (Lausanne).* **9**, 407 (2018).
35. Evers, I., De Valk, H., Mol, B., Ter Braak, E. & Visser, G. Macrosomia despite good glycaemic control in Type I diabetic pregnancy; results of a nationwide study in The Netherlands. *Diabetologia* **45**, 1484–1489 (2002).
36. Law, G. R. *et al.* Analysis of Continuous Glucose Monitoring in Pregnant Women With Diabetes: Distinct Temporal Patterns of Glucose Associated With Large-for-Gestational-Age Infants. *Diabetes Care* **38**, 1319–1325 (2015).
37. Murphy, H. R. *et al.* Effectiveness of continuous glucose monitoring in pregnant women with diabetes: Randomised clinical trial. *Bmj* **337**, 907–910 (2008).
38. Rafat, D. & Ahmad, J. HbA1c in pregnancy. *Diabetes Metab. Syndr. Clin. Res. Rev.* **6**, 59–64 (2012).
39. Middleton, P., Crowther, C. A. & Simmonds, L. Different intensities of glycaemic control for pregnant women with pre-existing diabetes. *Cochrane Database Syst. Rev.* **2016**, (2016).
40. Weykamp, C. HbA1c: A review of analytical and clinical aspects. *Ann. Lab. Med.* **33**, 393–400 (2013).
41. Diabetes Control and Complications Trial Research Group. The Effect of Intensive Treatment of Diabetes on the Development and Progression of Long-

Term Complications in Insulin-Dependent Diabetes Mellitus. *N. Engl. J. Med.* **329**, 977–986 (1993).
42. ACOG. Clinical Management Guidelines for Obstetrician – Gynecologists - Pre-existing Diabetes. *Obstet. Gynecol.* **132**, e229–e248 (2018).
43. ACOG. Clinical Management Guidelines for Obstetrician – Gynecologists - GDM. *Obstet. Gynecol.* **131**, e49–e64 (2018).
44. Nankervis, A. *et al.* ADIPS Consensus Guidelines for the Testing and Diagnosis of Gestational Diabetes Mellitus in Australia. *Australas. Diabetes Pregnancy Soc.* 1–8 (2008).
45. McIntyre, H. D. & Flack, J. R. Consensus statement on diabetes control in preparation for pregnancy. *Med. J. Aust.* **181**, 326 (2004).
46. McElduff, A. *et al.* The Australasian Diabetes in Pregnancy Society consensus guidelines for the management of type 1 and type 2 diabetes in relation to pregnancy. *Med. J. Aust.* **183**, 373–377 (2005).
47. Feig, D. S. *et al.* 2018 Clinical Practice Guidelines Diabetes and Pregnancy Diabetes Canada Clinical Practice Guidelines Expert Committee Pre-Existing Diabetes Preconception and During Pregnancy. *Can J Diabetes* **42**, S255-282 (2018).
48. Blumer, I. *et al.* Diabetes and pregnancy: An endocrine society clinical practice guideline. *J. Clin. Endocrinol. Metab.* **98**, 4227–4249 (2013).
49. Langer, O. Glycemic targets for the optimal treatment of GDM. *Clin. Obstet. Gynecol.* **56**, 788–802 (2013).
50. Bancroft, K., Tuffnell, D. J., Mason, G. C., Rogerson, L. J. & Mansfield, M. A randomised controlled pilot study of the management of gestational impaired glucose tolerance. *Br. J. Obstet. Gynaecol.* **107**, 959–963 (2000).
51. Hawkins, J. S., Casey, B. M. & Lo, J. Y. Monitoring in Women With Diet-Treated Gestational Diabetes. *Obstet. Gynecol.* **113**, 1307–1312 (2009).
52. Varner, M. W. Efficacy of home glucose monitoring in diabetic pregnancy. *Obstet. Gynecol. Surv.* **39**, 427–429 (1984).
53. National Institute for Health and Care Excellence. Type 1 Diabetes in Adults: Diagnosis and Management, NG17 Guidelines. 1–89 (2015).
54. Advani, A. Positioning time in range in diabetes management. *Diabetologia* **63**, 242–252 (2020).
55. Battelino, T. *et al.* Clinical targets for continuous glucose monitoring data interpretation: Recommendations from the international consensus on time in range. *Diabetes Care* **42**, 1593–1603 (2019).
56. Feig, D. S. *et al.* Continuous glucose monitoring in pregnant women with type 1 diabetes (CONCEPTT): a multicentre international randomised controlled trial. *Lancet* **390**, 2347–2359 (2017).
57. Kestilä, K. K., Ekblad, U. U. & Rönnemaa, T. Continuous glucose monitoring versus self-monitoring of blood glucose in the treatment of gestational diabetes mellitus. *Diabetes Res. Clin. Pract.* **77**, 174–179 (2007).
58. Wei, Q. *et al.* Effect of a CGMS and SMBG on Maternal and Neonatal Outcomes in Gestational Diabetes Mellitus: A Randomized Controlled Trial. *Sci. Rep.* **6**, 1–9 (2016).
59. Alfadhli, E., Osman, E. & Basri, T. Use of a real time continuous glucose monitoring system as an educational tool for patients with gestational diabetes. *Diabetol. Metab. Syndr.* **8**, 1–7 (2016).
60. Kristensen, K. *et al.* Continuous glucose monitoring in pregnant women with type 1 diabetes: an observational cohort study of 186 pregnancies. *Diabetologia* **62**, 1143–1153 (2019).
61. Scott, E. M., Feig, D. S., Murphy, H. R. & Law, G. R. Continuous glucose monitoring in pregnancy: Importance of analyzing temporal profiles to understand clinical outcomes. *Diabetes Care* **43**, 1178–1184 (2020).
62. Law, G. R. *et al.* Suboptimal nocturnal glucose control is associated with large

for gestational age in treated gestational diabetes mellitus. *Diabetes Care* **42**, 810–815 (2019).
63. Secher, A. L., Ringholm, L., Andersen, H. U., Damm, P. & Mathiesen, E. R. The effect of real-time continuous glucose monitoring in pregnant women with diabetes A randomized controlled trial. *Diabetes Care* **36**, 1877–1883 (2013).
64. Gauster, M., Desoye, G., Tötsch, M. & Hiden, U. The placenta and gestational diabetes mellitus. *Curr. Diab. Rep.* **12**, 16–23 (2012).
65. Chen, D. B. & Zheng, J. Regulation of Placental Angiogenesis. *Microcirculation* **21**, 15–25 (2014).
66. Evain-Brion, D. & Malassine, A. Human placenta as an endocrine organ. *Growth Horm. IGF Res.* **13**, 34–37 (2003).
67. Clark, A. R., Lin, M., Tawhai, M., Saghian, R. & James, J. L. Multiscale modelling of the feto-placental vasculature. *Interface Focus* **5**, (2015).
68. Wang, Y. & Zhao, S. *Vascular Biology of the Placenta*. *Colloquium Series on Integrated Systems Physiology: From Molecule to Function* (2010).
69. Jones, R. E. & Lopez, K. H. *Human reproductive biology*. (Elsevier Academic Press, 2006). doi:10.1016/s0890-6238(96)90010-6.
70. Woods, L., Perez-Garcia, V. & Hemberger, M. Regulation of Placental Development and Its Impact on Fetal Growth—New Insights From Mouse Models. *Front. Endocrinol. (Lausanne).* **9**, (2018).
71. Apps, R. *et al.* Genome-wide expression profile of first trimester villous and extravillous human trophoblast cells. *Placenta* **32**, 33–43 (2011).
72. Enders, A. C. A comparative study of the fine structure of the trophoblast in several hemochorial placentas. *Am. J. Anat.* **116**, 29–68 (1965).
73. Degner, K., Magness, R. R. & Shah, D. M. Establishment of the Human Uteroplacental Circulation: A Historical Perspective. *Reprod. Sci.* **24**, 753–761 (2017).
74. Ng, S. W. *et al.* Endometrial decidualization: The primary driver of pregnancy health. *Int. J. Mol. Sci.* **21**, 1–20 (2020).
75. Kingdom, J., Huppertz, B., Seaward, G. & Kaufmann, P. Development of the placental villous tree and its consequences for fetal growth. *Eur. J. Obstet. Gynecol. Reprod. Biol.* **92**, 35–43 (2000).
76. Jaffe, R., Jauniaux, E. & Hustin, J. Maternal circulation in the first-trimester human placenta - Myth or reality? *Am. J. Obstet. Gynecol.* **176**, 695–705 (1997).
77. Jauniaux, E., Jurkovic, D. & Campbell, S. In vivo investigations of the anatomy and the physiology of early human placental circulations. *Ultrasound Obstet. Gynecol.* **1**, 435–445 (1991).
78. Roberts, V. H. J. *et al.* Early first trimester uteroplacental flow and the progressive disintegration of spiral artery plugs: New insights from contrast-enhanced ultrasound and tissue histopathology. *Hum. Reprod.* **32**, 2382–2393 (2017).
79. Saghian, R., Bogle, G., James, J. L. & Clark, A. R. Establishment of maternal blood supply to the placenta: Insights into plugging, unplugging and trophoblast behaviour from an agent-based model. *Interface Focus* **9**, (2019).
80. Demir, R., Seval, Y. & Huppertz, B. Vasculogenesis and angiogenesis in the early human placenta. *Acta Histochem.* **109**, 257–265 (2007).
81. Charnock-Jones, D. S., Kaufmann, P. & Mayhew, T. M. Aspects of human fetoplacental vasculogenesis and angiogenesis. I. Molecular regulation. *Placenta* **25**, 103–113 (2004).
82. Armulik, A., Abramsson, A. & Betsholtz, C. Endothelial/pericyte interactions. *Circ. Res.* **97**, 512–523 (2005).
83. Kim, K. R., Sung, C. O., Kwon, T. J., Lee, J. & Robboy, S. J. Defective pericyte recruitment of villous stromal vessels as the possible etiologic cause of hydropic change in complete hydatidiform mole. *PLoS One* **10**, e0122266 (2015).
84. Sebire, N. J. & Talbert, D. The role of intraplacental vascular smooth muscle in

the dynamic placenta: A conceptual framework for understanding uteroplacental disease. *Med. Hypotheses* **58**, 347–351 (2002).
85. Fong, G.-H., Rossant, J., Gertsenstein, M. & Breitman, M. L. Role of the Flt-1 receptor tyrosine kinase in regulating the assembly of vascular endothelium. *Nature* **376**, 66–70 (1995).
86. Carmeliet, P. *et al.* Abnormal blood vessel development and lethality in embryos lacking a single VEGF allele. *Nature* **380**, 435–439 (1996).
87. Shalaby, F. *et al.* Failure of blood-island formation and vasculogenesis in Flk-1-deficient mice. *Nature* **376**, 62–66 (1995).
88. Pepper, M. S., Ferrara, N., Orci, L. & Montesano, R. Vascular endothelial growth factor (VEGF) induces plasminogen activators and plasminogen activator inhibitor-1 in microvascular endothelial cells. *Biochem. Biophys. Res. Commun.* **181**, 902–906 (1991).
89. Unemori, E. N., Ferrara, N., Bauer, E. A. & Amento, E. P. Vascular endothelial growth factor induces interstitial collagenase expression in human endothelial cells. *J. Cell. Physiol.* **153**, 557–562 (1992).
90. Zheng, J. *et al.* Activation of multiple signaling pathways is critical for fibroblast growth factor 2- and vascular endothelial growth factor-stimulated ovine fetoplacental endothelial cell proliferation. *Biol. Reprod.* **78**, 143–150 (2008).
91. Teichert, M. *et al.* Pericyte-expressed Tie2 controls angiogenesis and vessel maturation. *Nat. Commun.* **8**, 16106 (2017).
92. Sweeney, M. & Foldes, G. It Takes Two: Endothelial-Perivascular Cell Cross-Talk in Vascular Development and Disease. *Front. Cardiovasc. Med.* **5**, 1–14 (2018).
93. Charnock-Jones, D. S. & Burton, G. J. Placental vascular morphogenesis. *Best Pract. Res. Clin. Obstet. Gynaecol.* **14**, 953–968 (2000).
94. Seval, Y., Korgun, E. T. & Demir, R. Hofbauer Cells in Early Human Placenta: Possible Implications in Vasculogenesis and Angiogenesis. *Placenta* **28**, 841–845 (2007).
95. Vuorela, P. *et al.* Expression of Vascular Endothelial Growth Factor and Placenta Growth Factor in Human Placenta1. *Biol. Reprod.* **56**, 489–494 (1997).
96. Arany, E. & Hill, D. J. Fibroblast growth factor-2 and fibroblast growth factor receptor-1 mRNA expression and peptide localization in placentae from normal and diabetic pregnancies. *Placenta* **19**, 133–142 (1998).
97. Vuorela, P. *et al.* Expression of Vascular Endothelial Growth Factor and Placenta Growth Factor in Human Placenta1. *Biol. Reprod.* **56**, 489–494 (1997).
98. Matjila, M., Millar, R., van der Spuy, Z. & Katz, A. The Differential Expression of Kiss1, MMP9 and Angiogenic Regulators across the Feto-Maternal Interface of Healthy Human Pregnancies: Implications for Trophoblast Invasion and Vessel Development. *PLoS One* **8**, e63574 (2013).
99. Matjila, M., Millar, R., van der Spuy, Z. & Katz, A. The Differential Expression of Kiss1, MMP9 and Angiogenic Regulators across the Feto-Maternal Interface of Healthy Human Pregnancies: Implications for Trophoblast Invasion and Vessel Development. *PLoS One* **8**, e63574 (2013).
100. Loegl, J. *et al.* Pigment epithelium-derived factor (PEDF): a novel trophoblast-derived factor limiting feto-placental angiogenesis in late pregnancy. *Angiogenesis* **19**, 373–388 (2016).
101. Hughes, C. C. W. Endothelial-stromal interactions in angiogenesis. *Curr. Opin. Hematol.* **15**, 204–209 (2008).
102. Reyes, L., Wolfe, B. & Golos, T. Hofbauer Cells: Placental Macrophages of Fetal Origin. *Results Probl. Cell Differ.* **62**, 45–60 (2017).
103. Loegl, J. *et al.* Hofbauer cells of M2a, M2b and M2c polarization may regulate feto-placental angiogenesis. *Reproduction* **152**, 447–455 (2016).
104. Thomas, J. R. *et al.* Phenotypic and functional characterization of first-trimester human placental macrophages, Hofbauer cells. *J. Exp. Med.* **218**, (2020).

105. Demir, R. *et al.* Sequential expression of VEGF and its receptors in human placental villi during very early pregnancy: differences between placental vasculogenesis and angiogenesis. *Placenta* **25**, 560–572 (2004).
106. Martin, D., Galisteo, R. & Gutkind, J. S. CXCL8/IL8 stimulates vascular endothelial growth factor (VEGF) expression and the autocrine activation of VEGFR2 in endothelial cells by activating NFkappaB through the CBM (Carma3/Bcl10/Malt1) complex. *J. Biol. Chem.* **284**, 6038–6042 (2009).
107. Petreaca, M. L., Yao, M., Liu, Y., DeFea, K. & Martins-Green, M. Transactivation of Vascular Endothelial Growth Factor Receptor-2 by Interleukin-8 (IL-8/CXCL8) Is Required for IL-8/CXCL8-induced Endothelial Permeability. *Mol. Biol. Cell* **18**, 5014–5023 (2007).
108. Stamatovic, S. M., Keep, R. F., Mostarica-Stojkovic, M. & Andjelkovic, A. V. CCL2 Regulates Angiogenesis via Activation of Ets-1 Transcription Factor1. *J. Immunol.* **177**, 2651 LP – 2661 (2006).
109. Chu, L.-H., Lee, E., Bader, J. S. & Popel, A. S. Angiogenesis interactome and time course microarray data reveal the distinct activation patterns in endothelial cells. *PLoS One* **9**, e110871 (2014).
110. Lien, M.-Y. *et al.* Chemokine CCL4 Induces Vascular Endothelial Growth Factor C Expression and Lymphangiogenesis by miR-195-3p in Oral Squamous Cell Carcinoma . *Frontiers in Immunology* vol. 9 (2018).
111. Wu, Y., Li, Y.-Y., Matsushima, K., Baba, T. & Mukaida, N. CCL3-CCR5 Axis Regulates Intratumoral Accumulation of Leukocytes and Fibroblasts and Promotes Angiogenesis in Murine Lung Metastasis Process1. *J. Immunol.* **181**, 6384–6393 (2008).
112. Salcedo, R. *et al.* Human endothelial cells express CCR2 and respond to MCP-1: direct role of MCP-1 in angiogenesis and tumor progression. *Blood* **96**, 34–40 (2000).
113. Burton, G. J., Woods, A. W., Jauniaux, E. & Kingdom, J. C. P. Rheological and physiological consequences of conversion of the maternal spiral arteries for uteroplacental blood flow during human pregnancy. *Placenta* **30**, 473–482 (2009).
114. Brugger, B. A., Guettler, J. & Gauster, M. Go with the flow—trophoblasts in flow culture. *Int. J. Mol. Sci.* **21**, 1–13 (2020).
115. Kupper, N., Pritz, E., Siwetz, M., Guettler, J. & Huppertz, B. Placental villous explant culture 2.0: Flow culture allows studies closer to the in vivo situation. *Int. J. Mol. Sci.* **22**, (2021).
116. Paszkowiak, J. J. & Dardik, A. Arterial wall shear stress: observations from the bench to the bedside. *Vasc. Endovascular Surg.* **37**, 47–57 (2003).
117. Lecarpentier, E. *et al.* Computational Fluid Dynamic Simulations of Maternal Circulation: Wall Shear Stress in the Human Placenta and Its Biological Implications. *PLoS One* **11**, e0147262 (2016).
118. Acharya, G., Sonesson, S. E., Flo, K., Räsänen, J. & Odibo, A. Hemodynamic aspects of normal human feto-placental (umbilical) circulation. *Acta Obstetricia et Gynecologica Scandinavica* vol. 95 672–682 (2016).
119. Tun, W. M., Yap, C. H., Saw, S. N., James, J. L. & Clark, A. R. Differences in placental capillary shear stress in fetal growth restriction may affect endothelial cell function and vascular network formation. *Sci. Rep.* **9**, (2019).
120. Morley, L. C., Beech, D. J., Walker, J. J. & Simpson, N. A. B. Emerging concepts of shear stress in placental development and function. *Mol. Hum. Reprod.* **25**, 1–11 (2019).
121. James, J. L., Saghian, R., Perwick, R. & Clark, A. R. Trophoblast plugs: impact on utero-placental haemodynamics and spiral artery remodelling. *Hum. Reprod.* **33**, 1430–1441 (2018).
122. Daskalakis, G. *et al.* Placental pathology in women with gestational diabetes. *Acta Obstet. Gynecol. Scand.* **87**, 403–407 (2008).

123. Bhattacharjee, D. *et al.* Histopathological study with immunohistochemical expression of vascular endothelial growth factor in placentas of hyperglycemic and diabetic women. *J. Lab. Physicians* **9**, 227–233 (2017).
124. Meng, Q. *et al.* Expressions of VEGF-A and VEGFR-2 in placentae from GDM pregnancies. *Reprod. Biol. Endocrinol.* **14**, (2016).
125. Akarsu, S., Bagirzade, M., Omeroglu, S. & Büke, B. Placental vascularization and apoptosis in Type-1 and gestational DM. *J. Matern. Neonatal Med.* **30**, 1045–1050 (2017).
126. Burton, G. J. & Tham, S. W. Formation of vasculo-syncytial membranes in the human placenta. *J. Dev. Physiol.* **18**, 43–47 (1992).
127. Blundell, C. *et al.* A microphysiological model of the human placental barrier. *Lab Chip* **16**, 3065–3073 (2016).
128. Burton, G. J. & Fowden, A. L. The placenta: a multifaceted, transient organ. *Philos. Trans. R. Soc. London. Ser. B, Biol. Sci.* **370**, 20140066 (2015).
129. Troncoso, F. *et al.* Gestational diabetes mellitus is associated with increased pro-migratory activation of vascular endothelial growth factor receptor 2 and reduced expression of vascular endothelial growth factor receptor 1. *PLoS One* **12**, (2017).
130. Stoz, F., Schuhmann, R. A. & Schultz, R. Morphohistometric investigations of placentas of diabetic patients in correlation to the metabolic adjustment of the disease. *J. Perinat. Med.* **16**, 211–216 (1988).
131. Jirkovská, M. *et al.* The branching pattern of villous capillaries and structural changes of placental terminal villi in type 1 diabetes mellitus. *Placenta* **33**, 343–351 (2012).
132. Calderon, I. M. P. *et al.* Morphometric study of placental villi and vessels in women with mild hyperglycemia or gestational or overt diabetes. *Diabetes Res. Clin. Pract.* **78**, 65–71 (2007).
133. Higgins, M., Felle, P., Mooney, E. E., Bannigan, J. & McAuliffe, F. M. Stereology of the placenta in type 1 and type 2 diabetes. *Placenta* **32**, 564–569 (2011).
134. Jirkovská, M. *et al.* Topological properties and spatial organization of villous capillaries in normal and diabetic placentas. *J. Vasc. Res.* **39**, 268–278 (2002).
135. Björk, O. & Persson, B. Villous structure in different parts of the cotyledon in placentas of insulin-dependent diabetic women: A morphometric study. *Acta Obstet. Gynecol. Scand.* **63**, 37–43 (1984).
136. Mayhew, T. M., Sørensen, F. B., Klebe, J. G. & Jackson, M. R. Growth and maturation of villi in placentae from well-controlled diabetic women. *Placenta* **15**, 57–65 (1994).
137. Mayhew, T. M., Sorensen, F. B., Klebe, J. G. & Jackson, M. R. The effects of mode of delivery and sex of newborn on placental morphology in control and diabetic pregnancies. *J. Anat.* **183**, 545–552 (1993).
138. Babawale, M. O. *et al.* Effects of gestational diabetes on junctional adhesion molecules in human term placental vasculature. *Diabetologia* **43**, 1185–1196 (2000).
139. Jauniaux, E., Moscoso, J. G., Vanesse, M., Campbell, S. & Driver, M. Perfusion fixation for placental morphologic investigation. *Hum. Pathol.* **22**, 442–449 (1991).
140. Ogawa, M. *et al.* Standard curves of placental weight and fetal/placental weight ratio in Japanese population: difference according to the delivery mode, fetal sex, or maternal parity. *Eur. J. Obstet. Gynecol. Reprod. Biol.* **206**, 225–231 (2016).
141. Kalisch-Smith, J. I., Simmons, D. G., Dickinson, H. & Moritz, K. M. Review: Sexual dimorphism in the formation, function and adaptation of the placenta. *Placenta* **54**, 10–16 (2017).
142. Gorkem, U., Togrul, C. & Arslan, E. Relationship between elevated serum level of placental growth factor and status of gestational diabetes mellitus. *J. Matern.*

Neonatal Med. **0**, 1–5 (2019).
143. Ong, C. Y. T., Lao, T. T., Spencer, K. & Nicolaides, K. H. Maternal serum level of placental growth factor in diabetic pregnancies. *J. Reprod. Med. Obstet. Gynecol.* **49**, 477–480 (2004).
144. El-Tarhouny, S. A., Almasry, S. M., Elfayomy, A. K., Baghdadi, H. & Habib, F. A. Placental growth factor and soluble Fms-like tyrosine kinase 1 in diabetic pregnancy: A possible relation to distal villous immaturity. *Histol. Histopathol.* **29**, 259–272 (2014).
145. Eleftheriades, M. *et al.* Elevated placental growth factor concentrations at 11-14 weeks of gestation to predict gestational diabetes mellitus. *Metabolism.* **63**, 1419–1425 (2014).
146. Syngelaki, A., Kotecha, R., Pastides, A., Wright, A. & Nicolaides, K. H. First-trimester biochemical markers of placentation in screening for gestational diabetes mellitus. *Metabolism.* **64**, 1485–1489 (2015).
147. Gasiorowska, A. *et al.* Maternal factors, ultrasound and placental function parameters in early pregnancy as predictors of birth weight in low-risk populations and among patients with pre-gestational diabetes. *Ginekol. Pol.* **90**, 388–395 (2019).
148. Nadarajah, V. D., Min, R. G. L. Y., Judson, J. P., Jegasothy, R. & Ling, E. H. P. Maternal plasma soluble fms-like tyrosine kinase-1 and placental growth factor levels as biochemical markers of gestational hypertension for Malaysian mothers. *J. Obstet. Gynaecol. Res.* **35**, 855–863 (2009).
149. Pietro, L. *et al.* Vascular endothelial growth factor (VEGF) and VEGF-receptor expression in placenta of hyperglycemic pregnant women. *Placenta* **31**, 770–780 (2010).
150. Madazli, R. *et al.* The incidence of placental abnormalities, maternal and cord plasma malondialdehyde and vascular endothelial growth factor levels in women with gestational diabetes mellitus and nondiabetic controls. *Gynecol. Obstet. Invest.* **65**, 227–232 (2008).
151. Zhao, B., Han, X., Meng, Q. & Luo, Q. Early second trimester maternal serum markers in the prediction of gestational diabetes mellitus. *J. Diabetes Investig.* **9**, 967–974 (2018).
152. Lang, U. *et al.* Uterine blood flow—a determinant of fetal growth. *Eur. J. Obstet. Gynecol. Reprod. Biol.* **110**, S55–S61 (2003).
153. Huynh, J. *et al.* Type 1, type 2 and gestational diabetes mellitus differentially impact placental pathologic characteristics of uteroplacental malperfusion. *Placenta* **36**, 1161–1166 (2015).
154. Starikov, R. *et al.* Comparison of placental findings in type 1 and type 2 diabetic pregnancies. *Placenta* **35**, 1001–1006 (2014).
155. Pietryga, M. *et al.* Abnormal uterine Doppler is related to vasculopathy in pregestational diabetes mellitus. *Circulation* **112**, 2496–2500 (2005).
156. Salvesen, D. R. *et al.* Placental and fetal Doppler velocimetry in pregnancies complicated by maternal diabetes mellitus. *Am. J. Obstet. Gynecol.* **168**, 645–652 (1993).
157. Zimmermann, P., Kujansuu, E. & Tuimala, R. Doppler flow velocimetry of the uterine and uteroplacental circulation in pregnancies complicated by insulin-dependent diabetes mellitus. *J. Perinat. Med.* **22**, 137–147 (1994).
158. Wong, C.-H., Chen, C.-P., Sun, F.-J. & Chen, C.-Y. Comparison of placental three-dimensional power Doppler indices and volume in the first and the second trimesters of pregnancy complicated by gestational diabetes mellitus. *J. Matern. neonatal Med. Off. J. Eur. Assoc. Perinat. Med. Fed. Asia Ocean. Perinat. Soc. Int. Soc. Perinat. Obstet.* **32**, 3784–3791 (2019).
159. Vajnerova, O., Kafka, P., Kratzerova, T., Chalupsky, K. & Hampl, V. Pregestational diabetes increases fetoplacental vascular resistance in rats. *Placenta* **63**, 32–38 (2018).

160. Moran, M. *et al.* Novel placental ultrasound assessment: potential role in pre-gestational diabetic pregnancy. *Placenta* **35**, 639–644 (2014).
161. Eriksson, U. J. & Jansson, L. Diabetes in pregnancy: decreased placental blood flow and disturbed fetal development in the rat. *Pediatr. Res.* **18**, 735–738 (1984).
162. Surányi, A. *et al.* Placental three-dimensional power Doppler indices in mid-pregnancy and late pregnancy complicated by gestational diabetes mellitus. *Prenat. Diagn.* **33**, 952–958 (2013).
163. Chen, S.-J., Chen, C.-P., Sun, F.-J. & Chen, C.-Y. Comparison of Placental Three-Dimensional Power Doppler Vascular Indices and Placental Volume in Pregnancies with Small for Gestational Age Neonates. *J. Clin. Med.* **8**, (2019).
164. Rejniak, K. A., Kliman, H. J. & Fauci, L. J. A computational model of the mechanics of growth of the villous trophoblast bilayer. *Bull. Math. Biol.* **66**, 199–232 (2004).
165. Phillips, J. K. *et al.* Impact of experimental diabetes on the maternal uterine vascular remodeling during rat pregnancy. *Reprod. Sci.* **19**, 322–331 (2012).
166. Burke, S. D., Dong, H., Hazan, A. D. & Croy, B. A. Aberrant endometrial features of pregnancy in diabetic NOD mice. *Diabetes* **56**, 2919–2926 (2007).
167. Björk, O., Persson, B., Stangenberg, M. & Václavínková, V. Spiral artery lesions in relation to metabolic control in diabetes mellitus. *Acta Obstet. Gynecol. Scand.* **63**, 123–127 (1984).
168. Lecarpentier, E. *et al.* Fluid Shear Stress Promotes Placental Growth Factor Upregulation in Human Syncytiotrophoblast Through the cAMP-PKA Signaling Pathway. *Hypertens. (Dallas, Tex. 1979)* **68**, 1438–1446 (2016).
169. Burton, G. J., Charnock-Jones, D. S. & Jauniaux, E. Regulation of vascular growth and function in the human placenta. *Reproduction* **138**, 895–902 (2009).
170. Aardema, M. W., Oosterhof, H., Timmer, A., Van Rooy, I. & Aarnoudse, J. G. Uterine artery Doppler flow and uteroplacental vascular pathology in normal pregnancies and pregnancies complicated by pre-eclampsia and small for gestational age fetuses. *Placenta* **22**, 405–411 (2001).
171. Ferrazzi, E. *et al.* Uterine doppler velocimetry and placental hypoxic-ischemic lesion in pregnancies with fetal intrauterine growth restriction. *Placenta* **20**, 389–394 (1999).
172. Tun, W. M., Yap, C. H., Saw, S. N., James, J. L. & Clark, A. R. Differences in placental capillary shear stress in fetal growth restriction may affect endothelial cell function and vascular network formation. *Sci. Rep.* **9**, (2019).
173. Gaillard, R., Steegers, E. A. P., Tiemeier, H., Hofman, A. & Jaddoe, V. W. V. Placental Vascular Dysfunction, Fetal and Childhood Growth, and Cardiovascular Development. *Circulation* **128**, 2202–2210 (2013).
174. Rizzo, G. *et al.* Role of first-trimester umbilical vein blood flow in predicting large-for-gestational age at birth. *Ultrasound Obstet. Gynecol.* **56**, 67–72 (2020).
175. Michelsen, T. M. *et al.* Uteroplacental Glucose Uptake and Fetal Glucose Consumption: A Quantitative Study in Human Pregnancies. *J. Clin. Endocrinol. Metab.* **104**, 873–882 (2019).
176. Opheim, G. L. *et al.* The impact of umbilical vein blood flow and glucose concentration on blood flow distribution to the fetal liver and systemic organs in healthy pregnancies. *FASEB J.* **34**, 12481–12491 (2020).
177. Adanaş Aydın, G., Özdemir Akdur, P. & Özgen, G. The effect of glucose tolerance test on fetoplacental circulation. *Taiwan. J. Obstet. Gynecol.* **60**, 723–727 (2021).
178. Mone, F. *et al.* Fetal umbilical artery Doppler pulsatility index and childhood neurocognitive outcome at 12 years. *BMJ Open* **6**, e008916 (2016).
179. Widnes, C., Flo, K., Wilsgaard, T., Kiserud, T. & Acharya, G. Sex differences in umbilical artery Doppler indices: a longitudinal study. *Biol. Sex Differ.* **9**, 16 (2018).

180. Adedo, A. A., Arogundade, R. A., Okunowo, A. A., Idowu, B. M. & Oduola-Owoo, L. T. Comparative Study of the Umbilical Artery Doppler Indices of Healthy and Growth-Restricted Foetuses in Lagos. *J. West African Coll. Surg.* **12**, 63–69 (2022).
181. Haugen, G., Bollerslev, J. & Henriksen, T. Human umbilical and fetal cerebral blood flow velocity waveforms following maternal glucose loading: a cross-sectional observational study. *Acta Obstet. Gynecol. Scand.* **95**, 683–689 (2016).
182. Pardo, F. *et al.* Role of equilibrative adenosine transporters and adenosine receptors as modulators of the human placental endothelium in gestational diabetes mellitus. *Placenta* **34**, 1121–1127 (2013).
183. Echeverria, C. *et al.* Endothelial dysfunction in pregnancy metabolic disorders. *Biochim. Biophys. Acta - Mol. Basis Dis.* **1866**, 165414 (2020).
184. Figueroa, R. *et al.* Alterations in relaxation to lactate and H2O2in human placental vessels from gestational diabetic pregnancies. *Am. J. Physiol. Circ. Physiol.* **278**, H706–H713 (2000).
185. Zhou, J. *et al.* Potential Role of Hyperglycemia in Fetoplacental Endothelial Dysfunction in Gestational Diabetes Mellitus. *Cell. Physiol. Biochem.* **39**, 1317–1328 (2016).
186. Meigs, J. B., Hu, F. B., Rifai, N. & Manson, J. E. Biomarkers of Endothelial Dysfunction and Risk of Type 2 Diabetes Mellitus. *JAMA* **291**, 1978–1986 (2004).
187. Sultan, S. A. *et al.* The Role of Maternal Gestational Diabetes in Inducing Fetal Endothelial Dysfunction. *J. Cell. Physiol.* **230**, 2695–2705 (2015).
188. Bell, A. W. & Ehrhardt, R. A. Regulation of placental nutrient transport and implications for fetal growth. *Nutr. Res. Rev.* **15**, 211–230 (2002).
189. Bell, A. W., Hay, W. W. J. & Ehrhardt, R. A. Placental transport of nutrients and its implications for fetal growth. *J. Reprod. Fertil. Suppl.* **54**, 401–410 (1999).
190. Dumolt, J. H., Powell, T. L. & Jansson, T. Placental Function and the Development of Fetal Overgrowth and Fetal Growth Restriction. *Obstet. Gynecol. Clin. North Am.* **48**, 247–266 (2021).
191. Brett, K. E., Ferraro, Z. M., Yockell-Lelievre, J., Gruslin, A. & Adamo, K. B. Maternal–Fetal Nutrient Transport in Pregnancy Pathologies: The Role of the Placenta. *International Journal of Molecular Sciences* vol. 15 16153–16185 (2014).
192. Nicholas P. Illsley, M. U. B. Human placental glucose transport in fetoplacental growth and metabolism. *Biochim. Biophys. Acta - Mol. Basis Dis.* **1866**, 139–148 (2018).
193. Jansson, T., Wennergren, M. & Illsley, N. P. Glucose transporter protein expression in human placenta throughout gestation and in intrauterine growth retardation. *J. Clin. Endocrinol. Metab.* **77**, 1554–1562 (1993).
194. Brown, K., Heller, D. S., Zamudio, S. & Illsley, N. P. Glucose transporter 3 (GLUT3) protein expression in human placenta across gestation. *Placenta* **32**, 1041–1049 (2011).
195. Ericsson, A., Hamark, B., Powell, T. L. & Jansson, T. Glucose transporter isoform 4 is expressed in the syncytiotrophoblast of first trimester human placenta. *Hum. Reprod.* **20**, 521–530 (2005).
196. Stanirowski, P. J. *et al.* Impact of pre-gestational and gestational diabetes mellitus on the expression of glucose transporters GLUT-1, GLUT-4 and GLUT-9 in human term placenta. *Endocrine* **55**, 799–808 (2017).
197. Gaither, K., Quraishi, A. N. & Illsley, N. P. Diabetes alters the expression and activity of the human placental GLUT1 glucose transporter. *J. Clin. Endocrinol. Metab.* **84**, 695–701 (1999).
198. Janzen, C. *et al.* Placental glucose transporter 3 (GLUT3) is up-regulated in human pregnancies complicated by late-onset intrauterine growth restriction.

Placenta **34**, 1072–1078 (2013).
199. Cleal, J. K., Lofthouse, E. M., Sengers, B. G. & Lewis, R. M. A systems perspective on placental amino acid transport. *J. Physiol.* **596**, 5511–5522 (2018).
200. Cleal, J. K. *et al.* Facilitated transporters mediate net efflux of amino acids to the fetus across the basal membrane of the placental syncytiotrophoblast. *J. Physiol.* **589**, 987–997 (2011).
201. Day, P. E. L. *et al.* Partitioning of glutamine synthesised by the isolated perfused human placenta between the maternal and fetal circulations. *Placenta* **34**, 1223–1231 (2013).
202. Kuruvilla, A. G. *et al.* Altered activity of the system A amino acid transporter in microvillous membrane vesicles from placentas of macrosomic babies born to diabetic women. *J. Clin. Invest.* **94**, 689–695 (1994).
203. Jansson, T., Ekstrand, Y., Björn, C., Wennergren, M. & Powell, T. L. Alterations in the Activity of Placental Amino Acid Transporters in Pregnancies Complicated by Diabetes . *Diabetes* **51**, 2214–2219 (2002).
204. Mahendran, D. *et al.* Amino acid (System A) transporter activity in microvillous membrane vesicles from the placentas of appropriate and small for gestational age babies. *Pediatr. Res.* **34**, 661–665 (1993).
205. Castillo-Castrejon, M. & Powell, T. L. Placental nutrient transport in gestational diabetic pregnancies. *Front. Endocrinol. (Lausanne).* **8**, 1–9 (2017).
206. Magnusson, A. L., Waterman, I. J., Wennergren, M., Jansson, T. & Powell, T. L. Triglyceride Hydrolase Activities and Expression of Fatty Acid Binding Proteins in the Human Placenta in Pregnancies Complicated by Intrauterine Growth Restriction and Diabetes. *J. Clin. Endocrinol. Metab.* **89**, 4607–4614 (2004).
207. Lindegaard, M. L. S., Damm, P., Mathiesen, E. R. & Nielsen, L. B. Placental triglyceride accumulation in maternal type 1 diabetes is associated with increased lipase gene expression. *J. Lipid Res.* **47**, 2581–2588 (2006).
208. PrabhuDas, M. *et al.* Immune mechanisms at the maternal-fetal interface: perspectives and challenges. *Nature immunology* vol. 16 328–334 (2015).
209. Mezouar, S., Katsogiannou, M., Ben Amara, A., Bretelle, F. & Mege, J.-L. Placental macrophages: Origin, heterogeneity, function and role in pregnancy-associated infections. *Placenta* **103**, 94–103 (2021).
210. Hoo, R., Nakimuli, A. & Vento-Tormo, R. Innate Immune Mechanisms to Protect Against Infection at the Human Decidual-Placental Interface. *Front. Immunol.* **11**, 1–15 (2020).
211. Jabrane-Ferrat, N. & Siewiera, J. The up side of decidual natural killer cells: new developments in immunology of pregnancy. *Immunology* **141**, 490–497 (2014).
212. Granot, I., Gnainsky, Y. & Dekel, N. Endometrial inflammation and effect on implantation improvement and pregnancy outcome. *REPRODUCTION* **144**, 661–668 (2012).
213. Challis, J. R. *et al.* Inflammation and Pregnancy. *Reprod. Sci.* **16**, 206–215 (2009).
214. Commins, S. P., Borish, L. & Steinke, J. W. Immunologic messenger molecules: cytokines, interferons, and chemokines. *J. Allergy Clin. Immunol.* **125**, S53-72 (2010).
215. Saito, S. Cytokine network at the feto-maternal interface. *J. Reprod. Immunol.* **47**, 87–103 (2000).
216. Liu, H. *et al.* Chemokines in Gestational Diabetes Mellitus. *Front. Immunol.* **13**, 1–13 (2022).
217. Dutta, S. & Sengupta, P. Defining pregnancy phases with cytokine shift. *J. Pregnancy Reprod.* **1**, 1–3 (2017).
218. Zhang, S. *et al.* Regulation and Function of Chemokines at the Maternal–Fetal Interface . *Frontiers in Cell and Developmental Biology* vol. 10 (2022).
219. Du, M. R., Wang, S. C. & Li, D. J. The integrative roles of chemokines at the

maternal-fetal interface in early pregnancy. *Cell. Mol. Immunol.* **11**, 438–448 (2014).
220. Barke, T. L. *et al.* Gestational diabetes mellitus is associated with increased CD163 expression and iron storage in the placenta. *Am. J. Reprod. Immunol.* **80**, e13020 (2018).
221. Sisino, G. *et al.* Diabetes during pregnancy influences Hofbauer cells, a subtype of placental macrophages, to acquire a pro-inflammatory phenotype. *Biochim. Biophys. Acta - Mol. Basis Dis.* **1832**, 1959–1968 (2013).
222. Joerink, M., Rindsjö, E., van Riel, B., Alm, J. & Papadogiannakis, N. Placental macrophage (Hofbauer cell) polarization is independent of maternal allergen-sensitization and presence of chorioamnionitis. *Placenta* **32**, 380–385 (2011).
223. Young, O. M. *et al.* Toll-like Receptor-Mediated Responses by Placental Hofbauer Cells (HBCs): A Potential Pro-Inflammatory Role for Fetal M2 Macrophages. *Am. J. Reprod. Immunol.* **73**, 22–35 (2015).
224. Barke, T. L. *et al.* Gestational diabetes mellitus is associated with increased CD163 expression and iron storage in the placenta. *Am. J. Reprod. Immunol.* **80**, e13020 (2018).
225. Roszer, T. Understanding the Mysterious M2 Macrophage through Activation Markers and Effector Mechanisms. *Mediators Inflamm.* **2015**, 1–16 (2015).
226. Gensel, J. C. & Zhang, B. Macrophage activation and its role in repair and pathology after spinal cord injury. *Brain Res.* **1619**, 1–11 (2015).
227. Sironi, M. *et al.* Differential regulation of chemokine production by Fcgamma receptor engagement in human monocytes: association of CCL1 with a distinct form of M2 monocyte activation (M2b, Type 2). *J. Leukoc. Biol.* **80**, 342–349 (2006).
228. Orme, J. & Mohan, C. Macrophage subpopulations in systemic lupus erythematosus. *Discov. Med.* **13**, 151–158 (2012).
229. Martinez, F. O., Sica, A., Mantovani, A. & Locati, M. Macrophage activation and polarization. *Front. Biosci. - Landmark* **13**, 453–461 (2008).
230. Bhatnagar, J. *et al.* Zika Virus RNA Replication and Persistence in Brain and Placental Tissue. *Emerg. Infect. Dis.* **23**, 405–414 (2017).
231. de Noronha, L. *et al.* Zika Virus Infection at Different Pregnancy Stages: Anatomopathological Findings, Target Cells and Viral Persistence in Placental Tissues. *Front. Microbiol.* **9**, 2266 (2018).
232. Lewis, S. H., Reynolds-Kohler, C., Fox, H. E. & Nelson, J. A. HIV-1 in trophoblastic and villous Hofbauer cells, and haematological precursors in eight-week fetuses. *Lancet (London, England)* **335**, 565–568 (1990).
233. El Costa, H. *et al.* ZIKA virus reveals broad tissue and cell tropism during the first trimester of pregnancy. *Sci. Rep.* **6**, 35296 (2016).
234. Berbudi, A., Rahmadika, N., Tjahjadi, A. I. & Ruslami, R. Type 2 Diabetes and its Impact on the Immune System. *Curr. Diabetes Rev.* **16**, 442–449 (2020).
235. Donath, M. Y. & Shoelson, S. E. Type 2 diabetes as an inflammatory disease. *Nat. Rev. Immunol.* **11**, 98–107 (2011).
236. Wedekind, L. & Belkacemi, L. Altered cytokine network in gestational diabetes mellitus affects maternal insulin and placental–fetal development. *J. Diabetes Complications* **30**, 1393–1400 (2016).
237. Lu, J., Liu, J., Li, L., Lan, Y. & Liang, Y. Cytokines in type 1 diabetes: mechanisms of action and immunotherapeutic targets. *Clin. Transl. Immunol.* **9**, e1122 (2020).
238. McElwain, C. J., McCarthy, F. P. & McCarthy, C. M. Gestational Diabetes Mellitus and Maternal Immune Dysregulation: What We Know So Far. *Int. J. Mol. Sci.* **22**, 4261 (2021).
239. Altinova, A. E. *et al.* Circulating concentrations of adiponectin and tumor necrosis factor-α in gestational diabetes mellitus. *Gynecol. Endocrinol.* **23**, 161–165 (2007).

240. López-Tinoco, C. *et al.* Cytokine profile, metabolic syndrome and cardiovascular disease risk in women with late-onset gestational diabetes mellitus. *Cytokine* **58**, 14–19 (2012).
241. McLachlan, K. A., O'Neal, D., Jenkins, A. & Alford, F. P. Do adiponectin, TNFα, leptin and CRP relate to insulin resistance in pregnancy? Studies in women with and without gestational diabetes, during and after pregnancy. *Diabetes. Metab. Res. Rev.* **22**, 131–138 (2006).
242. Salmi, A., Zaki, M. N., Zakaria, Nor Aliza, G. & Rasool, H. G. Arterial stiffness, inflammatory and pro-atherogenic markers in gestational diabetes mellitus. *Vasa* **41**, 96–104 (2012).
243. Palik, E. *et al.* Elevated serum acylated (biologically active) ghrelin and resistin levels associate with pregnancy-induced weight gain and insulin resistance. *Diabetes Res. Clin. Pract.* **76**, 351–357 (2007).
244. Gueuvoghlanian-Silva, B. Y. *et al.* Profile of Inflammatory Mediators in Gestational Diabetes Mellitus: Phenotype and Genotype. *Am. J. Reprod. Immunol.* **67**, 241–250 (2012).
245. Montazeri, S., Nalliah, S. & Radhakrishnan, A. K. Is there a genetic variation association in the IL-10 and TNF α promoter gene with gestational diabetes mellitus? *Hereditas* **147**, 94–102 (2010).
246. Gomes, C. P. *et al.* Cytokine Levels in Gestational Diabetes Mellitus: a Systematic Review of the Literature. *Am. J. Reprod. Immunol.* **69**, 545–557 (2013).
247. Kuzmicki, M. *et al.* Circulating pro- and anti-inflammatory cytokines in Polish women with gestational diabetes. *Horm. Metab. Res. = Horm. und Stoffwechselforsch. = Horm. Metab.* **40**, 556–560 (2008).
248. Georgiou, H. M. *et al.* Screening for biomarkers predictive of gestational diabetes mellitus. *Acta Diabetol.* **45**, 157–165 (2008).
249. Tagoma, A. *et al.* Plasma cytokines during pregnancy provide insight into the risk of diabetes in the gestational diabetes risk group. *J. Diabetes Investig.* **13**, 1596–1606 (2022).
250. Kirwan, J. P. *et al.* TNF-alpha is a predictor of insulin resistance in human pregnancy. *Diabetes* **51**, 2207–2213 (2002).
251. Sisino, G. *et al.* Diabetes during pregnancy influences Hofbauer cells, a subtype of placental macrophages, to acquire a pro-inflammatory phenotype. *Biochim. Biophys. Acta - Mol. Basis Dis.* **1832**, 1959–1968 (2013).
252. Yu, J. *et al.* Assessment of the number and function of macrophages in the placenta of gestational diabetes mellitus patients. *J. Huazhong Univ. Sci. Technol. - Med. Sci.* **33**, 725–729 (2013).
253. Schliefsteiner, C. *et al.* Human Placental Hofbauer Cells Maintain an Anti-inflammatory M2 Phenotype despite the Presence of Gestational Diabetes Mellitus. *Front. Immunol.* **8**, 888 (2017).
254. Aye, I. L. M. H. *et al.* Increasing maternal body mass index is associated with systemic inflammation in the mother and the activation of distinct placental inflammatory pathways. *Biol. Reprod.* **90**, 129 (2014).
255. Chambers, M. A., Moylan, J. S., Smith, J. D., Goodyear, L. J. & Reid, M. B. Stretch-stimulated glucose uptake in skeletal muscle is mediated by reactive oxygen species and p38 MAP-kinase. *J. Physiol.* **587**, 3363–3373 (2009).
256. Tsai, R.-Y. *et al.* Ultra-low dose naloxone restores the antinociceptive effect of morphine in pertussis toxin-treated rats and prevents glutamate transporter downregulation by suppressing the p38 mitogen-activated protein kinase signaling pathway. *Neuroscience* **159**, 1244–1256 (2009).
257. Ho, R. C., Alcazar, O., Fujii, N., Hirshman, M. F. & Goodyear, L. J. p38gamma MAPK regulation of glucose transporter expression and glucose uptake in L6 myotubes and mouse skeletal muscle. *Am. J. Physiol. Regul. Integr. Comp. Physiol.* **286**, R342-9 (2004).

258. Jones, H. N., Jansson, T. & Powell, T. L. IL-6 stimulates system A amino acid transporter activity in trophoblast cells through STAT3 and increased expression of SNAT2. *Am. J. Physiol. Cell Physiol.* **297**, C1228-35 (2009).
259. Aye, I. L. M. H., Jansson, T. & Powell, T. L. Interleukin-1β inhibits insulin signaling and prevents insulin-stimulated system A amino acid transport in primary human trophoblasts. *Mol. Cell. Endocrinol.* **381**, 46–55 (2013).
260. Tan, Q. *et al.* Potential roles of IL-1 subfamily members in glycolysis in disease. *Cytokine Growth Factor Rev.* **44**, 18–27 (2018).
261. Marko, D. M. *et al.* Interleukin-6 Treatment Results in GLUT4 Translocation and AMPK Phosphorylation in Neuronal SH-SY5Y Cells. *Cells* **9**, (2020).
262. Sáez, T., de Vos, P., Kuipers, J., Sobrevia, L. & Faas, M. M. Fetoplacental endothelial exosomes modulate high D-glucose-induced endothelial dysfunction. *Placenta* **66**, 26–35 (2018).
263. Cawyer, C. *et al.* Hyperglycemia impairs cytotrophoblast function via stress signaling. *Am. J. Obstet. Gynecol.* **211**, 541.e1-541.e8 (2014).
264. Cawyer, C. *et al.* Attenuation of hyperglycemia-induced apoptotic signaling and anti-angiogenic milieu in cultured cytotrophoblast cells. *Hypertens. Pregnancy* **35**, 159–169 (2016).
265. Han, C. S. *et al.* Glucose and metformin modulate human first trimester trophoblast function: A model and potential therapy for diabetes-associated uteroplacental insufficiency. *Am. J. Reprod. Immunol.* **73**, 362–371 (2015).
266. Esposito, C. *et al.* Long-term exposure to high glucose up-regulates VCAM-induced endothelial cell adhesiveness to PBMC. *Kidney Int.* **59**, 1842–1849 (2001).
267. Williams, B., Gallacher, B., Patel, H. & Orme, C. Glucose-induced protein kinase C activation regulates vascular permeability factor mRNA expression and peptide production by human vascular smooth muscle cells in vitro. *Diabetes* **46**, 1497–1503 (1997).
268. Natarajan, R., Bai, W., Lanting, L., Gonzales, N. & Nadler, J. Effects of high glucose on vascular endothelial growth factor expression in vascular smooth muscle cells. *Am. J. Physiol. - Hear. Circ. Physiol.* **273**, (1997).
269. Hulme, C. H. *et al.* Identification of the functional pathways altered by placental cell exposure to high glucose: Lessons from the transcript and metabolite interactome. *Sci. Rep.* **8**, 1–11 (2018).
270. Al-Awar, A. *et al.* Experimental Diabetes Mellitus in Different Animal Models. *J. Diabetes Res.* **2016**, 9051426 (2016).
271. Eckmann, M., Sheng, Q., Baldwin H, S. & Lister, R. L. Maternal Hyperglycemia Induces Changes in Gene Expression and Morphology in Mouse Placentas. *Gynecol. Reprod. Heal.* **5**, (2021).
272. Qin, Y. *et al.* Hyperglycemia results in significant pathophysiological changes of placental spiral artery remodeling and angiogenesis, further contributing to congenital defects. *Front. Biosci. - Landmark* **26**, 965–976 (2021).
273. Elshennawy, A. T. M. Effect of Gestational Diabetes on Gross Morphology, Histology and Histochemistry of Human Placenta. *Endocrinol. Metab. Syndr.* **05**, 1–13 (2016).
274. Edu, A. *et al.* Placenta changes in pregnancy with gestational diabetes. *Rom. J. Morphol. Embryol.* **57**, 507–512 (2016).
275. Lehtoranta, L. *et al.* Placental structural abnormalities have detrimental hemodynamic consequences in a rat model of maternal hyperglycemia. *Placenta* **44**, 54–60 (2016).
276. Nielsen, L. R. *et al.* Hypoglycemia in pregnant women with type 1 diabetes: Predictors and role of metabolic control. *Diabetes Care* **31**, 9–14 (2008).
277. Ter Braak, E. W. M. T., Evers, I. M., Erkelens, D. W. & Visser, G. H. A. Maternal hypoglycemia during pregnancy in type 1 diabetes: Maternal and fetal consequences. *Diabetes. Metab. Res. Rev.* **18**, 96–105 (2002).

278. Vadakekut, E. S., McCoy, S. J. B. & Payto, M. E. Association of maternal hypoglycemia with low birth weight and low placental weight: A retrospective investigation. *J. Am. Osteopath. Assoc.* **111**, 148–152 (2011).
279. Joy, N. G. *et al.* Effects of acute hypoglycemia on inflammatory and pro-atherothrombotic biomarkers in individuals with type 1 diabetes and healthy individuals. *Diabetes Care* **33**, 1529–1535 (2010).
280. Razavi Nematollahi, L. *et al.* Proinflammatory cytokines in response to insulin-induced hypoglycemic stress in healthy subjects. *Metabolism.* **58**, 443–448 (2009).
281. Davis, I. C., Ahmadizadeh, I., Randell, J., Younk, L. & Davis, S. N. Understanding the impact of hypoglycemia on the cardiovascular system. *Expert Rev. Endocrinol. Metab.* **12**, 21–33 (2017).
282. Mitsui, T. *et al.* Upregulation of angiogenic factors via protein kinase c and hypoxia-induced factor-1a pathways under high-glucose conditions in the placenta. *Acta Med. Okayama* **72**, 359–367 (2018).
283. Cvitic, S., Desoye, G. & Hiden, U. Glucose, Insulin, and Oxygen Interplay in Placental Hypervascularisation in Diabetes Mellitus. *Biomed Res. Int.* **2014**, (2014).
284. Hiden, U. *et al.* Insulin control of placental gene expression shifts from mother to foetus over the course of pregnancy. *Diabetologia* **49**, 123–131 (2006).
285. Hiden, U., Glitzner, E., Hartmann, M. & Desoye, G. Insulin and the IGF system in the human placenta of normal and diabetic pregnancies. *J. Anat.* **215**, 60–68 (2009).
286. Lindsay, R. S. *et al.* Inverse changes in fetal insulin-like growth factor (IGF)-1 and IGF binding protein-1 in association with higher birth weight in maternal diabetes. *Clin. Endocrinol. (Oxf).* **66**, 322–328 (2007).
287. Westgate, J. A. *et al.* Hyperinsulinemia in cord blood in mothers with type 2 diabetes and gestational diabetes mellitus in New Zealand. *Diabetes Care* **29**, 1345–1350 (2006).
288. Nelson, S. M., Coan, P. M., Burton, G. J. & Lindsay, R. S. Placental structure in type 1 diabetes: Relation to fetal insulin, leptin, and IGF-I. *Diabetes* **58**, 2634–2641 (2009).
289. Grissa, O. *et al.* Growth factor concentrations and their placental mRNA expression are modulated in gestational diabetes mellitus: Possible interactions with macrosomia. *BMC Pregnancy Childbirth* **10**, (2010).
290. Hajagos-Tóth, J., Ducza, E., Samavati, R., Vari, S. G. & Gaspar, R. Obesity in pregnancy: A novel concept on the roles of adipokines in uterine contractility. *Croat. Med. J.* **58**, 96–104 (2017).
291. Miao, M. *et al.* Influence of maternal overweight, obesity and gestational weight gain on the perinatal outcomes in women with gestational diabetes mellitus. *Sci. Rep.* **7**, (2017).
292. Mierzyński, R., Poniedziałek-Czajkowska, E., Dłuski, D. & Leszczyńska-Gorzelak, B. The role of new adipokines in gestational diabetes mellitus pathogenesis. *Ginekol. Pol.* **89**, 210–215 (2018).
293. Pérez-Pérez, A. *et al.* Leptin action in normal and pathological pregnancies. *J. Cell. Mol. Med.* **22**, 716–727 (2018).
294. Islami, D., Bischof, P. & Chardonnens, D. Modulation of placental vascular endothelial growth factor by leptin and hCG. *Mol. Hum. Reprod.* **9**, 395–398 (2003).
295. Sierra-Honigmann, M. R. *et al.* Biological action of leptin as an angiogenic factor. *Science (80-.).* **281**, 1683–1686 (1998).
296. Jones, H. N., Jansson, T. & Powell, T. L. Full-length adiponectin attenuates insulin signaling and inhibits insulin-stimulated amino Acid transport in human primary trophoblast cells. *Diabetes* **59**, 1161–1170 (2010).
297. Mouillet, J. F., Ouyang, Y., Coyne, C. B. & Sadovsky, Y. MicroRNAs in placental

health and disease. *Am. J. Obstet. Gynecol.* **213**, S163–S172 (2015).
298. Assmann, T. S., Recamonde-Mendoza, M., De Souza, B. M. & Crispim, D. MicroRNA expression profiles and type 1 diabetes mellitus: Systematic review and bioinformatic analysis. *Endocr. Connect.* **6**, 773–790 (2017).
299. Pordzik, J. *et al.* Significance of circulating microRNAs in diabetes mellitus type 2 and platelet reactivity: Bioinformatic analysis and review. *Cardiovasc. Diabetol.* **18**, 1–19 (2019).
300. Ibarra, A., Vega-Guedes, B., Brito-Casillas, Y. & Wägner, A. M. Diabetes in pregnancy and microRNAs: Promises and limitations in their clinical application. *Non-coding RNA* **4**, (2018).
301. Zhu, Y. *et al.* Profiling maternal plasma microRNA expression in early pregnancy to predict gestational diabetes mellitus. *Int. J. Gynecol. Obstet.* **130**, 49–53 (2015).
302. Cao, Y. L., Jia, Y. J., Xing, B. H., Shi, D. D. & Dong, X. J. Plasma microRNA-16-5p, -17-5p and -20a-5p: Novel diagnostic biomarkers for gestational diabetes mellitus. *J. Obstet. Gynaecol. Res.* **43**, 974–981 (2017).
303. Pheiffer, C., Dias, S., Rheeder, P. & Adam, S. Decreased Expression of Circulating miR-20a-5p in South African Women with Gestational Diabetes Mellitus. *Mol. Diagnosis Ther.* **22**, 345–352 (2018).
304. Wander, P. L. *et al.* Circulating early- and mid-pregnancy microRNAs and risk of gestational diabetes. *Diabetes Res. Clin. Pract.* **132**, 1–9 (2017).
305. Tryggestad, J. B. *et al.* Influence of gestational diabetes mellitus on human umbilical vein endothelial cell miRNA. *Clin. Sci.* **130**, 1955–1967 (2016).
306. Zhao, C. *et al.* Early second-trimester serum miRNA profiling predicts gestational diabetes mellitus. *PLoS One* **6**, (2011).
307. Théry, C. *et al.* Minimal information for studies of extracellular vesicles 2018 (MISEV2018): a position statement of the International Society for Extracellular Vesicles and update of the MISEV2014 guidelines. *J. Extracell. Vesicles* **7**, (2018).
308. Mulcahy, L. A., Pink, R. C. & Carter, D. R. F. Routes and mechanisms of extracellular vesicle uptake. *J. Extracell. Vesicles* **3**, (2014).
309. Lu, K.-C., Zhang, Y. & Song, E. Extracellular RNA: mechanisms of it's transporting into target cells. *ExRNA* **1**, 22 (2019).
310. Boon, R. A. & Vickers, K. C. Intercellular Transport of MicroRNAs Reinier. *Arterioscler. Thromb. Vasc. Biol.* **33**, 186–192 (2013).
311. Salomon, C. *et al.* Gestational diabetes mellitus is associated with changes in the concentration and bioactivity of placenta-derived exosomes in maternal circulation across gestation. *Diabetes* **65**, 598–609 (2016).
312. Gillet, V. *et al.* MiRNA Profiles in Extracellular Vesicles from Serum Early in Pregnancies Complicated by Gestational Diabetes Mellitus. *J. Clin. Endocrinol. Metab.* **104**, 5157–5169 (2019).
313. Wang, Y. *et al.* MiR-122 targets VEGFC in bladder cancer to inhibit tumor growth and angiogenesis. *Am. J. Transl. Res.* **8**, 3056–3066 (2016).
314. Yan, X.-C. *et al.* miR-342-5p Is a Notch Downstream Molecule and Regulates Multiple Angiogenic Pathways Including Notch, Vascular Endothelial Growth Factor and Transforming Growth Factor β Signaling. *J. Am. Heart Assoc.* **5**, (2016).
315. Malassiné, A., Frendo, J. L. & Evain-Brion, D. A comparison of placental development and endocrine functions between the human and mouse model. *Hum. Reprod. Update* **9**, 531–539 (2003).
316. Barry, J. S. & Anthony, R. V. The pregnant sheep as a model for human pregnancy. *Theriogenology* **69**, 55–67 (2008).
317. Costa, J. *et al.* The Role of the 3Rs for Understanding and Modeling the Human Placenta. *Journal of Clinical Medicine* vol. 10 (2021).
318. Grigsby, P. L. Animal Models to Study Placental Development and Function

throughout Normal and Dysfunctional Human Pregnancy. *Semin. Reprod. Med.* **34**, 11–16 (2016).
319. Swanson, A. M. & David, A. L. Animal models of fetal growth restriction: Considerations for translational medicine. *Placenta* **36**, 623–630 (2015).
320. Jawerbaum, A. & White, V. Animal Models in Diabetes and Pregnancy. *Endocr. Rev.* **31**, 680–701 (2010).
321. Miller, R. K. *et al.* Human placental explants in culture: Approaches and assessments. *Placenta* **26**, 439–448 (2005).
322. Simán, C. M., Sibley, C. P., Jones, C. J. P., Turner, M. A. & Greenwood, S. L. The functional regeneration of syncytiotrophoblast in cultured explants of term placenta. *Am. J. Physiol. - Regul. Integr. Comp. Physiol.* **280**, 1116–1122 (2001).
323. Sato, B. L., Ward, M. A., Astern, J. M., Kendal-Wright, C. E. & Collier, A. C. Validation of murine and human placental explant cultures for use in sex steroid and phase II conjugation toxicology studies. *Toxicol. Vitr. an Int. J. Publ. Assoc. with BIBRA* **29**, 103–112 (2015).
324. Hertz, R. Choriocarcinoma of Women Maintained in Serial Passage in Hamster and Rat. *Proc. Soc. Exp. Biol. Med.* **102**, 77–81 (1959).
325. Graham, C. H. *et al.* Establishment and Characterization of First Trimester Human Trophoblast Cells with Extended Lifespan. *Exp. Cell Res.* **206**, 204–211 (1993).
326. Wice, B., Menton, D., Geuze, H. & Schwartz, A. L. Modulators of cyclic AMP metabolism induce syncytiotrophoblast formation in vitro. *Exp. Cell Res.* **186**, 306–316 (1990).
327. Bode, C. J. *et al.* In vitro models for studying trophoblast transcellular transport. *Methods Mol. Med.* **122**, 225–239 (2006).
328. Liu, F., Soares, M. J. & Audus, K. L. Permeability properties of monolayers of the human trophoblast cell line BeWo. *Am. J. Physiol.* **273**, C1596-604 (1997).
329. Pattillo, R. A. & Gey, G. O. The establishment of a cell line of human hormone-synthesizing trophoblastic cells in vitro. *Cancer Res.* **28**, 1231–1236 (1968).
330. Pattillo, R. A., Ruckert, A. C. F., Hussa, R. O., Bernstein, R. A. & Delfs, E. The JAr cell line - continuous human multi-hormone production and controls. *Vitr. Cell. Dev. Biol. – Plant* **6**, 398–399 (1971).
331. Abou-Kheir, W., Barrak, J., Hadadeh, O. & Daoud, G. HTR-8/SVneo cell line contains a mixed population of cells. *Placenta* **50**, 1–7 (2017).
332. Kliman, H. J., Nestler, J. E., Sermasi, E., Sanger, J. M. & Strauss III, J. F. Purification, Characterization, and in vitro Differentiation of Cytotrophoblasts from Human Term Placentae*. *Endocrinology* **118**, 1567–1582 (1986).
333. Nursalim, Y. N. S., Groom, K. M., Blenkiron, C. & Chamley, L. W. A simple method to isolate term trophoblasts and maintain them in extended culture. *Placenta* **108**, 1–10 (2021).
334. Taylor, P. V & Hancock, K. W. VIABILITY OF HUMAN TROPHOBLAST IN VITRO. *BJOG An Int. J. Obstet. Gynaecol.* **80**, 834–838 (1973).
335. Rothbauer, M. *et al.* A comparative study of five physiological key parameters between four different human trophoblast-derived cell lines. *Sci. Rep.* **7**, 5892 (2017).
336. Almeida, M. P. O. *et al.* Susceptibility of human villous (BeWo) and extravillous (HTR-8/SVneo) trophoblast cells to Toxoplasma gondii infection is modulated by intracellular iron availability. *Parasitol. Res.* **118**, 1559–1572 (2019).
337. Turco, M. Y. *et al.* Trophoblast organoids as a model for maternal–fetal interactions during human placentation. *Nature* **564**, 263–267 (2018).
338. Sheridan, M. A. *et al.* Establishment and differentiation of long-term trophoblast organoid cultures from the human placenta. *Nat. Protoc.* **15**, 3441–3463 (2020).
339. Okae, H. *et al.* Derivation of Human Trophoblast Stem Cells. *Cell Stem Cell* **22**, 50-63.e6 (2018).

340. Haider, S. *et al.* Self-Renewing Trophoblast Organoids Recapitulate the Developmental Program of the Early Human Placenta. *Stem Cell Reports* **11**, 537–551 (2018).
341. Cherubini, M., Erickson, S. & Haase, K. Modelling the human placental interface in vitro—A review. *Micromachines* **12**, (2021).
342. Nishiguchi, A. *et al.* In vitro placenta barrier model using primary human trophoblasts, underlying connective tissue and vascular endothelium. *Biomaterials* **192**, 140–148 (2019).
343. Kreuder, A.-E. *et al.* Inspired by the human placenta: a novel 3D bioprinted membrane system to create barrier models. *Sci. Rep.* **10**, 15606 (2020).
344. Whitesides, G. M. The origins and the future of microfluidics. *Nature* **442**, 368–373 (2006).
345. Mancini, V. & Pensabene, V. Organs-on-chip models of the female reproductive system. *Bioengineering* **6**, 1–16 (2019).
346. Lee, J. S. *et al.* Placenta-on-A-chip: A novel platform to study the biology of the human placenta. *J. Matern. Neonatal Med.* **29**, 1046–1054 (2016).
347. Blundell, C. *et al.* Placental Drug Transport-on-a-Chip: A Microengineered In Vitro Model of Transporter-Mediated Drug Efflux in the Human Placental Barrier. *Adv. Healthc. Mater.* **7**, 1700786 (2018).
348. Haase, K., Gillrie, M. R., Hajal, C. & Kamm, R. D. Pericytes Contribute to Dysfunction in a Human 3D Model of Placental Microvasculature through VEGF-Ang-Tie2 Signaling. *Adv. Sci.* **6**, 1900878 (2019).
349. Offeddu, G. S. *et al.* An on-chip model of protein paracellular and transcellular permeability in the microcirculation. *Biomaterials* **212**, 115–125 (2019).
350. Nuzzo, A. M. *et al.* Altered expression of G1/S phase cell cycle regulators in placental mesenchymal stromal cells derived from preeclamptic pregnancies with fetal-placental compromise. *Cell Cycle* **16**, 200–212 (2017).
351. Lermant, A. *et al.* Development of a human iPSC-derived placental barrier-on-chip model. *iScience* **26**, (2023).
352. Mandt, D. *et al.* Fabrication of biomimetic placental barrier structures within a microfluidic device utilizing two-photon polymerization. *Int. J. Bioprinting* **4**, 1–12 (2018).
353. Mosavati, B., Oleinikov, A. V & Du, E. Development of an Organ-on-a-Chip-Device for Study of Placental Pathologies. *International Journal of Molecular Sciences* vol. 21 (2020).
354. Pemathilaka, R. L., Caplin, J. D., Aykar, S. S., Montazami, R. & Hashemi, N. N. Placenta-on-a-Chip: In Vitro Study of Caffeine Transport across Placental Barrier Using Liquid Chromatography Mass Spectrometry. *Glob. Challenges* **3**, 1800112 (2019).
355. Pu, Y., Gingrich, J. & Veiga-Lopez, A. A 3-dimensional microfluidic platform for modeling human extravillous trophoblast invasion and toxicological screening. *Lab Chip* **21**, 546–557 (2021).
356. Yin, F. *et al.* A 3D human placenta-on-a-chip model to probe nanoparticle exposure at the placental barrier. *Toxicol. Vitr. an Int. J. Publ. Assoc. with BIBRA* **54**, 105–113 (2019).
357. Zhu, Y. *et al.* Placental Barrier-on-a-Chip: Modeling Placental Inflammatory Responses to Bacterial Infection. *ACS Biomater. Sci. Eng.* **4**, 3356–3363 (2018).
358. Perinatal Institute. Gestation Related Optimal Weight (GROW) Calculator. https://www.gestation.net/cc/about.htm (2022).
359. Kennedy, M. G. Circulating miRNAs as key regulators of placental vascular dysfunction and altered fetal growth in pregnancies complicated by diabetes. (University of Leeds, 2022).
360. Pelekanos, R. A. *et al.* Isolation and expansion of mesenchymal stem/stromal cells derived from human placenta tissue. *J. Vis. Exp.* **2016**, 1–3 (2016).
361. Mancini, V. Multiparametric analysis of embryonic, glial and endothelial cells

cultured in microfluidic systems in standard or pertubed states. (University of Leeds, 2020).
362. Cherubini, M. *et al.* Flow in fetoplacental microvessels in vitro enhances perfusion, barrier function, and matrix stability. *bioRxiv* 2023.07.19.549736 (2023) doi:10.1101/2023.07.19.549736.
363. Cherubini, M. & Haase, K. A Bioengineered Model for Studying Vascular-Pericyte Interactions of the Placenta. *Methods Mol. Biol.* **2608**, 409–423 (2023).
364. Fluigent. Why is it important to control shear stress in your microfluidic experiments? https://www.fluigent.com/resources-support/expertise/expertise-reviews/microfluidic-cell-biology/controling-shear-stress/ (2023).
365. Doering, C. R. & Gibbon, J. D. *Applied Analysis of the Navier-Stokes Equations*. (Cambridge University Press, 1995).
366. Huang, Y., Qian, J.-Y., Cheng, H. & Li, X.-M. Effects of shear stress on differentiation of stem cells into endothelial cells. *World J. Stem Cells* **13**, 894–913 (2021).
367. Szalóki, G. & Goda, K. Compensation in multicolor flow cytometry. *Cytom. Part A* **87**, 982–985 (2015).
368. McKinnon, K. M. Flow Cytometry: An Overview. *Curr. Protoc. Immunol.* **120**, 5.1.1-5.1.11 (2018).
369. Mccoy, J. P. *Molecular Biology Immunophenotyping*. (Humana New York, 2019). doi:https://doi.org/10.1007/978-1-4939-9650-6.
370. Nakatsu, M. N., Davis, J. & Hughes, C. C. W. Optimized fibrin gel bead assay for the study of angiogenesis. *J. Vis. Exp.* 186 (2007) doi:10.3791/186.
371. Clavane, E. M., Taylor, H. A., Cubbon, R. M. & Meakin, P. J. Endothelial Cell Fibrin Gel Angiogenesis Bead Assay. in *Angiogenesis. Methods in Molecular Biology.* (ed. Benest, A. V) 321–327 (Springer US, 2022). doi:10.1007/978-1-0716-2059-5_25.
372. Boussommier-Calleja, A. *et al.* The effects of monocytes on tumor cell extravasation in a 3D vascularized microfluidic model. *Biomaterials* **198**, 180–193 (2019).
373. Holder, B. S., Tower, C. L., Abrahams, V. M. & Aplin, J. D. Syncytin 1 in the human placenta. *Placenta* **33**, 460–466 (2012).
374. Kerby, A., Graham, N., Wallworth, R., Batra, G. & Heazell, A. Development of dynamic image analysis methods to measure vascularisation and syncytial nuclear aggregates in human placenta. *Placenta* **120**, 65–72 (2022).
375. Matlock, B. Assessment of Nucleic Acid Purity. *Tech. Bull. NanoDrop Spectrophotometers* 1–2 (2015).
376. Ye, J. *et al.* Primer-BLAST: a tool to design target-specific primers for polymerase chain reaction. *BMC Bioinformatics* **13**, 134 (2012).
377. Madeira, F. *et al.* Search and sequence analysis tools services from EMBL-EBI in 2022. *Nucleic Acids Res.* gkac240 (2022) doi:10.1093/nar/gkac240.
378. Lv, Y. *et al.* Identification of reference genes for qRT-PCR in granulosa cells of healthy women and polycystic ovarian syndrome patients. *Sci. Rep.* **7**, 6961 (2017).
379. Yan, Y., Peng, H., Wang, P., Wang, H. & Dong, M. Increased expression of fatty acid binding protein 4 in preeclamptic Placenta and its relevance to preeclampsia. *Placenta* **39**, 94–100 (2016).
380. Inglis, S., Christensen, D., Wilson, D. I., Kanczler, J. M. & Oreffo, R. O. C. Human endothelial and foetal femur-derived stem cell co-cultures modulate osteogenesis and angiogenesis. *Stem Cell Res. Ther.* **7**, 1–16 (2016).
381. Keller, C., Keller, P., Marshal, S. & Pedersen, B. K. IL-6 gene expression in human adipose tissue in response to exercise--effect of carbohydrate ingestion. *J. Physiol.* **550**, 927–931 (2003).
382. Ye, J. *et al.* JCAD Promotes Progression of Nonalcoholic Steatohepatitis to Liver Cancer by Inhibiting LATS2 Kinase Activity. *Cancer Res.* **77**, 5287–5300 (2017).

383. Ma, S. *et al.* PDGF-D−PDGFRβ signaling enhances IL-15–mediated human natural killer cell survival. *Proc. Natl. Acad. Sci.* **119**, e2114134119 (2022).
384. Böhrnsen, F. & Schliephake, H. Supportive angiogenic and osteogenic differentiation of mesenchymal stromal cells and endothelial cells in monolayer and co-cultures. *Int. J. Oral Sci.* **8**, 223–230 (2016).
385. Sugimoto, A. *et al.* Piezo type mechanosensitive ion channel component 1 functions as a regulator of the cell fate determination of mesenchymal stem cells. *Sci. Rep.* **7**, 1–14 (2017).
386. Wang, C. *et al.* Efficient Differentiation of Bone Marrow Mesenchymal Stem Cells into Endothelial Cells in Vitro. *Eur. J. Vasc. Endovasc. Surg.* **55**, 257 (2018).
387. Eastman, A. W. & Yuan, Z.-C. Development and validation of an rDNA operon based primer walking strategy applicable to de novo bacterial genome finishing . *Frontiers in Microbiology* vol. 5 (2015).
388. Dobin, A. *et al.* STAR: ultrafast universal RNA-seq aligner. *Bioinformatics* **29**, 15–21 (2013).
389. Liao, Y., Smyth, G. K. & Shi, W. featureCounts: an efficient general purpose program for assigning sequence reads to genomic features. *Bioinformatics* **30**, 923–930 (2014).
390. Love, M. I., Huber, W. & Anders, S. Moderated estimation of fold change and dispersion for RNA-seq data with DESeq2. *Genome Biol.* **15**, 550 (2014).
391. Stevens, J. R., Herrick, J. S., Wolff, R. K. & Slattery, M. L. Power in pairs: assessing the statistical value of paired samples in tests for differential expression. *BMC Genomics* **19**, 953 (2018).
392. Liao, Y., Wang, J., Jaehnig, E. J., Shi, Z. & Zhang, B. WebGestalt 2019: gene set analysis toolkit with revamped UIs and APIs. *Nucleic Acids Res.* **47**, W199–W205 (2019).
393. Consortium, G. O. The Gene Ontology resource: enriching a GOld mine. *Nucleic Acids Res.* **49**, D325–D334 (2021).
394. Ashburner, M. *et al.* Gene ontology: tool for the unification of biology. The Gene Ontology Consortium. *Nat. Genet.* **25**, 25–29 (2000).
395. Kanehisa, M., Furumichi, M., Sato, Y., Ishiguro-Watanabe, M. & Tanabe, M. KEGG: integrating viruses and cellular organisms. *Nucleic Acids Res.* **49**, D545–D551 (2021).
396. Kanehisa, M. Toward understanding the origin and evolution of cellular organisms. *Protein Sci.* **28**, 1947–1951 (2019).
397. Kanehisa, M. & Goto, S. KEGG: kyoto encyclopedia of genes and genomes. *Nucleic Acids Res.* **28**, 27–30 (2000).
398. Thomas, P. D. *et al.* PANTHER: A library of protein families and subfamilies indexed by function. *Genome Res.* **13**, 2129–2141 (2003).
399. Gillespie, M. *et al.* The reactome pathway knowledgebase 2022. *Nucleic Acids Res.* **50**, D687–D692 (2022).
400. Krämer, A., Green, J., Pollard, J. J. & Tugendreich, S. Causal analysis approaches in Ingenuity Pathway Analysis. *Bioinformatics* **30**, 523–530 (2014).
401. Krämer, A., Green, J., Pollard, J. & Tugendreich, S. Causal analysis approaches in ingenuity pathway analysis. *Bioinformatics* **30**, 523–530 (2014).
402. Szklarczyk, D. *et al.* STRING v11: protein–protein association networks with increased coverage, supporting functional discovery in genome-wide experimental datasets. *Nucleic Acids Res.* **47**, D607–D613 (2019).
403. Shannon, P. *et al.* Cytoscape: a software environment for integrated models of biomolecular interaction networks. *Genome Res.* **13**, 2498–2504 (2003).
404. Bader, G. D. & Hogue, C. W. V. An automated method for finding molecular complexes in large protein interaction networks. *BMC Bioinformatics* **4**, 2 (2003).
405. Nepusz, T., Yu, H. & Paccanaro, A. Detecting overlapping protein complexes in protein-protein interaction networks. *Nat. Methods* **9**, 471–472 (2012).

406. Vento-tormo, R. *et al.* Single-cell reconstruction of the early maternal – fetal interface in humans. *Nature* **563**, 347–353 (2022).
407. Pantazi, P. *et al.* Placental macrophage responses to viral and bacterial ligands and the influence of fetal sex. *iScience* **25**, 105653 (2022).
408. Tang, Z. *et al.* Isolation of hofbauer cells from human term placentas with high yield and purity. *Am. J. Reprod. Immunol.* **66**, 336–348 (2011).
409. Martinez, F. O., Gordon, S., Locati, M. & Mantovani, A. Transcriptional Profiling of the Human Monocyte-to-Macrophage Differentiation and Polarization: New Molecules and Patterns of Gene Expression. *J. Immunol.* **177**, 7303–7311 (2006).
410. NCBI. Gene Expression Omnibus. https://www.ncbi.nlm.nih.gov/geo/.
411. EMBL-EBI. ArrayExpress. https://www.ebi.ac.uk/biostudies/arrayexpress.
412. NCBI. About GEO2R. https://www.ncbi.nlm.nih.gov/geo/info/geo2r.html (2023).
413. Illumina. GenomeStudio Gene Expression Module v1.0 User Guide. (2008).
414. Blighe, K., Rana, S., Turkes, E., Ostendorf, B. & Lewis, M. EnhancedVolcano: Publication-ready volcano plots with enhanced colouring and labeling. https://github.com/kevinblighe/EnhancedVolcano (2020).
415. Xu, S. *et al.* Use ggbreak to Effectively Utilize Plotting Space to Deal With Large Datasets and Outliers . *Frontiers in Genetics* vol. 12 (2021).
416. Sobrevia, L. *et al.* Insulin therapy and fetoplacental vascular function in gestational diabetes mellitus. *Experimental Physiology* (2015) doi:10.1113/expphysiol.2014.082743.
417. Wyatt, A. W., Steinert, J. R. & Mann, G. E. Modulation of the l-arginine/nitric oxide signalling pathway in vascular endothelial cells. *Biochem. Soc. Symp.* **71**, 143–156 (2004).
418. Valent, A. M., Choi, H., Kolahi, K. S. & Thornburg, K. L. Hyperglycemia and gestational diabetes suppress placental glycolysis and mitochondrial function and alter lipid processing. *FASEB J. Off. Publ. Fed. Am. Soc. Exp. Biol.* **35**, e21423 (2021).
419. Nteeba, J. *et al.* Poorly controlled diabetes mellitus alters placental structure, efficiency, and plasticity. *BMJ Open Diabetes Res. Care* **8**, 1–12 (2020).
420. Hulme, C. H. *et al.* The effect of high glucose on lipid metabolism in the human placenta. *Sci. Rep.* **9**, 14114 (2019).
421. Russo, V. C., Higgins, S., Werther, G. A. & Cameron, F. J. Effects of Fluctuating Glucose Levels on Neuronal Cells In Vitro. *Neurochem. Res.* **37**, 1768–1782 (2012).
422. Risso, A., Mercuri, F., Quagliaro, L., Damante, G. & Ceriello, A. Intermittent high glucose enhances apoptosis in human umbilical vein endothelial cells in culture. *Am. J. Physiol. Metab.* **281**, E924–E930 (2001).
423. Chen, B., Jia, Y., Lu, D. & Sun, Z. Acute glucose fluctuation promotes in vitro intestinal epithelial cell apoptosis and inflammation via the NOX4/ROS/JAK/STAT3 signaling pathway. *Exp Ther Med* **22**, 688 (2021).
424. Thomas, M. G., Marwood, R. M., Parsons, A. E. & Parsons, R. B. The effect of foetal bovine serum supplementation upon the lactate dehydrogenase cytotoxicity assay: Important considerations for in vitro toxicity analysis. *Toxicol. Vitr. an Int. J. Publ. Assoc. with BIBRA* **30**, 300–308 (2015).
425. Smith, S. C., Baker, P. N. & Symonds, E. M. Increased placental apoptosis in intrauterine growth restriction. *Am. J. Obstet. Gynecol.* **177**, 1395–1401 (1997).
426. Chen, C.-P., Bajoria, R. & Aplin, J. D. Decreased vascularization and cell proliferation in placentas of intrauterine growth-restricted fetuses with abnormal umbilical artery flow velocity waveforms. *Am. J. Obstet. Gynecol.* **187**, 764–769 (2002).
427. Higgins, L. *et al.* Maternal obesity and its effect on placental cell turnover. *J. Matern. Neonatal Med.* **26**, 783–788 (2013).
428. Arnholdt, H., Meisel, F., Fandrey, K. & Löhrs, U. Proliferation of villous

trophoblast of the human placenta in normal and abnormal pregnancies. *Virchows Arch. B. Cell Pathol. Incl. Mol. Pathol.* **60**, 365–372 (1991).
429. Chiu, P. M., Ngan, Y. S., Khoo, U. S. & Cheung, A. N. Y. Apoptotic activity in gestational trophoblastic disease correlates with clinical outcome: assessment by the caspase-related M30 CytoDeath antibody. *Histopathology* **38**, 243–249 (2001).
430. Koch, C. M. *et al.* A Beginner's Guide to Analysis of RNA Sequencing Data. *Am. J. Respir. Cell Mol. Biol.* **59**, 145–157 (2018).
431. Schulze, F. *et al.* Inhibition of IL-1beta improves Glycaemia in a Mouse Model for Gestational Diabetes. *Sci. Rep.* **10**, 1–11 (2020).
432. Aribi, M. *et al.* Relationship between interleukin-1beta and lipids in type 1 diabetic patients. *Med. Sci. Monit. Int. Med. J. Exp. Clin. Res.* **13**, CR372-8 (2007).
433. Xu, Y. *et al.* The expression of FoxO1 in placenta and omental adipose tissue of gestational diabetes mellitus. *Exp. Clin. Endocrinol. diabetes Off. journal, Ger. Soc. Endocrinol. [and] Ger. Diabetes Assoc.* **122**, 287–294 (2014).
434. Kristiansen, O. P. & Mandrup-Poulsen, T. Interleukin-6 and Diabetes: The Good, the Bad, or the Indifferent? *Diabetes* **54**, S114–S124 (2005).
435. Rehman, K. *et al.* Role of Interleukin-6 in Development of Insulin Resistance and Type 2 Diabetes Mellitus. *Crit. Rev. Eukaryot. Gene Expr.* **27**, 229–236 (2017).
436. Pan, X., Kaminga, A. C., Wen, S. W. & Liu, A. Chemokines in Prediabetes and Type 2 Diabetes: A Meta-Analysis . *Frontiers in Immunology* vol. 12 (2021).
437. Cimini, F. A. *et al.* Circulating IL-8 levels are increased in patients with type 2 diabetes and associated with worse inflammatory and cardiometabolic profile. *Acta Diabetol.* **54**, 961–967 (2017).
438. Shanmugam, N. *et al.* Increased expression of cyclooxygenase-2 in human pancreatic islets treated with high glucose or ligands of the advanced glycation endproduct-specific receptor (AGER), and in islets from diabetic mice. *Diabetologia* **49**, 100–107 (2006).
439. Persaud, S. J., Burns, C. J., Belin, V. D. & Jones, P. M. Glucose-Induced Regulation of COX-2 Expression in Human Islets of Langerhans. *Diabetes* **53**, S190 LP-S192 (2004).
440. Redondo, S. *et al.* Overproduction of cyclo-oxygenase-2 (COX-2) is involved in the resistance to apoptosis in vascular smooth muscle cells from diabetic patients: a link between inflammation and apoptosis. *Diabetologia* **54**, 190–199 (2011).
441. Burke, K. T. *et al.* Transport of maternal cholesterol to the fetus is affected by maternal plasma cholesterol concentrations in the Golden Syrian hamster. *J. Lipid Res.* **50**, 1146–1155 (2009).
442. Madsen, E. M., Lindegaard, M. L. S., Andersen, C. B., Damm, P. & Nielsen, L. B. Human placenta secretes apolipoprotein B-100-containing lipoproteins. *J. Biol. Chem.* **279**, 55271–55276 (2004).
443. Kamper, M. *et al.* Estrogen-enhanced apical and basolateral secretion of apolipoprotein B-100 by polarized trophoblast-derived BeWo cells. *Biochimie* **138**, 116–123 (2017).
444. Woodfin, A., Voisin, M.-B. & Nourshargh, S. PECAM-1: A Multi-Functional Molecule in Inflammation and Vascular Biology. *Arterioscler. Thromb. Vasc. Biol.* **27**, 2514–2523 (2007).
445. Li, Y. *et al.* Preeclampsia does not alter vascular growth and expression of CD31 and vascular endothelial cadherin in human placentas. *J. Histochem. Cytochem. Off. J. Histochem. Soc.* **63**, 22–31 (2015).
446. Xu, S. *et al.* The novel coronary artery disease risk gene JCAD/KIAA1462 promotes endothelial dysfunction and atherosclerosis. *Eur. Heart J.* **40**, 2398–2408 (2019).
447. Jones, P. D. *et al.* JCAD, a Gene at the 10p11 Coronary Artery Disease Locus,

Regulates Hippo Signaling in Endothelial Cells. *Arterioscler. Thromb. Vasc. Biol.* **38**, 1711–1722 (2018).
448. Tanaka, M. *et al.* The endothelial adrenomedullin-RAMP2 system regulates vascular integrity and suppresses tumour metastasis. *Cardiovasc. Res.* **111**, 398–409 (2016).
449. Yamauchi, A. *et al.* Functional differentiation of RAMP2 and RAMP3 in their regulation of the vascular system. *J. Mol. Cell. Cardiol.* **77**, 73–85 (2014).
450. Koyama, T. *et al.* Vascular endothelial adrenomedullin-RAMP2 system is essential for vascular integrity and organ homeostasis. *Circulation* **127**, 842–853 (2013).
451. McVicar, C. M., Rice-McCaldin, A., Curtis, T., Stitt, A. W. & Gardiner, T. A. Angiogenesis Induced by EGF Is Mediated by Autocrine VEGF. *Invest. Ophthalmol. Vis. Sci.* **48**, 1379 (2007).
452. Kilari, S. *et al.* Endothelial cell-specific chemotaxis receptor (ECSCR) enhances vascular endothelial growth factor (VEGF) receptor-2/kinase insert domain receptor (KDR) activation and promotes proteolysis of internalized KDR. *J. Biol. Chem.* **288**, 10265–10274 (2013).
453. Akakabe, Y. *et al.* Ecscr regulates insulin sensitivity and predisposition to obesity by modulating endothelial cell functions. *Nat. Commun.* **4**, 2389 (2013).
454. Tan, V. P. & Miyamoto, S. HK2/hexokinase-II integrates glycolysis and autophagy to confer cellular protection. *Autophagy* **11**, 963–964 (2015).
455. Roberts, D. J. & Miyamoto, S. Hexokinase II integrates energy metabolism and cellular protection: Akting on mitochondria and TORCing to autophagy. *Cell Death Differ.* **22**, 248–257 (2015).
456. Gray, S. M., Page, L. C. & Tong, J. Ghrelin regulation of glucose metabolism. *J. Neuroendocrinol.* **31**, e12705 (2019).
457. Poher, A.-L., Tschöp, M. H. & Müller, T. D. Ghrelin regulation of glucose metabolism. *Peptides* **100**, 236–242 (2018).
458. Fondacci, C. *et al.* Alterations of human placental epidermal growth factor receptor in intrauterine growth retardation. *J. Clin. Invest.* **93**, 1149–1155 (1994).
459. Dackor, J., Caron, K. M. & Threadgill, D. W. Placental and embryonic growth restriction in mice with reduced function epidermal growth factor receptor alleles. *Genetics* **183**, 207–218 (2009).
460. Kashimata, M., Hiramatsu, M. & Minami, N. Effect of streptozotocin-induced diabetes on epidermal growth factor receptors in rat liver plasma membrane. *Biochim. Biophys. Acta* **923**, 496–500 (1987).
461. Jaworek, J. & Konturek, S. J. Distribution, release, and secretory activity of epidermal growth factor in the pancreas. *Int. J. Pancreatol. Off. J. Int. Assoc. Pancreatol.* **6**, 189–205 (1990).
462. Kasayama, S., Ohba, Y. & Oka, T. Epidermal growth factor deficiency associated with diabetes mellitus. *Proc. Natl. Acad. Sci. U. S. A.* **86**, 7644–7648 (1989).
463. Lee, H. Y. *et al.* Epidermal growth factor increases insulin secretion and lowers blood glucose in diabetic mice. *J. Cell. Mol. Med.* **12**, 1593–1604 (2008).
464. Elmasri, H. *et al.* Endothelial cell-fatty acid binding protein 4 promotes angiogenesis: role of stem cell factor/c-kit pathway. *Angiogenesis* **15**, 457–468 (2012).
465. Zhang, J. *et al.* Interleukin 6 (IL-6) and Tumor Necrosis Factor α (TNF-α) Single Nucleotide Polymorphisms (SNPs), Inflammation and Metabolism in Gestational Diabetes Mellitus in Inner Mongolia. *Med. Sci. Monit. Int. Med. J. Exp. Clin. Res.* **23**, 4149–4157 (2017).
466. Yan, J.-Y. & Wang, X.-J. [Expression and significance of adipocyte fatty acid-binding protein in placenta, serum and umbilical cord blood in preeclampsia]. *Zhonghua Fu Chan Ke Za Zhi* **45**, 885–890 (2010).
467. Yan, Y., Peng, H., Wang, P., Wang, H. & Dong, M. Increased expression of fatty

acid binding protein 4 in preeclamptic Placenta and its relevance to preeclampsia. *Placenta* **39**, 94–100 (2016).
468. Basak, S., Das, M. K., Srinivas, V. & Duttaroy, A. K. The interplay between glucose and fatty acids on tube formation and fatty acid uptake in the first trimester trophoblast cells, HTR8/SVneo. *Mol. Cell. Biochem.* **401**, 11–19 (2014).
469. Patro-Małysza, J. *et al.* FABP4 in gestational diabetes—association between mothers and offspring. *J. Clin. Med.* **8**, (2019).
470. Ortega-Senovilla, H. *et al.* Gestational diabetes mellitus causes changes in the concentrations of adipocyte fatty acid-binding protein and other adipocytokines in cord blood. *Diabetes Care* **34**, 2061–2066 (2011).
471. Kralisch, S. *et al.* Serum levels of adipocyte fatty acid binding protein are increased in gestational diabetes mellitus. *Eur. J. Endocrinol.* **160**, 33–38 (2009).
472. Zhang, Y. *et al.* Changes in serum adipocyte fatty acid-binding protein in women with gestational diabetes mellitus and normal pregnant women during mid- and late pregnancy. *J. Diabetes Investig.* **7**, 797–804 (2016).
473. Hara, T. *et al.* Targeted Disruption of JCAD (Junctional Protein Associated With Coronary Artery Disease)/KIAA1462, a Coronary Artery Disease-Associated Gene Product, Inhibits Angiogenic Processes In Vitro and In Vivo. *Arterioscler. Thromb. Vasc. Biol.* **37**, 1667–1673 (2017).
474. Chen, B. *et al.* Systematic Identification of Hub Genes in Placenta Accreta Spectrum Based on Integrated Transcriptomic and Proteomic Analysis. *Front. Genet.* **11**, 551495 (2020).
475. Romacho, T., Sánchez-Ferrer, C. F. & Peiró, C. Visfatin/Nampt: An adipokine with cardiovascular impact. *Mediators Inflamm.* **2013**, (2013).
476. Tsai, P. J. S., Davis, J., Thompson, K. & Bryant-Greenwood, G. Visfatin/Nampt and SIRT1: Roles in postterm delivery in pregnancies associated with obesity. *Reprod. Sci.* **22**, 1028–1036 (2015).
477. Noureldeen, A. F. H., Qusti, S. Y., Al-Seeni, M. N. & Bagais, M. H. Maternal leptin, adiponectin, resistin, visfatin and tumor necrosis factor-alpha in normal and gestational diabetes. *Indian J. Clin. Biochem.* **29**, 462–470 (2014).
478. Lewandowski, K. C. *et al.* Elevated serum levels of visfatin in gestational diabetes: A comparative study across various degrees of glucose tolerance. *Diabetologia* **50**, 1033–1037 (2007).
479. Telejko, B. *et al.* Visfatin in gestational diabetes: serum level and mRNA expression in fat and placental tissue. *Diabetes Res. Clin. Pract.* **84**, 68–75 (2009).
480. Tsiotra, P. C. *et al.* Circulating adipokines and mRNA expression in adipose tissue and the placenta in women with gestational diabetes mellitus. *Peptides* **101**, 157–166 (2018).
481. Zhang, J. *et al.* Platelet-derived growth factor D promotes the angiogenic capacity of endothelial progenitor cells. *Mol Med Rep* **19**, 125–132 (2019).
482. Wang, H., Nian, L., Li, Z. & Lu, C. Inhibiting PDGF-D alleviates the symptoms of HELLP by suppressing NF-κB activation. *J. Mol. Endocrinol.* **66**, 233–243 (2021).
483. Uutela, M. *et al.* PDGF-D induces macrophage recruitment, increased interstitial pressure, and blood vessel maturation during angiogenesis. *Blood* **104**, 3198–3204 (2004).
484. Uras, N. *et al.* CD31 and Factor VIII in angiogenesis of normal and pre-eclamptic human placentas. *J. Obstet. Gynaecol. J. Inst. Obstet. Gynaecol.* **32**, 533–536 (2012).
485. Hayes, E. K. *et al.* Adverse Fetal and Neonatal Outcomes Associated with a Life-Long High Fat Diet: Role of Altered Development of the Placental Vasculature. *PLoS One* **7**, e33370 (2012).
486. Sirico, A. *et al.* Placental diabesity: placental VEGF and CD31 expression

according to pregestational BMI and gestational weight gain in women with gestational diabetes. *Arch. Gynecol. Obstet.* (2022) doi:10.1007/s00404-022-06673-3.

487. Vangrieken, P. *et al.* Hypoxia-induced mitochondrial abnormalities in cells of the placenta. *PLoS One* **16**, e0245155 (2021).
488. Scheele, C. *et al.* Altered regulation of the PINK1 locus: a link between type 2 diabetes and neurodegeneration? *FASEB J. Off. Publ. Fed. Am. Soc. Exp. Biol.* **21**, 3653–3665 (2007).
489. Kadmiel, M., Matson, B. C., Espenschied, S. T., Lenhart, P. M. & Caron, K. M. Loss of receptor activity-modifying protein 2 in mice causes placental dysfunction and alters PTH1R regulation. *PLoS One* **12**, 1–12 (2017).
490. Weston, C. *et al.* Modulation of glucagon receptor pharmacology by receptor activity-modifying protein-2 (RAMP2). *J. Biol. Chem.* **290**, 23009–23022 (2015).
491. Hayashi, K. G., Hosoe, M., Sakumoto, R. & Takahashi, T. Temporo-spatial expression of adrenomedullin and its receptors in the bovine placenta. *Reprod. Biol. Endocrinol.* **11**, 1–14 (2013).
492. Gao, H., Liebenthal, D. A., Yallampalli, U. & Yallampalli, C. Adrenomedullin promotes rat trophoblast stem cell differentiation. *Biol. Reprod.* **91**, 1–6 (2014).
493. Li, L., Tang, F. & O, W. S. Coexpression of adrenomedullin and its receptor component proteins in the reproductive system of the rat during gestation. *Reprod. Biol. Endocrinol.* **8**, 130 (2010).
494. Makino, Y., Shibata, K., Makino, I., Kangawa, K. & Kawarabayashi, T. Alteration of the adrenomedullin receptor components gene expression associated with the blood pressure in pregnancy-induced hypertension. *J. Clin. Endocrinol. Metab.* **86**, 5079–5082 (2001).
495. Zhou, Y.-B. *et al.* Adrenomedullin attenuates vascular calcification in fructose-induced insulin resistance rats. *Acta Physiol.* **207**, 437–446 (2013).
496. Hiragushi, K. *et al.* The role of adrenomedullin and receptors in glomerular hyperfiltration in streptozotocin-induced diabetic rats. *Kidney Int.* **65**, 540–550 (2004).
497. Han, C. S. *et al.* Glucose and metformin modulate human first trimester trophoblast function: a model and potential therapy for diabetes-associated uteroplacental insufficiency. *Am. J. Reprod. Immunol.* **73**, 362–371 (2015).
498. Madonna, R., Geng, Y. J., Shelat, H., Ferdinandy, P. & De Caterina, R. High glucose-induced hyperosmolarity impacts proliferation, cytoskeleton remodeling and migration of human induced pluripotent stem cells via aquaporin-1. *Biochim. Biophys. Acta - Mol. Basis Dis.* **1842**, 2266–2275 (2014).
499. El-Remessy, A. B., Abou-Mohamed, G., Caldwell, R. W. & Caldwell, R. B. High glucose-induced tyrosine nitration in endothelial cells: Role of eNOS uncoupling and aldose reductase activation. *Investig. Ophthalmol. Vis. Sci.* **44**, 3135–3143 (2003).
500. Madonna, R. *et al.* High glucose-induced hyperosmolarity contributes to COX-2 expression and angiogenesis: Implications for diabetic retinopathy. *Cardiovasc. Diabetol.* **15**, 1–14 (2016).
501. Palmer, M. E., Watson, A. L. & Burton, G. J. Morphological analysis of degeneration and regeneration of syncytiotrophoblast in first trimester placental villi during organ culture. *Hum. Reprod.* **12**, 379–382 (1997).
502. Heazell, A., Harris, L., Forbes, K. & Crocker, I. Placental cell turnover in health and disease. *Rev. Gynaecol. Perinat. Pract.* **6**, 80–86 (2006).
503. Crocker, I. P., Tansinda, D. M. & Baker, P. N. Altered cell kinetics in cultured placental villous explants in pregnancies complicated by pre-eclampsia and intrauterine growth restriction. *J. Pathol.* **204**, 11–18 (2004).
504. Crocker, I. P., Tansinda, D. M., Jones, C. J. P. & Baker, P. N. The Influence of Oxygen and Tumor Necrosis Factor-α on the Cellular Kinetics of Term Placental Villous Explants in Culture. *J. Histochem. Cytochem.* **52**, 749–757 (2004).

505. Hsieh, Y.-S. *et al.* Is the level of serum lactate dehydrogenase a potential biomarker for glucose monitoring with type 2 diabetes mellitus? . *Frontiers in Endocrinology* vol. 13 (2022).
506. Alcazar, O., Tiedge, M. & Lenzen, S. Importance of lactate dehydrogenase for the regulation of glycolytic flux and insulin secretion in insulin-producing cells. *Biochem. J.* **352**, 373–380 (2000).
507. S. Vaidya, S., W. Walsh, S. & M. Gerk, P. Application of Human Placental Villous Tissue Explants to Study ABC Transporter Mediated Efflux of 2,4-Dinitrophenyl-S-Glutathione. *Curr. Pharm. Biotechnol.* **12**, 814–823 (2012).
508. Sooranna, S. R., Oteng-Ntim, E., Meah, R., Ryder, T. A. & Bajoria, R. Characterization of human placental explants: Morphological, biochemical and physiological studies using first and third trimester placenta. *Hum. Reprod.* **14**, 536–541 (1999).
509. Sibley, C. P. Treating the dysfunctional placenta. *J. Endocrinol.* **234**, R81–R97 (2017).
510. Leung, D. N., Smith, S. C., To, K. F., Sahota, D. S. & Baker, P. N. Increased placental apoptosis in pregnancies complicated by preeclampsia. *Am. J. Obstet. Gynecol.* **184**, 1249–1250 (2001).
511. Belkacemi, L., Kjos, S., Nelson, D. M., Desai, M. & Ross, M. G. Reduced apoptosis in term placentas from gestational diabetic pregnancies. *J. Dev. Orig. Health Dis.* **4**, 256–265 (2013).
512. Ehlers, E., Talton, O. O., Schust, D. J. & Schulz, L. C. Placental structural abnormalities in gestational diabetes and when they develop: A scoping review. *Placenta* **116**, 58–66 (2021).
513. Zhang, L. *et al.* Gestational Diabetes Mellitus-Associated Hyperglycemia Impairs Glucose Transporter 3 Trafficking in Trophoblasts Through the Downregulation of AMP-Activated Protein Kinase . *Frontiers in Cell and Developmental Biology* vol. 9 (2021).
514. Wang, Z. *et al.* Effects of glucose and osmotic pressure on the proliferation and cell cycle of human chorionic trophoblast cells. *Open life Sci.* **17**, 1418–1428 (2022).
515. Aires, M. B. & Dos Santos, A. C. V. Effects of maternal diabetes on trophoblast cells. *World J. Diabetes* **6**, 338–344 (2015).
516. Hulme, C. H. Understanding placental function in pregnancies complicated by Diabetes mellitus: a systems biology approach. (University of Manchester, 2016).
517. Augustin, R. The protein family of glucose transport facilitators: It's not only about glucose after all. *IUBMB Life* **62**, 315–333 (2010).
518. Freedman, A. A. *et al.* Associations Between Features of Placental Morphology and Birth Weight in Dichorionic Twins. *Am. J. Epidemiol.* **188**, 518–526 (2019).
519. Garvey, W. T., Maianu, L., Hancock, J. A., Golichowski, A. M. & Baron, A. Gene expression of GLUT4 in skeletal muscle from insulin-resistant patients with obesity, IGT, GDM, and NIDDM. *Diabetes* **41**, 465–475 (1992).
520. James-Allan, L. B., Arbet, J., Teal, S. B., Powell, T. L. & Jansson, T. Insulin stimulates GLUT4 trafficking to the syncytiotrophoblast basal plasma membrane in the human placenta. *J. Clin. Endocrinol. Metab.* **104**, 4225–4238 (2019).
521. Colomiere, M., Permezel, M., Riley, C., Desoye, G. & Lappas, M. Defective insulin signaling in placenta from pregnancies complicated by gestational diabetes mellitus. *Eur. J. Endocrinol.* **160**, 567–578 (2009).
522. Carayannopoulos, M. O. *et al.* GLUT8 is a glucose transporter responsible for insulin-stimulated glucose uptake in the blastocyst. *Proc. Natl. Acad. Sci. U. S. A.* **97**, 7313–7318 (2000).
523. Maria, Z., Campolo, A. R. & Lacombe, V. A. Diabetes Alters the Expression and Translocation of the Insulin-Sensitive Glucose Transporters 4 and 8 in the Atria. *PLoS One* **10**, e0146033 (2015).

524. Stanirowski, P. J. *et al.* Differential Expression of Glucose Transporter Proteins GLUT-1, GLUT-3, GLUT-8 and GLUT-12 in the Placenta of Macrosomic, Small-for-Gestational-Age and Growth-Restricted Foetuses. *Journal of Clinical Medicine* vol. 10 (2021).
525. Limesand, S. W., Regnault, T. R. H. & Hay, W. W. J. Characterization of glucose transporter 8 (GLUT8) in the ovine placenta of normal and growth restricted fetuses. *Placenta* **25**, 70–77 (2004).
526. Adastra, K. L. *et al.* Slc2a8 deficiency in mice results in reproductive and growth impairments. *Biol. Reprod.* **87**, 49 (2012).
527. Janzen, C. *et al.* Humanin (HN) and glucose transporter 8 (GLUT8) in pregnancies complicated by intrauterine growth restriction. *PLoS One* **13**, e0193583 (2018).
528. Hahn, T. *et al.* Hyperglycemia regulates the glucose-transport system of clonal choriocarcinoma cells in vitro. A potential molecular mechanism contributing to the adjunct effect of glucose in tumor therapy. *Int. J. cancer* **78**, 353–360 (1998).
529. Li, H., Gu, Y., Zhang, Y., Lucas, M. J. & Wang, Y. High glucose levels down-regulate glucose transporter expression that correlates with increased oxidative stress in placental trophoblast cells in vitro. *J. Soc. Gynecol. Investig.* **11**, 75–81 (2004).
530. Sun, Y., Asnicar, M., Saha, P. K., Chan, L. & Smith, R. G. Ablation of ghrelin improves the diabetic but not obese phenotype of ob/ob mice. *Cell Metab.* **3**, 379–386 (2006).
531. Song, T.-R. *et al.* Dysregulated miRNAs contribute to altered placental glucose metabolism in patients with gestational diabetes via targeting GLUT1 and HK2. *Placenta* **105**, 14–22 (2021).
532. Morishima, M., Horikawa, K. & Funaki, M. Cardiomyocytes cultured on mechanically compliant substrates, but not on conventional culture devices, exhibit prominent mitochondrial dysfunction due to reactive oxygen species and insulin resistance under high glucose. *PLoS One* **13**, e0201891 (2018).
533. Zhao, D. *et al.* Orphan nuclear transcription factor TR3/Nur77 regulates microvessel permeability by targeting endothelial nitric oxide synthase and destabilizing endothelial junctions. *Proc. Natl. Acad. Sci. U. S. A.* **108**, 12066–12071 (2011).
534. Kang, J. I. *et al.* Pro-angiogenic Ginsenosides F1 and Rh1 Inhibit Vascular Leakage by Modulating NR4A1. *Sci. Rep.* **9**, 1–13 (2019).
535. Villota, S. D., Toledo-Rodriguez, M. & Leach, L. Compromised barrier integrity of human feto-placental vessels from gestational diabetic pregnancies is related to downregulation of occludin expression. *Diabetologia* **64**, 195–210 (2021).
536. Cvitic, S. *et al.* Human fetoplacental arterial and venous endothelial cells are differentially programmed by gestational diabetes mellitus, resulting in cell-specific barrier function changes. *Diabetologia* **61**, 2398–2411 (2018).
537. Ciborowski, M. *et al.* Potential first trimester metabolomic biomarkers of abnormal birth weight in healthy pregnancies. *Prenat. Diagn.* **34**, 870–877 (2014).
538. Dubé, E. *et al.* Modulation of Fatty Acid Transport and Metabolism by Maternal Obesity in the Human Full-Term Placenta1. *Biol. Reprod.* **87**, 1-11,14 (2012).
539. Song, L., Wang, N., Peng, Y., Sun, B. & Cui, W. Placental lipid transport and content in response to maternal overweight and gestational diabetes mellitus in human term placenta. *Nutr. Metab. Cardiovasc. Dis.* **32**, 692–702 (2022).
540. Visiedo, F. *et al.* High glucose levels reduce fatty acid oxidation and increase triglyceride accumulation in human placenta. *Am. J. Physiol. - Endocrinol. Metab.* **305**, 205–212 (2013).
541. Nikolova, V. *et al.* Changes in LXR signaling influence early-pregnancy lipogenesis and protect against dysregulated fetoplacental lipid homeostasis. *Am. J. Physiol. Metab.* **313**, E463–E472 (2017).

542. Xu, S. & Cao, X. Interleukin-17 and its expanding biological functions. *Cell. Mol. Immunol.* **7**, 164–174 (2010).
543. Moore, K. W., Malefyt, R. D. W., Robert, L. & Garra, A. O. Interleukin -10 and the Interleukin -10 Receptor. *Mol. Cell. Biol.* **1**, 683–765 (2001).
544. Bhattacharjee, A. *et al.* IL-4 and IL-13 employ discrete signaling pathways for target gene expression in alternatively activated monocytes/macrophages. *Free Radic. Biol. Med.* **54**, 1–16 (2013).
545. Audrito, V., Messana, V. G. & Deaglio, S. NAMPT and NAPRT: Two Metabolic Enzymes With Key Roles in Inflammation. *Front. Oncol.* **10**, 1–17 (2020).
546. Dimitriadis, E., White, C. A., Jones, R. L. & Salamonsen, L. A. Cytokines, chemokines and growth factors in endometrium related to implantation. *Hum. Reprod. Update* **11**, 613–630 (2005).
547. Bowen, J. M., Chamley, L., Mitchell, M. D. & Keelan, J. A. Cytokines of the Placenta and Extra-placental Membranes: Biosynthesis, Secretion and Roles in Establishment of Pregnancy in Women. *Placenta* **23**, 239–256 (2002).
548. Raghupathy, R. Cytokines as key players in the pathophysiology of preeclampsia. *Med. Princ. Pract. Int. J. Kuwait Univ. Heal. Sci. Cent.* **22 Suppl 1**, 8–19 (2013).
549. Hannan, N. J. & Salamonsen, L. A. Role of chemokines in the endometrium and in embryo implantation. *Curr. Opin. Obstet. Gynecol.* **19**, 266–272 (2007).
550. Parrott, M. S., von Versen-Hoeynck, F., Ness, R. B., Markovic, N. & Roberts, J. M. System A amino acid transporter activity in term placenta is substrate specific and inversely related to amino acid concentration. *Reprod. Sci.* **14**, 687–693 (2007).
551. Dimasuay, K. G., Boeuf, P., Powell, T. L. & Jansson, T. Placental Responses to Changes in the Maternal Environment Determine Fetal Growth . *Frontiers in Physiology* vol. 7 (2016).
552. Yang, Y. *et al.* Transcriptomic Profiling of Human Placenta in Gestational Diabetes Mellitus at the Single-Cell Level. *Front. Endocrinol. (Lausanne).* **12**, 679582 (2021).
553. Binder, A. M., LaRocca, J., Lesseur, C., Marsit, C. J. & Michels, K. B. Epigenome-wide and transcriptome-wide analyses reveal gestational diabetes is associated with alterations in the human leukocyte antigen complex. *Clin. Epigenetics* **7**, 1–12 (2015).
554. Tang, L., Li, P. & Li, L. Whole transcriptome expression profiles in placenta samples from women with gestational diabetes mellitus. *J. Diabetes Investig.* **11**, 1307–1317 (2020).
555. Uusküla, L. *et al.* Mid-Gestational Gene Expression Profile in Placenta and Link to Pregnancy Complications. *PLoS One* **7**, (2012).
556. Deyssenroth, M. A. *et al.* Expression of placental regulatory genes is associated with fetal growth. *J. Perinat. Med.* **45**, 887–893 (2017).
557. Cox, B. *et al.* A Co-expression Analysis of the Placental Transcriptome in Association with Maternal Pre-pregnancy BMI and Newborn Birth Weight. *Front. Genet.* **10**, 1–13 (2019).
558. de Onis, M. *et al.* Worldwide implementation of the WHO Child Growth Standards. *Public Health Nutr.* **15**, 1603–1610 (2012).
559. Chiswick, C. *et al.* Effect of metformin on maternal and fetal outcomes in obese pregnant women (EMPOWaR): a randomised, double-blind, placebo-controlled trial. *lancet. Diabetes & Endocrinol.* **3**, 778–786 (2015).
560. Rosen, H. *et al.* Delivery outcomes of large-for-gestational-age newborns stratified by the presence or absence of gestational diabetes mellitus. *Int. J. Gynaecol. Obstet. Off. organ Int. Fed. Gynaecol. Obstet.* **141**, 120–125 (2018).
561. Tsu, B. V *et al.* Diverse viral proteases activate the NLRP1 inflammasome. *Elife* **10**, e60609 (2021).
562. Sun, Y., Zhao, J., Sun, X. & Ma, G. Identification of TNFAIP8 as an Immune-

Related Biomarker Associated With Tumorigenesis and Prognosis in Cutaneous Melanoma Patients . *Frontiers in Genetics* vol. 12 (2021).
563. Ponder, K. G. & Boise, L. H. The prodomain of caspase-3 regulates its own removal and caspase activation. *Cell Death Discov.* **5**, 56 (2019).
564. Mudde, A. C. A., Booth, C. & Marsh, R. A. Evolution of Our Understanding of XIAP Deficiency. *Front. Pediatr.* **9**, (2021).
565. Madeleneau, D. *et al.* Transcriptomic analysis of human placenta in intrauterine growth restriction. *Pediatr. Res.* **77**, 799–807 (2015).
566. Crossey, P. A., Pillai, C. C. & Miell, J. P. Altered placental development and intrauterine growth restriction in IGF binding protein-1 transgenic mice. *J. Clin. Invest.* **110**, 411–418 (2002).
567. Forbes, K. & Westwood, M. The IGF axis and placental function: A mini review. *Horm. Res.* **69**, 129–137 (2008).
568. Akhabir, L. & Sandford, A. Genetics of interleukin 1 receptor-like 1 in immune and inflammatory diseases. *Curr. Genomics* **11**, 591–606 (2010).
569. Tokunaga, R. *et al.* CXCL9, CXCL10, CXCL11/CXCR3 axis for immune activation - A target for novel cancer therapy. *Cancer Treat. Rev.* **63**, 40–47 (2018).
570. Rouault, C. *et al.* Roles of Chemokine Ligand-2 (CXCL2) and Neutrophils in Influencing Endothelial Cell Function and Inflammation of Human Adipose Tissue. *Endocrinology* **154**, 1069–1079 (2013).
571. Ivetic, A., Hoskins Green, H. L. & Hart, S. J. L-selectin: A Major Regulator of Leukocyte Adhesion, Migration and Signaling. *Front. Immunol.* **10**, 1068 (2019).
572. Zhang, Y. *et al.* TIPARP is involved in the regulation of intraocular pressure. *Commun. Biol.* **5**, 1386 (2022).
573. Hu, X. *et al.* Depletion of Ars2 inhibits cell proliferation and leukemogenesis in acute myeloid leukemia by modulating the miR-6734-3p/p27 axis. *Leukemia* **33**, 1090–1101 (2019).
574. Takahashi, D. T. *et al.* Topoisomerase I (TOP1) dynamics: conformational transition from open to closed states. *Nat. Commun.* **13**, 59 (2022).
575. Wang, Q. *et al.* Hapln2 in Neurological Diseases and Its Potential as Therapeutic Target . *Frontiers in Aging Neuroscience* vol. 11 (2019).
576. Zhang, R. *et al.* FcgRIII Deficiency and FcgRIIb Defeciency Promote Renal Injury in Diabetic Mice. *Biomed Res. Int.* **2019**, 3514574 (2019).
577. Towne, J. E. *et al.* Interleukin-36 (IL-36) ligands require processing for full agonist (IL-36α, IL-36β, and IL-36γ) or antagonist (IL-36Ra) activity. *J. Biol. Chem.* **286**, 42594–42602 (2011).
578. Deyssenroth, M. A. *et al.* Whole-transcriptome analysis delineates the human placenta gene network and its associations with fetal growth. *BMC Genomics* **18**, 520 (2017).
579. Münzberg, H. & Heymsfield, S. B. New Insights into the Regulation of Leptin Gene Expression. *Cell Metab.* **29**, 1013–1014 (2019).
580. Xiao, C., Wang, Y. & Fan, Y. Bioinformatics Analysis Identifies Potential Related Genes in the Pathogenesis of Intrauterine Fetal Growth Retardation. *Evol. Bioinforma.* **18**, (2022).
581. Wu, J. *et al.* Regulation of the urea cycle by CPS1 O-GlcNAcylation in response to dietary restriction and aging. *J. Mol. Cell Biol.* **14**, mjac016 (2022).
582. Chen, J. *et al.* PDGF-D promotes cell growth, aggressiveness, angiogenesis and EMT transformation of colorectal cancer by activation of Notch1/Twist1 pathway. *Oncotarget* **8**, 9961–9973 (2017).
583. Kiriko Kaneko *et al.* Identification of a novel erythroid-specific enhancer for the ALAS2 gene and its loss-of-function mutation which is associated with congenital sideroblastic anemia. *Haematologica* **99**, 252–261 (2014).
584. Furuhashi, M., Saitoh, S., Shimamoto, K. & Miura, T. Fatty Acid-Binding Protein 4 (FABP4): Pathophysiological Insights and Potent Clinical Biomarker of

Metabolic and Cardiovascular Diseases. *Clin. Med. Insights. Cardiol.* **8**, 23–33 (2014).
585. Kenny, L. C. *et al.* Advanced maternal age and adverse pregnancy outcome: evidence from a large contemporary cohort. *PLoS One* **8**, e56583 (2013).
586. Li, G. *et al.* Incidence and Risk Factors of Gestational Diabetes Mellitus: A Prospective Cohort Study in Qingdao, China. *Front. Endocrinol. (Lausanne).* **11**, 636 (2020).
587. Roca-Rodríguez, M. D., Ramos-García, P., López-Tinoco, C. & Aguilar-Diosdado, M. Significance of Serum-Plasma Leptin Profile during Pregnancy in Gestational Diabetes Mellitus: A Systematic Review and Meta-Analysis. *Journal of Clinical Medicine* vol. 11 (2022).
588. McMinn, J. *et al.* Unbalanced Placental Expression of Imprinted Genes in Human Intrauterine Growth Restriction. *Placenta* **27**, 540–549 (2006).
589. Obeidat, R. A. *et al.* Maternal and fetal serum leptin levels and their association with maternal and fetal variables and labor: A cross-sectional study. *Ann. Med. Surg.* **72**, 103050 (2021).
590. Wiznitzer, A. *et al.* Cord leptin level and fetal macrosomia. *Obstet. Gynecol.* **96**, 707–713 (2000).
591. White, V. *et al.* Leptin modulates nitric oxide production and lipid metabolism in human placenta. *Reprod. Fertil. Dev.* **18**, 425–432 (2006).
592. Lee, J.-H. *et al.* Identification of Pre-Diabetic Biomarkers in the Progression of Diabetes Mellitus. *Biomedicines* vol. 10 (2022).
593. Urbantat, R. M. *et al.* The CXCL2/IL8/CXCR2 Pathway Is Relevant for Brain Tumor Malignancy and Endothelial Cell Function. *Int. J. Mol. Sci.* **22**, (2021).
594. Cho, J. G., Lee, A., Chang, W., Lee, M.-S. & Kim, J. Endothelial to Mesenchymal Transition Represents a Key Link in the Interaction between Inflammation and Endothelial Dysfunction. *Front. Immunol.* **9**, 294 (2018).
595. Stefanie Swietlik. Examining the possibility of an endothelialmesenchymal transition in placenta. (University of Manchester, 2015).
596. Scott, E. M., Murphy, H. R. & Myers, J. MAGIC (Maternal Glucose in Pregnancy) - Understanding the glycemic profile of pregnancy , intensive CGM glucose profiling and its relationship to fetal growth . An observational study protocol. 1–12 (2023).
597. Kedziora, S. M. *et al.* Placental Transcriptome Profiling in Subtypes of Diabetic Pregnancies Is Strongly Confounded by Fetal Sex. *Int. J. Mol. Sci.* **23**, (2022).
598. Uzelac, P. S. *et al.* Dysregulation of Leptin and Testosterone Production and Their Receptor Expression in the Human Placenta with Gestational Diabetes Mellitus. *Placenta* **31**, 581–8 (2010).
599. Asmat, U., Abad, K. & Ismail, K. Diabetes mellitus and oxidative stress—A concise review. *Saudi Pharm. J.* **24**, 547–553 (2016).
600. Teramo, K. & Piñeiro-Ramos, J. D. Fetal chronic hypoxia and oxidative stress in diabetic pregnancy. Could fetal erythropoietin improve offspring outcomes? *Free Radic. Biol. Med.* **142**, 32–37 (2019).
601. Drake, P. M., Red-Horse, K. & Fisher, S. J. Reciprocal chemokine receptor and ligand expression in the human placenta: Implications for cytotrophoblast differentiation. *Dev. Dyn.* **229**, 877–885 (2004).
602. Red-Horse, K., Drake, P. M., Gunn, M. D. & Fisher, S. J. Chemokine Ligand and Receptor Expression in the Pregnant Uterus: Reciprocal Patterns in Complementary Cell Subsets Suggest Functional Roles. *Am. J. Pathol.* **159**, 2199–2213 (2001).
603. Drake, P. M. *et al.* Human Placental Cytotrophoblasts Attract Monocytes and Cd56bright Natural Killer Cells via the Actions of Monocyte Inflammatory Protein 1α. *J. Exp. Med.* **193**, 1199–1212 (2001).
604. Pantham, P., Aye, I. L. M. H. & Powell, T. L. Inflammation in maternal obesity and gestational diabetes mellitus. *Placenta* **36**, 709–715 (2015).

605. Fakonti, G., Pantazi, P., Bokun, V. & Holder, B. Placental Macrophage (Hofbauer Cell) Responses to Infection During Pregnancy: A Systematic Scoping Review. *Frontiers in immunology* vol. 12 756035 (2021).
606. Chávez-Galán, L., Olleros, M. L., Vesin, D. & Garcia, I. Much more than M1 and M2 macrophages, there are also CD169+ and TCR+ macrophages. *Front. Immunol.* **6**, 1–15 (2015).
607. Saqib, U. *et al.* Phytochemicals as modulators of M1-M2 macrophages in inflammation. *Oncotarget* **9**, 17937–17950 (2018).
608. Hu, X. L., Yang, Y. & Hunt, J. S. Differential distribution of interleukin-1α and interleukin-1β proteins in human placentas. *J. Reprod. Immunol.* **22**, 257–268 (1992).
609. Benyo, D. F., Miles, T. M. & Conrad, K. P. Hypoxia stimulates cytokine production by villous explants from the human placenta. *J. Clin. Endocrinol. Metab.* **82**, 1582–1588 (1997).
610. Kameda, T. *et al.* Production of interleukin-6 by normal human trophoblast. *Placenta* **11**, 205–213 (1990).
611. Hla, T. & Neilson, K. Human cyclooxygenase-2 cDNA. *Proc. Natl. Acad. Sci. U. S. A.* **89**, 7384–7388 (1992).
612. Mrizak, I. *et al.* Placental infiltration of inflammatory markers in gestational diabetic women. *Gen. Physiol. Biophys.* **33**, 169–176 (2014).
613. Kleiblova, P. *et al.* Expression of adipokines and estrogen receptors in adipose tissue and placenta of patients with gestational diabetes mellitus. *Mol. Cell. Endocrinol.* **314**, 150–156 (2010).
614. Benyo, D. F., Smarason, A., Redman, C. W. G., Sims, C. & Conrad, K. P. Expression of inflammatory cytokines in placentas from women with preeclampsia. *J. Clin. Endocrinol. Metab.* **86**, 2505–2512 (2001).
615. Yockey, L. J. & Iwasaki, A. Interferons and Proinflammatory Cytokines in Pregnancy and Fetal Development. *Immunity* **49**, 397–412 (2018).
616. Nadeau-Vallée, M. *et al.* A critical role of interleukin-1 in preterm labor. *Cytokine Growth Factor Rev.* **28**, 37–51 (2016).
617. Paquette, A. G. *et al.* Placental transcriptomic signatures of spontaneous preterm birth. *Am. J. Obstet. Gynecol.* **228**, 73.e1-73.e18 (2022).
618. Hedderson, M. M., Ferrara, A. & Sacks, D. A. Gestational diabetes mellitus and lesser degrees of pregnancy hyperglycemia: association with increased risk of spontaneous preterm birth. *Obstet. Gynecol.* **102**, 850–856 (2003).
619. Dissanayake, W. C., Oh, J. K., Sorrenson, B. & Shepherd, P. R. Glucose regulates expression of pro-inflammatory genes, IL-1β and IL-12, through a mechanism involving hexosamine biosynthesis pathway-dependent regulation of α-E catenin. *Biosci. Rep.* **41**, (2021).
620. Hill, J. R., Kwon, G., Marshall, C. A. & McDaniel, M. L. Hyperglycemic levels of glucose inhibit interleukin 1 release from RAW 264.7 murine macrophages by activation of protein kinase C. *J. Biol. Chem.* **273**, 3308–3313 (1998).
621. Young, O. M. *et al.* Toll-like Receptor-Mediated Responses by Placental Hofbauer Cells (HBCs): A Potential Pro-Inflammatory Role for Fetal M2 Macrophages. *Am. J. Reprod. Immunol.* **73**, 22–35 (2015).
622. Svensson-Arvelund, J. *et al.* The Human Fetal Placenta Promotes Tolerance against the Semiallogeneic Fetus by Inducing Regulatory T Cells and Homeostatic M2 Macrophages. *J. Immunol.* **194**, 1534–1544 (2015).
623. Zajac, E. *et al.* Angiogenic capacity of M1- and M2-polarized macrophages is determined by the levels of TIMP-1 complexed with their secreted proMMP-9. *Blood* **122**, 4054–4067 (2013).
624. Jeon, G.-H. *et al.* 117: The expression of CD36 in preterm and term pregnancies. *Am. J. Obstet. Gynecol.* **206**, S64–S65 (2012).
625. Lager, S. *et al.* Protein expression of fatty acid transporter 2 is polarized to the trophoblast basal plasma membrane and increased in placentas from

overweight/obese women. *Placenta* **40**, 60–66 (2016).
626. Jablonski, K. A. *et al.* Novel Markers to Delineate Murine M1 and M2 Macrophages. *PLoS One* **10**, e0145342 (2015).
627. Zhang, B., Yang, Y., Yi, J., Zhao, Z. & Ye, R. Hyperglycemia modulates M1/M2 macrophage polarization via reactive oxygen species overproduction in ligature-induced periodontitis. *J. Periodontal Res.* **56**, 991–1005 (2021).
628. Lin, J., Kong, Q., Hao, W. & Hu, W. High glucose contributes to the polarization of peritoneal macrophages to the M2 phenotype in vivo and in vitro. *Mol. Med. Rep.* **22**, 127–134 (2020).
629. Jetten, N. *et al.* Anti-inflammatory M2, but not pro-inflammatory M1 macrophages promote angiogenesis in vivo. *Angiogenesis* **17**, 109–118 (2014).
630. Maruyama, K. *et al.* Interleukin-1βUpregulates Cardiac Expression of Vascular Endothelial Growth Factor and its Receptor KDR/flk-1 via Activation of Protein Tyrosine Kinases. *J. Mol. Cell. Cardiol.* **31**, 607–617 (1999).
631. Alagappan, V. K. T. *et al.* Proinflammatory cytokines upregulate mRNA expression and secretion of vascular endothelial growth factor in cultured human airway smooth muscle cells. *Cell Biochem. Biophys.* **43**, 119–129 (2005).
632. Fahey, E. & Doyle, S. L. IL-1 family cytokine regulation of vascular permeability and angiogenesis. *Front. Immunol.* **10**, 1–15 (2019).
633. Tamura, K., Sakurai, T. & Kogo, H. Relationship between prostaglandin E2 and vascular endothelial growth factor (VEGF) in angiogenesis in human vascular endothelial cells. *Vascul. Pharmacol.* **44**, 411–416 (2006).
634. Ingman, K., Cookson, V. J. K. W., Jones, C. J. P. & Aplin, J. D. Characterisation of Hofbauer Cells in First and Second Trimester Placenta: Incidence, Phenotype, Survival in vitro and Motility. *Placenta* **31**, 535–544 (2010).
635. Dusza, H. M. *et al.* Experimental human placental models for studying uptake, transport and toxicity of micro- and nanoplastics. *Sci. Total Environ.* **860**, 160403 (2023).
636. Lang, I. *et al.* Heterogeneity of microvascular endothelial cells isolated from human term placenta and macrovascular umbilical vein endothelial cells. *Eur. J. Cell Biol.* **82**, 163–173 (2003).
637. Lang, I. *et al.* Human fetal placental endothelial cells have a mature arterial and a juvenile venous phenotype with adipogenic and osteogenic differentiation potential. *Differentiation* **76**, 1031–1043 (2008).
638. Lang, I. *et al.* Immunohistochemical evidence for the heterogeneity of maternal and fetal vascular endothelial cells in human full-term placenta. *Cell Tissue Res.* **274**, 211–218 (1993).
639. Morley, L. C. *et al.* Piezo1 channels are mechanosensors in human fetoplacental endothelial cells. *Mol. Hum. Reprod.* **24**, 510–520 (2018).
640. Castrechini, N. M. *et al.* Mesenchymal stem cells in human placental chorionic villi reside in a vascular Niche. *Placenta* **31**, 203–212 (2010).
641. Demir, R., Kayisli, U. A., Cayli, S. & Huppertz, B. Sequential Steps During Vasculogenesis and Angiogenesis in the Very Early Human Placenta. *Placenta* **27**, 535–539 (2006).
642. Wu, M. *et al.* Comparison of the Biological Characteristics of Mesenchymal Stem Cells Derived from the Human Placenta and Umbilical Cord. *Sci. Rep.* **8**, 5014 (2018).
643. Du, W. J. *et al.* Heterogeneity of proangiogenic features in mesenchymal stem cells derived from bone marrow, adipose tissue, umbilical cord, and placenta. *Stem Cell Res. Ther.* **7**, 1–11 (2016).
644. Kinzer, M. *et al.* Mesenchymal stromal cells from the human placenta promote neovascularization in a mouse model in vivo. *Placenta* **35**, 517–519 (2014).
645. Mathew, S. A. & Bhonde, R. Mesenchymal stromal cells isolated from gestationally diabetic human placenta exhibit insulin resistance, decreased

clonogenicity and angiogenesis. *Placenta* **59**, 1–8 (2017).
646. Gao, Z., Wang, N. & Liu, X. Human placenta mesenchymal stem cell-derived exosome shuttling microRNA-130b-3p from gestational diabetes mellitus patients targets ICAM-1 and perturbs human umbilical vein endothelial cell angiogenesis. *Acta Diabetol.* **59**, 1091–1107 (2022).
647. Boss, A. L., Chamley, L. W., Brooks, A. E. S. & James, J. L. Differences in human placental mesenchymal stromal cells may impair vascular function in FGR. *Reproduction* **162**, 319–330 (2021).
648. Umapathy, A. *et al.* Mesenchymal Stem/Stromal Cells from the Placentae of Growth Restricted Pregnancies Are Poor Stimulators of Angiogenesis. *Stem Cell Rev. Reports* **16**, 557–568 (2020).
649. Boss, A. L., Brooks, A. E. S., Chamley, L. W. & James, J. L. Influence of culture media on the derivation and phenotype of fetal-derived placental mesenchymal stem/stromal cells across gestation. *Placenta* **101**, 66–74 (2020).
650. de Groot, C. J., Chao, V. A., Roberts, J. M. & Taylor, R. N. Human endothelial cell morphology and autacoid expression. *Am. J. Physiol.* **268**, H1613-20 (1995).
651. DeCicco-Skinner, K. L. *et al.* Endothelial cell tube formation assay for the in vitro study of angiogenesis. *J. Vis. Exp.* e51312 (2014) doi:10.3791/51312.
652. Voyta, J. C., Via, D. P., Butterfield, C. E. & Zetter, B. R. Identification and isolation of endothelial cells based on their increased uptake of acetylated-low density lipoprotein. *J. Cell Biol.* **99**, 2034–2040 (1984).
653. Wu, C. C. *et al.* Synergism of biochemical and mechanical stimuli in the differentiation of human placenta-derived multipotent cells into endothelial cells. *J. Biomech.* **41**, 813–821 (2008).
654. Chen, C. Y. C. Y. C. P. *et al.* Human placenta-derived multipotent mesenchymal stromal cells involved in placental angiogenesis via the PDGF-BB and STAT3 pathways. *Biol. Reprod.* **93**, 1–10 (2015).
655. Qi, Y.-X., Han, Y. & Jiang, Z.-L. Mechanobiology and Vascular Remodeling: From Membrane to Nucleus. *Adv. Exp. Med. Biol.* **1097**, 69–82 (2018).
656. König, J. *et al.* Amnion-derived mesenchymal stromal cells show angiogenic properties but resist differentiation into mature endothelial cells. *Stem Cells Dev.* **21**, 1309–1320 (2011).
657. König, J. *et al.* Placental mesenchymal stromal cells derived from blood vessels or avascular tissues: what is the better choice to support endothelial cell function? *Stem Cells Dev.* **24**, 115–131 (2015).
658. Oswald, J. *et al.* Mesenchymal stem cells can be differentiated into endothelial cells in vitro. *Stem Cells* **22**, 377–384 (2004).
659. Pankajakshan, D., Kansal, V. & Agrawal, D. K. In vitro differentiation of bone marrow derived porcine mesenchymal stem cells to endothelial cells. *J. Tissue Eng. Regen. Med.* **7**, 911–920 (2013).
660. Yu, S. *et al.* First trimester placental mesenchymal stem cells improve cardiac function of rat after myocardial infarction via enhanced neovascularization. *Heliyon* **7**, e06120 (2021).
661. Bai, K., Huang, Y., Jia, X., Fan, Y. & Wang, W. Endothelium oriented differentiation of bone marrow mesenchymal stem cells under chemical and mechanical stimulations. *J. Biomech.* **43**, 1176–1181 (2010).
662. Fischer, L. J. *et al.* Endothelial Differentiation of Adipose-Derived Stem Cells: Effects of Endothelial Cell Growth Supplement and Shear Force. *J. Surg. Res.* **152**, 157–166 (2009).
663. Janeczek Portalska, K. *et al.* Endothelial Differentiation of Mesenchymal Stromal Cells. *PLoS One* **7**, (2012).
664. Shojaei, S., Tafazzoli-Shahdpour, M., Shokrgozar, M. A. & Haghighipour, N. Effects of mechanical and chemical stimuli on differentiation of human adipose-derived stem cells into endothelial cells. *Int. J. Artif. Organs* **36**, 663–673 (2013).
665. Wang, H. *et al.* Shear stress induces endothelial differentiation from a murine

embryonic mesenchymal progenitor cell line. *Arterioscler. Thromb. Vasc. Biol.* **25**, 1817–1823 (2005).
666. Wang, P. *et al.* Shear stress promotes differentiation of stem cells from human exfoliated deciduous teeth into endothelial cells via the downstream pathway of VEGF-Notch signaling. *Int. J. Mol. Med.* **42**, 1827–1836 (2018).
667. Yuan, L., Sakamoto, N., Song, G. & Sato, M. High-level shear stress stimulates endothelial differentiation and VEGF secretion by human mesenchymal stem cells. *Cell. Mol. Bioeng.* **6**, 220–229 (2013).
668. Zhang, P., Baxter, J., Vinod, K., Tulenko, T. N. & Di Muzio, P. J. Endothelial differentiation of amniotic fluid-derived stem cells: Synergism of biochemical and shear force stimuli. *Stem Cells Dev.* **18**, 1299–1308 (2009).
669. Vellasamy, S., Sandrasaigaran, P., Vidyadaran, S., George, E. & Ramasamy, R. Isolation and characterisation of mesenchymal stem cells derived from human placenta tissue. *World J. Stem Cells* **4**, 53–61 (2012).
670. Dominici, M. *et al.* Minimal criteria for defining multipotent mesenchymal stromal cells. The International Society for Cellular Therapy position statement. *Cytotherapy* (2006) doi:10.1080/14653240600855905.
671. Shalaby, F. *et al.* A requirement for Flk1 in primitive and definitive hematopoiesis and vasculogenesis. *Cell* **89**, 981–990 (1997).
672. Fong, G.-H., Zhang, L., Bryce, D.-M. & Peng, J. Increased hemangioblast commitment, not vascular disorganization, is the primary defect in flt-1 knock-out mice. *Development* **126**, 3015–3025 (1999).
673. Goncharov, N. V, Nadeev, A. D., Jenkins, R. O. & Avdonin, P. V. Markers and Biomarkers of Endothelium: When Something Is Rotten in the State. *Oxid. Med. Cell. Longev.* **2017**, 9759735 (2017).
674. Zanetta, L. *et al.* Expression of Von Willebrand factor, an endothelial cell marker, is up-regulated by angiogenesis factors: a potential method for objective assessment of tumor angiogenesis. *Int. J. cancer* **85**, 281–288 (2000).
675. Olofsson, B., Porsch, H. & Heldin, P. Knock-Down of CD44 Regulates Endothelial Cell Differentiation via NFκB-Mediated Chemokine Production. *PLoS One* **9**, e90921 (2014).
676. Trochon, V. *et al.* Evidence of involvement of CD44 in endothelial cell proliferation, migration and angiogenesis in vitro. *Int. J. Cancer* **66**, 664–668 (1996).
677. Saalbach, A., Wetzig, T., Haustein, U. F. & Anderegg, U. Detection of human soluble Thy-1 in serum by ELISA. Fibroblasts and activated endothelial cells are a possible source of soluble Thy-1 in serum. *Cell Tissue Res.* **298**, 307–315 (1999).
678. Jurisic, G., Iolyeva, M., Proulx, S. T., Halin, C. & Detmar, M. Thymus cell antigen 1 (Thy1, CD90) is expressed by lymphatic vessels and mediates cell adhesion to lymphatic endothelium. *Exp. Cell Res.* **316**, 2982–2992 (2010).
679. Airas, L. *et al.* Differential regulation and function of CD73, a glycosyl-phosphatidylinositol-linked 70-kD adhesion molecule, on lymphocytes and endothelial cells. *J. Cell Biol.* **136**, 421–431 (1997).
680. Lin, C. S., Xin, Z. C., Dai, J. & Lue, T. F. Commonly used mesenchymal stem cell markers and tracking labels: Limitations and challenges. *Histol. Histopathol.* **28**, 1109–1116 (2013).
681. Qian, H., Le Blanc, K. & Sigvardsson, M. Primary mesenchymal stem and progenitor cells from bone marrow lack expression of CD44 protein. *J. Biol. Chem.* **287**, 25795–25807 (2012).
682. Lee, D.-H. *et al.* Isolation and expansion of synovial CD34(-)CD44(+)CD90(+) mesenchymal stem cells: comparison of an enzymatic method and a direct explant technique. *Connect. Tissue Res.* **52**, 226–234 (2011).
683. Nassiri, F. *et al.* Endoglin (CD105): A Review of its Role in Angiogenesis and Tumor Diagnosis, Progression and Therapy. *Anticancer Res.* **31**, 2283 LP –

2290 (2011).
684. Qian, H., Yang, L., Zhao, W., Chen, H. & He, S. A comparison of CD105 and CD31 expression in tumor vessels of hepatocellular carcinoma by tissue microarray and flow cytometry. *Exp. Ther. Med.* **16**, 2881–2888 (2018).
685. Kong, D.-H., Kim, Y. K., Kim, M. R., Jang, J. H. & Lee, S. Emerging Roles of Vascular Cell Adhesion Molecule-1 (VCAM-1) in Immunological Disorders and Cancer. *Int. J. Mol. Sci.* **19**, (2018).
686. Vestweber, D. VE-cadherin: the major endothelial adhesion molecule controlling cellular junctions and blood vessel formation. *Arterioscler. Thromb. Vasc. Biol.* **28**, 223–232 (2008).
687. Crisan, M. *et al.* Perivascular Multipotent Progenitor Cells in Human Organs. *Ann. N. Y. Acad. Sci.* **1176**, 118–123 (2009).
688. Leroyer, A. S. *et al.* CD146 (Cluster of Differentiation 146). *Arterioscler. Thromb. Vasc. Biol.* **39**, 1026–1033 (2019).
689. Wu, C. C., Liu, F. L., Sytwu, H. K., Tsai, C. Y. & Chang, D. M. CD146+ mesenchymal stem cells display greater therapeutic potential than CD146- cells for treating collagen-induced arthritis in mice. *Stem Cell Res. Ther.* **7**, 1–13 (2016).
690. Deosarkar, S. P., Bhatt, P., Lewis, C. J. & Goetz, D. J. A quantitative real-time PCR approach for the detection and characterization of endothelial cells in whole blood. *Ann. Biomed. Eng.* (2011) doi:10.1007/s10439-011-0354-x.
691. Marelli-Berg, F. M., Clement, M., Mauro, C. & Caligiuri, G. An immunologist's guide to CD31 function in T-cells. *J. Cell Sci.* **126**, 2343–2352 (2013).
692. Lin, G. *et al.* Defining stem and progenitor cells within adipose tissue. *Stem Cells Dev.* **17**, 1053–1063 (2008).
693. Barber, C. L. & Iruela-Arispe, M. L. The ever-elusive endothelial progenitor cell: Identities, functions and clinical implications. *Pediatr. Res.* **59**, 26–32 (2006).
694. Sidney, L. E., Branch, M. J., Dunphy, S. E., Dua, H. S. & Hopkinson, A. Concise Review: Evidence for CD34 as a Common Marker for Diverse Progenitors. *Stem Cells* **32**, 1380–1389 (2014).
695. Siemerink, M. J. *et al.* CD34 marks angiogenic tip cells in human vascular endothelial cell cultures. *Angiogenesis* **15**, 151–163 (2012).
696. Tsuneki, M. & Madri, J. A. CD44 regulation of endothelial cell proliferation and apoptosis via modulation of CD31 and VE-cadherin expression. *J. Biol. Chem.* **289**, 5357–5370 (2014).
697. Sawano, A. *et al.* Flt-1, vascular endothelial growth factor receptor 1, is a novel cell surface marker for the lineage of monocyte-macrophages in humans. *Blood* **97**, 785–791 (2001).
698. Shibuya, M. Vascular endothelial growth factor receptor-1 (VEGFR-1/Flt-1): a dual regulator for angiogenesis. *Angiogenesis* **9**, 225–230 (2006).
699. Cleal, J. K., Day, P., Hanson, M. A. & Lewis, R. M. Measurement of Housekeeping Genes in Human Placenta. *Placenta* **30**, 1002–1003 (2009).
700. Spiegelman, B. M. & Farmer, S. R. Decreases in tubulin and actin gene expression prior to morphological differentiation of 3T3 Adipocytes. *Cell* **29**, 53–60 (1982).
701. Dugina, V. B., Shagieva, G. S., Shakhov, A. S. & Alieva, I. B. The Cytoplasmic Actins in the Regulation of Endothelial Cell Function. *Int. J. Mol. Sci.* **22**, (2021).
702. Xin, X. *et al.* Hepatocyte growth factor enhances vascular endothelial growth factor-induced angiogenesis in vitro and in vivo. *Am. J. Pathol.* **158**, 1111–1120 (2001).
703. Meng, F. *et al.* In vitro fluidic systems: Applying shear stress on endothelial cells. *Med. Nov. Technol. Devices* **15**, 100143 (2022).
704. Wong, A. K., LLanos, P., Boroda, N., Rosenberg, S. R. & Rabbany, S. Y. A Parallel-Plate Flow Chamber for Mechanical Characterization of Endothelial Cells Exposed to Laminar Shear Stress. *Cell. Mol. Bioeng.* **9**, 127–138 (2016).

705. Yoshimura, K. *et al.* Characterization of freshly isolated and cultured cells derived from the fatty and fluid portions of liposuction aspirates. *J. Cell. Physiol.* **208**, 64–76 (2006).
706. Varma, M. J. O. *et al.* Phenotypical and functional characterization of freshly isolated adipose tissue-derived stem cells. *Stem Cells Dev.* **16**, 91–104 (2007).
707. Campagnolo, P. *et al.* Human adult vena saphena contains perivascular progenitor cells endowed with clonogenic and proangiogenic potential. *Circulation* **121**, 1735–1745 (2010).
708. Gerhardt, H. & Betsholtz, C. Endothelial-pericyte interactions in angiogenesis. *Cell Tissue Res.* **314**, 15–23 (2003).
709. Lin, C.-S. & Lue, T. F. Defining vascular stem cells. *Stem Cells Dev.* **22**, 1018–1026 (2013).
710. Thomas, J. R., Naidu, P., Appios, A. & McGovern, N. The Ontogeny and Function of Placental Macrophages . *Frontiers in Immunology* vol. 12 (2021).
711. Ben Amara, A. *et al.* Placental macrophages are impaired in chorioamnionitis, an infectious pathology of the placenta. *J. Immunol.* **191**, 5501–5514 (2013).
712. Blaschitz, A. *et al.* Vascular endothelial expression of indoleamine 2,3-dioxygenase 1 forms a positive gradient towards the feto-maternal interface. *PLoS One* **6**, e21774 (2011).
713. in 't Anker, P. S. *et al.* Isolation of Mesenchymal Stem Cells of Fetal or Maternal Origin from Human Placenta. *Stem Cells* **22**, 1338–1345 (2004).
714. Kusuma, G. D. *et al.* Mesenchymal stem cells reside in a vascular niche in the decidua basalis and are absent in remodelled spiral arterioles. *Placenta* **36**, 312–321 (2015).
715. Mathews, S. *et al.* Propagation of pure fetal and maternal mesenchymal stromal cells from terminal chorionic villi of human term placenta. *Sci. Rep.* **5**, 10054 (2015).
716. Zhu, Y. *et al.* Placental mesenchymal stem cells of fetal and maternal origins demonstrate different therapeutic potentials. *Stem Cell Res. Ther.* **5**, 48 (2014).
717. Chen, K. *et al.* Human Decidual Mesenchymal Stem Cells Obtained From Early Pregnancy Improve Cardiac Revascularization Postinfarction by Activating Ornithine Metabolism . *Frontiers in Cardiovascular Medicine* vol. 9 (2022).
718. Elsafadi, M. *et al.* Transgelin is a TGFβ-inducible gene that regulates osteoblastic and adipogenic differentiation of human skeletal stem cells through actin cytoskeleston organization. *Cell Death Dis.* **7**, 1–14 (2016).
719. Brun, J. *et al.* Smooth Muscle-Like Cells Generated from Human Mesenchymal Stromal Cells Display Marker Gene Expression and Electrophysiological Competence Comparable to Bladder Smooth Muscle Cells. *PLoS One* **10**, e0145153 (2015).
720. Gu, W. *et al.* Smooth muscle cells differentiated from mesenchymal stem cells are regulated by microRNAs and suitable for vascular tissue grafts. *J. Biol. Chem.* **293**, 8089–8102 (2018).
721. Wang, Z., Wang, D.-Z., Pipes, G. C. T. & Olson, E. N. Myocardin is a master regulator of smooth muscle gene expression. *Proc. Natl. Acad. Sci.* **100**, 7129–7134 (2003).
722. Zeisberg, M. & Neilson, E. G. Review series personal perspective Biomarkers for epithelial-mesenchymal transitions. **119**, 1429–1437 (2009).
723. Alimperti, S. & Andreadis, S. T. CDH2 and CDH11 act as regulators of stem cell fate decisions. *Stem Cell Res.* **14**, 270–282 (2015).
724. Sakimoto, S. *et al.* CD44 expression in endothelial colony-forming cells regulates neurovascular trophic effect. *JCI insight* **2**, e89906 (2017).
725. Silva, L. P. D. *et al.* Neovascularization Induced by the Hyaluronic Acid-Based Spongy-Like Hydrogels Degradation Products. *ACS Appl. Mater. Interfaces* **8**, 33464–33474 (2016).
726. Rios de la Rosa, J. M. *et al.* Binding and Internalization in Receptor-Targeted

Carriers: The Complex Role of CD44 in the Uptake of Hyaluronic Acid-Based Nanoparticles (siRNA Delivery). *Adv. Healthc. Mater.* **8**, 1901182 (2019).
727. Ode, A. *et al.* CD73 and CD29 concurrently mediate the mechanically induced decrease of migratory capacity of mesenchymal stromal cells. *Eur. Cell. Mater.* **22**, 26–42 (2011).
728. Li, Q. *et al.* CD73(+) Mesenchymal Stem Cells Ameliorate Myocardial Infarction by Promoting Angiogenesis. *Front. cell Dev. Biol.* **9**, 637239 (2021).
729. Allard, B. *et al.* Anti-CD73 therapy impairs tumor angiogenesis. *Int. J. Cancer* **134**, 1466–1473 (2014).
730. Halldorsson, S., Lucumi, E., Gómez-Sjöberg, R. & Fleming, R. M. T. Advantages and challenges of microfluidic cell culture in polydimethylsiloxane devices. *Biosens. Bioelectron.* **63**, 218–231 (2015).
731. Wang, X., Bove, A. M., Simone, G. & Ma, B. Molecular Bases of VEGFR-2-Mediated Physiological Function and Pathological Role. *Front. Cell Dev. Biol.* **8**, 1–12 (2020).
732. Kroll, J. & Waltenberger, J. VEGF-A induces expression of eNOS and iNOS in endothelial cells via VEGF receptor-2 (KDR). *Biochem. Biophys. Res. Commun.* **252**, 743–746 (1998).
733. Liu, Z. *et al.* Endothelial nitric oxide synthase is dynamically expressed during bone marrow stem cell differentiation into endothelial cells. *Am. J. Physiol. - Hear. Circ. Physiol.* **293**, 1760–1765 (2007).
734. Wang, Y. *et al.* Interplay between integrins and FLK-1 in shear stress-induced signaling. *Am. J. Physiol. - Cell Physiol.* **283**, 1540–1547 (2002).
735. Byzova, T. V *et al.* A mechanism for modulation of cellular responses to VEGF: activation of the integrins. *Mol. Cell* **6**, 851–860 (2000).
736. Heiss, C., Rodriguez-Mateos, A. & Kelm, M. Central role of eNOS in the maintenance of endothelial homeostasis. *Antioxid. Redox Signal.* **22**, 1230–1242 (2015).
737. Aboalola, D. & Han, V. K. M. Different Effects of Insulin-Like Growth Factor-1 and Insulin-Like Growth Factor-2 on Myogenic Differentiation of Human Mesenchymal Stem Cells. *Stem Cells Int.* **2017**, 8286248 (2017).
738. Lin, S. *et al.* IGF-1 promotes angiogenesis in endothelial cells/adipose-derived stem cells co-culture system with activation of PI3K/Akt signal pathway. *Cell Prolif.* **50**, (2017).
739. Li, J. *et al.* Piezo1 integration of vascular architecture with physiological force. *Nature* **515**, 279–282 (2014).
740. Pathak, M. M. *et al.* Stretch-activated ion channel Piezo1 directs lineage choice in human neural stem cells. *Proc. Natl. Acad. Sci.* **111**, 16148–16153 (2014).
741. Zhou, T. *et al.* Piezo1/2 mediate mechanotransduction essential for bone formation through concerted activation of NFAT-YAP1-ß-catenin. *Elife* **9**, e52779 (2020).
742. Tonelli, F. M. P. *et al.* Stem cells and calcium signaling. *Adv. Exp. Med. Biol.* **740**, 891–916 (2012).
743. Sen, A. & Ta, M. Altered Adhesion and Migration of Human Mesenchymal Stromal Cells under Febrile Temperature Stress Involves NF-κβ Pathway. *Sci. Rep.* **10**, 4473 (2020).
744. Dahal, S., Huang, P., Murray, B. T. & Mahler, G. J. Endothelial to mesenchymal transformation is induced by altered extracellular matrix in aortic valve endothelial cells. *J. Biomed. Mater. Res. Part A* **105**, 2729–2741 (2017).
745. Piera-Velazquez, S. & Jimenez, S. A. Endothelial to Mesenchymal Transition: Role in Physiology and in the Pathogenesis of Human Diseases. *Physiol. Rev.* **99**, 1281–1324 (2019).
746. Dyer, L. A., Pi, X. & Patterson, C. The role of BMPs in endothelial cell function and dysfunction. *Trends Endocrinol. Metab.* **25**, 472–480 (2014).
747. Ma, L., Lu, M.-F., Schwartz, R. J. & Martin, J. F. Bmp2 is essential for cardiac

cushion epithelial-mesenchymal transition and myocardial patterning. *Development* **132**, 5601–5611 (2005).
748. McCulley, D. J., Kang, J.-O., Martin, J. F. & Black, B. L. BMP4 is required in the anterior heart field and its derivatives for endocardial cushion remodeling, outflow tract septation, and semilunar valve development. *Dev. Dyn. an Off. Publ. Am. Assoc. Anat.* **237**, 3200–3209 (2008).
749. Medici, D. & Kalluri, R. Endothelial-mesenchymal transition and its contribution to the emergence of stem cell phenotype. *Semin. Cancer Biol.* **22**, 379–384 (2012).
750. Jansson, T., Ekstrand, Y., Wennergren, M. & Powell, T. L. Placental glucose transport in gestational diabetes mellitus. *Am. J. Obstet. Gynecol.* **184**, 111–116 (2001).
751. Nathan, D. M. *et al.* Translating the A1C assay into estimated average glucose values. *Diabetes Care* **31**, 1473–1478 (2008).
752. Law, G. R. *et al.* Translating HbA1c measurements into estimated average glucose values in pregnant women with diabetes. *Diabetologia* **60**, 618–624 (2017).
753. Hempel, A. *et al.* High glucose concentrations increase endothelial cell permeability via activation of protein kinase C alpha. *Circ. Res.* **81**, 363–371 (1997).
754. He, X. *et al.* High glucose protects mesenchymal stem cells from metformin-induced apoptosis through the AMPK-mediated mTOR pathway. *Sci. Rep.* **9**, 17764 (2019).
755. Tsai, T. L., Manner, P. A. & Li, W. J. Regulation of mesenchymal stem cell chondrogenesis by glucose through protein kinase C/transforming growth factor signaling. *Osteoarthr. Cartil.* **21**, 368–376 (2013).
756. Cramer, C. *et al.* Persistent high glucose concentrations alter the regenerative potential of mesenchymal stem cells. *Stem Cells Dev.* **19**, 1875–1884 (2010).
757. Cheng, N.-C., Hsieh, T.-Y., Lai, H.-S. & Young, T.-H. High glucose-induced reactive oxygen species generation promotes stemness in human adipose-derived stem cells. *Cytotherapy* **18**, 371–383 (2016).
758. Hankamolsiri, W. *et al.* The effects of high glucose on adipogenic and osteogenic differentiation of gestational tissue-derived MSCs. *Stem Cells Int.* **2016**, (2016).
759. Mannino, G. *et al.* Effects of High Glucose Concentration on Pericyte-Like Differentiated Human Adipose-Derived Mesenchymal Stem Cells. *International Journal of Molecular Sciences* vol. 22 (2021).
760. Hayashi, J. N. *et al.* Effects of glucose on migration, proliferation and tube formation by vascular endothelial cells. *Virchows Arch. B Cell Pathol. Incl. Mol. Pathol.* **60**, 245–252 (1991).
761. Lee, C.-H. *et al.* High glucose induces human endothelial dysfunction through an Axl-dependent mechanism. *Cardiovasc. Diabetol.* **13**, 53 (2014).
762. Eskens, B. J. M., Zuurbier, C. J., van Haare, J., Vink, H. & van Teeffelen, J. W. G. E. Effects of two weeks of metformin treatment on whole-body glycocalyx barrier properties in db/db mice. *Cardiovasc. Diabetol.* **12**, 175 (2013).
763. Uddin, M. A., Akhter, M. S., Kubra, K.-T., Siejka, A. & Barabutis, N. Metformin in acute respiratory distress syndrome: An opinion. *Experimental gerontology* vol. 145 111197 (2021).
764. Tauseef, M. *et al.* Metformin Prevents High Glucose Induced Disruption of Coronary Artery Endothelial Barrier Function and Accelerates Wound Healing Via Regulating Junctional Protein, VE-Cadherin. *FASEB J.* **33**, 512.5-512.5 (2019).
765. Rasio, E. A., Bendayan, M. & Goresky, C. A. Effect of reduced energy metabolism and reperfusion on the permeability and morphology of the capillaries of an isolated rete mirabile. *Circ. Res.* **64**, 243–254 (1989).

766. Shawkat, H., Westwood, M.-M. & Mortimer, A. Mannitol: a review of its clinical uses. *Contin. Educ. Anaesth. Crit. Care Pain* **12**, 82–85 (2012).
767. Han, C., Yang, F., Guo, S. & Zhang, J. Hypertonic Saline Compared to Mannitol for the Management of Elevated Intracranial Pressure in Traumatic Brain Injury: A Meta-Analysis . *Frontiers in Surgery* vol. 8 (2022).
768. Roquilly, A. *et al.* Effect of Continuous Infusion of Hypertonic Saline vs Standard Care on 6-Month Neurological Outcomes in Patients with Traumatic Brain Injury: The COBI Randomized Clinical Trial. *JAMA - J. Am. Med. Assoc.* **325**, 2056–2066 (2021).
769. Rocha e Silva, M., Braga, G. A., Prist, R., Velasco, I. T. & Grança, E. S. Isochloremic hypertonic solutions for severe hemorrhage. *J. Trauma* **35**, 200–205 (1993).
770. Kang, J. H. *et al.* Mechanobiological Adaptation to Hyperosmolarity Enhances Barrier Function in Human Vascular Microphysiological System. *Adv. Sci.* **10**, 2206384 (2023).
771. Rao, G. M. Serum electrolytes and osmolality in diabetes mellitus. *Indian J. Med. Sci.* **46**, 301–303 (1992).
772. Singer, D. L., Drolette, M. E., Hurwitz, D. & Freinkel, N. Serum Osmolality and Glucose in Maturity Onset Diabetes Mellitus. *Arch. Intern. Med.* **110**, 758–762 (1962).
773. Lemmey, H. A. L. *et al.* Hyperglycaemia disrupts conducted vasodilation in the resistance vasculature of db/db mice. *Vascul. Pharmacol.* **103**–**105**, 29–35 (2018).
774. Kim, J. *et al.* Umbilical cord mesenchymal stromal cells affected by gestational diabetes mellitus display premature aging and mitochondrial dysfunction. *Stem Cells Dev.* **24**, 575–586 (2015).
775. Moseley, K. F., Doyle, M. E. & Jan De Beur, S. M. Diabetic serum from older women increases adipogenic differentiation in mesenchymal stem cells. *Endocr. Res.* **43**, 155–165 (2018).
776. Dwi Putra, S. E. *et al.* Being Born Large for Gestational Age is Associated with Increased Global Placental DNA Methylation. *Sci. Rep.* **10**, 1–10 (2020).
777. Byford, A. R., Forbes, K. & Scott, E. M. Glucose Treatment Targets in Pregnancy - A Review of Evidence and Guidelines. *Curr. Diabetes Rev.* **18**, (2022).
778. NHS. National Pregnancy in Diabetes Audit Report 2016: England, Wales and the Isle of Man. 5678 (2016).
779. Lee, T. T. M. *et al.* AiDAPT: automated insulin delivery amongst pregnant women with type 1 diabetes: a multicentre randomized controlled trial - study protocol. *BMC Pregnancy Childbirth* **22**, 282 (2022).
780. Stewart, Z. A. *et al.* Closed-Loop Insulin Delivery during Pregnancy in Women with Type 1 Diabetes. *N. Engl. J. Med.* **375**, 644–654 (2016).
781. Stewart, Z. A. *et al.* Day-and-night closed-loop insulin delivery in a broad population of pregnant women with type 1 diabetes: A randomized controlled crossover trial. *Diabetes Care* **41**, 1391–1399 (2018).
782. NHS England. Saving Babies' Lives Version 3.1. (2023).
783. Murphy, H. R. *et al.* Characteristics and outcomes of pregnant women with type 1 and type 2 diabetes: national population based 5-year cohort study. *Lancet Diabetes Endocrinol. - Press* (2020).
784. Davies, A. *et al.* Protocol for a multi-site randomised controlled feasibility study investigating intermittently scanned blood continuous glucose monitoring use for gestational diabetes: the RECOGNISE study. *Pilot Feasibility Stud.* **9**, 1–14 (2023).
785. Byford, A., Walsh, K., Holder, B., Scott, E. M. & Forbes, K. Temporal periods of mild hyperglycaemia in pregnancies complicated by gestational diabetes and LGA alter placental transcriptomic networks associated with vascularisation and

M2 hofbauer cell polarisation. *Endocr. Abstr.* **86**, (2022).
786. Dandona, P. Minimizing Glycemic Fluctuations in Patients with Type 2 Diabetes: Approaches and Importance. *Diabetes Technol. Ther.* **19**, 498–506 (2017).
787. Ciechanowska, A., Gora, I. M., Sabalinska, S. & Ladyzynski, P. The Effect of High and Variable Glucose on the Viability of Endothelial Cells Co-Cultured with Smooth Muscle Cells. *Int. J. Mol. Sci.* **23**, (2022).
788. National Institute for Health and Care Excellence. Diagnosis and management of type 1 diabetes in adults (NG17). (2022).
789. National Institute for Health and Care Excellence. Type 2 diabetes in adults (NG28). (2022) doi:10.1002/9781119950424.ch5.
790. Zhang, J., Li, H., Fan, B., Xu, W. & Zhang, X. Extracellular vesicles in normal pregnancy and pregnancy-related diseases. *J. Cell. Mol. Med.* **24**, 4377–4388 (2020).
791. Holder, B. *et al.* Macrophage Exosomes Induce Placental Inflammatory Cytokines: A Novel Mode of Maternal-Placental Messaging. *Traffic* **17**, 168–178 (2016).
792. Kennedy, M. *et al.* miR-1-3p and miR-133-3p are altered in maternal serum EVs and placenta in pregnancies complicated by gestational diabetes with large-for-gestational age babies. *Endocr. Abstr.* (2019) doi:10.1530/endoabs.65.p349.
793. Cartland, S., Scott, E., Saravanan, P., Simpson, N. & Forbes, K. Altered levels of extracellular vesicle miRNAs in the circulation of women with gestational diabetes is linked to altered placental development and increased fetal growth. *Placenta* **69**, e5–e11 (2018).
794. Rice, G. E. *et al.* The effect of glucose on the release and bioactivity of exosomes from first trimester trophoblast cells. *J. Clin. Endocrinol. Metab.* **100**, E1280–E1288 (2015).
795. Yamamoto, J. M. *et al.* Maternal glycaemic control and risk of neonatal hypoglycaemia in Type 1 diabetes pregnancy: a secondary analysis of the CONCEPTT trial. *Diabet. Med.* **36**, 1046–1053 (2019).
796. Malinowski, R. M. *et al.* Pancreatic β-cells respond to fuel pressure with an early metabolic switch. *Sci. Rep.* **10**, 1–11 (2020).
797. Rumala, C. Z. *et al.* Exposure of Pancreatic β-Cells to Excess Glucose Results in Bimodal Activation of mTORC1 and mTOR-Dependent Metabolic Acceleration. *iScience* **23**, 100858 (2020).
798. Nakano, H. *et al.* Glucose inhibits cardiac muscle maturation through nucleotide biosynthesis. *Elife* **6**, 1–23 (2017).
799. Torimoto, K. *et al.* Glucose consumption of vascular cell types in culture: toward optimization of experimental conditions. *Am. J. Physiol. Physiol.* **322**, C73–C85 (2021).
800. Malek, A. M., Goss, G. G., Jiang, L., Izumo, S. & Alper, S. L. Mannitol at clinical concentrations activates multiple signaling pathways and induces apoptosis in endothelial cells. *Stroke* **29**, 2631–2640 (1998).

Appendix

Appendix 1 – Final supplement concentrations in endothelial growth medium 2 (EGM-2).

Media Supplement	Final Supplement Concentration
Fetal Calf Serum (FCS)	0.02 mL/mL
Ascorbic Acid	1 µg/mL
Hydrocortisone	0.2 µg/mL
Long R3 Insulin-like Growth Factor 1 (IGF-1)	20 ng/mL
Heparin	22.5 µg/mL
Epidermal Growth Factor (EGF; recombinant human)	5 ng/mL
Basic Fibroblast Growth Factor (FGF; recombinant human)	10 ng/mL
VEGF-A (recombinant human)	0.5 ng/mL

Appendix 2 - Concentrations of supplements in VascuLife VEGF Endothelial Medium (Rh – recombinant human).

Media Supplement	Final Supplement Concentration
rh FGF basic	5 ng/mL
Ascorbic Acid	50 µg/mL
Hydrocortisone Hemisuccinate	1 µg/mL
FBS LifeFactor	2%
L-Glutamine	10 mM
rh IGF-1	15 ng/mL
rh EGF	5 ng/mL
rh VEGF	5 ng/mL
Heparin Sulfate	0.75U/mL
Antimicrobial supplement: *Gentamicin* *Amphotericin B*	 30 mg/mL 15 µg/mL

Appendix 3 - Concentrations of supplements in FibroLife S2 Medium (Rh – recombinant human).

Media Supplement	Final Supplement Concentration
rh FGF basic	5 ng/mL
Ascorbic Acid	50 µg/mL
Hydrocortisone Hemisuccinate	1 µg/mL
FBS LifeFactor	2%
L-Glutamine	7.5 mM
rh Insulin	5 µg/mL
Antimicrobial supplement: *Gentamicin* *Amphotericin B*	 30 mg/mL 15 µg/mL

Appendix 4 - Tissue processing program for term placental tissue and placental explants.

Reagent	Time (hh:mm)	
	Term tissue	Explants
70% EtOH	03:30	03:30
90% EtOH	03:30	03:30
100% EtOH	01:00	00:45
100% EtOH	01:00	00:45
100% EtOH	01:00	00:45
100% EtOH	01:00	00:45
100% EtOH	01:00	00:45
Xylene	01:00	00:30
Xylene	01:00	00:30
Xylene	01:00	00:30
Paraffin Wax	02:00	01:00
Paraffin Wax	02:00	01:00

Appendix 5 – Significant differentially expressed genes (DEGs) altered by 7 mM glucose in placental explants following acute glucose treatments for 48 hours. Genes significantly upregulated or downregulated ($p<0.05$, Log2FC -0.5< or >0.5) in placental explants cultured in constant 7 mM glucose compared to fluctuating 5/5.5 mM glucose for 48 hours. The Ensembl IDs and associated gene symbol (if available) are noted.

Ensembl ID	Gene Symbol	Log_2FC	P Value
ENSG00000279901		4.758602549	0.022955985
ENSG00000248385	TARM1	4.558466381	0.010090045
ENSG00000273888	FRMD6-AS1	4.047577009	0.042304306
ENSG00000254979		4.02260467	0.026515523
ENSG00000215887	ZNF859P	3.911542958	0.014670758
ENSG00000243543	WFDC6	3.842388383	0.040522921
ENSG00000204334	ERICH2	3.770909589	0.013777266
ENSG00000185156	MFSD6L	3.75366258	0.037005884
ENSG00000214643	DEFB133	3.674077211	0.04126769
ENSG00000252242	RNU7-115P	3.521264523	0.039732247
ENSG00000260126		3.447351633	0.000212347
ENSG00000124019	FAM124B	3.442410944	0.001275372
ENSG00000215237		3.413922149	0.029680207
ENSG00000005187	ACSM3	3.333865272	0.01228044
ENSG00000249753		3.217218128	0.04045208
ENSG00000174469	CNTNAP2	3.193200087	0.004944113
ENSG00000267174		3.186805221	0.013766308
ENSG00000264057		3.071906648	0.026690947
ENSG00000152580	IGSF10	2.8890633	0.004808519
ENSG00000153898	MCOLN2	2.721551745	0.021755943
ENSG00000281571		2.669494826	0.029058332
ENSG00000236994	YBX1P9	2.657370321	0.043527452
ENSG00000173894	CBX2	2.548418787	0.008547735
ENSG00000155659	VSIG4	2.527551334	0.013174631
ENSG00000266941		2.526025885	0.047087158
ENSG00000204352	C9orf129	2.514619071	0.041963526
ENSG00000238150		2.511039146	0.041905646
ENSG00000266283		2.477799791	0.049692801
ENSG00000113396	SLC27A6	2.356267641	0.020965571
ENSG00000153294	ADGRF4	2.352803578	0.020647979
ENSG00000258429	PDF	2.339725596	0.033881432
ENSG00000185306	C12orf56	2.334901791	0.011247478
ENSG00000156096	UGT2B4	2.288768541	0.033988228
ENSG00000164749	HNF4G	2.187500233	0.04027704
ENSG00000131477	RAMP2	2.019689649	0.004797885
ENSG00000099260	PALMD	2.004761862	0.002971963
ENSG00000134762	DSC3	1.998211876	0.024484244
ENSG00000269526	ERVV-1	1.954927556	0.041031844

ENSG00000162636	FAM102B	1.952835514	0.049425652
ENSG00000275162		1.927979739	0.006065005
ENSG00000238468	RNU7-14P	1.907891523	0.009680563
ENSG00000263257		1.870923932	0.038461675
ENSG00000147606	SLC26A7	1.869225133	0.034480943
ENSG00000152086	TUBA3E	1.854333085	0.021382739
ENSG00000186723	OR10H1	1.776374732	0.02306443
ENSG00000168916	ZNF608	1.766854808	0.028972363
ENSG00000267313	KC6	1.731246265	0.044614699
ENSG00000259479	SORD2P	1.724792995	0.029969847
ENSG00000170323	FABP4	1.704141057	0.001374824
ENSG00000196872	CRACDL	1.696867407	0.048246289
ENSG00000249751	ECSCR	1.687172747	0.044793975
ENSG00000112232	KHDRBS2	1.660053427	0.03246557
ENSG00000226987		1.644260758	0.038628417
ENSG00000203258		1.628624389	0.040503147
ENSG00000072694	FCGR2B	1.627657729	0.009940011
ENSG00000147036	LANCL3	1.624483512	0.021377191
ENSG00000185614	INKA1	1.617282128	0.046281436
ENSG00000037749	MFAP3	1.614395182	0.046222007
ENSG00000226124	FTCDNL1	1.604927916	0.01145013
ENSG00000083454	P2RX5	1.599774598	0.027673033
ENSG00000258659	TRIM34	1.582829973	0.013258623
ENSG00000064115	TM7SF3	1.497547187	0.026546057
ENSG00000107719	PALD1	1.420841788	0.03822645
ENSG00000226499		1.308667341	0.021819733
ENSG00000214357	NEURL1B	1.278429918	0.031047495
ENSG00000058804	NDC1	1.263477653	0.028677898
ENSG00000122176	FMOD	1.259121522	0.04856894
ENSG00000158828	PINK1	1.24814603	0.03843604
ENSG00000090776	EFNB1	1.247819628	0.03682553
ENSG00000159640	ACE	1.228429098	0.041715789
ENSG00000075188	NUP37	1.212871251	0.046943244
ENSG00000142494	SLC47A1	1.212826071	0.034514946
ENSG00000008853	RHOBTB2	1.191251432	0.031219484
ENSG00000165757	JCAD	1.15042256	0.00710357
ENSG00000260430		1.127155389	0.043375979
ENSG00000101311	FERMT1	1.125073495	0.031139073
ENSG00000174718	RESF1	1.118050507	0.025902199
ENSG00000259366		1.112751382	0.026725413
ENSG00000112769	LAMA4	1.083116822	0.022995104
ENSG00000070190	DAPP1	1.057479284	0.039757796
ENSG00000085871	MGST2	1.054271849	0.007080645
ENSG00000126785	RHOJ	1.037392904	0.048642228
ENSG00000120279	MYCT1	1.026560329	0.017915113
ENSG00000224877	NDUFAF8	1.023101911	0.036404268

ENSG00000261371	PECAM1	1.022098106	0.036329244
ENSG00000170917	NUDT6	0.996840699	0.035130401
ENSG00000144645	OSBPL10	0.987108851	0.022241342
ENSG00000137210	TMEM14B	0.962794675	0.014278
ENSG00000182405	PGBD4	0.954380149	0.035041675
ENSG00000172172	MRPL13	0.929841228	0.014139922
ENSG00000108387	SEPTIN4	0.90314955	0.043919427
ENSG00000099953	MMP11	0.898698279	0.045380161
ENSG00000187118	CMC1	0.895108443	0.017618995
ENSG00000124466	LYPD3	0.875624375	0.047163899
ENSG00000069122	ADGRF5	0.865311821	0.035414389
ENSG00000100593	ISM2	0.846453247	0.003907937
ENSG00000135218	CD36	0.844584355	0.017714661
ENSG00000111726	CMAS	0.830505971	0.043922252
ENSG00000175274	TP53I11	0.82644552	0.045507104
ENSG00000074660	SCARF1	0.806956582	0.049024905
ENSG00000122378	PRXL2A	0.80181127	0.037169851
ENSG00000111907	TPD52L1	0.79793909	0.043181518
ENSG00000181031	RPH3AL	0.784592347	0.040011706
ENSG00000166557	TMED3	0.774119053	0.02829421
ENSG00000185361	TNFAIP8L1	0.758525104	0.047545863
ENSG00000187266	EPOR	0.754702772	0.03559575
ENSG00000092850	TEKT2	0.72470648	0.036717627
ENSG00000153721	CNKSR3	0.698439437	0.018884877
ENSG00000048140	TSPAN17	0.686225084	0.035280106
ENSG00000111913	RIPOR2	0.612970758	0.049929284
ENSG00000130520	LSM4	0.588690372	0.041799696
ENSG00000104886	PLEKHJ1	0.588149457	0.040019932
ENSG00000105854	PON2	0.576078729	0.029169286
ENSG00000171345	KRT19	0.570050643	0.014021511
ENSG00000186994	KANK3	0.569843784	0.047906723
ENSG00000100342	APOL1	0.566670246	0.019022654
ENSG00000196743	GM2A	0.559809976	0.042698377
ENSG00000129757	CDKN1C	0.543538887	0.015901615
ENSG00000004799	PDK4	0.532816534	0.049515589
ENSG00000183077	AFMID	0.532698128	0.024794949
ENSG00000172590	MRPL52	0.516732833	0.049570048
ENSG00000125730	C3	-0.510534562	0.021474619
ENSG00000150093	ITGB1	-0.511035695	0.013163199
ENSG00000086015	MAST2	-0.514788177	0.013163199
ENSG00000008513	ST3GAL1	-0.515926698	0.014143656
ENSG00000133657	ATP13A3	-0.519750451	0.01179552
ENSG00000074964	ARHGEF10L	-0.522593661	0.049698957
ENSG00000134668	SPOCD1	-0.52499027	0.032091469
ENSG00000100906	NFKBIA	-0.52965119	0.033163415
ENSG00000087087	SRRT	-0.530623204	0.043964883

ENSG00000142871	CCN1	-0.531765092	0.04180847
ENSG00000196218	RYR1	-0.560196469	0.046102624
ENSG00000096070	BRPF3	-0.563089064	0.023450043
ENSG00000105559	PLEKHA4	-0.563305637	0.03453058
ENSG00000109323	MANBA	-0.564390377	0.041916784
ENSG00000196684	HSH2D	-0.56858871	0.035765794
ENSG00000049323	LTBP1	-0.56909961	0.030091612
ENSG00000154175	ABI3BP	-0.575272341	0.02155091
ENSG00000132510	KDM6B	-0.576298341	0.037780405
ENSG00000184557	SOCS3	-0.578165175	0.024387583
ENSG00000143333	RGS16	-0.591034352	0.042368678
ENSG00000168621	GDNF	-0.596330354	0.033163618
ENSG00000184014	DENND5A	-0.604300597	0.043179587
ENSG00000198900	TOP1	-0.604347873	0.045177698
ENSG00000079308	TNS1	-0.613139937	0.026348198
ENSG00000197594	ENPP1	-0.613403513	0.024592459
ENSG00000179832	MROH1	-0.614469386	0.020048832
ENSG00000113389	NPR3	-0.615994879	0.029853024
ENSG00000120738	EGR1	-0.621919502	0.038615403
ENSG00000010818	HIVEP2	-0.622712698	0.024960323
ENSG00000175084	DES	-0.627483272	0.01635447
ENSG00000102265	TIMP1	-0.627524096	0.039217017
ENSG00000176170	SPHK1	-0.628069441	0.028826076
ENSG00000081041	CXCL2	-0.628945615	0.020693757
ENSG00000185359	HGS	-0.633148305	0.038911279
ENSG00000175592	FOSL1	-0.633471914	0.030374495
ENSG00000074410	CA12	-0.63544177	0.035689608
ENSG00000169429	CXCL8	-0.636600533	0.014427092
ENSG00000214193	SH3D21	-0.640395648	0.042857063
ENSG00000107099	DOCK8	-0.641833055	0.046782966
ENSG00000160323	ADAMTS13	-0.642116473	0.016345084
ENSG00000196611	MMP1	-0.647418412	0.020601978
ENSG00000095383	TBC1D2	-0.652485117	0.043935126
ENSG00000162889	MAPKAPK2	-0.655310472	0.043028662
ENSG00000051523	CYBA	-0.655508591	0.038880794
ENSG00000103723	AP3B2	-0.658634599	0.022527897
ENSG00000165895	ARHGAP42	-0.660431478	0.021552959
ENSG00000133247	KMT5C	-0.664249515	0.017341107
ENSG00000180448	ARHGAP45	-0.67760495	0.032601053
ENSG00000125148	MT2A	-0.683284022	0.035941789
ENSG00000156831	NSMCE2	-0.683643554	0.044993747
ENSG00000159399	HK2	-0.686795572	0.019742926
ENSG00000101335	MYL9	-0.692057379	0.04596463
ENSG00000137331	IER3	-0.700272764	0.007081396
ENSG00000178860	MSC	-0.711580722	0.044417397
ENSG00000168542	COL3A1	-0.718768171	0.008900737

ENSG00000250397		-0.72283666	0.013306813
ENSG00000122861	PLAU	-0.724822436	0.023880528
ENSG00000047648	ARHGAP6	-0.725503744	0.021616075
ENSG00000157766	ACAN	-0.733398086	0.039301558
ENSG00000251562	MALAT1	-0.741114579	0.03852839
ENSG00000129667	RHBDF2	-0.743710736	0.038899528
ENSG00000246089		-0.74914953	0.005419754
ENSG00000266586		-0.750600009	0.031346523
ENSG00000112096	SOD2	-0.75235593	0.011498881
ENSG00000104765	BNIP3L	-0.752878518	0.026478072
ENSG00000026508	CD44	-0.754295236	0.005352573
ENSG00000171017	LRRC8E	-0.756284177	0.043013627
ENSG00000083857	FAT1	-0.757556195	0.046450396
ENSG00000108691	CCL2	-0.75757111	0.017034332
ENSG00000166483	WEE1	-0.781829762	0.017034332
ENSG00000270533		-0.784613648	0.046752523
ENSG00000270441	LAMB2P1	-0.787760999	0.035968811
ENSG00000117266	CDK18	-0.787764156	0.028345456
ENSG00000042062	RIPOR3	-0.790335929	0.03251634
ENSG00000156273	BACH1	-0.795278137	0.045327386
ENSG00000152503	TRIM36	-0.795495267	0.022276451
ENSG00000197355	UAP1L1	-0.799310664	0.010220776
ENSG00000101115	SALL4	-0.801817342	0.010760356
ENSG00000163735	CXCL5	-0.803586729	0.004739587
ENSG00000106624	AEBP1	-0.806027001	0.014985767
ENSG00000153904	DDAH1	-0.809037468	0.032034478
ENSG00000166670	MMP10	-0.841145532	0.005324783
ENSG00000134644	PUM1	-0.844117069	0.032560091
ENSG00000170345	FOS	-0.847698798	0.009916537
ENSG00000221878	PSG7	-0.853692434	0.03309329
ENSG00000128016	ZFP36	-0.858064516	0.009637477
ENSG00000136244	IL6	-0.868414347	0.014428601
ENSG00000073756	PTGS2	-0.868837976	0.002685991
ENSG00000148204	CRB2	-0.877206407	0.015409537
ENSG00000125740	FOSB	-0.886738614	0.007920696
ENSG00000101400	SNTA1	-0.912682142	0.033726482
ENSG00000163739	CXCL1	-0.917889854	0.006301246
ENSG00000172530	BANP	-0.923136478	0.006128132
ENSG00000163734	CXCL3	-0.930384134	0.006252173
ENSG00000197140	ADAM32	-0.93129183	0.047441088
ENSG00000144810	COL8A1	-0.936229893	0.049298162
ENSG00000136560	TANK	-0.944728324	0.021114674
ENSG00000162892	IL24	-0.94855088	0.005154745
ENSG00000121281	ADCY7	-0.950062757	0.044315047
ENSG00000165379	LRFN5	-0.952037208	0.028305406
ENSG00000244586	WNT5A-AS1	-0.952451547	0.044276677

ENSG00000161640	SIGLEC11	-0.954599874	0.047885277
ENSG00000197558	SSPOP	-0.963495652	0.015218085
ENSG00000180747	SMG1P3	-0.96627515	0.020089222
ENSG00000175985	PLEKHD1	-0.967073414	0.011530315
ENSG00000169826	CSGALNACT2	-0.980284076	0.037418256
ENSG00000105835	NAMPT	-0.984464559	0.002867751
ENSG00000100121	GGTLC2	-0.989111235	0.004812404
ENSG00000006283	CACNA1G	-1.006585762	0.030364823
ENSG00000184205	TSPYL2	-1.009595505	0.039694271
ENSG00000008710	PKD1	-1.009675476	0.026074951
ENSG00000140403	DNAJA4	-1.014050428	0.028786323
ENSG00000205795	CYS1	-1.028362437	0.03130073
ENSG00000115009	CCL20	-1.028538711	0.016270284
ENSG00000049656	CLPTM1L	-1.036009806	0.041718104
ENSG00000163673	DCLK3	-1.037642255	0.015909278
ENSG00000105989	WNT2	-1.046114727	0.011015078
ENSG00000131044	TTLL9	-1.061665883	0.046422735
ENSG00000144802	NFKBIZ	-1.065220128	0.012975865
ENSG00000157423	HYDIN	-1.07819004	0.030962987
ENSG00000157017	GHRL	-1.080569102	0.021166448
ENSG00000100626	GALNT16	-1.082539603	0.038248104
ENSG00000158220	ESYT3	-1.085050848	0.008897447
ENSG00000260860		-1.087673001	0.012466685
ENSG00000112149	CD83	-1.102983628	0.04537208
ENSG00000267505		-1.103003763	0.03667844
ENSG00000149435	GGTLC1	-1.112277285	0.014238008
ENSG00000007384	RHBDF1	-1.137164594	0.039999986
ENSG00000029153	ARNTL2	-1.149986734	0.023565513
ENSG00000253200		-1.156988738	0.028895789
ENSG00000258384	RCCD1-AS1	-1.159585552	0.042875926
ENSG00000110944	IL23A	-1.175560068	0.018696119
ENSG00000235501	CNN3-DT	-1.203386764	0.035524022
ENSG00000140983	RHOT2	-1.203467803	0.043104514
ENSG00000186193	SAPCD2	-1.210737044	0.042773462
ENSG00000233009	NALCN-AS1	-1.224300745	0.039647677
ENSG00000257674		-1.225973709	0.045806286
ENSG00000125538	IL1B	-1.233200397	0.000431421
ENSG00000164171	ITGA2	-1.238501302	0.028014684
ENSG00000105737	GRIK5	-1.23943003	0.022355902
ENSG00000134343	ANO3	-1.272119188	0.005203994
ENSG00000006071	ABCC8	-1.273225495	0.027668325
ENSG00000183458	PKD1P3	-1.276728727	0.0239894
ENSG00000280399		-1.287389604	0.031867222
ENSG00000168246	UBTD2	-1.308974723	0.039107874
ENSG00000253669	GASAL1	-1.343257028	0.034293162
ENSG00000104320	NBN	-1.346397442	0.037513825

ENSG00000132702	HAPLN2	-1.349515236	0.023672511
ENSG00000187997	C17orf99	-1.383378006	0.046386665
ENSG00000171094	ALK	-1.404952825	0.022829452
ENSG00000166448	TMEM130	-1.40742093	0.036589881
ENSG00000233186	KLF4P1	-1.408611972	0.025249456
ENSG00000138741	TRPC3	-1.412376767	0.048756307
ENSG00000236493	EIF2S2P3	-1.416525907	0.039092159
ENSG00000173369	C1QB	-1.422997262	0.023859747
ENSG00000176887	SOX11	-1.439514531	0.02346707
ENSG00000152784	PRDM8	-1.452554858	0.047089702
ENSG00000184313	MROH7	-1.463740417	0.022441731
ENSG00000078053	AMPH	-1.464156479	0.039958093
ENSG00000036448	MYOM2	-1.473713557	0.028182722
ENSG00000117479	SLC19A2	-1.476900716	0.031336622
ENSG00000142102	PGGHG	-1.480123885	0.049370858
ENSG00000196557	CACNA1H	-1.497651538	0.043732225
ENSG00000114124	GRK7	-1.504291886	0.029767424
ENSG00000059378	PARP12	-1.508711534	0.038196718
ENSG00000115419	GLS	-1.510730122	0.029989849
ENSG00000159086	PAXBP1	-1.516545906	0.044006277
ENSG00000126368	NR1D1	-1.520313128	0.035126759
ENSG00000228399		-1.521080037	0.03018281
ENSG00000121769	FABP3	-1.54584567	0.037204059
ENSG00000140044	JDP2	-1.547306074	0.044836296
ENSG00000048405	ZNF800	-1.560298809	0.049789107
ENSG00000171621	SPSB1	-1.562656926	0.036640603
ENSG00000125144	MT1G	-1.583849109	0.013307699
ENSG00000167842	MIS12	-1.585655104	0.044675048
ENSG00000173200	PARP15	-1.597512448	0.018040572
ENSG00000123358	NR4A1	-1.603969293	0.00976169
ENSG00000178038	ALS2CL	-1.608812504	0.034412639
ENSG00000176358	TAC4	-1.617595858	0.045440387
ENSG00000170340	B3GNT2	-1.622051779	0.048358642
ENSG00000248795		-1.623426527	0.023742043
ENSG00000178031	ADAMTSL1	-1.633647125	0.03396598
ENSG00000280113		-1.646585898	0.015622672
ENSG00000163659	TIPARP	-1.649209559	0.021241367
ENSG00000176903	PNMA1	-1.667565622	0.045785357
ENSG00000133065	SLC41A1	-1.668557844	0.044766635
ENSG00000161132		-1.676478503	0.047003322
ENSG00000227775		-1.681455899	0.046979871
ENSG00000165802	NSMF	-1.684775202	0.029915725
ENSG00000232871	SEC1P	-1.693862238	0.020830921
ENSG00000123610	TNFAIP6	-1.722582258	0.014016536
ENSG00000038358	EDC4	-1.731438239	0.039021244
ENSG00000213440	H2AZP1	-1.735873183	0.04370762

ENSG00000065268	WDR18	-1.742767106	0.045603878
ENSG00000242860	RN7SL180P	-1.75032183	0.025082334
ENSG00000073150	PANX2	-1.753869634	0.031887783
ENSG00000166863	TAC3	-1.759173681	0.034411698
ENSG00000250390		-1.761638278	0.03555382
ENSG00000241360	PDXP	-1.762164988	0.022369464
ENSG00000171051	FPR1	-1.768506851	0.042463764
ENSG00000270706	PRMT1P1	-1.795325851	0.049511546
ENSG00000224950		-1.803555248	0.007864301
ENSG00000198121	LPAR1	-1.804517709	0.047070051
ENSG00000071994	PDCD2	-1.809972477	0.041261046
ENSG00000253519		-1.841808021	0.031654678
ENSG00000100191	SLC5A4	-1.852647456	0.025943117
ENSG00000136449	MYCBPAP	-1.853996557	0.011378356
ENSG00000172548	NIPAL4	-1.860540941	0.029796834
ENSG00000129195	PIMREG	-1.860968117	0.042308385
ENSG00000240771	ARHGEF25	-1.876246655	0.04940245
ENSG00000160796	NBEAL2	-1.890339196	0.02602107
ENSG00000233576	HTR3C2P	-1.929675732	0.043040134
ENSG00000147234	FRMPD3	-1.930072403	0.023639512
ENSG00000106410	NOBOX	-1.931075681	0.047611965
ENSG00000146216	TTBK1	-1.940058646	0.038179535
ENSG00000175513	TSGA10IP	-1.957078515	0.02216985
ENSG00000119946	CNNM1	-1.960761061	0.022619557
ENSG00000197249	SERPINA1	-1.964170826	0.010181537
ENSG00000167257	RNF214	-1.966717115	0.049384188
ENSG00000132661	NXT1	-1.969114886	0.035785664
ENSG00000268496		-1.976020549	0.016775478
ENSG00000230061	TRPM2-AS	-1.990828677	0.03717638
ENSG00000273507		-2.005534107	0.041976234
ENSG00000237429		-2.006448476	0.01245131
ENSG00000163286	ALPG	-2.017697556	0.016381025
ENSG00000132437	DDC	-2.033115253	0.048331016
ENSG00000188365		-2.036878675	0.027229464
ENSG00000140598	EFL1	-2.05871045	0.036428014
ENSG00000229266	POM121L8P	-2.074591144	0.022143825
ENSG00000155330	C16orf87	-2.077124174	0.043392378
ENSG00000254884	PRR13P2	-2.087090597	0.013650144
ENSG00000112837	TBX18	-2.091625197	0.047890121
ENSG00000220581	VN1R12P	-2.094578595	0.010672021
ENSG00000277156	TOMM40P1	-2.104327662	0.049917325
ENSG00000140379	BCL2A1	-2.129917423	0.01434803
ENSG00000137558	PI15	-2.130000464	0.001226265
ENSG00000234042		-2.132161943	0.004133115
ENSG00000263766	KPNB1-DT	-2.135561463	0.030938095
ENSG00000222714	RN7SKP38	-2.139777314	0.042926076

ENSG00000285556		-2.1747645	0.027308349
ENSG00000152433	ZNF547	-2.20721591	0.041072271
ENSG00000228615	CENPNP2	-2.222435911	0.007076184
ENSG00000237846		-2.226466779	0.045600663
ENSG00000213866	YBX1P10	-2.228474609	0.043310751
ENSG00000153093	ACOXL	-2.238747668	0.044480439
ENSG00000111087	GLI1	-2.267066657	0.026081668
ENSG00000198326	TMEM239	-2.293693516	0.02826254
ENSG00000234773		-2.296172517	0.003992109
ENSG00000211452	DIO1	-2.332141169	0.046804219
ENSG00000130294	KIF1A	-2.338452942	0.026625675
ENSG00000197067	OR2T32P	-2.34378194	0.003371588
ENSG00000280767		-2.346831954	0.036445207
ENSG00000213779		-2.35479697	0.03597587
ENSG00000206120	EGFEM1P	-2.360075532	0.02167502
ENSG00000108641	B9D1	-2.362685045	0.029109885
ENSG00000269481		-2.383823843	0.039479071
ENSG00000182218	HHIPL1	-2.384464872	0.026810494
ENSG00000268049		-2.386937727	0.005685161
ENSG00000239483	RPS15AP16	-2.387723995	0.042071876
ENSG00000169314	C22orf15	-2.396351679	0.008882191
ENSG00000225025	KIF4CP	-2.401969021	0.027695392
ENSG00000215263		-2.402090111	0.028589308
ENSG00000114270	COL7A1	-2.4022393	0.047514879
ENSG00000241233	KRTAP5-8	-2.408757936	0.049249238
ENSG00000261644	CYLD-AS1	-2.41798911	0.028686326
ENSG00000227960		-2.437524722	0.031752585
ENSG00000236200	KDM4A-AS1	-2.444637045	0.048439499
ENSG00000026751	SLAMF7	-2.451844244	0.000358115
ENSG00000228307	OR2S1P	-2.461842142	0.040653137
ENSG00000228559		-2.467638017	0.023686301
ENSG00000206814	Y_RNA	-2.490414262	0.027484207
ENSG00000110881	ASIC1	-2.497580502	0.024189927
ENSG00000284959		-2.508225182	0.044899569
ENSG00000170962	PDGFD	-2.528187149	0.035585109
ENSG00000272397		-2.529748994	0.043645826
ENSG00000175463	TBC1D10C	-2.534768512	0.022923048
ENSG00000225447	RPS15AP10	-2.537556152	0.044874941
ENSG00000235979		-2.538499757	0.040957473
ENSG00000147697	GSDMC	-2.551563399	0.049880306
ENSG00000277632	CCL3	-2.558965808	0.044996347
ENSG00000267924		-2.574643145	0.040832991
ENSG00000273258		-2.598257487	0.015887474
ENSG00000183273	CCDC60	-2.616564689	0.047165146
ENSG00000084674	APOB	-2.636833339	0.008989683
ENSG00000204860	FAM201A	-2.645769192	0.043690004

ENSG00000186867	QRFPR	-2.664104568	0.02623324
ENSG00000239351	NPM1P29	-2.668217841	0.036028026
ENSG00000270379	HEATR9	-2.68924561	0.040232128
ENSG00000143632	ACTA1	-2.698819637	0.016289219
ENSG00000266076		-2.701097519	0.03515265
ENSG00000186710	CFAP73	-2.704343756	0.03111132
ENSG00000240045	STRIT1	-2.719714095	0.038906133
ENSG00000227242		-2.730648061	0.017293611
ENSG00000237331	XIAP-AS1	-2.747336916	0.032555148
ENSG00000237872	POU5F1P4	-2.748647459	0.024096801
ENSG00000204179	PTPN20	-2.762353316	0.042690295
ENSG00000188404	SELL	-2.77675976	0.023096586
ENSG00000130413	STK33	-2.790149425	0.02656852
ENSG00000227933		-2.790932306	0.003553252
ENSG00000182257	PRR34	-2.810777839	0.014111096
ENSG00000248550	OTX2-AS1	-2.816976202	0.048838471
ENSG00000262870	CYCSP40	-2.822340923	0.042261147
ENSG00000284727		-2.827720999	0.019205544
ENSG00000229931	ATXN1-AS1	-2.830889514	0.019450165
ENSG00000273724		-2.843925973	0.021054024
ENSG00000158578	ALAS2	-2.851524791	0.016554138
ENSG00000237788		-2.855239936	0.009427792
ENSG00000115616	SLC9A2	-2.889357555	0.027637759
ENSG00000228882	CICP9	-2.891459763	0.043672663
ENSG00000205710	C17orf107	-2.907065534	0.017399673
ENSG00000167414	GNG8	-2.909030077	0.047956554
ENSG00000130711	PRDM12	-2.913721715	0.035182156
ENSG00000199732	Y_RNA	-2.923973591	0.013793995
ENSG00000248796	MED15P8	-2.987937078	0.049108187
ENSG00000255583		-2.98928509	0.003966449
ENSG00000267275	KLF2-DT	-3.002661159	0.04009095
ENSG00000241577		-3.021416926	0.045453073
ENSG00000004468	CD38	-3.03087002	0.027347678
ENSG00000230661	YY1P1	-3.041256029	0.026989534
ENSG00000091583	APOH	-3.050072382	0.026121295
ENSG00000233579	KRT8P15	-3.072084493	0.024520969
ENSG00000125872	LRRN4	-3.079368824	0.028953258
ENSG00000263934	SNORD3A	-3.079862007	0.007642302
ENSG00000249188	ENPP7P1	-3.084586446	0.040588882
ENSG00000227790	SPECC1P1	-3.090618408	0.033484686
ENSG00000105675	ATP4A	-3.096387182	0.004202852
ENSG00000198944	SOWAHA	-3.109532071	0.04039
ENSG00000211891	IGHE	-3.117287095	0.049718647
ENSG00000108684	ASIC2	-3.133704184	0.004924393
ENSG00000258636		-3.145747852	0.041005501
ENSG00000155875	SAXO1	-3.148359575	0.019331131

ENSG00000268510	IFNL3P1	-3.156584652	0.048207323
ENSG00000263154		-3.16383716	0.020338204
ENSG00000232485	RPL37A-DT	-3.172148375	0.039242723
ENSG00000242067	RPL9P28	-3.172670238	0.015741962
ENSG00000114805	PLCH1	-3.189922662	0.03328192
ENSG00000171819	ANGPTL7	-3.220964861	0.036080306
ENSG00000274594		-3.261246111	0.024301064
ENSG00000204710	SPDYC	-3.279583414	0.04608219
ENSG00000174145	NWD2	-3.281212336	0.042899844
ENSG00000285694		-3.290250381	0.027879484
ENSG00000231468	PRDX3P2	-3.32037211	0.024552996
ENSG00000246777		-3.332514303	0.046751199
ENSG00000219926	OR7E104P	-3.352036602	0.043837897
ENSG00000198488	B3GNT6	-3.352825276	0.021196774
ENSG00000280035		-3.38427555	0.037056114
ENSG00000272892		-3.387304912	0.009756799
ENSG00000243081		-3.413094957	0.013421706
ENSG00000279296	PRAL	-3.420836442	0.004495087
ENSG00000182397	DNM1P46	-3.444079132	0.035101175
ENSG00000243365	RN7SL278P	-3.460768059	0.031464451
ENSG00000138028	CGREF1	-3.472802357	0.024393448
ENSG00000253433	NCRNA00250	-3.498173935	0.026617797
ENSG00000162383	SLC1A7	-3.50102512	0.04289421
ENSG00000215397	SCRT2	-3.506783141	0.028402141
ENSG00000275591	XKR5	-3.528060404	0.030221237
ENSG00000124205	EDN3	-3.56865962	0.018155094
ENSG00000138798	EGF	-3.572051046	0.024427775
ENSG00000165113	GKAP1	-3.623886796	0.005596348
ENSG00000254893	RAP1BL	-3.630389984	0.030466673
ENSG00000104059	FAM189A1	-3.636798071	0.024999029
ENSG00000234231	ANAPC1P4	-3.641991911	0.02956629
ENSG00000259964	THSD4-AS1	-3.643903069	0.028950019
ENSG00000278869		-3.693417305	0.023744195
ENSG00000261873	SMIM36	-3.708562439	0.032577239
ENSG00000188199	NUTM2B	-3.724355451	0.018783326
ENSG00000262223		-3.730704265	0.026378118
ENSG00000263718	SEPTIN9-DT	-3.734382083	0.01510481
ENSG00000255221	CARD17	-3.742618127	0.035076281
ENSG00000117971	CHRNB4	-3.755164975	0.011941988
ENSG00000252366	RNA5SP367	-3.759003452	0.013908458
ENSG00000130700	GATA5	-3.764679071	0.00183252
ENSG00000101251	SEL1L2	-3.770067029	0.043750577
ENSG00000186451	SPATA12	-3.798274737	0.045781612
ENSG00000234377	OBI1-AS1	-3.81436461	0.028601893
ENSG00000202058	RN7SKP80	-3.820418882	0.007600302
ENSG00000253521	HPYR1	-3.82476965	0.045394845

ENSG00000260386	LDC1P	-3.832862651	0.020063857
ENSG00000230528	NOS2P3	-3.840476244	0.017137263
ENSG00000250764		-3.848341017	0.018851593
ENSG00000095627	TDRD1	-3.859659249	0.038412067
ENSG00000244593		-3.87520177	0.028929986
ENSG00000228192		-3.875971776	0.013686493
ENSG00000213461	RPL32P15	-3.879579169	0.047696993
ENSG00000215156		-3.904843333	0.008986804
ENSG00000225398	PGM5P4	-3.905079843	0.040168227
ENSG00000213509	PPIAP16	-3.929400365	0.02629545
ENSG00000170558	CDH2	-3.95735028	0.011618338
ENSG00000185958	FAM186A	-3.962024774	0.008930239
ENSG00000234753	FOXP4-AS1	-3.985927496	0.019673839
ENSG00000236501		-3.989968546	0.027452406
ENSG00000204335	SP5	-4.006036069	0.007100767
ENSG00000262732		-4.007186572	0.017293443
ENSG00000269959	SPACA6P-AS	-4.026236095	0.008582101
ENSG00000269243		-4.038370481	0.01131355
ENSG00000196860	TOMM20L	-4.043397931	0.014013564
ENSG00000230180	RPL12P49	-4.080567333	0.036396518
ENSG00000060709	RIMBP2	-4.082375352	0.01351344
ENSG00000258524	NT5CP1	-4.094318514	0.041953892
ENSG00000228929	RPS13P2	-4.100841632	0.004098176
ENSG00000268061	NAPA-AS1	-4.105974145	0.009611466
ENSG00000226321	CROCC2	-4.125918036	0.043579752
ENSG00000211892	IGHG4	-4.189791101	0.014764136
ENSG00000224014		-4.200827936	0.039357027
ENSG00000254780		-4.214987218	0.047272244
ENSG00000095713	CRTAC1	-4.216555685	0.010821906
ENSG00000180245	RRH	-4.22246471	0.009071368
ENSG00000250432	FAM242C	-4.230862967	0.020957453
ENSG00000198134	PTMAP9	-4.276920342	0.02709012
ENSG00000172724	CCL19	-4.300141788	0.024535009
ENSG00000166664	CHRFAM7A	-4.317982715	0.020777156
ENSG00000237351	ITPK1P1	-4.329425036	0.004672353
ENSG00000239291		-4.336980134	0.008225262
ENSG00000222032		-4.366526527	0.042512616
ENSG00000251010		-4.430104256	0.01915734
ENSG00000258713	C20orf141	-4.468675808	0.00803477
ENSG00000284196		-4.486535737	0.008900992
ENSG00000228149	RPL3P1	-4.50087298	0.010984835
ENSG00000250120	PCDHA10	-4.515565522	0.021196576
ENSG00000125780	TGM3	-4.561448942	0.039576886
ENSG00000139865	TTC6	-4.589377365	0.045275183
ENSG00000015520	NPC1L1	-4.603525866	0.003012584
ENSG00000234381	MED15P7	-4.649487345	0.027530706

ENSG00000214970		-4.710694137	0.034487632
ENSG00000196376	SLC35F1	-4.802545901	0.004027729
ENSG00000198445	CCT8L2	-4.816350581	0.011044011
ENSG00000163352	LENEP	-4.839904973	0.027362854
ENSG00000070985	TRPM5	-4.955795204	0.003730511
ENSG00000255520		-4.984614959	0.017206567
ENSG00000256963		-5.00690072	0.00076069
ENSG00000169218	RSPO1	-5.481583398	0.000417693
ENSG00000261226		-5.571156504	0.000492695
ENSG00000102854	MSLN	-5.723054765	7.98E-05

Appendix 6 – Significant differentially expressed long non-coding RNAs (lncRNAs) altered by 7 mM glucose in placental explants following acute glucose treatments for 48 hours. LncRNAs significantly upregulated or downregulated ($p<0.05$, Log2FC -0.5< or >0.5) in placental explants cultured in constant 7 mM glucose compared to fluctuating 5/5.5 mM glucose for 48 hours. The Ensembl IDs and associated gene symbol (if available) are noted.

Ensembl ID	Gene Symbol	Log_2FC	P Value
ENSG00000227082	LINC02798	3.563147511	0.016387821
ENSG00000238284	LINC01448	3.294421798	0.044531488
ENSG00000254242		2.89667393	0.039506911
ENSG00000228824	MIR4500HG	1.939201619	0.047955386
ENSG00000251580	LINC02482	1.893907014	0.000289233
ENSG00000204929		1.484878755	0.00940901
ENSG00000163364	LINC01116	1.288367075	0.014235623
ENSG00000259070	LINC00639	-1.170374564	3.03E-05
ENSG00000254300	LINC01111	-1.298062157	0.011044188
ENSG00000242512	LINC01206	-1.517690564	0.036050352
ENSG00000248150	LINC02150	-1.758289899	0.046218459
ENSG00000214894	LINC00243	-1.858536587	0.024289555
ENSG00000259664	LINC02254	-2.072273575	0.023592086
ENSG00000260737	LINC01227	-2.220928168	0.044355179
ENSG00000182376		-2.257464344	0.036329189
ENSG00000227467	LINC01537	-2.362716236	0.048600169
ENSG00000225762	LINC01389	-2.609162923	0.047016132
ENSG00000272840		-2.644186848	0.03695853
ENSG00000253799	LINC01030	-2.872039741	0.030511304
ENSG00000253633		-3.138947924	0.014384553
ENSG00000226995	LINC00658	-3.302119495	0.04125261
ENSG00000223956	LINC01767	-3.356651453	0.034359392
ENSG00000249345	LINC02405	-3.474454892	0.033836685
ENSG00000262097	LINC02185	-3.492620047	0.019961527
ENSG00000263063		-3.873748919	0.033746003
ENSG00000249635		-3.973886412	0.011781134
ENSG00000272282	LINC02084	-4.505046589	0.008256063
ENSG00000269364	LINC01233	-4.51732604	0.012489366
ENSG00000236543		-4.941981967	0.033425771
ENSG00000230212		-4.999448402	0.003238656

Appendix 7 – Expression changes in Endothelial to Mesenchymal transition (EndMT) related genes in pMSCs cultured in control medium or differentiation medium for 11 days. The cycle threshold (Ct) values were inputted into an analysis spreadsheet provided by AnyGenes and carried out according to manufacturer's instructions. The Student's T-Test was used to determine statistical significance ($p<0.05$ considered statistically significant). A positive or negative gene expression variation was used to determine whether a gene was up- or down-regulated, respectively in pMSCs cultured in differentiation medium compared to control medium. **Red** highlight indicates genes that are upregulated in pMSCs cultured in differentiation medium (gene expression variation > 2) and **green** highlight indicates genes that are downregulated in pMSCs cultured in differentiation medium (gene expression variation < -2). Significant p values are highlighted in bold ($p<0.05$).

Gene Name	Expression variation	P Value
CDH5	-1.61	0.44580
ABL1	-1.19	0.66746
ACTA2	**-6.26**	**0.00093**
ACVR1	1.24	**0.02079**
AKT1	-1.08	0.88850
BMP2	**2.85**	**0.01452**
BMP4	1.23	0.65901
BMP7	-1.58	0.06967
CD34	1.98	0.26276
CDH2	**-16.13**	**0.00106**
CLDN5	1.12	0.79806
CNN1	**-11.26**	**0.00001**
COL1A1	-1.48	0.29066
CTGF	**-2.03**	0.11821
CTNNB1	-1.28	**0.04879**
DDR2	-1.22	0.17399
EDN1	-1.96	0.23298
EP300	-1.28	0.21671
F8	-1.27	0.57670
FGF2	**-5.48**	**0.00001**
FLT1	**14.63**	**0.00652**
FN1	-1.15	0.76281
GATA4	**-2.79**	0.26233
GSC	-1.65	0.12297
GSK3B	-1.13	0.53819
HGF	**28.12**	**0.00102**
HIF1A	-1.95	**0.01483**
ICAM2	-1.67	0.16637
IGF2	1.48	0.49423
IL1B	1.47	**0.03294**
ITGA5	1.06	0.23719
ITGAV	1.08	0.49092
ITGB1	-1.16	0.24408
ITGB3	-1.56	0.50160
JAG1	-1.31	0.76734
JAG2	-1.21	0.37998
KDR	**3.77**	**0.04661**
LEF1	**-2.20**	**0.04058**
MAPK1	-1.08	0.72364
MAPK14	-1.13	0.45803
MAPK3	1.33	0.05623

MMP2	**-2.72**	**0.01696**
MMP3	-1.66	0.70699
MMP9	**-3.35**	0.05526
MSX1	-1.24	0.46747
MSX2	-1.49	0.27320
MYOCD	**-16.52**	**0.00144**
NFATC1	1.55	0.20543
NFKB1	-1.32	0.05550
NOS3	-1.56	0.12250
NOTCH1	1.14	0.61147
NOTCH2	-1.47	0.15759
NOTCH3	1.14	0.54173
NOTCH4	-1.36	0.28603
PECAM1	-1.37	0.56913
PIK3CA	1.30	**0.00006**
PIK3R1	**-2.41**	**0.01829**
PRKCD	1.20	0.12211
SELE	-1.89	0.24961
SERPINE1	1.73	0.17069
SMAD2	-1.32	0.08556
SMAD3	-1.05	0.96871
SMAD4	-1.27	0.22701
SNAI1	1.24	0.33633
SNAI2	-1.32	0.50492
TAGLN	**-2.94**	**0.00188**
TCF3	-1.34	0.08917
TCF4	-1.19	0.62851
TGFB1	1.33	0.07781
TGFB2	1.34	0.60970
TGFB3	-1.01	0.82769
TGFBR1	-1.56	0.13408
TGFBR2	**5.72**	**0.00002**
TIE1	-1.58	0.17787
TNF	**-2.04**	0.09355
TWIST1	-1.13	0.85032
VEGFA	-1.49	0.15740
VIM	-1.07	0.93980
VTN	**-2.32**	**0.03891**
VWF	**-2.36**	0.05779
WNT11	**-2.49**	**0.04371**
WNT5A	-1.62	0.41409
ZEB1	**2.19**	**0.00465**
ZEB2	1.07	0.53685